

Aus dem Pathologischen Institut
Direktor: Prof. Dr. med. Thomas Kirchner
Ludwig-Maximilians-Universität München

**Funktionelle Genomik und zielgerichtete Therapie
maligner Tumoren**

vorgelegt von
Dr. med. Thomas Grünwald, Ph.D.
2017

Inhaltsverzeichnis

| | |
|---|-----------|
| 1 Zusammenfassung | 1 |
| 2 Einleitung | 3 |
| 3 Zielsetzung und Fragestellung | 5 |
| 4 Zusammenfassung und Diskussion themenbezogener eigener Arbeiten | 6 |
| 4.1 Silencing of LASP-1 influences zyxin localization, inhibits proliferation and reduces migration in breast cancer cells. | |
| 4.2 Overexpression of LASP-1 mediates migration and proliferation of human ovarian cancer cells and influences zyxin localization. | |
| 4.3 Nuclear localization and cytosolic overexpression of LASP-1 correlates with tumor size and nodal-positivity of human breast carcinoma. | |
| 4.4 Nuclear localisation of LASP-1 correlates with poor long-term survival in female breast cancer. | |
| 4.5 Loss of tumor suppressor mir-203 mediates overexpression of LIM and SH3 Protein 1 (LASP1) in high-risk prostate cancer thereby increasing cell proliferation and migration. | |
| 4.6 MondoA is highly overexpressed in acute lymphoblastic leukemia cells and modulates their metabolism, differentiation and survival. | |
| 4.7 STEAP1 is associated with the invasive and oxidative stress phenotype of Ewing tumors. | |
| 4.8 High STEAP1 expression is associated with improved outcome of Ewing's sarcoma patients. | |
| 4.9 Anti-oxidative stress response genes: bioinformatic analysis of their expression and relevance in multiple cancers. | |
| 4.10 The Zyxin-related protein thyroid receptor interacting protein 6 (TRIP6) is overexpressed in Ewing's sarcoma and promotes migration, invasion and cell growth. | |
| 4.11 First identification of Ewing's sarcoma-derived extracellular vesicles and exploration of their biological and potential diagnostic implications. | |
| 4.12 Robust diagnosis of Ewing sarcoma by immunohistochemical detection of super-enhancer-driven EWSR1-ETS targets. | |
| 4.13 Chimeric EWSR1-FLI1 regulates the Ewing sarcoma susceptibility gene EGR2 via a GGAA microsatellite. | |
| 5 Ausblick | 21 |
| 6 Literaturverzeichnis | 22 |
| 7 Danksagung | 29 |
| 8 Originalarbeiten | 30 |

1. Zusammenfassung

Ziel des vorliegenden Habilitationsprojekts war es, zu untersuchen, welche Strukturen sich in bestimmten Tumorentitäten als Angriffspunkte für eine Therapie und/oder als Biomarker eignen, ob sie funktionelle Relevanz für Tumorigenese und Metastasierung haben und über welche Mechanismen sie ihre Effekte ausüben.

Im Rahmen dieses Themenkomplexes wurde bei Mamma-, Ovarial- und Prostatakarzinomen erstmals gezeigt, dass das Zytoskelettprotein LASP1 in diesen Tumorentitäten stark überexprimiert ist und über die Regulation des Proteins Zyxin die Proliferation und Migration der Tumorzellen fördert (Frietsch et al., 2010; Grünwald et al., 2006, 2007a; Hailer et al., 2014), was mit einer signifikant schlechteren Prognose korrelierte (Frietsch et al., 2010; Grünwald et al., 2007b; Hailer et al., 2014). Ähnliche Beobachtungen wurden mit meinem Beitrag im Medulloblastomen gemacht (Traenka et al., 2010). Darüber hinaus lieferten meine Arbeiten den ersten Beleg dafür, dass LASP1 auch im Zellkern lokalisiert ist (Frietsch et al., 2010; Grünwald et al., 2007b) und damit wie LPP (Grünwald et al., 2009) und TRIP6 (Willier et al., 2011) zur Gruppe der nukleo-zytoplasmatischen Shuttle-Proteine gehört (Frietsch et al., 2010; Grünwald and Butt, 2008; Grünwald et al., 2007b; Orth et al., 2015; Vaman et al., 2015). In einer Folgearbeit verhalf ich zur Identifikation eines epigenetischen Mechanismus, der zur Überexpression von ZEB1 und damit zur verstärkten Metastasierung von Mammakarzinomen führt (Sahay et al., 2015). In weiteren Arbeiten trug ich zur metabolischen Charakterisierung von Mammakarzinomen bei, wodurch u. a. belegt wurde, dass deren Metastasen spezifische Veränderungen im Stoffwechsel aufweisen, die einer zielgerichteten Therapie zugänglich sind (Christen et al., 2016; Elia et al., 2017). Ähnliche Beobachtungen wurden von mir in der pädiatrischen akuten B lymphoblastischen Leukämiezellen gemacht, die den Glukose-Sensor MondoA stark überexprimieren und so ihre Glukoseaufnahme und Proliferation steigern (Wernicke et al., 2012). In einer weiteren Forschungsarbeit mit meinem Beitrag wurde gezeigt, dass LASP1 in chronisch myeloischen Leukämiezellen durch das Fusions-Onkoprotein BCR-ABL phosphoryliert wird und sich als Biomarker für das Monitoring der Aktivität von BCR-ABL-Inhibitoren eignet (Frietsch et al., 2014).

Ein weiterer Schwerpunkt des Habilitationsprojekts lag auf pädiatrischen Sarkomen wie dem Rhabdomyosarkom und dem Ewing Sarkom, die oft mit einer schlechten Prognose verbunden sind (Thiel et al., 2013, 2016). Ein besonderes Merkmal des

Ewing Sarkoms ist die Expression des Fusions-Onkoproteins *EWSR1-FLI1*, das als aberrierender Transkriptionsfaktor fungiert. In einer experimentellen Studie demonstrierte ich, dass die exosomale mRNA von *EWSR1-FLI1* als potentieller Biomarker im peripheren Blut dienen kann (Miller und Grünwald, 2015; Miller et al., 2013). In einer zusätzlichen Arbeit wurden zwei neue diagnostische Biomarker für Ewing Sarkome charakterisiert, deren Detektion mittels Immunhistochemie (IHC) eine einfache und robuste Abgrenzung von Ewing Sarkomen gegenüber anderen kleinrundzelligen Sarkomen ermöglicht (Baldauf et al., 2017).

Durch die Kombination von Genexpressions-Analysen und funktionellen Experimenten zeigte ich, dass die im Ewing Sarkom stark überexprimierte Oxidoreduktase *STEAP1* (Grünwald et al., 2012a) durch reaktive Sauerstoffspezies zum invasiven Wachstum und zum oxidativen Stress-Phänotyp von Ewing Sarkomen beiträgt (Grünwald et al., 2012b), was mit dem klinischen Outcome korrelierte (Grünwald et al., 2012c). In einer Folgearbeit mit meinem Beitrag wurde belegt, dass *STEAP1* als spezifische Zielstruktur einer Immuntherapie dienen kann (Grünwald et al., 2012a; Schirmer et al., 2016). Weiterführende bioinformatische Analysen wiesen zudem darauf hin, dass sich auch zahlreiche Karzinome durch einen oxidativen Stress-Phänotyp und eine kompensatorische Überaktivierung der Thioredoxin- und Glutathion-Systeme auszeichnen (Rotblat et al., 2013). In der Tat stellen spezifische Anpassungsmechanismen an Stressbedingungen einen Selektionsvorteil dar (Sannino et al., 2016). Diesbezüglich wurde in zwei Arbeiten mit meinem Beitrag gezeigt, dass die Proteine *YB1* und *G3BP1* in Sarkomzellen die Bildung von Stressgranula fördern, was die Metastasierung begünstigt (El-Naggar et al., 2015; Somasekharan et al., 2015).

Ein anderes im Ewing Sarkom stark überexprimierte Gen kodiert für den Zytoskelett-Regulator *TRIP6*, das dem durch *LASP1* regulierten Protein Zyxin strukturell ähnlich ist (Willier et al., 2011). In funktionellen Experimenten zeigte ich, dass die Überexpression von *TRIP6* mit verstärktem Tumorwachstum und Metastasierung von Ewing Sarkom-Zellen assoziiert ist (Grünwald et al., 2013). Zusätzlich trug ich zur funktionellen Charakterisierung von *EWSR1-FLI1*-induzierten Genen wie *GPR64*, *DKK2*, *CHM1* und *PAPPA* bei (Blaeschke et al., 2016; Hauer et al., 2013; Kirschner et al., 2017; Richter et al., 2013). Für *CHM1* und *PAPPA* konnten mit meinem Beitrag adoptive T Zell-Therapien entwickelt werden (Blaeschke et al., 2016; Kirschner et al., 2017), die teilweise bereits bei Ewing Sarkom-Patienten

eingesetzt werden (Thiel et al., 2017) und für die Fratrizid-Ereignisse durch einen neuen Biomarker vorhergesagt werden können (Kirschner et al., 2016).

Ewing Sarkome treten ca. 10-20x häufiger bei Europäern als bei Afrikanern auf. In einer weiteren Arbeit wurde hierfür einen ersten Erklärungsansatz beschrieben (Grünwald et al., 2015): So konnte ich mittels funktioneller Genomik zeigen wie EWSR1-FLI1 innerhalb eines bekannten Suszeptibilitäts-Locus mit einer regulatorischen Variante interagiert und so das Gen *EGR2* hochreguliert (Grünwald et al., 2015). Funktionelle Experimente demonstrierten, dass die Unterdrückung von *EGR2* die Proliferation von Ewing Sarkom-Zellen stark reduziert und in einem Mausmodell sogar zur Tumorregression führte. Dies könnte durch die Verknüpfung von *EGR2* mit dem fibroblast growth factor (FGF)-Signalweg bedingt sein, der das Wachstum von Ewing Sarkom-Zelllinien stark fördert (Grünwald et al., 2015). Eine vergleichende Untersuchung in öffentlichen Datensätzen ergab eine hochsignifikant erhöhte Frequenz der oben beschriebenen Risiko-Variante im Erbgut von Europäern im Vergleich zu Afrikanern (Grünwald et al., 2015). Diese Ergebnisse zeigen beispielhaft, wie das Zusammenspiel einer häufigen Keimbahn-Variante mit einem seltenen Onkogen wichtige Signalwege so modifizieren kann, dass schließlich die Tumorentstehung gefördert und das populationsspezifische Krebsrisiko erhöht wird (Grünwald and Delattre, 2016; Grünwald et al., 2016). Darüber hinaus wies die enge Verzahnung von *EGR2* mit dem FGF-Signalweg darauf hin, dass dessen Blockierung therapeutisch nutzbar sein könnte, was in einer Folgearbeit mit meinem Beitrag belegt wurde (Cidre-Aranaz et al., 2017). In einer von mir durchgeführten Delphi-Umfrage an 24 deutschsprachigen Universitäts-Kinderkliniken wurde zudem eine empirische Bewertung von experimentellen Therapien bei krebskranken Kindern erhoben (Grünwald et al., 2012d).

2. Einleitung

Eine der wahrscheinlich wichtigsten Herausforderungen für die moderne Medizin in der Behandlung von krebskranken Patienten liegt in der Transformation konventioneller Therapieschemata zu einer sich immer weiter differenzierenden personalisierten Medizin (Schilsky, 2010). Bahnbrechende technologische Entwicklungen haben es in den vergangenen 20 Jahren ermöglicht, Tumoren Genom- und Transkriptom-weit zu analysieren (Vucic et al., 2012). Durch ständig

sinkende Kosten und Weiterentwicklungen im Bereich der Bioinformatik werden solche „Omics“-Analysen in naher Zukunft ein Standardverfahren bei jedem krebskranken Patienten sein (Vucic et al., 2012). Es ist davon auszugehen, dass schon bald Genom-Sequenzierungen sowie die Interpretation der gewonnenen Daten mit entsprechenden „bench-top“-Geräten auf den Krankenstationen selbst innerhalb von wenigen Stunden für sehr geringe Kosten durchführbar sein werden. Eine wesentliche Aufgabe der forschenden Medizin liegt nun darin die teilweise patientenspezifischen (epi-)genetischen Veränderungen der Tumorzellen im Hinblick auf deren mögliche funktionelle Relevanz sowie Nutzbarkeit als Biomarker und/oder Zielstruktur einer individualisierten Krebstherapie zu bewerten (Rotblat und Grünwald, 2015). Diese Aufgaben fallen in den Bereich der funktionellen Genomik. Prominente Beispiele dafür, wie durch Forschungsergebnisse aus der funktionellen Genomik die Heilungsaussichten von Patienten maßgeblich verbessert werden konnten, sind der niedermolekulare Inhibitor Imatinib bei der chronisch myeloischen Leukämie (Druker et al., 2006) und beim gastrointestinalen Stromatumor (Demetri et al., 2002) sowie die Antikörper Trastuzumab und Pertuzumab beim HER2/neu-positiven Mammakarzinom (Swain et al., 2015). Stimuliert durch diese wichtigen Erfolge für die personalisierte Medizin wurden internationale Konsortien wie das ICGC (International Cancer Genome Consortium) mit dem Ziel gegründet, globale Ressourcen zu bündeln, um auch für seltene Krebserkrankungen hohe Fallzahlen an standardisiert analysierten Tumoren zu erreichen und die erhobenen Daten der Öffentlichkeit zur Verfügung zu stellen (Zhang et al., 2011). Hierbei zeigte sich, dass sich insbesondere hypermutierte Tumoren des Erwachsenenalters für neue immuntherapeutische Verfahren eignen (Neoantigene) (Gubin et al., 2015), wohingegen oligo-mutierte pädiatrische Tumoren eher subtilere Veränderungen aufweisen, die bei entsprechender funktioneller Charakterisierung dennoch neue Ansatzpunkte für eine individualisierte Therapie bieten können (Grünwald und Fulda, 2016). So ist bei kindlichen Tumoren davon auszugehen, dass die detaillierte Charakterisierung von Interaktionen aus Veränderungen der Keimbahn und den meist wenigen somatischen Mutationen eventuell zusätzliche Zielstrukturen identifizieren wird (Grünwald und Delattre, 2016; Grünwald et al., 2016).

Eine weitere wichtige Aufgabe der forschenden Medizin wird darin liegen, nicht nur die inter-individuellen Unterschiede der Patienten und korrespondierenden Tumoren zu verstehen, sondern auch die Mechanismen und klinischen Auswirkungen der

intra-tumoralen Heterogenität (Grünwald et al., 2011). Aus diesen Kernaufgaben der modernen Krebsmedizin ergeben sich wichtige Fragestellungen zur klinischen und funktionellen Bedeutung von tumorspezifischen Veränderungen, die im Rahmen der hier zusammengefassten experimentellen Arbeiten behandelt wurden.

3. Zielsetzung und Fragestellung

Ziel dieses Habilitationsprojekts war es, mittels funktioneller Genomik neue Angriffspunkte und Biomarker für eine schonende Therapie von Patienten mit malignen Tumoren zu identifizieren und zu charakterisieren. Die Schwerpunkte lagen dabei im Erwachsenenbereich auf gynäkologischen und urologischen Tumoren und bei kindlichen Krebserkrankungen auf Sarkomen. Im Speziellen wurden folgende Fragestellungen angegangen:

1. Welche Strukturen eignen sich in den jeweiligen Tumorentitäten als therapeutische Angriffspunkte?
2. Welche Strukturen eignen sich in den jeweiligen Tumorentitäten als diagnostische, prognostische und/oder prädiktive Biomarker?
3. Haben die identifizierten Strukturen funktionelle Relevanz für Tumorigenese und Metastasierung?
4. Über welche Mechanismen üben diese Strukturen ihre Effekte aus?

4. Zusammenfassung und Diskussion themenbezogener eigener Arbeiten

4.1 Silencing of LASP-1 influences zyxin localization, inhibits proliferation and reduces migration in breast cancer cells

Thomas G. P. Grünewald, Ulrike Kämmerer, Elfriede Schulze, Detlev Schindler, Arnd Hönig, Michael Zimmer, Elke Butt

Exp Cell Res. 2006; 312:974–82.

Tomasetto *et al.* haben 1995 die Überexpression von *LASP1* mRNA in humanen Mammakarzinomen anhand von Northern blots nachgewiesen (Tomasetto *et al.*, 1995a). Unklar blieb jedoch die Funktion von *LASP1* für diese Tumoren.

In der unter 4.1 genannten Studie wurde die hohe Expression von *LASP1* in Mammakarzinomen mittels Immunhistochemie (IHC) bestätigt sowie eine Reihe von funktionellen Experimenten durchgeführt. So wurde gezeigt, dass sich die Herunterregulation von *LASP1* in Mammakarzinom-Zelllinien mittels RNA-Interferenz stark inhibierend auf die Migration auswirkt, wohingegen die ektopische Überexpression in Mesangialzellen der australischen Beutelratte die Motilität deutlich steigerte (Grünewald *et al.*, 2006). Diese Ergebnisse deuteten auf eine wichtige Rolle von *LASP1* im Hinblick auf Metastasierung hin und darauf, dass eine gewisse Menge an *LASP1* in fokalen Kontakten für ein normales Migrationsverhalten notwendig ist, zumal die artifizielle Überexpression von *LASP1* in Mammakarzinom-Zellen, die ohnehin schon *LASP1* überexprimieren, ebenfalls zu einer Hemmung der Migration führte.

Darüber hinaus wurde gezeigt, dass der knockdown von *LASP1* zu einer stark verringerten Proliferation und Arretierung des Zellzyklus in der G2-Phase führt. Diese in Mammakarzinom-Zelllinien gewonnenen Erkenntnisse wurden mehrfach in anderen Tumorentitäten bestätigt (Orth *et al.*, 2015). In weiterführenden Experimenten zeigte sich, dass der Verlust von *LASP1* an fokalen Kontakten auch zum Verlust des nukleo-zytoplasmatischen Shuttle-Proteins Zyxin führt, das dann vermehrt im Zellkern lokalisiert ist. Interessanterweise wird Zyxin in Ewing Sarkomen nur sehr gering exprimiert und ist dort ebenfalls nur diffus im Zytoplasma verteilt, statt sich in Aktin-reichen Zelladhäsionsplaques anzusammeln (Amsellem *et al.*, 2005). Ein Zyxin-Gentransfer in EWSR1-FLI1-transformierte Fibroblasten führte dagegen zur Akkumulation von Zyxin an fokalen Kontakten und zu einer verringerten

Proliferationsrate. Deshalb wurde Zyxin in Ewing Sarkomen bereits als Tumorsuppressor-Protein beschrieben (Amsellem et al., 2005).

Dies könnte im Umkehrschluss bedeuten, dass Tumorzellen, die LASP1 stark überexprimieren, vermehrt Zyxin an fokale Kontakte rekrutieren und dadurch Zyxin bei der Ausübung der Tumorsuppressor-Funktion behindern (Grünwald und Butt, 2008).

4.2 Overexpression of LASP-1 mediates migration and proliferation of human ovarian cancer cells and influences zyxin localization

Thomas G. P. Grünwald, Ulrike Kämmerer, Christiane Winkler, Detlev Schindler, Albert Sickmann, Arnd Hönig, Elke Butt

Br J Cancer. 2007; 96:296–305.

Die unter 4.1 beschriebene Arbeit legte nahe, dass die Überexpression von LASP1 zur Aggressivität von Mammakarzinomen beiträgt (Grünwald et al., 2006). In der unter 4.2 genannten Folgearbeit wurde untersucht, ob ähnliche Effekte auch bei Ovarialkarzinomen vorliegen. Tatsächlich ist LASP1 auch in verschiedenen Ovarialkarzinom-Zelllinien und primären Ovarialkarzinomen überexprimiert. In funktionellen Analysen konnte gezeigt werden, dass LASP1 auch in Ovarialkarzinom-Zelllinien zur Proliferation und zur Zellzyklus-Progression sowie zur Migration und Lokalisation von Zyxin an fokalen Kontakten beiträgt (Grünwald et al., 2007a). Interessanterweise hatte der LASP1 knockdown weder Einfluss auf das Aktin- noch auf das Tubulin-Zytoskelett, und ein knockdown von Zyxin alleine hatte auch keinen Einfluss auf die Migration von Ovarialkarzinom-Zelllinien. Diese Experimente wiesen darauf hin, dass der LASP1 über die Lokalisation von Zyxin hinausgehende Effekte auf die Migration haben könnte.

Zudem wurde mithilfe von 2D-Proteom-Gelelektrophoresen und anschließender Massenspektrometrie ein durch LASP1 differenziell reguliertes Protein gefunden – namentlich 14-3-3 σ (Grünwald et al., 2007a). Dabei scheint der knockdown von LASP1 zu einer verstärkten Expression von 14-3-3 σ zu führen, das als Tumorsuppressor die Zellzyklusprogression in der G2/M-Phase hemmt (Peng et al., 1997).

In weiterführenden Arbeiten wurde belegt, dass LASP1 ein direkter Bindungspartner von 14-3-3 σ ist und dass die durch LASP1 vermittelte Unterdrückung von 14-3-3 σ zur Aggressivität von Dickdarmkarzinomen beiträgt (Shao et al., 2016). Zudem erwies sich, dass eine gleichzeitige niedrige 14-3-3 σ - und hohe LASP1-Expression mit besonders schlechten Heilungsaussichten von Patienten mit Dickdarmkarzinomen einhergehen (Shao et al., 2016). Die LASP1-14-3-3 σ -Signalkaskade wurde deshalb als neue therapeutische Zielstruktur vorgeschlagen (Shao et al., 2016).

4.3 Nuclear localization and cytosolic overexpression of LASP-1 correlates with tumor size and nodal-positivity of human breast carcinoma

Thomas G. P. Grünwald*, Ulrike Kämmerer*, Michaela Kapp, Matthias Eck, Johannes Dietl, Elke Butt, Arnd Hönig (* geteilte Erstautorenschaft)
BMC Cancer. 2007; 7:198.

Die unter 4.1 beschriebene Studie belegte erstmals die hohe Expression von LASP1 in Mammakarzinomen (Grünwald et al., 2006). Um das Expressionsmuster und dessen klinische Relevanz besser zu charakterisieren, wurde die unter 4.3 genannte Folgearbeit durchgeführt. Diese ergab, dass die LASP1-Expression signifikant positiv mit dem klinischen Stadium von Patientinnen mit Mammakarzinomen korreliert. Da LASP1 sowohl Proliferation als auch Migration beeinflusst (Grünwald et al., 2006), erschien es plausibel, dass Mammakarzinome mit hoher LASP1-Expression häufig bereits zum Operationszeitpunkt metastasiert waren und einen großen Tumorquerschnitt erreichten. Zudem wurde in dieser Arbeit zum ersten Mal mittels konfokaler Mikroskopie sowie Western blots gezeigt, dass LASP1 nicht nur an fokalen Kontakten, sondern auch im Zellkern lokalisiert ist (Grünwald et al., 2007b), was LASP1 in die Familie der nukleo-zytoplasmatischen Shuttle-Proteine einreicht (Grünwald und Butt, 2008; Orth et al., 2015). LASP1 ist dabei nicht nur in Zellkernen von Tumorzellen nachweisbar, sondern auch in proliferierenden Zellen der Basalzellschicht der Epidermis, wohingegen nicht-proliferierende obere Epithelschichten keine nukleäre LASP1-Immunoreaktivität aufwiesen (Grünwald et al., 2007b). Die nukleäre Translokation von LASP1 könnte somit für die Proliferation von sowohl Tumor- als auch Normalgeweben bedeutsam sein.

Der genaue Mechanismus der nukleären Translokation von LASP1, welches selbst kein nukleäres Importsignal besitzt, wurde von Mihlan *et al.* beschrieben (Mihlan *et al.*, 2013): LASP1 muss mit einem weiteren nukleo-zytoplasmatischen Shuttle-Protein, ZO2, hetero-dimerisieren, um in den Zellkern zu gelangen (Mihlan *et al.*, 2013). Im Zellkern scheint LASP1 als Plattform für TGFβ-vermittelte Signalwege und SNAIL zu dienen (Duvall-Noelle *et al.*, 2016; Niu *et al.*, 2016), womit LASP1 direkt in Prozesse wie EMT (Epithelial to Mesenchymal Transition) involviert sein könnte. Die mögliche Assoziation der nukleären Translokation von LASP1 mit individuellen Zellzyklusphasen wurde in einer Folgestudie untersucht (siehe 4.4).

4.4 Nuclear localisation of LASP-1 correlates with poor long-term survival in female breast cancer

Jochen J. Frietsch*, Thomas G. P. Grünwald*, Sabrina Jasper, Ulrike Kämmerer, Sabine Herterich, Michaela Kapp, Arnd Hönig, Elke Butt (* geteilte Erstautorenschaft)
Br J Cancer. 2010; 102:1645–53.

In Vorarbeiten (siehe 4.3) konnte gezeigt werden, dass LASP1 mit dem Nodalstatus und der Tumogröße korreliert und dass LASP1 auch im Zellkern lokalisiert ist (Grünwald *et al.*, 2007b).

In der Folgearbeit (4.4) wurde nun experimentell belegt, dass die Kernlokalisation von LASP1 stark mit bestimmten Zellzyklusphasen assoziiert ist: Während in der G1-Phase nur relativ wenig LASP1 im Zellkern vorkommt, wird es vermehrt in der S-Phase nachgewiesen, und am stärksten in der G2/M-Phase (Frietsch *et al.*, 2010). Diese Beobachtung korrespondierte mit dem Befund, dass der knockdown von LASP1 in Ovarial- und Mammakarzinom-Zelllinien zu einem Zellzyklus-Arrest in der G2-Phase führt (Grünwald *et al.*, 2006, 2007a). In einer großen Patienten Kohorte konnte zudem belegt werden, dass es insbesondere der LASP1-Kernstatus ist, der mit dem Gesamtüberleben von Mammakarzinom-Patientinnen korreliert (Frietsch *et al.*, 2010). Ähnliche Korrelationen wurden mittlerweile an zahlreichen weiteren Tumorentitäten nachgewiesen (Orth *et al.*, 2015).

In frühen Arbeiten zu LASP1 wurde darüber spekuliert (Tomasetto *et al.*, 1995b, 1995a), ob die hohe LASP1-Expression in Mammakarzinomen möglicherweise mit einer Amplifikation des *LASP1*-Genlocus und/oder dem Verlust von p53, das *LASP1*

als direktes transkriptionelles Zielgen hat (Wang et al., 2009), zusammenhängt. In der unter 4.4 genannten Studie konnte erstmals gezeigt werden, dass die Dysregulation von *LASP1* weder mit einer möglichen Genamplifikation noch dem Verlust von *TP53* assoziiert ist. Tatsächlich zeigte die genetische Analyse von 63 mikro-dissezierten histologischen Schnittpräparaten mit anschließender qRT-PCR eine Amplifikation des *LASP1*-Gens in nur einem Fall (1 von 63; 1,6 %) (Frietsch et al., 2010). Folglich wird die *LASP1*-Überexpression in den meisten Mammakarzinomen vermutlich eher durch transkriptionelle Regulation als durch Genamplifikation hervorgerufen und ist somit als aktiver Prozess in der Tumorigenese anzusehen.

4.5 Loss of tumor suppressor mir-203 mediates overexpression of LIM and SH3 Protein 1 (LASP1) in high-risk prostate cancer thereby increasing cell proliferation and migration

Amelie Hailer*, Thomas G. P. Grünewald*, Martin Orth, Cora Reiss, Burkhard Kneitz, Martin Spahn, Elke Butt (* geteilte Erstautorenschaft)
Oncotarget. 2014; 5:4144–53.

Das Prostatakarzinom gehört zu den häufigsten Krebserkrankungen der westlichen Welt. Trotz seiner Häufigkeit existieren derzeit keine verlässlichen molekularen Biomarker für die Vorhersage, ob ein Patient einen indolenten oder aggressiven Subtyp dieser Erkrankung entwickeln wird (Sboner et al., 2010). Patienten werden daher häufig übertherapiert, was eine erhebliche Therapie-assozierte Morbidität bedingt (Daskivich et al., 2011). In der unter 4.5 genannten Arbeit wurde an einem Kollektiv von definierten „high-risk“ Prostatakarzinomen untersucht, ob *LASP1* einen Beitrag zum aggressiven Verhalten der Tumoren hat. In der Tat konnte gezeigt werden, dass *LASP1* insbesondere in Metastasen sowie in einer Subgruppe von high-risk Prostatakarzinomen überexprimiert ist (Hailer et al., 2014). Mittels Gene-Set-Enrichment-Analysen (GSEA) konnte in verfügbaren Genexpressions-Microarraydaten gezeigt werden, dass die *LASP1*-Überexpression mit einer Aktivierung von Signalwegen einhergeht, die in Zellmigrationsprozesse involviert sind. In funktionellen Experimenten wurde demonstriert, dass die Suppression von *LASP1* in Prostatakarzinom-Zelllinien mit einer verringerten Zellmigration und

Zellproliferation assoziiert ist (Hailer et al., 2014). In dem Patientenkollektiv korrelierte sowohl die zytoplasmatische als auch die nukleäre Immunoreaktivität von LASP1 mit einem signifikant schnelleren biochemischen Progress sowie dem Verlust der Tumorsuppressor-micro-RNA 203 (mir-203) (Hailer et al., 2014). Von mir-203 ist bekannt, dass sie physiologisch in die Unterdrückung der LASP1-Expression involviert ist (Orth et al., 2015). Zwei unabhängige Arbeiten bestätigten kürzlich, dass LASP1 bei der Karzinogenese und Progression von Prostatakarzinomen eine wichtige Rolle spielt (Dejima et al., 2017; Sun et al., 2017).

Diese Ergebnisse deuten darauf hin, dass LASP1 eventuell als zusätzlicher Biomarker für die Risikoabschätzung und damit Therapieplanung von Patienten mit Prostatakarzinomen dienen könnte.

4.6 MondoA is highly overexpressed in acute lymphoblastic leukemia cells and modulates their metabolism, differentiation and survival

Caroline M. Wernicke, Günther H. S. Richter, Beate C. Beinvogl, Stephanie Plehm, Anna-Melissa Schlitter, Obul R. Bandapalli, Olivia Prazeres da Costa, Uwe E. Hattenhorst, Ines Volkmer, Martin S. Staege, Irene Esposito, Stefan Burdach, Thomas G. P. Grünewald

Leuk Res. 2012; 36:1185–92.

Die akute lymphoblastische B-Zell Leukämie (common ALL, cALL) ist die häufigste Krebserkrankung bei Kindern. Obwohl die cALL bei der Mehrzahl der Patienten gut behandelt und sogar dauerhaft geheilt werden kann, ist die Prognose insbesondere bei Rückfällen ungünstig. In vielen Fällen kommen dann Hochdosis-Chemotherapien und Stammzelltransplantationen zum Einsatz, die mit erheblicher akuter und chronischer Toxizität verbunden sind (Wernicke et al., 2011). Um neue therapeutische Zielstrukturen zu erfassen, die in cALL-Zellen, aber kaum in Normalgeweben exprimiert werden, führten wir eine umfangreiche Genexpressionsanalyse mit Affymetrix Microarrays durch. Diese ergab, dass der Transkriptionsfaktor MondoA (alias MLXIP) besonders hoch in cALL-Zellen gebildet wird (Wernicke et al., 2012). In funktionellen Experimenten konnte gezeigt werden, dass der Knockdown von MondoA mit einer verminderten Glucoseaufnahme und Proliferation von cALL-Zellen einhergeht. Zudem hemmt die Unterdrückung von

MondoA das klonogene Wachstum. Durch Transkriptom-Analysen konnte belegt werden, dass MondoA zur Aufrechterhaltung eines unreifen Phänotyps sowie zur Apoptose-Resistenz beiträgt (Wernicke et al., 2012). Ähnliche Effekte wurden in einer Folgestudie in Neuroblastomen beschrieben, wo die MondoA-Überexpression mit besonders schlechtem Gesamtüberleben assoziiert ist (Carroll et al., 2015). MondoA könnte deshalb sowohl bei der cALL als auch beim Neuroblastom als sinnvolle Zielstruktur für eine gerichtete Tumortherapie sowie als Biomarker für die Prognoseabschätzung dienen.

4.7 STEAP1 is associated with the invasive and oxidative stress phenotype of Ewing tumors

Thomas G. P. Grünwald, Isabelle Diebold, Irene Esposito, Stephanie Plehm, Kristina Hauer, Uwe Thiel, Patricia da Silva-Buttkus, Frauke Neff, Rebekka Unland, Carsten Müller-Tidow, Colette Zobywalski, Katharina Lohrig, Urs Lewandrowski, Albert Sickmann, Olivia Prazeres da Costa, Agnes Görlach, Andrea Cossarizza, Elke Butt, Günther H. S. Richter, Stefan Burdach

Mol Cancer Res. 2012; 10:52–65.

Ewing Sarkome sind die zweithäufigsten malignen Knochentumore des Kindes- und Jugendalters (Sand et al., 2015). Trotz bislang erzielter Fortschritte in der Behandlung beträgt die Fünf-Jahres-Überlebensrate für Patienten mit disseminierter Erkrankung weniger als 30% (Gaspar et al., 2015). Außerdem sind derzeitige multimodale Therapie-Protokolle mit erheblicher akuter und chronischer Toxizität verbunden, weshalb schonendere und gleichzeitig effektivere Therapiestrategien unbedingt notwendig sind (Burdach und Jürgens, 2002; Potratz et al., 2012).

Ein besonderes Merkmal des Ewing Sarkoms ist die pathognomonische Expression von chimären Transkriptionsfaktoren, die durch eine Fusion des *EWSR1*-Gens (Ewing sarcoma breakpoint region 1) mit verschiedenen Mitgliedern der *ETS*-Genfamilie (erythroblast transformation specific) entstehen (in 85 % der Fälle *FLI1*, in 10 % *ERG*) (Riggi und Stamenkovic, 2007). *EWSR1-FLI1* und *EWSR1-EGR* sind aberrierende Transkriptionsfaktoren, die an GGAA-Motive im Erbgut binden und entweder aktivierende oder supprimierende Wirkung auf Zielgene haben. Beide Fusionsonkogene induzieren erhebliche Veränderungen im Transkriptom, die in ihrer

Gesamtheit den malignen und hochaggressiven Phänotyp von Ewing Sarkomen ausmachen (Delattre et al., 1992; Gangwal et al., 2008; Guillou et al., 2009). Außer *EWSR1-ETS*-Genfusionen kommen beim Ewing Sarkomen kaum weitere rekurrende somatische Mutationen vor, weshalb das Ewing Sarkom eine der genetisch stabilsten Tumorentitäten darstellt (Brohl et al., 2014; Crompton et al., 2014; Tirode et al., 2014). Dies ist für die Charakterisierung einer stabil exprimierten und durch *EWSR1-ETS* induzierten tumorexklusiven Expressionssignatur von großer Bedeutung.

Trotz der hochspezifischen Expression der chimären *EWSR1-ETS*-Fusionsproteine, die nur in Ewing Sarkom-Zellen vorhanden sind und prinzipiell ideale Angriffspunkte für zielgerichtete Therapien darstellen würden, ist die Entwicklung von spezifischen Therapien gegen *EWSR1-ETS*-Fusionsproteine aus nachfolgenden Gründen erschwert:

(1) *EWSR1-ETS*-Fusionsproteine sind nur schlecht löslich, was strukturelle Analysen mittels Kristallographie oder Kernspinresonanz, die zur Konzipierung und Herstellung von sog. *small molecules* notwendig sind, stark beeinträchtigt (Uren und Toretsky, 2005). (2) *EWSR1-ETS*-Fusionsproteine sind kaum immunogen. (3) *EWSR1-ETS*-Fusionsproteine sind im Zellkern lokalisiert und haben keine enzymatische Funktion. Alternativ zu diesen Ansätzen stellen spezifische *EWSR1-ETS*-Zielgene einen Ansatzpunkt zur Entwicklung einer schonenden und effektiveren Therapie dar. Mittels funktioneller Genomik ist es in den letzten Jahren gelungen, einige *EWSR1-ETS*-Zielgene, die im Ewing Sarkom stark, aber gleichzeitig im Normalgewebe kaum exprimiert sind, zu identifizieren und funktionell zu charakterisieren (Blaeschke et al., 2016; Hauer et al., 2013; Kirschner et al., 2017; Richter et al., 2013).

So konnte gezeigt werden, dass die im Ewing Sarkom stark überexprimierte Oxidoreduktase STEAP1 (six-transmembrane epithelial antigen of the prostate 1) (Grünwald et al., 2012a) durch reaktive Sauerstoffspezies (ROS) zum invasiven Wachstum und zum oxidativen Stress-Phänotyp von Ewing Sarkomen beiträgt (Grünwald et al., 2012b). Interessanterweise fehlt STEAP1 im Gegensatz zu anderen STEAP-Proteinen eine N-terminale Oxidoreduktase-Domäne (Grünwald et al., 2012a). Dennoch kann STEAP1 über eine spezielle Eisen-Reaktion zur ROS-Produktion beitragen (Kim et al., 2016).

Durch Transkriptom-Analysen konnte gezeigt werden, dass STEAP1 die drei Gene *MMP1*, *DTX3L* und *ADIPOR1* über eine gesteigerte ROS-Produktion hochreguliert

(Grünewald et al., 2012b). Funktionelle Experimente belegten, dass der individuelle knockdown von MMP1, DTX3L oder ADIPOR1 teilweise den Phänotyp des STEAP1 knockdowns kopiert. Zusammengefasst weisen diese Daten darauf hin, dass sich STEAP1 aufgrund seiner hohen Expression in Ewing Sarkomen im Vergleich zu Normalgeweben sowie seines Beitrags zum aggressiven Verhalten dieser Tumorentität als neue therapeutische Zielstruktur eignen könnte (Grünewald et al., 2012b, 2012a).

4.8 High STEAP1 expression is associated with improved outcome of Ewing's sarcoma patients

Thomas G. P. Grünewald*, Andreas Ranft*, Irene Esposito*, Patricia da Silva-Buttkus, Michaela Aichler, Daniel Baumhoer, Karl-Ludwig Schäfer, Laura Ottaviano, Christopher Poremba, Gernot Jundt, Heribert Jürgens, Uta Dirksen, Günther H.S. Richter, Stefan Burdach (* geteilte Erstautorenschaft)

Ann Oncol 2012; 23:2185–90.

In der unter 4.7 genannten Arbeit wurde gezeigt, dass STEAP1 zum oxidativen Stress-Phänotyp von Ewing Sarkomen beiträgt, was in Modellsystemen zu einer erhöhten Invasivität der Tumorzellen führt. Unklar blieb jedoch die klinische Relevanz von STEAP1 für Ewing Sarkome. Es wurde deshalb die unter 4.8 beschriebene Folgestudie zur Untersuchung des prognostischen und/oder prädiktiven Potentials von STEAP1 initiiert. Dazu wurden insgesamt 114 Primärtumoren mittels IHC auf STEAP1 gefärbt und die Immunoreaktivität wurde semiquantitativ von drei unabhängigen Beobachtern bewertet. Ein Abgleich mit klinischen Daten ergab, dass überraschenderweise eine erhöhte STEAP1-Expression mit einem verbesserten Gesamtüberleben assoziiert ist. Multivariate Cox-Regressions-Analysen belegten dabei, dass dieser Zusammenhang nicht durch andere bekannte klinische Prognoseparameter bedingt ist. Weiterführende Experimente zeigten, dass der knockdown von STEAP1 in Ewing Sarkom-Zelllinien zu einem verringerten Ansprechen der Tumorzellen auf die Chemotherapeutika Doxorubicin und Etoposid führt. Interessanterweise verbesserte sich das Ansprechen auf diese beiden Chemotherapeutika, die regelmäßig bei Ewing Sarkom-Patienten zum Einsatz kommen (Gaspar et al., 2015), wenn die intrazellulären Level der reaktiven

Sauerstoffspezies erhöht waren (Grünewald et al., 2012c). Dies legt nahe, dass die beobachtete Korrelation der erhöhten STEAP1-Expression mit einem besseren Gesamtüberleben durch ein besseres Ansprechen auf Chemotherapeutika bedingt sein könnte. Obschon diese Hypothese noch validiert werden muss, konnte bereits in einer anderen Studie ein ähnlicher Zusammenhang einer erhöhten STEAP1-Expression mit einem besseren klinischen Verlauf bei Patienten mit Dickdarmkarzinomen beobachtet werden (Lee et al., 2016). Aufgrund seiner präferenziellen Expression in Tumorgeweben im Vergleich zu Normalgeweben wird STEAP1 derzeit intensiv als neue Zielstruktur für antibody-drug-conjugates und für Zell-basierte Immuntherapien untersucht (Grünewald et al., 2012a). In einer Folgearbeit wurde bereits demonstriert, dass STEAP1 als spezifische Zielstruktur einer adoptiven Immuntherapie für Ewing Sarkome dienen kann (Grünewald et al., 2012a; Schirmer et al., 2016).

4.9 Anti-oxidative stress response genes: bioinformatic analysis of their expression and relevance in multiple cancers

Barak Rotblat*, Thomas G. P. Grünewald*, Gabriel Leprivier*, Gerry Melino, Richard A. Knight (* geteilte Erstautorenschaft)

Oncotarget. 2013 Dec; 4(12):2577-90

In den unter 4.7 und 4.8 beschriebenen Arbeiten wurde gezeigt, dass ein erhöhter intrazellulärer oxidativer Stress zum aggressiven Phänotyp von Ewing Sarkomen beitragen kann, diese u. U. aber auch für ROS-abhängige Chemotherapeutika sensibilisiert. In der unter 4.9 benannten Folgearbeit wurde dieser Ansatz systematisch in Genexpressionsdaten 994 maligner Tumoren und 353 Normalgeweben analysiert (Rotblat et al., 2013). Im Speziellen wurden die Genexpressionsprofile von 285 sogenannten „oxidative stress genes“ miteinander verglichen und mit hierarchischem Clustering in Gruppen zugeordnet. Hierdurch konnte eine Signatur aus 116 Genen identifiziert werden, die in vielen Karzinomen im Vergleich zu Normalgeweben hochgradig überexprimiert werden (Rotblat et al., 2013). Gene-set Enrichment-Analysen dieser Gene zeigten, dass sie hauptsächlich im Thioredoxin- und Glutathion-System involviert sind und somit zur Kompensation von oxidativem Stress beitragen könnten (Rotblat et al., 2013). Durch Abgleich mit

klinischen Daten konnte gezeigt werden, dass die Überexpression verschiedener Schlüsselfaktoren dieser Signalwege wie *TXN* und *GCLC* im nicht-kleinzelligen Lungenkarzinom mit einem signifikant schlechteren Gesamtüberleben einhergeht (Rotblat et al., 2013). Das kompensatorische Anti-Oxidantien-System maligner Tumoren könnte also als therapeutischer Angriffspunkt genutzt werden (Rotblat et al., 2013), da sich eine Inhibition dieser Kompensationssysteme wahrscheinlich negativ auf das Tumorwachstum auswirken würde (Gorrini et al., 2013).

4.10 The Zyxin-related protein thyroid receptor interacting protein 6 (TRIP6) is overexpressed in Ewing's sarcoma and promotes migration, invasion and cell growth

Thomas G. P. Grünwald*, Semjon Willier*, Dirk Janik, Rebekka Unland, Cora Reiss, Olivia Prazeres da Costa, Thorsten Buch, Uta Dirksen, Günther H. S. Richter, Frauke Neff, Stefan Burdach, Elke Butt (* geteilte Erstautorenschaft)

Biol Cell. 2013; 105:535–47

Die Mitglieder der Zyxin-Proteinfamilie sind in vielfältige zelluläre Funktionen eingebunden. Hierbei nehmen sie, teilweise funktionell redundant, Einfluss auf zytoplasmatische und nukleäre Prozesse (Willier et al., 2011). In der unter 4.10 genannten Studie konnte durch Analyse von öffentlich verfügbaren Microarraydaten belegt werden, dass lediglich das Protein TRIP6 (thyroid receptor interacting protein 6) aus der Zyxin-Proteinfamilie in Ewing Sarkomen deutlich überexprimiert ist (Grünwald et al., 2013). TRIP6 dient, neben seiner Funktion in der Organisation des Zytoskeletts, auch nukleär als Kotranskriptionsfaktor und als Kofaktor in der Telomerprotektion. Vielfach wurde eine Implikation dieses multifunktionellen Adapterproteins in maligne Prozesse dokumentiert (Willier et al., 2011). Die Überexpression von TRIP6 in Ewing Sarkomen ist jedoch unabhängig von EWSR1-FLI1. Eine Bindung von EWSR1-FLI1 an eine putative Bindungsstelle im Promotor von *TRIP6* konnte nicht nachgewiesen werden (Grünwald et al., 2013).

Die Analyse von Microarrays nach Herunterregulation von TRIP6 in Ewing Sarkom-Zelllinien identifizierte mehrere Signalwege, welche mit Proliferation und Invasivität assoziiert sind und die nach knockdown von TRIP6 vermindert aktiviert werden (Grünwald et al., 2013). Die für verschiedene Malignome relevanten Proteine *RDX*,

CD164 und *CRYZ* konnten als Zielgene des Kotranskriptionsfaktors *TRIP6* mithilfe von qRT-PCR validiert werden (Grünewald et al., 2013). Durch Verringerung der Proteinmenge von *TRIP6* in Ewing Sarkomen mittels RNA-Interferenz kam es zu deutlich reduziertem klonogenem Wachstum und Migration der Zellen *in vitro*. Nach induzierbarem *TRIP6*-knockdown konnte eine verminderte Tumorigenese und hepatische Metastasierung *in vivo* beobachtet werden (Grünewald et al., 2013). Zusammengefasst deuten diese Daten auf eine Beteiligung von *TRIP6* in der Pathogenese des Ewing Sarkoms und insbesondere beim Prozess der Metastasierung hin. Somit legen diese Ergebnisse eine weitere Evaluierung von *TRIP6* als Biomarker oder molekulare Zielstruktur für therapeutische Ansätze in Ewing Sarkomen nahe (Grünewald et al., 2013). In der Tat belegte eine andere Studie kürzlich, dass *TRIP6* als putatives Zielgen des RhoA-Signalwegs eine Rolle in Prozessen der Zytoskelett-Organisation haben könnte (Katschnig et al., 2017), die bei Migrations- und Metastasierungsprozessen eine wichtige Rolle spielen.

4.11 First identification of Ewing's sarcoma-derived extracellular vesicles and exploration of their biological and potential diagnostic implications

Isabella V. Miller, Graca Raposo, Ulrich Welsch, Olivia Prazeres da Costa, Uwe Thiel, Maria Lebar, Martina Maurer, Hans-Ulrich Bender, Irene von Luettichau, Günther H. S. Richter, Stefan Burdach, Thomas G. P. Grünewald
Biol Cell. 2013; 105:289–303.

Derzeit arbeiten mehrere Gruppen intensiv an der Entwicklung von Biomarkern für die minimal-residual-disease (MRD)-Diagnostik des Ewing Sarkoms. Einen möglichen Ansatzpunkt stellen hierbei zirkulierende freie Desoxynukleinsäuren (cfDNA) dar, mit besonderem Augenmerk auf durch *EWSR1-ETS* kodierte patientenspezifische cfDNAs. Tatsächlich konnte bereits gezeigt werden, dass mit digital-droplet PCR-Technologien ein Monitoring von Ewing Sarkom-Patienten anhand von Patienten-spezifischer *EWSR1-ETS* cfDNA möglich ist (Krumbholz et al., 2016). Ein anderer von uns verfolgter Ansatz besteht in der Detektion sogenannter extrazellulärer Vesikel, u. a. den Exosomen, die von den meisten Zellen abgeschieden werden und einen *RNA-Fingerprint* ihrer jeweiligen Ursprungszelle beherbergen (Miller und Grünewald, 2015). So konnte bereits gezeigt werden, dass

Ewing Sarkom-Zellen mRNAs der Fusionsonkogene in Exosomen verpacken und abscheiden, und dass die exosomalen mRNAs von *EWSR1-FLI1* und *STEAP1* potentielle Biomarker im peripheren Blut darstellen (Miller und Grünwald, 2015; Miller et al., 2013).

4.12 Robust diagnosis of Ewing sarcoma by immunohistochemical detection of super-enhancer-driven EWSR1-ETS targets

Michaela C. Baldauf*, Martin F. Orth*, Marlene Dallmayer*, Aruna Marchetto, Julia S. Gerke, Rebeca Alba Rubio, Merve M. Kiran, Julian Musa, Maximilian M. L. Knott, Shunya Ohmura, Jing Li, Nusret Akpolat, Ayse N. Akatli, Özlem Özen, Uta Dirksen, Wolfgang Hartmann, Enrique de Alava, Daniel Baumhoer, Giuseppina Sannino, Thomas Kirchner, Thomas G. P. Grünwald (* geteilte Erstautorenschaft)

Oncotarget. 2017 Aug DOI 10.18632/oncotarget.20098, Advance Online Publication.

Ewing Sarkome wurden erstmals 1921 vom amerikanischen Pathologen James Ewing beschrieben (Ewing, 2006). Fast 100 Jahre nach der Erstbeschreibung durch James Ewing ist die Histogenese dieses undifferenzierten kleinrundzelligen Tumors immer noch ungeklärt (Kovar et al., 2016). Einige Studien weisen auf eine Entstehung aus mesenchymalen Stammzellen hin, die entweder vom Mesoderm oder der Neuralleiste abstammen (von Levetzow et al., 2011; Tirode et al., 2007). Der undifferenzierte Phänotyp der Ewing Sarkom-Zellen bereitet in der histopathologischen Diagnostik oftmals Probleme in der Abgrenzung zu anderen kleinrundzelligen Sarkomen. In der unter 4.12 genannten Arbeit wurden mittels vergleichender Transkriptomanalysen von Ewing Sarkomen und 20 sogenannten „morphological mimics“ drei Kandidaten-Biomarker (ATP1A1, GLG1 und BCL11B) identifiziert (Baldauf et al., 2017). Funktionelle und bioinformatische Analysen belegten dabei, dass diese drei Gene kaum in Normalgeweben exprimiert werden und dass ihre Expression durch die Bindung von *EWSR1-FLI1* an benachbarte GGAA-Mikrosatelliten mit Charakteristika von Super-Enhancern angetrieben wird. Die spezifische Expression der drei Gene wurde mittels IHC in einem tissue-microarray bestätigt. Systematische Analysen der Expressionslevel in den verschiedenen Tumorentitäten ergaben, dass die Expression von BCL11B und/oder GLG1 bei CD99-positiven Tumoren in diesem tissue-microarray eine Spezifität von

mindestens 96 % für Ewing Sarkome erreicht (Baldauf et al., 2017). Darüber hinaus wurde durch diese Studie gezeigt, dass EWSR1-NFATc2-positive kleinrundzellige Sarkome von klassischen EWSR1-ETS-positiven Ewing Sarkomen abgrenzen sind und sehr wahrscheinlich eine eigenständige Tumorentität darstellen (Baldauf et al., 2017).

4.13 Chimeric EWSR1-FLI1 regulates the Ewing sarcoma susceptibility gene EGR2 via a GGAA microsatellite

Thomas G. P. Grünwald, Virginie Bernard, Pascale Gilardi-Hebenstreit, Virginie Raynal, Didier Surdez, Marie-Ming Aynaud, Olivier Mirabeau, Florencia Cidre-Aranaz, Franck Tirode, Sakina Zaidi, Gaelle Perot, Annelinie H. Jonker, Carlo Lucchesi, Marie-Cécile Le Deley, Odile Oberlin, Perrine Marec-Bérard, Amélie S. Véron, Stephanie Reynaud, Eve Lapouble, Valentina Boeva, Thomas Rio Frio, Javier Alonso, Smita Bhatia, Gaelle Pierron, Geraldine Cancel-Tassin, Olivier Cussenot, David G. Cox, Lindsay M. Morton, Mitchell J. Machiela, Stephen J. Chanock, Patrick Charnay, Olivier Delattre

Nat Genet. 2015; 47:1073–8.

Ewing Sarkome kommen circa 10-20x häufiger bei Europäern als bei Afrikanern vor (Worch et al., 2011), was auf einen starken Beitrag der Keimbahnvariabilität, also der angeborenen genetischen Varianten im menschlichen Erbgut, zur Tumorentstehung hinweist. Vor diesem Hintergrund identifizierte eine Genom-weite Assoziationsstudie (GWAS) drei Stellen im Erbgut von Europäern, die zum Ewing Sarkom prädisponieren (Postel-Vinay et al., 2012). Unklar blieb jedoch, wie diese sogenannten Suszeptibilitäts-Loci das Risiko für Ewing Sarkome erhöhen. In der unter 4.13 genannten Studie wurde hierfür ein erster mechanistischer Erklärungsansatz beschrieben: Es konnte gezeigt werden, wie der für Ewing Sarkome charakteristische Transkriptionsfaktor EWSR1-FLI1, der durch eine erworbene somatische Mutation entsteht, innerhalb eines Suszeptibilitäts-Locus mit einer angeborenen regulatorischen Variante interagiert und so das Suszeptibilitäts-Gen *EGR2* (*early growth response-2*) hochreguliert (Grünwald und Delattre, 2016; Grünwald et al., 2015). Interessanterweise liegt diese regulatorische Variante in einem GGAA-Mikrosatelliten. GGAA-Mikrosatelliten sind sich wiederholende

Nukleinsäuren in unserem Erbgut, denen oft keinerlei Funktion zugesprochen wird, die aber insbesondere von EWSR1-FLI1 benutzt werden, um die Expression spezifischer Gene anzutreiben (Riggi et al., 2014). Die genannte regulatorische Variante modifiziert dabei einen bestimmten GGAA-Mikrosatelliten derart, dass die Bindung von EWSR1-FLI1 und somit die Expression von EGR2 in Ewing Sarkom-Zellen stark gesteigert werden (Grünwald et al., 2015). In funktionellen Experimenten wurde beobachtet, dass die Unterdrückung von EGR2 die Zellteilungsrate von Ewing Sarkom-Zellen hemmt und in einem Mausmodell sogar zur Rückbildung der Tumoren führt. Weitere funktionelle Analysen zeigten, dass EGR2 „downstream“ des fibroblast growth factor (FGF)-Signalwegs agiert, der das Wachstum von Ewing Sarkom Zelllinien stark fördert (Grünwald et al., 2015). Eine vergleichende Untersuchung in öffentlichen verfügbaren Datensätzen verschiedener humaner Populationen ergab eine hochsignifikant erhöhte Frequenz dieser Risiko-Variante im Erbgut von Europäern im Vergleich zu Afrikanern. Diese häufige angeborene Erbgutvariante bleibt jedoch solange bedeutungslos, bis durch eine zusätzliche erworbene Mutation das Fusionsonkogen EWSR1-FLI1 in bestimmten Zellen entsteht (Grünwald et al., 2015).

EGR2 stellt somit ein Suszeptibilitäts-Gen für das Ewing Sarkom dar, dessen EWSR1-FLI1-abhängige Überexpression in Ewing Sarkomen durch eine Risiko-Variante innerhalb eines GGAA-Mikrosatelliten vermittelt wird (Grünwald et al., 2015). Diese Studie demonstriert somit beispielhaft, wie eine angeborene Suszeptibilitäts-Variante der Keimbahn unser Verständnis über die Funktionsweise einer Krebsart-spezifischen erworbenen Mutation (EWSR1-FLI1) erweitern kann. Sie zeigt auch, wie das Zusammenspiel einer häufigen Keimbahn-Variante mit einem seltenen Onkogen wichtige Signalwege so modifizieren kann, dass schließlich die Tumorentstehung gefördert und möglicherweise das populationsspezifische Krebsrisiko erhöht wird. Darüber hinaus weist die enge Verzahnung von *EGR2* mit dem FGF-Signalweg darauf hin, dass die Blockierung dieses Signalwegs therapeutisch genutzt werden könnte (Cidre-Aranaz et al., 2017).

5. Ausblick

Im vorliegenden Habilitationsprojekt wurden mittels funktioneller Genomik verschiedene potentielle Zielstrukturen in malignen Tumoren charakterisiert und ihre mögliche Eignung als Biomarker bewertet. Ein Schwerpunkt lag dabei auf dem nukleo-zytoplasmatische Shuttle-Protein LASP1, das u. a. in humanen Mamma- und Ovarialkarzinomen sowie einer Untergruppe an high-risk Prostatakarzinomen stark überexprimiert ist und mit einem schlechteren klinischen Verlauf der betroffenen Patienten korreliert. Analoge Beobachtungen wurden auch in Medulloblastomen gemacht (Traenka et al., 2010). Unklar bleibt jedoch, über welchen Mechanismus LASP1 die Zellzyklusprogression und Migration fördert und ob dieser einer zielgerichteten Therapie zugänglich ist. Ein weiterer Schwerpunkt dieses Habilitationsprojekts lag auf der Identifikation von neuen Zielstrukturen im Ewing Sarkom. Hier wurden insbesondere STEAP1, TRIP6 und EGR2 untersucht. Diese Proteine sind in Ewing Sarkomen stark überexprimiert und fördern den aggressiven Phänotyp dieser Erkrankung. Aufgrund seiner membranständigen Lokalisation scheint insbesondere STEAP1 eine attraktive immuntherapeutisch nutzbare Zielstruktur zu sein (Grünwald et al., 2012a; Schirmer et al., 2016). Durch seine Funktion als Oxidoreduktase und die hierdurch bedingten erhöhten intrazellulären ROS-Level könnte STEAP1 zudem als prädiktiver Biomarker für das Ansprechen auf ROS-abhängige Chemotherapeutika dienen. Da STEAP1 im Prostata- und Mammakarzinom ebenfalls stark überexprimiert ist (Grünwald et al., 2012a), stellt sich die Frage, ob STEAP1 auch hier mit dem klinischen Verlauf und/oder dem Ansprechen auf Chemotherapeutika assoziiert ist. Zudem wurden in diesem Habilitationsprojekt neue potentielle Biomarker für die Diagnostik und die Verlaufskontrolle in der IHC am Tumorgewebe bzw. im peripheren Blut identifiziert, deren Eignung in größer angelegten Studien prospektiv validiert werden soll.

Durch funktionelle Genomik und Integration von Keimbahn-Genomik mit somatischen Mutationsprofilen wurden im Ewing Sarkom erste Erklärungsansätze für das epidemiologische Inzidenzmuster sowie ein möglicher Beitrag des FGF-Signalwegs zur Pathogenese dieser Erkrankung aufgedeckt (Grünwald et al., 2015). Inwieweit andere Signalwege eine Rolle bei der Keimbahn-Prädisposition zum Ewing Sarkom spielen und ob diese therapeutisch nutzbar sind, muss in nachfolgenden Studien geklärt werden. Wir planen, diese und weitere Fragestellungen der funktionellen Genomik in zukünftigen Arbeiten anzugehen.

6. Literaturverzeichnis

Amsellem, V., Kryszke, M.-H., Hervy, M., Subra, F., Athman, R., Leh, H., Brachet-Ducos, C., and Auclair, C. (2005). The actin cytoskeleton-associated protein zyxin acts as a tumor suppressor in Ewing tumor cells. *Exp. Cell Res.* 304, 443–456.

Baldauf, M.C., Orth, M.F., Dallmayer, M., Marchetto, A., Gerke, J.S., Rubio, R.A., Kiran, M.M., Musa, J., Knott, M.M.L., Ohmura, S., et al. (2017). Robust diagnosis of Ewing sarcoma by immunohistochemical detection of super-enhancer-driven EWSR1-ETS targets. *Oncotarget*, Epub DOI 10.18632/oncotarget.20098.

Blaeschke, F., Thiel, U., Kirschner, A., Thiede, M., Rubio, R.A., Schirmer, D., Kirchner, T., Richter, G.H.S., Mall, S., Klar, R., et al. (2016). Human HLA-A*02:01/CHM1+ allo-restricted T cell receptor transgenic CD8+ T cells specifically inhibit Ewing sarcoma growth in vitro and in vivo. *Oncotarget* 7, 43267–43280.

Brohl, A.S., Solomon, D.A., Chang, W., Wang, J., Song, Y., Sindiri, S., Patidar, R., Hurd, L., Chen, L., Shern, J.F., et al. (2014). The Genomic Landscape of the Ewing Sarcoma Family of Tumors Reveals Recurrent STAG2 Mutation. *PLoS Genet.* 10, e1004475.

Burdach, S., and Jürgens, H. (2002). High-dose chemoradiotherapy (HDC) in the Ewing family of tumors (EFT). *Crit. Rev. Oncol. Hematol.* 41, 169–189.

Carroll, P.A., Diolaiti, D., McFerrin, L., Gu, H., Djukovic, D., Du, J., Cheng, P.F., Anderson, S., Ulrich, M., Hurley, J.B., et al. (2015). Deregulated Myc requires MondoA/MLx for metabolic reprogramming and tumorigenesis. *Cancer Cell* 27, 271–285.

Christen, S., Lorendeau, D., Schmieder, R., Broekaert, D., Metzger, K., Veys, K., Elia, I., Buescher, J.M., Orth, M.F., Davidson, S.M., et al. (2016). Breast Cancer-Derived Lung Metastases Show Increased Pyruvate Carboxylase-Dependent Anaplerosis. *Cell Rep.* 17, 837–848.

Cidre-Aranaz, F., Grünwald, T.G.P., Surdez, D., García-García, L., Carlos Lázaro, J., Kirchner, T., González-González, L., Sastre, A., García-Miguel, P., López-Pérez, S.E., et al. (2017). EWS-FLI1-mediated suppression of the RAS-antagonist Sprouty 1 (SPRY1) confers aggressiveness to Ewing sarcoma. *Oncogene* 36, 766–776.

Crompton, B.D., Stewart, C., Taylor-Weiner, A., Alexe, G., Kurek, K.C., Calicchio, M.L., Kiezun, A., Carter, S.L., Shukla, S.A., Mehta, S.S., et al. (2014). The Genomic Landscape of Pediatric Ewing Sarcoma. *Cancer Discov.* 4, 1326–1341.

Daskivich, T.J., Chamie, K., Kwan, L., Labo, J., Palvolgyi, R., Dash, A., Greenfield, S., and Litwin, M.S. (2011). Overtreatment of men with low-risk prostate cancer and significant comorbidity. *Cancer* 117, 2058–2066.

Dejima, T., Imada, K., Takeuchi, A., Shiota, M., Leong, J., Tombe, T., Tam, K., Fazli, L., Naito, S., Gleave, M.E., et al. (2017). Suppression of LIM and SH3 Domain Protein 1 (LASP1) Negatively Regulated by Androgen Receptor Delays Castration Resistant Prostate Cancer Progression. *The Prostate* 77, 309–320.

Delattre, O., Zucman, J., Plougastel, B., Desmaze, C., Melot, T., Peter, M., Kovar, H., Joubert, I., de Jong, P., and Rouleau, G. (1992). Gene fusion with an ETS DNA-binding domain caused by chromosome translocation in human tumours. *Nature* 359, 162–165.

Demetri, G.D., von Mehren, M., Blanke, C.D., Van den Abbeele, A.D., Eisenberg, B., Roberts, P.J., Heinrich, M.C., Tuveson, D.A., Singer, S., Janicek, M., et al. (2002). Efficacy and safety of imatinib mesylate in advanced gastrointestinal stromal

tumors. *N. Engl. J. Med.* 347, 472–480.

Druker, B.J., Guilhot, F., O'Brien, S.G., Gathmann, I., Kantarjian, H., Gattermann, N., Deininger, M.W.N., Silver, R.T., Goldman, J.M., Stone, R.M., et al. (2006). Five-year follow-up of patients receiving imatinib for chronic myeloid leukemia. *N. Engl. J. Med.* 355, 2408–2417.

Duvall-Noelle, N., Karwandyar, A., Richmond, A., and Raman, D. (2016). LASP-1: a nuclear hub for the UHRF1-DNMT1-G9a-Snail1 complex. *Oncogene* 35, 1122–1133.

Elia, I., Broekaert, D., Christen, S., Boon, R., Radaelli, E., Orth, M.F., Verfaillie, C., Grünwald, T.G.P., and Fendt, S.-M. (2017). Proline metabolism supports metastasis formation and could be inhibited to selectively target metastasizing cancer cells. *Nat. Commun.* 11, 15267.

El-Naggar, A.M., Veinotte, C.J., Cheng, H., Grünwald, T.G.P., Negri, G.L., Somasekharan, S.P., Corkery, D.P., Tirode, F., Mathers, J., Khan, D., et al. (2015). Translational Activation of HIF1 α by YB-1 Promotes Sarcoma Metastasis. *Cancer Cell* 27, 682–697.

Ewing, J. (2006). The Classic: Diffuse endothelioma of bone. *Proceedings of the New York Pathological Society.* 1921;12:17. *Clin. Orthop.* 450, 25–27.

Frietsch, J.J., Grünwald, T.G.P., Jasper, S., Kammerer, U., Herterich, S., Kapp, M., Honig, A., and Butt, E. (2010). Nuclear localisation of LASP-1 correlates with poor long-term survival in female breast cancer. *Br. J. Cancer* 102, 1645–1653.

Frietsch, J.J., Kastner, C., Grünwald, T.G.P., Schweigel, H., Nollau, P., Ziermann, J., Clement, J.H., La Rosée, P., Hochhaus, A., and Butt, E. (2014). LASP1 is a novel BCR-ABL substrate and a phosphorylation-dependent binding partner of CRKL in chronic myeloid leukemia. *Oncotarget* 5, 5257–5271.

Gangwal, K., Sankar, S., Hollenhorst, P.C., Kinsey, M., Haroldsen, S.C., Shah, A.A., Boucher, K.M., Watkins, W.S., Jorde, L.B., Graves, B.J., et al. (2008). Microsatellites as EWS/FLI response elements in Ewing's sarcoma. *Proc. Natl. Acad. Sci. U. S. A.* 105, 10149–10154.

Gaspar, N., Hawkins, D.S., Dirksen, U., Lewis, I.J., Ferrari, S., Le Deley, M.-C., Kovar, H., Grimer, R., Whelan, J., Claude, L., et al. (2015). Ewing Sarcoma: Current Management and Future Approaches Through Collaboration. *J. Clin. Oncol.* 33, 3036–3046.

Gorrini, C., Harris, I.S., and Mak, T.W. (2013). Modulation of oxidative stress as an anticancer strategy. *Nat. Rev. Drug Discov.* 12, 931–947.

Grünwald, T.G.P., and Butt, E. (2008). The LIM and SH3 domain protein family: structural proteins or signal transducers or both? *Mol. Cancer* 7, 31.

Grünwald, T.G.P., and Delattre, O. (2016). Cooperation between somatic mutations and germline susceptibility variants in tumorigenesis - a dangerous liaison. *Mol. Cell. Oncol.* 3, e1086853.

Grünwald, T.G.P., and Fulda, S. (2016). Editorial: Biology-Driven Targeted Therapy of Pediatric Soft-Tissue and Bone Tumors: Current Opportunities and Future Challenges. *Front. Oncol.* 6, 39.

Grünwald, T.G., Pasedag, S.M., and Butt, E. (2009). Cell Adhesion and Transcriptional Activity - Defining the Role of the Novel Protooncogene LPP. *Transl. Oncol.* 2, 107–116.

Grünwald, T.G.P., Kammerer, U., Schulze, E., Schindler, D., Honig, A., Zimmer, M., and Butt, E. (2006). Silencing of LASP-1 influences zyxin localization, inhibits

proliferation and reduces migration in breast cancer cells. *Exp. Cell Res.* 312, 974–982.

Grünewald, T.G.P., Kammerer, U., Winkler, C., Schindler, D., Sickmann, A., Honig, A., and Butt, E. (2007a). Overexpression of LASP-1 mediates migration and proliferation of human ovarian cancer cells and influences zyxin localisation. *Br. J. Cancer* 96, 296–305.

Grünewald, T.G.P., Kammerer, U., Kapp, M., Eck, M., Dietl, J., Butt, E., and Honig, A. (2007b). Nuclear localization and cytosolic overexpression of LASP-1 correlates with tumor size and nodal-positivity of human breast carcinoma. *BMC Cancer* 7, 198.

Grünewald, T.G.P., Herbst, S.M., Heinze, J., and Burdach, S. (2011). Understanding tumor heterogeneity as functional compartments--superorganisms revisited. *J. Transl. Med.* 9, 79.

Grünewald, T.G.P., Bach, H., Cossarizza, A., and Matsumoto, I. (2012a). The STEAP protein family: versatile oxidoreductases and targets for cancer immunotherapy with overlapping and distinct cellular functions. *Biol. Cell* 104, 641–657.

Grünewald, T.G.P., Diebold, I., Esposito, I., Plehm, S., Hauer, K., Thiel, U., da Silva-Buttkus, P., Neff, F., Unland, R., Müller-Tidow, C., et al. (2012b). STEAP1 is associated with the invasive and oxidative stress phenotype of Ewing tumors. *Mol. Cancer Res. MCR* 10, 52–65.

Grünewald, T.G.P., Ranft, A., Esposito, I., da Silva-Buttkus, P., Aichler, M., Baumhoer, D., Schaefer, K.L., Ottaviano, L., Poremba, C., Jundt, G., et al. (2012c). High STEAP1 expression is associated with improved outcome of Ewing's sarcoma patients. *Ann. Oncol.* 23, 2185–2190.

Grünewald, T.G.P., Greulich, N., Kontny, U., Frühwald, M., Rutkowski, S., Kordes, U., Scheurlen, W., Schmidt, W., Stachel, D., Metzler, M., et al. (2012d). Targeted therapeutics in treatment of children and young adults with solid tumors: an expert survey and review of the literature. *Klin. Padiatr.* 224, 124–131.

Grünewald, T.G.P., Willier, S., Janik, D., Unland, R., Reiss, C., Prazeres da Costa, O., Buch, T., Dirksen, U., Richter, G.H.S., Neff, F., et al. (2013). The Zyxin-related protein thyroid receptor interacting protein 6 (TRIP6) is overexpressed in Ewing's sarcoma and promotes migration, invasion and cell growth. *Biol. Cell* 105, 535–547.

Grünewald, T.G.P., Bernard, V., Gilardi-Hebenstreit, P., Raynal, V., Surdez, D., Aynaud, M.-M., Mirabeau, O., Cidre-Aranaz, F., Tirode, F., Zaidi, S., et al. (2015). Chimeric EWSR1-FLI1 regulates the Ewing sarcoma susceptibility gene EGR2 via a GGAA microsatellite. *Nat. Genet.* 47, 1073–1078.

Grünewald, T.G.P., Gilardi-Hebenstreit, P., Charnay, P., and Delattre, O. (2016). [Cooperation between a somatic mutation and a genetic susceptibility variant in Ewing sarcoma]. *Med. Sci. MS* 32, 323–326.

Gubin, M.M., Artyomov, M.N., Mardis, E.R., and Schreiber, R.D. (2015). Tumor neoantigens: building a framework for personalized cancer immunotherapy. *J. Clin. Invest.* 125, 3413–3421.

Guillon, N., Tirode, F., Boeva, V., Zynovyev, A., Barillot, E., and Delattre, O. (2009). The oncogenic EWS-FLI1 protein binds in vivo GGAA microsatellite sequences with potential transcriptional activation function. *PloS One* 4, e4932.

Hailer, A., Grünewald, T.G.P., Orth, M., Reiss, C., Kneitz, B., Spahn, M., and Butt, E. (2014). Loss of tumor suppressor mir-203 mediates overexpression of LIM and

SH3 Protein 1 (LASP1) in high-risk prostate cancer thereby increasing cell proliferation and migration. *Oncotarget* 5, 4144–4153.

Hauer, K., Calzada-Wack, J., Steiger, K., Grünwald, T.G.P., Baumhoer, D., Plehm, S., Buch, T., Prazeres da Costa, O., Esposito, I., Burdach, S., et al. (2013). DKK2 mediates osteolysis, invasiveness, and metastatic spread in Ewing sarcoma. *Cancer Res.* 73, 967–977.

Katschnig, A.M., Kauer, M.O., Schwentner, R., Tomazou, E.M., Mutz, C.N., Linder, M., Sibilia, M., Alonso, J., Aryee, D.N.T., and Kovar, H. (2017). EWS-FLI1 perturbs MRTFB/YAP-1/TEAD target gene regulation inhibiting cytoskeletal autoregulatory feedback in Ewing sarcoma. *Oncogene*, Epub, DOI 10.1038/onc.2017.202.

Kim, K., Mitra, S., Wu, G., Berka, V., Song, J., Yu, Y., Poget, S., Wang, D.-N., Tsai, A.-L., and Zhou, M. (2016). Six-Transmembrane Epithelial Antigen of Prostate 1 (STEAP1) Has a Single b Heme and Is Capable of Reducing Metal Ion Complexes and Oxygen. *Biochemistry (Mosc.)* 55, 6673–6684.

Kirschner, A., Thiede, M., Blaeschnke, F., Richter, G.H.S., Gerke, J.S., Baldauf, M.C., Grünwald, T.G.P., Busch, D.H., Burdach, S., and Thiel, U. (2016). Lysosome-associated membrane glycoprotein 1 predicts fratricide amongst T cell receptor transgenic CD8+ T cells directed against tumor-associated antigens. *Oncotarget* 7, 56584–56597.

Kirschner, A., Thiede, M., Grünwald, T.G.P., Alba Rubio, R., Richter, G.H.S., Kirchner, T., Busch, D.H., Burdach, S., and Thiel, U. (2017). Pappalysin-1 T cell receptor transgenic allo-restricted T cells kill Ewing sarcoma in vitro and in vivo. *Oncoimmunology* 6, e1273301.

Kovar, H., Amatruda, J., Brunet, E., Burdach, S., Cidre-Aranaz, F., de Alava, E., Dirksen, U., van der Ent, W., Grohar, P., Grünwald, T.G.P., et al. (2016). The second European interdisciplinary Ewing sarcoma research summit--A joint effort to deconstructing the multiple layers of a complex disease. *Oncotarget* 7, 8613–8624.

Krumbholz, M., Hellberg, J., Steif, B., Bäuerle, T., Gillmann, C., Fritscher, T., Agaimy, A., Frey, B., Juengert, J., Wardemann, E., et al. (2016). Genomic EWSR1 Fusion Sequence as Highly Sensitive and Dynamic Plasma Tumor Marker in Ewing Sarcoma. *Clin. Cancer Res.* 22, 4356–4365.

Lee, C.-H., Chen, S.-L., Sung, W.-W., Lai, H.-W., Hsieh, M.-J., Yen, H.-H., Su, T.-C., Chiou, Y.-H., Chen, C.-Y., Lin, C.-Y., et al. (2016). The Prognostic Role of STEAP1 Expression Determined via Immunohistochemistry Staining in Predicting Prognosis of Primary Colorectal Cancer: A Survival Analysis. *Int. J. Mol. Sci.* 17, 592.

von Levetzow, C., Jiang, X., Gwye, Y., von Levetzow, G., Hung, L., Cooper, A., Hsu, J.H.-R., and Lawlor, E.R. (2011). Modeling Initiation of Ewing Sarcoma in Human Neural Crest Cells. *PLoS ONE* 6, e19305.

Mihlan, S., Reiβ, C., Thalheimer, P., Herterich, S., Gaetzner, S., Kremerskothen, J., Pavenstädt, H.J., Lewandrowski, U., Sickmann, A., and Butt, E. (2013). Nuclear import of LASP-1 is regulated by phosphorylation and dynamic protein-protein interactions. *Oncogene* 32, 2107–2113.

Miller, I.V., and Grünwald, T.G.P. (2015). Tumour-derived exosomes: Tiny envelopes for big stories. *Biol. Cell* 107, 287–305.

Miller, I.V., Raposo, G., Welsch, U., Prazeres da Costa, O., Thiel, U., Lebar, M., Maurer, M., Bender, H.-U., von Luettichau, I., Richter, G.H.S., et al. (2013). First

identification of Ewing's sarcoma-derived extracellular vesicles and exploration of their biological and potential diagnostic implications. *Biol. Cell* 105, 289–303.

Niu, Y., Shao, Z., Wang, H., Yang, J., Zhang, F., Luo, Y., Xu, L., Ding, Y., and Zhao, L. (2016). LASP1-S100A11 axis promotes colorectal cancer aggressiveness by modulating TGF β /Smad signaling. *Sci. Rep.* 6, 26112.

Orth, M.F., Cazes, A., Butt, E., and Grünewald, T.G.P. (2015). An update on the LIM and SH3 domain protein 1 (LASP1): a versatile structural, signaling, and biomarker protein. *Oncotarget* 6, 26–42.

Peng, C.Y., Graves, P.R., Thoma, R.S., Wu, Z., Shaw, A.S., and Piwnica-Worms, H. (1997). Mitotic and G2 checkpoint control: regulation of 14-3-3 protein binding by phosphorylation of Cdc25C on serine-216. *Science* 277, 1501–1505.

Postel-Vinay, S., Véron, A.S., Tirode, F., Pierron, G., Reynaud, S., Kovar, H., Oberlin, O., Lapouble, E., Ballet, S., Lucchesi, C., et al. (2012). Common variants near TARDBP and EGR2 are associated with susceptibility to Ewing sarcoma. *Nat. Genet.* 44, 323–327.

Potratz, J., Dirksen, U., Jürgens, H., and Craft, A. (2012). Ewing sarcoma: clinical state-of-the-art. *Pediatr. Hematol. Oncol.* 29, 1–11.

Richter, G.H.S., Fasan, A., Hauer, K., Grünewald, T.G.P., Berns, C., Rössler, S., Naumann, I., Staegge, M.S., Fulda, S., Esposito, I., et al. (2013). G-Protein coupled receptor 64 promotes invasiveness and metastasis in Ewing sarcomas through PGF and MMP1. *J. Pathol.* 230, 70–81.

Riggi, N., and Stamenkovic, I. (2007). The Biology of Ewing sarcoma. *Cancer Lett.* 254, 1–10.

Riggi, N., Knoechel, B., Gillespie, S.M., Rheinbay, E., Boulay, G., Suvà, M.L., Rossetti, N.E., Boonseng, W.E., Oksuz, O., Cook, E.B., et al. (2014). EWS-FLI1 utilizes divergent chromatin remodeling mechanisms to directly activate or repress enhancer elements in Ewing sarcoma. *Cancer Cell* 26, 668–681.

Rotblat, B., and Grünewald, T.G.P. (2015). Translating cancer-omics into function. *Biol. Cell* 00, 1–2.

Rotblat, B., Grünewald, T.G.P., Leprivier, G., Melino, G., and Knight, R.A. (2013). Anti-oxidative stress response genes: bioinformatic analysis of their expression and relevance in multiple cancers. *Oncotarget* 4, 2577–2590.

Sahay, D., Leblanc, R., Grünewald, T.G.P., Ambatipudi, S., Ribeiro, J., Clézardin, P., and Peyruchaud, O. (2015). The LPA1/ZEB1/miR-21-activation pathway regulates metastasis in basal breast cancer. *Oncotarget* 6, 20604–20620.

Sand, L., Szuhai, K., and Hogendoorn, P. (2015). Sequencing Overview of Ewing Sarcoma: A Journey across Genomic, Epigenomic and Transcriptomic Landscapes. *Int. J. Mol. Sci.* 16, 16176–16215.

Sannino, G., Pasqualini, L., Ricciardelli, E., Montilla, P., Soverchia, L., Ruggeri, B., Falcinelli, S., Renzi, A., Ludka, C., Kirchner, T., et al. (2016). Acute stress enhances the expression of neuroprotection- and neurogenesis-associated genes in the hippocampus of a mouse restraint model. *Oncotarget* 7, 8455–8465.

Sboner, A., Demichelis, F., Calza, S., Pawitan, Y., Setlur, S.R., Hoshida, Y., Perner, S., Adam, H.-O., Fall, K., Mucci, L.A., et al. (2010). Molecular sampling of prostate cancer: a dilemma for predicting disease progression. *BMC Med. Genomics* 3, 8.

Schilsky, R.L. (2010). Personalized medicine in oncology: the future is now. *Nat. Rev. Drug Discov.* 9, 363–366.

Schirmer, D., Grünwald, T.G.P., Klar, R., Schmidt, O., Wohlleber, D., Rubí, R.A., Uckert, W., Thiel, U., Bohne, F., Busch, D.H., et al. (2016). Transgenic antigen-specific, HLA-A*02:01-allo-restricted cytotoxic T cells recognize tumor-associated target antigen STEAP1 with high specificity. *Oncoimmunology* 5, e1175795.

Shao, Z., Cai, Y., Xu, L., Yao, X., Shi, J., Zhang, F., Luo, Y., Zheng, K., Liu, J., Deng, F., et al. (2016). Loss of the 14-3-3 σ is essential for LASP1-mediated colorectal cancer progression via activating PI3K/AKT signaling pathway. *Sci. Rep.* 6, 25631.

Somasekharan, S.P., El-Naggar, A., Leprivier, G., Cheng, H., Hajee, S., Grünwald, T.G.P., Zhang, F., Ng, T., Delattre, O., Evdokimova, V., et al. (2015). YB-1 regulates stress granule formation and tumor progression by translationally activating G3BP1. *J. Cell Biol.* 208, 913–929.

Sun, W., Guo, L., Shao, G., Liu, X., Guan, Y., Su, L., and Zhao, S. (2017). Suppression of LASP-1 attenuates the carcinogenesis of prostatic cancer cell lines: Key role of the NF- κ B pathway. *Oncol. Rep.* 37, 341–347.

Swain, S.M., Baselga, J., Kim, S.-B., Ro, J., Semiglazov, V., Campone, M., Ciruelos, E., Ferrero, J.-M., Schneeweiss, A., Heeson, S., et al. (2015). Pertuzumab, trastuzumab, and docetaxel in HER2-positive metastatic breast cancer. *N. Engl. J. Med.* 372, 724–734.

Thiel, U., Koscielniak, E., Blaesche, F., Grünwald, T.G.P., Badoglio, M., Diaz, M.A., Paillard, C., Prete, A., Ussowicz, M., Lang, P., et al. (2013). Allogeneic stem cell transplantation for patients with advanced rhabdomyosarcoma: a retrospective assessment. *Br. J. Cancer* 109, 2523–2532.

Thiel, U., Wawer, A., von Luettichau, I., Bender, H.-U., Blaesche, F., Grünwald, T.G.P., Steinborn, M., Röper, B., Bonig, H., Klingebiel, T., et al. (2016). Bone marrow involvement identifies a subgroup of advanced Ewing sarcoma patients with fatal outcome irrespective of therapy in contrast to curable patients with multiple bone metastases but unaffected marrow. *Oncotarget* 7, 70959–70968.

Thiel, U., Schober, S., Einspieler, I., Kirschner, A., Thiede, M., Schrimmer, D., Gall, K., Blaesche, F., Rubio, R.A., Grünwald, T.G.P., et al. (2017). Ewing Sarcoma Partial Regression without GvHD by Chondromodulin-I/HLA-A*02:01-Specific Allorestricted T Cell Receptor Transgenic T Cells. *Oncolimmunology* 6, e1312239.

Tirode, F., Laud-Duval, K., Prieur, A., Delorme, B., Charbord, P., and Delattre, O. (2007). Mesenchymal stem cell features of Ewing tumors. *Cancer Cell* 11, 421–429.

Tirode, F., Surdez, D., Ma, X., Parker, M., Le Deley, M.C., Bahrami, A., Zhang, Z., Lapouble, E., Grossetete-Lalami, S., Rusch, M., et al. (2014). Genomic Landscape of Ewing Sarcoma Defines an Aggressive Subtype with Co-Association of STAG2 and TP53 Mutations. *Cancer Discov.* 4, 1342–1353.

Tomasetto, C., Moog-Lutz, C., Régnier, C.H., Schreiber, V., Basset, P., and Rio, M.C. (1995a). Lasp-1 (MLN 50) defines a new LIM protein subfamily characterized by the association of LIM and SH3 domains. *FEBS Lett.* 373, 245–249.

Tomasetto, C., Régnier, C., Moog-Lutz, C., Mattei, M.G., Chenard, M.P., Lidereau, R., Basset, P., and Rio, M.C. (1995b). Identification of four novel human genes amplified and overexpressed in breast carcinoma and localized to the q11-q21.3 region of chromosome 17. *Genomics* 28, 367–376.

Traenka, C., Remke, M., Korshunov, A., Bender, S., Hielscher, T., Northcott, P.A., Witt, H., Ryzhova, M., Felsberg, J., Benner, A., et al. (2010). Role of LIM and SH3 protein 1 (LASP1) in the metastatic dissemination of medulloblastoma. *Cancer*

Res. 70, 8003–8014.

Uren, A., and Toretsky, J.A. (2005). Ewing's sarcoma oncoprotein EWS-FLI1: the perfect target without a therapeutic agent. *Future Oncol.* 1, 521–528.

Vaman, V.S.A., Poppe, H., Houben, R., Grünwald, T.G.P., Goebeler, M., and Butt, E. (2015). LASP1, a Newly Identified Melanocytic Protein with a Possible Role in Melanin Release, but Not in Melanoma Progression. *PloS One* 10, e0129219.

Vucic, E.A., Thu, K.L., Robison, K., Rybaczyk, L.A., Chari, R., Alvarez, C.E., and Lam, W.L. (2012). Translating cancer 'omics' to improved outcomes. *Genome Res.* 22, 188–195.

Wang, B., Feng, P., Xiao, Z., and Ren, E.-C. (2009). LIM and SH3 protein 1 (Lasp1) is a novel p53 transcriptional target involved in hepatocellular carcinoma. *J. Hepatol.* 50, 528–537.

Wernicke, C.M., Grünwald, T.G.P., Juenger, H., Kuci, S., Kuci, Z., Koehl, U., Mueller, I., Doering, M., Peters, C., Lawitschka, A., et al. (2011). Mesenchymal stromal cells for treatment of steroid-refractory GvHD: a review of the literature and two pediatric cases. *Int. Arch. Med.* 4, 27.

Wernicke, C.M., Richter, G.H.S., Beinvogl, B.C., Plehm, S., Schlitter, A.M., Bandapalli, O.R., Prazeres da Costa, O., Hattenhorst, U.E., Volkmer, I., Staeger, M.S., et al. (2012). MondoA is highly overexpressed in acute lymphoblastic leukemia cells and modulates their metabolism, differentiation and survival. *Leuk. Res.* 36, 1185–1192.

Willier, S., Butt, E., Richter, G.H.S., Burdach, S., and Grünwald, T.G.P. (2011). Defining the role of TRIP6 in cell physiology and cancer. *Biol. Cell* 103, 573–591.

Worch, J., Cyrus, J., Goldsby, R., Matthay, K.K., Neuhaus, J., and DuBois, S.G. (2011). Racial differences in the incidence of mesenchymal tumors associated with EWSR1 translocation. *Cancer Epidemiol. Biomark. Prev.* 20, 449–453.

Zhang, J., Baran, J., Cros, A., Guberman, J.M., Haider, S., Hsu, J., Liang, Y., Rivkin, E., Wang, J., Whitty, B., et al. (2011). International Cancer Genome Consortium Data Portal--a one-stop shop for cancer genomics data. *Database J. Biol. Databases Curation* 2011, bar026.

7. Danksagung

Mein besonderer Dank gilt meinen bisherigen wissenschaftlichen und ärztlichen Mentoren, Frau Prof. Dr. rer. nat Elke Butt, Herrn Prof. Dr. med. Stefan Burdach, Herrn Prof. Dr. Olivier Delattre, und insbesondere Herrn Prof. Dr. med. Thomas Kirchner für seine großartige Unterstützung meiner Forschung und meiner Ausbildung zum Pathologen. Der Deutschen Krebshilfe danke ich für die Förderung im Rahmen des Max-Eder Nachwuchs-Programms.

8. Originalarbeiten

available at www.sciencedirect.com
SCIENCE @ **DIRECT**®
www.elsevier.com/locate/yexcr

Research Article

Silencing of LASP-1 influences zyxin localization, inhibits proliferation and reduces migration in breast cancer cells

Thomas G.P. Grunewald^a, Ulrike Kammerer^b, Elfriede Schulze^a, Detlef Schindler^c,
Arnd Honig^b, Michael Zimmer^a, Elke Butt^{a,*}

^aInstitute of Clinical Biochemistry and Pathobiochemistry, University of Würzburg, Grobühlstr. 12, D-97080 Würzburg, Germany

^bDepartment of Obstetrics and Gynecology, University of Würzburg, Josef-Schneider-Str. 4, D-97080 Würzburg, Germany

^cDepartment of Human Genetics, University of Würzburg, Biozentrum, Am Hubland, D-97074 Würzburg, Germany

ARTICLE INFORMATION

Article Chronology:

Received 25 July 2005

Revised version received

10 November 2005

Accepted 13 December 2005

Available online 23 January 2006

ABSTRACT

LIM and SH3 protein (LASP-1), initially identified from human breast cancer, is a specific focal adhesion protein involved in cell migration. LASP-1 is an actin binding protein, which also interacts with the proline-rich domains of zyxin, a scaffolding protein required for cell movement and gene transcription.

In the present work, we analyzed the effect of LASP-1 on different human breast cancer cell lines. Transfection with LASP-1-specific siRNA resulted in a reduced protein level of LASP-1 in BT-20 and MCF-7 cell lines. The siRNA-treated cells were arrested in G2/M phase of cell cycle, and proliferation of the tumor cells was suppressed by 30–50% corresponding to around 50% of the cells being transfected successfully as seen by immunofluorescence. In addition, tumor cells showed a 50% reduced migration after siRNA treatment, while overexpression of LASP-1 in non-tumor PTK-2 cells, which do not express endogenous LASP-1, resulted in a significant increase in cell motility. LASP-1 silencing is accompanied with a reduced binding of the LASP-1 binding partner zyxin to focal contacts without changes in actin stress fiber organization as observed in immunofluorescence experiments.

The data provide evidence for an essential role of LASP-1 in tumor cell growth and migration, possibly by influencing the localization of zyxin.

© 2005 Elsevier Inc. All rights reserved.

Keywords:

Breast cancer

MCF-7

BT-20

Metastasis

LASP-1

Zyxin

Migration

siRNA

Cell cycle

Focal contacts

Introduction

Breast cancer is the most frequent malignancy among women and ranks first as a cause of cancer deaths among women at ages 20 to 59 years [1]. Despite the use of endocrine therapy, systemic chemotherapy and novel approaches such as treatment with trastuzumab (Herceptin®), the outcome of metastatic breast cancer has not substantially improved. Metastatic disease remains generally incurable with a median

survival time of only a few years [2,3], hence additional therapeutic modalities are required to improve treatment. To improve the outcome, new therapies are required, and genes that are overexpressed in metastatic cancer cells are promising targets for novel therapeutic targets.

LASP-1 (Lim and SH3 domain protein) was initially identified from a cDNA library of breast cancer metastases, and the gene was mapped to human chromosome 17q21 [4,5]. Human LASP-1 encodes a protein of 261 amino acids

* Corresponding author. Fax: +49 931 3293630.

E-mail address: butt@klin-biochem.uni-wuerzburg.de (E. Butt).

containing an N-terminal LIM domain followed by two actin binding sites and a C-terminal src homology SH3 domain. The actin binding domains in the core of the LASP-1 protein mediate an interaction between LASP-1 and the actin cytoskeleton at cell membrane extensions, but not along the actin stress fibers [6–9]. The SH3 domain at the C-terminus is involved in protein–protein interactions through binding to proline-rich sequences, specifically with zyxin, lipoma preferred partner (LPP) and vasodilator stimulated phosphoprotein (VASP) [9,10]. Although the specific cellular functions of LASP-1 have not been defined, the protein–protein interactions mediated by the LIM and SH3 domains can be regarded as scaffolds for the formation of complexes of higher order.

LASP-1 is a cAMP- and cGMP-depending signaling protein [8]. In rabbit parietal cells, elevation of intracellular cAMP induced a partial translocation of LASP-1 to the apically directed F-actin-rich intracellular canalculus, which is the site of active HCl secretion [11,12]. Moreover, phosphorylation resulted in a translocation of the protein from the membrane to the cytosol and was associated with reduced cell migration [8]. In addition, LASP-1 expression has been reported to be increased in metastatic breast cancer, suggesting that over-expression of LASP-1 may be involved in the migratory process of these cells [4]. Surprisingly, both increase in LASP-1, and depletion in COS-7, HEK293 and MCF-7 cells inhibited basal and growth-factor-stimulated cell migration [13].

In this study, we demonstrate that LASP-1 is highly over-expressed in breast cancer tissue and metastatic breast cancer cells. Silencing of the LASP-1 gene by RNAi technique retarded cell proliferation and cell migration of breast cancer cells *in vitro* without influencing the expression of other proteins related to the LASP-1 signaling pathway. Furthermore, the knock-down of LASP-1 severely affected zyxin localization.

Materials and methods

Tissue samples

The studies were performed with approval of the Ethics Committee of the University of Wuerzburg. Tissue samples of 10 archival cases each of ductal carcinoma *in situ* (DCIS) without any invasive component, invasive breast carcinoma and lymph node metastases of breast carcinoma as well as three samples of normal breast tissue from reduction mammoplasty were obtained from the Department of Pathology of the University of Wuerzburg and reviewed by a pathologist to confirm the diagnosis.

Immunohistochemistry

For immunohistochemical staining procedures, endogenous peroxidase was blocked by incubation in 0.1% hydrogen peroxide in PBS for 5 min. The slides were then incubated with the polyclonal anti-LASP antibody diluted 1:1000 in “antibody diluent” (DAKO, Hamburg, Germany) followed by the EnVision/rabbit detection system (DAKO). Histogreen (Linaris, Wertheim, Germany) was used as the chromogen, and cells were counterstained with hematoxylin (Sigma, Deisenhofen, Germany).

Cell culture conditions

Cell lines were obtained from Cell Line Services (Heidelberg, Germany) and grown at 1×10^5 cells/ml in a plastic cell culture flask in a humidified incubator under 5% CO₂ atmosphere. BT-20 and MCF-7 cells derived from human breast carcinoma were cultured in HBCA medium (Biochrom, Berlin, Germany). PTK-2 cells (Potorous tridactylis kidney) were grown in DMEM medium, 2 mM glutamine (Life Technologies, Karsruhe, Germany). HUVEC (human umbilical vein endothelial cells) were cultured in endothelial cell basal medium EBM (Cambrex Bio Science Walkersville, MD). The HUVEC cell lines were kindly supplied by the Department of Nephrology, University of Wuerzburg, Germany.

All media contained 10% heat-inactivated fetal bovine serum (PAA, Linz, Austria) and 1% streptomycin/ampicillin (Invitrogen, Karsruhe, Germany) and were cultured at 37°C in a humidified atmosphere of 5% CO₂/95% air. Cells were checked routinely and found to be free of contamination by bacteria or fungi.

siRNA preparation and transfection

Expression of human and mouse LASP-1 was knocked down with siRNA duplexes targeting the sequence 5'-AAG GTG AAC TGT CTG GAT AAG-3' (bases 49–69), 5'-CUUAUCCAGA-CAGUUCACCdTdT-3'. For silencing of the human enabled homolog *Drosophila* gene (ENAH), the following siRNA sequence was used: (bases 204–224), 5'-CUGUGUAGCUU-GAUUGUACdTdT-3'. A BLAST search against the complete human and mouse genomes verified that the selected sequences were specific for the respective target genes. The scrambled Neuropilin 1 (NP1) 5'-AGAGAUGUAGUCG-CUCGCUdTdT-3' was used as a control that targeted no known mRNA sequences. All siRNAs were obtained from Dharmacon RNA Technologies (Lafayette, CO). The siControl Non-Targeting siRNA from Dharmacon could not be used in our cell system due to toxic effects.

Cells in the exponential growth phase were plated in six-well plates at a density of 0.5×10^5 cells/well, grown for 24 h and transfected with 1 µg siRNA in reduced serum medium OPTI-MEM-I (Gibco, Paisley, UK) according to the manufacturer's protocol in 30–50% confluence. For the formation of the siRNA–lipid complexes, 3 µl siRNA stock solution (20 µM) was diluted in 100 µl OPTI-MEM, mixed with 3 µl Metafectene (Biontex, Munich, Germany) in 100 µl OPTI-MEM and incubated at room temperature for 17 min. Subsequently, the culture medium was removed and replaced by 1 ml OPTI-MEM-I and the siRNA–lipid complexes (1.2 ml total volume).

After 4 h of incubation at 37°C, 1.2 ml of cell culture medium with 20% fetal bovine serum was added, and incubation was continued for 36–56 h. For control cells, Metafectene alone and/or 1 µg siRNA scrambled NP1 oligonucleotides were used.

At least three independent experiments were performed for each cell line, and representative results are shown.

Cell proliferation assay

For proliferation assay, cells were transfected as described. At the time points indicated, cells were

trypsinized, and cell numbers were determined by a Coulter Counter (Beckman, Fullerton, CA). Experiments were performed in triplicate for each time point. Cell viability was evaluated by counting trypan-blue-positive and -negative cells under a phase-contrast microscope (Zeiss Axiovert, Aalen, Germany).

Western blot analysis

For Western blotting, cells were prepared by lysing in Laemmli sample buffer, and equal amounts of protein, according to the cell count, were resolved by 12% SDS-PAGE. After blotting on nitrocellulose membrane and blocking with 3% nonfat dry milk in 10 mM Tris, pH 7.5, 100 mM NaCl, 0.1% (w/v) Tween 20, the membrane was first incubated with the antibodies raised against LASP-1 (1:10,000) [8], caspase-3 (1:1000) (New England Biolabs, Frankfurt, Germany), VASP M4 (1:1000) (Nanotools, Tuebingen, Germany) or PKA (1:1000) (Abcam, Cambridge, UK) followed by incubation with horseradish-peroxidase-coupled goat anti-rabbit IgG (Biorad, Munich, Germany), diluted 1:5000 and detected by ECL or ECL plus (Amersham Biosciences, Freiburg, Germany). For Mena, the primary mouse monoclonal antibody was used at a dilution of 1:2000 (BD Bioscience, San Diego, CA) followed by a secondary horseradish-peroxidase-coupled goat anti-mouse IgA antibody diluted 1:5000 (Sigma, Deisenhofen, Germany). For zyxin, mouse hybridoma supernatant (kind gift of Dr. J. Wehland, GBF Braunschweig, Germany) [14] was used at a dilution of 1:100 followed by a secondary horseradish-peroxidase-coupled goat anti-mouse IgA antibody diluted 1:5000. Protein bands were visualized by autoradiography. Quantification of signal transduction by densitometry was carried out using the Odyssey system (Li-Cor, Bad Homburg, Germany).

Annexin V analysis

For apoptosis detection, cells were stained with anti-Annexin V-FITC (BD Pharmingen, Heidelberg, Germany) following the manufacturer's instructions. In brief, cells were harvested 1 h after transfection, washed twice in ice-cold PBS and resuspended in Annexin V-binding buffer at 1×10^6 cells/ml. Two microliters of the Annexin V-FITC antibody and 2 μ l of propidium iodide (10 μ g/ml) were added to 100 μ l of cell suspension and incubated for 15 min at room temperature. Cells were then washed once in binding buffer, resuspended in 200 μ l binding buffer and immediately analyzed in a FACS-Scan Cytometer (Becton Dickinson, Heidelberg). A total of 10,000 cells per sample were evaluated for specific staining. Results were analyzed using the WinMDI-software (Version 2.8, ©Joseph Trotter).

FACS

For cell cycle analysis, BT-20 cells were harvested 44 h after LASP-1 siRNA transfection. The cells were pelleted and stained with DAPI (Sigma, Deisenhofen, Germany) at a final concentration of 2 μ g/ml in permeabilizing buffer containing 0.1 M Tris-HCl pH 7.4, 0.154 M NaCl, 0.5 mM

MgCl₂, 1 mM CaCl₂, 0.1% NP-40 and 0.2% BSA in ddH₂O for 30 min at 4°C in the dark. Bivariate flow histograms were recorded on an analytical dual-laser equipped cytometer (LSR1, Becton Dickinson Biosciences, Heidelberg, Germany) using UV excitation. Resulting cell cycle distributions were quantitated with the MPLUS AV software (Phoenix Flow Systems, San Diego, CA). For technical details, see [15].

Immunofluorescence

For immunofluorescence microscopy, cells were grown on glass chamber slides, fixed in 4% (w/v) paraformaldehyde in PBS, permeabilized with 0.1% (w/v) Triton X-100 in PBS and then stained with affinity-purified LASP-1 antibody (1:2000) followed by secondary Cy3-labeled anti-rabbit antibody (Dianova, Hamburg, Germany) or mouse Zyxin hybridoma supernatant (1:10) followed by secondary FITC-labeled goat anti-mouse antibody (Sigma, Deisenhofen, Germany). Oregon green phalloidin (Molecular Probes, Leiden, The Netherlands) was used for actin staining.

Migration experiments

Cells were cultured in medium in 25 cm² flasks to approximately 30–40% confluence and transfected with 2.5 μ g LASP-1 siRNA or 2.5 μ g WT LASP-1 pcDNA3 (8) using 10 μ l Metafectene. After 48 h of incubation and overnight starving, 1×10^5 cells per 100 μ l incubation medium (with 1 mM MgCl₂) were seeded in the upper chamber of BSA-coated 8 μ M pore size transwell chambers (Corning star, Cambridge, MA). Cells were allowed to migrate through the porous membrane for 4 h at 37°C. Cells remaining at the upper surface were completely removed using a cotton carrier. The lower surfaces of the membranes were then stained in a solution of 1% (w/v) crystal violet in 2% ethanol for 30 s and rinsed afterwards in distilled water. Cell-associated crystal violet was extracted by incubation in 10% acetic acid for 20 min and measured at 595 nm absorbance.

Results

LASP-1 is overexpressed in breast cancer tissue

To assess the role of LASP-1 in breast cancer, we examined its expression in benign breast tissue, in breast samples containing ductal carcinoma in situ (DCIS), in primary breast cancer and breast cancer metastases in the lymph node. Immunohistochemistry clearly allowed to localize LASP-1 expression in the myoepithelial cells of normal breast tissue, while luminal epithelial cells were LASP-1-negative in all normal breast tissues in ductus as well as in acini (Fig. 1A). In samples containing DCIS, weak but clear LASP-1-positive hyperplastic epithelial cells could be seen next to the LASP-1-positive myoepithelial cells (Fig. 1B). In all samples containing invasive breast cancer, a strong positivity of the tumor cells for LASP-1 was seen (Fig. 1C).

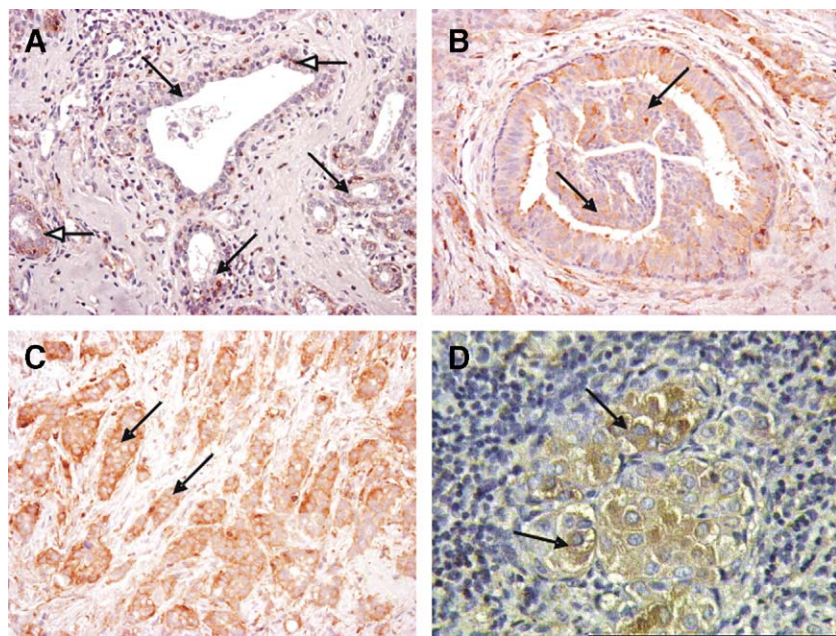


Fig. 1 – Immunohistochemical staining of normal and cancerous breast tissue samples at different stages of tumor development. LASP-1 was detected using anti-LASP-1 rabbit polyclonal antibody in paraffin-embedded tissue samples. (A) Normal breast tissue with two ducti in the center and the acini at the left and right sides. LASP-1 is positive in the myoepithelial cells (white head arrow) surrounding the LASP-1-negative luminal epithelia cells (black arrow). (B) In DCIS, LASP-1 is expressed within the hyperplastic areas (arrows). (C) In breast cancer, all cancer cells are intensively stained positive for LASP (Arrows). (D) In lymph node metastases, breast cancer cells are intensively stained for LASP-1. LASP-1-positive structures are seen in brown (DAB). All sections were counterstained with hematoxylin. Magnification $\times 400$ (A–C) and $\times 630$ (D).

No correlation was seen between the overexpression of LASP-1 in malignant breast tissue and histologic subtype (lobular and invasive ductal carcinoma), tumor size or

nodal status respectively (not shown). In addition to primary lesions, all lymph node metastases showed a marked overexpression of LASP-1 (Fig. 1D).

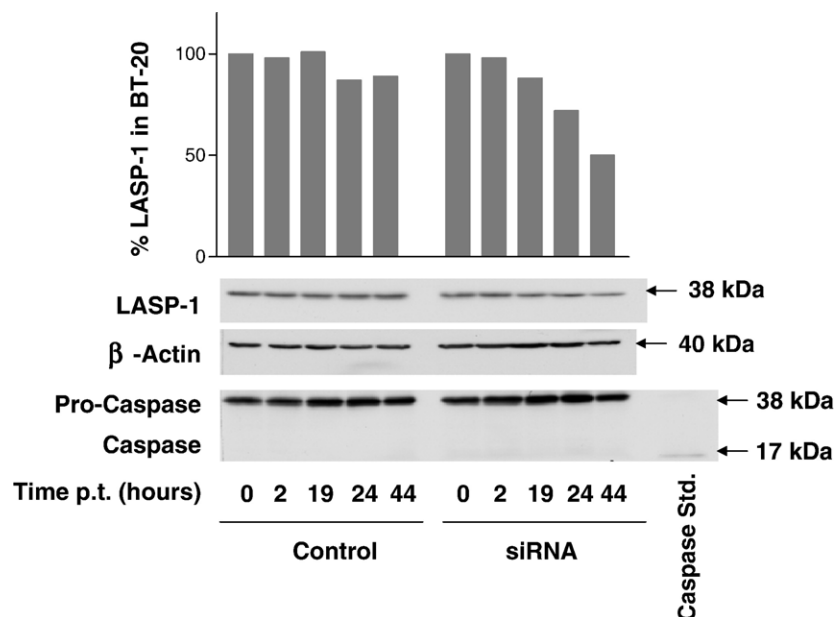


Fig. 2 – LASP-1 knock-down. A total of 50,000 cells of the BT-20 breast cancer cell line were plated and allowed to grow for 24 h (until 40% confluence). siRNA LASP-1 was transfected into cells in a concentration of 60 nM. Cells were harvested after 2, 19, 24 and 44 h of siRNA LASP-1 treatment. Total cell protein was analyzed by Western blot with antibodies against LASP-1, β -actin and caspase-3. Control cells were treated with scrambled NP1 siRNA. Upper panel: densitometric quantification of the LASP-1 Western blot analysis standardized to β -actin.

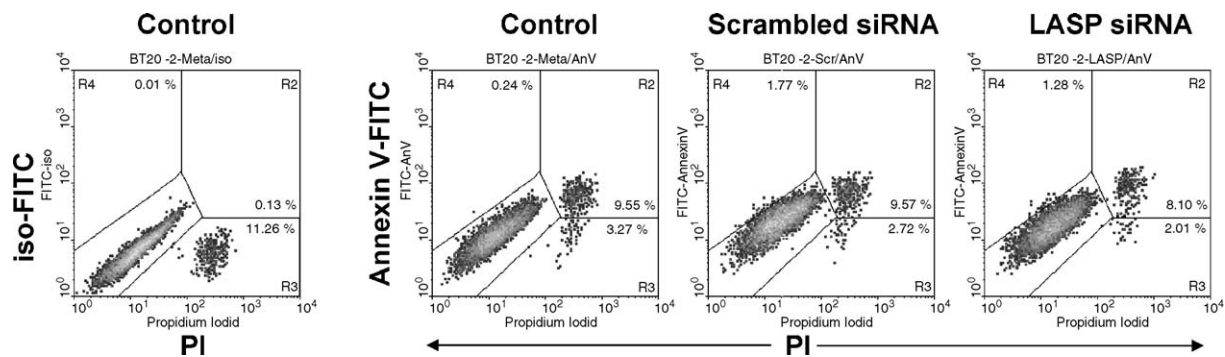


Fig. 3 – LASP-1 siRNA treatment does not induce apoptosis. A total of 1×10^6 cells/ml was stained with Annexin V-FITC and analyzed by FACS. No significantly higher rate of apoptosis (around 2%) was observed in siRNA LASP-1-treated BT-20 cells compared to cells transfected with scrambled siRNA NP1 or Metafectene alone (Control), respectively. PI, propidium iodide stain.

Silencing of LASP-1 in BT-20 and MCF-7 cells inhibits proliferation in vitro

To study the possible role of LASP-1 in breast cancer, we performed knock-down of the gene in the breast cancer cell lines BT-20 and MCF-7 by siRNA. The effect of siRNA transfection on the expression of LASP-1 was followed by Western blot analysis 24 h and 44 h after transfection. The amount of LASP-1 protein, standardized to β -actin, was reduced up to 50% after 44 h (Fig. 2) compared to the scrambled NP1 siRNA-transfected control cells. This corresponds to around 50% of the cells being transfected successfully as seen by immunofluorescence. In parallel to the protein knock-down, we observed a slower proliferation rate in LASP-1 siRNA-transfected cells compared to controls (Fig. 4A). The viability of cells was similar in both cultures as trypan blue staining detected no more than 5–8% dead cells in all experiments. To test whether the decreased proliferation could be due to apoptosis, we carried out a Western blot analysis with an anti-caspase-3 antibody. The antibody recognizes both the non-active pro-caspase-3 (38 kDa) and the active cleaved caspase-3 protein (17 kDa). As shown in Fig. 2, treatment of BT-20 cells with the LASP-1 siRNA duplex produced no active caspase 3. To rule out caspase-independent apoptosis pathways, we also performed Annexin V staining. Analysis of the FACS data (Fig. 3) showed no significant cell death in response to LASP-1 siRNA treatment. Similar results were obtained with MCF-7 cells (data not shown).

To ensure that the observed antiproliferative effect was due to specific knock-down of LASP-1, BT-20 cells were transfected with siRNA against human Drosophila enabled protein (ENAH), a protein also known to bind to zyxin in focal contacts and to be involved in cell motility [16]. Western blot analysis revealed an almost total loss of ENAH protein after ENAH siRNA treatment in BT-20 cells without affecting cell proliferation (Fig. 5A), whereas the knock-down of LASP-1 displayed a decreased proliferation rate (Figs. 4A and 5B).

Western blot analysis was performed to further examine the specificity of the siRNA treatment. Since LASP-1 acts as a scaffolding protein, we assessed the protein levels of the LASP-1 cytoskeletal interacting partners VASP, zyxin and actin as well as the level of protein kinase A (known to phosphorylate LASP-1

and ENAH) before and after siRNA LASP-1 and siRNA ENAH treatment. The data revealed no change in protein expression of the interacting proteins after LASP-1 silencing (Figs. 2, 5 and 6).

Downregulation of LASP-1 induces G2 phase accumulation in BT-20 cells

We next analyzed cell cycle distributions of siRNA-treated BT-20 cells using flow cytometry. After incubation with LASP-1 siRNA for 44 h, the proportion of cells accumulated in the G2 phase amounted to 33.6% (Fig. 4B), whereas the same cells treated with scrambled

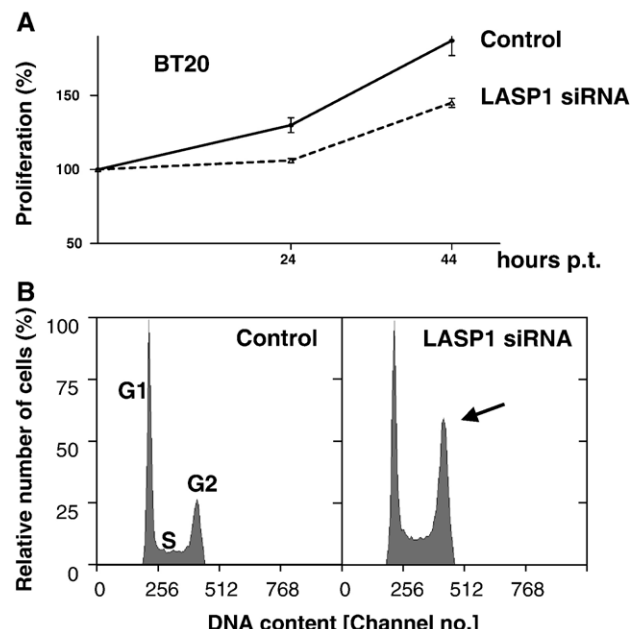


Fig. 4 – LASP-1 siRNA treatment impairs BT-20 cell proliferation by inducing G2 phase accumulation. (A) BT-20 cells were transfected with siRNA LASP-1 or scrambled NP1 siRNA (Control). After the indicated periods of time, the cells were harvested, and their total number was determined using a Coulter counter. (B) FACS analysis of LASP-1 siRNA-treated BT-20 cells shows G2 phase accumulation as opposed to the same cells transfected with scrambled NP1 siRNA.

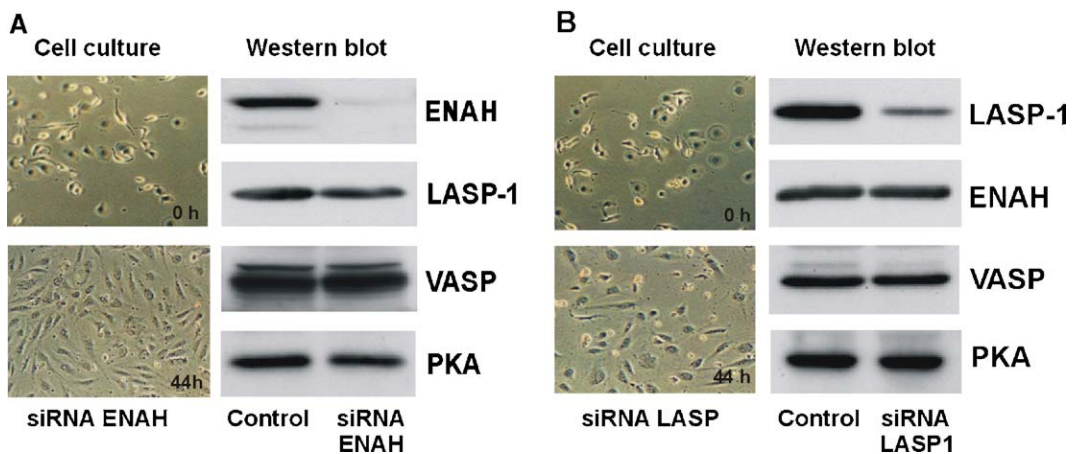


Fig. 5 – Inhibition of cell proliferation is specific for LASP-1 silencing. BT-20 cells were treated with either ENAH siRNA (A) or LASP-1 siRNA (B). 44 h post-transfection, cells were photographed, harvested and counted to visualise reduced proliferation of siRNA LASP-1 treated cells (Cell culture). Western blot analysis was performed to assess the expression of LASP-1, ENAH, VASP and PKA in cell extracts from siRNA LASP-treated and scrambled NP1 siRNA control cells showing comparable protein levels between knock-down and control cells.

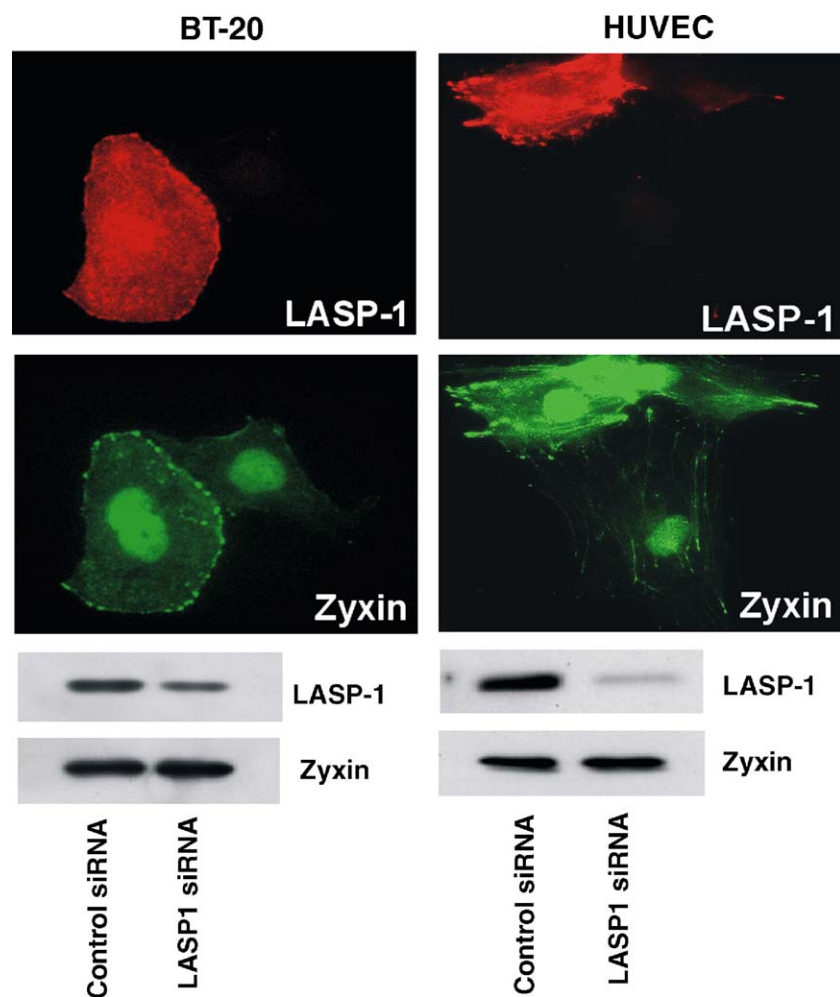


Fig. 6 – LASP-1 is required for zyxin localization at focal adhesions. Immunofluorescence images of LASP-1 (red) and zyxin (green) in siRNA LASP-1-treated BT-20 cells. Cells were stained with primary polyclonal antibody against LASP-1 and with mouse zyxin hybridoma supernatant. Western blot analysis was performed to assess LASP-1 and zyxin levels in cell extract aliquots from LASP-1 siRNA and scrambled NP1 siRNA-treated BT-20 cells above.

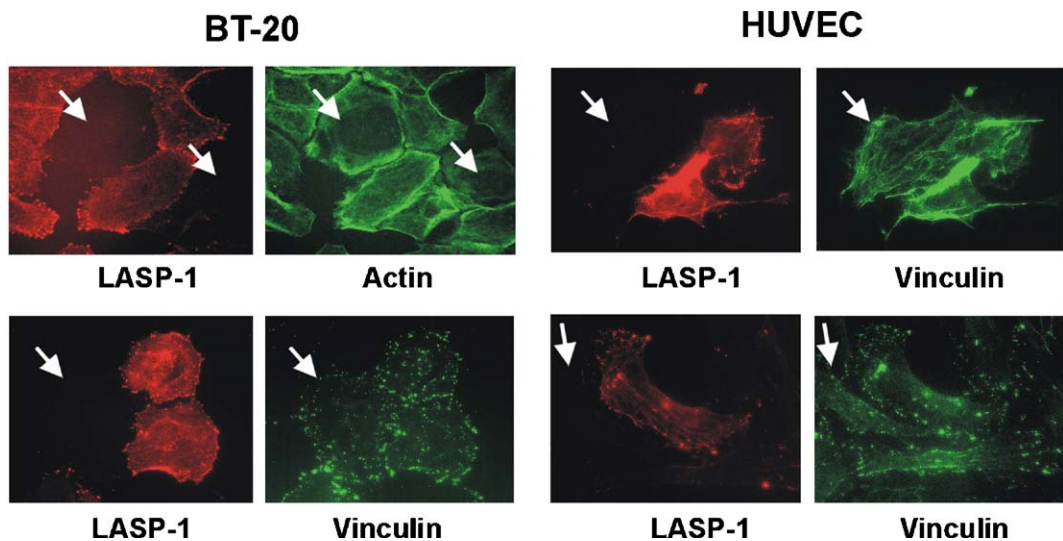


Fig. 7 – LASP-1 silencing is not influencing actin and vinculin localization. Immunofluorescence images of BT-20 cells and HUVEC transfected with siRNA LASP-1 and stained with antibodies against LASP-1 (red), vinculin (green) and actin (green). Shown are representative sections of a mixed population of both LASP-1 downregulated cells (arrows) and non-infected cells demonstrating no changes in actin and vinculin distribution of cells lacking LASP-1.

NP1 siRNA as a control had only 23.3% G2 phase proportion. Upon mock transfection, 23.4% of cells arrested in G2 phase, while the G2 phase proportion was 22.8% without transfection. The S phase fractions were comparable for LASP-1 and scrambled NP1 siRNA treatments (38.0 and 33.5%, respectively). Similar results were obtained in three independent experiments.

Silencing of LASP-1 results in reduced zyxin binding to focal adhesions

LASP-1 has previously been shown to localize to sites of cell adhesion and to interact with zyxin and actin [9,10]. To assess

whether silencing of LASP-1 affects these binding partners, siRNA LASP-1-treated BT-20 cells were stained with phalloidin green against actin or mouse anti-zyxin hybridoma supernatant and an FITC-labeled secondary antibody. In LASP-1, siRNA-transfected cells zyxin was absent from the focal adhesions, while the cellular level of zyxin remained unchanged as confirmed by Western blot analysis (Fig. 6). However, the absence of zyxin from focal contacts did not lead to changes in focal adhesion morphology as visualized by vinculin staining (Fig. 7). Likewise, the actin filament was not disturbed—less actin bundles, a blurred network of shorter filaments and some F-actin aggregates are typical for highly

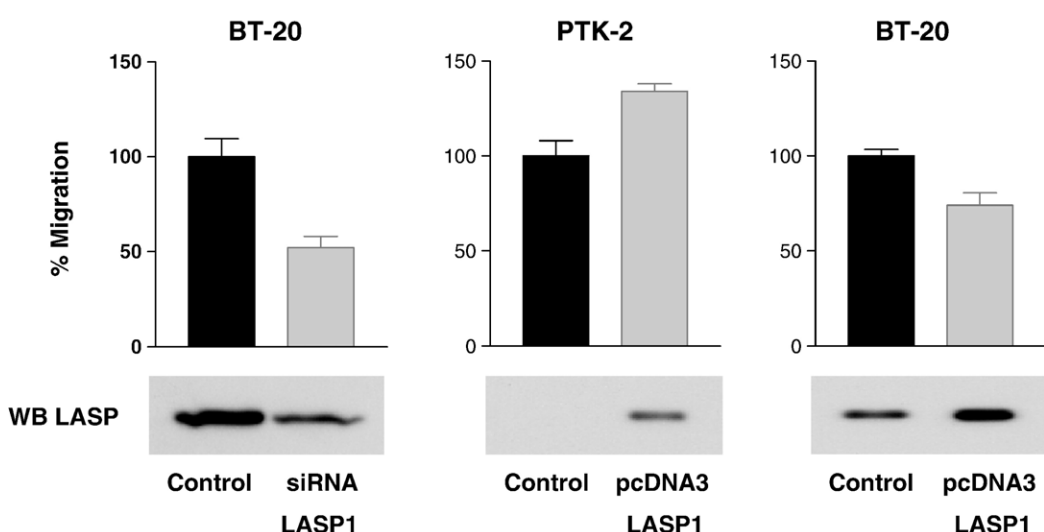


Fig. 8 – LASP-1 is necessary for cell migration. BT-20 cells and PTK-2 cells were transfected with LASP-1 siRNA, scrambled NP1 siRNA (Control), wild-type LASP-1 pcDNA3 or empty vector (Control pcDNA3). Migration was measured over 4 h in a Transwell® cell culture chamber. At least four chambers from three different experiments were analyzed. Each bars represent the mean ± SD. Corresponding Western blots of control cells, LASP-1 siRNA-transfected cells or LASP-1 pcDNA3-transfected cells probed with anti-LASP-1 polyclonal antibody are shown in the lower panel.

metastatic cancer cell lines [17]. Similar results were obtained with HUVEC demonstrating a loss of zyxin at the sites of focal contacts without changing cellular zyxin protein levels (Fig. 6). Interestingly, zyxin could still be detected along the actin stress fibers in HUVEC (co-localization of zyxin/actin not shown), an observation that is consistent with earlier results demonstrating LASP-1 presence only in the focal adhesion plaques and lamellopodia but not along the actin stress fibers [9,12].

Overexpression of LASP-1 in non-cancer cells increases cell migration

Although the function of LASP-1 is not known, recent results suggest an important role for the protein in cell adhesion and migration [8,13]. To directly examine the function of LASP-1 on cell motility, we performed migration experiments in a modified Boyden chamber with BT-20 cells either transfected with LASP-1 siRNA to downregulate the protein or BT-20 and PTK-2 cells transiently transfected with wild-type LASP-1 pcDNA3 plasmid to overexpress the protein. Cells were seeded in the upper chamber of a transwell polycarbonate membrane. After 4 h, those cells that had migrated through the porous membrane were counted. Depletion of LASP-1 in BT-20 cells strongly reduced cell migration (Fig. 8), while exogenous expression of LASP-1 in non-cancer PTK-2 cells, containing no detectable level of LASP-1, caused a significant increase in cell motility (Fig. 8), suggesting that LASP-1 is necessary for cell migration.

Surprisingly, amplification of LASP-1 in BT-20 breast cancer cells also inhibited cell motility (Fig. 8). Most likely, the amplification of LASP-1 in cancer cells already overexpressing this scaffolding protein (10-fold overexpression in case of BT-20 compared to human mesangial cells, data not shown) leads to disrupted pathways and changes in the cytoskeleton structure which influences cell migration. A similar effect of reduced motility in cancer cells has been observed by Lin and co-workers in MCF-7 cells [13]. Additional experiments to transfet wild-type LASP-1 pcDNA3 plasmid in normal human mesangial cells failed, while amplification of LASP-1 in primary human umbilical vein endothelial cells (HUVEC) exhibited only a slight but not significant increase in cell migration, most likely due to the very slow motility rate of these cells (Butt E; unpublished results).

Discussion

Cell migration and the controlled assembly and disassembly of focal adhesions are a highly integrated multistep process and a central feature in the molecular pathology of cancer [18]. To date, more than 50 different adhesion proteins have been identified that regulate the rate and organization of actin polymerization and focal adhesion turnover in protrusion. LASP-1 has been shown to interact with lipoma preferred partner (LPP) and zyxin, both of which can influence actin filament dynamics. The binding occurs between the C-terminal SH3 domain of LASP-1 and the N-terminal proline-rich domains of zyxin and LPP [8,13]. We found that depletion of LASP-1 from breast cancer BT-20 cells strongly inhibits cell migration, while amplification of wild-type LASP-1 in normal

kidney cells of rat kangaroo (PTK-2) stimulated cell motility, pointing to an important role of the protein for metastasis. However, cell adhesion and spreading are not affected by LASP-1 silencing as demonstrated by Lin and co-workers [13]. In the same study, LASP-1 was shown to be involved in cell migration upon growth factor stimulation, whereas treatment of cells with apoptosis-inducing reagents resulted in phosphorylation of LASP-1 at Tyr-171 and relocalization of the protein from focal adhesions to the periphery of the cell, leading to cell death. In an earlier published work, overexpression of LASP-1 mRNA in metastatic lymph nodes derived from breast cancer patients and the co-amplification of the gene together with HER-2/neu (c-erbB2) in 12% of mammary tumors were demonstrated [4,19]. And just recently, an IGF-I induced expression of the LASP-1 gene in MCF-7 cells was described [20]. Concordant with the published findings on mRNA level, our immunohistochemical data show LASP-1 to be absent from benign breast gland epithelial cells, while LASP-1 expression is detectable in DCIS and to very high levels in breast carcinoma and lymph node metastasis. These own and the published data are emphasizing the important role for LASP-1 for cancer metastasis.

An additional observation underscores the importance of LASP-1 in cancer. Recent studies have shown LASP-1 to be transcriptionally upregulated in response to the morphogen Sonic Hedgehog [21]. Disruption of the Hedgehog signaling cascade leads to a number of developmental disorders and plays a key role in the formation of a range of human cancers. In this context, it is interesting to note that zyxin also has been identified as a differentially transcribed gene in several types of cancer by microarray technology [22].

Zyxin is localized primarily at focal adhesion plaques and plays a central role in actin filament polymerization in mammalian cells [23]. Silencing of zyxin in HeLa cells resulted in significantly reduced actin stress fibers [24], whereas under cyclic stretch zyxin only dissociated from focal contacts and accumulated in the nucleus, without affecting vinculin or actin filaments [25]. In our immunofluorescence experiments, we observed a diffuse cytoplasmic localization of zyxin without protein loss and without changes in either vinculin distribution or actin stress fiber organization after LASP-1 knockdown, demonstrating the importance of LASP-1 for binding and recruiting zyxin to focal adhesions. The decreased cell motility after LASP-1 silencing can be explained by the functional loss of zyxin as a scaffolding protein that facilitates the formation of molecular complexes to promote site-specific actin assembly required for cell movement. This is in agreement with previous findings using a non-genetic approach and injecting a peptide derived from the N-terminus of zyxin to displace zyxin from its normal subcellular location, thus leading to reduced cell migration [26].

Recent work has shown that zyxin also shuttles through the nucleus – most likely by association with other LIM proteins – and may regulate gene transcription [27–29]. During mitosis, a fraction of zyxin becomes associated with the tumor suppressor h-warts at the mitotic apparatus [30]. H-warts is a key player in mitosis in mammalian cells, and loss of its function disrupts normal cell cycle regulation possibly leading to tumor development [31]. In BT-20 cells transfected with LASP-1 siRNA, zyxin has been shown to dissociate from focal

adhesion plaques and to distribute diffusely into the cytoplasm. It is therefore likely that part of zyxin enters the nucleus, binds to h-warts and leads to G2 cell cycle arrest and inhibits proliferation as observed after LASP-1 silencing.

In summary, our observations suggest an expanded role for LASP-1 in proliferation and breast cancer cell migration. Further studies will define the potential of LASP-1 antibody as an independent marker for diagnosis of breast cancer as well as a marker for prognosis of this disease.

Acknowledgments

We thank Richard Friedl for expert flow cytometric measurements, M. Kapp for excellent technical assistance and M. Eck (Dept. of Pathology, University of Wuerzburg) for pathohistological guidance. This study was supported by the Deutsche Krebshilfe 106219 to E.B. and A. H.

REFERENCES

[1] A. Jemal, T. Murray, E. Ward, A. Samuels, R.C. Tiwari, A. Ghafoor, E.J. Feuer, M.J. Thun, *Cancer statistics, 2005*, CA Cancer J. Clin. 55 (2005) 10–30.

[2] P.A. Greenberg, G.N. Hortobagyi, T.L. Smith, L.D. Ziegler, D.K. Frye, A.U. Buzdar, Long-term follow-up of patients with complete remission following combination chemotherapy for metastatic breast cancer, *J. Clin. Oncol.* 14 (1996) 2197–2205.

[3] C.K. Osborne, Tamoxifen in the treatment of breast cancer, *N. Engl. J. Med.* 339 (1998) 1609–1618.

[4] C. Tomasetto, C. Moog-Lutz, C.H. Regnier, V. Schreiber, P. Basset, M.C. Rio, LASP-1 (MLN 50) defines a new LIM protein subfamily characterized by the association of LIM and SH3 domains, *FEBS Lett.* 373 (1995) 245–249.

[5] C. Tomasetto, C. Regnier, C. Moog-Lutz, M.G. Mattei, M.P. Chenard, R. Liderau, P. Basset, M.C. Rio, Identification of four novel human genes amplified and overexpressed in breast carcinoma and localized to the q11–q21.3 region of chromosome 17, *Genomic* 28 (1995) 367–376.

[6] V. Schreiber, C. Moog-Lutz, C.H. Regnier, M.P. Chenard, H. Boeuf, J.L. Vonesch, C. Tomasetto, M.C. Rio, LASP-1, a novel type of actin-binding protein accumulating in cell membrane extensions, *Mol. Med.* 4 (1998) 675–687.

[7] S.C. Chew, X. Chen, J.A. Parente, S. Tarrer, C. Okamoto, H.Y. Qin, LASP-1 binds to non-muscle F-actin in vitro and is localized within multiple sites of dynamic actin assembly in vivo, *J. Cell Sci.* 115 (2002) 4787–4799.

[8] E. Butt, S. Gambaryan, N. Göttfert, A. Galler, K. Marcus, H.E. Meyer, Actin binding of human LIM and SH3 protein is regulated by cAMP- and cGMP-dependent protein kinase phosphorylation on serine 146, *J. Biol. Chem.* 278 (2003) 15601–15607.

[9] C. Keicher, S. Gambaryan, E. Schulze, K. Marcus, H.E. Meyer, E. Butt, Phosphorylation of mouse LASP-1 on threonine 156 by cAMP- and cGMP-dependent protein kinase, *Biochem. Biophys. Res. Commun.* 24 (2004) 308–316.

[10] B. Li, L.B. Zhuang, B. Trueb, Zyxin interacts with the SH3 domains of the cytoskeletal proteins LIM-nebulette and LASP-1, *J. Biol. Chem.* 279 (2004) 20401–20410.

[11] C.S. Chew, J.R. Parente, C.J. Zhou, E. Baranco, X. Chen, LASP-1 is a regulated phosphoprotein within the cAMP-signaling pathway in the gastric parietal cell, *J. Physiol.* 275 (1998) C56–C67.

[12] C.S. Chew, J.A. Parente, X. Chen, C. Chaponnier, R.S. Cameron, The LIM and SH3 domain containing protein, LASP-1, may link the cAMP-signaling pathway with dynamic membrane restructuring activities in ion transporting epithelia, *J. Cell Sci.* 113 (2000) 2035–2045.

[13] H.Y. Lin, Z.Y. Park, D. Lin, A.A. Brahmbhatt, M. Rio, J.R. Yates, R.L. Klemke, Regulation of cell migration and survival by focal adhesion targeting of LASP-1, *J. Cell Biol.* 165 (2004) 421–432.

[14] K. Rottner, M. Krause, M. Gimona, J.V. Small, J. Wehland, Zyxin is not colocalized with VASP at lamellipodial Tipps and exhibits different dynamics to vinculin, paxillin and VASP in focal adhesions, *Mol. Biol. Cell* 12 (2000) 3013–3103.

[15] D. Schindler, H. Hoehn, Flow cytometric testing for syndromes with chromosomal instability, in: R.D. Wegner (Ed.), *Diagnostic Cytogenetics*, Springer, Berlin, 1999, pp. 269–281.

[16] M. Reinhard, T. Jarchau, U. Walter, Actin-bases motility. Stopp and go with Ena/VASP proteins, *Trends Biochem. Sci.* 4 (2001) 243–249.

[17] C.R. Liu, C.S. Ma, J.Y. Ning, J.F. You, S.L. Liao, J. Zheng, Differential thymosin beta 10 expression levels and actin filament organisation in tumor cell lines with different metastatic potential, *Chin. Med. J.* 117 (2004) 213–218.

[18] A.J. Ridley, M.A. Schwartz, K. Burridge, R.A. Firtel, M.H. Ginsberg, G. Borisy, J.T. Parsons, A.R. Horwitz, Cell migration: integrating signals from front to back, *Science* 302 (2003) 1704–1709.

[19] I. Bieche, C. Tomasetto, H. Regnier, C. Moog-Lutz, M.C. Rio, R. Liderau, Two distinct amplified regions at 17q11–q21 involved in human primary breast cancer, *Cancer Res.* 56 (1996) 3886–3890.

[20] G. Loughran, M. Huigslot, P.A. Kiely, L.M. Smith, S. Floud, V. Aylton, R. O’Connor, Gene expression profiles in cells transformed by overexpression of the IGF-1 receptor, *Oncogene* 24 (2005) 6185–6193.

[21] W.J. Ingram, C.A. Wicking, S.M. Grimmond, A.R. Forrest, B.J. Wainwright, Novel genes regulated by sonic Hedgehog in pluripotent mesenchymal cells, *Oncogene* 21 (2002) 8196–8205.

[22] Y. Wang, I.V. Tetko, M.A. Hall, E. Frank, A. Facius, K.F. Mayer, H. W. Mewes, Gene selection from microarray data for cancer classification—A machine learning approach, *Comput. Biol. Chem.* 29 (2005) 37–46.

[23] M.C. Beckerle, Zyxin: zinc fingers at sites of cell adhesion, *Bioassays* 19 (1997) 949–957.

[24] E. Griffith, A.S. Coutts, D.M. Black, RNAi knock-down of the focal adhesion protein TES reveals its role in actin stress fibre organisation, *Cell Motil. Cytoskelet.* 60 (2005) 140–152.

[25] M. Cattaruzza, C. Latrich, M. Hecker, Focal adhesion protein zyxin is a mechanosensitive modulator of gene expression in vascular muscle cells, *Hypertension* 43 (2004) 726–730.

[26] B.E. Drees, K.M. Andrews, M.C. Beckerle, Molecular dissection of zyxin function reveals its involvement in cell motility, *J. Cell Biol.* 147 (1999) 1549–1560.

[27] D.A. Nix, J. Fradelizi, S. Bockholt, B. Menichi, D. Louvard, E. Friedrich, M.C. Beckerle, Targeting of zyxin to sites of actin membrane interaction and to nucleus, *J. Biol. Chem.* 276 (2001) 34759–34767.

[28] Y. Wang, T.D. Gilmore, Zyxin and Paxillin proteins: focal adhesion plaque LIM domain proteins go nuclear, *Biochim. Biophys. Acta* 1593 (2003) 115–120.

[29] J.L. Kadrmas, M.C. Beckerle, The LIM domain: from the cytoskeleton to the nucleus, *Nat. Rev., Mol. Cell Biol.* 5 (2004) 920–931.

[30] T. Hirota, T. Morisaki, Y. Nishiyama, T. Marumoto, K. Tada, T. Hara, N. Masuko, M. Inagaki, K. Hatakeyama, H. Saya, Zyxin, a regulator of actin filament assembly, targets the mitotic apparatus by interacting with h-warts/LATS1 tumor suppressor, *J. Cell Biol.* 5 (2000) 1073–1086.

[31] S. Iida, T. Hirota, T. Morisaki, T. Marumoto, T. Hara, S. Kuninaka, S. Honda, K. Kosai, M. Kawasumi, D.C. Pallas, H. Saya, Tumor suppressor WARTS ensures genomic integrity by regulating both mitotic progression and tetraploidy checkpoint function, *Oncogene* 23 (2004) 5266–5274.

Overexpression of LASP-1 mediates migration and proliferation of human ovarian cancer cells and influences zyxin localisation

TGP Grunewald¹, U Kammerer², C Winkler³, D Schindler⁴, A Sickmann³, A Honig² and E Butt^{*,1}

¹Institute of Clinical Biochemistry and Pathobiochemistry, University of Wurzburg, Grombuehlstr. 12, D-97080 Wurzburg, Germany; ²Department of Obstetrics and Gynecology, University of Wurzburg, Josef-Schneider-Str. 4, D-97080 Wurzburg, Germany; ³Protein Mass Spectrometry and Functional Proteomics Group, Rudolf-Virchow-Center for Experimental Biomedicine, Versbacher Straße 9, 97078 Wurzburg, Germany and ⁴Department of Human Genetics, University of Wurzburg, Biozentrum am Hubland, D-97074 Wurzburg, Germany

LIM and SH3 protein 1 (LASP-1), initially identified from human breast cancer, is a specific focal adhesion protein involved in cell proliferation and migration. In the present work, we analysed the effect of LASP-1 on biology and function of human ovarian cancer cell line SKOV-3 using small interfering RNA technique (siRNA). Transfection with LASP-1-specific siRNA resulted in a reduced protein level of LASP-1 in SKOV-3 cells. The siRNA-treated cells were arrested in G₂/M phase of the cell cycle and proliferation of the tumour cells was suppressed by 60–90% corresponding to around 70% of the cells being transfected successfully as seen by immunofluorescence. Moreover, transfected tumour cells showed a 40% reduced migration. LASP-1 silencing is accompanied by a reduced binding of the LASP-1-binding partner zyxin to focal contacts without changes in actin stress fibre and microtubule organisation or focal adhesion morphology as observed by immunofluorescence. In contrast, silencing of zyxin is not influencing cell migration and had neither influence on LASP-1 expression nor actin cytoskeleton and focal contact morphology suggesting that LASP-1 is necessary and sufficient for recruiting zyxin to focal contacts. The data provide evidence for an essential role of LASP-1 in tumour cell growth and migration, possibly through influencing zyxin localization.

British Journal of Cancer (2007) **96**, 296–305. doi:10.1038/sj.bjc.6603545 www.bjancer.com

Published online 9 January 2007

© 2007 Cancer Research UK

Keywords: LASP-1; ovarian cancer; zyxin; 14-3-3; SKOV-3; migration

Ovarian cancer is the sixth most common cancer among women worldwide, with estimated 190 000 new cases and 114 000 deaths caused through this neoplasm each year (Parkin *et al*, 2001). Epithelial ovarian cancer represents 90–95% of all ovarian tumours (Auersperg *et al*, 2001; Quirk and Natarajan, 2005), which is detected in 60.6% cases in advanced stages of disease due to unspecific or absent symptoms in early stages. Although tremendous efforts have been undertaken to improve the therapeutic outcome, ovarian cancer still remains the most lethal malignoma among gynaecological tumours of women in the western world, given that only 35% of ovarian cancer patients show a 5-year survival (Legge *et al*, 2005).

About 90% of all epithelial ovarian tumours are sporadic and are diagnosed in women without germline mutations in known susceptibility loci. However, the remaining cases are heritable. Data from several international studies suggest that patients with a loss of heterozygosity of the BRCA1 and BRCA2 genes, which are located on 17q21 and found in hereditary forms of breast cancer, have a 6–61-fold increased lifetime risk of ovarian cancer compared with general population rates (Antoniou *et al*, 2003).

The Lim and SH3 domain protein LASP-1 was initially identified from a cDNA library of breast cancer metastases. The gene was also mapped to human chromosome 17q21 in a region that is altered in 20–30% of human breast cancers (Tomasetto *et al*, 1995a,b), suggesting that it could play a role in tumour development and metastasis of breast and ovarian cancer.

Human LASP-1 encodes a membrane-associated protein of 261 amino acids containing an N-terminal LIM domain, followed by two actin-binding sites and a C-terminal src homology SH3 domain. The actin-binding domains in the core of the LASP-1 protein mediate an interaction between LASP-1 and actin at cell membrane extensions, but not along the actin stress fibres (Schreiber *et al*, 1998; Chew *et al*, 2002; Butt *et al*, 2003; Keicher *et al* 2004; Nakagawa *et al*, 2006). The exact cellular function of LASP-1 is still not known, but the protein has previously been reported to localise within multiple sites of dynamic actin assembly such as focal contacts, focal adhesions, lamellipodia, membrane ruffles and pseudopodia (Tomasetto *et al*, 1995a; Chew *et al*, 1998, 2000, 2002; Lin *et al*, 2004).

The SH3 domain at the C-terminus is involved in protein–protein interactions through binding to proline-rich sequences, specifically with zyxin, pallidin, lipoma preferred partner (LPP) and vasodilator-stimulated phosphoprotein (VASP) (Keicher *et al*, 2004; Li *et al*, 2004; Rachlin and Otey, 2006).

Moreover, recent data showed that LASP-1 specifically interacts via its nebulin-like repeats with Krp1, a focal adhesion protein

*Correspondence: Dr E Butt;
E-mail: butt@klin-biochem.uni-wuerzburg.de

Received 24 August 2006; revised 21 November 2006; accepted 21 November 2006; published online 9 January 2007

involved in cell migration. Mutation analysis of LASP-1 demonstrates that its SH3 domain is necessary for pseudopodial extension and invasion (Spence *et al*, 2006). Thus the protein–protein interactions mediated by the LIM and SH3 domains can be regarded as scaffolds for the formation of complexes of higher order.

LASP-1 is a cAMP- and cGMP-dependent protein kinase substrate with a specific phosphorylation site on serine 146 (Butt *et al*, 2003). In rabbit parietal cells, elevation of intracellular cAMP by forskolin induced a partial translocation of LASP-1 to the apically directed F-actin-rich intracellular canalculus, which is the site of active HCl secretion (Chew *et al*, 1998, 2000). Beyond this, phosphorylation on serine 146 resulted in translocation of the protein from the membrane to the cytosol and was followed by reduced cell migration (Butt *et al*, 2003). It has also been shown that the SH3 domain of LASP-1 interacts with the N-terminus of Ableson tyrosine kinase and that phosphorylation of LASP-1 at tyrosine 171 is associated with the loss of LASP-1 from focal adhesions and the initiation of cell death, but without changes in dynamic of migratory processes (Lin *et al*, 2004).

In addition, LASP-1 expression has been reported to be increased in metastatic breast cancer, suggesting that overexpression of LASP-1 may be involved in the migratory process of these cells (Tomasetto *et al*, 1995a). Surprisingly, both increase and depletion of LASP-1 in COS-7, HEK293 and MCF-7 cells inhibited basal and growth factor-stimulated cell migration (Lin *et al*, 2004).

Interestingly, recent work has shown, that knock-down of LASP-1 in metastatic breast cancer cell lines BT-20 and MCF-7 results in a strong inhibition of proliferation and migration and leads to a reduction of zyxin at focal contacts through absence of LASP-1 (Grunewald *et al*, 2006).

In this study we demonstrate that LASP-1 is highly overexpressed in ovarian cancer tissue and metastatic ovarian cancer cell lines. Silencing of the LASP-1 gene by RNA interference in the ovarian cancer cell line SKOV-3 reduced cell proliferation and cell migration *in vitro* without influencing the actin cytoskeleton, microtubule polymerisation and focal adhesion morphology. Furthermore, the knock-down of LASP-1 severely affected zyxin localisation.

MATERIALS AND METHODS

Tissue samples

The studies were performed with approval of the Ethics Committee of the University of Wurzburg. Tissue samples of 26 archival cases each of serous epithelial ovarian carcinomas with and without invasive components (obtained from the Department of Pathology of the University of Wurzburg and reviewed by a pathologist to confirm the diagnosis), as well as two samples of ascitic fluid containing ovarian cancer cells of women with metastatic ovarian cancer were analysed.

Immunohistochemistry

For immunohistochemical staining procedures, endogenous peroxidase was blocked by incubation in 0.1% hydrogen peroxide in PBS for 5 min. The slides were then incubated with the polyclonal anti-LASP-1 antibody (Butt *et al*, 2003) diluted 1:1000 in 'antibody diluent' (DAKO, Hamburg, Germany), followed by the EnVision/rabbit detection system (DAKO). Histogreen (Linaris, Wertheim, Germany) was used as the chromogen and cells were counterstained with haematoxylin (Sigma, Deisenhofen, Germany).

Cell culture conditions

Cell lines (SKOV-3, OAW-42 and PA-1) were obtained from the Cell Line Services (Heidelberg, Germany) and grown at 1×10^5

cells ml^{-1} in a plastic cell culture flask in a humidified incubator at 37°C under 5% CO₂ atmosphere in RPMI 1640 medium (PAA, Linz, Austria) containing 10% heat-inactivated foetal bovine serum (PAA) and 1% streptomycin/ampicillin (Invitrogen, Karlsruhe, Germany). For primary tumour cell culture, effusions (20–500 ml) were centrifuged, cell pellets washed twice in PBS (Biochrom, Berlin, Germany), resuspended in RPMI 1640 medium supplemented as described and then seeded on the bottom of a cell culture flask. After 1 h, all nonadherent (mostly leucocytes) cells were washed away and adherent tumour cells cultured in RPMI 1640/10%FCS/streptomycin/ampicillin. Contaminating fibroblasts were deleted by trypsin treatment every other day and the remaining tumour cell monolayer was cultured until homogeneous morphology of the cells (passage 3–4) was reached. Cells were checked routinely and found to be free of contamination by bacteria or fungi.

small interfering RNA preparation and transfection

Expression of human LASP-1 was knocked down with siRNA duplexes targeting the sequence 5'-AAG GTG AAC TGT CTG GAT AAG-3' (bases 49–69), 5'-CUUAUCCAGACAGUUCACCDdTdT-3'. The control siRNA 5'-AGAGAUGUAUGUCGCUCGCUdTdT-3' targeting no known mRNA sequence was used as a control. Both siRNAs were obtained from Dharmacon RNA Technologies (Lafayette, CO, USA). The siControl nontargeting siRNA from Dharmacon could not be used in our cell system owing to toxic effects. A BLAST search against the complete human and murine genome verified that the selected sequences were specific for the respective target gene.

Cells in the exponential phase of growth were plated in six-well plates at a density of 0.5×10^5 cells/well, grown for 24 h and transfected with 1 μg (60 nm) siRNA in reduced serum medium OPTI-MEM-I (Gibco, Paisley, UK) at 30–50% confluence. For the formation of the siRNA–lipid complexes, 3 μl siRNA stock solution (20 μM) was diluted in 100 μl OPTI-MEM, mixed with 3 μl Metafectene (Biontex, Munich, Germany) in 100 μl OPTI-MEM and incubated at room temperature for 17 min. Subsequently, the culture medium was removed and replaced by 1 ml OPTI-MEM-I and the siRNA–lipid complexes (1.2 ml total volume). After 4 h incubation at 37°C, 1.2 ml of cell culture medium with 20% foetal bovine serum was added, and incubation was continued for 36–56 h. For control cells, Metafectene alone (MOCK-transfection) and/or 1 μg scrambled control-siRNA were used.

Silencing of zyxin was achieved with Hs_ZYX_1_HP validated siRNA at a final concentration of 10 nm using HiPerfect transfection reagent (Qiagen, Hilden, Germany) according to the manufacturer's directions. For zyxin control experiments, non-silencing control siRNA, Alexa Fluor 488 labelled, provided by Qiagen, was used.

At least three independent experiments were performed for each cell line, and representative results are shown.

Cell proliferation assay

For proliferation assay, cells were transfected as described. At the time points indicated, cells were trypsinised and cell numbers were determined by a Coulter counter (Beckman, Fullerton, CA, USA). Experiments were performed in triplicate for each time point. Cell viability was evaluated by counting trypan blue-positive and -negative cells under a phase-contrast microscope (Zeiss Axiovert, Aalen, Germany).

Western blot analysis

For Western blotting, cells were prepared by lysing in Laemmli sample buffer and equal amounts of protein, according to the cell count, were resolved by 12% SDS-PAGE. After blotting on

nitrocellulose membrane and blocking with 3% nonfat dry milk in 10 mM Tris, pH 7.5, 100 mM NaCl and 0.1% (w/v) Tween 20, the membrane was first incubated with the antibodies raised against LASP-1 (1:10 000) (Butt *et al*, 2003), caspase-3 (1:1000) (New England Biolabs, Frankfurt, Germany) or mouse zyxin hybridoma supernatant (1:100; kind gift from Dr J Wehland, GBF Braunschweig, Germany; Rottner *et al*, 2000), followed by incubation with horseradish peroxidase-coupled goat anti-rabbit IgG or goat anti mouse IgG (Biorad, Munich, Germany), diluted 1:5000 and detection by ECL or ECL plus (Amersham Biosciences, Freiburg, Germany). Protein bands were visualised by autoradiography. Quantification of the signals was carried out by densitometry using the Odyssey system (Li-Cor, Bad Homburg, Germany).

FACS

For cell cycle analysis, SKOV-3 cells were harvested 48 h after LASP-1 siRNA transfection. The cells were pelleted and stained with DAPI (Sigma) at a final concentration of 2 μ g ml⁻¹ in permeabilisation buffer containing 0.1 M Tris-HCl, pH 7.4, 0.154 M NaCl, 0.5 mM MgCl₂, 1 mM CaCl₂, 0.1% NP-40 and 0.2% BSA in ddH₂O for 30 min at 4°C in the dark. Bivariate flow histograms were recorded on an analytical, dual-laser-equipped cytometer (LSR1, Becton Dickinson Biosciences, Heidelberg, Germany) using UV excitation. Resulting cell cycle distributions were quantified with the MPLUS AV software (Phoenix Flow Systems, San Diego, CA, USA). For technical details, see Schindler and Hoehn (1999).

Two-dimensional-gelelectrophoreses and mass spectrometry

Isoelectric focusing for two-dimensional (2D) gel electrophoresis was performed using the Protean IEF cell from Biorad (Munich, Germany) according to the instructions of the manufacturer. The SKOV-3 homogenate (about 200 μ g protein) was solubilised for 15 min by sonication in 320 μ l lysis buffer containing 7 M urea, 2 M thiourea, 4% (w/v) CHAPS, 15 mM DTT (electrophoresis grade), 0.5% carrier ampholytes, pH 3–10. Pellet homogenate was loaded on a 17-cm immobilised IPG strip, pH 3–10 and resolved overnight at 50 V. Focussing was carried out for 1 h at 250 V, 1 h at 500 V and 15 h at 7000 V. After equilibration in 50 mM Tris, pH 8.9, 6 M urea, 30% (w/v) glycerol and 2% (w/v) SDS, gels were immediately applied to a vertical 10% SDS gel without a stacking gel. Electrophoresis was carried out at 8°C with a constant current of 40 mA per gel. Proteins were visualised by Coomassie Brilliant Blue R-250 (Sigma) staining.

Gel pieces were washed two times alternating with 50 mM ammonium hydrogen carbonate buffer and 25 mM ammonium hydrogen carbonate buffer with 50% acetonitrile. Proteins were reduced with 10 mM DTT for 30 min at 56°C and subsequently alkylated by incubation with 20 mM iodoacetamide at room temperature for 30 min. Again samples were washed as described before. Gel pieces were shrunken in a SpeedVac (Thermo Electron, Dreieich, Germany) and rehydrated with 12.5 ng of trypsin in 50 mM ammonium hydrogen carbonate buffer. Digestion was performed by incubation at 37°C overnight. The resulting peptides were extracted by application of 15 μ l of 5% formic acid for 10 min.

Separation of complex peptide mixtures was achieved by using reversed-phase chromatography. For nano-LC-ESI-MS/MS experiments, a setup consisting of an autosampler (Famos, Dionex, Idstein, Germany) and precolumn concentration (Switchos, Dionex) before nano-LC separation (Ultimate, Dionex) was used. Precolumns (300- μ m inner diameter \times 1-mm length) and separation columns (75 μ m inner diameter \times 150-mm length, C18 PepMapTM) were purchased from Dionex. Gradient elution was performed using a linear gradient from 5 to 50% solvent B (84% acetonitrile, 0.1% formic acid) during a period of 2 h. Solvent A

was 0.1% formic acid in water. Separation was followed by rinsing the column with 95% B for 5 min before equilibration to 5% solvent B before the next separation cycle.

Peptides were directly eluted into an ESI mass spectrometer. For mass spectrometric analysis, an ESI linear ion trap LTQ (Thermo Electron, Dreieich, Germany), using distal-coated fused silica tips (New Objective, Woburn, MA, USA), spray voltage was set around 1800 V. A survey scan (m/z 350–2000) was followed by five MS/MS scans fragmenting the five most intensive peptide signals.

Mass spectra were transformed into peak lists in dta or mgf format using the wo in-house software solution raw2dta (Boehm *et al*, 2004). Generated data were processed in parallel with the search algorithms SequestTM, Version 27 (Yates *et al*, 1995) and MascotTM, Version 2.1.6 (Perkins *et al*, 1999). For sequence alignment, the swissprot database from October 2005 was used. As fixed modification, carbamidomethylation of cysteine residues was used, and as variable modification oxidation of methionine residues was selected. As filter criteria for Sequest we accepted in the first instance only positive peptide hits with a minimum cross-correlation factor of 2.5, a CN value of 0.25, and a preliminary ranking of one. For the Mascot algorithm the minimum score was set to 40 for each peptide. Only protein hits that were identified with these parameters by both algorithms and had at minimum two identified peptides were accepted. Additionally, all significant hits were revised manually.

Immunfluorescence

For immunfluorescence microscopy, cells were grown on glass chamber slides, fixed in 4% (w/v) paraformaldehyde in PBS, permeabilised with 0.1% (w/v) Triton X-100 in PBS and then stained with affinity-purified LASP-1 antibody (1:2000, 1 h), followed by secondary Cy3-labelled anti-rabbit antibody (1:500, 30 min) (Dianova, Hamburg, Germany) or mouse zyxin hybridoma supernatant (1:10, 2 h), followed by secondary Cy2 labelled goat anti mouse antibody (1:500, 1 h) (Dianova). Oregon green phalloidin (Molecular Probes, Leiden, The Netherlands) was used for actin staining. Tubulin was stained with an anti- α -tubulin antibody (3 μ g ml⁻¹) (Calbiochem, Darmstadt, Germany). DNA was counterstained with DAPI (1:2500) (Calbiochem) for 2 min.

Migration experiments

Cells were cultured in medium in 25 cm² flasks to approximately 30–40% confluence and transfected with 10 nM zyxin siRNA or 30 nM LASP-1 siRNA (Keicher *et al*, 2004) using 10 μ l Metafectene. After 48 h incubation and overnight starving, 1 \times 10⁵ cells in 100 μ l incubation medium (with 1 mM MgCl₂) were seeded in the upper chamber of BSA-coated 8 μ m pore size transwell Boyden chambers (Corning star, Cambridge, MA, USA). Cells were allowed to migrate through the porous membrane for 4 h at 37°C. Cells remaining at the upper surface were completely removed using a cotton carrier. The lower surfaces of the membranes were then stained in a solution of 1% (w/v) crystal violet in 2% ethanol for 30 s and rinsed afterwards in distilled water. Cell-associated crystal violet was extracted by incubation in 10% acetic acid for 20 min and measured at 595 nm absorbance.

RESULTS

LASP-1 is overexpressed in ovarian cancer tissue

To assess the role of LASP-1 in ovarian cancer, we examined its expression in 26 ovarian cancer samples from different patients with or without invasive components. Immunohistochemistry clearly allowed to localise LASP-1 expression in 14 out of 26 malignant ovarian tissues (53.8%). Strong immunoreactivity was observed in nine cases (Figure 1A), whereas five probes showed a

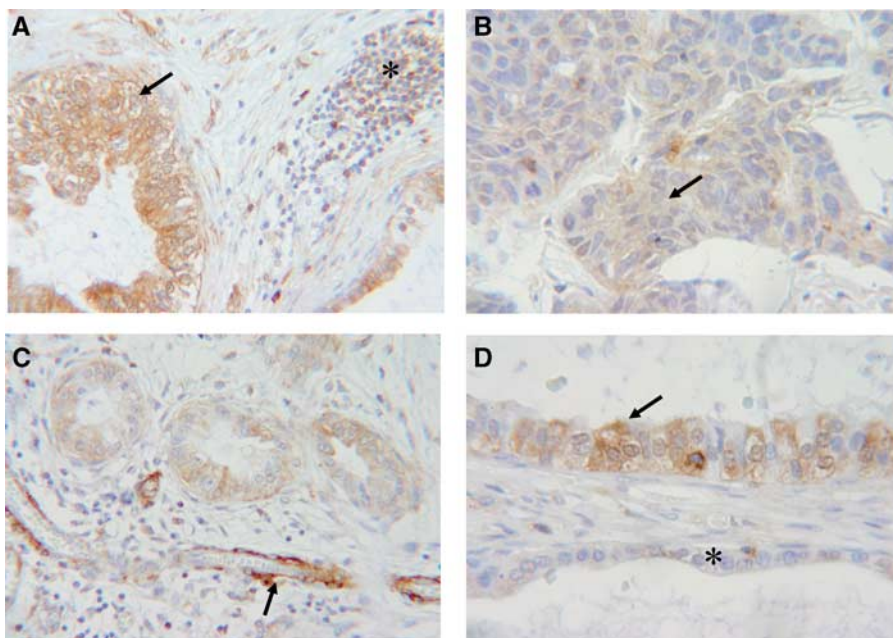


Figure 1 Immunohistochemical staining of cancerous ovarian tissue. LASP-1 was detected using anti-LASP-1 rabbit polyclonal antibody in paraffin-embedded tissue samples. **(A)** Ovarian cancer tissue with two cystic structures containing malignant cells, which are strongly LASP-1 positive (arrow), and an LASP-1-negative lymphocytic inflammation (star). **(B)** Infiltrating tumour cells displaying medium LASP-1 expression (arrow). **(C)** Three ductus with malignant epithelial cells and medium LASP-1 expression and a blood vessel in longitudinal cut with vascular smooth muscle cells showing strong LASP-1 positivity (arrow). **(D)** Two epithelial strata separated through connective tissue. The arrow indicates malignant LASP-1-positive and the star benign LASP-1-negative epithelial cells. LASP-1⁺ cells are stained in brown (DAB). All sections were counterstained with haematoxylin.

medium to low LASP-1 expression (Figure 1B) and 12 specimens (46.2%) were considered to be LASP-1 negative.

Normal benign epithelial cells were LASP-1-negative in all ovarian tissues even when malignant epithelial cancer cells close to these normal epithelial cells displayed a strong positivity for LASP-1 (Figure 1D).

In analogy to previous findings in myoepithelial cells of human breast tissue (Grunewald *et al*, 2006), a massive overexpression in vascular smooth muscle cells could be observed (Figure 1C).

LASP-1 is strongly expressed in ovarian cancer cell lines

In order to study the significance of LASP-1 overexpression in ovarian cancer, we tested three ovarian cancer cell lines (SKOV-3, OAW-42 and PA-1) as well as two primary cell cultures derived from ascitic fluid of patients with peritoneal metastatic ovarian cancer for LASP-1 expression. Loading was standardised to 3×10^5 cells per slot and controlled by β -actin loading control signal intensity.

Only the three ovarian cancer cell lines showed a high LASP-1 signal, whereas the two primary cell lines were LASP-1 negative (Figure 2). Interestingly, the solid primary ovarian cancer tissue preparations of these two patients showed intensive LASP-1 staining (data not shown).

We chose SKOV-3 cells as a cellular model for ovarian cancer because in these cells the BRCA1 and BRCA2 genes, which are located next to the LASP-1 gene on chromosome 17q21, are upregulated (Rauh-Adelmann *et al*, 2000).

Silencing of LASP-1 in SKOV-3 cells inhibits proliferation *in vitro*

To investigate the function of LASP-1 in the ovarian cancer cell line SKOV-3, we performed a knock-down of the gene using the powerful RNAi technique. The effect of siRNA transfection on the

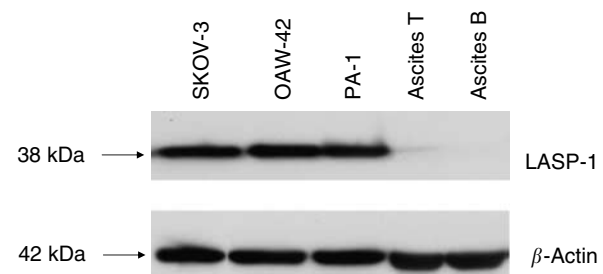


Figure 2 Western blot of different ovarian cancer cell lines. A total of 200 000 cells from established ovarian cancer cell lines (SKOV-3, OAW-42 and PA-1), as well as primary cells derived from ascitic fluid of two patients (ascitis T and B) with peritoneal metastatic ovarian cancer, were analysed for LASP-1 expression by Western blot. Loading was controlled by β -actin Western blot.

expression of LASP-1 was followed by Western blot analysis 0, 24, 48 and 53 h after transfection. The amount of LASP-1 protein, standardised to β -actin, was reduced up to 58% after 48 h (Figure 3, lower panel) compared with the control siRNA-transfected control cells. This corresponds to around 70% of the cells being transfected successfully as seen by immunofluorescence. Parallel to the protein knock-down, we observed a slower proliferation rate in LASP-1 siRNA-transfected cells compared with control cells (Figure 3, upper panel). The viability of cells was similar in both cultures as trypan blue staining detected no more than 5–8% dead cells in all experiments. To test whether the decreased proliferation could be due to apoptosis, we carried out a Western blot analysis with an anti-caspase-3 antibody. The antibody recognises both the non-active pro-caspase-3 (38 kDa) and the active cleaved caspase-3 protein (17 kDa). As shown in Figure 4B, treatment of SKOV-3 cells with the LASP-1 siRNA duplex produced no active caspase-3,

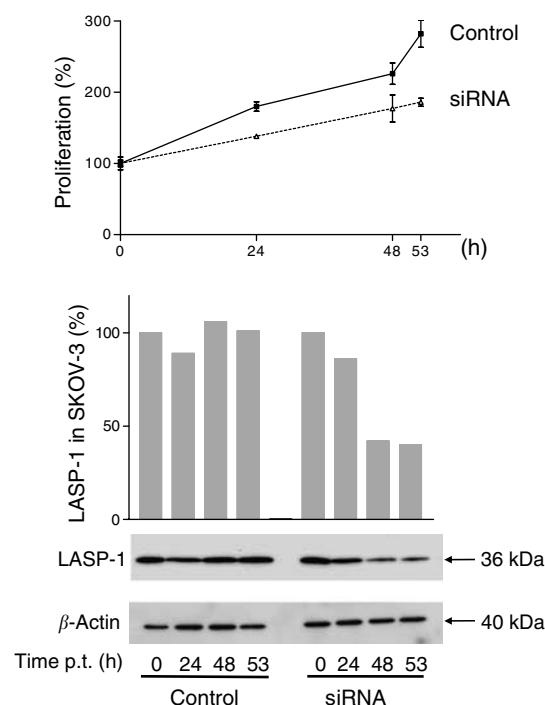


Figure 3 Silencing of LASP-1 in SKOV-3 cells inhibits proliferation. A total of 40 000 cells of the SKOV-3 cells were plated and allowed to grow for 24 h (up to 40% confluence). Small interfering RNA LASP-1 was transfected into cells in a concentration of 60 nM. Cells were harvested after 0, 24, 44 and 53 h of siRNA treatment. Control cells were treated with control siRNA. Upper panel: treatment with siRNA LASP-1 impairs SKOV-3 cell proliferation. After the indicated periods of time, the cells were harvested, and their total number was determined using a Coulter counter. Lower panel: Densitometric quantification and Western blot analysis of LASP-1 expression standardised to β -actin at the corresponding time points shows a reduction of LASP-1 expression of about 60% 44 h after transfection with siRNA LASP-1.

indicating that apoptosis might not explain the reduced proliferation.

Downregulation of LASP-1 induces G2 phase accumulation in SKOV-3 cells

We next analysed cell cycle distributions of siRNA-treated SKOV-3 cells using flow cytometry. After incubation with LASP-1 siRNA for 48 h, the proportion of cells accumulating in the G₂ phase amounted to 19.4% (Figure 4A), whereas the same cells treated with Metafectene alone (MOCK transfection) as a control had only 6.7% G₂ phase proportion. Conversely, the G₁ fraction decreased from 73.4% in MOCK-treated cells to 48% in LASP-1-silenced SKOV-3 cells. The S phase fraction for siRNA LASP-1-treated cells was 32.6% and for MOCK transfection 19.9%, respectively. Similar results were obtained in three independent experiments indicating that in LASP-1-silenced SKOV-3 cells mitotic progression cannot proceed normally. However, immunofluorescence staining of α -tubulin and DNA in the cells reveal no reduced tubulin polymerisation in the LASP-1-silenced cells arrested in G₂/M phase (Figure 4C).

Knock-down of LASP-1 results in protein changes of glycolytic metabolism and cell cycle regulation

Under LASP-1 knock-down conditions it might be necessary for the maintenance of cellular steady state to upregulate alternative

proteins to overcome functionally the loss of LASP-1. We used 2D gel electrophoreses to resolve the homogenate of SKOV-3 cells before and after LASP-1 silencing. Subtractive analysis of the two gels showed a high degree of similarity, however, at least five proteins have been identified to become up-, or respectively downregulated by LASP-1 silencing in three independent experiments: pyruvate kinase (up), enolase-1 (down), glucose dehydrogenase (down), 14-3-3 (up) and heat-shock protein (Hsp) 27 (up) (Figure 5).

Silencing of LASP-1 results in reduced zyxin binding to focal adhesions

LASP-1 has previously been shown to localise to sites of cell adhesion and to interact with zyxin and actin (Chew *et al*, 2002; Li *et al*, 2004). To assess whether silencing of LASP-1 affects these binding partners, siRNA-treated SKOV-3 cells were stained with phalloidin green against actin or mouse anti-zyxin hybridoma supernatant. In LASP-1 siRNA-transfected cells, zyxin was absent from focal adhesions, whereas the cellular level of zyxin remained unchanged as confirmed by Western blot analysis (Figure 6). However, absence of zyxin from focal contacts did not lead to changes in focal adhesion morphology as visualized by vinculin staining (Figure 6). Likewise, actin filament assembly was not disturbed (Figure 6), despite less actin bundles, a blurred network of shorter filaments and some F-actin aggregates are typical for highly metastatic cancer cell lines (Liu *et al*, 2004).

Silencing of zyxin does not change LASP-1 localisation or focal adhesion morphology

As knock-down of LASP-1 is altering zyxin localisation, we further assessed the interaction of both proteins in a reverse experiment by knocking down zyxin. Transfection of SKOV-3 with zyxin-specific siRNA dramatically reduced zyxin expression down to 10–20%, while the cellular level of LASP-1 and β -actin remained unchanged as confirmed by Western blot analysis (Figure 7). Immunofluorescence of the zyxin-silenced cells illustrated lack of zyxin at the focal adhesions without altering the position of LASP-1 (Figure 7), suggesting that LASP-1 is necessary for the positioning and recruiting of zyxin to focal adhesions. Other focal adhesion proteins, for example, β -actin (Figure 7) and vinculin (data not shown), were unaffected by the zyxin knock-down.

Silencing of LASP-1, but not of zyxin, decreases cell migration

Although the exact function of LASP-1 is not known, recent results suggest an important role for this protein in cell adhesion and migration (Butt *et al*, 2003; Lin *et al*, 2004; Grunewald *et al*, 2006; Nakagawa *et al*, 2006). To directly examine the relevance of LASP-1 for cell motility we performed migration experiments in a modified Boyden chamber with SKOV-3 cells either transfected with LASP-1 siRNA or zyxin siRNA to downregulate the respective protein. Cells were seeded in the upper chamber of a transwell polycarbonate membrane. After 4 h, those cells that had migrated through the porous membrane were counted. Depletion of LASP-1 in SKOV-3 cells strongly reduced cell migration, while zyxin knock-down had no influence on cell migration (Figure 8) suggesting that LASP-1 acts as a positive regulator for cell motility.

DISCUSSION

Cell migration and controlled assembly and disassembly of focal adhesions are highly integrated multistep processes and a central feature in the molecular pathology of cancer (Ridley *et al*, 2003). To date, more than 50 different adhesion proteins that regulate the

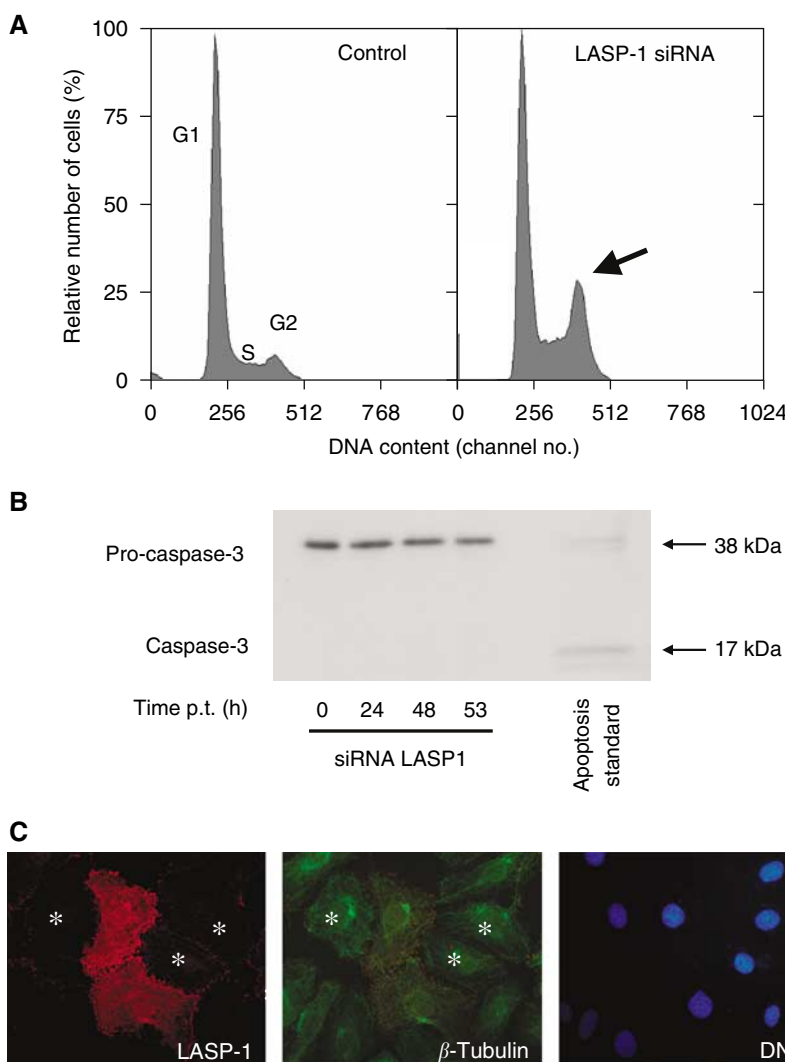


Figure 4 LASP-1 siRNA treatment of SKOV-3 cells induces G₂ phase accumulation without triggering apoptosis. **(A)** SKOV-3 cells were transfected with siRNA LASP-1 and transfection reagent Metafectene or treated only with Metafectene (MOCK transfection). After 48 h, the cells were harvested and prepared for flow cytometric cell cycle analysis. LIM and SH3 protein 1 (LASP-1) siRNA-treated cells show G₂ phase accumulation as opposed to the same cells with MOCK transfection. **(B)** Several hours after siRNA LASP-1 treatment, cells were harvested and prepared for Western blot analysis using an anti-caspase-3 antibody, the antibody recognises both the nonactive pro-caspase-3 (38 kDa) and the active cleaved caspase-3 protein (17 kDa). No active caspase-3 could be detected. **(C)** Immunofluorescence of LASP-1 (red), α -tubulin (green) and DNA (blue) of siRNA LASP-1-transfected (*) and nontransfected SKOV-3 cells.

rate and organisation of actin polymerisation and focal adhesion turnover have been identified.

In earlier publications, overexpression of LASP-1 mRNA in metastatic lymph nodes derived from breast cancer patients, as well as the co-amplification of the gene together with HER-2/neu (c-erbB2) were demonstrated (Chew *et al*, 1998; Legge *et al*, 2005). Two additional observations underscore the importance of LASP-1 in cancer. First, altered expression of LASP-1 is associated with the MLL gene in acute myeloid leukaemia (Strehl *et al*, 2003). Second, recent studies have shown LASP-1 to be transcriptionally upregulated in response to the morphogen Sonic Hedgehog (Ingram *et al*, 2002).

Consistent with these data, we just recently described the overexpression of LASP-1 to very high levels in breast carcinomas and lymph node metastases (Grunewald *et al*, 2006). The functional significance of LASP-1 in cancer metastasis is further supported by the presented data showing high LASP-1 expression

in ovarian cancer tissue and reduced cell migration in ovarian cancer cells depleted of LASP-1. The absence of LASP-1 in cultures of primary ovarian cancer cells in contrast to established cell lines may reflect a downregulation of LASP-1 in the nonmigratory floating ascites cells which will be reverted after several passages of adherent cell culture. Comparable observations are published for LASP-1 in human mesenchymal stem cells showing an upregulation of the protein during later passages (Sun *et al*, 2006).

During LASP-1 silencing we observed reduced cell cycle progression and an induced G₂/M phase accumulation of the cells without disrupted normal mitotic microtubule polymerisation. This was accompanied by the upregulation and downregulation of several proteins. The differentially expressed proteins pyruvate kinase, enolase-1 and glucose dehydrogenase are part of the glycolytic metabolism and their regulation correlates well with the cell cycle arrest in G₂/M after LASP-1 silencing. Furthermore, pyruvate kinase and glucose dehydrogenase have been suspected

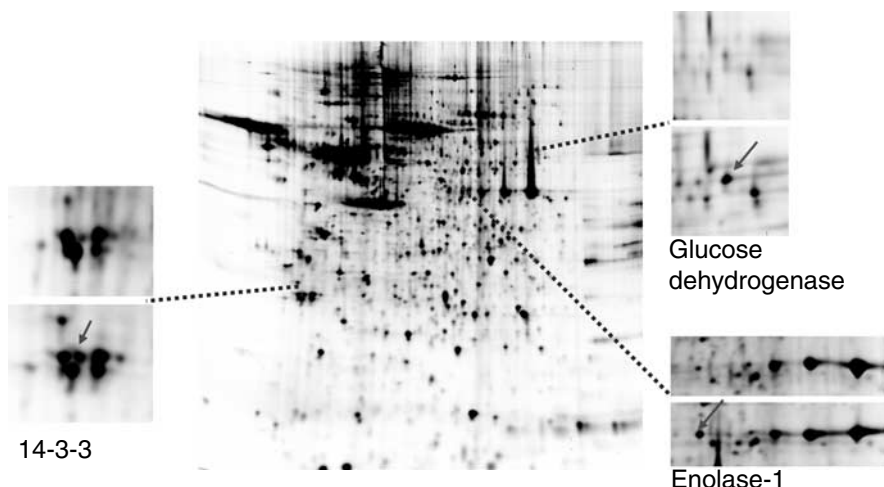


Figure 5 Two-dimensional gel of SKOV-3 proteins after LASP-1 silencing. Sections are showing differences between cellular proteins from control (upper panel) and LASP-1 knock-down (lower panel) SKOV-3 cells. Proteins were separated on nonlinear IPG-strips, pH 3–10. Two dimensional gels were stained with Coomassie blue. Proteins were identified following tryptic digestion and analysis of the resulting peptides by ESI-MS/MS.

to be highly important for tumour cell metabolism (Altenberg and Greulich, 2004). Pyruvate kinase is one of the proteins to be upregulated in cancer cells gaining energy by means of aerobic glycolysis, which is a characteristic of a number of cancer entities (Gatenby and Gillies, 2004). In addition, pyruvate kinase has been identified as a proteomic marker of cancer progression in breast cancer (Isidoro *et al*, 2005). The glycolytic enzyme enolase-1 as well as HSP27, two additional proteins identified in the 2D-gel experiments, are associated with high metastatic activity in breast cancer cells (Espana *et al*, 2005; Zhang *et al*, 2005).

14-3-3, found to be upregulated after LASP-1 depletion in ovarian cancer cells, has been implicated in cell cycle deregulation. The 14-3-3 proteins are a family of highly conserved DNA-binding proteins, which associate with the centrosomes during mitosis and are inhibitors of G₂/M progression at the mitotic and G₂ cell cycle checkpoint (Pietromonaco *et al*, 1996; Wang and Shakes, 1996; Hermeking *et al*, 1997; Peng *et al*, 1997; Alvarez *et al*, 2002). Overexpression of 14-3-3 led to cell cycle arrest in cell culture models (Tzivion *et al*, 2006) and, therefore, might contribute to the observed G₂ arrest in ovarian cancer cells lacking LASP-1.

Heat-shock proteins are molecular chaperons and are induced during cellular stress. Upregulation of HSP27 after LASP-1 silencing correlates well with increased survival by inhibiting key effectors of the apoptotic pathway (Concannon *et al*, 2003).

So far, the identified proteins are regulated in response to cell cycle arrest, but do not substitute for LASP-1 after silencing.

Recently, several LASP-1-binding partners have been identified. Along with zyxin (Li *et al*, 2004) and actin (Schreiber *et al*, 1998), LASP-1 interacts with Krp1 (Spence *et al*, 2006), palladin (Rachlin and Otey 2006), lipoma-preferred partner (LPP) and VASP (Keicher *et al*, 2004), which all can influence actin filament dynamics and pseudopodial elongation. In the case of palladin, LPP and zyxin, the binding occurs between the C-terminal SH3 domain of LASP-1 and the N-terminal proline-rich domains of these proteins, whereas in the case of Krp1, binding is observed between the nebulin-like repeats of LASP-1 and the N-terminal BTB/POZ domain of Krp1. The interaction of LASP-1 and Krp1 is crucial for pseudopodial elongation in fibroblasts in absence of fibronectin and results in their colocalisation with F-actin at the tips of extending pseudopodia (Spence *et al*, 2006).

Zyxin is localised primarily at focal adhesion plaques and plays a central role in actin filament polymerisation in mammalian cells (Beckerle, 1997).

Silencing of zyxin in HeLa cells resulted in significantly reduced actin stress fibres (Griffith *et al*, 2005), whereas under cyclic stretch zyxin only dissociated from focal contacts and accumulated in the nucleus, without affecting vinculin or actin filaments (Cattaruzza *et al*, 2004). Recent data show that in genetically zyxin-deficient fibroblasts, focal adhesions are depleted from Mena and VASP, and that cells lacking zyxin display deficits in actin cytoskeleton remodelling (Hoffman *et al*, 2006). In our immunofluorescence experiments with LASP-1-deficient SKOV-3 cells, we observed a diffuse cytoplasmic localisation of zyxin without protein loss and without changes in either vinculin distribution nor actin stress fibre organisation, emphasising the importance of LASP-1 for binding and recruiting zyxin to focal adhesions.

The loss of zyxin at the sites of focal contacts without changing cellular zyxin protein levels is not restricted to cancer cells, but was also observed in human umbilical vein endothelial cells (Grunewald *et al*, 2006). Interestingly, in these cells, zyxin could still be detected along the actin stress fibres, indicating the potential existence of another zyxin-recruiting protein along actin stress fibres since earlier results detected LASP-1 only in the focal adhesion plaques (Chew *et al*, 2002; Butt *et al*, 2003).

In our zyxin knock-down experiments, neither changes in LASP-1 localisation, actin cytoskeleton, microtubule polymerisation nor vinculin distribution were detectable suggesting that zyxin does not change focal adhesion morphology. This is concordant with the fact that genetically zyxin-deficient fibroblasts show even enhanced adhesion to surface and increased integrin expression (Hoffman *et al*, 2006). In synopsis, our LASP-1 and zyxin silencing studies have demonstrated that LASP-1 is necessary for recruiting zyxin to focal contacts.

The decreased cell motility after LASP-1 silencing can be explained by the functional loss of zyxin as a scaffolding protein that facilitates the formation of molecular complexes to promote site-specific actin assembly required for cell migration. This is in agreement with previous findings using a nongenetic approach and injecting a peptide derived from the N-terminus of zyxin to displace zyxin from its normal subcellular location thus leading to reduced cell migration (Drees *et al*, 1999). On the other hand, the knock-down of zyxin in SKOV-3 cells had no influence on cell migration while genetically zyxin-deficient fibroblasts display enhanced migration (Hoffman *et al*, 2006). These contrary effects have not been fully elucidated yet.

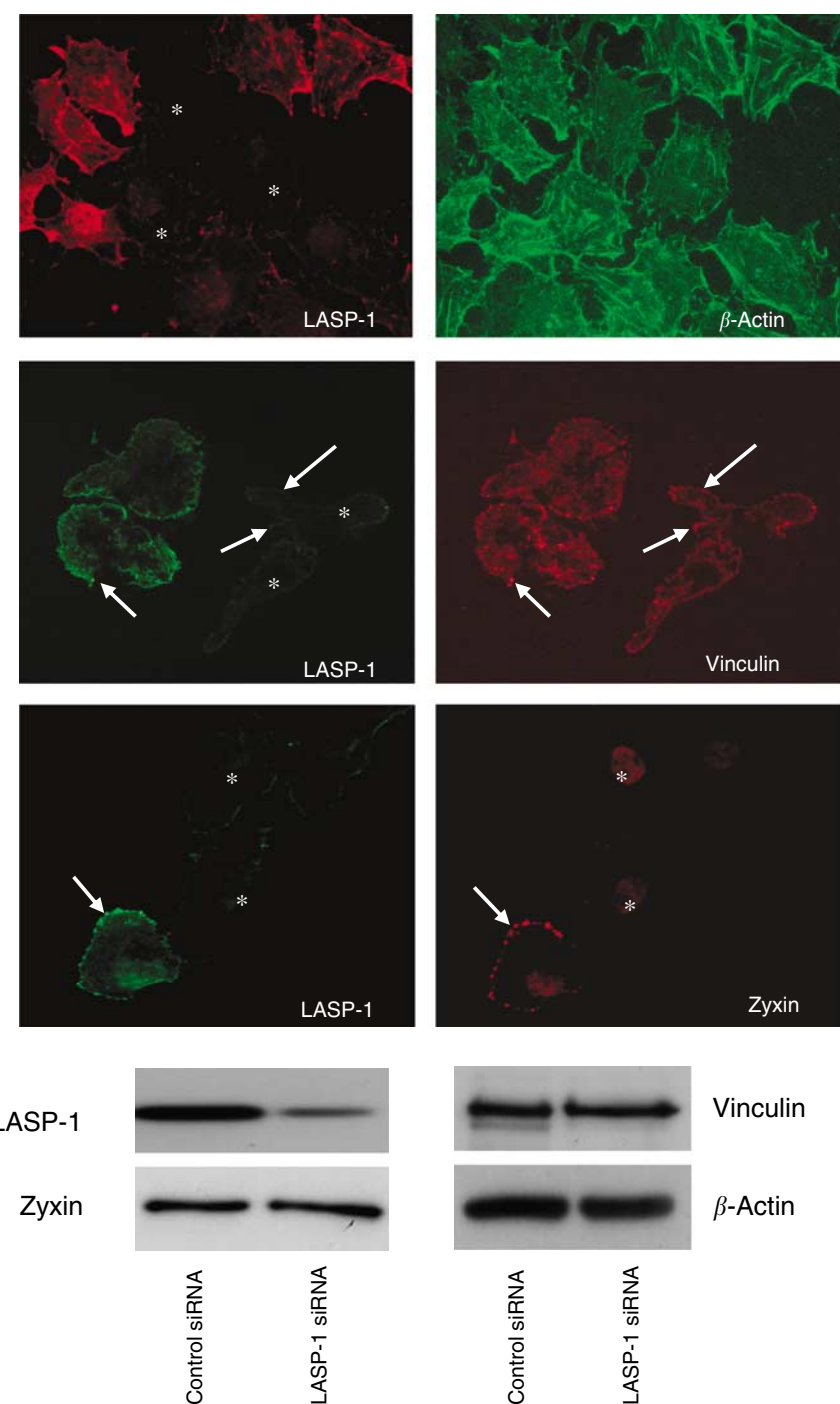


Figure 6 LIM and SH3 protein 1 (LASP-1) is required for zyxin localisation at focal adhesions. Immunofluorescent images of LASP-1, zyxin, vinculin and β -actin in siRNA LASP-1-treated SKOV-3 cells. Focal adhesions are marked with white arrows. Positions of downregulated cells are marked with stars. Western blot (WB) analysis to assess LASP-1 and zyxin levels in the LASP-1 siRNA and control siRNA-treated SKOV-3 cells were performed from the corresponding immunofluorescent cell extracts.

Recent work has shown that zyxin also shuttles through the nucleus – most likely by association with other LIM proteins – and may regulate gene transcription (Nix *et al*, 2001; Wang and Gilmore, 2003; Kadoma and Beckerle, 2004). During mitosis, a fraction of zyxin becomes associated with the tumour suppressor h-warts at the mitotic apparatus (Hirota *et al*, 2000). h-warts is a key player in mitosis in mammalian cells and loss of its function disrupts normal cell cycle regulation, possibly leading to tumour

development (Iida *et al*, 2004). In SKOV-3 cells transfected with LASP-1 siRNA, zyxin has been shown to dissociate from focal adhesion plaques and to distribute diffusely into the cytoplasm. It is, therefore, likely that part of zyxin enters the nucleus, binds to h-warts and leads to G_2 cell cycle arrest and inhibition of proliferation as observed after LASP-1 silencing.

Interestingly, in Ewing tumour cells, zyxin is only expressed at very low levels and remains diffusely distributed throughout the

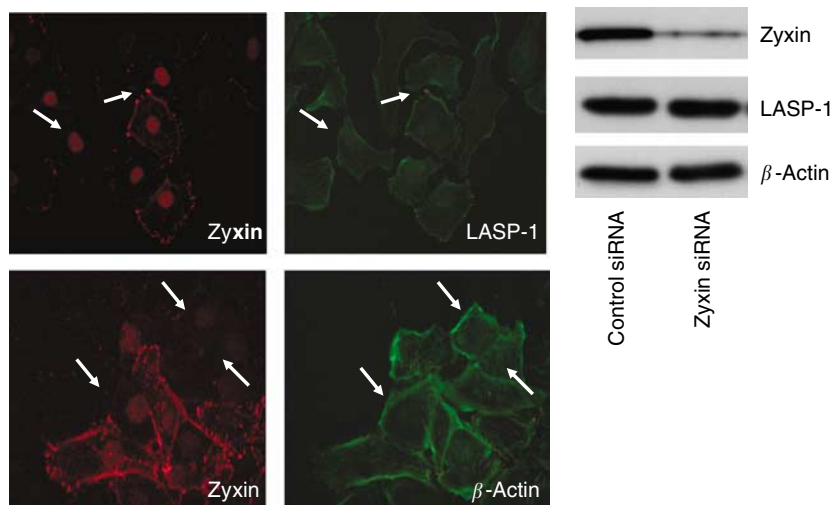


Figure 7 Zyxin silencing is not influencing actin and LASP-1 localisation. Immunofluorescent images of SKOV-3 cells transfected with siRNA zyxin and stained with antibodies against LASP-1 and β -actin. Shown are representative sections of a mixed population of both, zyxin downregulated cells and nontransfected cells, demonstrating no changes in actin and LASP-1 distribution of cells lacking zyxin.

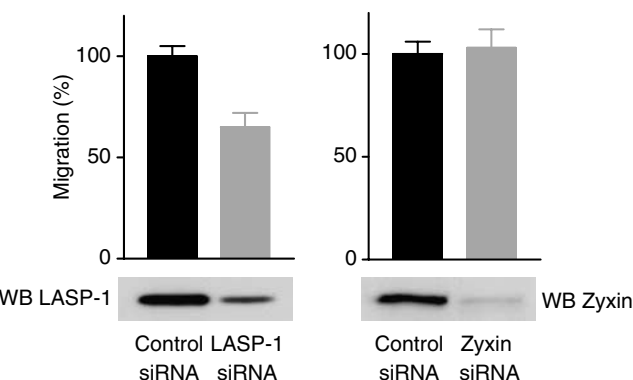


Figure 8 LIM and SH3 protein 1 is necessary for cell migration. SKOV-3 cells were transfected with LASP-1 siRNA, zyxin siRNA or control siRNA. Migration was measured over 4 h in a Transwell® cell culture chamber. At least four chambers from three different experiments were analysed (P -values significantly different from that of Control by t -test; $P < 0.001$). Each bar represents the mean \pm s.d. Corresponding Western blots of control cells and LASP-1 siRNA-transfected or zyxin siRNA-transfected cells are shown in the lower panel.

cytoplasm instead of concentrating in actin-rich dynamic structures. Zyxin gene transfer into EWS-FLI1-transformed fibroblasts

elicits reconstitution of zyxin-rich focal adhesions and leads to decreased cell motility and inhibition of anchorage independent tumour growth, indicating that zyxin has tumour suppressor activity in these cells (Amsellem et al, 2005).

Similar to findings in human breast cancer (Grunewald et al, 2006), our immunofluorescence experiments have shown that absence of LASP-1 in focal contacts dramatically influences zyxin distribution. In reverse, tumour cells, that are overexpressing LASP-1, could functionally inhibit zyxin from shuttling into the nucleus and acting as a tumour suppressor through increased recruiting of zyxin to focal contacts by LASP-1. In summary, our observations suggest an expanded role for LASP-1 in proliferation and cancer cell migration. Further studies will define the potential of LASP-1 as an independent marker for diagnosis of cancer, as well as a marker for prognosis of this disease.

ACKNOWLEDGEMENTS

We thank Richard Friedl for expert flow cytometric measurements, Michaela Kapp, Elfriede Schulze and Sabrina Jaspers for excellent technical assistance and Matthias Eck (Department of Pathology, University of Wurzburg) for pathohistological guidance. This study was supported by Deutsche Krebshilfe 106219 to EB and AH.

REFERENCES

Altenberg B, Greulich KO (2004) Genes of glycolysis are ubiquitously overexpressed in 24 cancer classes. *Genomics* 84: 1014–1020

Alvarez D, Novac O, Callejo M, Ruiz MT, Price GB, Zannis-Hadjopoulos M (2002) 14-3-3 sigma is a criciform DNA binding protein and associates in vivo with origins of DNA replication. *J Cell Biochem* 87: 197–207

Amsellem V, Kryszke MH, Hervy M, Subra F, Athman R, Leh H, Brachet-Ducos C, Auclair C (2005) The actin cytoskeleton-associated protein zyxin acts as a tumour suppressor in Ewing tumour cells. *Exp Cell Res* 304: 443–456

Antoniou A, Pharoah PD, Narod S, Risch HA, Eiford JE, Hopper JL (2003) Average risk of breast and ovarian cancer associated with BRCA1 and BRCA2 mutations detected in case series unselected for family history: a combined analysis of 22 studies. *Am J Hum Genet* 72: 1117–1130

Auersperg N, Wong AS, Choi KC, Kang SK, Leung PC (2001) Ovarian surface epithelium: biology, endocrinology, and pathology. *Endocr Rev* 22: 255–288

Beckerle MC (1997) Zyxin: zinc fingers at sites of cell adhesion. *Bioessays* 19: 949–957

Boehm AM, Galvin RP, Sickmann A (2004) Extractor for ESI quadrupole TOF tandem MS data enabled for high throughput batch processing. *BMC Bioinformatics* 5: 162–166

Butt E, Gambaryan S, Göttfert N, Galler A, Marcus K, Meyer HE (2003) Actin binding of human LIM and SH3 protein is regulated by cAMP- and

cGMP-dependent protein kinase phosphorylation on serine 146. *J Biol Chem* **278**: 15601–15607

Cattaruzza M, Lattrich C, Hecker M (2004) Focal adhesion protein zyxin is a mechanosensitive modulator of gene expression in vascular smooth muscle cells. *Hypertension* **43**: 726–730

Chew CS, Chen X, Parente JA, Tarrer S, Okamoto C, Qin HY (2002) Lasp-1 binds to non-muscle F-actin *in vitro* and is localized within multiple sites of dynamic actin assembly *in vivo*. *J Cell Sci* **115**: 4787–4799

Chew CS, Parente JA, Chen X, Chaponnier C, Cameron RS (2000) The LIM and SH3 domain containing protein, lasp-1, may link the cAMP-signaling pathway with dynamic membrane restructuring activities in ion transporting epithelia. *J Cell Sci* **113**: 2035–2045

Chew CS, Parente JR, Zhou CJ, Baranco E, Chen X (1998) Lasp-1 is a regulated phosphoprotein within the cAMP-signaling pathway in the gastric parietal cell. *J Physiol* **275**: C56–C67

Concannon CG, Gorman AM, Samali A (2003) On the role of Hsp27 in regulating apoptosis. *Apoptosis* **8**: 61–70

Drees BE, Andrews KM, Beckerle MC (1999) Molecular dissection of zyxin function reveals its involvement in cell motility. *J Cell Biol* **147**: 1549–1560

Espana L, Martin B, Aragues R, Chiva C, Oliva B, Andreu D, Sierra A (2005) Bcl-x(L)-mediated changes in metabolic pathways of breast cancer cells: from survival in the blood stream to organ-specific metastasis. *Am J Pathol* **167**: 1125–1137

Gatenby RA, Gillies RJ (2004) Why do cancers have high aerobic glycolysis? *Nat Rev Cancer* **4**: 891–899

Griffith E, Coutts AS, Black DM (2005) RNAi knock-down of the focal adhesion protein TES reveals its role in actin stress fibre organisation. *Cell Mot Cytoskelet* **60**: 140–152

Grunewald TG, Kammerer U, Schulze E, Schindler D, Honig A, Zimmer M, Butt E (2006) Silencing of LASP-1 influences zyxin localization, inhibits proliferation and reduces migration in breast cancer cells. *Exp Cell Res* **312**: 974–982

Hermeking H, Lengauer C, Polyak K, He TC, Zhang L, Thiagalingam S, Kinzler KW, Vogelstein B (1997) 14-3-3 sigma is p53-regulated inhibitor of G₂/M progression. *Mol Cell* **1**: 3–11

Hirota T, Morisaki T, Nishiyama Y, Marumoto T, Tada K, Hara T, Masuko N, Inagaki M, Hatakeyama K, Saya H (2000) Zyxin, a regulator of actin filament assembly, targets the mitotic apparatus by interacting with h-warts/LATS1 tumour suppressor. *J Cell Biol* **5**: 1073–1086

Hoffman LM, Jensen CJ, Kloeker S, Wang CL, Yoshigi M, Beckerle MC (2006) Genetic ablation of zyxin causes Mena/VASP mislocalization, increased motility, and deficits in actin remodelling. *J Cell Biol* **172**: 771–782

Iida S, Hirota T, Morisaki T, Marumoto T, Hara T, Kuninaka S, Honda S, Kosai K, Kawasaji M, Pallas DC, Saya H (2004) Tumour suppressor WARTS ensures genomic integrity by regulating both mitotic progression and tetraploidy checkpoint function. *Oncogene* **23**: 5266–5274

Isidoro A, Casado E, Redondo A, Acebo P, Espinosa E, Alonso AM, Cejas P, Hardisson D, Fresno Vara JA, Belda-Iniesta C, Gonzales-Baron M, Cuevas JM (2005) Breast carcinomas fulfill the Warburg hypothesis and provide metabolic markers of cancer prognosis. *Carcinogenesis* **26**: 2095–2104

Ingram WJ, Wicking CA, Grimmond SM, Forrest AR, Wainwright BJ (2002) Novel genes regulated by sonic Hedgehog in pluripotent mesenchymal cells. *Oncogene* **21**: 8196–8205

Kadomas JL, Beckerle MC (2004) The LIM domain: from the cytoskeleton to the nucleus. *Nat Rev Mol Cel Biol* **5**: 920–931

Keicher C, Gambaryan S, Schulze E, Marcus K, Meyer HE, Butt E (2004) Phosphorylation of mouse LASP-1 on threonine 156 by cAMP- and cGMP-dependent protein kinase. *Biochem Biophys Res Com* **24**: 308–316

Legge F, Ferrandina G, Salutari V, Scambia G (2005) Biological characterization of ovarian cancer: prognostic and therapeutic implications. *Ann Oncol* **16**: 95–101

Li B, Zhuang LB, Trueb B (2004) Zyxin interacts with the SH3 domains of the cytoskeletal proteins LIM-nebulette and Lasp-1. *J Bio Chem* **279**: 20401–20410

Lin HY, Park ZY, Lin D, Brahmbhatt AA, Rio M, Yates JR, Klemke RL (2004) Regulation of cell migration and survival by focal adhesion targeting of LASP-1. *J Cell Biol* **165**: 421–432

Liu CR, Ma CS, Ning JY, You JF, Liao SL, Zheng J (2004) Differential thymosin beta 10 expression levels and actin filament organisation in tumour cell lines with different metastatic potential. *Chin Med J* **117**: 213–218

Nakagawa H, Terasaki AG, Suzuki H, Ohashi K, Miyamoto S (2006) Short-term retention of actin filament binding proteins on lamellipodial actin bundles. *FEBS Lett* **580**: 3223–3228

Nix DA, Fradelizi J, Bockholt S, Menichi B, Louvard D, Friedrich E, Beckerle MC (2001) Targeting of zyxin to sites of actin membrane interaction and to nucleus. *J Biol Chem* **276**: 34759–34767

Parkin DM, Bray F, Pisani P (2001) Estimating the world cancer burden: Globocan 2000. *Int J Cancer* **94**: 153–156

Peng CY, Graves PR, Thoma RS, Wu Z, Shaw AS, Piwnica-Worms H (1997) Mitotic and G2 checkpoint control: regulation of 14-3-3 protein binding by phosphorylation of Cdc25C on serine-216. *Science* **277**: 1501–1505

Perkins DN, Pappin DJ, Creasy DM, Cottrell JS (1999) Probability-based protein identification by searching sequence databases using mass spectrometry data. *Electrophoresis* **20**: 3551–3567

Pietromonaco SF, Seluja GA, Aitken A, Elias L (1996) Association of 14-3-3 proteins with centrosomes. *Blood Cells Mol Dis* **22**: 225–237

Quirk JT, Natarajan N (2005) Ovarian cancer incidence in the United States, 1992–1999. *Gynecol Oncol* **97**: 519–523

Rachlin AS, Otey CA (2006) Identification of pallidin isoforms and characterization of an isoform-specific interaction between LASP-1 and pallidin. *J Cell Sci* **119**: 995–1004

Rauh-Adelmann C, Kin-Mang L, Sabeti N, Long JP, Mok SC, Ho S (2000) Altered expression of BRCA1, BRCA2 and newly identified BRCA2 exon 12 deletion variant in malignant human ovarian, prostate, and breast cancer cell lines. *28*: 236–246

Ridley AJ, Schwartz MA, Burridge K, Firtel RA, Ginsberg MH, Borisy G, Parsons JT, Horwitz AR (2003) Cell migration: integrating signals from front to back. *Science* **302**: 1704–1709

Rottner K, Krause M, Gimona M, Small JV, Wehland J (2000) Zyxin is not colocalized with VASP at lamellipodial tips and exhibits different dynamics to vinculin, paxillin and VASP in focal adhesions. *Mol Biol Cell* **12**: 3103–3113

Schindler D, Hoehn H (1999) Flow cytometric testing for syndromes with chromosomal instability. In *Diagnostic Cytogenetics* Wegner RD (ed) pp 269–281. Berlin: Springer

Schreiber V, Moog-Lutz C, Regnier CH, Chenard MP, Boeuf H, Vonesch JL, Tomasetto C, Rio MC (1998) Lasp-1, a novel type of actin-binding protein accumulating in cell membrane extensions. *Mol Med* **4**: 675–687

Spence HJ, McGarry L, Chew CS, Carragher NO, Scott-Carragher LA, Yuan Z, Croft DR, Olson MF, Frame M, Ozanne BW (2006) AP-1 differentially expressed proteins Krp1 and fibronectin cooperatively enhance Rho-ROCK-independent mesenchymal invasion by altering the function, localization, and activity of nondifferentially expressed proteins. *Mol and Cell Biol* **26**: 1480–1495

Strehl S, Borkhardt A, Slany R, Fuchs UE, König K, Haas OA (2003) The human LASP1 gene is fused to MLL in an acute myeloid leukemia with t(11;17)(q23;q21). *Oncogene* **22**: 157–160

Sun HJ, Bahk YY, Choi YR, Shim JH, Han SH, Lee JW (2006) A proteomic analysis during serial subculture and osteogenic differentiation of human mesenchymal stem cells. *J Orthop Res* **24**: 2059–2071

Tomasetto C, Moog-Lutz C, Regnier CH, Schreiber V, Basset P, Rio MC (1995b) Lasp-1 (MLN 50) defines a new LIM protein subfamily characterized by the association of LIM and SH3 domains. *FEBS Lett* **373**: 245–249

Tomasetto C, Regnier C, Moog-Lutz C, Mattei MG, Chenard MP, Lidereau R, Basset P, Rio MC (1995a) Identification of four novel human genes amplified and overexpressed in breast carcinoma and localized to the q11–q21.3 region of chromosome 17. *Genomics* **28**: 367–376

Tzivion G, Gupta VS, Kaplun L, Balan V (2006) 14-3-3 proteins as potential oncogenes. *Semin Cancer Biol* **16**: 203–213

Wang W, Shakes DC (1996) Molecular evolution of the 14-3-3 protein family. *J Mol Evol* **43**: 384–398

Wang Y, Gilmore TD (2003) Zyxin and paxillin proteins: focal adhesion plaque LIM domain proteins go nuclear. *Biochem Biophys Acta* **1593**: 115–120

Yates III JR, Eng JK, McCormack AL, Schieltz D (1995) Method to correlate tandem mass spectra of modified peptides to amino acid sequences in the protein database. *Anal Chem* **67**: 1426–1436

Zhang D, Tai LK, Wong LL, Chiu LL, Sethi SK, Koay ES (2005) Proteomic study reveals that proteins involved in metabolic and detoxification pathways are highly expressed in HER-2/neu-positive breast cancer. *Mol Cell Proteomics* **4**: 1686–1696

Research article

Open Access

Nuclear localization and cytosolic overexpression of LASP-1 correlates with tumor size and nodal-positivity of human breast carcinoma

Thomas GP Grunewald^{†1}, Ulrike Kammerer^{†2}, Michaela Kapp²,
Matthias Eck³, Johannes Dietl², Elke Butt^{*1} and Arnd Honig²

Address: ¹Institute of Clinical Biochemistry and Pathobiochemistry, University of Wuerzburg, Grobuehlstr. 12, D-97080 Wuerzburg, Germany,

²Department of Obstetrics and Gynecology, University of Wuerzburg, Josef-Schneider-Str. 4, D-97080 Wuerzburg, Germany and ³Institute of Pathology, University of Wuerzburg, Josef-Schneider-Str. 2, D-97080 Wuerzburg, Germany

Email: Thomas GP Grunewald - Thgruenewald@web.de; Ulrike Kammerer - frak057@mail.uni-wuerzburg.de;
Michaela Kapp - M.Kapp@mail.uni.wuerzburg.de; Matthias Eck - Math.Eck@gmx.de; Johannes Dietl - frauenklinik@mail.uni-wuerzburg.de;
Elke Butt* - butt@klin-biochem.uni-wuerzburg.de; Arnd Honig - arnd_honig@hotmail.com

* Corresponding author †Equal contributors

Published: 23 October 2007

Received: 13 July 2007

BMC Cancer 2007, 7:198 doi:10.1186/1471-2407-7-198

Accepted: 23 October 2007

This article is available from: <http://www.biomedcentral.com/1471-2407/7/198>

© 2007 Grunewald et al; licensee BioMed Central Ltd.

This is an Open Access article distributed under the terms of the Creative Commons Attribution License (<http://creativecommons.org/licenses/by/2.0>), which permits unrestricted use, distribution, and reproduction in any medium, provided the original work is properly cited.

Abstract

Background: LIM and SH3 protein 1 (LASP-1), initially identified from human breast cancer, is a specific focal adhesion protein involved in cell proliferation and migration, which was reported to be overexpressed in 8–12 % of human breast cancers and thought to be exclusively located in cytoplasm.

Methods: In the present work we analyzed the cellular and histological expression pattern of LASP-1 and its involvement in biological behavior of human breast cancer through correlation with standard clinicopathological parameters and expression of c-erbB2 (HER-2/neu), estrogen- (ER) and progesterone-receptors (PR). For this purpose immunohistochemical staining intensity and percentage of stained cells were semi-quantitatively rated to define a LASP-1 immunoreactive score (LASP-1-IRS). LASP-1-IRS was determined in 83 cases of invasive ductal breast carcinomas, 25 ductal carcinomas in situ (DCIS) and 18 fibroadenomas. Cellular LASP-1 distribution and expression pattern was visualized by immunofluorescence and confocal microscopy and assessed through separate Western blots of nuclear and cytosol preparations of BT-20, MCF-7, MDA-MB231, and ZR-75/1 breast cancer cells.

Results: Statistical analysis revealed that the resulting LASP-1-IRS was significantly higher in invasive carcinomas compared to fibroadenomas ($p = 0.0176$). Strong cytoplasmatic expression of LASP-1 was detected in 55.4 % of the invasive carcinomas, which correlated significantly with nuclear LASP-1-positivity ($p = 0.0014$), increased tumor size ($p = 0.0159$) and rate of nodal-positivity ($p = 0.0066$). However, levels of LASP-1 expression did not correlate with average age at time point of diagnosis, histological tumor grading, c-erbB2-, ER- or PR-expression.

Increased nuclear localization and cytosolic expression of LASP-1 was found in breast cancer with higher tumor stage as well as in rapidly proliferating epidermal basal cells. Confocal microscopy and separate Western blots of cytosolic and nuclear preparations confirmed nuclear localization of LASP-1.

Conclusion: The current data provide evidence that LASP-1 is not exclusively a cytosolic protein, but is also detectable within the nucleus. Increased expression of LASP-1 *in vivo* is present in breast carcinomas with higher tumor stage and therefore may be related with worse prognosis concerning patients' overall survival.

Background

Breast cancer is the most frequent malignancy among women and ranks first as cause of cancer deaths among women at ages between 20 to 59 years [1]. Despite the use of endocrine therapy, systemic chemotherapy and novel approaches such as treatment with trastuzumab (Herceptin®), outcome of metastatic breast cancer has not substantially improved. Metastatic disease remains generally incurable with a median survival time of only a few years [2,3]. Thus, new therapeutic modalities are required to improve the outcome. Genes that are overexpressed in metastatic cancer cells are promising targets for novel therapeutic agents.

The LIM and SH3 domain protein LASP-1 was initially identified from a cDNA library of breast cancer metastases. The gene was mapped to human chromosome 17q21 in a region that is altered in 20–30% of human breast cancers [4,5], suggesting that it could play a role in tumor development and metastases of breast cancer.

Human LASP-1 encodes a membrane-bound protein of 261 amino acids containing one N-terminal LIM domain, followed by two actin-binding sites and a C-terminal src homology SH3 domain. The actin-binding domains in the core of LASP-1 mediate an interaction between LASP-1 and actin at cell membrane extensions, but not along actin stress fibers [6-10].

Recent data showed an additional interaction of LASP-1 via its nebulin like actin-binding repeats with kelch related protein 1 (Krp1), a focal adhesion protein involved in cell migration. The exact cellular function of LASP-1 is not known yet, but the protein has previously been reported to localize within multiple sites of dynamic actin assembly such as focal contacts, focal adhesions, lamellipodia, membrane ruffles and pseudopodia [4,7,11-13].

The C-terminal SH3 domain of LASP-1 is involved in protein-protein interactions through binding to proline-rich sequences, specifically with zyxin, palladin, lipoma preferred partner (LPP) and vasodilator stimulated phosphoprotein (VASP) [9,14,15]. Mutation analysis of LASP-1 led to the conclusion that its SH3 domain is necessary for pseudopodial extension and invasion [16].

Although no binding partner for the LIM domain of LASP-1 has been identified so far, previous data have shown that the zinc-finger module in the LIM domain of LASP-1 is an morphologically and perhaps functionally independent folding-unit of this protein harboring the possibility of direct binding to DNA [17].

Moreover, LASP-1 is substrate of Abelson tyrosine kinase. Abelson tyrosine kinase is strongly involved in carcinogenesis of hematopoietic tumors, such as B-cell lymphomas [18]. Phosphorylation of LASP-1 at tyrosine 171 is associated with loss of LASP-1 from focal adhesion points and the initiation of cell death, but without changes in dynamics of migratory processes [13]. In addition, phosphorylation of LASP-1 at serine 146 by cAMP- and cGMP-dependent protein kinases resulted in a translocation of the protein from membrane to cytosol and was followed by reduced cell migration [8]. All these protein-protein interactions mediated by the LIM and SH3 domains can be regarded as scaffolds for the formation of higher order complexes and suggest that LASP-1 could be part of important signaling pathways and a structural protein as well.

LASP-1 expression has been reported to be increased in metastatic breast cancer, suggesting that overexpression of LASP-1 may be involved in the migratory process of these cells [4]. Interestingly, knock-down of LASP-1 by RNA-interference in metastatic breast cancer cell lines BT-20 and MCF-7, as well as in the ovarian cancer cell line SKOV-3 resulted in a strong inhibition of proliferation, migration and in cell cycle arrest in G2-phase without induction of apoptosis or necrosis. Furthermore, LASP-1 silencing was accompanied by a reduced binding of the LASP-1 binding partner zyxin to focal contacts.

Reversely, artificial overexpression of LASP-1 in non-neoplastic PTK2 (Porous tridactylis kidney) cells hardly expressing endogenous LASP-1, resulted in a acceleration of migration [19,20].

In this study we demonstrate that LASP-1 is not only a cytosolic, but also a nuclear located protein, which is highly overexpressed in breast cancer tissue compared to benign fibroadenomas. Furthermore, we provide evidence that its cytosolic overexpression and nuclear localization correlates significantly with tumor size and nodal-positivity of human breast carcinomas.

Methods

Tissue samples

The studies were performed with approval of the Ethics Committee of the University of Wuerzburg. Paraffin embedded tissue samples of 126 archival cases with confirmed histological diagnosis were obtained from the department of Pathology of the University of Wuerzburg.

We analyzed 25 cases of ductal carcinoma in situ without any invasive component (DCIS), 83 invasive ductal breast carcinomas and 18 fibroadenomas as well as three samples of normal breast tissue from reduction mammoplasty.

The patients with invasive breast carcinomas were aged from 32 to 96 (mean 58.6 ± 13.52) years. In this study all carcinomas, which were mainly collected from patients undergoing wide excisions, have been classified according to criteria of the WHO and recorded as invasive ductal carcinomas by a pathologist. Grading of malignancy of ductal carcinomas was evaluated according to the Scarff, Bloom and Richardson criteria with guidelines as suggested by Nottingham City Hospital Pathologists [21]. Tumor staging was performed according to parameters of the TNM system [22].

Immunohistochemistry

For immunohistochemical staining procedures tissue sections were cut from regular paraffin embedded tissue at 2–3 μm . Sections were placed onto APES (3-amino-propyl-triethoxy-silane; Roth, Karlsruhe, Germany) coated slides, dewaxed in xylene, rehydrated in graded ethanol and in TRIS-buffered saline (TBS; 25 mM TRIS/HCl, pH 7.4, 137 mM NaCl, 2.7 mM KCl). For antigen retrieval, sections were subjected to heat pretreatment by boiling it in 0.01 M of sodium citrate buffer (pH 6.0) for 10 min in a microwave oven (600Watt/sec.). Endogenous peroxidase was blocked by incubation in 0.1% hydrogen peroxide in PBS for 5 min. Slides were then incubated with the polyclonal anti-LASP-1 antibody [8] diluted 1:1000 in "antibody diluent" (DAKO, Hamburg, Germany) followed by EnVision/rabbit detection system (DAKO, Hamburg, Germany). 3,3'-Diaminobenzidine (DAB; DAKO, Hamburg, Germany) was used as chromogen and sections were counterstained in hematoxylin (Mayers, Sigma, Deisenhofen, Germany), dehydrated through graded ethanol and embedded in Entelan (Merck, Darmstadt, Germany).

Evaluation of immunohistochemical LASP-1 staining and LASP-1-IRS

To assess the role of LASP-1 in human breast cancer, we examined its expression in 83 breast carcinoma samples from patients selected randomly from January 2000 to December 2006 with or without invasive components.

Semi-quantitative evaluation of LASP-1 immunostaining was carried out by three independent observers (TG, UK and EB) through defining of the percentage of positive cells and the staining intensity as described below. In most of all cases ($> 90\%$) the independently determined LASP-1-IRS was consistent within all observers. In the rare event of divergent evaluation, a consensus was found. For positive controls we used breast cancer sections previously described as highly LASP-1-positive [19]. In negative controls with omitted primary antibody or with pre-immune serum no staining was observed.

Scoring of cytosolic LASP-1 expression was carried out in analogy to scoring of hormone receptor Immune Reactive

Score (IRS) ranging from 0–12 according to Remmele et al. [23], which is used routinely in surgical pathology for the quantification of hormone receptor expression in mammary carcinoma.

The percentage of LASP-1-positive stained cells was scored in five grades (grade 0 = 0–19%, grade 1 = 20–39%, grade 2 = 40–59%, grade 3 = 60–79% and grade 4 = 80–100% LASP-1 expressing tumor cells). The fraction of LASP-1-positive stained cells was scored after having examined 10 high-power fields (40 \times) of one section for each sample. In addition, the intensity of LASP-1 expression by the tumor cells was determined (grade 0 = none, grade 1 = low, grade 2 = moderate, grade 3 = strong). The multiplication of these two grading scores calculates the immunoreactive score for LASP-1 expression (LASP-1-IRS) in stained tissue (% LASP-1-positive tumor cells \times staining intensity = LASP-1-IRS). Examples for the very heterogeneous LASP-1 expression in invasive breast cancer are given in Figure 1.

For better statistical discrimination samples scored with cytosolic LASP-1-IRS < 5 were classified as LASP-1-negative, those with LASP-1-IRS > 5 or higher as LASP-1-positive.

Nuclear LASP-1-positivity was scored by determining percentage of positive nuclei regardless of cytosolic LASP-1 expression and staining intensity. In analogy to the scoring of the proliferation marker Ki67 samples were considered as nuclear-positive (NUC+) if 10% or more cells showed nuclear staining for LASP-1 [24].

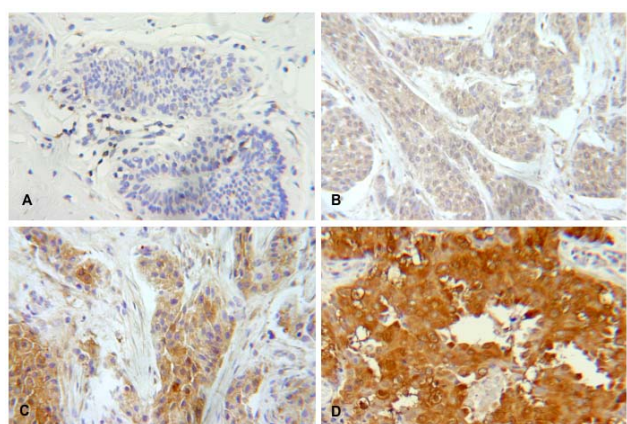


Figure 1
Heterogeneous LASP-1 expression in human invasive breast cancer. Immunohistochemical staining of different LASP-1 expression intensity levels in human invasive breast cancer samples (DAB, brown; magnification 100 \times). (A+B) low LASP-1-IRS (< 5). (C+D) medium to high LASP-1-IRS (> 5).

The immunomarkers c-erbB2 (HER-2/neu), estrogen receptor (ER) and progesterone receptor (PR) assessed in this study had been previously detected by standard immunohistochemistry and were drawn from the archival database of the Department of Pathology, Wuerzburg.

Statistical analysis

Graph Pad Prism software test statistics was used to assess LASP-1 expression and the categorical parameters of interest. Furthermore, multivariate non-parametric analysis was performed using Fisher's exact (F) and Mann-Whitney (M) test. In the statistical analysis invasive ductal carcinomas were sorted in groups depending on nodal-positive or nodal-negative status and small ($T_1 = \emptyset$ max. 2 cm) or larger tumor size ($> T_1$). This dichotomous graduation was made on the basis of a recent meta-analysis stating that the most beneficial prognostic criteria are nodal-negativity and a small tumor size at time point of diagnosis [25].

Further stratification of our tumor samples according to extent of nodal positivity and advanced tumor size was abandoned, since there are no additional major therapeutic implications [26].

Cell culture conditions

Cell lines (MCF-7, BT-20, MDA-MB231 and ZR-75/1) were obtained from Cell Line Services (Heidelberg, Germany) and grown at 1×10^5 cells/ml in a plastic cell culture flask in a humidified incubator at 37°C under 5% CO₂ atmosphere in HBCA-medium [27] containing 10% heat-inactivated fetal bovine serum (PAA, Linz, Austria) and 1% streptomycin/ampicillin (Invitrogen, Karlsruhe, Germany). Cells were cultured until homogeneous morphology of cells was reached (passage 3–4) since LASP-1 belongs to a group of several differential expressed proteins that are up-regulated after later passages [28].

Immunofluorescence and confocal imaging

For confocal microscopy, cells were grown until homogeneous morphology at a maximum of 70% confluence on glass chamber slides, fixed in 4% (w/v) paraformaldehyde in PBS, permeabilized with 0.1% (w/v) Triton X-100 in PBS, and then stained with affinity-purified LASP-1 antibody (1:2000) followed by secondary Cy3-labeled anti-rabbit antibody (1:500) (Dianova, Hamburg, Germany).

Fluorescence and transmission-DIC images were recorded on a modified confocal microscope (Leica SP5, Mannheim, Germany) with a 100× NA 1.4 objective (Leica, Wetzlar, Germany). Fluorescence was detected with SP5 spectral emission setting at 570–650 nm for the Cy3 and with the DIC-transmission channel. The images were recorded with 512 × 512 pixels with lateral resolution between 90 and 200 nm and a recording rate of 400 lines

per second. Each image was also line averaged 4 times and the entire frame was averaged twice for optimal signal to noise ratio. The images were converted to .tiff format and analyzed with Photoshop™ software.

Preparation of nuclear and cytosolic cell fractions

Human breast cancer cell lines were harvested at 80% confluence through trypsinization. Isolation of nuclei and cytosol was carried out using NE-PER Nuclear and Cytoplasmic Extraction Reagents (Pierce, Bonn, Germany) following the manufacturers instructions. Probes were solved in Laemmli sample buffer at a final concentration of 1×10^6 /ml and stored at -20°C before Western Blot electrophoresis.

Western blot analysis

For Western blotting cells were lysed in Laemmli sample buffer. Equal amounts of protein, according to cell count, were resolved by 12% SDS-PAGE. After blotting on nitrocellulose membrane and blocking with 3% nonfat dry milk in 10 mM Tris, pH 7.5, 100 mM NaCl, 0.1% (w/v) Tween 20, the membrane was first incubated with the antibody raised against LASP-1 (1:10000) [8] followed by incubation with horseradish peroxidase-coupled goat anti-rabbit IgG (Biorad, Munich, Germany), diluted 1:5000, and visualization was done using ECL (Amersham Biosciences, Freiburg, Germany). Protein bands were visualized by autoradiography. Quantification of autoradiography signals was carried out by densitometry using the ImageJ software (NIH, Bethesda, USA).

GAPDH was used as a specific cytosolic marker to exclude cytoplasmatic contamination of the nuclei preparation and was visualized by incubating NC membrane with polyclonal anti-GAPDH primary antibody (1:1000; Santa Cruz, Santa Cruz, USA). Anti Lamin A+C antibody (1: 50; Abcam, Cambridge, UK) served as a specific nuclear marker to exclude nuclear contamination in cytoplasmatic cell samples [29-31]. At least three independent experiments have been carried out and representative results are shown.

Results

LASP-1 is overexpressed in invasive breast cancer tissue

LASP-1 expression was detected in cytoplasm of tumor cells, leukocytes, myoepithelial cells and vascular smooth muscle cells, but not in stromal cells. Immunohistochemistry clearly allowed to localize LASP-1 expression in carcinoma cells of 76 malignant breast carcinomas (91.56 %), whereas in seven patients LASP-1 could not be detected in invasive neoplastic cells. Medium to high LASP-1-IRS (>5) was observed in 46 cases (55.4%), which were considered to be LASP-1-positive, while 37 probes (44.6%) showed a low LASP-1-IRS (<5) and were considered to be LASP-1-negative (Table 1 and Figure 2B). In

Table 1: Statistical analysis of LASP-1 expression in 83 breast cancer samples (in-CA), 25 ductal carcinomas in situ (DCIS) and 18 fibroadenomas (FIBRO). IRS: immune reactive score; n.s.: not significant

| LASP-1 + | | LASP-1 - | | IRS mean | IRS STDV | IRS Median | p-values (Fisher's exact) | |
|----------|----|----------|----|----------|----------|------------|---------------------------|--------------------|
| n | % | n | % | | | | | |
| FIBRO | 4 | 22.2 | 14 | 77.8 | 3.11 | 2.22 | 3 | 0.7315 n.s. |
| DCIS | 8 | 32 | 17 | 68 | 3.48 | 2.80 | 3 | 0.7315 n.s. |
| in-CA | 46 | 55.4 | 37 | 44.6 | 5.75 | 3.73 | 8 | 0.066 n.s. 0.0176* |

contrast, LASP-1 could not be detected in benign epithelial cells of reduction mammoplasty.

In analogy to previous findings in myoepithelial and vascular smooth muscle cells of human breast and ovarian tissue [19,20], LASP-1 overexpression could be observed in highly proliferating epidermal basal cells (Figure 3A), while cells of non-proliferating superficial layers or dermal connective tissue cells like fibroblasts showed only weak LASP-1 expression. Interestingly, strong nuclear LASP-1-positivity could be observed in about 29% of all breast carcinomas as well as in nuclei of epidermal basal cells (Figures 3A, 3B and 3C), whereas all other breast carcinoma nuclei were negative for LASP-1 and the cells only displayed perinuclear and cytosolic LASP-1 enrichment (Figure 3D).

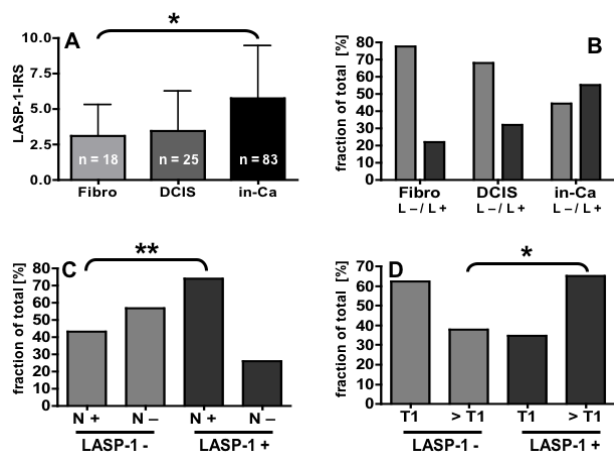


Figure 2
Graphical illustration of statistical LASP-1 distribution. (A) LASP-1-IRS (immunoreactive score) is significantly higher in invasive breast carcinomas (in-Ca) compared to fibroadenomas (Fibro). Error bars represent standard deviation. (B) Distribution of LASP-1-positivity (L+) and LASP-1-negativity (L-) in fibroadenomas, DCIS and invasive breast cancer. (C+D) Positive nodal status (N+) and tumor size (>T1) correlate significantly with LASP-1-positivity. Significant statistical differences are labeled with one star ($p < 0.05$) or two stars ($p < 0.01$).

In 89% of all tumor-samples, which were scored to be LASP-1-negative, LASP-1 was not detectable within the nucleus, while 43.5% of all LASP-1-positive specimens showed clear nuclear LASP-1 staining. Thus nuclear stain-

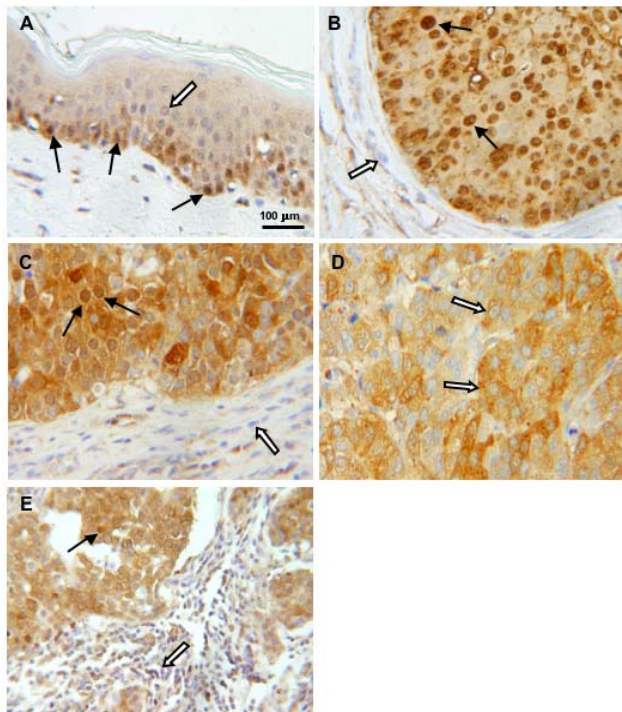


Figure 3
Histological expression pattern of LASP-1. Immunohistochemical staining of LASP-1 (DAB, brown, magnification 100 \times) in different cell types. White arrows indicate LASP-1-negative nuclei, black arrows LASP-1-positive nuclei. (A) LASP-1 is highly overexpressed in physiologically proliferating epidermal basal cells, compared to superficial epidermal strata or dermal connective tissue cells. (B+C) LASP-1 is localized abundantly in nuclei of invasive breast cancer cells compared to LASP-1-negative nuclei of stromal cells. (D) Invasive breast cancer cells with LASP-1-negative nuclei but perinuclear and cytosolic LASP-1 overexpression. (E) Nuclear and cytosolic LASP-1-positive breast cancer cells in direct neighborhood to infiltrating LASP-1-negative lymphocytes.

ing is correlated with cytosolic LASP-1 expression and significantly higher in LASP-1-positive cells compared to LASP-1-negative samples ($p = 0.0014$; Table 2).

However, two samples (2.4%) showed a very high nuclear LASP-1-positivity with concurrent low cytosolic staining (Figure 3B).

This nuclear staining is unlikely to be unspecific, because nuclei of other benign stromal cells like fibrocytes are LASP-1-negative, even when located right next to cancer cells (Figures 3B and 3C).

This observation is even more obvious in Figure 3E, showing strong LASP-1-positive nuclei and cytosol of human breast cancer cells in comparison to LASP-1-negative nuclei of neighboring infiltrating lymphocytes.

LASP-1 expression is significantly higher in invasive breast cancer compared to fibroadenomas and is correlated with TNM-staging

Comparison of average LASP-1 expression of fibroadenomas, DCIS and invasive breast cancer demonstrated that invasive cancer cells display significantly higher LASP-1 expression than fibroadenomas ($p = 0.0176$), as seen in Table 1 and Figure 2A. In contrast, staining intensity of LASP-1 in DCIS was not significantly higher than in

Table 2: Statistical analysis of LASP-1 distribution and expression in correlation to clinicopathological and biological parameters.
LASP-1 (L) protein expression was analyzed in 83 breast cancer samples. Associations with clinicopathological and biological parameters were analyzed using Mann-Whitney-test (M) and Fisher's exact test (F); n.s.: not significant.

| | Total (n = 83) | L + (n = 46) | | L - (n = 37) | | p-value (Test) |
|-----------------------|-------------------|-----------------|----|-----------------|----|-------------------|
| | | n | % | n | % | |
| Nodal status | | | | | | |
| N+ | 50 | 60.2 | 34 | 73.9 | 16 | 43.2 |
| N- | 33 | 39.9 | 12 | 26.1 | 21 | 56.8 |
| Tumor size | | | | | | |
| T1 | 39 | 47 | 16 | 34.8 | 23 | 62.2 |
| >T1 | 44 | 53 | 30 | 65.2 | 14 | 37.8 |
| Grading | | | | | | |
| G1 | 3 | 3.6 | 0 | 0 | 3 | 8.1 |
| G2 | 39 | 47 | 24 | 52.2 | 15 | 40.5 |
| G3 | 41 | 49.4 | 22 | 47.8 | 19 | 51.4 |
| c-erbB-2 | | | | | | |
| Her+ | 18 | 21.7 | 12 | 26.1 | 6 | 16.2 |
| Her- | 65 | 78.3 | 34 | 73.9 | 31 | 83.8 |
| Estrogen receptor | | | | | | |
| ER+ | 60 | 72.3 | 33 | 71.7 | 27 | 73 |
| | | | | | | 1.0 (F) |
| ER- | 23 | 27.7 | 13 | 28.3 | 10 | 27 |
| Progesterone receptor | | | | | | n.s. |
| PR+ | 51 | 61.5 | 26 | 56.5 | 25 | 67.6 |
| | | | | | | 0.3673 (F) |
| PR- | 32 | 38.5 | 20 | 43.5 | 12 | 32.4 |
| Nuclear positivity | | | | | | n.s. |
| NUC + | 24 | 29 | 20 | 43.5 | 4 | 11 |
| | | | | | | 0.0014 (F) |
| NUC - | 59 | 71 | 26 | 56.5 | 33 | 89 |
| | | | | | | ** |

fibroadenomas, but also not significantly lower than in invasive breast cancer (Table 1 and Figures 2A and 2B).

To evaluate the clinical relevance of the heterogeneous LASP-1 expression, LASP-1-IRS was compared to clinicopathological and biological parameters. Positive correlations were found between LASP-1-IRS and TNM-staging regarding tumor size T ($p = 0.0159$) and nodal-positivity ($p = 0.0066$; Table 2) (Figures 2C and 2D). No correlation was found with age at time of surgery (Table 3), grading, ER- and PR-positivity and HER-2/neu-expression (Table 2).

To evaluate the possible relevance of LASP-1 as a prognostic marker for lymph node metastasis in human breast cancer disease, a contingency test was performed and prognostic indices were calculated. Sensitivity of LASP-1-IRS-scoring to predict node-positivity is 85% with a specificity of 36.4%, (positive and negative predictive value 73.9 vs. 51.3%, respectively).

LASP-1 is detectable within the nucleus by confocal microscopy

To further assess the cellular expression pattern of LASP-1, we performed confocal and non-confocal microscopy of immunofluorescence labeled LASP-1 in the breast cancer cell line BT-20. The immunofluorescence images showed a variable cellular expression pattern of the protein. In addition to the reported localization of LASP-1 (white arrows) to focal contacts and tips of lamellipodia (Figure 4A) [4,7,11-13], LASP-1 was detected in the cytosol (Figure 4C), perinuclear (Figures 4B and 4D) and nuclear (Figures 4B and 4E). This is in accordance to the LASP-1 localization observed in the breast tissue samples (Figure 3). A similar immunohistochemical staining pattern was detected in MCF-7 breast cancer cells and SKOV-3 ovarian cancer cells (data not shown).

LASP-1 is detectable in nuclear fractions of various breast cancer cell lines by Western blotting

To verify the nuclear localization of LASP-1, MCF-7, BT-20, MDA-MB231 and ZR-75/1 breast cancer cells were separated in cytosolic and nuclear fractions and assessed by Western blot. Equal amounts of protein, according to

Table 3: Statistical analysis of LASP-1 (L) expression in relation to age. FIBRO: fibroadenome (n = 18); DCIS: ductal carcinomas in situ (n = 25); in-CA: invasive breast cancer (n = 83).

| | FIBRO | | DCIS | | in-CA | |
|----------------|-------|------|------|------|-------|------|
| | L + | L - | L + | L - | L + | L - |
| Age (yrs) mean | 40.8 | 40 | 54.1 | 54.5 | 61.1 | 55.1 |
| STDEV | 8.9 | 16.1 | 11.6 | 13.7 | 13.7 | 11.9 |

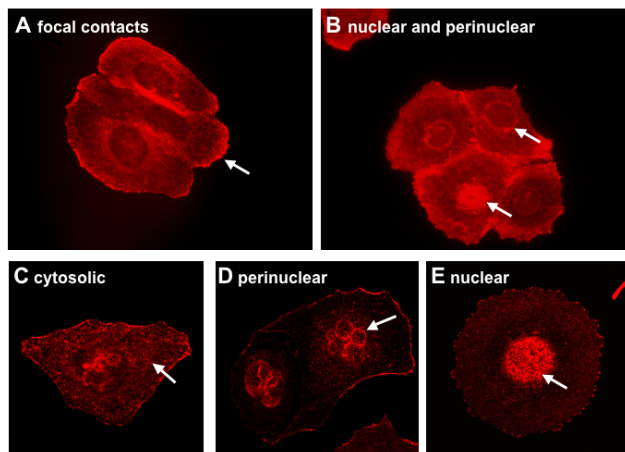


Figure 4
Cellular LASP-1 expression pattern visualized by confocal microscopy. Non-confocal (A+B) and confocal (C-E) microscopy of LASP-1 immunostaining in BT-20 breast cancer cells revealed that LASP-1 (red) is mainly detectable in focal contacts (A) and in the cytosol (C). In addition, more than 30% of the cells show a nuclear staining (B+E), and in some cells a peri-nuclear localization of LASP-1 is visible (B+D).

cell count, were resolved by 12% SDS-PAGE and blotted on nitrocellulose membrane. As seen in Figure 5, LASP-1 is clearly detectable in the nuclei of human breast cancer cell lines MCF-7 and BT-20, while nuclei of MDA-MB231 and ZR-75/1 cells were found to be negative for LASP-1 in the nuclear fraction. GAPDH was used as a specific cytosolic marker to exclude cytoplasmatic contamination of nuclei samples during preparation. Reversely Lamin A+C served as a specific nuclear marker to exclude nuclear contamination in cytoplasmatic cell fractions (Figure 5).

Discussion

In the present work we investigated for the first time the expression of LASP-1 in a series of 83 invasive breast carcinomas at protein level and compared the data to clinically established breast cancer parameters. We found that the degree of immunohistochemical staining correlated significantly with nodal metastasis and tumor size but seems to be independent of other parameters such as age, grading and estrogen or progesterone receptor status.

In contrast to earlier publications, demonstrating the co-amplification of the LASP-1 gene together with HER-2/neu (c-erbB2) [4,32], our statistical analysis revealed no relation between LASP-1 protein level and HER-2/neu protein expression.

A previous study also showed that LASP-1 mRNA is over-expressed in only 8–12% of all human breast cancers [5].

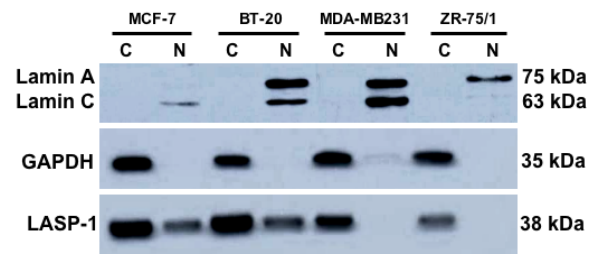


Figure 5
Western Blot of nuclear and cytosolic fractions of the cancer cell lines MCF-7, BT-20, MDA-MB231 and ZR-75/1. LASP-1 is detectable in nuclear (N) as well as in cytoplasmic (C) cell fractions of breast cell lines MCF-7 and BT-20, but not in the nucleus of MDA-MB231 and ZR-75/1 cells. GAPDH was used as a cytoplasmic marker, Lamin A + C as nuclear markers to exclude contamination during cell fraction isolation.

However, our immunohistochemical analysis provide evidence that the LIM and SH3 domain protein is highly expressed (LASP-1-positive) in 55.4% of all tested breast cancer samples. This discrepancy could be due to the fact that Tomasetto et al. [4] used total surgical specimens for their mRNA isolation, containing undefined amounts of LASP-1 free benign tissue, while our data focused on malign cells only.

Consistent with the high expression of LASP-1 in breast tumors recent data demonstrated the functional significance of LASP-1 for cancer metastasis. Silencing of LASP-1 by RNAi in highly LASP-1 expressing human breast and ovarian cancer cells led to reduced cell proliferation, migration and to cell cycle arrest in G2-phase [19,20].

These experiments are supported by our present study proving the significantly higher expression of LASP-1 in invasive breast carcinomas compared to benign fibroadenomas. The rate of strongly LASP-1 expressing samples of invasive ductal carcinomas amounted 55.4% (LASP-1-IRS > 5). Moreover, statistical analysis provided evidence for a positive correlation of cytosolic as well as nuclear LASP-1-positivity with tumor size and nodal-positivity indicating an important role of LASP-1 in proliferation and migration.

These data resemble those of another focal adhesion protein, ENAH. ENAH is a member of the ENAH/VASP protein family, which regulates cell migration and actin-cytoskeleton organization at focal contacts. Like LASP-1, ENAH is not detectable in benign breast epithelium, but is weakly expressed in low-risk benign diseases like fibroadenomas and strongly expressed in invasive breast

cancers. Similar to LASP-1, there is a significant correlation of ENAH-expression and tumor size ($p < 0.05$) [33]. In contrast to LASP-1, siRNA induced ENAH-knock-down does not affect cell proliferation while LASP-1 silencing resulted in strong inhibition of cell growth and migration [19]. Thus, it is likely that among several focal adhesion proteins which are overexpressed in breast cancer LASP-1 has more regulatory function than others.

In a recent investigation, a cDNA microarray was used to establish a prognostic index for nodal-positive breast cancer [34]. Similar to our study, all 20 patients were LASP-1-positive, albeit LASP-1 was found to be one out of five genes being under-expressed in patients that died within 5 years after surgery. This is in part differing from our results demonstrating a correlation between high LASP-1 protein levels and nodal-positivity. However, in many cases there are significant discrepancies between the measured mRNA levels and protein data indicating post-transcriptional mechanism of regulation and stabilization [35].

In the present work we provide evidence for LASP-1 being not only a cytosolic, but also a nuclear protein. By our immunohistochemical stainings LASP-1 was detectable in nuclei of 29% of all investigated breast carcinomas independent of its actual cytosolic expression. Images taken with confocal microscopy confirmed nuclear localization of LASP-1 within the nucleus in BT-20 and MCF-7 breast cancer cells. Although these monoclonal cell lines are genetically identical, immunostaining demonstrated a variable cytosolic and nuclear LASP-1 localization, possibly dependent on cell cycle. Western blot analysis verified nuclear LASP-1 localization in MCF-7 and BT-20 cells while breast cancer cell lines MDA-MB231 and ZR-75/1 only displayed a cytosolic but no nuclear LASP-1 localization. Cell line ZR-75/1 is known to be highly estrogen and progesterone dependent [36] and was found to have the highest c-erbB2-expression among eight characterized breast- and four ovarian-cancer cell lines [37], whereas MDA-MB231 cells are ER- and PR-receptor negative and express HER-2/neu only at very low levels [38]. However, in our study LASP-1-IRS as well as nuclear LASP-1-positivity did not correlate with ER-, PR- or HER-2/neu-expression.

Previous data have shown that the zinc-finger containing LIM domain of LASP-1 is a morphologically and perhaps functionally independent folding-unit offering the possibility of direct binding to DNA [17]. In general, LIM domains are specialized double zinc-finger motifs interacting with many different proteins in association with the cytoskeleton and even form homeodomains to become nuclear transcription factors [39,40]. No hetero- or homodimerization of LASP-1 has been reported yet [9].

However, LASP-1 binding partner zyxin is a LIM domain containing protein known to be a nuclear shuttle protein involved in cell migration and cell cycle control [41,42], which could act as a potential interaction partner of LASP-1 in cell core.

In our present study we could demonstrate that LASP-1 is not only highly expressed in fast proliferating malignant tumor cells, but also in proliferating regenerative epidermal basal cells, while slowly proliferating dermal fibroblasts are LASP-1-negative. This observation is consistent with previous findings showing that LASP-1 expression positively influences tumor cell proliferation [19,20]. However, preliminary results show no correlation between the well-known proliferation marker Ki67 and LASP-1 expression (data not shown). Nevertheless, previous publications have shown that Ki67 expression is often considered as false positive and is inferior in evaluating tumor proliferation activity compared to standardized mitotic index at optimal cut-off points. This implies that evaluation of patients' prognosis by Ki67 expression has to be appraised with caution [43].

Further statistical calculations with contingency tests demonstrated that according to our data, postoperative relevance of LASP-1 expression for prediction of nodal-positivity has a sensitivity of about 85%, suggesting that LASP-1 could be used as a predictive marker for lymph node metastasis together with other markers like the superior method of sentinel lymph node biopsy with an average sensitivity of about 95% [44]. Thus postoperative non-invasive LASP-1 scoring in primary tumor tissue could accomplish node-positivity prediction as an additional marker to invasive sentinel node biopsy, especially in cases of negative sentinel node biopsy or if patients reject invasive sentinel node biopsy.

Conclusion

This study is the first description of LASP-1 as a nuclear protein, whose cytosolic expression and nuclear localization correlates *in vivo* with tumor size and nodal positivity of human invasive ductal carcinoma of the breast. In summary, our observations suggest an expanded role for LASP-1 in biological breast cancer behavior. Further prospective studies will be necessary to define the potential of LASP-1 as an independent marker for diagnosis of cancer as well as a marker for prognosis of this disease.

Competing interests

The author(s) declare that they have no competing interests.

Authors' contributions

TG, UK and AH drafted and wrote the manuscript, designed and coordinated the study, evaluated the immu-

nohistochemical data and performed statistical analyses, EB participated in its design and carried out immunofluorescence and confocal microscopy, MK carried out the immunohistological stainings and Western blots, ME provided histopathological and immunohistological guidance, JD participated in the design of the study and provided patients' data. All authors read and approved the final manuscript.

Acknowledgements

We thank Prof. Greg Harms for the use of and help with the confocal microscope. Thanks also to Petra Thalheimer for technical assistance and Barbara Lechner for her helpful comments and corrections on the manuscript. This study was supported by Deutsche Krebshilfe 106219 to E.B. and A.H.

References

- Jemal A, Murray T, Ward E, Samuels A, Tiwari RC, Ghafoor A, Feuer EJ, Thun MJ: **Cancer statistics, 2005.** *CA Cancer J Clin* 2005, **55**(1):10-30.
- Greenberg PA, Hortobagyi GN, Smith TL, Ziegler LD, Frye DK, Buzdar AU: **Long-term follow-up of patients with complete remission following combination chemotherapy for metastatic breast cancer.** *J Clin Oncol* 1996, **14**(8):2197-2205.
- Osborne CK: **Tamoxifen in the treatment of breast cancer.** *N Engl J Med* 1998, **339**(22):1609-1618.
- Tomasetto C, Moog-Lutz C, Regnier CH, Schreiber V, Basset P, Rio MC: **Lasp-1 (MLN 50) defines a new LIM protein subfamily characterized by the association of LIM and SH3 domains.** *FEBS Lett* 1995, **373**(3):245-249.
- Tomasetto C, Regnier C, Moog-Lutz C, Mattei MG, Chenard MP, Lidereau R, Basset P, Rio MC: **Identification of four novel human genes amplified and overexpressed in breast carcinoma and localized to the q11-q21.3 region of chromosome 17.** *Genomics* 1995, **28**(3):367-376.
- Schreiber V, Moog-Lutz C, Regnier CH, Chenard MP, Boeuf H, Vonesch JL, Tomasetto C, Rio MC: **Lasp-1, a novel type of actin-binding protein accumulating in cell membrane extensions.** *Mol Med* 1998, **4**(10):675-687.
- Chew CS, Chen X, Parente JA Jr., Tarrer S, Okamoto C, Qin HY: **Lasp-1 binds to non-muscle F-actin in vitro and is localized within multiple sites of dynamic actin assembly in vivo.** *J Cell Sci* 2002, **115**(Pt 24):4787-4799.
- Butt E, Gambaryan S, Gottfert N, Galler A, Marcus K, Meyer HE: **Actin binding of human LIM and SH3 protein is regulated by cGMP- and cAMP-dependent protein kinase phosphorylation on serine 146.** *J Biol Chem* 2003, **278**(18):15601-15607.
- Keicher C, Gambaryan S, Schulze E, Marcus K, Meyer HE, Butt E: **Phosphorylation of mouse LASP-1 on threonine 156 by cAMP- and cGMP-dependent protein kinase.** *Biochem Biophys Res Commun* 2004, **324**(1):308-316.
- Nakagawa H, Terasaki AG, Suzuki H, Ohashi K, Miyamoto S: **Short-term retention of actin filament binding proteins on lamellipodial actin bundles.** *FEBS Lett* 2006, **580**(13):3223-3228.
- Chew CS, Parente JA Jr., Zhou C, Baranco E, Chen X: **Lasp-1 is a regulated phosphoprotein within the cAMP signaling pathway in the gastric parietal cell.** *Am J Physiol* 1998, **275**(1 Pt 1):C56-67.
- Chew CS, Parente JA Jr., Chen X, Chaponnier C, Cameron RS: **The LIM and SH3 domain-containing protein, lasp-1, may link the cAMP signaling pathway with dynamic membrane restructuring activities in ion transporting epithelia.** *J Cell Sci* 2000, **113** (Pt 11):2035-2045.
- Lin YH, Park ZY, Lin D, Brahmbhatt AA, Rio MC, Yates JR 3rd, Klemke RL: **Regulation of cell migration and survival by focal adhesion targeting of Lasp-1.** *J Cell Biol* 2004, **165**(3):421-432.
- Li B, Zhuang L, Trueb B: **Zyxin interacts with the SH3 domains of the cytoskeletal proteins LIM-nebulette and Lasp-1.** *J Biol Chem* 2004, **279**(19):20401-20410.
- Rachlin AS, Otey CA: **Identification of palladin isoforms and characterization of an isoform-specific interaction between Lasp-1 and palladin.** *J Cell Sci* 2006, **119**(Pt 6):995-1004.
- Spence HJ, McGarry L, Chew CS, Carragher NO, Scott-Carragher LA, Yuan Z, Croft DR, Olson MF, Frame M, Ozanne BW: **AP-1 differentially expressed proteins Krp1 and fibronectin cooperatively enhance Rho-ROCK-independent mesenchymal invasion by altering the function, localization, and activity of nondifferentially expressed proteins.** *Mol Cell Biol* 2006, **26**(4):1480-1495.
- Hammarstrom A, Berndt KD, Sillard R, Adermann K, Otting G: **Solution structure of a naturally-occurring zinc-peptide complex demonstrates that the N-terminal zinc-binding module of the Lasp-1 LIM domain is an independent folding unit.** *Biochemistry* 1996, **35**(39):12723-12732.
- Jumaa H, Hendriks RVW, Reth M: **B cell signaling and tumorigenesis.** *Annu Rev Immunol* 2005, **23**:415-445.
- Grunewald TG, Kammerer U, Schulze E, Schindler D, Honig A, Zimmer M, Butt E: **Silencing of LASP-1 influences zyxin localization, inhibits proliferation and reduces migration in breast cancer cells.** *Exp Cell Res* 2006, **312**(7):974-982.
- Grunewald TG, Kammerer U, Winkler C, Schindler D, Sickmann A, Honig A, Butt E: **Overexpression of LASP-1 mediates migration and proliferation of human ovarian cancer cells and influences zyxin localisation.** *Br J Cancer* 2007, **96**(2):296-305.
- Dalton LW, Pinder SE, Elston CE, Ellis IO, Page DL, Dupont WD, Blamey RW: **Histologic grading of breast cancer: linkage of patient outcome with level of pathologist agreement.** *Mod Pathol* 2000, **13**(7):730-735.
- Singletary SE, Connolly JL: **Breast cancer staging: working with the sixth edition of the AJCC Cancer Staging Manual.** *CA Cancer J Clin* 2006, **56**(1):37-47; quiz 50-1.
- Remmeli WV, Stegner HE: **[Recommendation for uniform definition of an immunoreactive score (IRS) for immunohistochemical estrogen receptor detection (ER-ICA) in breast cancer tissue].** *Pathologe* 1987, **8**(3):138-140.
- Tan PH, Bay BH, Yip G, Selvarajan S, Tan P, Wu J, Lee CH, Li KB: **Immunohistochemical detection of Ki67 in breast cancer correlates with transcriptional regulation of genes related to apoptosis and cell death.** *Mod Pathol* 2005, **18**(3):374-381.
- Soerjomataram I, Louwman MW, Ribot JG, Roukema JA, Coebergh JW: **An overview of prognostic factors for long-term survivors of breast cancer.** *Breast Cancer Res Treat* 2007. [Epub ahead of print]
- Goldhirsch A, Glick JH, Gelber RD, Coates AS, Thurlimann B, Senn HJ: **Meeting highlights: international expert consensus on the primary therapy of early breast cancer 2005.** *Ann Oncol* 2005, **16**(10):1569-1583.
- Calvo F, Brower M, Carney DN: **Continuous culture and soft agarose cloning of multiple human breast carcinoma cell lines in serum-free medium.** *Cancer Res* 1984, **44**(10):4553-4559.
- Sun HJ, Bahk YY, Choi YR, Shim JH, Han SH, Lee JW: **A proteomic analysis during serial subculture and osteogenic differentiation of human mesenchymal stem cell.** *J Orthop Res* 2006, **24**(11):2059-2071.
- Gerace L, Blobel G: **The nuclear envelope lamina is reversibly depolymerized during mitosis.** *Cell* 1980, **19**(1):277-287.
- Gerace L, Blum A, Blobel G: **Immunocytochemical localization of the major polypeptides of the nuclear pore complex-lamina fraction. Interphase and mitotic distribution.** *J Cell Biol* 1978, **79**(2 Pt 1):546-566.
- Glass CA, Glass JR, Taniura H, Hasel KW, Blevitt JM, Gerace L: **The alpha-helical rod domain of human lamins A and C contains a chromatin binding site.** *Embo J* 1993, **12**(11):4413-4424.
- Bieche I, Tomasetto C, Regnier CH, Moog-Lutz C, Rio MC, Lidereau R: **Two distinct amplified regions at 17q11-q21 involved in human primary breast cancer.** *Cancer Res* 1996, **56**(17):3886-3890.
- Di Modugno F, Mottolese M, Di Benedetto A, Conidi A, Novelli F, Perracchio L, Venturoli I, Botti C, Jager E, Santoni A, Natali PG, Nistico P: **The cytoskeleton regulatory protein hMena (ENAH) is overexpressed in human benign breast lesions with high risk of transformation and human epidermal growth factor receptor-2-positive/hormonal receptor-negative tumors.** *Clin Cancer Res* 2006, **12**(5):1470-1478.

34. Asaka S, Fujimoto T, Akaishi J, Ogawa K, Onda M: **Genetic prognostic index influences patient outcome for node-positive breast cancer.** *Surg Today* 2006, **36**(9):793-801.
35. Griffin TJ, Gygi SP, Ideker T, Rist B, Eng J, Hood L, Aebersold R: **Complementary profiling of gene expression at the transcriptome and proteome levels in *Saccharomyces cerevisiae*.** *Mol Cell Proteomics* 2002, **1**(4):323-333.
36. Pfeffer U, Fecarotta E, Castagnetta L, Vidali G: **Estrogen receptor variant messenger RNA lacking exon 4 in estrogen-responsive human breast cancer cell lines.** *Cancer Res* 1993, **53**(4):741-743.
37. Kammerer U, Thanner F, Kapp M, Dietl J, Sutterlin M: **Expression of tumor markers on breast and ovarian cancer cell lines.** *Anti-cancer Res* 2003, **23**(2A):1051-1055.
38. Lacroix M, Leclercq G: **Relevance of breast cancer cell lines as models for breast tumours: an update.** *Breast Cancer Res Treat* 2004, **83**(3):249-289.
39. David IB, Breen JJ, Toyama R: **LIM domains: multiple roles as adapters and functional modifiers in protein interactions.** *Trends Genet* 1998, **14**(4):156-162.
40. Bach I: **The LIM domain: regulation by association.** *Mech Dev* 2000, **91**(1-2):5-17.
41. Beckerle MC: **Zyxin: zinc fingers at sites of cell adhesion.** *Bioessays* 1997, **19**(11):949-957.
42. Kadrmas JL, Beckerle MC: **The LIM domain: from the cytoskeleton to the nucleus.** *Nat Rev Mol Cell Biol* 2004, **5**(11):920-931.
43. Jalava P, Kuopio T, Juntti-Patinen L, Kotkansalo T, Krongqvist P, Collan Y: **Ki67 immunohistochemistry: a valuable marker in prognosis but with a risk of misclassification: proliferation subgroups formed based on Ki67 immunoreactivity and standardized mitotic index.** *Histopathology* 2006, **48**(6):674-682.
44. Cserni G: **Evaluation of sentinel lymph nodes in breast cancer.** *Histopathology* 2005, **46**(6):697-702.

Pre-publication history

The pre-publication history for this paper can be accessed here:

http://www.biomedcentral.com/1471-2407/7/198/pre_pub

Publish with **BioMed Central** and every scientist can read your work free of charge

"BioMed Central will be the most significant development for disseminating the results of biomedical research in our lifetime."

Sir Paul Nurse, Cancer Research UK

Your research papers will be:

- available free of charge to the entire biomedical community
- peer reviewed and published immediately upon acceptance
- cited in PubMed and archived on PubMed Central
- yours — you keep the copyright

Submit your manuscript here:
http://www.biomedcentral.com/info/publishing_adv.asp



Nuclear localisation of LASP-1 correlates with poor long-term survival in female breast cancer

JJ Frietsch^{1,4}, TGP Grunewald^{2,4}, S Jasper¹, U Kammerer³, S Herterich¹, M Kapp³, A Honig³ and E Butt^{*,1}

¹Institute for Clinical Biochemistry and Pathobiochemistry, University of Wuerzburg, Grombuehlstr. 12, 97080 Wuerzburg, Germany; ²Department of Pediatrics, Children's Cancer Research Center (CCRC), Laboratory of Functional Genomics and Transplantation Biology, Klinikum rechts der Isar, Technische Universität München, Kölner Platz 1, 80804 Munich, Germany; ³Department of Obstetrics and Gynecology, University of Wuerzburg, Josef-Schneider Str 4, 97080 Wuerzburg, Germany

BACKGROUND: LIM and SH3 protein 1 (LASP-1) is a nucleo-cytoplasmatic signalling protein involved in cell proliferation and migration and is upregulated in breast cancer *in vitro* studies have shown that LASP-1 might be regulated by prostate-derived ETS factor (PDEF), p53 and/or *LASP1* gene amplification. This current study analysed the prognostic significance of LASP-1 on overall survival (OS) in 177 breast cancer patients and addressed the suggested mechanisms of LASP-1-regulation.

METHODS: Nucleo-cytoplasmatic LASP-1-positivity of breast carcinoma samples was correlated with long-term survival, clinicopathological parameters, Ki67-positivity and PDEF expression. Rate of *LASP1* amplification was determined in micro-dissected primary breast cancer cells using quantitative RT-PCR. Cell-phase dependency of nuclear LASP-1-localisation was studied in synchronised cells. In addition, LASP-1, PDEF and p53 expression was compared in cell lines of different tumour entities to define principles for LASP-1-regulation.

RESULTS: We showed that LASP-1 overexpression is not due to *LASP1* gene amplification. Moreover, no correlation between p53-mutations or PDEF-expression and LASP-1-status was observed. However, nuclear LASP-1-localisation in breast carcinomas is increased during proliferation with peak in G2/M-phase and correlated significantly with Ki67-positivity and poor OS.

CONCLUSION: Our results provide evidence that nuclear LASP-1-positivity may serve as a negative prognostic indicator for long-term survival of breast cancer patients.

British Journal of Cancer (2010) **102**, 1645–1653. doi:10.1038/sj.bjc.6605685 www.bjancer.com

Published online 11 May 2010

© 2010 Cancer Research UK

Keywords: LASP-1; Ki67; PDEF; p53; breast cancer

Breast cancer is expected to account for 26% of all new cancer cases among women in the western world of which 89% will survive 5 years after diagnosis (Jemal *et al*, 2007). In spite of the significant improvements in diagnostic and therapeutic modalities for the treatment of cancer patients, metastasis still composes the major cause of mortality being responsible for 60% of breast cancer deaths (Hanahan and Weinberg, 2000). Metastatic disease remains generally incurable with a median survival time of only a few years. Regardless of the increase in its incidence, mortality related to breast cancer is decreasing because of raised awareness and screening, as well as multidisciplinary treatment. The introduction of endocrine therapy and the treatment with trastuzumab (Herceptin) in patients with HER-2/neu overexpression reduced the rates of recurrence by 50% and significantly improved survival (Widakowich *et al*, 2007). Nevertheless, breast cancer remains a multi-step process linked to more than one single molecular alteration. Therefore, elucidating genes that are overexpressed in breast cancer cells may yield promising targets for novel therapeutic agents (Mauriac *et al*, 2005).

*Correspondence: Dr E Butt;
E-mail: butt@klin-biochem.uni-wuerzburg.de

⁴These authors contributed equally to this work.

Received 2 March 2010; revised 26 March 2010; accepted 12 April 2010;
published online 11 May 2010

The LIM and SH3 domain protein (LASP-1) was initially identified from a cDNA library of breast cancer metastases. It became the first member of a newly defined LIM-protein subfamily of the nebulin group characterised by the combined presence of LIM and SH3 domains (Grunewald and Butt, 2008). LASP-1 is localised within multiple sites of dynamic F-actin assembly such as focal contacts, lamellipodia and membrane ruffles it binds to the specific shuttle proteins Zyxin and lipoma preferred partner (LPP) and is involved in cell migration and proliferation (Schreiber *et al*, 1998; Chew *et al*, 2002; Butt *et al*, 2003; Nakagawa *et al*, 2006). Silencing of LASP-1 by RNA-interference in various cancer cell lines resulted in strong inhibition of proliferation and migration with cell cycle arrest in G2/M-phase (Grunewald *et al*, 2006, 2007b).

LIM and SH3 protein 1 mRNA is expressed ubiquitously at low basal levels in all normal human tissues, but is overexpressed in metastatic human breast cancer (Grunewald and Butt, 2008) and ovarian cancer (Grunewald *et al*, 2007b; Dimova *et al*, 2009). In a recent case-control study, LASP-1-expression correlated significantly with tumour size and nodal-positivity (Grunewald *et al*, 2007a). Albeit the protein is predominantly situated at focal adhesions, nuclear localisation of the protein could be clearly detected by confocal microscopy and western blots of cytosolic and nuclear preparations from various breast cancer cell lines (Grunewald *et al*, 2007a). These data prompted us to further

investigate the long-term survival in relation to nuclear and cytosolic LASP-1-localisation in a large well-characterised cohort of breast cancer patients and to analyse the nuclear LASP-1-localisation in the different phases of the cell cycle.

In invasive breast cancer cells, LASP-1-expression was significantly inversely affected by prostate-derived ETS factor (PDEF), a transcription factor known to repress a variety of genes that are possibly involved in oncogenesis, such as the apoptosis regulator survivin (Ghaderohi *et al*, 2007) and the pro-invasive protease uPA (Turner *et al*, 2008).

Real-time PCR analysis confirmed upregulation of *LASP1* mRNA in PDEF-deficient invasive and highly metastatic breast cancer cells (MBA-MB-231, BT-549), while in the non-invasive MCF-7 breast cancer cell line, endogenously expressing PDEF, a reduced LASP-1 protein level was detected (Turner *et al*, 2008).

In a study conducted with hepatocellular carcinoma (HCC), LASP-1 was repressed by wild-type p53 at the transcriptional level (Wang *et al*, 2009). Functional negative p53 mutations led to increased LASP-1-expression and to a more aggressive HCC phenotype (Wang *et al*, 2009).

In this study, we aimed to determine whether the PDEF level or mutations of the tumour suppressor p53 represent a general mechanism of LASP-1 deregulation in human cancer. Thus, we analysed several tumour cell lines of different entities as well as breast cancer tissue for LASP-1-expression in correlation to PDEF protein concentration and p53 status.

As *LASP1* gene amplification was reported earlier in one breast cancer cell line (Tomasetto *et al*, 1995b) and in 40% of crude extracts of lymph nodes derived from metastatic breast cancer (Tomasetto *et al*, 1995a) and was accounted for the principal cause of LASP-1 overexpression, we also re-analysed the rate of *LASP1* gene amplification in individual micro-dissected primary breast cancer cells. It is noteworthy that the *LASP1* gene maps to a region (17q12) that is altered in 20–30% of human breast cancers (Tomasetto *et al*, 1995a, b) and tumours bearing amplifications of 17q11–21 are associated with an adverse prognosis because of increased resistance to chemotherapy and endocrine therapy (Ross and Fletcher, 1999).

MATERIALS AND METHODS

Tissue samples

The studies were performed with approval of the ethics committee of the University of Wuerzburg. Paraffin-embedded tissue samples of surgical biopsies from 177 patients with invasive breast cancer were obtained from the Department of Pathology of the University of Wuerzburg. The patients were aged from 32 to 85 (mean 55.3 ± 11.9) years. All carcinomas were mainly collected from patients that underwent wide excisions.

Grading of malignancy of ductal carcinomas was evaluated according to the Scarff, Bloom and Richardson criteria as suggested by Nottingham City Hospital Pathologists (Dalton *et al*, 2000). Tumour staging was performed according to parameters of the TNM system (Singletary and Connolly, 2006).

Ten paraffin-embedded breast tissue samples from reduction mammoplasties were used as control tissue to obtain reference DNA for the evaluation of the quantitative RT-PCR results.

Immunohistochemistry

For immunohistochemical staining procedures tissue sections were cut from regular paraffin-embedded tissue at $2-3\ \mu\text{m}$. Sections were placed onto APES (3-amino-propyltriethoxy-silane; Roth, Karlsruhe, Germany) coated slides, dewaxed twice in xylene for 10 min, rehydrated in graded ethanol (two changes in 96%, one change in 70%, one change with distilled water) and in

TRIS-buffered saline (25 mM TRIS/HCl, pH 7.4, 137 mM NaCl, 2.7 mM KCl) for 1 min each. For antigen retrieval, sections were subjected to heat pretreatment by boiling in 0.01 M of sodium citrate buffer (pH 6.0) for 5 min in a microwave oven (800 W s^{-1}). Endogenous peroxidase was blocked by incubation in 3.0% hydrogen peroxide in methyl alcohol for 5 min, washed in PBS and incubated in Beriglobin (Aventis Behring GmbH, Marburg, Germany) 1:10 in PBS at room temperature (RT) for 15 min to prevent unspecified attachments. Slides were then incubated with the polyclonal anti-LASP-1 antibody (Butt *et al*, 2003) diluted 1:1000 in antibody diluent (DAKO, Hamburg, Germany) or with Ki67 antibody (DAKO) diluted 1:100 in antibody diluent at 4 °C overnight followed by EnVision/rabbit detection system (DAKO) for 30 min at RT. 3,3'-Diaminobenzidine (DAB; DAKO) was used as chromogen and sections were counterstained in haematoxylin (Mayers, Sigma, Deisenhofen, Germany), dehydrated through graded ethanol (in the inverse way as described above) and embedded in Entelan (Merck, Darmstadt, Germany). The specificity of the LASP-1 antibody is shown in Supplementary Figure 1.

For PDEF staining, slices were incubated in Beriglobin, diluted 1:50 in PBS at RT for 15 min before incubation with polyclonal anti-PDEF antibody (Invitrogen, Karlsruhe, Germany) diluted 1:50 in 'antibody diluent' (DAKO) at 4 °C overnight. After washing with PBS, the slides were incubated for 15 min with biotinylated secondary antibody followed by 15 min incubation with streptavidin-HRP (both LSAB2 system DAKO). The specificity of the PDEF antibody is shown in Supplementary Figure 2.

Evaluation of immunohistochemical LASP-1 staining and LASP-1-IRS

After staining procedure, the slides were screened and scored as previously described (Grunewald *et al*, 2007a). To assess the role of LASP-1 in human breast cancer, we examined its expression in 177 breast carcinoma samples from patients selected randomly from January 1985 to December 2007. Semi-quantitative evaluation of LASP-1 immunostaining was carried out by defining the percentage of positive cells and the staining intensity as described below. For positive controls, breast cancer sections previously described as highly LASP-1-positive (Grunewald *et al*, 2006, 2007a) were used. No staining was observed in negative controls with omitted primary antibody or with pre-immune serum (data not shown).

Scoring of cytosolic LASP-1-expression was carried out in analogy to the scoring of hormone receptor Immune Reactive Score (IRS) ranging from 0 to 12 according to Remmeli *et al* (Remmeli and Stegner, 1987), which is used routinely in surgical pathology for the quantification of hormone receptor expression in mammary carcinoma.

The percentage of LASP-1-positive stained cells was scored in five grades (grade 0 = 0–19%, grade 1 = 20–39%, grade 2 = 40–59%, grade 3 = 60–79% and grade 4 = 80–100% LASP-1-expressing tumour cells) by examining 10 high-power fields ($\times 40$ magnification) in each tissue sample. In addition, the intensity of LASP-1-expression by the tumour cells was determined (score 0 = none, score 1 = low, score 2 = moderate, score 3 = strong). The multiplication of these two grading scores (% LASP-1-positive tumour cells \times staining intensity) calculates the immunoreactive score for LASP-1-expression (LASP-1-IRS). Examples for the very heterogeneous LASP-1-expression in invasive breast cancer are given in Figure 1.

For better statistical discrimination, samples scored with cytosolic LASP-1-IRS < 5 were classified as LASP-1-negative, those with LASP-1-IRS > 5 as LASP-1-positive.

Nuclear LASP-1-staining was scored by determining percentage of positive nuclei regardless of cytosolic LASP-1-expression and cytosolic staining intensity. Samples were considered as nuclear-positive when 10% or more cells showed nuclear LASP-1 staining.

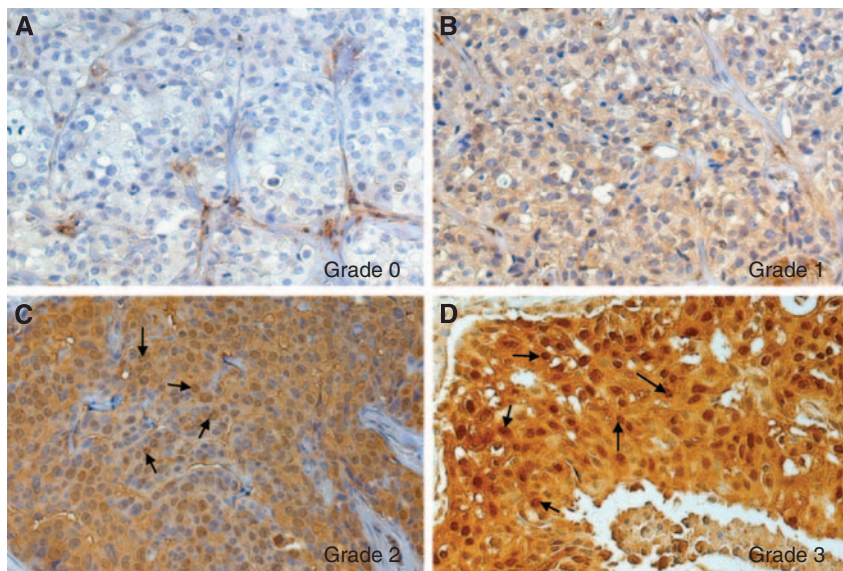


Figure 1 Representative images of heterogeneous LASP-1-expression in human invasive breast cancer. Immunohistochemical staining of LASP-1 (DAB, brown, magnification $\times 20$). (A) No LASP-1-expression (grade 0). (B) Low LASP-1-expression (grade 1). (C) Medium LASP-1-expression (grade 2). (D) High LASP-1-expression (grade 3). Arrows in (C) and (D) point to LASP-1-positive nuclei.

Examples for nuclear LASP-1 staining are observed in Figures 1C and D.

The immunomarkers c-erbB2 (HER-2/neu), oestrogen receptor and progesterone receptor assessed in this study had been previously detected by standard immunohistochemistry and were drawn from the archival database of the Department of Pathology of the University of Wuerzburg.

Scoring of Ki67-positivity

Immunohistochemical scoring was performed by counting 10 randomly selected $40 \times$ high-power fields containing representative sections of tumour and calculated as the percentage of positively stained cells to total cells by counting at least 1000 malignant cells. Ki67 $\geq 10\%$ nuclear staining was required for a positive classification (Tan *et al*, 2005).

Statistical analysis

Associations between nuclear or cytosolic LASP-1-localisation were evaluated by multivariate non-parametric analysis using Fisher's exact (F) and Mann-Whitney (M) test. These tests were conducted using Graph Pad Prism Software for Windows (GraphPad Software, Inc., La Jolla, CA, USA). $P < 0.05$ were regarded as statistically significant.

Tissue preparation, micro-dissection, DNA preparation

In all, 64 formalin-fixed paraffin-embedded breast cancer tissue samples of the patient cohort and 10 control breast tissues were placed onto PEN-membrane coated slides (polyethylene naphthalate; Leica, Wetzlar, Germany) were deparaffinised (two changes of xylene, two changes of 96% ethanol, one change of 70% ethanol, one change with distilled water, 1 min each). After staining with haematoxylin for 90 s and eosin for 60 s, all sections were rinsed 3 \times with distilled water. The slides were then air-dried at RT and used for micro-dissection. Incubation and staining times were kept as short as possible to enhance DNA recovery and proteinase K digestion (Godfrey *et al*, 2000; Ehrig *et al*, 2001).

Laser capture micro-dissection was performed using the Laser MicroBeam System (Leica LMD 6000; Leica). Tumour tissue

(2.0–2.5 mm²) was captured into the lid of a 0.5 ml reaction tube and digested with 30 μ l proteinase K digestion buffer (50 mM Tris, pH 8.1; 1 mM ethylenediamine tetraacetic acid; 0.5% Tween 20; 3 mU ml⁻¹ proteinase K). Subsequently, the tubes were closed in this inverted position and incubated for 50–60 h at 37 °C. Undigested debris was removed by centrifugation at 14 000 g for 5 min, and proteinase K was inactivated by incubation at 95 °C for 10 min. The samples can be stored safely for months at –20 °C (Lehmann and Kreipe, 2001).

Quantitative RT-PCR

Quantitative analysis of genomic *LASP1* DNA was performed by monitoring the increase in fluorescence of the dye SYBR Green (SYBR Green Supermix, Bio-Rad, Munich, Germany) using the iCycler iQ System (Bio-Rad).

Primers were designed to meet specific criteria by using Primer3 software (<http://frodo.wi.mit.edu>) (Rozen and Skaletsky, 2000) and were obtained from Operon Biotechnologie GmbH (Cologne, Germany). The sequences of the primers used for *LASP1* DNA amplification were 5'-TGTCTCTGACTGGTGCCT-3', and 5'-TG ATCTGGCCTGGGTCTTC-3'. Primers for GAPDH were used as internal reference gene: 5'-ATCAAGAAGGTGGTGAAGCAG-3' and 5'-TACTCCTTGGAGGCCATGTG-3'.

SYBR Green PCR was performed in optical caps for a 96-well tray (Bio-Rad) using a 25 μ l final reaction mixture containing 1 μ l of each primer pair (stock 5 μ M), 1 μ l of the micro-dissected lysed tissue sample, 12.5 μ l iQ SYBR Green (Bio-Rad) and sterile water. The reaction mixture was preheated at 95 °C for 5 min, followed by 40 cycles at 95 °C, 57 °C and 72 °C for 30 s each.

All amplification curves generated with SYBR Green from stained tissue showed the typical sigmoid curve. In every run, a negative control was included to exclude false-positive results. Melting curve analysis was implemented to ensure the correct PCR product. Each tissue sample was analysed at least twice for *LASP1* and twice for *GAPDH*.

The relative gene copy number was evaluated on the basis of the threshold cycles (C_T values) of the gene of interest $C_T(LASP1)$ and of the internal reference gene $C_T(GAPDH)$.

The $C_T(GAPDH)/C_T(LASP1)$ ratio in benign control breast tissues will reflect non-amplified *LASP1* conditions. In case of a

LASP1 gene amplification in tumour samples, the threshold cycle number will decrease while the values for the $C_T(GAPDH)/C_T(LASP1)$ ratio will increase. The reference range from 10 micro-dissected normal breast tissues was determined as 0.9699 ± 0.0743 . Therefore, the expectation interval can be calculated as: $\mu \pm 2s = (0.821278502 \leftrightarrow 1.118530727)$ with μ (arithmetic mean) and s (s.d.).

Cell lines and cell culture conditions

Hepatocellular carcinoma cell lines Hep-3B and Hep-G2, breast cancer cell lines BT-20, MCF-7 and MDA-MB-231, urothelial cancer cell lines T24 and RT-4, glioblastoma cell lines U251MG, U138MG and U87MG, medulloblastoma cell lines DAOY and D283 as well as chorioncarcinoma cell lines JEG-3 and JAR were obtained from Cell Line Services (Heidelberg, Germany) and grown in plastic cell culture flasks in a humidified incubator at 37°C under 5% CO_2 atmosphere in RPMI 1640 medium containing 10% heat-inactivated fetal bovine serum (PAA, Linz, Austria) and 1% streptomycin/ampicillin (Invitrogen). Cells were cultured until homogeneous morphology of cells was reached (passage 3–4) because *LASP1* belongs to a group of several differential expressed proteins that are upregulated after later passages (Sun *et al*, 2006).

p53 Mutations

Cell lines with known p53 mutations are listed in the database: <http://p53.free.fr>. All mutations result in a non-functional p53 protein: <http://p53.iarc.fr>.

Cell cycle synchronisation and FACS analysis

BT-20 cells were rendered quiescent (G_0) by serum deprivation in RPMI 1640 with 0.1% FCS for 24 h followed by incubation with medium supplemented with 10% FCS to allow cell cycle re-entry in G_1 . To block S-phase transition, cells were incubated in medium supplemented with 10% FCS and $2\text{ }\mu\text{g ml}^{-1}$ aphidicolin for 24 h (Sigma). To synchronise the culture at G_2/M phase, cells in the S-phase were released in RPMI 1640 medium supplemented with 10% FCS for 12 h.

Cell cycle distribution was monitored by propidium iodide staining and measuring fluorescence in a FACScan 2 (Becton Dickinson, Heidelberg, Germany). BT-20 cells were harvested by trypsinisation and fixed in 70% ethanol (4°C) for 1 h followed by incubation in a solution containing $50\text{ }\mu\text{g ml}^{-1}$ RNase in PBS for 30 min. For staining, $50\text{ }\mu\text{g ml}^{-1}$ propidium iodide was added for another 30 min. Cells were analysed by FACS, and the proportion in G_0/G_1 , S and G_2/M phases was estimated using Modfit cell cycle analysis programme. Measurements were performed on at least three independent synchronisation experiments.

Preparation of nuclear and cytosolic cell fractions

Human breast cancer cell lines were harvested at 80% confluence through trypsinisation. Isolation of nuclei and cytosol was carried out using NE-PER nuclear and cytoplasmic extraction Reagents (Pierce, Bonn, Germany) following the manufacturer's instructions. Samples were solved in Laemmli sample buffer at a final concentration of $1 \times 10^6\text{ ml}^{-1}$ and stored at -20°C before western blot electrophoresis.

Western blot analysis

For western blotting, cells were lysed in Laemmli sample buffer. Equal amounts of protein, according to cell count, were resolved by 12% SDS-PAGE. After blotting on nitrocellulose membrane and blocking with 3% non-fat dry milk in 10 mM Tris, pH 7.5,

100 mM NaCl, 0.1% (w/v) Tween 20, the membrane was incubated with the antibody raised against *LASP-1* (1:20 000) (Butt *et al*, 2003) or PDEF antibody (1:1000) followed by incubation with horseradish peroxidase-coupled goat anti-rabbit IgG (Bio-Rad), diluted 1:5000, and visualised by ECL (Amersham Biosciences, Freiburg, Germany). Quantification of autoradiography signals was carried out by densitometry using the ImageJ software (NIH, Bethesda, MD, USA).

GAPDH (1:1000; Santa Cruz, Heidelberg, Germany) was used as a specific cytosolic marker to exclude cytoplasmic contamination of the nuclei preparation. Anti-Lamin A + C antibody (1:50; Abcam, Cambridge, UK) served as a specific nuclear marker to exclude nuclear contamination in cytoplasmic cell samples. At least three independent experiments have been carried out and representative results are shown.

RESULTS

Overexpression of *LASP-1* in breast cancer is not due to gene amplification

As increasing amounts of contaminating non-malignant cells lead to a significant decrease in detection sensitivity (Kallioniemi *et al*, 1994), we used individual micro-dissected breast cancer cells to examine the *LASP1* copy number in DNA samples from 64 patients with known invasive breast carcinoma selected randomly from January 2000 to December 2007.

We detected only 1 out of 64 tissue samples (1.5%) with a $C_T(GAPDH)/C_T(LASP1)$ ratio higher than the expectation interval, showing a negligible rate of *LASP1* gene amplification. Therefore, the observed overexpression of the *LASP-1* protein in more than 55% of human breast cancers (Grunewald *et al*, 2007a) is likely due to reasons distinct from gene amplification.

LASP-1 overexpression neither correlates with PDEF expression nor with p53 mutations

Commonly, the inner layer of benign ductal luminal epithelial cells show a high nuclear PDEF staining while in invasive ductal carcinoma, a weak PDEF staining is detected mainly in the cytosol (Feldman *et al*, 2003), (Figure 2). To determine whether the reported reciprocal effect of PDEF on *LASP-1* in non-invasive and invasive breast cancer cell lines (Turner *et al*, 2008) is transferable to breast tumour patient samples, we evaluated 35 primary breast cancer tissues for PDEF expression; 17 with known high (≥ 8) *LASP-1* IRS and 18 specimens with low (≤ 3) *LASP-1*-IRS.

In all 35 tested human breast cancer samples, we observed a comparable cytosolic PDEF localisation without significant differences in staining intensity. Only two out of the tested samples showed in parts additional nuclear PDEF staining. No correlation between the PDEF levels in invasive ductal carcinoma and high or low *LASP-1* expression could be detected.

When examining tumour cell lines of different entities, an overall PDEF expression is observed that does not correlate *per se* with low *LASP-1* protein concentration (Figure 3). For example, while the PDEF levels are similar in all three tested breast cancer cell lines (MDA-MB-231, BT-20, MCF-7) *LASP-1* expression is only reduced in MCF-7 cells. Analogous differences are also observed with glioblastoma and chorioncarcinoma cell lines (Figure 3).

To test whether *LASP1* is transcriptionally regulated by p53, we analysed several human cancer cell lines of different tumour entities with and without known p53 mutations for *LASP-1*-expression by western blot. All mutations result in a functionally inactive tumour suppressor. In summary, the analysis showed no correlation between high *LASP-1*-expression and p53 mutations (Figure 3). For instance, in spite of the total loss of function because of an additional stop codon in the p53 gene of the

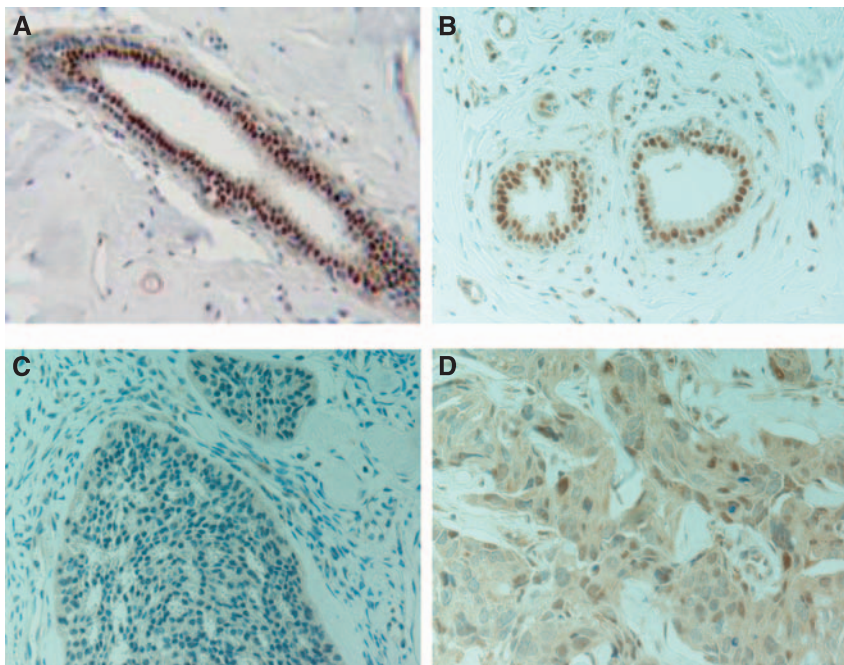


Figure 2 Immunohistochemical staining of PDEF (DAB, brown, magnification $\times 400$) in benign breast tissue (**A** and **B**) and invasive ductal breast cancer samples (**C** and **D**) showing a nuclear PDEF staining in normal tissue and a more cytosolic PDEF localisation in tumour cells.

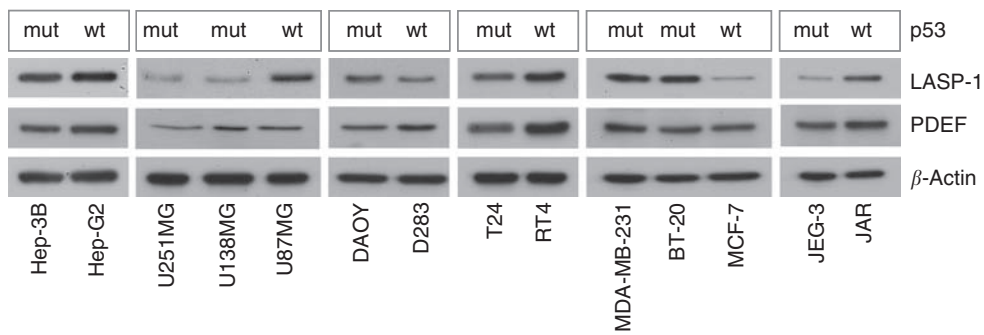


Figure 3 PDEF and LASP-1 protein expression in various cancer cell lines with (mut) and without (wt) known p53 mutations that lead to functionally inactive tumour suppressor protein. β -Actin blotting was used as a control for equal protein loading. Cell lines: hepatocellular carcinoma (Hep-G2, Hep-3B), glioblastoma (U251, U13898, U87), medulloblastoma (DAOY, D283), urothelial carcinoma (T24, RT4), breast cancer (MDA-MB-231, BT-20, MCF-7) and chorioncarcinoma (JEG-3, JAR). There is neither a correlation between PDEF and LASP-1 expression nor between LASP-1 protein levels and p53 mutations.

urothelial cell line T24, both, *p53* wild-type RT-4 and *p53* mutant T24 urothelial cancer cell lines express high levels of LASP-1. In contrast, the chorioncarcinoma cell line JEG-3 with a *p53* mutation and the breast carcinoma cell line MCF-7-expressing wild-type *p53* show low LASP-1-expression.

Nuclear localisation of LASP-1 correlates with poor long-term survival

In an earlier case-control study, a strong cytoplasmic staining for LASP-1 was detected in $>55\%$ of the invasive tumours, which correlated significantly with increased tumour size and rate of nodal-positivity. In addition, we observed a distinct nuclear LASP-1-localisation pattern that was absent in benign tissue (Grunewald *et al*, 2007a).

We therefore performed a retrospective study (January 1985 until December 2007) with samples of 177 archival cases of confirmed histological diagnosis of invasive breast carcinomas to

evaluate the long-term survival of breast tumour patients in relation to nuclear and cytoplasmic LASP-1-positivity.

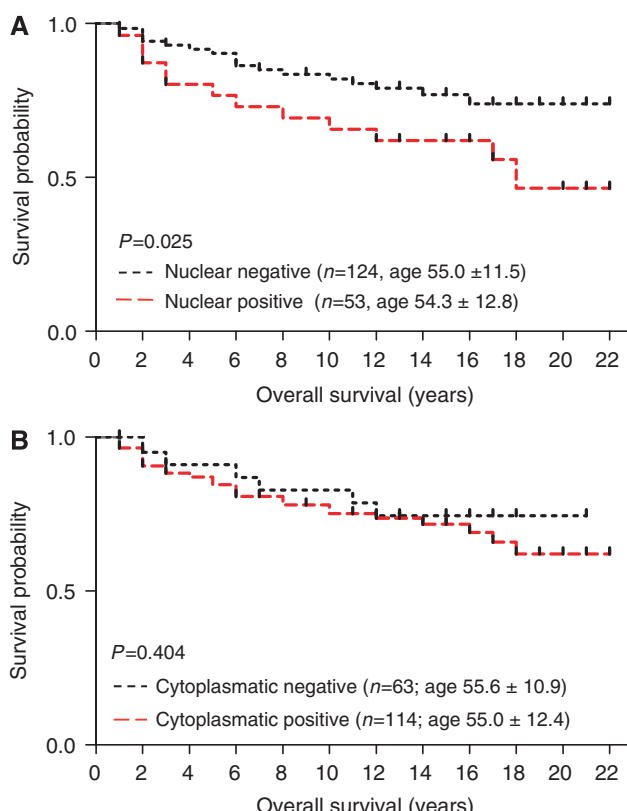
Cytoplasmic LASP-1 protein expression was detected in 95% of the breast carcinomas; thereof 31% showed an additional nuclear LASP-1 staining (Figure 1, Table 1). A low cytoplasmic expression correlated with negative/low nuclear staining and a high cytoplasmic LASP-1-expression with high nuclear localisation (Table 1).

The prognostic effect of nuclear and cytosolic LASP-1 staining was further tested using the Kaplan-Meier survival analysis. There was a significant correlation ($P=0.025$) between patients with positive nuclear LASP-1 staining and poor overall survival (OS) (Figure 4A, Table 2) while there was no significant association between OS and cytoplasmic LASP-1 staining (Figure 4B, $P=0.404$). Surprisingly, a relationship between high positive nuclear staining and low grading ($P=0.025$) was observed, whereas all other clinical parameters analysed (i.e., nodal status, oestrogen and progesterone receptor status, recurrence) did not correlate with nuclear LASP-1-localisation (Table 3).

Table 1 Analysis of overall survival in relation to LASP-1 staining intensity

| LASP-1 staining intensity | No. of patients | Positive nuclear LASP-1 staining | No. of deceased patients | Overall survival (%) |
|---------------------------|-----------------|----------------------------------|--------------------------|----------------------|
| Score 0 | 9 | 0 (0%) | 0 | 100 |
| Score 1 | 46 | 6 (13%) | 7 | 84.8 |
| Score 2 | 109 | 46 (42.2%) | 27 | 75.2 |
| Score 3 | 13 | 4 (28.5%) | 4 | 69.2 |
| Total | 177 | 56 (31%) | 38 | 89.6 |

Abbreviation: LASP-1 = LIM and SH3 protein 1.

**Figure 4** Outcome of patients with nuclear and cytosolic LASP-1 localisation. Kaplan-Meier plots measuring patients OS in years against cumulative survival for nuclear (A) and cytosolic (B) LASP-1 staining. The analysis included patients diagnosed from 1985 to 2007 ($n=177$). Nuclear LASP-1-positivity is associated with poor OS.**Table 2** Analysis of overall survival in relation to nuclear LASP-1-positivity

| Nuclear LASP-1-positivity | No. of patients | No. of deceased patients | Overall survival (%) |
|---------------------------|-----------------|--------------------------|----------------------|
| No | 121 | 21 | 82.6 |
| Yes | 56 | 17 | 69.6 |

Abbreviation: LASP-1 = LIM and SH3 protein 1.

Rate of nuclear LASP-1-localisation increases during proliferation and augments in G2/M phase

There are two facts regarding LASP-1 that seem to be linked: (a) the prominent nuclear localisation of LASP-1 in primary breast

Table 3 Univariate analysis of positive nuclear LASP-1 staining and clinicopathological parameters

| Parameters | Positive nuclear LASP-1 staining | P-value |
|----------------------|----------------------------------|----------|
| Nodal status | | |
| N+ ($n=83$) | 31 (37.3%) | 0.2 (F) |
| N- ($n=94$) | 25 (26.6%) | |
| Tumour size | | |
| Tis ($n=3$) | 0 (0.0%) | |
| T1 ($n=108$) | 37 (34.3%) | |
| T2 ($n=51$) | 15 (29.4%) | |
| T3 ($n=5$) | 2 (40.0%) | |
| T4 ($n=10$) | 2 (20.0%) | |
| Metastasis | | |
| M+ ($n=6$) | 1 (16.7%) | |
| M- ($n=171$) | 55 (32.2%) | |
| Grading | | |
| G1 ($n=7$) | 4 (57.1%) | 0.03 (M) |
| G2 ($n=69$) | 27 (39.1%) | |
| G3 ($n=45$) | 9 (20.0%) | |
| Recurrence | | |
| Yes ($n=36$) | 8 (22.2%) | 0.38 (F) |
| No ($n=87$) | 27 (31.0%) | |
| ER | | |
| ER+ ($n=98$) | 28 (28.6%) | 0.3 (F) |
| ER- ($n=62$) | 23 (37.1%) | |
| Progesteron receptor | | |
| PR+ ($n=86$) | 22 (25.6%) | 0.13 (F) |
| PR- ($n=71$) | 27 (38.0%) | |
| HER2/neu | | |
| Her+ ($n=27$) | 6 (33.3%) | 0.77 (F) |
| Her- ($n=47$) | 18 (28.1%) | |

Abbreviations: ER = oestrogen receptor; F = Fisher's exact test; LASP-1 = LIM and SH3 protein 1; M = Mann-Whitney Test; PR = progesterone receptor. Statistical significance is assumed when $P<0.05$.

cancer (Figure 1) (Grunewald *et al*, 2007a) and (b) cell cycle arrest at G2/M accompanied by reduced cell proliferation after knock-down of LASP-1 in breast carcinoma cell lines (Grunewald *et al*, 2006). Therefore, it was tempting to speculate that the rate of nuclear LASP-1-localisation might be cell cycle dependent. To test this hypothesis, BT-20 cell lysates were subjected to cytoplasmic and nuclear fractioning. Purity of the fractions was confirmed by probing western blot membranes for the nucleus marker Lamin A + B and the cytoplasmic marker GAPDH. Figure 5A shows that there was virtually no cross-contamination.

In cells with an asynchronous cell cycle, in non-proliferating G0 phase cells (resting/senescent) and in G1 phase cells (G1/S-checkpoint), LASP-1 was found primarily within the cytoplasm (95%) (Figures 5A and B). During proliferation (S-phase) the nuclear LASP-1 concentration increased up to 10% and reached a peak at G2/M phase (G2/M) although the overall LASP-1 protein level did not change (data not shown).

As LPP and Zyxin are known binding partners of LASP-1 (Keicher *et al*, 2004; Li *et al*, 2004) and are discussed as possible shuttle proteins to transfer LASP-1 into the nucleus we also controlled their distribution during cell cycle phases. Consistently, like LASP-1, both proteins showed a cell phase-dependent nuclear increase in G2/M (Figure 5B) without changes in absolute protein concentration. All cell cycle phases were controlled by flow cytometry (Figure 5C).

To further validate the influence of nuclear LASP-1 occurrence on cell proliferation, we quantified the number of positive stained

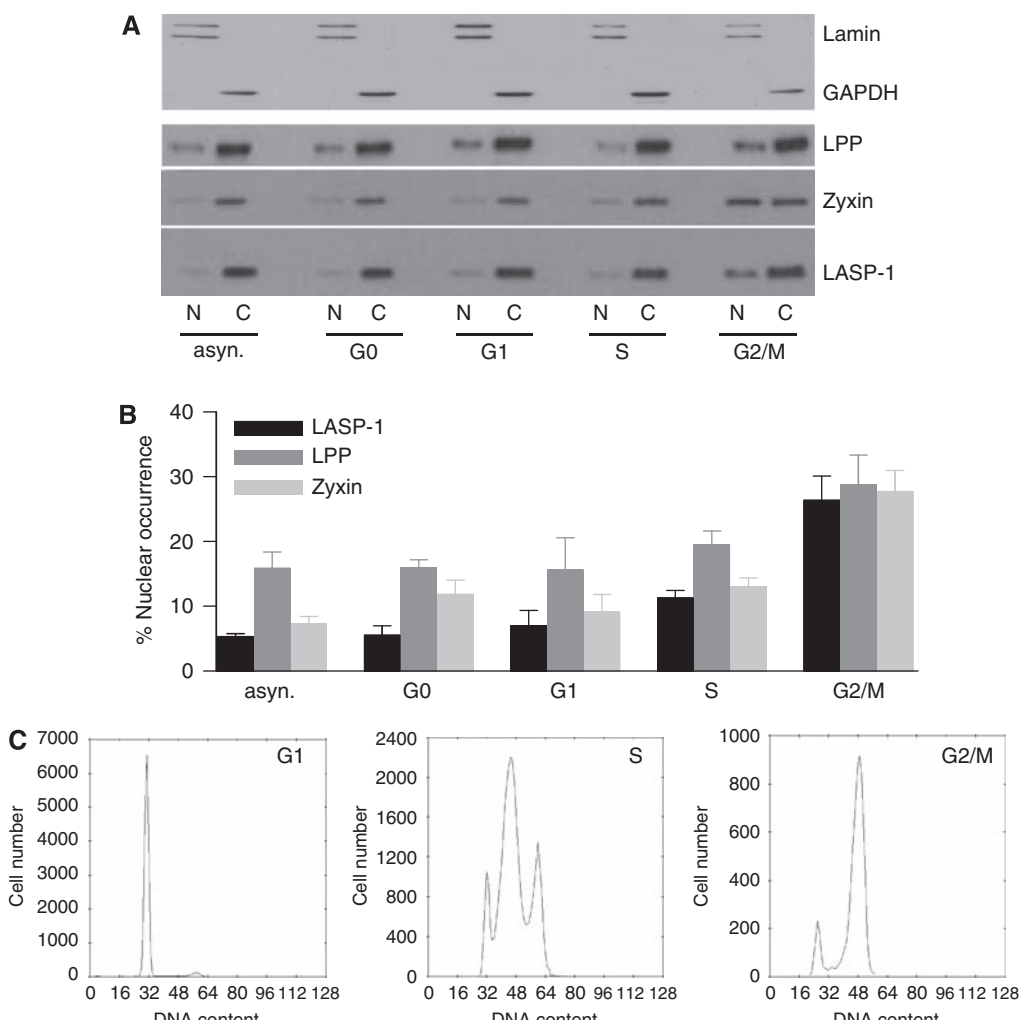


Figure 5 Cell cycle-dependent nuclear and cytosolic LASP-1 distribution. **(A)** Western blotting of nuclear (N) and cytosolic (C) proteins levels of LPP, Zyxin and LASP-1 in BT-20 cells synchronised to G0, G1, S and G2/M phase. Purity of nuclear and cytosolic fractions was controlled by Lamin A + B and GAPDH western blots, respectively. **(B)** Percentage of nuclear LPP, Zyxin and LASP-1 protein concentration (expressed as percentage of total cellular LPP, Zyxin and LASP-1 protein levels, respectively) plotted against cell cycle phases. **(C)** Flow-cytometric analysis of cell cycle phases (propidium iodide staining of total DNA).

cells for the proliferation marker Ki67 in 30 breast cancer tissue samples with known high LASP-1 IRS ≥ 8 and either nuclear or cytosolic LASP-1 localisation.

Although only 30.7% of the invasive ductal carcinoma samples with cytosolic LASP-1 expression are positive for Ki67 staining, 68.7% of the breast cancer tissues with nuclear LASP-1 occurrence show positive staining for the proliferation marker Ki67 (χ^2 test; $P=0.04$).

DISCUSSION

The *LASP1* gene was initially identified from a cDNA library of metastatic axillary lymph nodes (MLN) from human breast cancer and therefore called *MLN50*. The gene was mapped to chromosomal region 17q11-q21.3, a region known to contain the *c-erbB-2* (HER-2/neu) and the *BRCA1* oncogene and to be altered in 20–30% of all breast cancers (Tomasetto *et al*, 1995a, b). Since its discovery in 1995, several experimental approaches have been carried out to determine the cause of LASP-1 overexpression and its regulatory mechanisms. For instance, LASP-1 overexpression was reported to be due to *LASP1* gene amplification detected in 12 out of 98 tested whole breast cancer samples (Bieche *et al*, 1996)

while Tomasetto *et al* detected an amplification of *LASP1* only in one (BT-474) out of eight different breast cancer cell lines (Tomasetto *et al*, 1995b). Others observed deregulation of normal LASP-1-expression in relation to changes in PDEF and urokinase-type plasminogen activator (uPA) concentration or because of loss of p53 tumour suppressor activity (Turner *et al*, 2008; Salvi *et al*, 2009; Wang *et al*, 2009).

However, in this work, we analysed the expression pattern of LASP-1 in primary invasive breast cancers using micro-dissected tissues. Our data clearly show that the *LASP1* gene is not amplified in the vast majority of human breast cancers (only 1 out of 64 cases), suggesting that LASP-1 overexpression is mediated through transcriptional regulation rather than gene amplification. In the context of transcriptional regulation, we revealed that LASP-1 overexpression does not correlate *per se* with defects in the tumour suppressor protein p53 transcriptionally repressing LASP-1 (Wang *et al*, 2009). Although the data for the regulation of *LASP1* gene expression by p53 are convincing, there are clearly additional mechanisms involved in LASP-1 protein upregulation such as transcriptional cofactors and decay rates than just functional defects in p53.

As for PDEF, we could not confirm an association between low PDEF protein expression and high LASP-1 levels although

Turner *et al* showed that re-expression of PDEF in cells with low PDEF protein expression resulted in reduced LASP-1 levels (Turner *et al*, 2008).

However, PDEF mRNA concentration and protein expression in breast cancer cell lines is discussed controversially. As reported earlier, PDEF protein detection did not always correspond to PDEF mRNA levels. Although some studies showed increased PDEF mRNA (Turcotte *et al*, 2007) or protein expression in invasive ductal carcinoma (Sood *et al*, 2007) others observed reduced protein expression in breast cancer cells (Feldman *et al*, 2003; Doane *et al*, 2006; Ghadesshi *et al*, 2007; Turner *et al*, 2008). Recently, this discrepancy was explained by the identification of two microRNAs in human breast tumour samples that directly repressed PDEF protein expression in spite of the detection of high PDEF mRNA concentration (Findlay *et al*, 2008).

In a recent paper by Grunewald *et al*, LASP-1 was reported to be highly expressed in invasive breast carcinomas compared with fibroadenomas. Strong cytoplasmic staining for LASP-1 was found in 55.4% of the invasive breast tumours (Grunewald *et al*, 2007a). In addition to the reported localisation at focal contacts and lamellipodia, a perinuclear and nuclear distribution of the protein was observed. These data hint to a potential additional signalling function of LASP-1 as a shuttle protein thereby transducing growth signals from the sites of cellular contacts with the ECM into the nucleus.

In support of this hypothesis, this work shows a cell cycle-dependent increase of nuclear LASP-1 during the mitotic G2/M phase in proliferating tumour cells (Figure 5C) while serum-starved quiescent cells (G0) as well as cells in G1 and S-phase show only minor levels of the protein in the nucleus. Our observations are consistent with earlier data showing a specific cell cycle arrest at G2/M and inhibition of cell proliferation after LASP-1 knock-down in breast and ovarian cancer cell lines (Grunewald *et al*, 2006, 2007a, b). In reverse, a high LASP-1 concentration in the nucleus would show sustained cell proliferation. In fact, we found that approximately 70% of the patient samples with nuclear LASP-1 staining were positive for the cell proliferation marker Ki67 while only 30% of the patients with cytosolic LASP-1 expression showed positive Ki67 staining.

Consistently, earlier studies revealed a correlation between LASP-1-expression and tumour size as well as nodal-positivity in human breast carcinoma (Grunewald *et al*, 2007a). The present continuative long-term follow-up strengthens the assumed link between increased nuclear LASP-1-localisation and poor survival of patients with breast cancer suggesting an effect of nuclear LASP-1 on cell proliferation, especially because the absolute amount of cytosolic LASP-1-expression does not correlate with patients' OS.

Unexpectedly, we found a high nuclear localisation of LASP-1 in differentiated G1 tumours while in parallel nuclear LASP-1 abundance was correlated with worse prognosis. It is possible that tumours with a high nuclear LASP-1-expression represent a subgroup with poor survival irrespective of the grading. This could, for example, be due to a decreased response to endocrine or chemotherapeutic treatment. However, the number of available G1 tumours was very low. Therefore, we will not draw definitive conclusions regarding these data.

On the molecular level, the zinc-finger containing LIM-domain of LASP-1 offers a possibility for direct binding to DNA (Hammarstrom *et al*, 1996). LASP-1 may even form heterodomains to become a nuclear transcription factor (Kadomas and Beckerle, 2004).

Although LASP-1 sequence analysis revealed no nuclear localisation signal, the classical import pathway for the nucleus (Kutay and Guttinger, 2005), LASP-1 binds to the well-characterised shuttle proteins and transcription factors LPP and Zyxin that are upregulated in a wide variety of human cancers (Beckerle, 1997; Petit *et al*, 2003; Keicher *et al*, 2004; Li *et al*, 2004; Grunewald *et al*, 2009). For Zyxin, it is known that during mitosis a fraction of the cytoplasmic-dispersed protein becomes phosphorylated (most likely by Cdc2 kinase) and associates with the tumour suppressor h-warts (LATS1), a key governor of G2/M-progression, at the mitotic apparatus (Hirota *et al*, 2000).

Our data suggest that pathophysiological localisation of LASP-1 in the nucleus of malignant cells may induce mitosis and thereby enhance cell proliferation, possibly in concert with Zyxin and LPP. Further work will be needed to identify the nuclear shuttle partner(s) of LASP-1, the mechanism of nuclear translocation and the regulation of cell cycle progression.

The present continuative long-term follow-up provides evidence for the relation of increased nuclear LASP-1-localisation and poor survival of patients leading to the question whether nuclear LASP-1-positivity defines a subgroup of patients with unfavourable prognosis that is not responding to conventional treatment approaches. Future work is on the way to elucidate the precise molecular and clinical effect of LASP-1 nuclear overexpression.

ACKNOWLEDGEMENTS

We thank Dr Christian Korn for his help with the LEICA laser micro-dissection microscope and Petra Thalheimer for technical assistance.

Supplementary Information accompanies the paper on British Journal of Cancer website (<http://www.nature.com/bjc>)

REFERENCES

Beckerle MC (1997) Zyxin: zinc fingers at sites of cell adhesion. *Bioessays* **19**: 949–957

Bieche I, Tomasetto C, Regnier CH, Moog-Lutz C, Rio MC, Lidereau R (1996) Two distinct amplified regions at 17q11-q21 involved in human primary breast cancer. *Cancer Res* **56**: 3886–3890

Butt E, Gambaryan S, Gottfert N, Galler A, Marcus K, Meyer HE (2003) Actin binding of human LIM and SH3 protein is regulated by cGMP- and cAMP-dependent protein kinase phosphorylation on serine 146. *J Biol Chem* **278**: 15601–15607

Chew CS, Chen X, Parente Jr JA, Tarrer S, Okamoto C, Qin HY (2002) Lasp-1 binds to non-muscle F-actin *in vitro* and is localized within multiple sites of dynamic actin assembly *in vivo*. *J Cell Sci* **115**: 4787–4799

Dalton LW, Pinder SE, Elston CE, Ellis IO, Page DL, Dupont WD, Blamey RW (2000) Histologic grading of breast cancer: linkage of patient outcome with level of pathologist agreement. *Mod Pathol* **13**: 730–735

Dimova I, Orsetti B, Negre V, Rouge C, Ursule L, Lasorsa L, Dimitrov R, Doganov N, Toncheva D, Theillet C (2009) Genomic markers for ovarian cancer at chromosomes 1, 8 and 17 revealed by array CGH analysis. *Tumori* **95**: 357–366

Doane AS, Danso M, Lal P, Donaton M, Zhang L, Hudis C, Gerald WL (2006) An estrogen receptor-negative breast cancer subset characterized by a hormonally regulated transcriptional program and response to androgen. *Oncogene* **25**: 3994–4008

Ehrig T, Abdulkadir SA, Dintzis SM, Milbradt J, Watson MA (2001) Quantitative amplification of genomic DNA from histological tissue sections after staining with nuclear dyes and laser capture microdissection. *J Mol Diagn* **3**: 22–25

Feldman RJ, Sementchenko VI, Gayed M, Fraig MM, Watson DK (2003) Pdef expression in human breast cancer is correlated with invasive potential and altered gene expression. *Cancer Res* **63**: 4626–4631

Findlay VJ, Turner DP, Moussa O, Watson DK (2008) MicroRNA-mediated inhibition of prostate-derived Ets factor messenger RNA translation affects prostate-derived Ets factor regulatory networks in human breast cancer. *Cancer Res* **68**: 8499–8506

Ghaderohi A, Pan D, Fayazi Z, Hicks DG, Winston JS, Li F (2007) Prostate-derived Ets transcription factor (PDEF) downregulates survivin expression and inhibits breast cancer cell growth *in vitro* and xenograft tumor formation *in vivo*. *Breast Cancer Res Treat* **102**: 19–30

Godfrey TE, Kim SH, Chavira M, Ruff DW, Warren RS, Gray JW, Jensen RH (2000) Quantitative mRNA expression analysis from formalin-fixed, paraffin-embedded tissues using 5' nuclease quantitative reverse transcription-polymerase chain reaction. *J Mol Diagn* **2**: 84–91

Grunewald TG, Butt E (2008) The LIM and SH3 domain protein family: structural proteins or signal transducers or both? *Mol Cancer* **7**: 31

Grunewald TG, Kammerer U, Kapp M, Eck M, Dietl J, Butt E, Honig A (2007a) Nuclear localization and cytosolic overexpression of LASP-1 correlates with tumor size and nodal-positivity of human breast carcinoma. *BMC Cancer* **7**: 198

Grunewald TG, Kammerer U, Schulze E, Schindler D, Honig A, Zimmer M, Butt E (2006) Silencing of LASP-1 influences zyxin localization, inhibits proliferation and reduces migration in breast cancer cells. *Exp Cell Res* **312**: 974–982

Grunewald TG, Kammerer U, Winkler C, Schindler D, Sickmann A, Honig A, Butt E (2007b) Overexpression of LASP-1 mediates migration and proliferation of human ovarian cancer cells and influences zyxin localisation. *Br J Cancer* **96**: 296–305

Grunewald TG, Pasedag SM, Butt E (2009) Cell adhesion and transcriptional activity—defining the role of the novel protooncogene LPP. *Transl Oncol* **2**: 107–116

Hammarstrom A, Berndt KD, Sillard R, Adermann K, Otting G (1996) Solution structure of a naturally-occurring zinc-peptide complex demonstrates that the N-terminal zinc-binding module of the Lasp-1 LIM domain is an independent folding unit. *Biochemistry* **35**: 12723–12732

Hanahan D, Weinberg RA (2000) The hallmarks of cancer. *Cell* **100**: 57–70

Hirota T, Morisaki T, Nishiyama Y, Marumoto T, Tada K, Hara T, Masuko N, Inagaki M, Hatakeyama K, Saya H (2000) Zyxin, a regulator of actin filament assembly, targets the mitotic apparatus by interacting with h-warts/LATS1 tumor suppressor. *J Cell Biol* **149**: 1073–1086

Jemal A, Siegel R, Ward E, Murray T, Xu J, Thun MJ (2007) Cancer statistics, 2007. *CA Cancer J Clin* **57**: 43–66

Kadomas JL, Beckerle MC (2004) The LIM domain: from the cytoskeleton to the nucleus. *Nat Rev Mol Cell Biol* **5**: 920–931

Kallioniemi OP, Kallioniemi A, Piper J, Isola J, Waldman FM, Gray JW, Pinkel D (1994) Optimizing comparative genomic hybridization for analysis of DNA sequence copy number changes in solid tumors. *Genes Chromosomes Cancer* **10**: 231–243

Keicher C, Gambaryan S, Schulze E, Marcus K, Meyer HE, Butt E (2004) Phosphorylation of mouse LASP-1 on threonine 156 by cAMP- and cGMP-dependent protein kinase. *Biochem Biophys Res Commun* **324**: 308–316

Kutay U, Guttinger S (2005) Leucine-rich nuclear-export signals: born to be weak. *Trends Cell Biol* **15**: 121–124

Lehmann U, Kreipe H (2001) Real-time PCR analysis of DNA and RNA extracted from formalin-fixed and paraffin-embedded biopsies. *Methods (San Diego, CA)* **25**: 409–418

Li B, Zhuang L, Trueb B (2004) Zyxin interacts with the SH3 domains of the cytoskeletal proteins LIM-nebulette and Lasp-1. *J Biol Chem* **279**: 20401–20410

Mauriac L, Debled M, MacGrogan G (2005) When will more useful predictive factors be ready for use? *Breast (Edinburgh, Scotland)* **14**: 617–623

Nakagawa H, Terasaki AG, Suzuki H, Ohashi K, Miyamoto S (2006) Short-term retention of actin filament binding proteins on lamellipodial actin bundles. *FEBS Lett* **580**: 3223–3228

Petit MM, Meulemans SM, Van de Ven WJ (2003) The focal adhesion and nuclear targeting capacity of the LIM-containing lipoma-preferred partner (LPP) protein. *J Biol Chem* **278**: 2157–2168

Remmeli W, Stegner HE (1987) Recommendation for uniform definition of an immunoreactive score (IRS) for immunohistochemical estrogen receptor detection (ER-ICA) in breast cancer tissue. *Pathologe* **8**: 138–140

Ross JS, Fletcher JA (1999) The HER-2/neu oncogene: prognostic factor, predictive factor and target for therapy. *Semin Cancer Biol* **9**: 125–138

Rozen S, Skaletsky H (2000) Primer3 on the WWW for general users and for biologist programmers. *Methods Mol Biol (Clifton, NJ)* **132**: 365–386

Salvi A, Bongarzone I, Micciche F, Arici B, Barlati S, De Petro G (2009) Proteomic identification of LASP-1 down-regulation after RNAi urokinase silencing in human hepatocellular carcinoma cells. *Neoplasia (New York, NY)* **11**: 207–219

Schreiber V, Moog-Lutz C, Regnier CH, Chenard MP, Boeuf H, Vonesch JL, Tomasetto C, Rio MC (1998) Lasp-1, a novel type of actin-binding protein accumulating in cell membrane extensions. *Mol Med* **4**: 675–687

Singletary SE, Connolly JL (2006) Breast cancer staging: working with the sixth edition of the AJCC cancer staging manual. *CA Cancer J Clin* **56**: 37–47; quiz 50–1

Sood AK, Saxena R, Groth J, Desouki MM, Cheewakriangkrai C, Rodabaugh KJ, Kasyapa CS, Geradts J (2007) Expression characteristics of prostate-derived Ets factor support a role in breast and prostate cancer progression. *Human Pathol* **38**: 1628–1638

Sun HJ, Bahk YY, Choi YR, Shim JH, Han SH, Lee JW (2006) A proteomic analysis during serial subculture and osteogenic differentiation of human mesenchymal stem cell. *J Orthop Res* **24**: 2059–2071

Tan PH, Bay BH, Yip G, Selvarajan S, Tan P, Wu J, Lee CH, Li KB (2005) Immunohistochemical detection of Ki67 in breast cancer correlates with transcriptional regulation of genes related to apoptosis and cell death. *Mod Pathol* **18**: 374–381

Tomasetto C, Moog-Lutz C, Regnier CH, Schreiber V, Bassett P, Rio MC (1995a) Lasp-1 (MLN 50) defines a new LIM protein subfamily characterized by the association of LIM and SH3 domains. *FEBS Lett* **373**: 245–249

Tomasetto C, Regnier C, Moog-Lutz C, Mattei MG, Chenard MP, Lidereau R, Bassett P, Rio MC (1995b) Identification of four novel human genes amplified and overexpressed in breast carcinoma and localized to the q11-q21.3 region of chromosome 17. *Genomics* **28**: 367–376

Turcotte S, Forget MA, Beauseigle D, Nassif E, Lapointe R (2007) Prostate-derived Ets transcription factor overexpression is associated with nodal metastasis and hormone receptor positivity in invasive breast cancer. *Neoplasia (New York, NY)* **9**: 788–796

Turner DP, Findlay VJ, Kirven AD, Moussa O, Watson DK (2008) Global gene expression analysis identifies PDEF transcriptional networks regulating cell migration during cancer progression. *Mol Biol Cell* **19**: 3745–3757

Wang B, Feng P, Xiao Z, Ren EC (2009) LIM and SH3 protein 1 (Lasp1) is a novel p53 transcriptional target involved in hepatocellular carcinoma. *J Hepatol* **50**: 528–537

Widakowich C, de Azambuja E, Gil T, Cardoso F, Dinh P, Awada A, Piccart-Gebhart M (2007) Molecular targeted therapies in breast cancer: where are we now? *Int J Biochem Cell Biol* **39**: 1375–1387

Loss of tumor suppressor mir-203 mediates overexpression of LIM and SH3 Protein 1 (LASP1) in high-risk prostate cancer thereby increasing cell proliferation and migration

Amelie Hailer^{1,*}, Thomas GP Grunewald^{2,*}, Martin Orth¹, Cora Reiss¹, Burkhard Kneitz³, Martin Spahn³ and Elke Butt¹

¹ Institute for Clinical Biochemistry and Pathobiochemistry, University Clinic of Wuerzburg, Grobmuehlstrasse 12, 97080 Wuerzburg, Germany

² INSERM Unit 830, Genetics and Biology of Cancers, Institute Curie Research Center, 26 rue d'Ulm, 75248 Paris, France

³ Urology and Pediatric Urology, University Clinic of Wuerzburg, Oberduerrbacher Strasse 6, 97080 Wuerzburg, Germany

* These authors contributed equally to this work

Correspondence to: Elke Butt, **email:** butt@klin-biochem.uni-wuerzburg.de

Keywords: LASP1, prostate cancer, mir-203, PSA, LNCaP

Received: March 18, 2014

Accepted: April 25, 2014

Published: April 27, 2014

This is an open-access article distributed under the terms of the Creative Commons Attribution License, which permits unrestricted use, distribution, and reproduction in any medium, provided the original author and source are credited.

ABSTRACT

Several studies have linked overexpression of the LIM and SH3 domain protein 1 (LASP1) to progression of breast, colon, liver, and bladder cancer. However, its expression pattern and role in human prostate cancer (PCa) remained largely undefined.

Analysis of published microarray data revealed a significant overexpression of LASP1 in PCa metastases compared to parental primary tumors and normal prostate epithelial cells. Subsequent gene-set enrichment analysis comparing LASP1-high and -low PCa identified an association of LASP1 with genes involved in locomotory behavior and chemokine signaling. These bioinformatic predictions were confirmed *in vitro* as the inducible short hairpin RNA-mediated LASP1 knockdown impaired migration and proliferation in LNCaP prostate cancer cells.

By immunohistochemical staining and semi-quantitative image analysis of whole tissue sections we found an enhanced expression of LASP1 in primary PCa and lymph node metastases over benign prostatic hyperplasia. Strong cytosolic and nuclear LASP1 immunoreactivity correlated with PSA progression. Conversely, qRT-PCR analyses for mir-203, which is a known translational suppressor of LASP1 in matched RNA samples revealed an inverse correlation of LASP1 protein and mir-203 expression. Collectively, our results suggest that loss of mir-203 expression and thus uncontrolled LASP1 overexpression might drive progression of PCa.

INTRODUCTION

Prostate cancer (PCa) is the most frequent cancer of men in the western world [1]. Although many PCa are rather indolent tumors and remain clinically stable for many years or even decades and do not require any treatment, more aggressive PCa subtypes metastasize early and are associated with dismal outcome [2-4]. In 1986, introduction of prostate specific antigen (PSA) testing has significantly improved early diagnosis of PCa [5]. However, although high serum PSA levels may correlate

with PCa aggressiveness [6], PSA testing has caused a stage shift to less aggressive PCa. Over-detection and over-treatment are the main drawbacks of PSA-testing and unintentionally affect patients' quality of life [7]. Consequently, there is an urgent need for prognostic biomarkers to discriminate indolent from highly aggressive PCa in order to better guide an individual patient's treatment.

Recently, Erho et al. [8] developed and validated a PCa genomic classifier set with 22 markers that predicts metastatic progression better than clinicopathologic

variables. The LIM and SH3 protein 1 (LASP1) is one of these markers.

LASP1 is a nucleo-cytosolic shuttling protein involved in migration, adhesion, proliferation and cell cycle progression of many cancers [9]. LASP1 was initially identified from a cDNA library of breast cancer metastases and the corresponding protein is overexpressed in more than 50% of all breast cancers [10-12]. Besides its function as a structural scaffolding protein at sites of actin assembly such as invadopodia and membrane ruffles [13], LASP1 likely acts as a signaling molecule transducing information from the cytoplasm into the nucleus [14]. LASP1 is expressed in virtually all normal tissues [9], but overexpressed in many cancer entities such as the aggressive pediatric brain tumor medulloblastoma [15] as well as breast [12], ovarian [16] and colorectal carcinoma [17]. Moreover, LASP1 overexpression correlates with adverse outcome in these cancer entities suggesting an oncogenic function of LASP1 [12, 15, 17]. Expression of LASP1 is regulated i) by tumor suppressor p53 on the genomic level as shown for hepatocellular carcinoma [18] and ii) on the protein level by microRNA mir-203 as described for esophageal squamous cell carcinoma [19], breast cancer [20], and PCa [21, 22].

Here, we investigated the LASP1 expression pattern in a large series of surgically treated high-risk PCa samples ($n=161$) and correlated LASP1 protein levels with mir-203 expression levels in a subset of the same tumors ($n=138$).

In addition, we investigated the effect of RNA interference mediated LASP1 knockdown in a metastatic PCa cell line.

Our data demonstrate for the first time that LASP1 is overexpressed in a subset of high-risk PCa and that this expression correlates with PSA progression. qRT-PCR revealed a correlation between high LASP1 protein levels and reduced mir-203 expression in the PCa tissue samples. Cell culture experiments underline the more proliferative and migratory PCa phenotype in high LASP1 expressing cells.

These data might represent a first step toward characterizing LASP1 as a promising novel candidate biomarker to discriminate indolent from aggressive PCa.

RESULTS

LASP1 mRNA expression is increased in prostate cancer metastases and is associated with pathways involved in cell migration

As LASP1 is overexpressed in several cancer entities [15-17], we assessed the LASP1 mRNA expression pattern in publicly available microarray datasets. Specifically, microarray data of primary PCa ($n=61$) and PCa metastases ($n=25$) were compared with normal prostate tissue ($n=18$). As displayed in Figure 1A,

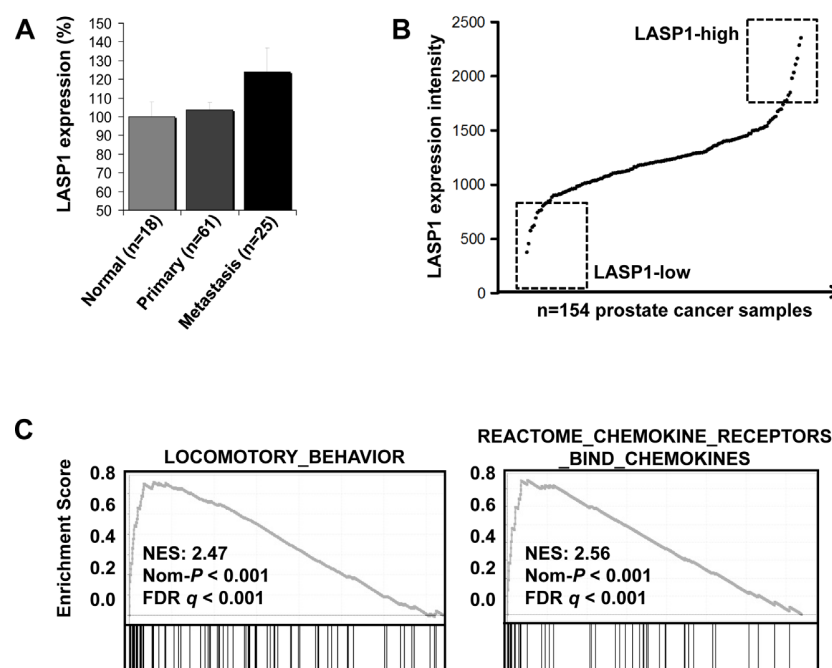


Figure 1: LASP1 mRNA expression is increased in prostate cancer metastases and is associated with pathways involved in cell migration A: LASP1 is significantly overexpressed in PCa metastases compared to parental primary tumors and normal prostate epithelial cells ($p=0.028$; Student's t test metastasis versus normal and primary). B: Gene expression signatures in the top 10 LASP1-high versus top 10 LASP1-low PCa samples by gene-set enrichment analysis (GSEA). C: GSEA analysis of the PCa microarray data, showing significant enrichment of genes involved in locomotory behaviour and chemokine signaling.

Table 1: Patient characteristics (n=161)

| Parameters | Median |
|--|----------------|
| Age at surgery, years (range) | 65.9 (43-81) |
| Mean follow-up, months (range) | 47.14 (1-105) |
| Nuclear LASP1 positivity | 56 (34.78%) |
| LASP1-IRS positivity | 39 (24.22%) |
| Clinical failure/ clinical recurrence | 19 (11.80%) |
| Mean preoperative PSA (ng/ml) (range) | 48.07 (20-160) |
| Death for any reason | 22 (13.66%) |
| Cancer related death (CRD) | 10 (6.21%) |
| Cancer specific survival, months (range) | 43.7 (14-63) |
| Biochemical progression / PSA progression | 41 (25.47%) |
| Average time to PSA progression, months (range) | 22.8 (1-54) |
| Average time to clinical progression, months (range) | 26.79 (3-89) |
| Gleason score | |
| 6 | 3 (1.86%) |
| 7 | 49 (30.43%) |
| 8 | 52 (32.3%) |
| 9 | 43 (26.71%) |
| 10 | 14 (8.7%) |
| Pathological tumor stage | |
| pT2 | 23 (14.29%) |
| pT3a | 44 (27.33%) |
| pT3b | 67 (41.61%) |
| pT4 | 27 (16.77%) |
| Lymph node positive | 59 (36.65%) |

LASP1 is significantly ($p=0.028$) overexpressed in PCa metastases compared to normal tissues and the primary tumor.

To investigate LASP1 correlated pathways, we analyzed a large PCa microarray study ($n=154$) for LASP1 expression. As displayed in Figure 1B, LASP1 is

moderately expressed in most PCa samples but appears to be overexpressed in about 15% of PCa samples (designated as LASP1-high). Subsequently, we compared the gene expression signatures in the top 10 LASP1-high versus top 10 LASP1-low PCa samples (Figure 1B and Supplemental Table 1) by gene-set enrichment analysis

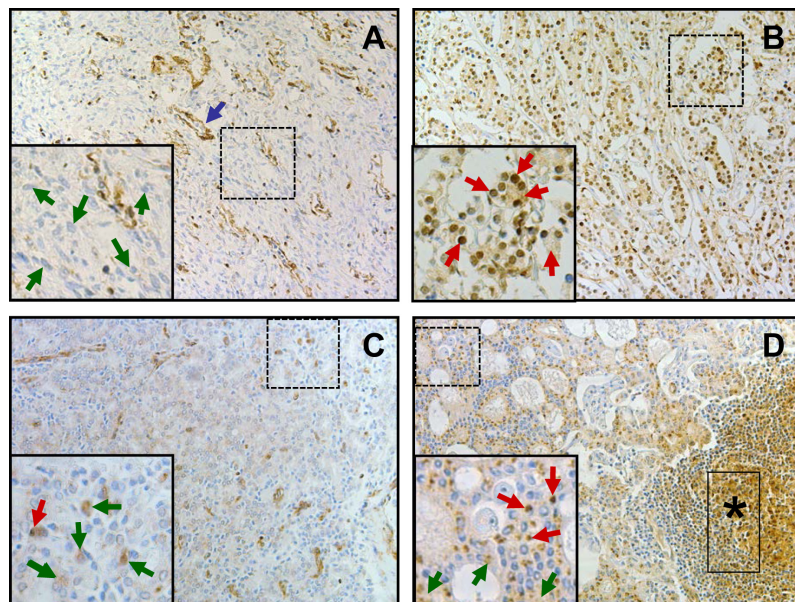


Figure 2: LASP1 protein expression is elevated in metastatic prostate cancer A: Representative immunostaining of BPH: most hyperplastic cells are LASP1 negative, both, for cytosol and nucleus (green arrows). Smooth muscle cells of blood vessels are positive for LASP1 (blue arrow). B: Representative PCa immunostaining (Gleason 8): most cells display positive LASP1 staining, both, for cytosol (IRS 4) and nuclei (red arrows). C and D: Prostate cancer (Gleason 8) with corresponding LNM, respectively: in PCa most cells are weak positive for cytosolic LASP1 staining (IRS 1) (green arrows). Few cells show additional positive nuclear LASP1 staining (red arrow). Compared to the primary tumor shown in C, in LNM (D) the overall cytosolic LASP1 staining (IRS 4) (green arrows) and the amount of cells with additional LASP1 positive nuclei (red arrows) are increased. LASP1 positive lymphocytes are marked with a black asterisk. (DAB, brown, magnification x40)

Table 2: LASP1 and mir-203 expression in BPH, PCa and LNM

| | Positive LASP1 nucleus ($\geq 10\%$) | Mean Nuclear staining (range) | Positive LASP1 (IRS>5) | Median IRS (range) | ΔCT mir-203 (subset) |
|-------------|---|--|------------------------------|--------------------------|------------------------------------|
| BPH (n=15) | 1 (6.7%) | 3.3 (0-13) | 1 (6.7%) | 2 (0-6) | -0.54 ± 0.16 (15) |
| PCa (n=161) | 56 (34.8%) | 16.3 (0-95) | 39 (24.2%) | 3 (0-12) | -1.54 ± 0.12 (138) |
| LNM (n=17) | 5 (29.4%) | 12.5 (2-50) | 2 (11.8%) | 4 (1-11) | -2.39 ± 0.26 (12) |

(GSEA). GSEA revealed that LASP1 overexpression in clinical PCa samples is strongly correlated ($p<0.001$) with

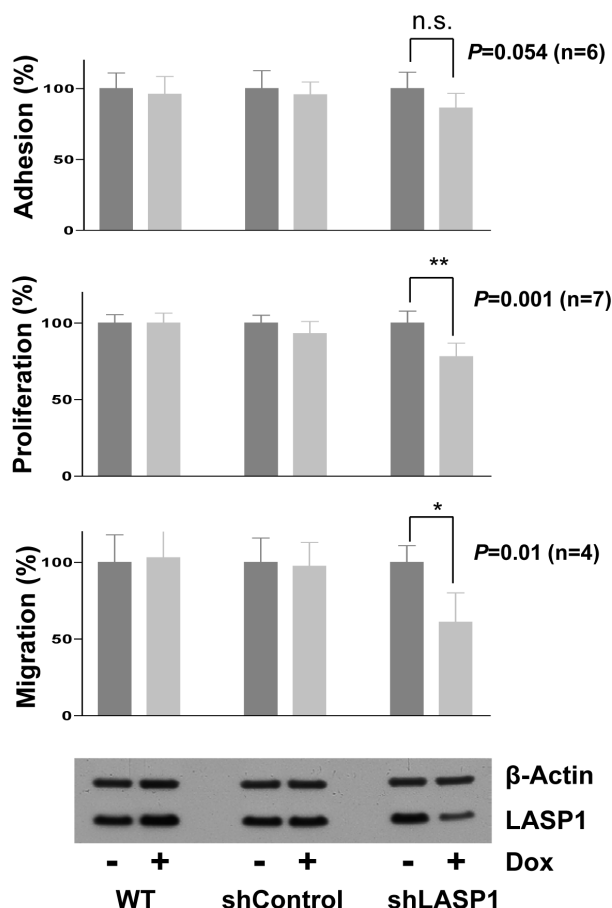


Figure 3: Silencing of LASP1 impairs proliferation and migration of prostate cancer cells *in vitro*. Used were non-transfected LNCaP wild type cells (WT) and cells stably transfected with control shRNA or shRNA against LASP1. Adhesion: After 4 days LASP1 knockdown, cells were seeded in 48-well plates and incubated for 7.5h. Adherent cells were counted using CellTiterGlo®. Proliferation: Cells were seeded in T25 flasks. Knockdown was induced with doxycycline (Dox) and cells were counted after 4 days. Migration: After 4 days LASP1 knockdown, cells were seeded in modified Boyden chambers and incubated for 4 h. Migrated cells were fixed, stained with crystal violet and absorbance was measured. Bar plots represent mean \pm SEM; p, Student's *t* test, *versus* control. LASP1 knockdown efficiency was controlled by Western blot. Actin is shown as loading control.

gene signatures involved in locomotory behaviour and chemokine signaling (Figure 1C). Collectively, these data indicate that LASP1 overexpression is associated with a more aggressive PCa phenotype.

LASP1 protein expression is elevated in metastatic prostate cancer

To validate our findings on LASP1 overexpression in a subset of PCa samples on protein level, we investigated the LASP1 protein expression pattern by immunohistochemistry (IHC) in specimens from 15 benign prostatic hyperplasias (BPH), 161 high-risk PCa derived from patients with pre-treatment PSA >20 ng/ml who underwent radical prostatectomy, and 17 corresponding lymph node metastases (LNM). Representative samples for the observed LASP1 immunoreactivity are shown in Figure 2. Analysis of the Immune Reactive Scores (IRS) revealed that the median expression of LASP1 increases from BPH (IRS 2.0 ± 1) to PCa (IRS 3.0 ± 2) and LNM (IRS 4.0 ± 1). Interestingly, only PCa and LNM showed very high IRS values up to 12 while in BPH, the IRS maximum is 6. Accordingly, a low cytosolic LASP1 expression correlated with negative/low nuclear staining and a high cytosolic expression with high nuclear LASP1 immunoreactivity ($p=0.0001$, Table 2). These analyses confirmed an increase of LASP1 protein levels in metastatic high-risk PCa.

Silencing of LASP1 impairs proliferation and migration of prostate cancer cells *in vitro*

To functionally assess the role of LASP1 in high-risk PCa, we used the LNCaP cell line, which is commonly used as an *in vitro* model for metastasized PCa [23]. LNCaP cells were stably transfected with inducible shRNA against LASP1 or a control shRNA. Doxycycline-induced LASP1 knockdown was confirmed for every experiment by Western blot (WB) and showed an average silencing of LASP1 of about 50% (Figure 3, lowest panel).

Proliferation was assessed by cell counting and revealed a significant inhibition of cell proliferation up to 31% upon LASP1 silencing (Figure 3). Similar results were obtained using a CellTiter-Glo® Luminescent assay

Table 3: Univariate analysis of positive nuclear LASP1 localisation and cytosolic LASP1 staining with clinicopathological parameters (n=161)

| Parameters (No. patients) | Positive nuclear LASP1 ($\geq 10\%$) | p-value | Positive cytosolic LASP1 (IRS >5) | p-value |
|---|---|-------------------------------------|---|-------------------------------------|
| Nodal status N+ (59) N- (102) | 16 (27.1%) 40 (39.2%) | 0.13 (F) | 7 (11.9%) 32 (31.4%) | 0.007 (F) |
| Tumour size pT2 (23) pT3a (44) pT3b (67) pT4 (27) | 11 (47.8%) 16 (36.4%) 19 (28.4%) 10 (37.0%) | 0.33 (M) | 11 (47.8%) 13 (29.5%) 9 (13.4%) 6 (22.2%) | 0.012 (M) |
| Gleason Score 6 (3) 7 (49) 8 (52) 9 (43) 10 (14) | 1 (33.3%) 18 (36.7%) 24 (46.2%) 9 (20.9%) 4 (28.6%) | 0.16 (M) | 0 (0.0%) 11 (22.4%) 15 (28.8%) 10 (23.3%) 3 (21.4%) | 0.84 (M) |
| Recurrence (19) PSA progress (41) Cancer related death (10) | 5 (26.3%) 22 (53.7%) 3 (30%) | 0.35 (LT) 0.02 (LT) 0.54 (LT) | 6 (31.6%) 16 (34.1%) 5 (50%) | 0.54 (LT) 0.04 (LT) 0.10 (LT) |

(F) Fisher's exact test, (M) Mann-Whitney-U-test; (LT) Log-rank test; statistical significance is assumed at $p < 0.05$.

(data not shown).

Since LASP1 has been shown to promote cell motility and metastasis in other tumor entities [17, 24] we analyzed cell migration and adhesion of LNCaP cells before and after LASP1 silencing with a modified

Boyden-chamber and an adhesion assay, respectively. We observed a strong reduction in migratory potential by 39% upon LASP1 silencing but no significant effect on adhesion (Figure 3). Taken together, these data provide evidence that LASP1 is functionally involved in PCa cell proliferation and migration.

Cytosolic and nuclear LASP positivity correlate with PSA progress

The prognostic impact of cytosolic and nuclear LASP1 immunoreactivity was tested using Kaplan-Meier survival analyses. We found a significant correlation between PSA recurrence, both, with nuclear LASP1

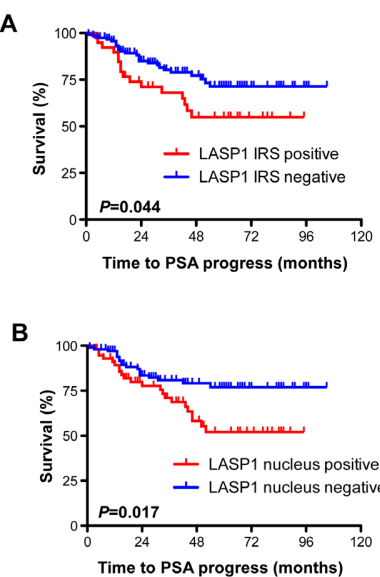


Figure 4: Cytosolic and nuclear LASP1 positivity correlate with PSA progress A: Kaplan-Meier plot displaying patients' probability for PSA progress stratified by cytosolic LASP1 positivity (IRS>5) and negativity (IRS<5) B: Kaplan-Meier plot displaying patients' probability for PSA progress stratified by nuclear LASP1 positivity (NUC $\geq 10\%$) and negativity (NUC<10%).

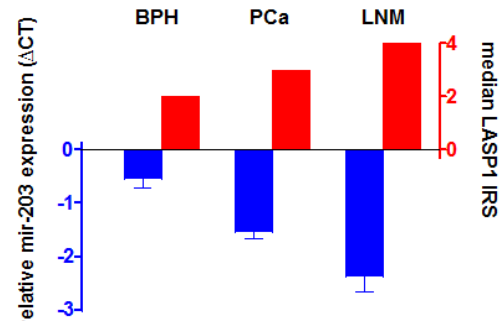


Figure 5: miR-203 levels are reduced in prostate cancer Reduced miR-203 levels correspond to enhanced LASP1 protein concentrations. miR-203 expression was analysed by qRT-PCR. Relative miR-203 expression values are presented as mean \pm SEM.

positivity ($p=0.017$) and with strong LASP1 IRS ($p=0.044$) (Figure 4). These statistical associations were confirmed by univariate analysis (Table 3). For cancer related death (CRD), we failed to attend significance between cytosolic LASP1 levels and this parameter ($p=0.1$, Table 3). However, the overall number of deceased persons ($n=10$) was too low for a statistically robust conclusion on CRD (Table 1). Univariate analysis of the data revealed no correlation between Gleason score and high cytosolic or nuclear LASP1 immunoreactivity (Table 3). In synopsis, LASP1 protein expression correlates with PSA progress.

mir-203 levels are reduced in prostate cancer

To investigate the role of mir-203 on LASP1 expression in PCa, we assessed the mir-203 levels for a subset of our cohort described in Table 2 (15 BPH, 138 high-risk PCa and 12 corresponding PCa/LNM) by qRT-PCR and matched the RNA data with the LASP1 IRS values determined by IHC (Table 2). For PCa a significant correlation between high cytosolic LASP1 protein levels (IRS >5) as well as high nuclear LASP1 levels (NUC $\geq 10\%$) and reduced mir-203 expression is observed ($p=0.002$ and $p=0.038$, respectively). Expression levels of mir-203 are significantly reduced from BPH over PCa ($p=0.006$) to LNM ($p=0.036$) while in return LASP1 protein levels are increased, supporting the hypothesis of LASP1 as a potential marker for aggressive PCa (Figure 5).

DISCUSSION

Current clinical staging is unable to accurately identify PCa subsets that are prone to progress to aggressive lethal disease, even if high Gleason scores and elevated PSA levels are used as combined prognostic markers [25]. This has contributed to a serious dilemma of overtreatment [26]. In the present study we identified LASP1 as a potential new prognostic PCa biomarker since the protein is significantly overexpressed in PCa compared with BPH ($p=0.03$) in our cohort. Moreover, analysis of 17 specimens of PCa and their corresponding LNM exhibited higher LASP1 levels in metastases, which points to a role of LASP1 in tumor progression. In addition, we analyzed LASP1 expression in high-risk PCa (Gleason score >8 and PSA >20 ng/ml) and correlated the immunoreactive LASP1 scores with clinicopathological data, which yielded a significant correlation between cytosolic and nuclear LASP1 levels and PSA progression. Similarly, a correlation between nuclear LASP1 localisation and poor overall survival is observed in breast cancer [11]. For colorectal cancer [17] and medulloblastoma [15] no distinct differentiation between cytosolic and nuclear LASP1 positivity was performed but patient survival was again inversely correlated with global LASP1 expression.

Unexpectedly, no correlation with clinical progression is observed in our study (Table 3). However, on average it lasts 8 years from PSA progression to clinically overt metastasis [27]. Our median study follow up was 4 years, which might explain, at least in part, the lack of statistically association of LASP1 levels with clinical progression in our cohort.

In support of our observations in primary PCa, we found a functional role of LASP1 in LNCaP cells. Besides a moderate reduction of cell proliferation, we observed an impaired migration of LNCaP cells upon inducible shRNA-mediated LASP1 knockdown. These *in vitro* results correspond to the *in silico* predictions derived from our GSEA of microarrays of primary PCa, which showed an association of LASP1 expression with transcriptional signatures involved in locomotory pathways. In analogy, reduced cellular migration upon LASP1 knockdown was observed in medulloblastoma [15], breast cancer [24], and colorectal cancer [17]. Consistently, in several cancer entities such as breast cancer [20], bladder cancer [28], squamous cell carcinoma [19] and now PCa, increased LASP1 protein levels are connected to reduced mir-203 RNA levels and concomitant enhanced cell proliferation and migration.

Notably, in parallel to our experiments, Erho et al. identified LASP1 as one out of 22 marker in a PCa genomic classifier (GC) [8]. The study revealed that 60% of clinical high-risk patients would be reclassified as low-risk with a cumulative incidence of metastasis of only 2.4% at 5 years post radical prostatectomy. Conversely, patients with the highest GC score had nearly 10 times higher cumulative incidence of metastasis by 5 years. The value of this GC in routine clinical practice was assessed in two additional studies [29] [30].

In summary, our results suggest that LASP1 overexpression, most likely mediated by the loss of mir-203 expression, is involved in progression and metastasis of PCa. These data add further functional support for LASP1 being part of the new GC set that discriminates indolent from more aggressive PCa subtypes.

METHODS

Tissue samples and study population

Patients' clinicopathologic characteristics are summarized in Table 1. 161 archived paraffin-embedded tissue samples from human prostate cancer (PCa) with confirmed histological diagnoses (radical prostatectomy), 17 corresponding lymph node metastases (LNM) and samples of 15 benign prostatic hyperplasia (BPH) were obtained from the Department of Pathology of the University of Karlsruhe, Germany [31]. All studies were performed with the approval of the Institutional Review

board of the Universities of Wuerzburg and Karlsruhe and complied with national laws and the declaration of Helsinki. Grading of PCa malignancy was evaluated according to the Gleason score [32]. Tumor staging was conducted according to parameters of the TNM classification system [4]. Follow-up was performed every 3 months for the first 2 years after surgery, every 6 months in the following 3 years, and annually thereafter. Clinical recurrence is the clinical failure after prostatectomy defined either as histologically proven local recurrence or distant metastasis confirmed by a CT or bone scan that had the date of failure. Biochemical progression/PSA progression was defined as PSA ≥ 0.2 ng/ml on 2 consecutive follow-up visits.

Microarray and gene-set enrichment analyses (GSEA)

To compare LASP1 mRNA expression in malignant and normal prostate tissue publicly available microarray data of primary (n=61) and metastatic PCa (n=25) as well as normal prostate tissue (n=18) were retrieved from the Gene Expression Omnibus (GEO; accession numbers: GSE6604, GSE6605, GSE6606, Affymetrix HG-U95Av2 arrays). In addition a much larger publicly available gene expression data of a study analyzing n=154 individual PCa samples was retrieved from the GEO (accession number: GSE17951, Affymetrix HG-U133Aplus2.0 microarrays) for pathway analyses. Expression data were manually revised for their correct annotations and simultaneously normalized by Robust Multi-array Average (RMA) [33, 34] using custom brainarray (v15 and v17 ENTREZG) CDF files yielding one optimized probe-set for each gene corresponding to the ENTREZ gene ID as described elsewhere [35]. To identify pathways and biological processes associated with LASP1 overexpression in PCa we applied a gene-set enrichment analysis (GSEA) on the normalized microarray data [36]. GSEA was performed with 1000 permutations using a pre-ranked list composed of the log2-transformed fold changes of the median gene expression values comparing the top 10 LASP1-high with the top 10 LASP1-low PCa samples (Supplemental Table 1).

Immunohistochemistry

For immunostaining, sections were placed onto SuperFrost® slides (Langenbrinck, Emmendingen, Germany), dewaxed in xylene, rehydrated in graded ethanol and in dH₂O. For antigen retrieval, sections were subjected to heat pre-treatment by boiling in 0.01 M of sodium citrate buffer (pH 6.0) for 10 min in a microwave oven (750 Watt/sec.). Endogenous peroxidase was blocked by incubation in 0.1% hydrogen peroxide in PBS for 5 min. Slides were then incubated with the polyclonal anti-

LASP1 antibody [37] diluted 1:1000 in “antibody diluent” (DAKO, Hamburg, Germany) followed by EnVision/rabbit detection system (DAKO, Hamburg, Germany). All immunohistological samples were evaluated by two independent scientists for defining of the percentage of LASP1 positive cells and the cytosolic immunoreactivity. Scoring of cytosolic LASP1 expression was carried out in analogy to the scoring of the hormone receptor Immune Reactive Score (IRS), ranging from 0-12 according to Remmeli et al. and is described in detail for LASP1 in breast cancer [12, 38]. For better statistical discrimination, samples scored with cytosolic LASP1-IRS <5 were classified as LASP1-negative and those with LASP1-IRS >5 as LASP1-positive. Nuclear LASP1 positivity: Nuclear LASP1 positivity was scored by determining the percentage of positive nuclei regardless of cytosolic LASP1 immunoreactivity. Samples were considered as nuclear-positive if 10% or more cells showed nuclear LASP1 staining.

Cell lines and culture conditions

PCa cell line LNCaP derived from a lymph node metastasis was purchased from American Type Culture Collection (ATCC, Manassas, USA). Cells were grown in plastic cell culture flasks at 37°C under 5% CO₂ atmosphere in RPMI 1640 medium (Life Technologies, Darmstadt, Germany) containing 10% heat-inactivated fetal bovine serum (FBS), 1% penicillin/streptomycin, 1% non-essential amino acids and 1% pyruvate (all Invitrogen, Darmstadt, Germany). Mycoplasma contamination was ruled out by PCR.

mir-203 - qRT-PCR

Total RNA was extracted from PCa, LNM and BPH tissues with Total RNA Extraction Kit (Life Technologies). The RNA concentration was determined with a Bioanalyser (Biorad, Munich, Germany). cDNA was synthesized according to the TaqMan miR Assay protocol (Life Technologies). Mature mir expression was quantified in tissue samples with TaqManR mir assay kits and an Applied Biosystems 7900 HT system. We followed the protocol provided in the manufacturer's instruction (Applied Biosystems, Foster City, CA, USA). The expression of RNU6B was used for normalization. Relative mir expression was calculated with the ΔCt -method (ΔCt sample = Ct RNU6B - Ct sample). Calculations were carried out assuming equal RNA-concentrations and complete efficacy of qRT-PCR.

RNA interference

For generation of an inducible LASP1 knockdown, LNCaP cells were infected with lentivirus (MOI: 1:10) containing a pTRIPZ vector with either a short hairpin RNA (shRNA) against LASP1 (clone V2THS-64686 mature antisense sequence 5'-GGCAAGTGGAAATATCTTATAT-3', Thermo Scientific) or respective non-targeting control shRNA. Successfully transduced LNCaP were selected in 0.5 µg/ml puromycin (Invitrogen). Knockdown efficiency upon doxycycline-treatment (0.5µg/ml) was confirmed by WB.

Lentivirus production: 5.5x10⁶ HEK293T cells were seeded into a 100 mm cell culture dish coated with 0.01% poly-L-lysine (Sigma-Aldrich, Deisenhofen, Germany) one day prior to transfection and cultured in DMEM (Invitrogen) supplemented with 10% FBS, 1% penicillin/streptomycin (both Invitrogen). Arrest-In™ (Thermo Scientific) was used as transfection reagent. DNA/Arrest-In™ complexes were formed by mixing 9 µg of the particular pTRIPZ vector DNA, with 28.5 µg of optimized packaging plasmid mix (pTLA1-Pak, pTLA1-Enz, pTLA1-Env, pTLA1-Rev and pTLA1-TOFF, all Open Biosystems, Thermo Scientific) in 1ml DMEM with 187.5 µg Arrest-In™ diluted in 1ml DMEM. Supernatant was harvested 48h and 72h after transfection and lentiviral particles were isolated by filtration and subsequent ultracentrifugation.

Western blot (WB)

Cells were lysed in Laemmli-buffer containing 10% β-mercaptoethanol (Sigma-Aldrich). Equal amounts of cells were resolved by 10% SDS-PAGE. After blotting on a nitrocellulose membrane (Schleicher&Schuell, Dassel, Germany) the membrane was blocked with 3% nonfat dry milk (Biorad) in TBS-T buffer (10 mM TRIS, 150 mM NaCl, 0.1% (w/v) Tween, pH 7.5). Then the membrane was incubated with a self-generated primary antibody against LASP1 [35] diluted 1:8000 and anti-β-Actin by Santa Cruz (Santa Cruz, CA, USA) diluted 1:2000. Finally the membrane was washed with TBS-T and incubated with the secondary antibody goat-anti-rabbit horseradish peroxidase-coupled and diluted 1:5000 (Biorad). The amount of detected protein was visualized by enhanced chemiluminescence (Amersham Biosciences, Freiburg, Germany) and autoradiography. Quantification of autoradiography signals was carried out by densitometry using the ImageJ software (NIH, Bethesda, USA).

Proliferation assays

Non-transduced LNCaP cells and cells stable transduced with control shRNA or shRNA against LASP1

were seeded in 48-well plates. Per well 1x10⁴ cells were seeded. After 24 h, medium was replaced by medium +/- doxycycline (0.5 µg/ml). 96h after knockdown induction, cells were counted with CellTiter-Glo® Luminescent Cell Viability Assay (Promega) following manufacturer's instruction. Assays were performed in 5 independent experiments, each with 6 replicates. In addition, the experiment was performed in T25 flasks and cells were counted with Neubauer chamber. Knockdown of LASP1 was confirmed in each experiment by WB.

Adhesion assay

To assess cell adhesion non transduced LNCaP cells and cells stable transduced with control shRNA or shRNA against LASP1 were grown for 96h in media (as described previously) +/- doxycycline (0.5µg/ml). Cells were seeded in 48-well plates, per well 4x10⁴ cells in 100µl media. Cells were allowed to attach for 7.5 h at 37°C (ca. 50 % adhesion of control cells). In 5 of 8 wells, non-adherent cells were removed by gentle washing with PBS and wells were refilled with 100 µl medium. Wells with non washed-off cells served as 100 % value of seeded cells. Cells were counted with CellTiter-Glo® Luminescent Cell Viability Assay (Promega) following manufacturer's instruction. Assays were performed in 6 independent experiments, (each with 5 replicates). Knockdown of LASP1 was comfirmed in each experiment by WB.

Migration assay

Cellular migration was assessed by a modified Boyden chamber assay (transwell chambers, Corning Star, Cambridge, MA, USA). Cells were serum-starved overnight, trypsinized, adjusted for viability, counted, and re-suspended in serum-free medium to a concentration of 1x10⁶ cells/ml. Before the experiment, the lower surface of the filter membrane (8 µM pore size) was coated for 15 min with 100 µl fibronectin solution (5 µg/ml; Sigma-Aldrich) as a chemo-attractant. The inner filter chambers were coated with 100 µl 10% FBS in RPMI medium for 30 min. 100 µl cell suspension was placed in the upper filter chambers. The chambers were placed in 24-well plates and cultured in 500 µl RPMI medium with 10% FBS for 4 h at 37°C to allow the cells to migrate through the porous membrane. Non-migrated cells from the top surface were removed using a cotton swab. Migrated cells at the lower surface of the membranes were stained in 200 µl 1% (w/v) crystal violet in 2% ethanol in a 24-well plate for 30 sec and rinsed twice afterwards in distilled water. Cell-associated crystal violet was extracted by incubating the membrane in 200 µl 10% acetic acid for 20 min and measured at 595 nm absorbance using a plate reader (Molecular Devices, Crawley, UK). Four independent experiments, each with 6 replicates, were performed

AUTHOR CONTRIBUTIONS

AH, EB and TGPG designed the study, drafted and wrote the paper, and designed the display items. MS supplied and organized tumor tissue and patients data. AH, MO and TGPG carried out bioinformatics analyses. AH, MO, CR and BK performed the experiments.

ACKNOWLEDGMENTS

We thank Mrs. Petra Thalheimer and Mrs. Michaela Kapp for excellent technical assistance.

FUNDING

This work was supported by grants from the Deutsche Forschungsgemeinschaft (DFG) to TGPG (GR3728/2-1) and to EB (BU740/6-2).

CONFLICT OF INTEREST

The authors declare no conflict of interest.

REFERENCES

1. Ferlay J, Shin HR, Bray F, Forman D, Mathers C and Parkin DM. Estimates of worldwide burden of cancer in 2008: GLOBOCAN 2008. *International journal of cancer Journal international du cancer.* 2010; 127(12):2893-2917.
2. Klotz L, Zhang L, Lam A, Nam R, Mamedov A and Loblaw A. Clinical results of long-term follow-up of a large, active surveillance cohort with localized prostate cancer. *J Clin Oncol.* 28(1):126-131.
3. Cooperberg MR, Carroll PR and Klotz L. Active surveillance for prostate cancer: progress and promise. *Journal of clinical oncology : official journal of the American Society of Clinical Oncology.* 2011; 29(27):3669-3676.
4. Cheng L, Montironi R, Bostwick DG, Lopez-Beltran A and Berney DM. Staging of prostate cancer. *Histopathology.* 2012; 60(1):87-117.
5. Welch HG and Albertsen PC. Prostate cancer diagnosis and treatment after the introduction of prostate-specific antigen screening: 1986-2005. *Journal of the National Cancer Institute.* 2009; 101(19):1325-1329.
6. Collette L, de Reijke TM and Schroder FH. Prostate specific antigen: a prognostic marker of survival in good prognosis metastatic prostate cancer? (EORTC 30892). *European urology.* 2003; 44(2):182-189; discussion 189.
7. Antonarakis ES, Feng Z, Trock BJ, Humphreys EB, Carducci MA, Partin AW, Walsh PC and Eisenberger MA. The natural history of metastatic progression in men with prostate-specific antigen recurrence after radical prostatectomy: long-term follow-up. *BJU Int.* 2012; 109(1):32-39.
8. Erho N, Crisan A, Vergara IA, Mitra AP, Ghadessi M, Buerki C, Bergstrahl EJ, Kollmeyer T, Fink S, Haddad Z, Zimmermann B, Sierociński T, Ballman KV, Triche TJ, Black PC, Karnes RJ, et al. Discovery and validation of a prostate cancer genomic classifier that predicts early metastasis following radical prostatectomy. *PLoS One.* 2013; 8(6):e66855.
9. Grunewald TG and Butt E. The LIM and SH3 domain protein family: structural proteins or signal transducers or both? *Mol Cancer.* 2008; 7:31.
10. Tomasetto C, Moog-Lutz C, Regnier CH, Schreiber V, Basset P and Rio MC. Lasp-1 (MLN 50) defines a new LIM protein subfamily characterized by the association of LIM and SH3 domains. *FEBS letters.* 1995; 373(3):245-249.
11. Frietsch JJ, Grunewald TG, Jasper S, Kammerer U, Herterich S, Kapp M, Honig A and Butt E. Nuclear localisation of LASP-1 correlates with poor long-term survival in female breast cancer. *Br J Cancer.* 2010; 102(11):1645-1653.
12. Grunewald TG, Kammerer U, Kapp M, Eck M, Dietl J, Butt E and Honig A. Nuclear localization and cytosolic overexpression of LASP-1 correlates with tumor size and nodal-positivity of human breast carcinoma. *BMC Cancer.* 2007; 7:198.
13. Nakagawa H, Terasaki AG, Suzuki H, Ohashi K and Miyamoto S. Short-term retention of actin filament binding proteins on lamellipodial actin bundles. *FEBS Lett.* 2006; 580(13):3223-3228.
14. Mihlan S, Reiss C, Thalheimer P, Herterich S, Gaetzner S, Kremerskothen J, Pavenstadt HJ, Lewandrowski U, Sickmann A and Butt E. Nuclear import of LASP-1 is regulated by phosphorylation and dynamic protein-protein interactions. *Oncogene.* 2013; 32(16):2107-2113.
15. Traenka C, Remke M, Korshunov A, Bender S, Hielscher T, Northcott PA, Witt H, Ryzhova M, Felsberg J, Benner A, Riester S, Scheurlen W, Grunewald TG, von Deimling A, Kulozik AE, Reifenberger G, et al. Role of LIM and SH3 protein 1 (LASP1) in the metastatic dissemination of medulloblastoma. *Cancer Res.* 2010; 70(20):8003-8014.
16. Grunewald TG, Kammerer U, Winkler C, Schindler D, Sickmann A, Honig A and Butt E. Overexpression of LASP-1 mediates migration and proliferation of human ovarian cancer cells and influences zyxin localisation. *Br J Cancer.* 2007; 96(2):296-305.
17. Zhao L, Wang H, Liu C, Liu Y, Wang X, Wang S, Sun X, Li J, Deng Y, Jiang Y and Ding Y. Promotion of colorectal cancer growth and metastasis by the LIM and SH3 domain protein 1. *Gut.* 2010; 59(9):1226-1235.
18. Wang B, Feng P, Xiao Z and Ren EC. LIM and SH3 protein 1 (Lasp1) is a novel p53 transcriptional target involved in hepatocellular carcinoma. *Journal of hepatology.* 2009; 50(3):528-537.

19. Takesita N, Mori M, Kano M, Hoshino I, Akutsu Y, Hanari N, Yoneyama Y, Ikeda N, Isozaki Y, Maruyama T, Akanuma N, Miyazawa Y and Matsubara H. miR-203 inhibits the migration and invasion of esophageal squamous cell carcinoma by regulating LASP1. *International journal of oncology*. 2012; 41(5):1653-1661.

20. Wang C, Zheng X, Shen C and Shi Y. MicroRNA-203 suppresses cell proliferation and migration by targeting BIRC5 and LASP1 in human triple-negative breast cancer cells. *J Exp Clin Cancer Res*. 2012; 31:58.

21. Viticchie G, Lena AM, Latina A, Formosa A, Gregersen LH, Lund AH, Bernardini S, Mauriello A, Miano R, Spagnoli LG, Knight RA, Candi E and Melino G. MiR-203 controls proliferation, migration and invasive potential of prostate cancer cell lines. *Cell cycle (Georgetown, Tex)*. 2011; 10(7):1121-1131.

22. Saini S, Majid S, Yamamura S, Tabatabai L, Suh SO, Shahryari V, Chen Y, Deng G, Tanaka Y, Dahiya R. Regulatory role of mir-203 in prostate cancer progression and metastasis. *Clin Cancer Res*. 2011; 17(16):5287-5298.

23. Carroll AG, Voeller HJ, Sugars L and Gelmann EP. p53 oncogene mutations in three human prostate cancer cell lines. *The Prostate*. 1993; 23(2):123-134.

24. Grunewald TG, Kammerer U, Schulze E, Schindler D, Honig A, Zimmer M and Butt E. Silencing of LASP-1 influences zyxin localization, inhibits proliferation and reduces migration in breast cancer cells. *Exp Cell Res*. 2006; 312(7):974-982.

25. Spahn M, Kneitz S, Scholz CJ, Stenger N, Rudiger T, Strobel P, Riedmiller H and Kneitz B. Expression of microRNA-221 is progressively reduced in aggressive prostate cancer and metastasis and predicts clinical recurrence. *Int J Cancer*. 2010; 127(2):394-403.

26. Loeb S, Roehl KA, Helfand BT and Catalona WJ. Complications of open radical retropubic prostatectomy in potential candidates for active monitoring. *Urology*. 2008; 72(4):887-891.

27. Pound CR, Partin AW, Eisenberger MA, Chan DW, Pearson JD and Walsh PC. Natural history of progression after PSA elevation following radical prostatectomy. *Jama*. 1999; 281(17):1591-1597.

28. Bo J, Yang G, Huo K, Jiang H, Zhang L, Liu D and Huang Y. microRNA-203 suppresses bladder cancer development by repressing bcl-w expression. *The FEBS journal*. 2011; 278(5):786-792.

29. Badani K, Thompson DJ, Buerki C, Davicioni E, Garrison J, Ghadessi M, Mitra AP, Wood PJ and Hornberger J. Impact of a genomic classifier of metastatic risk on postoperative treatment recommendations for prostate cancer patients: a report from the DECIDE study group. *Oncotarget*. 2013; 4(4):600-609.

30. Ross AE, Feng FY, Ghadessi M, Erho N, Crisan A, Buerki C, Sundi D, Mitra AP, Vergara IA, Thompson DJ, Triche TJ, Davicioni E, Bergstrahl EJ, Jenkins RB, Karnes RJ and Schaeffer EM. A genomic classifier predicting metastatic disease progression in men with biochemical recurrence after prostatectomy. *Prostate Cancer Prostatic Dis*. 2014; 17(1):64-69.

31. Spahn M, Joniau S, Gontero P, Fieuws S, Marchioro G, Tombal B, Kneitz B, Hsu CY, Van Der Eeckt K, Bader P, Frohneberg D, Tizzani A and Van Poppel H. Outcome predictors of radical prostatectomy in patients with prostate-specific antigen greater than 20 ng/ml: a European multi-institutional study of 712 patients. *European urology*. 2010; 58(1):1-7; discussion 10-11.

32. Gleason DF. Histologic grading of prostate cancer: a perspective. *Human pathology*. 1992; 23(3):273-279.

33. Irizarry RA, Hobbs B, Collin F, Beazer-Barclay YD, Antonellis KJ, Scherf U and Speed TP. Exploration, normalization, and summaries of high density oligonucleotide array probe level data. *Biostatistics*. 2003; 4(2):249-264.

34. Willier S, Butt E and Grunewald TG. Lysophosphatidic acid (LPA) signalling in cell migration and cancer invasion: a focussed review and analysis of LPA receptor gene expression on the basis of more than 1700 cancer microarrays. *Biol Cell*. 2013; 105(8):317-333.

35. Dai M, Wang P, Boyd AD, Kostov G, Athey B, Jones EG, Bunney WE, Myers RM, Speed TP, Akil H, Watson SJ and Meng F. Evolving gene/transcript definitions significantly alter the interpretation of GeneChip data. *Nucleic Acids Res*. 2005; 33(20):e175.

36. Subramanian A, Tamayo P, Mootha VK, Mukherjee S, Ebert BL, Gillette MA, Paulovich A, Pomeroy SL, Golub TR, Lander ES and Mesirov JP. Gene set enrichment analysis: a knowledge-based approach for interpreting genome-wide expression profiles. *Proceedings of the National Academy of Sciences of the United States of America*. 2005; 102(43):15545-15550.

37. Butt E, Gambaryan S, Gottfert N, Galler A, Marcus K and Meyer HE. Actin binding of human LIM and SH3 protein is regulated by cGMP- and cAMP-dependent protein kinase phosphorylation on serine 146. *J Biol Chem*. 2003; 278(18):15601-15607.

38. Remmele W and Stegner HE. [Recommendation for uniform definition of an immunoreactive score (IRS) for immunohistochemical estrogen receptor detection (ER-ICA) in breast cancer tissue]. *Der Pathologe*. 1987; 8(3):138-140.



MondoA is highly overexpressed in acute lymphoblastic leukemia cells and modulates their metabolism, differentiation and survival

Caroline M. Wernicke^a, Günther H.S. Richter^a, Beate C. Beinvogl^a, Stephanie Plehm^a, Anna M. Schlitter^b, Obul R. Bandapalli^{c,d}, Olivia Prazeres da Costa^e, Uwe E. Hattenhorst^f, Ines Volkmer^f, Martin S. Staegge^f, Irene Esposito^b, Stefan Burdach^a, Thomas G.P. Grunewald^{a,g,*}

^a Children's Cancer Research and Roman Herzog Comprehensive Cancer Center, Laboratory of Functional Genomics and Transplantation Biology, Klinikum rechts der Isar, Technische Universität München, Munich, Germany

^b Institute for Pathology, Technische Universität München, Munich, Germany

^c Department of Pediatric Oncology, Hematology and Immunology, University of Heidelberg, Germany

^d Molecular Medicine Partnership Unit (MMPU), Heidelberg, Germany

^e Institute for Medical Microbiology, Immunology and Hygiene, Technische Universität München, Munich, Germany

^f Department of Pediatrics, Children's Cancer Research Center, Martin-Luther-University Halle-Wittenberg, Halle, Germany

^g Medical Life Science and Technology Center, TUM Graduate School, Technische Universität München, Garching, Germany

ARTICLE INFO

Article history:

Received 27 March 2012

Received in revised form 17 May 2012

Accepted 21 May 2012

Available online 29 June 2012

Keywords:

MondoA

MondoB

Leukemia

Metabolism

Differentiation

Survival

Clonogenicity

ABSTRACT

Acute lymphoblastic leukemia (ALL) is the most common childhood cancer. To identify novel candidates for targeted therapy, we performed a comprehensive transcriptome analysis identifying MondoA (MLXIP) – a transcription factor regulating glycolysis – to be overexpressed in ALL compared to normal tissues. Using microarray-profiling, gene-set enrichment analysis, RNA interference and functional assays we show that MondoA overexpression increases glucose catabolism and maintains a more immature phenotype, which is associated with enhanced survival and clonogenicity of leukemia cells. These data point to an important contribution of MondoA to leukemia aggressiveness and make MondoA a potential candidate for targeted treatment of ALL.

© 2012 Elsevier Ltd. All rights reserved.

1. Introduction

Acute lymphoblastic leukemia (ALL) is the most common childhood cancer, of which common ALL (cALL) constitutes the most frequent entity carrying an early pre-B cell phenotype [1]. Although today cALL is associated with good survival, conventional therapies are accompanied with considerable toxicity [2]. Hence, targeted therapy may be key to reducing the toxic burden of cure [2–4].

To identify novel targets for therapy of cALL, we performed a transcriptome analysis of early pre-B cell ALL and fetal early pre-B cells (FEB) that revealed a novel signature of genes highly overexpressed in ALL [5]. One of the most prominent among them

was *MondoA* (alias MAX-like protein X (MLX) interacting protein, *MLXIP*) – the founding member of the basic helix-loop-helix leucine zipper transcription factors of the Mondo family, which have pleiotropic but functionally largely uncharacterized effects on cell metabolism [6]. *MondoA* is ubiquitously expressed with high expression in skeletal muscle [6]. Its paralog, *MondoB* (alias MLX interacting protein-like, *MLXIPL*, or carbohydrate responsive element-binding protein, *CHREBP*), is most highly expressed in the liver [7,8], where it regulates aerobic glycolysis, lipogenesis and nucleotide synthesis [9,10]. The N-termini of both proteins are conserved across family members and contain cytoplasmic localization and transcription activation domains [6,9]. It was recently proposed that a novel N-terminal domain might interact with glucose-6-phosphate to dictate the glucose response of Mondo family proteins [11]. *MondoA* forms heterodimers with MLX, a member of the MYC/MAX/MAD family of transcription factors [6,12–14]. This heterodimerization seems to be essential for its transcriptional function [6]. Recently, *MondoA:MLX* heterodimers have been discussed as a parallel network to MYC:MAX, which have broad effects

* Corresponding author at: Children's Cancer Research Center, Laboratory of Functional Genomics and Transplantation Biology, Klinikum rechts der Isar, Technische Universität München, Kölner Platz 1, 80804 Munich, Germany.

Tel.: +49.89.3068.5525; fax: +49.89.3068.3791.

E-mail address: thomas.grunewald@lrz.tum.de (T.G.P. Grunewald).

on cellular growth, proliferation and survival [15,16]. MondoA:MLX heterodimers are localized at the outer mitochondrial membrane where they are believed to sense the intracellular energy state since they may accumulate in the nucleus upon excess glucose availability, more precisely upon accumulation of glucose-6-phosphate as the first step in glycolysis, to guide an adaptive transcriptional response [11,14]. Accordingly, we hypothesized that MondoA may modulate the metabolic activity of leukemia cells and, hence, aimed to define its potential role for the malignant phenotype of ALL. In the current study, we show that MondoA is highly overexpressed in ALL compared to normal tissues and provide evidence that its overexpression not only enhances glucose consumption, but also contributes to the maintenance of a more immature phenotype, which is associated with increased survival and clonogenicity of leukemia cells.

2. Materials and methods

2.1. Cell lines and reagents

Human T cell lineage ALL lines LOUCY, HSB-2, DND-41, PEER, KE-37, ALL-SIL, HPB-ALL, P12-Ichikawa, JURKAT-J6, MOLT-4, TALL-1, JURKAT, BE13, and CCRF-CEM, and human B cell lineage ALL lines SKW6, cALL2, 697, SD-1, RS4;11, REH, and Nalm6 were obtained from the German Collection of Microorganisms and Cell Cultures (DSMZ) or ATCC (LGC standards). Hepatocellular carcinoma lines HepG2 and Hep3B were provided by Dr. Elke Butt (Institute for Clinical Biochemistry, University of Würzburg, Germany). Retrovirus packaging cell line PT67 was obtained from Takara Bio Europe/Clontech (Saint-Germain-en-Laye, France). Cells were grown in a humidified incubator at 37 °C in 5% CO₂ atmosphere in RPMI 1640 media (Invitrogen, Karlsruhe, Germany) containing 20% fetal bovine serum (Biochrom, Berlin, Germany), 1% glutamine, 100 µg/mL gentamicin (Invitrogen) and 200 mg/dL D-glucose. All cell lines were checked routinely for purity and mycoplasma contamination. All reagents were purchased from Sigma (Deisenhofen, Germany) if not otherwise specified.

2.2. Human samples

The Institutional Review Boards of the Universities of Halle-Wittenberg and Leipzig and of the Technische Universität München approved the current study. Patient-derived samples were obtained from the Departments of Pediatrics of the Universities of Halle-Wittenberg and Leipzig and the Technische Universität München according to legal guidelines of local authorities. Written informed consent was obtained from all donors and/or their legal guardians.

2.3. Preparation of acute lymphoblastic leukemia (ALL) cells and fetal early pre-B cells (FEB)

Pre-therapy cALL samples were obtained from bone marrow aspirates ($n=24$) or peripheral blood ($n=1$) of children treated according to the ALL-BFM study of the Society for Pediatric Oncology and Hematology (GPOH). Flow cytometric assessment of CD10 and CD19 confirmed the presence of leukemic blasts (>90% of cells) in each sample. FEB highly expressing the early B cell markers CD10 and CD19 were isolated from umbilical cord blood samples of healthy newborns. CD19⁺ cells were purified with CD19 Dynabeads (Dyna Biotech, Oslo, Norway) and magnetic cell sorting (MACS, Miltenyi Biotech, Bergisch Gladbach, Germany). Dynabeads were removed with DETACHaBEAD CD19 (Invitrogen). After detachment CD19⁺ cells were stained with anti-CD10-PE antibody (BD Biosciences, San Jose, CA) and subsequently with anti-PE microbeads and purified via MACS (both Miltenyi Biotech).

2.4. RNA extraction and quantitative real-time PCR (qRT-PCR)

RNA was isolated using the RNeasy kit (Qiagen, Düsseldorf, Germany). Gene expression was analyzed by qRT-PCR using TaqMan Universal PCR Master Mix with an AB 7300 Real-Time PCR System (Applied Biosystems, Darmstadt, Germany). Primers and probes were obtained as TaqMan Gene Expression Assays (Applied Biosystems, listed in Supplementary Data), which consisted of a FAM dye-labeled TaqMan MGB probe and two unlabeled PCR primers. The concentration of primers and probes were 900 and 250 nM, respectively. Results were normalized to the leukemia housekeeping gene *beta-2-microglobulin* (*B2M*) [17] and quantified by the ddCt-method.

2.5. Constructs, retroviral gene transfer and RNA interference (RNAi)

For stable silencing of MondoA, oligonucleotides of the short hairpin corresponding to a MondoA small interfering RNA (siRNA) were cloned into the

retroviral pSIREN-RetroQ vector (Takara Bio Europe/Clontech). Retroviral constructs were transfected by electroporation into PT67 packaging cells, and viral supernatant was isolated 48 h after transfection. Target cells (Nalm6) were infected in the presence of 4 µg/mL polybrene. Single-cell-cloned stable infectants were isolated after selection in 2 µg/mL puromycin for at least 7 days and were first used for subsequent assays after at least 7 additional days in culture without puromycin to avoid biases through acute infection and/or puromycin toxicity. The siRNA target sequences of Hs_MLXIP_1 (SI04144469) and Hs_MLXIP_3 (SI04371052) (Qiagen GmbH, Hilden, Germany) were 5'-CAGGACGATGACATGCTGTAT-3' and 5'-CACAGTTAGATCCAGTTGGA-3', respectively. As a control the corresponding shRNA of the AllStars negative control siRNA (#1027280, Qiagen) was used. Each experiment shown in this study, analyzing stably MondoA silenced Nalm6 cells (referred to as "pSImondoA" cells) compared to non-silenced Nalm6 cells (referred to as "pSInegative" cells), was performed with three independent infectants expressing either shMLXIP_1 or shMLXIP_3.

2.6. Microarray analysis

Total RNA was amplified and labeled using Affymetrix GeneChip Whole Transcript Sense Target Labeling Kit. cRNA was hybridized to Affymetrix Human Gene 1.0 ST arrays or HG-U133A arrays. Arrays were either RMA-normalized (Human Gene 1.0 ST) or scaled to the same target intensity of 500 (default setting) using the trimmed mean signal of all probe sets (HG-U133A). Quality assessment consisted of RNA degradation plots, Affymetrix control metrics, sample cross-correlation, and probe-level visualizations. RMA-normalization incorporated background correction, quantile normalization, and probe-level summation. Microarray data were deposited at the gene expression omnibus (GSE34670 and GSE33967). Subsequent analysis was carried out with signal intensities that were log2-transformed for equal representation of over- and underexpressed genes and then median centered to remove biases based on single expression values. Unsupervised hierarchical clustering [18] and principal component analysis were accomplished by use of Genesis [19]. For identification of differentially expressed genes we used significance analysis of microarrays (SAM) [20]. Gene-set enrichment analysis (GSEA) and pathway analyses were performed with the GSEA tool (<http://www.broad.mit.edu/gsea>) [21]. Comparison of independent published microarray studies was performed with the R2 microarray analysis and visualization platform (<http://r2.amc.nl>). All published datasets analyzed with the R2 platform were generated with Affymetrix HG-U133Plus2.0 microarrays and expression data were normalized with the MASS5.0 algorithm within the Affymetrix Expression Console.

2.7. Metabolism assay

Media turnover and metabolic activity of leukemia cells was assessed as follows: 3×10^6 pSInegative and pSImondoA Nalm6 infectants were incubated for 72 h in 20 mL RPMI 1640 media containing 200 mg/dL D-glucose and phenol red. Thereafter, metabolic activity was assessed by spectroscopic (IMPLEN GmbH, Munich, Germany) pH measurement in cell-free conditioned media (absorption measurement at 557 nm).

2.8. Analysis of glucose concentrations

Glucose levels of conditioned media were analyzed with a commercial Breeze 2 glucometer (Bayer Vital GmbH, Leverkusen, Germany) in an aliquot (5 µL) of cell-free conditioned media according to the manufacturer's protocol. Each measurement was performed in duplicate.

2.9. Flow cytometry

Cells were harvested, prepared and stained using propidium iodide for cell cycle analysis as previously described [22]. The annexin-V-PE/7-AAD (7-aminoactinomycin-D) apoptosis detection kit 1 (Becton Dickinson) was used to assess apoptosis and necrosis. Cluster of differentiation (CD) molecules were analyzed using antibodies (all Becton Dickinson) against CD10 (PE, Lot: 555375), CD19 (FITC, Lot: 560994), CD22 (FITC, Lot: 30141), and CD24 (PE, Lot: 23219). Samples were analyzed on a FACScalibur flow cytometer using Cellquest Pro (Becton Dickinson).

2.10. Assessment of clonogenicity

Clonogenicity was assessed with a commercial colony-forming assay (R&D Systems, Wiesbaden-Nordenstadt, Germany) as previously described [22].

2.11. Statistical analysis

Data were analyzed by unpaired two-tailed student's *t*-test, Spearman's rank correlation coefficient (r_s) and Fisher's exact test as indicated using Prism 5.0b (GraphPad Software). *p* values <0.05 were considered significant.

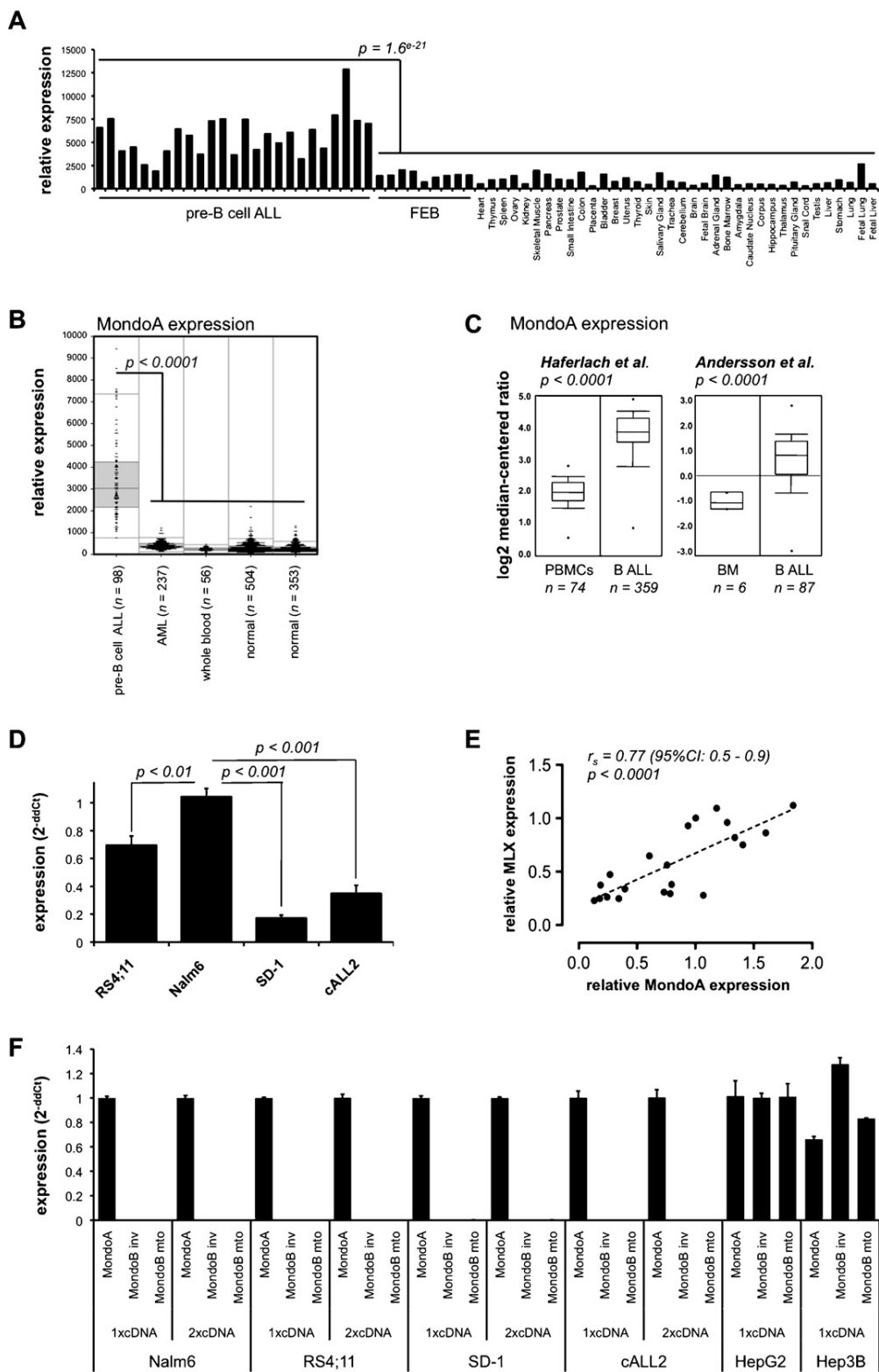


Fig. 1. MondoA is highly and stably overexpressed in leukemia. (A) MondoA expression in childhood early pre-B cell ALL, FEB and normal tissues (GSE34670, GSE2361). (B) Box-dot-plots showing MondoA expression in pre-B cell ALL (GSE7440), AML (GSE17855), whole blood (GSE6575), and normal tissues (GSE7307; GSE3526). (C) MondoA expression in primary B ALL, BM or PBMCs (GSE13204; GSE7186). Data were retrieved via oncomine™. (D) Summary of multiple ($n \geq 10$) expression analyses of B ALL lines. Mean \pm SEM. (E) Correlation of MondoA and MLX in 21 ALL lines (see methods). Two independent experiments. Dashed line = linear regression. Spearman's rank correlation coefficient (r_s). (F) MondoA and MondoB expression in Nalm6, RS4;11, SD-1, cALL2, HepG2 and Hep3B. Two different MondoB primer assays: MondoB inv/MondoB mto. Standard and double amount of cDNA ($1 \times / 2 \times$). Mean \pm SEM of two independent experiments; t -test.

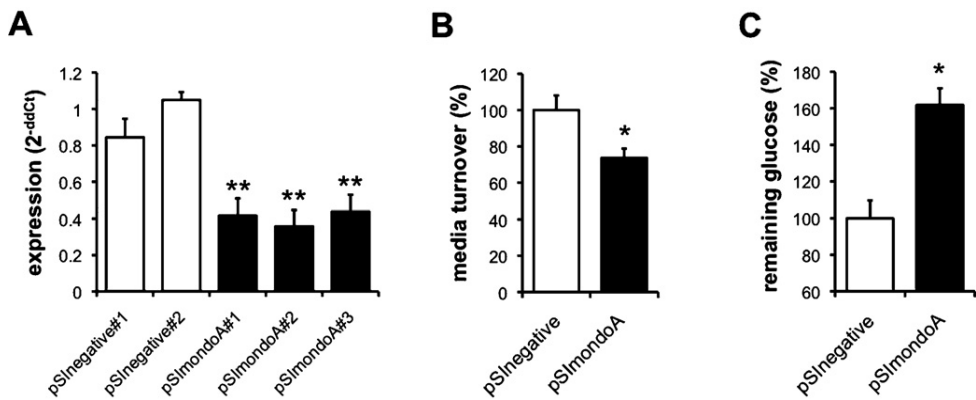


Fig. 2. MondoA expression increases metabolic activity. (A) MondoA expression in Nalm6 cells either expressing nonsense shRNA (clones #1 and #2, hereafter summarized as pSInegative) or specific MondoA shRNAs (clone #1 = shMLXIP_1 and clones #2 and #3 = shMLXIP_3; hereafter summarized as pSImondoA). Mean \pm SEM of at least four independent measurements. (B) Metabolic activity of pSInegative and pSImondoA cells (normalized to cell count). Mean \pm SEM of three independent experiments. (C) Remaining media D-glucose after 72 h. Mean \pm SEM of three independent experiments; * p $<$ 0.05, ** p $<$ 0.01; t-test.

3. Results

3.1. MondoA is highly and stably overexpressed in leukemia

Microarray analysis of 25 primary early pre-B cell ALL samples versus 9 highly purified FEB samples (fraction of CD10⁺ and CD19⁺ cells of >82%) (GSE34670) [5] revealed that MondoA is highly overexpressed in leukemia. This observation was extended by comparing our microarray data to those of a published study of 36 normal adult and fetal tissues (GSE2361) [23] (Fig. 1A). These data were further validated using the R2 microarray analysis and visualization tool (<http://r2:aml.nl>), comparing a pre-B cell ALL study with an acute myeloid leukemia (AML), a whole blood and two independent normal tissue studies (Fig. 1B) [24–26]. Additionally, MondoA overexpression in ALL was confirmed by reanalysis of two independent published microarray studies that directly compared B cell lineage ALL samples with peripheral blood mononuclear cells (PBMCs) and bone marrow (BM) (Fig. 1C) [27,28].

As B cell lineage ALL comprises the most common type of leukemia among children [3], we chose four B cell lineage ALL lines for further investigation – two with high (Nalm6, RS4;11) and two with relatively low (SD-1, cALL2) MondoA expression levels. As seen in Fig. 1D, MondoA is expressed in a remarkably stable fashion, with very little oscillation (note small error bars). Interestingly, the binding partner of MondoA, MLX, is strongly coexpressed with MondoA (r_s = 0.77, 95%CI: 0.5 to 0.9, p < 0.0001, n = 21; 7 B ALL and 14 T ALL lines) (Fig. 1E). However, the MondoA paralog MondoB [7,8] is neither expressed in the MondoA-high nor MondoA-low ALL lines (tested with two different MondoB primer assays and increasing cDNA employment). In contrast, MondoB can be readily detected in the human hepatocellular carcinoma lines HepG2 and Hep3B (positive controls) (Fig. 1F). Taken together, these data provide evidence that MondoA, but not MondoB, is highly and stably overexpressed in human ALL compared to AML and normal tissues including FEB, BM and PBMCs.

3.2. MondoA expression increases metabolic activity

To test the functional role of MondoA, we performed knockdown experiments. We generated single-cell-cloned MondoA-silencing and non-silencing cell lines of the highly MondoA expressing parental Nalm6 line [pSImondoA (either expressing shMLXIP_1 or shMLXIP_3, see Section 2) and pSInegative, respectively] (Fig. 2A). We first investigated the impact of MondoA knockdown on the metabolic activity and glucose utilization. MondoA-suppressed Nalm6 clones and respective controls were incubated in RPMI 1640

media containing 200 mg/dL D-glucose for 72 h and media turnover and media glucose levels were measured thereafter. As expected, constitutive MondoA knockdown reduced the metabolic activity of leukemia cells, which led to a higher amount of remaining non-metabolized glucose in the conditioned culture media (Fig. 2B–C).

3.3. MondoA knockdown promotes differentiation of leukemia cells

To gain a more functional insight, two different pSInegative Nalm6 clones and three different pSImondoA Nalm6 clones were subjected to a whole-transcriptome microarray analysis. MondoA knockdown differentially regulates 191 genes (mean log2 fold change \pm 0.5, p < 0.05, t-test) of which 49 genes were up- and 142 genes were downregulated (Fig. 3A and Supplementary Table 1). Surprisingly, gene-set enrichment analysis (GSEA) did not only reveal strong enrichment of gene-sets involved in metabolism, but a most significant enrichment of gene-sets involved in the maintenance of stemness, B cell differentiation as well as chemo/stress-resistance and survival (Fig. 3B and Supplementary Table 2). For instance, the gene-set STEMCELL_COMMON_DN (now renamed in RAMALHO_STEMNESS_DN) contains genes, which are usually depleted in embryonic, neural and hematopoietic stem cells [29], whereas the gene-set BLEO_HUMAN_LYMPH_HIGH_4HRS_UP comprises genes involved in DNA repair, cell cycle regulation, and apoptosis, which are differentially regulated in human lymphocytes 4 h following treatment with a high dose of bleomycin [30].

To validate these microarray data, we selected three up- and three downregulated genes of the 40 top-ranked genes (Fig. 3A), all of which have been previously associated with B cell lineage ALL and B cell activation and/or differentiation [31–38]. Their differential regulation upon MondoA knockdown was entirely confirmed on RNA or protein level by qRT-PCR or flow cytometry (Fig. 3C–D). Moreover, apart from these genes, whose regulation seemed to take place on the transcriptional level (microarrays), we also tested for the B cell marker CD24 [39], which was not significantly regulated on RNA level. Strikingly, we also found an upregulation of CD24 on protein level in MondoA suppressed Nalm6 cells. Together, these data suggest that MondoA knockdown results in a more differentiated leukemia phenotype (Fig. 3C–D).

3.4. MondoA enhances survival and clonogenicity of leukemia cells

Differentiation therapy is successfully employed to treat certain types of acute myeloid leukemia [40]. We therefore investigated

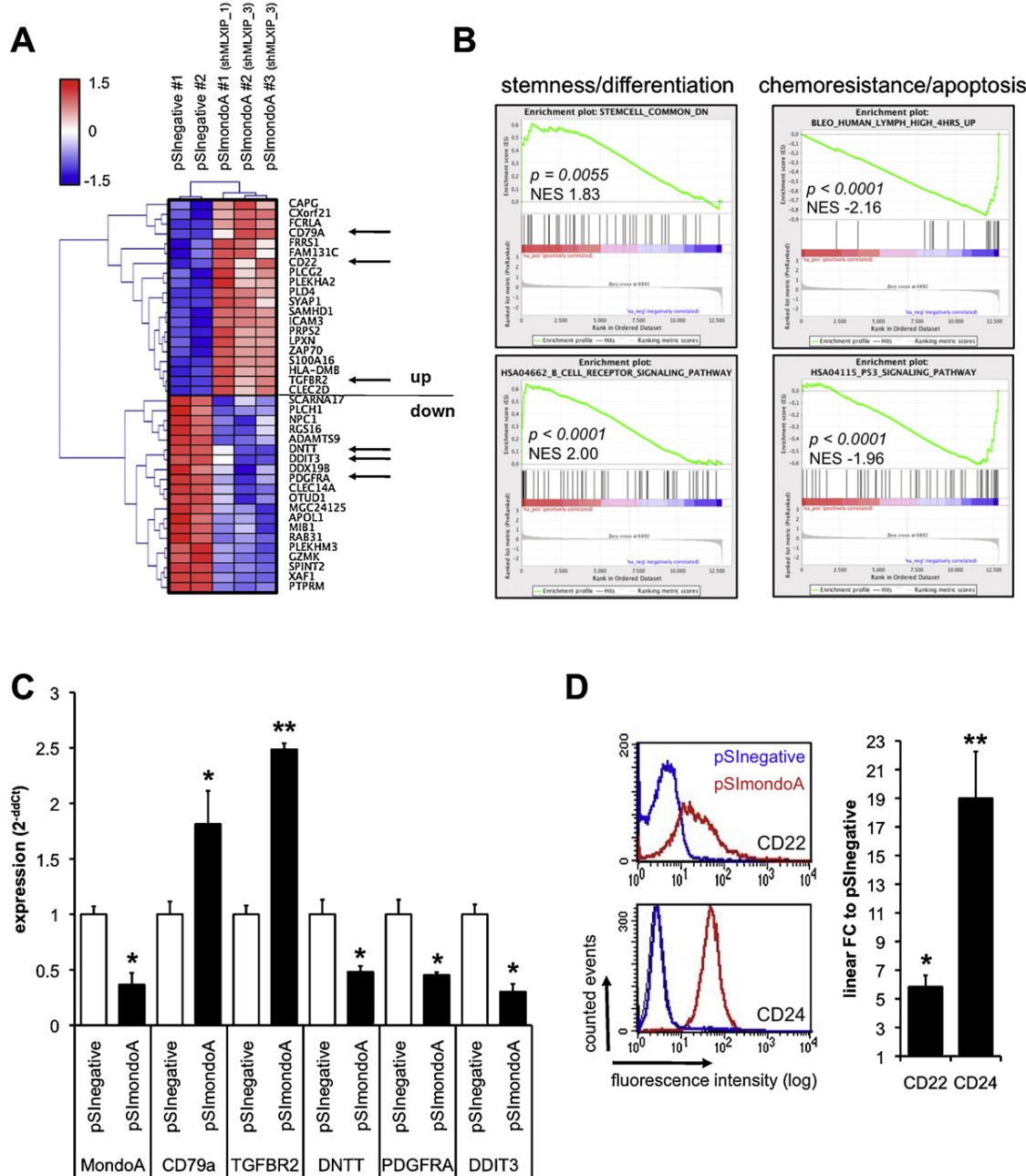


Fig. 3. MondoA knockdown promotes differentiation of leukemia cells. (A) Heatmap and hierarchical clustering of 40 top up- and downregulated genes. Arrows: genes selected for validation. (B) Enrichment plots of significantly enriched gene-sets. NES = normalized enrichment score. (C) Expression analysis of MondoA, CD79a, TGFBR2 (transforming growth factor beta receptor 2), DNTT (terminal deoxynucleotidyl-transferase), PDGFRA (platelet-derived growth factor receptor alpha), DDTT3 (DNA-damage-inducible transcript 3). Mean \pm SEM of at least two independent experiments. (D) Analysis of CD22 and CD24 by flow cytometry. Linear fold changes are mean \pm SEM of two independent experiments. * p < 0.05, ** p < 0.01; t -test.

whether the MondoA knockdown-mediated differentiation of ALL cells can mitigate the malignant phenotype in our model. We first conducted experiments addressing cell cycle progression and found no differences, as pSInegative and pSImondoA Nalm6 cells exhibited similar distributions of G1, S and G2/M phases (Fig. 4A).

Interestingly, MondoA knockdown downregulates genes sharing a significant overlap with a published expression signature of downregulated genes in primary childhood B cell lineage ALL that responded well to apoptosis-inducing therapy with glucocorticoids (Fig. 4B and Supplementary Table 3) [41]. This indicates that MondoA knockdown may shift gene expression toward a signature favoring apoptosis and reducing aggressiveness of leukemia cells. In

accordance, flow cytometric analysis of apoptosis and necrosis with annexin-V-PE and 7-AAD staining revealed that MondoA knockdown leads to increased rates of spontaneous cell death (Fig. 4C). In addition, clonogenicity of the MondoA-suppressed Nalm6 cells was significantly impaired (Fig. 4D).

4. Discussion

The current study aimed to determine the role of MondoA in ALL regarding glucose metabolism, growth and survival. Our results provide for the first time evidence that MondoA is highly

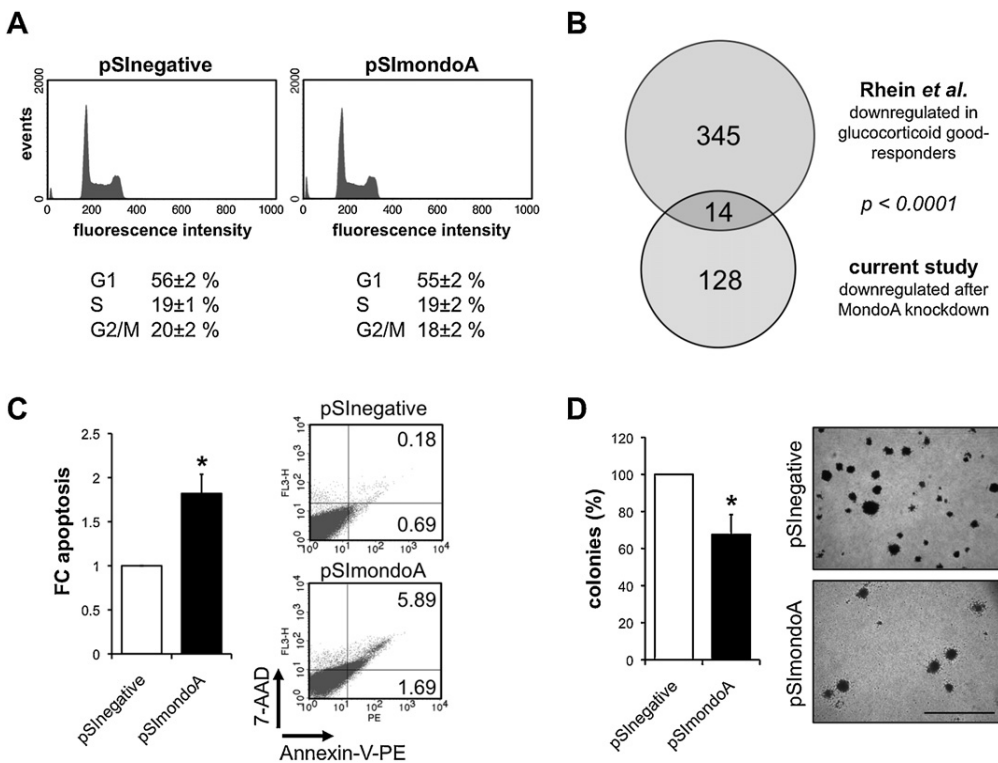


Fig. 4. MondoA enhances survival and clonogenicity of leukemia cells. (A) Cell cycle analysis (propidium iodide). Mean \pm SEM of three independent experiments. (B) Venn diagram: overlap between a published microarray study of childhood ALL and the current study (Supplementary Table 3). Fisher's exact test. (C) Summary of results of flow cytometric measurements of apoptotic cells. Mean \pm SEM of linear fold changes of two independent experiments. (D) Analysis of clonogenicity with colony-forming assays. Mean \pm SEM of three independent experiments. Scale bar = 1000 μ m. * $p < 0.05$; t-test.

overexpressed in ALL compared to normal tissues and that MondoA promotes glucose utilization of leukemia cells. Moreover, our data indicate that MondoA contributes to the maintenance of a more immature leukemia phenotype, which is linked with enhanced leukemia clonogenicity and survival.

So far, there are no reports on mutations involving *MondoA* or other alterations that might drive its overexpression. However, in preliminary experiments we found 6 conserved runt related transcription factor 1 (RUNX1) binding sites close to two methylation-prone CpG-islands in the *MondoA* promoter and a strong correlation of MondoA and RUNX1 expression in leukemia (Supplementary Figure 1 and Supplementary Table 4). Moreover, treatment of ALL cells with the demethylating agent zebularine increased MondoA expression (Supplementary Figure 1) suggesting that RUNX1 and/or MondoA promoter demethylation might play a role in MondoA overexpression.

Since MondoA is involved in glucose metabolism of many different cell types [12–14], we first examined an association of MondoA and glucose consumption. As expected, we found that MondoA knockdown decreases the metabolic activity and the overall glucose uptake of leukemia cells suggesting that MondoA overexpression may contribute to their highly glycolytic phenotype, which is a common feature of many cancers known as the Warburg effect [42]. As we did not detect any expression of MondoB in our leukemia cell lines, we conclude that MondoA, but not MondoB, is involved in the pathological metabolism of ALL.

However, our microarray and GSEA analyses revealed a hitherto unexpected role of MondoA in blocking leukemia cell differentiation as indicated by the differential expression of specific genes and proteins upon MondoA knockdown. Interestingly, these factors were previously associated with growth, B cell activation and differentiation as well as survival: for instance, TGFBR2

(transforming growth factor beta receptor 2) promotes cellular lineage fate decisions and terminal differentiation of many different cell types [33]. DNNT (terminal deoxynucleotidyltransferase) is expressed in normal and malignant pre-B and pre-T lymphocytes during early differentiation and contributes to the generation of antigen-receptor diversity [43]. In addition, DNNT has a strong anti-apoptotic function as its overexpression may contribute to resistance of leukemia cells to thiopurine-based chemotherapeutics [32]. Accordingly, downregulation of DNNT by MondoA knockdown may in part explain the increased cell death in our model. Similarly, DDIT3 (DNA-damage-inducible transcript 3, also known as CHOP-10 and GADD153) is involved in differentiation and survival of various tissues [31,34,35]. Moreover, PDGFR α (platelet-derived growth factor receptor alpha) is frequently overexpressed in childhood ALL [37] and often rearranged in myeloid and lymphoid neoplasms [36].

Furthermore, we detected an upregulation of the B cell markers CD22, CD24 and CD79a upon MondoA knockdown. This upregulation of differentiation markers [38,39,44] support the GSEA in silico prediction that MondoA overexpression maintains a more immature phenotype. In addition, enhanced CD24 expression may promote apoptosis in pre-B cells [45,46] converging with the fact that MondoA knockdown increases rates of spontaneous cell death and shifts gene expression toward a signature related to enhanced sensitivity of leukemia cells toward chemotherapy (GSEA, Table 1). Consistently, MondoA downregulation leads to decreased clonogenicity and to transcriptional changes similar to those seen in ALL samples derived from patients that responded well to treatment with glucocorticoids [41]. These data suggest that MondoA overexpression may contribute to a worse outcome of ALL patients because especially more immature cells with a leukemia stem-cell phenotype are believed to be therapy-resistant

and the main source of relapse [47]. Taking together our findings of less differentiation and enhanced survival and clonogenicity of leukemia cells through MondoA, the enrichment of genes involved in chemo-/stress-resistance in the GSEA and the anti-apoptotic and chemoresistance-conferring MondoA target genes such as DNTT, MondoA appears to be a promising therapeutic drug target. However, there is currently no drug available or under development that can specifically target MondoA.

In synopsis, our data hint to a contribution of MondoA to leukemia aggressiveness and to a possible role of MondoA as an attractive candidate for targeted treatment of ALL. Future studies will have to determine the pathways involved in regulation and functioning of MondoA and to evaluate MondoA as a therapeutic target and as a biomarker for ALL.

Role of the funding source

This work was supported by grants from the Deutsche Forschungsgemeinschaft (DFG GR3728/1-1 to TGPG, GHSR and SB; SFB TR-22 to OPdC), the Technische Universität München (KKF B08-05 to TGPG and KKF A09-02 to GHSR) and the Dr. Sepp und Hanne Sturm Gedächtnissstiftung of the Ministry of Health, City of Munich (to TGPG, GHSR, and SB). The study sponsors had no role in study design, collection, analysis and interpretation of data.

Conflict of interest

All authors declare no competing financial interests.

Acknowledgements

The authors thank Silke Bergmann for her help with the microarray analyses, Dr. Uwe Thiel for critical reading of the manuscript, and Dr. Elke Butt for providing the hepatocellular carcinoma cell lines.

Contributions: CMW, GHSR, SB and TGPG conceived the study. CMW and TGPG performed the experiments and interpreted the results. CMW and TGPG drafted and wrote the manuscript and designed the figures and the tables. BCB generated the highly purified FEB samples. IV and UEH contributed to the analysis of the primary cALL samples. SP performed the in silico promoter analysis. MSS and OPdC performed the microarray analyses. GHSR contributed part of the bioinformatic analysis. AMS and IE helped in data collection, provided pathological guidance and helped interpreting the results. ORB provided cell lines, protocols and experimental guidance. All authors read and approved the final manuscript.

Appendix A. Supplementary data

Supplementary data associated with this article can be found, in the online version, at <http://dx.doi.org/10.1016/j.leukres.2012.05.009>.

References

- Eden T. Aetiology of childhood leukaemia. *Cancer Treat Rev* 2010;36:286–97.
- Bourquin JP, Izraeli S. Where can biology of childhood ALL be attacked by new compounds? *Cancer Treat Rev* 2010;36:298–306.
- Pui CH, Carroll WL, Meshinchi S, Arceci RJ. Biology, risk stratification, and therapy of pediatric acute leukemias: an update. *J Clin Oncol* 2011;29:551–65.
- Grunewald TG, Greulich N, Kontny U, Fröhwald MC, Rutkowski S, Kordes U, et al. Targeted therapeutics in treatment of children and young adults with solid tumors: an expert survey and review of the literature. *Klin Padiatr* 2012;244:124–31.
- Richter G, Hattenhorst UE, Roessler S, Staeghe MS, Hansen G, Burdach S. Transcriptome analysis of pediatric cALL versus normal fetal B cells reveals a novel signature of the malignant phenotype. *Blood* 2005;106:1678–88.
- Billin AN, Eilers AL, Coulter KL, Logan JS, Ayer DE. MondoA, a novel basic helix-loop-helix-leucine zipper transcriptional activator that constitutes a positive branch of a max-like network. *Mol Cell Biol* 2000;20:8845–54.
- Iizuka K, Bruick RK, Liang G, Horton JD, Uyeda K. Deficiency of carbohydrate response element-binding protein (ChREBP) reduces lipogenesis as well as glycolysis. *Proc Natl Acad Sci U S A* 2004;101:7281–6.
- Ishii S, Iizuka K, Miller BC, Uyeda K. Carbohydrate response element binding protein directly promotes lipogenic enzyme gene transcription. *Proc Natl Acad Sci U S A* 2004;101:15597–602.
- Tong X, Zhao F, Mancuso A, Gruber JJ, Thompson CB. The glucose-responsive transcription factor ChREBP contributes to glucose-dependent anabolic synthesis and cell proliferation. *Proc Natl Acad Sci U S A* 2009;106:21660–5.
- Ma L, Tsatsos NG, Towle HC. Direct role of ChREBP, Mlx in regulating hepatic glucose-responsive genes. *J Biol Chem* 2005;280:12019–27.
- McFerrin LG, Atchley WR. A novel N-terminal domain may dictate the glucose response of monoo proteins. *PLoS One* 2012;7:e34803.
- Billin AN, Ayer DE. The Mlx network: evidence for a parallel Max-like transcriptional network that regulates energy metabolism. *Curr Top Microbiol Immunol* 2006;302:255–78.
- Sans CL, Satterwhite DJ, Stoltzman CA, Breen KT, Ayer DE. MondoA-Mlx heterodimers are candidate sensors of cellular energy status: mitochondrial localization and direct regulation of glycolysis. *Mol Cell Biol* 2006;26:4863–71.
- Stoltzman CA, Peterson CW, Breen KT, Muoio DM, Billin AN, Ayer DE. Glucose sensing by MondoA:Mlx complexes: a role for hexokinases and direct regulation of thioredoxin-interacting protein expression. *Proc Natl Acad Sci U S A* 2008;105:6912–7.
- Kadige MR, Elgort MG, Ayer DE. Coordination of glucose and glutamine utilization by an expanded Myc network. *Transcr* 2010;1:36–40.
- Sloan EJ, Ayer DE. Myc, monoo, and metabolism. *Genes Cancer* 2010;1:587–96.
- Beillard E, Pallisgaard N, van der Velden VH, Bi W, Dee R, van der Schoot E, et al. Evaluation of candidate control genes for diagnosis and residual disease detection in leukemia patients using 'real-time' quantitative reverse-transcriptase polymerase chain reaction (RQ-PCR) – a Europe against cancer program. *Leukemia* 2003;17:2474–86.
- Eisen MB, Spellman PT, Brown PO, Botstein D. Cluster analysis and display of genome-wide expression patterns. *Proc Natl Acad Sci U S A* 1998;95:14863–8.
- Sturm A, Quackenbush J, Trajanoski Z. Genesis: cluster analysis of microarray data. *Bioinformatics* 2002;18:207–8.
- Tusher VG, Tibshirani R, Chu G. Significance analysis of microarrays applied to the ionizing radiation response. *Proc Natl Acad Sci U S A* 2001;98:5116–21.
- Subramanian A, Tamayo P, Mootha VK, Mukherjee S, Ebert BL, Gillette MA, et al. Gene set enrichment analysis: a knowledge-based approach for interpreting genome-wide expression profiles. *Proc Natl Acad Sci U S A* 2005;102:15545–50.
- Grunewald TG, Diebold I, Esposito I, Plehm S, Hauer K, Thiel U, et al. STEAP1 is associated with the invasive and oxidative stress phenotype of Ewing tumors. *Mol Cancer Res* 2012;10:52–65.
- Ge X, Yamamoto S, Tsutsumi S, Midorikawa Y, Ihara S, Wang SM, et al. Interpreting expression profiles of cancers by genome-wide survey of breadth of expression in normal tissues. *Genomics* 2005;86:127–41.
- Balgobind BV, Van den Heuvel-Eibrink MM, De Menezes RX, Reinhardt D, Hollink IH, Arentsen-Peters ST, et al. Evaluation of gene expression signatures predictive of cytogenetic and molecular subtypes of pediatric acute myeloid leukemia. *Haematologica* 2011;96:221–30.
- Rhodes DR, Yu J, Shanker K, Deshpande N, Varambally R, Ghosh D, et al. Large-scale meta-analysis of cancer microarray data identifies common transcriptional profiles of neoplastic transformation and progression. *Proc Natl Acad Sci U S A* 2004;101:9309–14.
- Roth RB, Hevezzi P, Lee J, Willhite D, Lechner SM, Foster AC, et al. Gene expression analyses reveal molecular relationships among 20 regions of the human CNS. *Neurogenetics* 2006;7:67–80.
- Andersson A, Ritz C, Lindgren D, Eden P, Lassen C, Heldrup J, et al. Microarray-based classification of a consecutive series of 121 childhood acute leukemias: prediction of leukemic and genetic subtype as well as of minimal residual disease status. *Leukemia* 2007;21:1198–203.
- Haferlach T, Kohlmann A, Wieczorek L, Basso G, Krontie GT, Bene MC, et al. Clinical utility of microarray-based gene expression profiling in the diagnosis and subclassification of leukemia: report from the International Microarray Innovations in Leukemia Study Group. *J Clin Oncol* 2010;28:2529–37.
- Ramalho-Santos M, Yoon S, Matsuzaki Y, Mulligan RC, Melton DA. "Stemness": transcriptional profiling of embryonic and adult stem cells. *Science* 2002;298:597–600.
- Islah M, Li B, Kadura IA, Reid-Hubbard JL, Deahl JT, Altizer JL, et al. Comparison of gene expression changes induced in mouse and human cells treated with direct-acting mutagens. *Environ Mol Mutagen* 2004;44:401–19.
- Coutts M, Cui K, Davis KL, Keutzer JC, Szytowski AJ. Regulated expression and functional role of the transcription factor CHOP (GADD153) in erythroid growth and differentiation. *Blood* 1999;93:3369–78.
- Karim H, Hashemi J, Larsson C, Moshfegh A, Fotoohi AK, Albertoni F. The pattern of gene expression and gene dose profiles of 6-Mercaptopurine- and 6-Thioguanine-resistant human leukemia cells. *Biochem Biophys Res Commun* 2011;411:156–61.
- Massague J. TGF β in Cancer. *Cell* 2008;134:215–30.
- Maytin EV, Habener JF. Transcription factors C/EBP alpha, C/EBP beta, and CHOP (Gadd153) expressed during the differentiation program of keratinocytes in vitro and in vivo. *J Invest Dermatol* 1998;110:238–46.

[35] Pereira RC, Delany AM, Canalis E. CCAAT/enhancer binding protein homologous protein (DDIT3) induces osteoblastic cell differentiation. *Endocrinology* 2004;145:1952–60.

[36] Vladareanu AM, Muller-Tidow C, Bumbea H, Radesi S. Molecular markers guide diagnosis and treatment in Philadelphia chromosome-negative myeloproliferative disorders (review). *Oncol Rep* 2010;23:595–604.

[37] Yeoh EJ, Ross ME, Shurtleff SA, Williams WK, Patel D, Mahfouz R, et al. Classification, subtype discovery, and prediction of outcome in pediatric acute lymphoblastic leukemia by gene expression profiling. *Cancer Cell* 2002;1:133–43.

[38] Raponi S, De Propis MS, Intoppa S, Milani ML, Vitale A, Elia L, et al. Flow cytometric study of potential target antigens (CD19, CD20, CD22, CD33) for antibody-based immunotherapy in acute lymphoblastic leukemia: analysis of 552 cases. *Leuk Lymphoma* 2011;52:1098–107.

[39] Fang X, Zheng P, Tang J, Liu Y. CD24: from A to Z. *Cell Mol Immunol* 2010;7:100–3.

[40] Petrie K, Zelent A, Waxman S. Differentiation therapy of acute myeloid leukemia: past, present and future. *Curr Opin Hematol* 2009;16:84–91.

[41] Rhein P, Scheid S, Ratei R, Hagemeier C, Seeger K, Kirschner-Schwabe R, et al. Gene expression shift towards normal B cells, decreased proliferative capacity and distinct surface receptors characterize leukemic blasts persisting during induction therapy in childhood acute lymphoblastic leukemia. *Leukemia* 2007;21:897–905.

[42] Vander Heiden MG, Cantley LC, Thompson CB. Understanding the Warburg effect: the metabolic requirements of cell proliferation. *Science* 2009;324:1029–33.

[43] Thai TH, Kearney JF. Distinct and opposite activities of human terminal deoxynucleotidyltransferase splice variants. *J Immunol* 2004;173:4009–19.

[44] Chu PG, Arber DA. CD79: a review. *Appl Immunohistochem Mol Morphol* 2001;9:97–106.

[45] Taguchi T, Kiyokawa N, Mimori K, Suzuki T, Sekino T, Nakajima H, et al. Pre-B cell antigen receptor-mediated signal inhibits CD24-induced apoptosis in human pre-B cells. *J Immunol* 2003;170:252–60.

[46] Ju JH, Jang K, Lee KM, Kim M, Kim J, Yi JY, et al. CD24 enhances DNA damage-induced apoptosis by modulating NF- κ B signaling in CD44-expressing breast cancer cells. *Carcinogenesis* 2011;32:1474–83.

[47] Buss EC, Ho AD. Leukemia stem cells. *Int J Cancer* 2011;129:2328–36.

STEAP1 Is Associated with the Invasive and Oxidative Stress Phenotype of Ewing Tumors

Thomas G.P. Grunewald^{1,3}, Isabel Diebold⁴, Irene Esposito^{2,5}, Stephanie Plehm¹, Kristina Hauer¹, Uwe Thiel¹, Patricia da Silva-Buttkus⁵, Frauke Neff⁵, Rebekka Unland^{7,8}, Carsten Müller-Tidow⁷, Colette Zobywalski¹, Katharina Lohrig⁹, Urs Lewandrowski⁹, Albert Sickmann^{9,10}, Olivia Prazeres da Costa⁶, Agnes Görlach⁴, Andrea Cossarizza¹¹, Elke Butt¹², Günther H.S. Richter¹, and Stefan Burdach¹

Abstract

Ewing tumors comprise the second most common type of bone-associated cancer in children and are characterized by oncogenic EWS/FLI1 fusion proteins and early metastasis. Compelling evidence suggests that elevated levels of intracellular oxidative stress contribute to enhanced aggressiveness of numerous cancers, possibly including Ewing tumors. Using comprehensive microarray analyses and RNA interference, we identified the six-transmembrane epithelial antigen of the prostate 1 (STEAP1)—a membrane-bound mesenchymal stem cell marker of unknown function—as a highly expressed protein in Ewing tumors compared with benign tissues and show its regulation by EWS/FLI1. In addition, we show that STEAP1 knockdown reduces Ewing tumor proliferation, anchorage-independent colony formation as well as invasion *in vitro* and decreases growth and metastasis of Ewing tumor xenografts *in vivo*. Moreover, transcriptome and proteome analyses as well as functional studies revealed that STEAP1 expression correlates with oxidative stress responses and elevated levels of reactive oxygen species that in turn are able to regulate redox-sensitive and proinvasive genes. In synopsis, our data suggest that STEAP1 is associated with the invasive behavior and oxidative stress phenotype of Ewing tumors and point to a hitherto unanticipated oncogenic function of STEAP1. *Mol Cancer Res*; 10(1); 52–65. ©2011 AACR.

Introduction

Ewing tumors are highly metastatic bone-associated cancers of enigmatic histogenesis mostly affecting children. Established therapies still have limited success in advanced stages of the disease despite high toxicity (1). Thus, selective

and less toxic drugs are the prerequisites to reduce the toxic burden of cure.

Ewing tumors express chimeric EWS/ETS (Ewing sarcoma breakpoint region 1/E-twenty-six) fusion proteins derived from chromosomal translocations with EWS/FLI1 (Ewing sarcoma breakpoint region 1/friend leukemia virus integration 1) being the predominant one (85%). *EWS/FLI1* encodes an oncogenic transcription factor that determines the complex and highly malignant phenotype of Ewing tumors (2). Hence, the detailed functional characterization of the EWS/FLI1-induced transcriptome may be key to understand the underlying mechanisms of the disease and ultimately to halt its progression (3, 4).

Previously, we identified a specific expression signature of approximately 40 genes that are highly upregulated in Ewing tumors compared with benign tissues (3). Part of this signature is the six-transmembrane epithelial antigen of the prostate 1 (STEAP1)—a membrane-bound protein possibly contributing to transmembrane electron transfer (5, 6).

Among STEAP proteins, only STEAP1 is overexpressed in many carcinomas including prostate and bladder cancer, where it locates to plasma and endosomal membranes (6, 7), but its precise cellular function remains elusive. Recently, STEAP1 was validated as a bona fide marker for mesenchymal stem cells (MSC; ref. 8) supporting the relationship of Ewing tumors with MSCs (9). Moreover, STEAP1 mRNA

Authors' Affiliations: ¹Children's Cancer Research and Roman Herzog Comprehensive Cancer Center, Laboratory of Functional Genomics and Transplantation Biology, ²Institute of Pathology, Klinikum rechts der Isar, ³Medical Life Science and Technology Center, ⁴Experimental and Molecular Pediatric Cardiology, German Heart Center Munich; ⁵Institute of Pathology, Helmholtz-Zentrum München; ⁶Institute for Medical Microbiology, Immunology and Hygiene, Institute of Advanced Study, Technische Universität München, München; ⁷Department of Medicine, Hematology, and Oncology, and Interdisciplinary Center for Clinical Research (IZKF), University of Münster; ⁸Department of Pediatric Hematology and Oncology, University Children's Hospital Münster, Münster; ⁹Leibniz-Institut für Analytische Wissenschaften-ISAS e.V., Dortmund; ¹⁰Medical Proteome Center (MPC), Ruhr-University Bochum, Bochum, Germany; ¹¹Department of Biomedical Sciences, University of Modena and Reggio Emilia School of Medicine, Italy; and ¹²Institute for Clinical Biochemistry, University of Würzburg, Würzburg, Germany

Note: Supplementary data for this article are available at Molecular Cancer Research Online (<http://mcr.aacrjournals.org/>).

G.H.S. Richter and S. Burdach share senior authorship.

Corresponding Author: Thomas G.P. Grunewald, Technische Universität München, Körner Platz 1, Munich 80804, Germany. Phone: 4989-3068-5525; Fax: 4989-3068-3791; E-mail: thomas.grunewald@lrz.tum.de

doi: 10.1158/1541-7786.MCR-11-0524

©2011 American Association for Cancer Research.

circulates in peripheral blood (6, 10), and its detection in bone marrow of patients with Ewing tumors is indicative for occult Ewing tumor cells (11).

In contrast, STEAP1 mRNA is not detectable in blood of healthy donors and is hardly expressed in benign tissues, except for low amounts in urothelium and prostate (6, 10). Because of its high tumor specificity and membrane-bound localization, STEAP1 might serve as a promising candidate for targeted therapy (6, 10, 11). In accordance, monoclonal antibodies against STEAP1 inhibit growth of xenografted prostate and bladder cancer (12).

STEAP proteins are homologues of NADPH oxidases (NOX; refs. 13, 14), which are involved in cellular reactive oxygen species (ROS) metabolism and frequently overexpressed in cancer (15). Like NOX, all STEAP proteins, except for STEAP1, are equipped with an N-terminal NADP⁺ oxidoreductase (7, 13). In addition, all STEAP members contain a C-terminal ferric oxidoreductase. Thus, a role in cellular iron homeostasis is assumed for these proteins (16). However, in contrast to other STEAP proteins, STEAP1 does not facilitate iron uptake and reduction, suggesting another distinct function (7).

ROS play a key role in oncogenic signaling and elevated ROS levels are a salient feature of many highly invasive cancers (17, 18), possibly including Ewing tumors (19). Sound evidence suggests that many malignancies take advantage of a permanently active "oxidative stress phenotype" leading to enhanced invasiveness, which has been recognized as an additional hallmark of cancer (20). On the basis of its homology to NOX and its overexpression in highly metastatic cancers, we hypothesized that STEAP1 is involved in the invasive behavior and oxidative stress phenotype of Ewing tumors.

In the present study, we investigate the putative oncogenic function of STEAP1. We prove that *STEAP1* is induced by *EWS/FLI1* and that its expression promotes proliferation, invasiveness, anchorage-independent colony formation, tumorigenicity, and metastasis of Ewing tumors. Moreover, transcriptome and proteome analyses as well as functional studies reveal that STEAP1 expression is associated with elevated ROS levels that regulate ROS-sensitive signaling molecules and proinvasive genes via STAT1.

Materials and Methods

Cell lines and reagents

Ewing tumor cell lines (MHH-ES1, SK-ES1, RDES, SK-N-MC, TC-71), neuroblastoma lines (CHP126, MHH-NB11, SHSY5Y, SIMA), rhabdomyosarcoma cell line RH-30, and B-cell leukemia lines (Nalm6, 697, cALL2) were obtained from the German Collection of Microorganisms and Cell Cultures (DSMZ). A673 was purchased from American Type Culture Collection (LGC Standards). SB-KMS-KS1, previously described as SBSR-AKS, is an Ewing tumor cell line with a type 1 *EWS/FLI1* translocation established in our laboratory (4). Human MSCs L87 and V54.2 were immortalized with SV40 large T-antigen (4).

Retrovirus packaging cell line PT67 was obtained from Takara Bio Europe/Clontech. Cells were grown at 37°C in 5% CO₂ in a humidified atmosphere in RPMI-1640 (Invitrogen) containing 10% FBS (Biochrom), 1% glutamine, and 100 µg/mL gentamycin (Invitrogen). Cell lines were checked routinely for purity (*EWS/FLI1* translocation product, surface antigen, or HLA-phenotype) and Mycoplasma contamination. Reagents were purchased from Sigma, if not otherwise specified.

Quantitative real-time PCR

Gene expression was analyzed using TaqMan Universal PCR Master Mix, TaqMan Gene Expression Assays, and fluorescence detection with an AB 7300 Real-Time PCR System (Applied Biosystems). Results were normalized to glyceraldehyde-3-phosphate dehydrogenase (GAPDH) and quantified by the $\Delta\Delta C_t$ method. Primers are listed in Supplementary Methods.

RNA interference

Transfection was described previously (4). For siRNA, see Supplementary Methods.

Chromatin immunoprecipitation

Chromatin immunoprecipitation was essentially carried out as described (4). For primers, see Supplementary Methods.

Western blotting

Procedures were described previously (4). For antibodies, see Supplementary Methods. Specificity of the STEAP1 antibody was assessed previously (21, 22).

Tissue samples

The Institutional Review Board of the Technische Universität München (Munich, Germany) approved the current study. Archival tumor samples were obtained from the Department of Pathology of the Technische Universität München.

Histology and immunohistochemistry

Procedures were described previously (4). See Supplementary Methods.

Microarrays

Experiments were essentially carried out as described previously (4). See Supplementary Methods.

Two-dimensional gel electrophoresis and mass spectrometry

Two-dimensional (2D) isoelectric focusing/SDS-PAGE were essentially carried out as described previously (23). For spot selection and mass spectrometry, see Supplementary Methods.

Flow cytometry

Cells were stained 48 to 72 hours after transfection as described (24). Samples were analyzed on a FACScalibur

flow cytometer (Becton Dickinson). At least 30,000 events per sample were recorded. See Supplementary Methods.

Proliferation assays

Cell numbers were counted in real-time with a bioelectric xCELLigence instrument (Roche/ACEA Biosciences) monitoring impedance across gold micro-electrodes on the bottom of E-plates. Immediately after transfection with siRNA, 1.6×10^4 cells were seeded in wells in 200 μL media containing 10% FBS. Cellular impedance was measured periodically. Transfection efficacy was controlled by Western blot analysis and/or quantitative real-time PCR (qRT-PCR).

Invasion assays

A total of 5×10^5 transiently transfected cells in 500 μL serum-free media was seeded into the upper chambers of Matrigel-covered Transwell plates (Becton Dickinson). Bottom chambers contained 500 μL media with 10% FBS. After 48 hours, invading cells were stained with 4 $\mu\text{g}/\text{mL}$ CalceinAM (Becton Dickinson) in Hank's balanced salt solution and photographed with a Zeiss AxioCam MRm camera on a Zeiss Axiovert 100 microscope (Zeiss). The number of invading cells was normalized to proliferation as assessed with xCELLigence (Roche/ACEA Biosciences). *N*-Acetylcysteine (NAC) or H_2O_2 pretreatment of Matrigel plates did not affect invasiveness of untreated Ewing tumor cells plated subsequently.

Constructs and retroviral gene transfer

See Supplementary Methods.

Colony-forming assay

Procedures were described previously (4).

Mice and *in vivo* experiments

Immunodeficient $\text{Rag2}^{-/-}\gamma_c^{-/-}$ mice on a BALB/c background were obtained from the Central Institute for Experimental Animals (Kawasaki) and maintained under pathogen-free conditions in accordance with the institutional guidelines and approval by local authorities. Experiments were carried out in 6- to 16-week-old mice. For *in vivo* tumor growth, 3×10^6 Ewing tumor cells in 0.2 mL PBS were subcutaneously injected in groins. The amount of 2×10^6 to 5×10^6 cells has been previously reported to be optimal for assessment of local growth of Ewing tumor xenografts (4, 25). Mice bearing tumors greater than 10 mm in diameter (determined with a caliper) were considered positive (event). To analyze metastatic potential, tumor cells were injected intravenously. Five weeks later, mice were euthanized and metastasis was monitored in individual organs. All macroscopically visible metastases within an organ were counted. Tumors and affected tissues were excised for histology and gene expression analysis.

Measurement of ROS and mitochondrial mass

Procedures were described previously (26). See Supplementary Methods.

Glutathione assay

Cellular glutathione was assessed with a colorimetric assay kit following the manufacturer's instructions (Cayman Europe).

Electron microscopy

Procedures were described previously (27, 28).

Statistics

Unpaired two-tailed Student *t* test or independent one-sample *t* test were used; $P < 0.05$ was considered significant.

Results

STEAP1 is highly expressed in Ewing tumors and induced by EWS/FLI1

Previously, we identified STEAP1 in an Ewing tumor expression signature (3). To substantiate this observation, we matched our microarray data against those of neuroblastomas and a normal body map composed of benign fetal and adult tissues. As seen in Fig. 1A and B, STEAP1 is highly expressed in Ewing tumors but virtually not expressed in neuroblastomas and benign tissues. High STEAP1 expression in Ewing tumors was confirmed by qRT-PCR and Western blot analysis (Fig. 1C). To test whether EWS/ETS transcription factors can induce STEAP1, we transfected MSCs with *EWS/FLI1*-containing vectors and observed a 5- to 6-fold increase of STEAP1 expression in 2 MSC lines (L87 and V54.2; Fig. 1D). Vice versa, RNA interference-mediated EWS/FLI1 silencing in Ewing tumor cells reduced STEAP1 expression (Fig. 1E). Moreover, the *STEAP1* promoter contains 2 evolutionarily conserved ETS-binding sites ($-1,465$ and -250 bp upstream of the transcriptional start site), which proved to be enriched for FLI1 in chromatin immunoprecipitation (Fig. 1F). We next confirmed STEAP1 overexpression in primary Ewing tumors on protein level. As positive controls, we chose prostate cancer because of its known overexpression of STEAP1 (6). Figure 1G shows that among a series of tumors, which are usually included in the histologic differential diagnosis of Ewing tumors (29, 30), only Ewing tumors display very high STEAP1 levels. Consistently, the analysis of a sarcoma gene expression library (137 sarcomas; 14 entities) revealed that STEAP1 discriminates Ewing tumors from other sarcomas (sensitivity, 89.5%; specificity, 82.2%; ref. 31).

Knockdown of STEAP1 inhibits proliferation, invasion, anchorage-independent colony formation, tumorigenicity and metastasis of Ewing tumor cells

Because STEAP1 is overexpressed in Ewing tumors, we tested whether RNA interference-mediated STEAP1 silencing impacts the Ewing tumor phenotype. Using an xCELLigence instrument, we observed that STEAP1 knockdown reduced proliferation of Ewing tumor cells (Fig. 2A) without affecting rates of apoptosis and/or necrosis or inducing cell-cycle arrest (Supplementary Fig. S1). Moreover, STEAP1 silencing inhibited cellular invasiveness through Matrigel (Fig. 2B), whereas STEAP1 overexpression in Ewing tumor

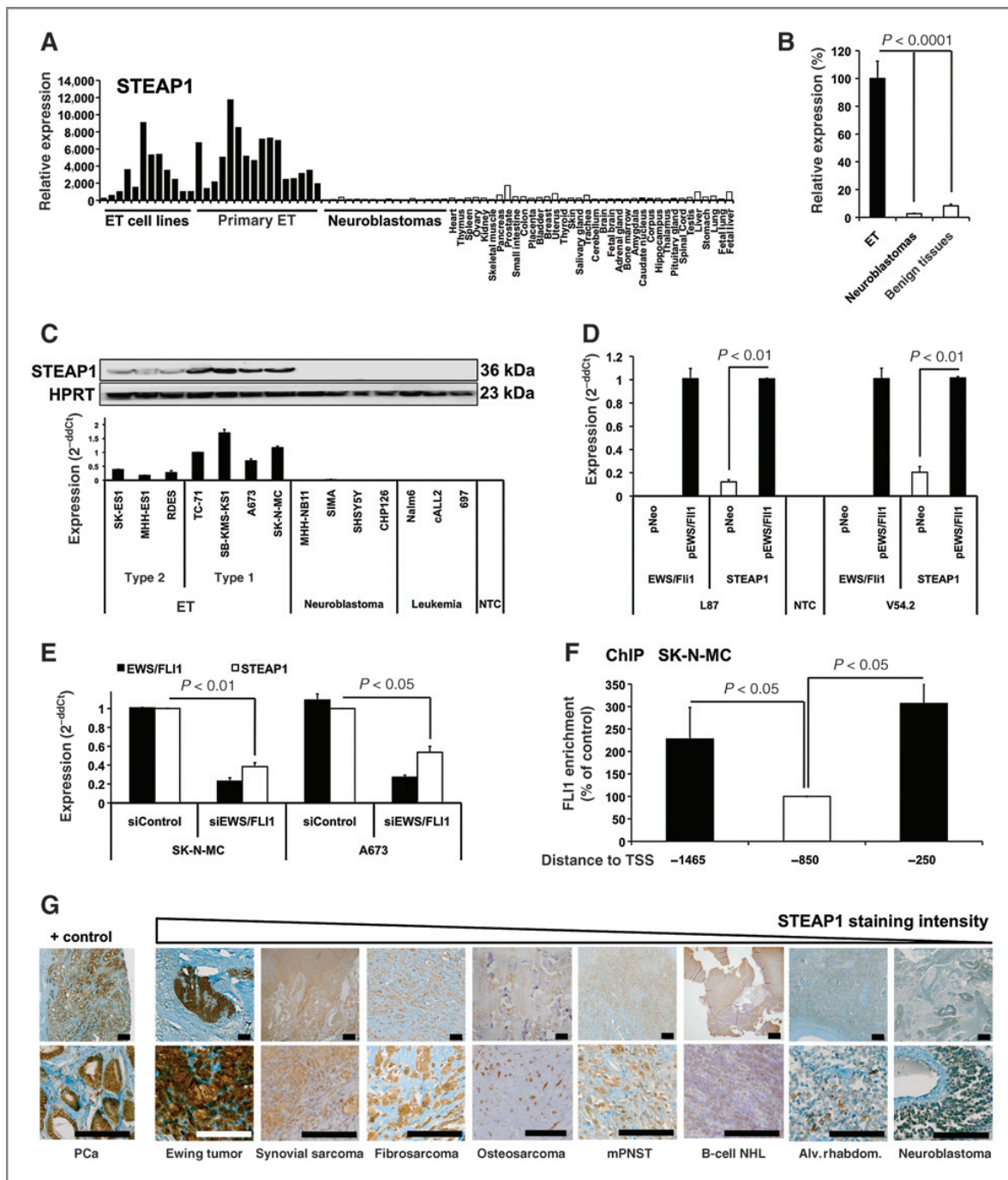


Figure 1. STEAP1 is highly expressed in Ewing tumors (ET) and induced by EWS/FLI1. **A** and **B**, RNA microarrays of 26 Ewing tumors and 16 neuroblastomas (GSE1824, GSE1825, GSE15757) compared with 36 benign tissues (GSE2361) for STEAP1 expression. Mean \pm SEM. **C**, quantification of STEAP1 by qRT-PCR and Western blot analysis in Ewing tumor (type 1 and 2 translocation), neuroblastoma, and leukemia cell lines. Mean \pm SEM of 3 experiments (duplicates/group). Loading control: hypoxanthine phosphoribosyltransferase 1 (HPRT); NTC, no template control. **D**, analysis of STEAP1 and EWS/FLI1 by qRT-PCR in MSCs (L87 and V54.2) transfected with pMSCVews/fli1 (pEWS/FLI1) or empty vector (pNEO). Mean \pm SEM of 3 experiments/cell line (duplicates/group). **E**, expression of STEAP1 and EWS/FLI1 in Ewing tumor cell lines after EWS/FLI1 silencing. Mean \pm SEM of 2 experiments/cell line (duplicates/group). **F**, chromatin immunoprecipitation (ChIP) of the STEAP1 promoter: FLI1 is enriched at the ETS consensus sites at -250 and $-1,465$ bp upstream of the transcriptional start site (TSS). The -850 -bp region is devoid of the ETS recognition sequences and served as negative control. Mean \pm SEM of 3 ChIPs; *t* test. **G**, immunohistochemistry for STEAP1 of prostate cancer (PCA), Ewing tumor, synovial sarcoma, sclerosing epithelioid fibrosarcoma, osteosarcoma, malignant peripheral nerve sheath tumor (mPNST), B-cell non-Hodgkin lymphoma (NHL), alveolar rhabdomyosarcoma (Alv. rhabdom), and neuroblastoma. Scale bars, 500 and 125 μ m.

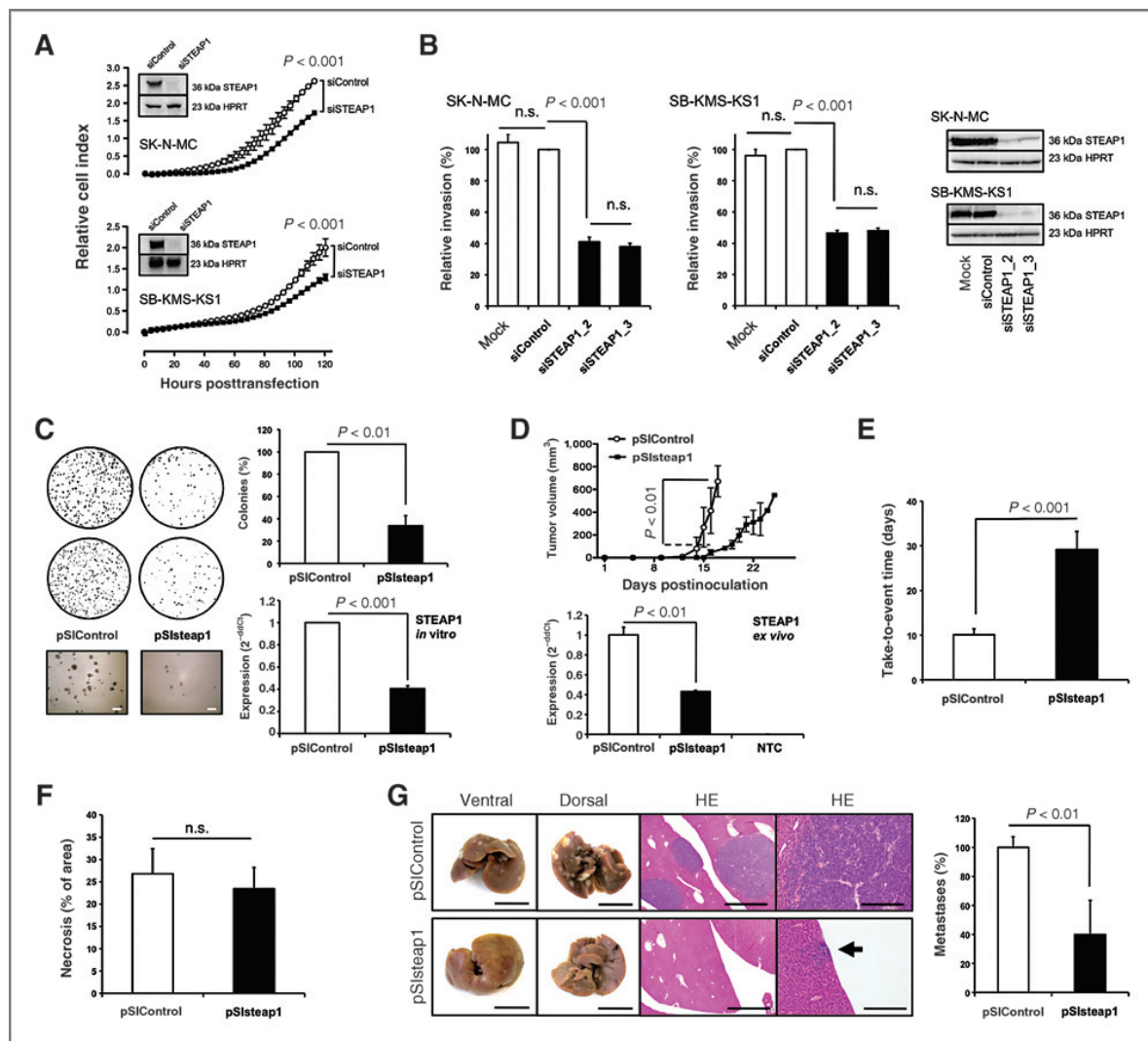


Figure 2. Knockdown of STEAP1 inhibits proliferation, invasion, anchorage-independent colony formation, tumorigenicity, and metastasis of Ewing tumor cells. **A**, analysis of proliferation of transfected Ewing tumor cells with xCELLigence. Cellular impedance is displayed as relative cell index. Mean \pm SEM of 2 experiments/cell line (heptaplicates/group). Western blot analysis was conducted 100 hours after transfection. **B**, analysis of invasiveness of SK-N-MC and SB-KMS-KS1 (transfected with siRNA 48 hours before seeding). Western blot analyses show STEAP1 knockdown efficacy. Mean \pm SEM of 3 experiments (pentaplicates/group). **C**, anchorage-independent colony formation of SK-N-MC with constitutive STEAP1 knockdown (pSiSTEAP1). Scale bars, 1,000 μm . Mean \pm SEM of 3 experiments (duplicates/group). **D**, tumorigenicity of SK-N-MC infectants (5 mice per group) and *ex vivo* confirmation of STEAP1 knockdown by qRT-PCR. Mean \pm SEM. **E**, combined analysis of tumor growth as take-to-event time of 3 experiments (14 mice pSiControl; 18 mice pSiSTEAP1). Mean \pm SEM. "Take" is the day when the tumor exceeded 2 mm and "event" when the tumor exceeded 10 mm in diameter. **F**, quantification of necrotic area (14 xenografts per group). Mean \pm SEM of 3 experiments. **G**, evaluation of metastatic potential of pSiSTEAP1 infectants (intravenously injected; 4 mice per group). All macroscopically visible metastases were counted and their small round blue phenotype was confirmed by histology (scale bar = 10 mm for macroscopy, 1,000 and 100 μm for histology; arrow, micrometastasis). Mean \pm SEM; *t* test. n.s., nonsignificant.

cells with low STEAP1 expression increased invasiveness and proliferation (Supplementary Fig. S1). Interestingly, STEAP1 levels correlated with invasiveness of different Ewing tumor cell lines (Supplementary Fig. S1). To evaluate the effect of long-term knockdown of STEAP1, we generated STEAP1 short hairpin RNA-expressing infectants of 2 Ewing tumor cell lines (SK-N-MC and SB-KMS-KS1).

Constitutive STEAP1 silencing reduced colony formation of Ewing tumor cells in methylcellulose in a dose-dependent manner (Fig. 2C and Supplementary Table S1). Consistently, these infectants exhibited delayed tumor growth in $\text{Rag}2^{-/-}\gamma_c^{-/-}$ mice (Fig. 2D and E). Persistence of STEAP1 knockdown was confirmed *ex vivo* in each xenograft (Fig. 2D). Comparing the xenografts with or without STEAP1

silencing, we did not find changes in immunohistochemistry for the apoptosis marker caspase-3 or for tumor-infiltrating macrophages (tested by MAC3; not shown). In addition, no differences in vascularization, quantified by CD31 staining (not shown), and in intratumoral necrosis were observed (Fig. 2F). Similarly to local tumor growth, experimental metastasis into the liver was diminished after STEAP1 knockdown (Fig. 2G). Although our cell lines showed a high propensity to metastasize into livers, we only noted kidney metastases in mice injected with control cells (pSIControl; not shown). Taken together, these results suggest that STEAP1 supports Ewing tumor growth and invasiveness.

STEAP1 silencing leads to adaptations in oxidative stress response systems

In accordance with data in HEK-293T cells (7), we did not find evidence for STEAP1 to impact iron uptake and reduction in Ewing tumors (Supplementary Fig. S2). However, to gain functional insight into how STEAP1 influences Ewing tumor malignancy, we conducted whole transcriptome microarrays (GSE26422) to identify concordantly regulated genes in A673 and SK-N-MC cells after STEAP1 silencing (minimum mean \log_2 fold change ± 0.32 ; maximum variation of 40% across siRNAs). STEAP1 knockdown differentially regulates 87 genes (41 upregulated and 46 downregulated; Fig. 3A and Supplementary Table S2). STEAP1-dependent gene regulation was confirmed on selected genes after STEAP1 knockdown (Fig. 3B) and STEAP1 overexpression (Supplementary Fig. S2).

Among the 40 top-regulated genes, 20% were assigned to the ubiquitin–proteasome system (UPS), suggesting that STEAP1 might play a role in protein modification that requires enhanced proteasomal decay. Consistently, gene set enrichment analysis (GSEA) revealed that STEAP1 silencing regulates gene sets involved in oxidative stress responses, type II conjugation, and proteolysis (Supplementary Table S3), which are part of the oxidative stress phenotype seen in cancer (32, 33).

In support of the prediction that changes in oxidative stress responses influence overall proteome composition, STEAP1 knockdown altered the protein levels of 121 spots (81 spots upregulated and 40 spots downregulated) of 845 spots detected in 2D gel electrophoresis of SK-N-MC cells (minimum linear fold change ± 2 in 3 independent experiments as assessed by densitometric analysis with PDquest Advanced; BioRad; $P < 0.05$).

The 24 most significantly regulated spots and 1 nonregulated control spot were excised for proteomic analysis. By mass spectrometry, 132 different proteins were identified, of which 17% were assigned to protein transport and folding, 13% to invasion, and 11% to the redox system according to their gene ontology (GO) annotations (Fig. 3C). Among these proteins are several redox enzymes such as peroxiredoxins and superoxide dismutases, which are dysregulated in a large cohort of cancers (15, 34). Moreover, endosomal redox stress response proteins (35, 36) were identified including T-complex chaperones, heat shock proteins, pro-

tein-disulfide isomerases as well as co-chaperones. Furthermore, we identified mediators of posttranscriptional mRNA processing such as heterogeneous nuclear ribonucleoproteins, THO complex proteins, and eukaryotic translation initiation factors (Supplementary Table S4). Notably, we found dysregulation of 2 of 6 key modules of the hexameric proteasomal ATPase (PSMC5 and PSMC6) and identified 2 further subunits (PSMC3 and PSMC4) in regulated spots by proteomic means as well as key modules of the proteolytic cavities of the proteasome and immunoproteasome (PSMA3, PSMB5, PSMB8, and PSMB9), which are critical for protein quality control upon oxidative stress (ref. 37; Supplementary Fig. S2). These data were confirmed by GSEA pathway analysis (Table 1). In summary, these analyses suggest that STEAP1 silencing leads to adaptations in oxidative stress response systems, supporting the hypothesis that STEAP1 is associated with the oxidative stress phenotype of Ewing tumors.

STEAP1 expression is associated with ROS levels of Ewing tumors cells

We next investigated whether the long-term knockdown of STEAP1 can lead to altered ROS levels. Indeed, constitutive STEAP1 silencing decreased ROS levels (Fig. 4A), whereas STEAP1 overexpression increased ROS levels (Fig. 4B) as quantified by dihydroethidium fluorescence. Moreover, STEAP1 knockdown reduced mitochondrial ROS without changing mitochondrial mass as quantified by MitoSOX Red and MitoTracker Green staining, respectively (Fig. 4C and D). Consistently, STEAP1 knockdown decreased the cellular pool of oxidized glutathione (glutathione disulfide) but increased the amount of reduced glutathione (GSH; Fig. 4E). Interestingly, reassessment of our microarray data revealed that STEAP1 is most prominently expressed in Ewing tumors among other NOX and STEAP proteins (Supplementary Fig. S3). It should be noted that we did not detect obvious morphologic changes of Ewing tumor cells and their mitochondria upon STEAP1 knockdown (Fig. 4F).

ROS are critical for Ewing tumor proliferation and invasiveness

Our data and recent discussion in the literature (19) indicate that ROS might promote Ewing tumor aggressiveness. In accordance, treatment of Ewing tumor cells with the antioxidant NAC reduced colony formation, proliferation, and invasiveness of Ewing tumor cells in a dose-dependent manner (Fig. 5A–C). Similar results have been obtained with PEGylated-superoxide dismutase and PEGylated-catalase (Supplementary Fig. S4). Reciprocally, treatment of STEAP1 silenced Ewing tumor cells with H_2O_2 rescued the invasive phenotype of STEAP1 knockdown cells (Fig. 5D).

We next tested whether STEAP1-regulated genes contribute to the oxidative stress phenotype observed. We choose MMP-1, ADIPOR1, and DTX3L for follow-up due to their high expression in Ewing tumors and their involvement in oxidative stress responses (34, 38, 39). Notably,

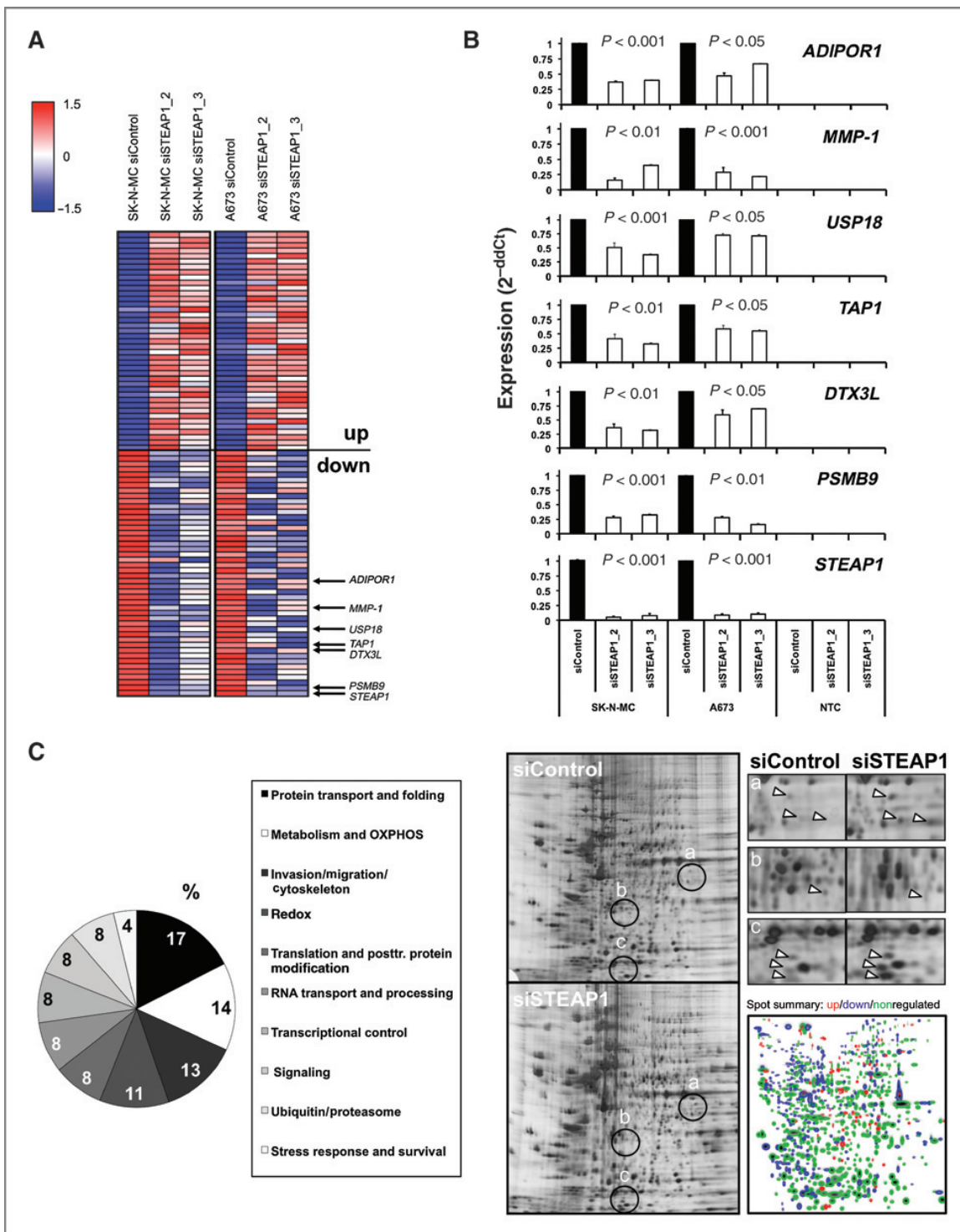


Figure 3. STEAP1 silencing leads to adaptations in oxidative stress response systems. A, heatmaps of differentially expressed genes after STEAP1 silencing (normalized median centered log₂ values) including genes selected for validation (arrows). B, validation of differential gene expression by qRT-PCR. *ADIPOR1*, adiponectin receptor 1; *MMP-1*, matrix metalloproteinase 1; *USP18*, ubiquitin-specific peptidase 18; *TAP1*, transporter 1, ATP-binding cassette, sub-family B; *DTX3L*, E3 ubiquitin-protein ligase deltex 3-like; *PSMB9*, proteasome subunit β -9. Mean \pm SEM of at least 2 experiments/cell line (duplicates/group); *t* test. C, left, distribution of functional GO annotations of differentially expressed proteins in SK-N-MC as identified by 2D gel electrophoresis and mass spectrometry 72 hours after RNA interference. Right, representative 2D gels of siControl and siSTEAP1, micrographs showing regulated spots (arrows), and the computational overlay summary of up, down, and nonregulated spots of 3 experiments.

Table 1. GSEA pathway analysis of differentially regulated proteins as identified by 2D gel electrophoresis and mass spectrometry

| Gene set name ^a | Function | K ^b | K ^c | K/K | P |
|---|--|----------------|----------------|------|--------|
| REACTOME_CHAPERONIN_MEDIATED_PROTEIN_FOLDING | Chaperonin-mediated protein folding | 50 | 7 | 0.14 | <0.001 |
| REACTOME_PREFOLDIN_MEDIATED_TRANSFER_OF_SUBSTRATE_TO_CCT_TRIC | Chaperonin-mediated protein folding | 28 | 7 | 0.25 | <0.001 |
| REACTOME_FORMATION_OF_TUBULIN_FOLDING_INTERMEDIATES_BY_CCT_TRIC | Chaperonin-mediated protein folding | 22 | 6 | 0.27 | <0.001 |
| KEGG_PROTEASOME | Proteasomal protein decay | 48 | 6 | 0.13 | <0.001 |
| REACTOME_SCF_BETA_TRCP_MEDIATED_DEGRADATION_OF_EMI1 | Ubiquitin ligase-mediated protein processing | 48 | 6 | 0.13 | <0.001 |
| REACTOME_SCF_SKP2_MEDIATED_DEGRADATION_OF_P27_P21 | Ubiquitin ligase-mediated protein processing | 52 | 6 | 0.12 | <0.001 |
| REACTOME_ASSOCIATION_OF_TRIC_CCT_WITH_TARGET_PROTEINS_DURING BIOSYNTHESIS | Chaperonin-mediated protein folding | 29 | 5 | 0.17 | <0.001 |
| REACTOME_METABOLISM_OF_PROTEINS | Translation, posttranslational modification, and protein folding | 215 | 12 | 0.06 | 0.024 |

^aREACTOME, BIOCARTA, and KEGG pathway gene sets were used for analysis.

^bK = number of genes in gene set.

^cK = number of genes in overlap.

expression of MMP-1, ADIPOR1, and DTX3L appeared to be ROS sensitive in Ewing tumor cells as H₂O₂ treatment induced their expression in a time-dependent manner (Fig. 5E). Moreover, H₂O₂ treatment rescued MMP-1, ADIPOR1, and DTX3L, but not STEAP1, expression in a dose-dependent manner implying that STEAP1 is upstream of ROS signaling whereas the other genes are potentially downstream (Fig. 5F). Interestingly, silencing of these genes reduced invasiveness through Matrigel (Fig. 5G), whereas only ADIPOR1 knockdown significantly reduced Ewing tumor proliferation (Fig. 5H). In summary, these data suggest that oxidative stress may support Ewing tumor aggressiveness possibly, in part, via enhanced expression of MMP-1, ADIPOR1, and DTX3L.

STEAP1 knockdown inhibits STAT1 activation

Using GSEA to search for common transcription factor motifs within the 87 differentially regulated genes after STEAP1 silencing, we identified STAT1 ($P = 0.07$) and its downstream cofactors, IFN response factors (IRF) 1, 2, 7, and 8 ($P < 0.05$; ref. 40) as top-ranked putative STEAP1 targets. Consistently, interrogation of the GSEA Molecular Signatures Database (C2; v3.0) with these 87 genes revealed a strong overrepresentation of gene sets involved in IFN signaling accompanying STEAP1 expression (Fig. 6A and B). Interestingly, STAT1, a downstream effector of ROS and IFNs (41), is predominantly expressed in Ewing tumors (Fig. 6C). Of note, alike STEAP1 silencing, STAT1 silencing reduced the expression of STEAP1 target genes but left STEAP1 expression unaffected. Moreover, the downregulation of these genes could (apart from MMP-1 in 2 of 3 cell lines tested) not be rescued by H₂O₂, suggesting that STAT1

may be downstream of ROS and STEAP1 (compare Figs. 6D and 5F). Indeed, STEAP1 silencing results in less phosphorylated STAT1, which can be rescued by exogenous H₂O₂ and IFN- γ (Fig. 6E). However, Ewing tumor cells virtually do not endogenously produce IFNs and STEAP1 silencing neither alters their expression nor their secretion as seen by microarray (Fig. 6F) and ELISPOT analyses (Supplementary Fig. S5). In summary, these data indicate that STEAP1 and ROS may, in part, mediate their transcriptional effects via IFN-independent activation of STAT1 (Fig. 6G).

Discussion

The current study assessed the involvement of STEAP1 in the invasive and oxidative stress phenotype of Ewing tumors. We show that *STEAP1* is induced by EWS/FLI1 and important for Ewing tumor malignancy. Moreover, our data support a model whereby STEAP1 expression is linked to the maintenance of oxidative stress of Ewing tumors and increased Ewing tumor aggressiveness, probably mediated via STAT1. We show that STEAP1 is highly expressed in Ewing tumors compared with benign tissues and a series of other sarcomas implying that STEAP1 could be used in routine pathology as an additional marker for Ewing tumor diagnosis.

Our data indicate that STEAP1 is important for anchorage-independent colony formation and invasiveness of Ewing tumor cells *in vitro* and for tumorigenicity and metastasis *in vivo*. Moreover, we show that STEAP1 expression correlates with increased cellular ROS levels, which in turn induce the redox-sensitive and proinvasive

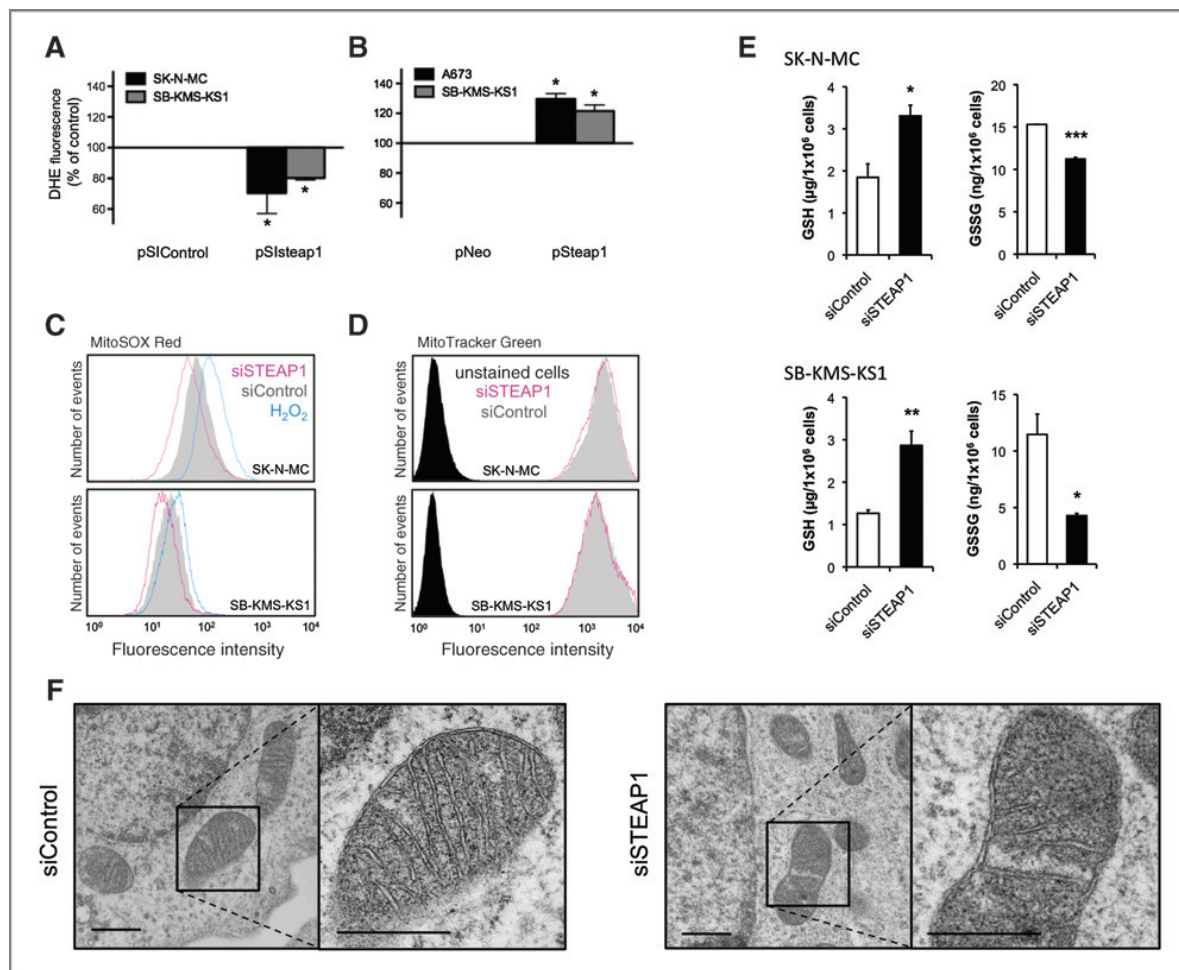


Figure 4. STEAP1 expression is associated with ROS levels of Ewing tumor cells. **A** and **B**, measurement of ROS with dihydroethidium (DHE) fluorescence after constitutive STEAP1 silencing (pSiSteap1) or STEAP1 overexpression (pSteap1). Mean \pm SEM of 3 experiments/cell line (octuplicates/group). Controls set as 100%. **C** and **D**, representative images of flow cytometric measurements of mitochondrial ROS (MitoSOX Red) and mitochondrial mass (MitoTracker Green) in Ewing tumor cells 72 hours after RNA interference. Minimum 30,000 events per group; 3 experiments/cell line. For positive control in MitoSOX Red staining, an aliquot of the cells was preincubated with 100 μmol/L hydrogen peroxide (H₂O₂; blue). **E**, analysis of reduced (GSH) and oxidized glutathione (glutathione disulfide; GSSG) 48 hours after transfection. Mean \pm SEM of 2 experiments/cell line. **F**, low-power electron micrographs of SK-N-MC 80 hours after transfection showing no differences in mitochondrial morphology (scale bars, 0.4 μm). *, P < 0.05; **, P < 0.01; ***, P < 0.001; t test.

genes *MMP-1*, *DTX3L*, and *ADIPOR1*. Consistently, Pan and colleagues found that STEAP1 overexpression promotes ROS-mediated hyperproliferation of thyroid epithelial cells (42).

ROS participate in oncogenic signaling and elevated ROS levels are a salient feature of aggressive cancers (17, 18). Disturbances in the delicate ROS balance can lead to protein misfolding, accumulation of dysfunctional proteins, and activation of cellular stress responses (36). In accordance, STEAP1 silencing provokes transcriptional and posttranscriptional adaptations of oxidative stress responses comprising the redox, chaperone, endopeptidase, and UPS. These observations are compatible with the hypothesis that STEAP1 is associated with an enhanced oxidative stress

phenotype in Ewing tumors. Consistently, we found that STEAP1 positively correlates with cytoplasmic and mitochondrial ROS levels. As mitochondrial morphology remained unaffected, we suppose that mitochondrial ROS levels change concomitantly with cytoplasmic ROS levels upon STEAP1-silencing, a mechanism also seen in the context of NOX proteins ("ROS-cross-talk"; ref. 43). The role of STEAP1 in ROS modulation is supported by *in silico* predictions and crystallography of STEAP proteins defining them as heme-containing redox enzymes (5, 13). Less aggressive ROS are well known to interact with heme iron of heme-containing proteins (15). Here, a nonenzymatic 2-electron oxidation of heme generates ferryl-heme and an unstable free radical that may be released as more aggressive

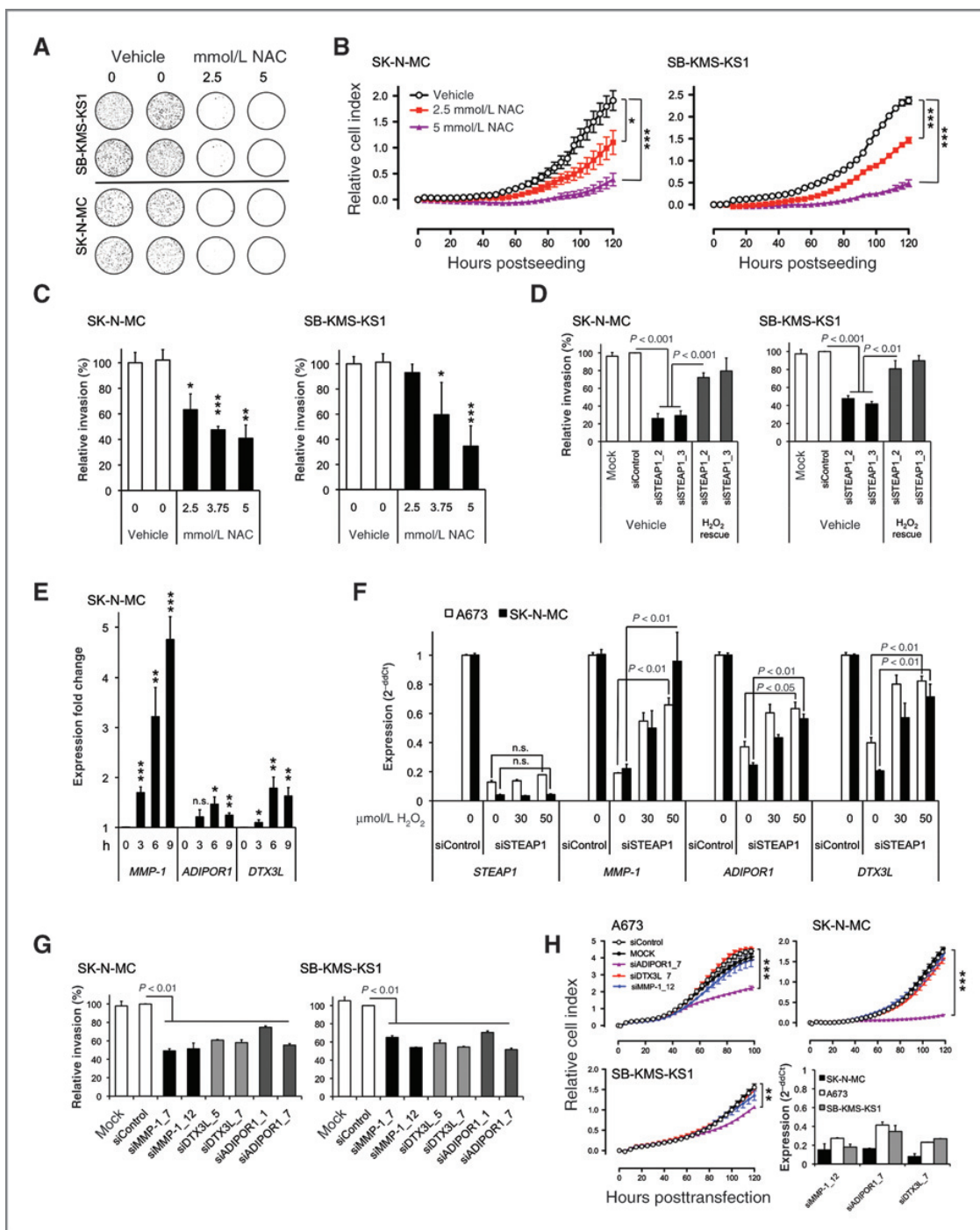


Figure 5. ROS are critical for Ewing tumor proliferation and invasiveness. **A**, colony formation of Ewing tumor cells treated with NAC or vehicle (H₂O). Images are representative for 3 experiments per cell line (duplicates/group). **B**, analysis of proliferation of SK-N-MC and SB-KMS-KS1 treated with NAC every 48 hours using xCELLigence. Mean \pm SEM of 2 experiments per cell line (quadruplicates/group). **C**, analysis of invasiveness of SK-N-MC and SB-KMS-KS1 treated with NAC. Mean \pm SEM of 2 experiments per cell line (pentaplicates/group). **D**, invasiveness of STEAP1-silenced SK-N-MC and SB-KMS-KS1 with/without H₂O₂ rescue. For H₂O₂ rescue, cells were treated periodically with H₂O₂ (cumulative dosage: 40 μ mol/L). Mean \pm SEM of 2 experiments per cell line (pentaplicates/group). **E**, MMP-1, ADIPOR1, and DTX3L expression in SK-N-MC treated with 50 μ mol/L H₂O₂ for 0 to 9 hours. Mean \pm SEM of 5 experiments (duplicates/group). **F**, analysis of STEAP1, MMP-1, ADIPOR1, and DTX3L expression in STEAP1-silenced A673 and SK-N-MC 6 hours after treatment with H₂O₂. Mean \pm SEM of at least 2 experiments per cell line (duplicates/group). **G**, invasiveness of SK-N-MC and SB-KMS-KS1 transfected 48 hours before seeding. Mean \pm SEM of 2 experiments per cell line (pentaplicates/group). **H**, analysis of proliferation of SK-N-MC and SB-KMS-KS1. Knockdown was confirmed by qRT-PCR (controls set as 1). Mean \pm SEM of 2 experiments per cell line (heptaplicates/group). *, P < 0.05; **, P < 0.01; ***, P < 0.001; †, P < 0.05; n.s., nonsignificant.

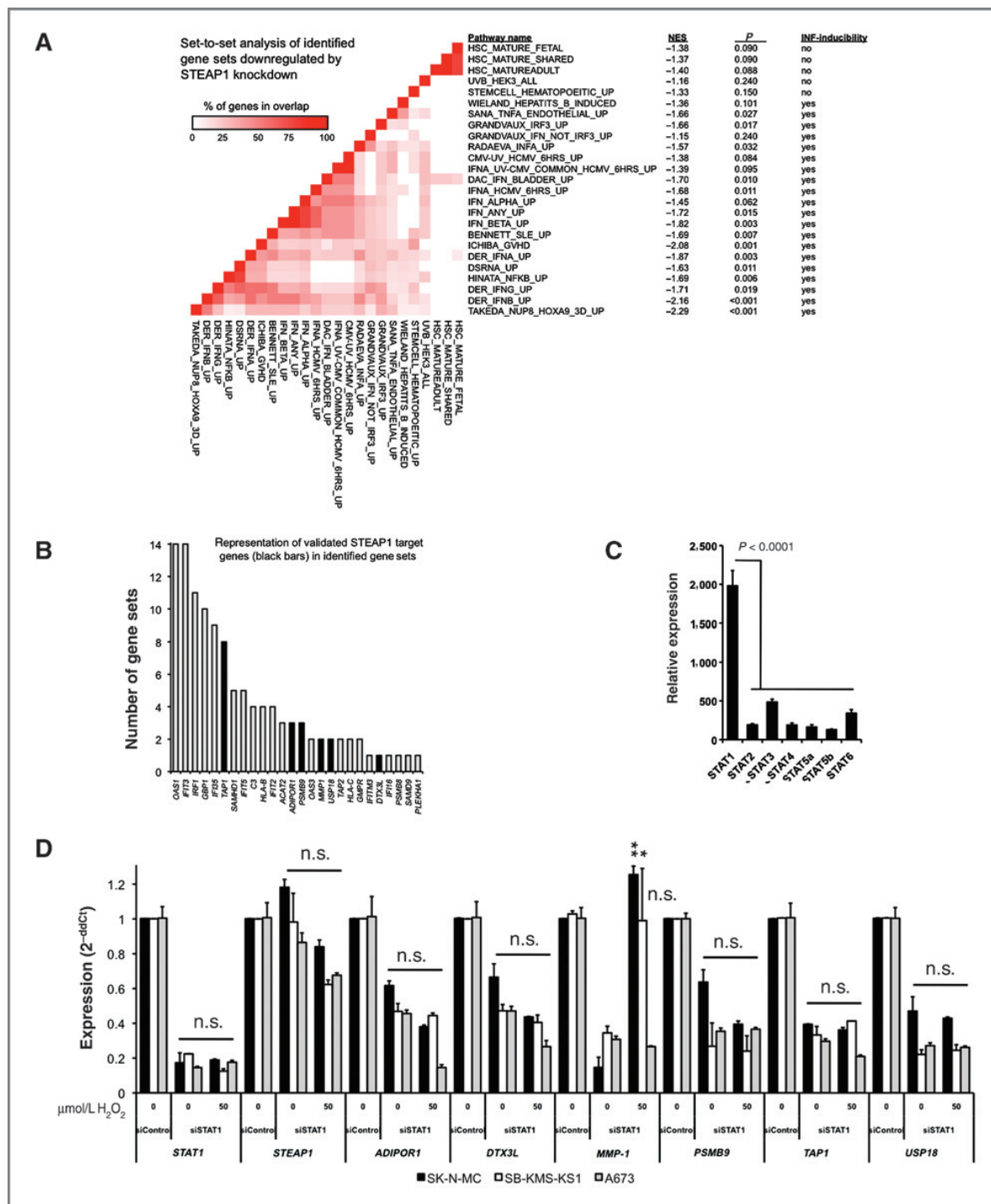


Figure 6. STEAP1 knockdown inhibits STAT1 activation. A, matrix diagram of the GSEA leading edge set-to-set analysis showing enrichment of IFN-related gene sets. NES, normalized enrichment score. B, gene-in-subset analysis reveals representation of validated STEAP1 target genes (black bars) within leading-edge genes. C, expression (mean \pm SEM) of different STAT proteins in 26 Ewing tumor microarrays. D, expression analysis of STEAP1 target genes by qRT-PCR 48 hours after STAT1 silencing and H_2O_2 treatment (50 $\mu\text{mol/L}$ for 6 hours).

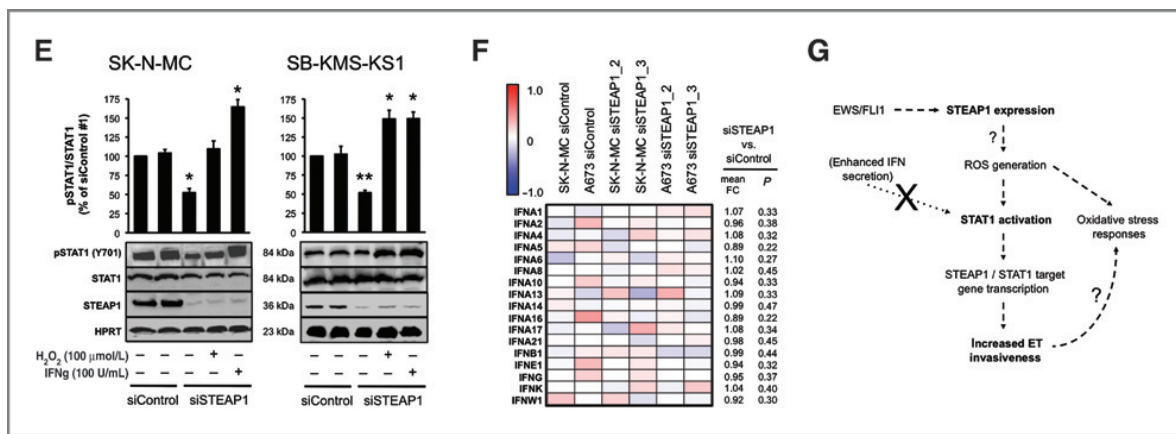


Figure 6. (Continued) E, Western blot and densitometric analysis of phospho-STAT1 (Y701) in Ewing tumor cells 48 hours after RNA interference and H_2O_2 (100 $\mu\text{mol/L}$) or IFN- γ (100 U/mL) stimulation (both 10 minutes). F, heatmap showing expression of IFN genes in Ewing tumor cells with/without STEAP1 silencing. G, simplified model of STEAP1-mediated target gene regulation. *, $P < 0.05$; **, $P < 0.01$; t test. FC, fold change; n.s., nonsignificant.

ROS in a site-specific manner depending on the localization of the protein (44, 45). As STEAP1 contains a ferric oxidoreductase, it is tempting to speculate that the protein generates ROS by itself (7, 42). However, although STEAP1 target genes appear to be downstream of ROS (Fig. 5F), it remains possible that part of STEAP1-induced ROS merely accompany upstream events involved in the STEAP1 phenotype.

Multiple studies proved that permanently elevated ROS levels activate prometastatic and proproliferative signaling in cancer (17, 19, 20). In agreement, we provide evidence that antioxidants reduce colony formation, proliferation, and invasion of Ewing tumor cells suggesting that Ewing tumors may benefit from an activated oxidative stress phenotype. Among STEAP1-regulated genes, we focused on *MMP-1*, *ADIPOR1*, and *DTX3L* all of which are implicated in ROS signaling. For instance, *MMP-1* has been shown to be highly ROS inducible (34, 46) and its overexpression increases invasiveness and metastasis of a variety of cancers (47). *ADIPOR1* is the cognate receptor for adiponectin, which stimulates proliferation of hematopoietic stem cells (48). Although the precise function of the ubiquitin ligase *DTX3L* is not defined, recent work suggests that *DTX3L* monoubiquitylates histone H4 lysine 91 and thereby protects DNA from ROS (39). Here, we show that these genes are highly inducible by ROS and regulated by STAT1. STAT1 had been traditionally viewed as a mere IFN signal transducer but has recently been linked with aggressiveness, therapy resistance, and oxidative stress responses of several cancers (49, 50). Consistently, we prove that the coordinated expression of *MMP-1*, *ADI-*

POR1, and *DTX3L* fosters the invasive and proliferative phenotype of Ewing tumors.

In summary, this work for the first time provides evidence that an activated oxidative stress phenotype enhances Ewing tumor malignancy: we show that STEAP1 overexpression promotes proliferation, invasiveness, anchorage-independent colony formation, tumorigenicity, and metastasis of Ewing tumors. Because STEAP1 is overexpressed in a wide variety of carcinomas, its oncogenic function may have general relevance for tumor progression and targeted therapy.

Disclosure of Potential Conflicts of Interest

No potential conflicts of interest were disclosed.

Acknowledgments

The authors thank Barbara Grunewald and Veit Buchholz for fruitful discussion and Ulrich Welsch for his help with electron microscopy.

Grant Support

This work was supported by the TU München (B08-05; A09-02), the Deutsche Forschungsgemeinschaft (GR3728/1.1, SFB/TR22, and EB740/6.1), the Wilhelm-Sander-Stiftung (2009.901.1), the Ministerium für Innovation, Wissenschaft und Technologie des Landes Nordrhein-Westfalen, the EU 7thFP Metoxia, the Bundesministerium für Bildung und Forschung (BMBF), and the Translational-Sarcoma-Research-Network supported by the BMBF (FK 01GM0870).

The costs of publication of this article were defrayed in part by the payment of page charges. This article must therefore be hereby marked *advertisement* in accordance with 18 U.S.C. Section 1734 solely to indicate this fact.

Received November 4, 2011; accepted November 7, 2011; published OnlineFirst November 11, 2011.

References

- Burdach S, Jurgens H. High-dose chemoradiotherapy (HDC) in the Ewing family of tumors (EFT). *Crit Rev Oncol Hematol* 2002;41:169–89.
- Delattre O, Zucman J, Melot T, Garau XS, Zucker JM, Lenoir GM, et al. The Ewing family of tumors—a subgroup of small-round-cell tumors defined by specific chimeric transcripts. *N Engl J Med* 1994;331:294–9.

3. Staeger MS, Hutter C, Neumann I, Foja S, Hattenhorst UE, Hansen G, et al. DNA microarrays reveal relationship of Ewing family tumors to both endothelial and fetal neural crest-derived cells and define novel targets. *Cancer Res* 2004;64:8213-21.
4. Richter GH, Plehm S, Fasan A, Rössler S, Unland R, Bennani-Baiti IM, et al. EZH2 is a mediator of EWS/FLI1 driven tumor growth and metastasis blocking endothelial and neuro-ectodermal differentiation. *Proc Natl Acad Sci U S A* 2009;106:5324-9.
5. Sendamari AK, Ohgami RS, Fleming MD, Lawrence CM. Structure of the membrane proximal oxidoreductase domain of human Steap3, the dominant ferrireductase of the erythroid transferrin cycle. *Proc Natl Acad Sci U S A* 2008;105:7410-5.
6. Hubert RS, Vivanco I, Chen E, Rastegar S, Leong K, Mitchell SC, et al. STEAP: a prostate-specific cell-surface antigen highly expressed in human prostate tumors. *Proc Natl Acad Sci U S A* 1999;96:14523-8.
7. Ohgami RS, Campagna DR, McDonald A, Fleming MD. The Steap proteins are metalloreductases. *Blood* 2006;108:1388-94.
8. Vaghjiani RJ, Talma S, Murphy CL. Six-transmembrane epithelial antigen of the prostate (STEAP1 and STEAP2)-differentially expressed by murine and human mesenchymal stem cells. *Tissue Eng Part A* 2009;15:2073-83.
9. Tirole F, Laud-Duval K, Prieur A, Delorme B, Charbord P, Delattre O. Mesenchymal stem cell features of Ewing tumors. *Cancer Cell* 2007;11:421-9.
10. Valenti MT, Dalle Carbonare L, Donatelli L, Bertoldi F, Giovanazzi B, Caliari F, et al. STEAP mRNA detection in serum of patients with solid tumors. *Cancer Lett* 2009;273:122-6.
11. Cheung IY, Feng Y, Danis K, Shukla N, Meyers P, Ladanyi M, et al. Novel markers of subclinical disease for Ewing family tumors from gene expression profiling. *Clin Cancer Res* 2007;13:6978-83.
12. Challita-Eid PM, Morrison K, Etessami S, An Z, Morrison KJ, Perez-Villar JJ, et al. Monoclonal antibodies to six-transmembrane epithelial antigen of the prostate-1 inhibit intercellular communication *in vitro* and growth of human tumor xenografts *in vivo*. *Cancer Res* 2007;67:5798-805.
13. Sanchez-Pulido L, Rojas AM, Valencia A, Martinez AC, Andrade MA. ACRATA: a novel electron transfer domain associated to apoptosis and cancer. *BMC Cancer* 2004;4:98.
14. von Rozycki T, Yen MR, Lende EE, Saier MH Jr. The YedZ family: possible heme binding proteins that can be fused to transporters and electron carriers. *J Mol Microbiol Biotechnol* 2004;8:129-40.
15. Lambeth JD. NOX enzymes and the biology of reactive oxygen. *Nat Rev Immunol* 2004;4:181-9.
16. Ohgami RS, Campagna DR, Greer EL, Antiochos B, McDonald A, Chen J, et al. Identification of a ferrireductase required for efficient transferrin-dependent iron uptake in erythroid cells. *Nat Genet* 2005;37:1264-9.
17. Szatrowski TP, Nathan CF. Production of large amounts of hydrogen peroxide by human tumor cells. *Cancer Res* 1991;51:794-8.
18. Grek CL, Tew KD. Redox metabolism and malignancy. *Curr Opin Pharmacol* 2010;10:362-8.
19. Smith DG, Maguire T, Burchill SA. Oxidative stress and therapeutic opportunities: focus on the Ewing's sarcoma family of tumors. *Expert Rev Anticancer Ther* 2011;11:229-49.
20. Luo J, Solimini NL, Elledge SJ. Principles of cancer therapy: oncogene and non-oncogene addiction. *Cell* 2009;136:823-37.
21. Klein A, Guhl E, Zollinger R, Tzeng YJ, Wessel R, Hummel M, et al. Gene expression profiling: cell cycle deregulation and aneuploidy do not cause breast cancer formation in WAP-SVT/t transgenic animals. *J Mol Med (Berl)* 2005;83:362-76.
22. Kobayashi H, Nagato T, Sato K, Aoki N, Kimura S, Murakami M, et al. Recognition of prostate and melanoma tumor cells by six-transmembrane epithelial antigen of prostate-specific helper T lymphocytes in a human leukocyte antigen class II-restricted manner. *Cancer Res* 2007;67:5498-504.
23. Grunewald TG, Kammerer U, Winkler C, Schindler D, Sickmann A, Honig A, et al. Overexpression of LASP-1 mediates migration and proliferation of human ovarian cancer cells and influences zyxin localization. *Br J Cancer* 2007;96:296-305.
24. Grunewald TG, Kammerer U, Schulze E, Schindler D, Honig A, Zimmer M, et al. Silencing of LASP-1 influences zyxin localization, inhibits proliferation and reduces migration in breast cancer cells. *Exp Cell Res* 2006;312:974-82.
25. Nelson L, Das SK, Hajdu SI. Human neuroblastoma in nude mice. *Cancer Res* 1975;35:2594-9.
26. Diebold I, Djordjevic T, Petry A, Hatzelmann A, Tenor H, Hess J, et al. Phosphodiesterase 2 mediates redox-sensitive endothelial cell proliferation and angiogenesis by thrombin via Rac1 and NADPH oxidase 2. *Circ Res* 2009;104:1169-77.
27. Chappell D, Dorfler N, Jacob M, Rehm M, Welsch U, Conzen P, et al. Glycocalyx protection reduces leukocyte adhesion after ischemia/reperfusion. *Shock* 2009;34:133-9.
28. Grunewald TG, von Luettichau I, Welsch U, Dörr HG, Höpner F, Kovacs K, et al. First report of ectopic ACTH syndrome and PTHrP-induced hypercalcemia due to a hepatoblastoma in a child. *Eur J Endocrinol* 2010;162:813-8.
29. Lessnick SL, Dei Tos AP, Sorensen PH, Dileo P, Baker LH, Ferrari S, et al. Small round cell sarcomas. *Semin Oncol* 2009;36:338-46.
30. Schmidt D, Harms D, Burdach S. Malignant peripheral neuroectodermal tumours of childhood and adolescence. *Virchows Arch A Pathol Anat Histopathol* 1985;406:351-65.
31. Baird K, Davis S, Antonescu CR, Harper UL, Walker RL, Chen Y, et al. Gene expression profiling of human sarcomas: insights into sarcoma biology. *Cancer Res* 2005;65:9226-35.
32. Acharya A, Das I, Chandhok D, Saha T. Redox regulation in cancer: a double-edged sword with therapeutic potential. *Oxid Med Cell Longev* 2010;3:23-34.
33. Landriscina M, Maddalena F, Laudiero G, Esposito F. Adaptation to oxidative stress, chemoresistance, and cell survival. *Antioxid Redox Signal* 2009;11:2701-16.
34. Nelson KK, Ranganathan AC, Mansouri J, Rodriguez AM, Providence KM, Rutter JL, et al. Elevated sod2 activity augments matrix metalloproteinase expression: evidence for the involvement of endogenous hydrogen peroxide in regulating metastasis. *Clin Cancer Res* 2003;9:424-32.
35. Buchberger A, Bukau B, Sommer T. Protein quality control in the cytosol and the endoplasmic reticulum: brothers in arms. *Mol Cell* 2010;40:238-52.
36. Grolach A, Klappa P, Kietzmann T. The endoplasmic reticulum: folding, calcium homeostasis, signaling, and redox control. *Antioxid Redox Signal* 2006;8:1391-418.
37. Seifert U, Bialy LP, Ebstein F, Bech-Otschir D, Voigt A, Schröter F, et al. Immunoproteasomes preserve protein homeostasis upon interferon-induced oxidative stress. *Cell* 2010;142:613-24.
38. Iwabu M, Yamauchi T, Okada-Iwabu M, Sato K, Nakagawa T, Funata M, et al. Adiponectin and AdipoR1 regulate PGC-1alpha and mitochondria by Ca(2+) and AMPK/SIRT1. *Nature* 2010;464:1313-9.
39. Yan Q, Dutt S, Xu R, Graves K, Juszczynski P, Manis JP, et al. BBAP monoubiquitylates histone H4 at lysine 91 and selectively modulates the DNA damage response. *Mol Cell* 2009;36:110-20.
40. Honda K, Takaoka A, Taniguchi T. Type I interferon [corrected] gene induction by the interferon regulatory factor family of transcription factors. *Immunity* 2006;25:349-60.
41. Simon AR, Rai U, Fanburg BL, Cochran BH. Activation of the JAK-STAT pathway by reactive oxygen species. *Am J Physiol* 1998;275:C1640-52.
42. Pan YZ, Li Y, Guo LR, Zhao YY, Zhao XJ. [Influence of expression of six transmembrane epithelial antigen of the prostate-1 on intracellular reactive oxygen species level and cell growth: an *in vitro* experiment]. *Zhonghua Yi Xue Za Zhi* 2008;88:641-4.
43. Daiber A. Redox signaling (cross-talk) from and to mitochondria involves mitochondrial pores and reactive oxygen species. *Biochim Biophys Acta* 2010;1797:897-906.

44. Galaris D, Skliada V, Barbouti A. Redox signaling and cancer: the role of "labile" iron. *Cancer Lett* 2008;266:21–9.

45. Chevion M. A site-specific mechanism for free radical induced biological damage: the essential role of redox-active transition metals. *Free Radic Biol Med* 1988;5:27–37.

46. Grange L, Nguyen MV, Lardy B, Derouazi M, Campion Y, Trocme C, et al. NAD(P)H oxidase activity of Nox4 in chondrocytes is both inducible and involved in collagenase expression. *Antioxid Redox Signal* 2006;8:1485–96.

47. Johansson N, Ahonen M, Kahari VM. Matrix metalloproteinases in tumor invasion. *Cell Mol Life Sci* 2000;57:5–15.

48. DiMascio L, Voermans C, Uqoewa M, Duncan A, Lu D, Wu J, et al. Identification of adiponectin as a novel hemopoietic stem cell growth factor. *J Immunol* 2007;178:3511–20.

49. Khodarev NN, Minn AJ, Efimova EV, Darga TE, Labay E, Beckett M, et al. Signal transducer and activator of transcription 1 regulates both cytotoxic and prosurvival functions in tumor cells. *Cancer Res* 2007;67:9214–20.

50. Schultz J, Koczan D, Schmitz U, Ibrahim SM, Pilch D, Landsberg J, et al. Tumor-promoting role of signal transducer and activator of transcription (Stat)1 in late-stage melanoma growth. *Clin Exp Metastasis* 2010;27:133–40.

Molecular Cancer Research



STEAP1 Is Associated with the Invasive and Oxidative Stress Phenotype of Ewing Tumors

Thomas G.P. Grunewald, Isabel Diebold, Irene Esposito, et al.

Mol Cancer Res 2012;10:52-65. Published OnlineFirst November 11, 2011.

Updated version Access the most recent version of this article at:
[doi:10.1158/1541-7786.MCR-11-0524](https://doi.org/10.1158/1541-7786.MCR-11-0524)

Supplementary Material Access the most recent supplemental material at:
<http://mcr.aacrjournals.org/content/suppl/2011/11/11/1541-7786.MCR-11-0524.DC1.html>

Cited Articles This article cites by 50 articles, 16 of which you can access for free at:
<http://mcr.aacrjournals.org/content/10/1/52.full.html#ref-list-1>

Citing articles This article has been cited by 5 HighWire-hosted articles. Access the articles at:
<http://mcr.aacrjournals.org/content/10/1/52.full.html#related-urls>

E-mail alerts [Sign up to receive free email-alerts](#) related to this article or journal.

Reprints and Subscriptions To order reprints of this article or to subscribe to the journal, contact the AACR Publications Department at
pubs@aacr.org.

Permissions To request permission to re-use all or part of this article, contact the AACR Publications Department at
permissions@aacr.org.

High STEAP1 expression is associated with improved outcome of Ewing's sarcoma patients

T. G. P. Grunewald^{1,2*}, A. Ranft^{3,†}, I. Esposito^{4,5,†}, P. da Silva-Buttkus⁵, M. Aichler⁵, D. Baumhoer⁶, K. L. Schaefer⁷, L. Ottaviano⁷, C. Poremba^{7,8}, G. Jundt⁶, H. Jürgens³, U. Dirksen³, G. H. S. Richter^{1,‡} & S. Burdach^{1,‡}

¹Children's Cancer Research and Roman Herzog Comprehensive Cancer Center, Laboratory of Functional Genomics and Transplantation Biology, Klinikum rechts der Isar, Technische Universität München, Munich; ²Medical Life Science and Technology Center, TUM Graduate School, Technische Universität München, Garching;

³Department of Pediatric Hematology and Oncology, University Hospital Münster, Münster; ⁴Institute of Pathology, Klinikum rechts der Isar, Technische Universität München, Munich; ⁵Institute of Pathology, Helmholtz-Zentrum München, Neuherberg, Germany; ⁶Bone Tumor Reference Center at the Institute of Pathology, University Hospital Basel, Basel, Switzerland; ⁷Institute of Pathology, Heinrich-Heine-University, Düsseldorf; ⁸Center of Histopathology, Cytology, and Molecular Diagnostics (CHCMD), Trier, Germany

Received 10 August 2011; revised 2 December 2011; accepted 5 December 2011

Background: Ewing's sarcoma (ES) is the second most common bone or soft-tissue sarcoma in childhood and adolescence and features a high propensity to metastasize. The six-transmembrane epithelial antigen of the prostate 1 (STEAP1) is a membrane-bound mesenchymal stem cell marker highly expressed in ES. Here, we investigated the role of STEAP1 as an immunohistological marker for outcome prediction in patients with ES.

Patients and methods: Membranous STEAP1 immunoreactivity was analyzed using immunohistochemistry in 114 primary pre-chemotherapy ES of patients diagnosed from 1983 to 2010 and compared with clinical parameters and patient outcome. Median follow-up was 3.85 years (range 0.43–17.51).

Results: A total of 62.3% of the ES samples displayed detectable STEAP1 expression with predominant localization of the protein at the plasma membrane. High membranous STEAP1 immunoreactivity was found in 53.5%, which correlated with better overall survival ($P = 0.021$). Accordingly, no or low membranous STEAP1 expression was identified as an independent risk factor in multivariate analysis (hazard ratio 2.65, $P = 0.036$).

Conclusion: High membranous STEAP1 expression predicts improved outcome and may help to define a specific subgroup of ES patients, who might benefit from adapted therapy regimens.

Key words: biomarker, Ewing's sarcoma, outcome, risk stratification, STEAP1

introduction

Ewing's sarcoma (ES) is a highly aggressive bone or soft-tissue cancer mostly affecting children and young adolescents [1–4]. Even though multimodal treatments have led to remarkable improvements in survival of patients with localized disease, prognosis of patients with metastatic disease remains poor with an event-free survival of <25% [4–7].

ES is characterized by *EWS-ETS* translocations [8] encoding aberrant transcription factors that determine the complex and highly malignant phenotype of this disease [9]. Although different variants of *EWS-ETS* fusion proteins exist, they fail to

provide reliable biomarkers for individual risk stratification [10, 11]. Several trials proved the clinicopathological parameters, tumor site, tumor volume, age at diagnosis, responsiveness to chemotherapy, and sites of metastatic disease, to have major prognostic value [10, 12, 13]. However, the currently available biological markers for ES are very limited [12, 14, 15]. Nevertheless, the discovery of novel prognostic and/or predictive biomarkers would potentially lead to a better understanding of tumor heterogeneity, enable individual risk stratification, and might help to guide targeted therapy [16–19].

We previously identified an expression signature comprising ~40 genes that are highly overexpressed in ES compared with normal tissues and that might constitute promising candidates for risk prediction and targeted therapy [9, 20]. Among them, we identified the six-transmembrane epithelial antigen of the prostate 1 (STEAP1), which is a membrane-bound channel protein possibly involved in transmembrane electron transfer [21, 22]. Apart from low amounts in prostate and urothelium,

*Correspondence to: Dr T. G. P. Grunewald, Children's Cancer Research and Roman Herzog Comprehensive Cancer Center, Laboratory of Functional Genomics and Transplantation Biology, Klinikum rechts der Isar, Technische Universität München, Kölner Platz 1, 80804 Munich, Germany. Tel: +49-89-3068-5525; Fax: +49-89-3068-3791; E-mail: thomas.grunewald@lrz.tum.de

†These authors contributed equally to this work.

‡Both authors contributed equally as senior authors.

STEAP1 is virtually not expressed in normal tissues [23, 24]. In contrast, STEAP1 is strongly overexpressed in many cancers including prostate, breast, and bladder carcinoma as well as ES [23–25]. STEAP1 messenger RNA (mRNA) circulates in peripheral blood of cancer patients [26] and its detection in bone marrow is indicative for occult residual tumor cells in patients with ES [27]. Moreover, STEAP1 was found to be a *bona fide* marker for human mesenchymal stem cells [28] lending support to the hypothesis of a mesenchymal origin of ES [29].

In addition, we recently showed that STEAP1 overexpression increases the invasive properties and intracellular levels of reactive oxygen species (ROS) of ES cells [24]. However, the diagnostic potential of STEAP1 for ES remained undetermined.

In the current study, we investigated the value of STEAP1 as an immunohistological marker for outcome prediction of patients with ES. We provide evidence that high membranous STEAP1 expression is associated with improved overall survival (OS). Moreover, high membranous STEAP1 immunoreactivity showed a trend toward a better histological tumor response to chemotherapy and, conversely, STEAP1-silenced ES cells were more resistant to chemotherapy *in vitro*. These data unravel a hitherto unanticipated role of STEAP1 as a promising independent biomarker for outcome prediction of ES.

materials and methods

study population, ES tissue samples, and tissue microarray

The Technische Universität München and the Universities of Basel, Düsseldorf, and Münster approved the current study. A total of 114 archival paraffin-embedded primary ES samples before treatment with confirmed histological diagnosis (reference pathology) were obtained from the Departments of Pathology of the Technische Universität München and the University of Düsseldorf as well as from the Bone Tumor Reference Center at the Institute of Pathology of the University of Basel. Representative formalin-fixed, paraffin-embedded tumor blocks were selected for either tissue microarray (TMA) construction at the Department of Pathology of the University of Düsseldorf (66 samples) or open procedures at the Departments of Pathology of the Technische Universität München (6 samples) and the University of Basel (42 samples). Each TMA slide contained reference tissues of ES xenografts with known STEAP1 expression as internal controls (see supplemental Methods, available at *Annals of Oncology* online).

Pertinent clinical data of patients were compiled from two sources: first, the Ewing trial center of the University Hospital Münster (93 patients enrolled in the CESS 81, CESS 86, EICESS 92, or EURO-E.W. I.N.G. 99 trials) and second, the Department of Pathology of the University of Basel (21 patients). Informed consent was obtained from all patients and/or their legal guardians. The study population included 60 males and 54 females with a median age of 16.9 years (range 0.6–59.8 years).

immunohistochemistry and evaluation of STEAP1 immunoreactivity

Immunohistochemistry (IHC) analyses were done on formalin-fixed, paraffin-embedded, pre-chemotherapy primary tumors. All tissue slides were collected at the Department of Pathology of the Technische

Universität München for immediate IHC staining. For IHC, 4-μm sections were cut and stained by an automated immunostainer with an iView DAB detection kit (Ventana Medical System, Tucson, AZ) according to the company's protocol. The following primary antibody was used: polyclonal rabbit anti-STEAP1 (1:50; H-105, sc-25514, Santa Cruz). Antigen retrieval was carried out by microwave treatment in Dako target retrieval solution, citrate, pH 6.0. Sections were counterstained with hematoxylin. For internal controls, we used tumors of xenografted ES cell lines with known STEAP1 mRNA and protein expression levels (see supplemental Methods and Figure S1, available at *Annals of Oncology* online). Specificity of the STEAP1 antibody was assessed previously by others [30, 31] and reassessed by us using immunoblot and indirect immunofluorescence, as previously described [32, 33] (see supplemental Methods and Figure S1, available at *Annals of Oncology* online). These control experiments further confirmed the specificity of the used STEAP1 antibody, in agreement with published findings on the STEAP1 protein [23, 24, 34]. Semi-quantitative evaluation of STEAP1 immunostaining was carried out in a blinded manner by a pathologist (IE) and two scientist experienced in histopathology (PS-B, MA) after having examined at least three high-power fields (40×) of one section for each sample. The intensity of membranous STEAP1 immunoreactivity was determined as grade 0 = none, grade 1 = faint, grade 2 = moderate, and grade 3 = strong (Figure 1). Intensity scoring was independently recorded and in case of disagreement determined by consensus. For better statistical discrimination, samples were classified into two groups as previously described [32, 35]: samples with grade 0 and 1 were classified as STEAP1 low and those with grade 2 and 3 as STEAP1 high.

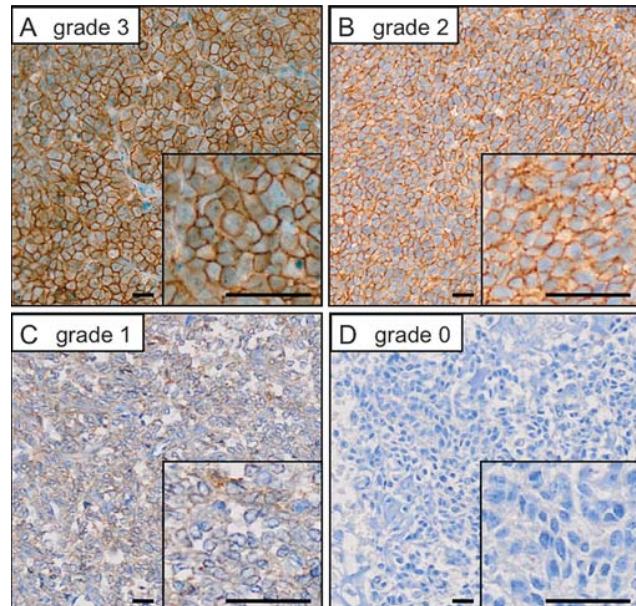


Figure 1. Examples of heterogeneous membranous six-transmembrane epithelial antigen of the prostate 1 (STEAP1) immunoreactivity in Ewing's sarcoma (ES): All samples depicted were located on the same tissue microarray slide and stained simultaneously by an automated immunostainer (see 'materials and methods' section). Membranous STEAP1 immunoreactivity (brown color) was scored according to reference ES with known STEAP1 expression levels, with grade 3 = strong (A), grade 2 = moderate (B), grade 1 = faint (C), and grade 0 = no immunoreactivity (D). Grades 3 and 2 were classified as STEAP1 high and grades 1 and 0 as STEAP1 low. Scale bars = 20 μm for overview and 80 μm for detail images.

statistical analyses

Statistical analyses were carried out with SPSS 19 (IBM Corporation, Armonk, NY) and SAS 9.2 (SAS Institute, Cary, NC). OS was estimated by the Kaplan–Meier method. OS time was defined as the interval between the date of diagnosis and the date of last follow-up or death. Living patients were censored at the date of most recent consultation. Group comparisons were calculated by log-rank test. Multivariate analyses were carried out by applying the Cox proportional hazard method. Differences in proportions between groups were evaluated by chi-square or Fisher's exact test. Significance level was set at $P < 0.05$ for two-sided testing. No alpha corrections were carried out for multiple testing. Outcome was analyzed on an exploratory basis.

results

STEAP1 is expressed in the majority of ES and mainly locates to plasma membranes

We first aimed to define the expression pattern of STEAP1 in ES. Of the 114 ES available for IHC, 71 displayed detectable membranous STEAP1 immunoreactivity (62.3%, grades 1–3). Examples of the differential membranous STEAP1 immunoreactivity are given in Figure 1. A total of 53.5% ($n = 61$) of the ES were scored as membranous STEAP1 high and 46.5% ($n = 53$) as membranous STEAP1 low; 24.6% (28 of 114) of the cases showed maximum membranous STEAP1 expression (grade 3; see Figure 1). In agreement with previous findings in breast, bladder, and prostate carcinoma [21, 23, 25], we noted a predominant plasma membranous localization of STEAP1 without defined apical or basal accentuation and mostly without cytoplasmic STEAP1 immunoreactivity. Only a few ES samples showed a faint to moderate cytoplasmic STEAP1 staining.

membranous STEAP1 expression and OS

We next aimed to determine whether membranous STEAP1 expression correlates with outcome of ES patients. Patient characteristics are given in Table 1. Univariate analysis on the predictive value of membranous STEAP1 immunoreactivity showed a lower survival rate in patients with ES classified as membranous STEAP1-low (5-year OS = 0.57; $n = 53$) when compared with membranous STEAP1-high cases (5-year OS = 0.79; $n = 61$) ($P = 0.021$) (Figure 2).

multivariate analysis

We next analyzed the impact of risk stratification in patients with membranous STEAP1-high ES compared with patients with membranous STEAP1-low ES to rule out a possible bias by favorable risk factor patterns in STEAP1-high cases. The multivariate analysis served to identify underlying factors that could influence prognosis. We included the known prognostic factors metastatic stage at diagnosis (M0, M1, M2), site (axial versus nonaxial), and age (<15 versus ≥ 15 years) [7, 12, 13] in the multivariate analysis. Eighty-three patients (72.8%) had localized disease (M0), 20 patients (17.5%) had pulmonary metastases (M1), and 11 patients (9.6%) had disseminated disease including other metastases than in lungs (M2). Sixty-six patients (57.9%) presented with an axial site ES and 48 patients (42.1%) with a non-axial site ES. Forty-six patients

Table 1. Patient characteristics ($n = 114$)

| Variable | Label | n (%) |
|--|----------------------------------|-----------|
| Sex | Male | 60 (52.6) |
| | Female | 54 (47.4) |
| Age at diagnosis | <15 years | 46 (40.4) |
| | ≥ 15 years | 68 (59.6) |
| Risk group | M0 (no metastases) | 83 (72.8) |
| | M1 (lung metastases) | 20 (17.5) |
| | M2 (other \pm lung metastases) | 11 (9.7) |
| Site | Axial | 66 (57.9) |
| | Non-axial | 48 (42.1) |
| Tumor volume ^a | <200 ml | 55 (71.4) |
| | ≥ 200 ml | 22 (28.6) |
| Histological response ^a | Good (<10% viable cells) | 46 (78.0) |
| | Poor ($\geq 10\%$ viable cells) | 13 (22.0) |
| Membranous six-transmembrane epithelial antigen of the prostate 1 expression | How | 53 (46.5) |
| | High | 61 (53.5) |

^aThese parameters relate to subsets of the study population.

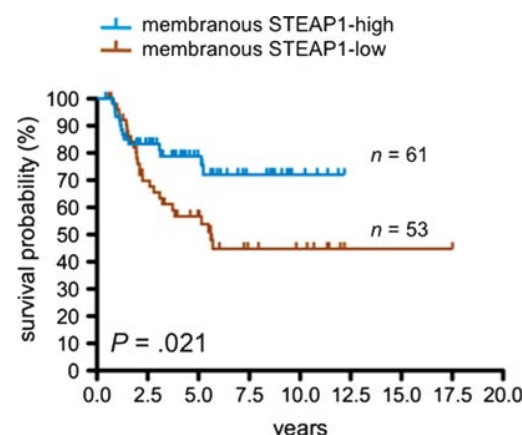


Figure 2. Six-transmembrane epithelial antigen of the prostate 1 (STEAP1) expression correlates with overall survival (OS): Kaplan–Meier estimates for OS probability for membranous STEAP1 expression ($n = 114$, $P = 0.021$). Log-rank test.

(40.4%) were aged <15 years, and 68 patients (59.6%) were aged ≥ 15 years at time of diagnosis.

The major risk factor was metastatic disease at diagnosis [M0: hazard ratio (HR) = 1.00; M1: HR = 2.19; M2: HR = 4.38; $P = 0.002$]. Membranous STEAP1-low expression (HR = 1.76; $P = 0.094$), age (≥ 15 years, HR = 1.69; $P = 0.135$), and primary axial tumor site (HR 1.30; $P = 0.435$) showed only a tendency or no major impact on survival ($n = 114$; Table 2).

In a second step, we analyzed the major group of patients with localized disease (M0; $n = 83$). Here, membranous STEAP1-low expression (HR = 2.59; $P = 0.036$) and age (≥ 15 years; HR = 3.39; $P = 0.030$) were major risk factors concerning survival in relation to primary axial tumor site (HR 1.76; $P = 0.218$) (Table 3), which most likely still only showed a

Table 2. Summary of results of the multivariate analysis in all patients ($n = 114$)

| Variable | Label | Risk ratio (95% CI) | P |
|------------------------------|------------------------------|------------------------|-------|
| Risk group | M0 (no metastases) | 1 | 0.002 |
| | M1 (lung metastases) | 2.19 (1.04–4.61) | 0.039 |
| | M2 (other ± lung metastases) | 4.38 (1.83–10.5) | 0.001 |
| Membranous STEAP1 expression | Low | 1.78 (0.91–3.48) | 0.094 |
| Age | ≥15 years | 1.69 (0.85–3.37) | 0.135 |
| Site | Axial | 1.30 (0.68–2.48) | 0.435 |

STEAP1, six-transmembrane epithelial antigen of the prostate 1 and CI, confidence interval.

Table 3. Summary of results of the multivariate analysis in patients with localized disease ($n = 83$)

| Variable | Label | Risk ratio (95% CI) | P |
|------------------------------|-----------|------------------------|-------|
| Membranous STEAP1 expression | Low | 2.59 (1.07–6.29) | 0.036 |
| Age | ≥15 years | 3.39 (1.13–10.2) | 0.030 |
| Site | Axial | 1.76 (0.72–4.31) | 0.218 |

STEAP1, six-transmembrane epithelial antigen of the prostate 1 and CI, confidence interval.

tendency on survival due to the limited size of our patient cohort.

Tumor volume: A tumor volume categorization (<200 versus ≥200 ml) was only available in 77 patients. Fifty-five patients (71.4%) had a tumor volume <200 ml and 22 patients (28.6%) had a tumor volume >200 ml. Multivariate analysis in this subcohort of 77 patients adding tumor volume as known prognostic factor to the other established prognostic factors described above (metastatic disease at diagnosis, age ≥15 years, and primary axial tumor site [7, 12, 13]) confirmed metastatic disease at diagnosis ($P = 0.002$) and membranous STEAP1-low expression ($HR = 2.65$; $P = 0.036$) as major risk factors.

association of STEAP1 expression with histological response to chemotherapy

Since high membranous STEAP1 immunoreactivity correlated with improved OS, we tested whether this observation is associated with a better response to treatment as estimated by Salzer-Kuntschik tumor regression states [36]. For 59 patients (51.8%), data were available for histological response following induction chemotherapy without concurrent early radiotherapy. Forty-six patients (78%) showed a good histological response (<10% viable tumor cells) and 13 patients (22%) a poor histological response (≥10% viable tumor cells); 80.6% of the patients with membranous STEAP1-high expression showed a good histological response compared with 73.9% of the patients with membranous STEAP1-low

Table 4. Summary of results of correlation of membranous STEAP1 immunoreactivity with tumor regression grade ($n = 59$)

| | | Histological response | | P |
|------------------------------|------|-----------------------|-----------|-------|
| | | Good | Poor | |
| Membranous STEAP1 expression | Low | 17 (73.9%) | 6 (26.1%) | 0.748 |
| | High | 29 (80.6%) | 7 (19.4%) | |

STEAP1, six-transmembrane epithelial antigen of the prostate 1.

expression ($P = 0.748$) (Table 4). To test whether differential STEAP1 expression may indeed alter response to chemotherapy *in vitro*, we transiently knocked down STEAP1 in cultured ES cells by RNA interference and assessed their rates of necrosis by flow cytometry. STEAP1-silenced ES cells treated with either doxorubicin or etoposide for 24 h exhibited lower rates of necrosis compared with ES cells with high STEAP1 expression ($P < 0.01$; *t*-test, $n = 4$) (Figure S2), indicating that low STEAP1 expression may confer ES cells with a more resistant phenotype to chemotherapy.

discussion

Combined modality treatment is crucial for successful therapy of patients with ES [7]. So far, various studies have identified metastatic state, tumor volume, tumor site, age, sex, and histological response to chemotherapy as important risk factors, with primary metastasis as the most unfavorable one [7, 12, 13, 37]. Although there is agreement that clinical management will benefit from biological markers that can guide therapeutic decisions [12], apart from the proliferation marker Ki67 [38, 39], there are no *bona fide* immunohistological markers available predicting outcome of patients with ES [12, 15].

This is, to the best of our knowledge, the first report evaluating the potential of STEAP1 for outcome prediction in ES. Regarding independent risk factors in our series, high membranous STEAP1 expression had a strong impact on OS in multivariate analysis.

Moreover, membranous STEAP1-high immunoreactivity showed a trend toward a better tumor response compared with membranous STEAP1-low immunoreactivity as estimated by Salzer-Kuntschik regression states. Even though this subsample tendency has to be validated in a larger cohort, it is noteworthy that high STEAP1 expression improves response of ES cells to chemotherapy *in vitro*. Hence, it is tempting to speculate that STEAP1 may exert a biological function that sensitizes ES to drugs such as doxorubicin and etoposide, which are essential components of current ES treatment protocols [40].

On the molecular level, STEAP1 is a homologue of NADPH oxidases [41, 42], which are involved in cellular ROS production and frequently overexpressed in cancer [43, 44]. Consistent with this notion, we recently demonstrated that STEAP1 overexpression in ES cells increases their intracellular ROS levels [24]. Similar observations were obtained by Pan et al. in thyroid epithelial cells [45]. Pharmacologically, multiple studies demonstrated that certain chemotherapeutics like

doxorubicin and etoposide become more potent at increased intracellular ROS levels [46, 47]. Moreover, radiotherapy is known to be more effective in combination with ROS-generating radiosensitizers [47, 48]. Thus, the apparent survival benefit seen in membranous STEAP1-high ES patients may be caused by elevated intracellular ROS levels of the ES cells, which might sensitize them to radiochemotherapy.

As outlined above, metastasis of ES is the most adverse clinical parameter indicative for dismal prognosis with a 5-year relapse-free survival of ~21% compared with 55% in patients with localized disease. Strikingly, the observed survival benefit of membranous STEAP1-high compared with membranous STEAP1-low immunoreactivity is similarly strong like the dramatic difference in survival indicated by localized versus metastatic disease. Hence, our data suggest that high membranous STEAP1 expression may be a property of an independent risk group of ES patients, who specifically might benefit from adapted radio-chemotherapy protocols.

Despite we are fully aware of the retrospective nature of this study and its associated limitations, STEAP1 may constitute a promising new biomarker for outcome prediction of ES patients, which is readily available due to standardized assessment by immunohistochemistry. Therefore, we strongly recommend to validate this observation in prospective studies and to experimentally elucidate the precise molecular role of STEAP1 in ES.

acknowledgements

We gratefully acknowledge the contribution of the participating Gesellschaft für Pädiatrische Onkologie und Hämatologie institutions and of the staff of the Ewing trial center Münster, Susanne Jabar and Regina Kloss. We thank Barbara Grunewald, Uwe Thiel, Stephanie Plehm, and Veit R. Buchholz for critical reading of the manuscript.

funding

Technische Universität München (KKF B08-05 to T.G. and A09-02 to G.R.); Dr. Sepp und Hanne Sturm Gedächtnisstiftung of the city of Munich (to T.G., G.R., and S.B.); TUM Graduate School (to T.G.); Deutsche Forschungsgemeinschaft (DFG GR3728/1-1 to T.G., G.R., and S.B.); Wilhelm-Sander-Stiftung (2009.901.1 to G.R. and S.B.); Deutsche Krebshilfe (50-2551-Jü3 and 50-2551-Jü4 to H.J.); BMBF (FK 01GM0870) to Translational Sarcoma Research Network; National Genome Network (NGFNplus) to IE's laboratory.

disclosure

The authors declare no conflict of interest.

references

1. Burdach S, Thiel U, Schöniger M et al. Total body MRI-governed involved compartment irradiation combined with high-dose chemotherapy and stem cell rescue improves long-term survival in Ewing tumor patients with multiple primary bone metastases. *Bone Marrow Transplant* 2010; 45(3): 483–489.
2. Burdach S. Treatment of advanced Ewing tumors by combined radiochemotherapy and engineered cellular transplants. *Pediatr Transplant* 2004; 8 (Suppl 5): 67–82.
3. Burdach S, Jurgens H. High-dose chemoradiotherapy (HDC) in the Ewing family of tumors (EFT). *Crit Rev Oncol Hematol* 2002; 41(2): 169–189.
4. Thiel U, Wawer A, Wolf P et al. No improvement of survival with reduced- versus high-intensity conditioning for allogeneic stem cell transplants in Ewing tumor patients. *Ann Oncol* 2011; 22(7): 1614–1621.
5. Burdach S, Jurgens H, Peters C et al. Myeloablative radiochemotherapy and hematopoietic stem-cell rescue in poor-prognosis Ewing's sarcoma. *J Clin Oncol* 1993; 11(8): 1482–1488.
6. Burdach S, Meyer-Bahlburg A, Laws HJ et al. High-dose therapy for patients with primary multifocal and early relapsed Ewing's tumors: results of two consecutive regimens assessing the role of total-body irradiation. *J Clin Oncol* 2003; 21(16): 3072–3078.
7. Haeusler J, Ranft A, Boelling T et al. The value of local treatment in patients with primary, disseminated, multifocal Ewing sarcoma (PDMES). *Cancer* 2010; 116(2): 443–450.
8. Delattre O, Zucman J, Melot T et al. The Ewing family of tumors—a subgroup of small-round-cell tumors defined by specific chimeric transcripts. *N Engl J Med* 1994; 331(5): 294–299.
9. Staeger MS, Hutter C, Neumann I et al. DNA microarrays reveal relationship of Ewing family tumors to both endothelial and fetal neural crest-derived cells and define novel targets. *Cancer Res* 2004; 64(22): 8213–8221.
10. Le Deley M-C, Delattre O, Schaefer K-L et al. Impact of EWS-ETS fusion type on disease progression in Ewing's sarcoma/peripheral primitive neuroectodermal tumor: prospective results from the cooperative Euro-E.W.I.N.G. 99 trial. *J Clin Oncol* 2010; 28(12): 1982–1988.
11. Ginsberg JP, de Alava E, Ladanyi M et al. EWS-FLI1 and EWS-ERG gene fusions are associated with similar clinical phenotypes in Ewing's sarcoma. *J Clin Oncol* 1999; 17(6): 1809–1814.
12. Riley RD, Burchill SA, Abrams KR et al. A systematic review and evaluation of the use of tumour markers in paediatric oncology: Ewing's sarcoma and neuroblastoma. *Health Technol Assess* 2003; 7(5): 1–162.
13. Cotterill SJ, Ahrens S, Paulussen M et al. Prognostic factors in Ewing's tumor of bone: analysis of 975 patients from the European Intergroup Cooperative Ewing's Sarcoma Study Group. *J Clin Oncol* 2000; 18(17): 3108–3114.
14. Bui MM, Han G, Acs G et al. Connexin 43 is a potential prognostic biomarker for Ewing sarcoma/primitive neuroectodermal tumor. *Sarcoma* 2011; 2011: 971050.
15. de Alava E, Antonescu CR, Panizo A et al. Prognostic impact of P53 status in Ewing sarcoma. *Cancer* 2000; 89(4): 783–792.
16. Lee CK, Lord SJ, Coates AS, Simes RJ. Molecular biomarkers to individualise treatment: assessing the evidence. *Med J Aust* 2009; 190(11): 631–636.
17. Nishio K, Arao T, Shimoyama T et al. Translational studies for target-based drugs. *Cancer Chemother Pharmacol* 2005; 56(Suppl 1): 90–93.
18. Grunewald TG, Herbst SM, Heinze J, Burdach S. Understanding tumor heterogeneity as functional compartments—superorganisms revisited. *J Transl Med* 2011; 9(1): 79.
19. Juergens H, Daw NC, Georger B et al. Preliminary efficacy of the anti-insulin-like growth factor type 1 receptor antibody fitumumab in patients with refractory Ewing sarcoma. *J Clin Oncol* 2011 Dec 1; 29(34): 4534–40. Epub 2011 Oct 24.
20. Thiel U, Pirson S, Müller-Spahn C et al. Specific recognition and inhibition of Ewing tumour growth by antigen-specific allo-restricted cytotoxic T cells. *Br J Cancer* 2011; 104(6): 948–956.
21. Challita-Eid PM, Morrison K, Etessami S et al. Monoclonal antibodies to six-transmembrane epithelial antigen of the prostate-1 inhibit intercellular communication in vitro and growth of human tumor xenografts in vivo. *Cancer Res* 2007; 67(12): 5798–5805.
22. Ohgami RS, Campagna DR, McDonald A, Fleming MD. The Steap proteins are metalloreductases. *Blood* 2006; 108(4): 1388–1394.

23. Hubert RS, Vivanco I, Chen E et al. STEAP: a prostate-specific cell-surface antigen highly expressed in human prostate tumors. *Proc Natl Acad Sci U S A* 1999; 96(25): 14523–14528.

24. Grunewald TG, Diebold I, Esposito I et al. STEAP1 is associated with the invasive and oxidative stress phenotype of Ewing tumors. *Mol Cancer Res* 2012; 10(1): 52–65.

25. Maia CJ, Socorro S, Schmitt F, Santos CR. STEAP1 is over-expressed in breast cancer and down-regulated by 17beta-estradiol in MCF-7 cells and in the rat mammary gland. *Endocrine* 2008; 34(1–3): 108–116.

26. Valenti MT, Dalle Carbonare L, Donatelli L et al. STEAP mRNA detection in serum of patients with solid tumours. *Cancer Lett* 2009; 273(1): 122–126.

27. Cheung IY, Feng Y, Danis K et al. Novel markers of subclinical disease for Ewing family tumors from gene expression profiling. *Clin Cancer Res* 2007; 13(23): 6978–6983.

28. Vaghjiani RJ, Talma S, Murphy CL. Six-transmembrane epithelial antigen of the prostate (STEAP1 and STEAP2)-differentially expressed by murine and human mesenchymal stem cells. *Tissue Eng Part A* 2009; 15(8): 2073–2083.

29. Tirode F, Laud-Duval K, Prieur A et al. Mesenchymal stem cell features of Ewing tumors. *Cancer Cell* 2007; 11(5): 421–429.

30. Klein A, Guhl E, Zollinger R et al. Gene expression profiling: cell cycle deregulation and aneuploidy do not cause breast cancer formation in WAP-SVT/t transgenic animals. *J Mol Med (Berl)* 2005; 83(5): 362–376.

31. Kobayashi H, Nagato T, Sato K et al. Recognition of prostate and melanoma tumor cells by six-transmembrane epithelial antigen of prostate-specific helper T lymphocytes in a human leukocyte antigen class II-restricted manner. *Cancer Res* 2007; 67(11): 5498–5504.

32. Grunewald TGP, Kammerer U, Kapp M et al. Nuclear localization and cytosolic overexpression of LASP-1 correlates with tumor size and nodal-positivity of human breast carcinoma. *BMC Cancer* 2007; 7: 198.

33. Grunewald TGP, Kammerer U, Winkler C et al. Overexpression of LASP-1 mediates migration and proliferation of human ovarian cancer cells and influences zyxin localisation. *Br J Cancer* 2007; 96(2): 296–305.

34. Hayashi S, Kumai T, Matsuda Y et al. Six-transmembrane epithelial antigen of the prostate and enhancer of zeste homolog 2 as immunotherapeutic targets for lung cancer. *J Transl Med* 2011; 9: 191.

35. Frietsch JJ, Grunewald TGP, Jasper S et al. Nuclear localisation of LASP-1 correlates with poor long-term survival in female breast cancer. *Br J Cancer* 2010; 102(11): 1645–1653.

36. Salzer-Kuntschik M, Brand G, Delling G. [Determination of the degree of morphological regression following chemotherapy in malignant bone tumors]. *Pathologe* 1983; 4(3): 135–141.

37. Rodríguez-Galindo C, Liu T, Krasin MJ et al. Analysis of prognostic factors in Ewing sarcoma family of tumors: review of St. Jude Children's Research Hospital studies. *Cancer* 2007; 110(2): 375–384.

38. López-Guerrero JA, Machado I, Scotlandi K et al. Clinicopathological significance of cell cycle regulation markers in a large series of genetically confirmed Ewing's sarcoma family of tumors. *Int J Cancer* 2011; 128(5): 1139–1150.

39. Mackintosh C, Ordóñez JL, García-Domínguez DJ et al. 1q gain and CDT2 overexpression underlie an aggressive and highly proliferative form of Ewing sarcoma. *Oncogene* 2011 Aug 8 [Epub ahead of print].

40. Juergens C, Weston C, Lewis I et al. Safety assessment of intensive induction with vincristine, ifosfamide, doxorubicin, and etoposide (VIDE) in the treatment of Ewing tumors in the EURO-E.W.I.N.G. 99 clinical trial. *Pediatr Blood Cancer* 2006; 47(1): 22–29.

41. Sanchez-Pulido L, Rojas AM, Valencia A et al. ACRATA: a novel electron transfer domain associated to apoptosis and cancer. *BMC Cancer* 2004; 4: 98.

42. von Rozycki T, Yen MR, Lende EE, Saier MH. The YedZ family: possible heme binding proteins that can be fused to transporters and electron carriers. *J Mol Microbiol Biotechnol* 2004; 8(3): 129–140.

43. Kamata T. Roles of Nox1 and other Nox isoforms in cancer development. *Cancer Sci* 2009; 100(8): 1382–1388.

44. Lambeth JD. NOX enzymes and the biology of reactive oxygen. *Nat Rev Immunol* 2004; 4(3): 181–189.

45. Pan YZ, Li Y, Guo LR et al. [Influence of expression of six transmembrane epithelial antigen of the prostate-1 on intracellular reactive oxygen species level and cell growth: an in vitro experiment]. *Zhonghua Yi Xue Za Zhi* 2008; 88(9): 641–644.

46. Mailloux RJ, Adjeitey CN, Harper ME. Genipin-induced inhibition of uncoupling protein-2 sensitizes drug-resistant cancer cells to cytotoxic agents. *PLoS One* 2010; 5(10): e13289.

47. Sun Y, St Clair DK, Xu Y et al. A NADPH oxidase-dependent redox signaling pathway mediates the selective radiosensitization effect of parthenolide in prostate cancer cells. *Cancer Res* 2010; 70(7): 2880–2890.

48. Girdhani S, Bhosle SM, Thulsidas SA et al. Potential of radiosensitizing agents in cancer chemo-radiotherapy. *J Cancer Res Ther* 2005; 1(3): 129–131.

Anti-oxidative stress response genes: bioinformatic analysis of their expression and relevance in multiple cancers

Barak Rotblat^{1,*}, Thomas G. P. Grunewald^{2,*}, Gabriel Leprivier^{3,*}, Gerry Melino^{1,4}, Richard A. Knight¹

¹ Medical Research Council, Toxicology Unit, Leicester University, Leicester, UK

² INSERM Unit 830 "Genetics and Biology of Cancer", Institut Curie Research Center, Paris, France

³ Department of Molecular Oncology, British Columbia Cancer Research Centre and Department of Pathology, University of British Columbia, Vancouver, BC, Canada

⁴ Department of Experimental Medicine and Surgery, Biochemistry IDI-IRCCS Laboratory, University of Rom 'Tor Vergata', Rome, Italy

* Equal contribution authors

Correspondence to: Barak Rotblat, **email:** br81@le.ac.uk

Keywords: anti-oxidant genes, glutathione, thioredoxin, breast cancer, lung cancer, NRF2, G6PD

Received: December 5, 2013

Accepted: December 15, 2013

Published: December 15, 2013

This is an open-access article distributed under the terms of the Creative Commons Attribution License, which permits unrestricted use, distribution, and reproduction in any medium, provided the original author and source are credited.

ABSTRACT:

Cells mount a transcriptional anti-oxidative stress (AOS) response program to scavenge reactive oxygen species (ROS) that arise from chemical, physical, and metabolic challenges. This protective program has been shown to reduce carcinogenesis triggered by chemical and physical insults. However, it is also hijacked by established cancers to thrive and proliferate within the hostile tumor microenvironment and to gain resistance against chemo- and radiotherapies. Therefore, targeting the AOS response proteins that are exploited by cancer cells is an attractive therapeutic strategy. In order to identify the AOS genes that are suspected to support cancer progression and resistance, we analyzed the expression patterns of 285 genes annotated for being involved in oxidative stress in 994 tumors and 353 normal tissues. Thereby we identified a signature of 116 genes that are highly overexpressed in multiple cancers while being only minimally expressed in normal tissues. To establish which of these genes are more likely to functionally drive cancer resistance and progression, we further identified those whose overexpression correlates with negative patient outcome in breast and lung carcinoma. Gene-set enrichment, gene ontology, network, and pathway analyses revealed that members of the thioredoxin and glutathione pathways are prominent components of this oncogenic signature and that activation of these pathways is common feature of many cancer entities. Interestingly, a large fraction of these AOS genes are downstream targets of the transcription factors NRF2, NF-kappaB, and FOXM1, and rely on NADPH for their enzymatic activities highlighting promising drug targets. We discuss these findings and propose therapeutic strategies that may be applied to overcome cancer resistance.

INTRODUCTION

The stressful biological conditions that exist within the tumor microenvironment exert strong adaptive pressure on cancer cells which in turn exploit endogenous pathways to reprogram their transcriptome, proteome, and

metabolism to survive and thrive under these conditions [1-6]. Therefore, proteins that facilitate these adaptation processes are attractive drug targets as they are expected to be active only in tumor tissues, which are exposed to stress, but not in non-stressed normal tissues [2, 7, 8]. Oxidative stress is commonly associated with cancer and cancer cells have been shown to promote expression of

ROS scavenging pathways in order to survive, proliferate, and resist radio- and chemotherapy [9-11]. While these basic biological principles have been extensively demonstrated and reviewed elsewhere [12], especially in the context of the transcription factor nuclear factor (erythroid-derived 2)-like 2 (NRF2 or NFE2L2) [13-15], it is still not clear which groups of AOS genes are overexpressed in multiple cancers compared with normal tissues. Similarly, it is as yet not defined which groups of AOS genes predict for bad prognosis and in different cancer entities.

Here, we systematically evaluated the mRNA expression patterns of all genes (n=285) annotated by GO(Gene Ontology) as being involved in 'oxidative stress' (including AOS genes) in publicly available microarray data sets and identified a sub-group of genes that is highly overexpressed in multiple cancers compared to normal tissues. Subsequently, by using multiple unsupervised analyses, we found that the glutathione and thioredoxin

pathways are significantly enriched among these genes. Interestingly, high expression of a significant number of these genes is negatively correlated with survival in breast and lung carcinoma, suggesting that they might play a protective role in cancer cells as opposed to merely reflecting a transcriptional response to oxidative stress. We discuss these genes, the regulators of their expression, their specific role in cancer, and possible therapeutic strategies that can hit these targets.

Identification of oxidative stress response genes highly expressed in multiple cancers: enrichment in glutathione and thioredoxin pathways-related genes

We wondered whether specific oxidative stress response genes are highly overexpressed in cancer as compared to normal tissues. Because we are primarily interested in how cancer cells adapt to their microenvironment found within solid tumors we focused our analysis on carcinomas as they constitute the most frequent type of solid tumors. Using hierarchical clustering, we observed that the 285 genes cluster into 6 clusters (hereafter referred to as "groups") (Figure 1; Table S1). Groups 2-5 were found to be cancer type specific (Figure 1; Table S1). While these may be interesting in the context of the corresponding cancers entity, they may also reflect genes highly expressed in the tissue of origin, and therefore will require further in-depth analysis. More interestingly, we identified a group of genes that is highly overexpressed in multiple cancers compared to normal tissues (group 6), as well as a group that is highly overexpressed in normal tissues compared to cancers (group 1).

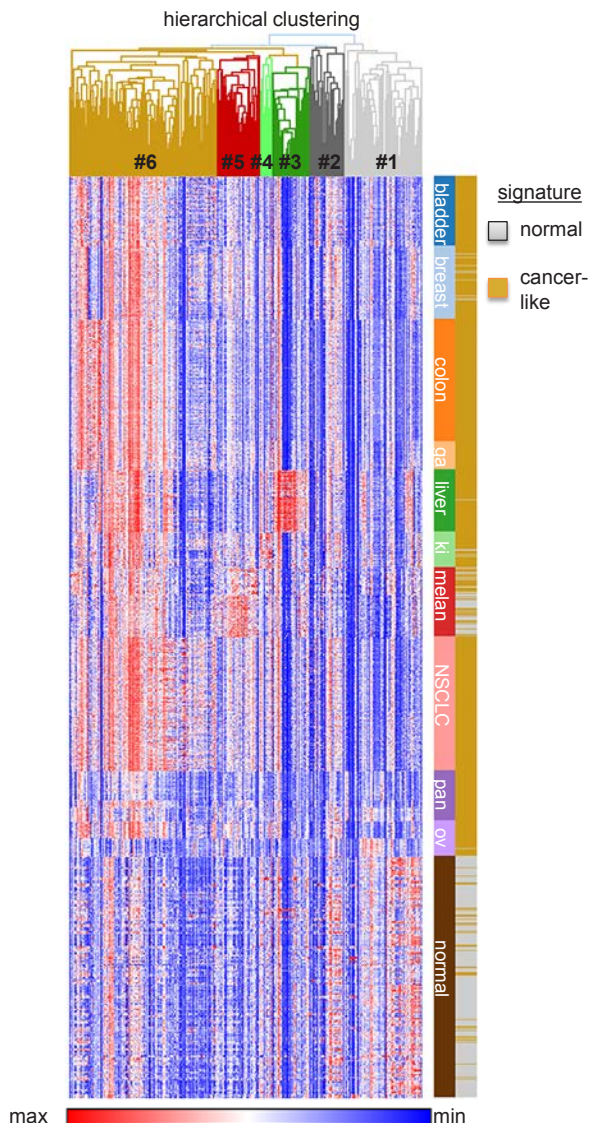


Figure 1: Gene expression patterns of 285 oxidative stress genes in 353 normal tissues and various carcinomas (total n=994, 10 different entities). Gene expression data were retrieved from the Gene Expression Omnibus (GEO; <http://www.ncbi.nlm.nih.gov/gds>) of published microarray studies (all Affymetrix HG-U133plus2.0). Normal tissue n=353 (GSE3526) [133]. Carcinomas: bladder n=102 (GSE31684, GSE7476), breast n=107 (GSE36774), colorectal n=177 (GSE17536), gastric cancer (ga) n=43 (GSE22377), liver (hepatocellular carcinoma) n=91 (GSE9843), kidney (ki) n=52 (GSE11151), melanoma (melan) n=101 (GSE10282, GSE15605), lung (non-small-cell lung cancer, NSCLC) n=196 (GSE37745), pancreas (pan) n=52 (GSE17891, GSE32676), ovary (ov) n=73 (GSE14001, GSE18520). All microarray data were normalized simultaneously by RMA [134] using custom brainarray (v15.0) ENTREZG CDF-files as previously described [132, 135, 136]. Hierarchical clustering of genes (1-Pearson correlation) and k-means clustering (2 signatures, 10,000 iterations) of microarray samples were performed with GENE-E software (<http://www.broadinstitute.org/cancer/software/GENE-E/index.html>). Gene expression data were log2 transformed for depiction in a heat-map.

Table 1: List of AOS response genes highly expressed in cancers which correlate with outcome in breast or lung cancer. The cancer AOS response signature was analyzed using bioprofiling.de GENE_SRV to identify cancers in which these genes have significant predictive power. Only genes that were found to correlate with survival are shown. Gene name, ENTREZ ID, microarray probeset ID and p value are provided. Kaplan-Meier plots for all the indicated genes are displayed in Figure S1-S3.

| Breast cancer | | ENTREZ ID | |
|----------------|----------|------------------|------------|
| | Gene | (probe ID) | P-value |
| Bad prognosis | BTG3 | 10950 (360504) | 0.00357 |
| | CASP3 | 836 (540397) | 0.0000453 |
| | CDC2 | 983 (5360092) | 0.0000105 |
| | ECT2 | 1894 (5420064) | 0.00012 |
| | EGLN1 | 54583 (6130168) | 0.00586 |
| | FOXM1 | 2305 (5390044) | 2.51E-08 |
| | G6PD* | 2539 (5700072) | 0.00748 |
| | GAPDH | 2597 (1940184) | 0.00321 |
| | HMOX1* | 3162 (6180100) | 0.000294 |
| | LONP1 | 9361 (870538) | 0.0031 |
| | NUDT1 | 4521 (6180369) | 0.0016 |
| | PRDX4* | 10549 (940131) | 0.00276 |
| | PSMB5 | 5693 (3610041) | 0.00337 |
| | SELS | 55829 (7100450) | 0.00844 |
| | SERPINE1 | 5054 (6840139) | 0.00167 |
| | SRXN1* | 140809 (3190176) | 0.00336 |
| | TXNRD1* | 7296 (6220603) | 0.00000169 |
| <hr/> | | | |
| Good prognosis | PON2 | 5445 (7040022) | 0.00457 |
| | SIRT1 | 23411 (6940021) | 0.00918 |
| <hr/> | | | |
| Lung cancer | | NCBI ID | |
| | NCBI ID | (probe ID) | P-value |
| Bad prognosis | COL1A1 | 1277 (926) | 0.000675 |
| | GAPDH | 2597 (1738) | 0.00185 |
| | GCLC* | 2729 (14771) | 0.00354 |
| | GSS* | 2937 (267) | 0.00934 |
| | NQO1* | 1728 (20812) | 0.0045 |
| | RNF7 | 9616 (12099) | 0.00439 |
| | STK24 | 8428 (10957) | 0.00195 |
| | TXN* | 7295 (10753) | 0.00789 |
| | TXNRD1* | 7296 (8394) | 0.00284 |
| <hr/> | | | |
| Good prognosis | NFKB1 | 4790 (3750) | 0.000849 |
| <hr/> | | | |
| * NRF2 targets | | | |

GO analysis using bioprofiling.de [16] (Table S2) confirmed that in both groups ‘response to oxidative stress’ and ‘response to hydrogen peroxide’ were the top two categories ($p<10-15$) confirming, as expected, that both lists (groups 1 and 6) are significantly enriched in genes involved in oxidative stress response. While the first two GO categories were similar between group 1 and group 6 the third was different. ‘Aging’ was the third identified GO category in the list of genes that are highly expressed in normal tissues (group 1) ($p<10-7$) while ‘cellular response to hydrogen peroxide’ ($p<10-12$) was the third category found in the list of genes that are highly expressed in cancer (group 6) (Table S2). It is interesting to note that the expression of AOS genes that are linked to aging is a feature of normal tissue in light of the discussion on the similarities and differences between expression of stress genes in cancer and aging [10, 17].

To identify possible common biological features of the genes represented in each of the two lists we next queried common protein folds of the encoded proteins. Using Interpro (bioprofiling.de; [16]) we found that the list of genes that are highly expressed in cancer (group 6) is significantly enriched ($p<10-6$; Table S3) in proteins that contain ‘Alkyl hydroperoxide reductase subunit C/ Thiol specific antioxidant’ domains, ‘Thioredoxin fold’, and ‘Thioredoxin like fold’, whereas the genes that are highly expressed in normal tissues (group 1) did not result in specifically enriched protein fold(s). Moreover, using pathway and network analysis (bioprofiling.de R_Spider; [18]), we found the ‘Glutathione metabolism’ pathway among the genes highly expressed in cancers (11 genes;

$p=0.01$) with a specific sub-group of 9 genes ($p<0.005$) whose products are known to interact with one another, such as glutamate cysteine ligase catalytic subunit (GCLC) and glutamate cysteine ligase modifier subunit (GCLM) (Figure 2A)[19]. Collectively, these analyses suggest that elevated glutathione synthesis and thioredoxin pathway activity are common features of cancer cells.

Identification of AOS response genes highly expressed in cancers which predict negative patient outcome

In order to identify possible drug targets within the list of genes that are up-regulated in cancer (group 6) we used the bioprofiling.de GENE_SRV tool that screens a list of genes against publicly available expression and patient survival data [20]. Specifically, this tool identifies cancer entities in which a particular gene signature is significantly enriched for predictors of patient outcome. We found significant predictive power of some genes in group 6 (highly expressed in cancers) in breast and lung cancers ($p=0.035$) and in chronic lymphocytic leukemia (CLL) ($p=0.037$). Since this study exclusively addresses AOS genes in solid tumors, we focus our discussion on the first two cancer entities. Kaplan-Meier plots for all genes that exhibited significant predictive power are summarized in Table 1 and Figure S1-3 (typical plots are shown in Figure 2B).

In lung cancer, 9 genes correlated with poor prognosis, including *GCLC*, *NAD(P)H dehydrogenase*

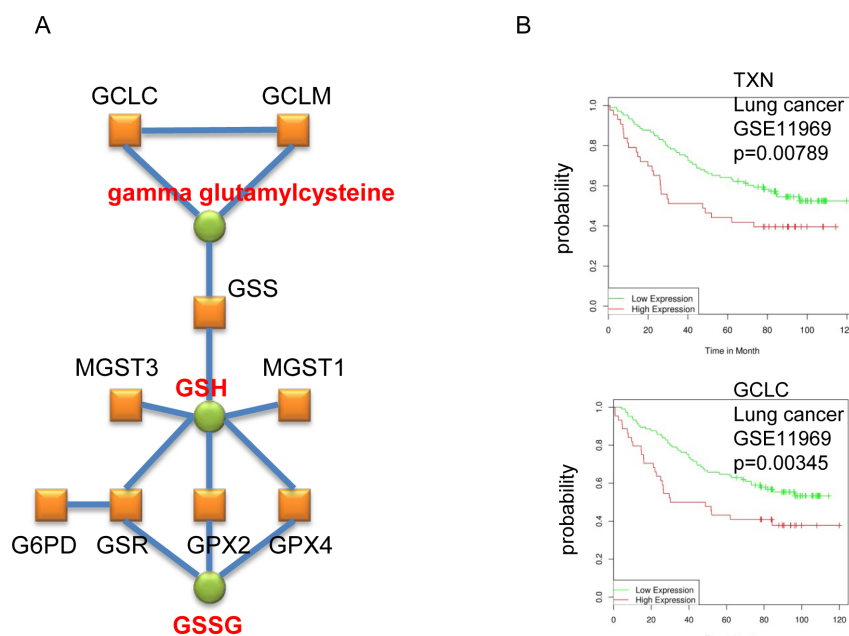


Figure 2: Enrichment of genes coding for enzymes involved in glutathione synthesis in the cancer AOS genes signature.
A. The depicted gene network was identified by R_SPIDER as statistically enriched in the list of genes that are highly expressed in cancers (group 6) (Table S1). Genes are represented by red boxes, known interactions between the corresponding proteins are displayed as blue lines and metabolites by green circles. B. Typical Kaplan-Meier plots are shown.

(quinone) 1 (*NQO1*) and thioredoxin (TXN), and 1 with good outcome (Figure 2B and Figure S1). In breast cancer, 17 genes were associated with poor prognosis, such as *glucose-6-phosphate dehydrogenase* (*G6PD*), *heme oxygenase (decycling) 1* (*HMOX1*) and *thioredoxin reductase 1* (*TXNRD1*), and only 2 with good outcome (Table 1 and Figure S2-S3). The finding that the majority of the genes are predictors for negative patient outcome supports the model that the AOS response genes, which are up-regulated in cancer, may facilitate cancer cell adaptation to the tumor environment and/or resistance to therapy. We therefore argue that the genes identified by our analyses as being highly overexpressed in carcinomas and correlating negatively with prognosis may constitute attractive drug targets as well, which will be further discussed below.

Relevance of the glutathione and thioredoxin pathways as essential components of multiple cancers and potential drug targets

Thioredoxin pathway

The thioredoxin system is highly conserved throughout evolution and we observed that multiple

members of this system are highly overexpressed in multiple cancers (Figure 1; group 6) and confer dismal prognosis in lung and breast cancers (Table 1 and Figure S1-S3). TXN is a small protein that reduces oxidized proteins and supports peroxiredoxin (PRDX)-mediated H₂O₂ clearance (Figure 3) [21]. It also positively regulates the activity of PTP1B, the phosphatase of the tyrosine kinase PDGF-beta, leading to increased PDGF-beta signaling [20] and it negatively regulates the tumor suppressor PTEN [22, 23]. These functions point to an oncogenic role of TXN.

In support to this notion, the expression of a number of TXN-related genes has been reported to predict negative patient outcome in multiple cancers [24]. Among the TXN-related genes we identified to be up-regulated in cancers (group 6), TXN expression was associated with reduced survival in various cancers, such as gastric, colorectal, non-small cell lung cancers and squamous cell carcinoma [25-27], whereas TXNRD1 expression was correlated with poor survival in breast cancer and squamous cell carcinoma [28, 29]. Furthermore, PRDX1 level was found to predict poor patient survival in non-small cell lung, ovarian, and breast cancers [30-32], and PRDX3 and PRDX4 expression were correlated with poor prognosis in hepatocellular carcinoma and squamous cell

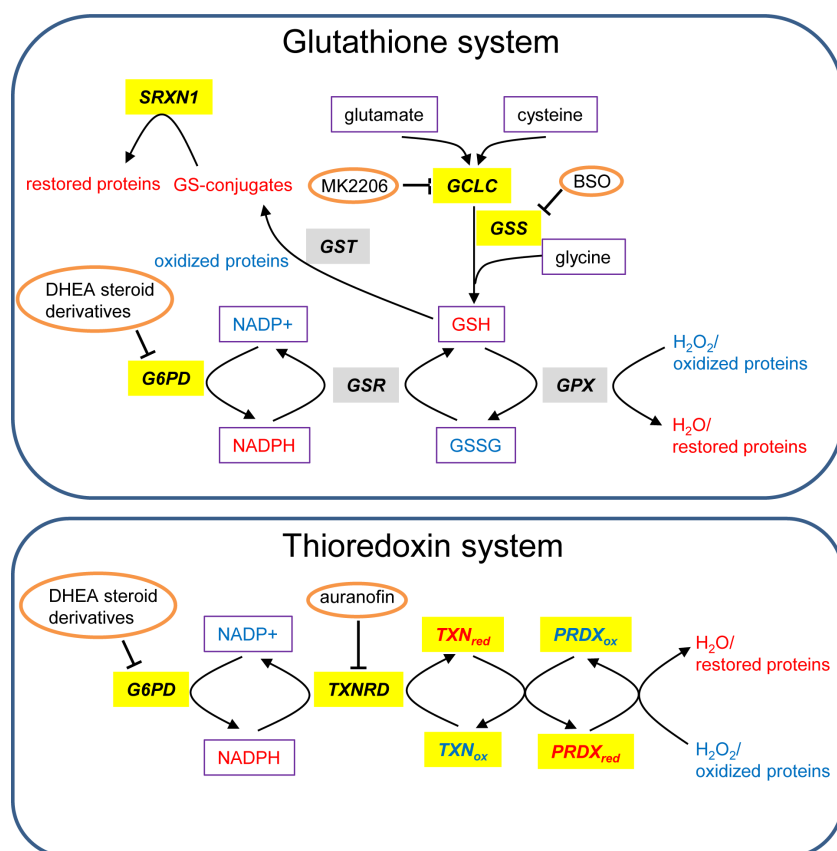


Figure 3: Glutathione and TXN systems. Genes that are highly expressed in tumors versus normal tissues are highlighted in gray and those associated with bad prognosis in lung or breast cancer are highlighted in yellow. The redox state of proteins and metabolites is depicted in color (red=reduced and blue=oxidized). Metabolites are boxed and inhibitors are circled. This scheme is adapted from [137].

carcinoma respectively [33, 34].

Among TXN pathway inhibitors, the TXN inhibitor PX-12 was shown to be well-tolerated in phase I trials [35]. However, in a phase II trial it exhibited limited therapeutic benefits possibly related to its pharmacokinetics [36], which prompted the development of better TXN inhibitors. An alternative strategy to inhibit TXN is to block TXN reductases [37], such as TXNRD1, that reduce and recycle TXN (Figure 3). TXNRD1 is an interesting drug target as its gene was found in our analysis to be up-regulated in cancers compared with normal tissues (Figure 1A; group 6). Moreover its high expression correlates with worse prognosis in both lung and breast cancer (Table 1 and Figure S1-S2). Indeed, its inhibitor Auranofin [38] can induce apoptosis and inhibit cancer cell growth *in vitro*, and is currently tested in clinical trials for CLL (phase II). Moreover, Auranofin was suggested to be used for treatment of glioblastoma [39], breast [40], lung [41-43], and other cancers [44]. Interestingly, Auranofin is an example of drug repurposing as it is a well-tolerated FDA-approved drug being already used for treatment of rheumatoid arthritis [38].

Glutathione pathway

Glutathione is the most abundant antioxidant in the cell and is involved in resistance of cancer cells to oxidative stress arising from detachment, hypoxia, radio- and chemotherapy [45-52]. GCLC and glutathione synthetase (GSS), whose genes were identified by our analysis to be highly overexpressed in cancers (Figure 2) and to confer bad prognosis in patients (Figure S1), are both essential enzymes catalyzing the synthesis of glutathione from glutamate, cysteine and glycine (Figure 3).

Previous reports have highlighted the clinical relevance for some of the glutathione-related genes we identified to be up-regulated in melanoma only (group 5) and in all cancers (group 6). The importance for glutathione S-transferase pi 1 (GSTP1) expression as a factor of bad prognosis and of poor response to chemotherapy has been reported in head and neck, gastric, colon, breast and ovarian cancers [53-60]. In addition, high GCLC and GCLM levels were associated with poor progression-free survival in diffuse large B-cell lymphoma [61], and glutathione peroxidase (GPX) activity was found to be specifically high in prostate and lung cancers compared to corresponding normal tissues [62, 63].

The glutathione pathway can be inhibited using specific drugs such as buthionine sulfoximine (BSO). The latter is a well-known inhibitor of GCLC [64] and has been shown to have only little adverse effects in humans [65, 66]. However, its efficacy as an anticancer drug is limited possibly due to bypass effects by other detoxification pathways such as the TXN pathway. In line with this notion, it was recently demonstrated that

only when both the glutathione and the TXN pathways were inhibited simultaneously, using BSO and Auranofin, respectively, there was significant inhibition of head and neck squamous cell carcinoma growth *in vitro* and *in vivo* [67]. The synergistic effects were efficiently blocked by N-acetyl cysteine (NAC), that replenishes glutathione, but not by catalase suggesting that the simultaneous inhibition of TXN and the glutathione pathways rather than reduction of total anti-oxidant cellular capacity is responsible for the growth inhibitory effect [67]. Similarly, it was shown that simultaneous inhibition of TXN and glutathione systems resulted in synergistic killing of lung cancer cells [41]. This was demonstrated using Auranofin and the AKT inhibitor MK2206, whose efficacy depends on the activity of KEAP1. KEAP1 is a known inhibitor of the transcription factor NRF2 that promotes the expression GCLC and other key enzymes in the glutathione synthesis pathway [68-71]. These data once more underscore that there is a synergistic effect caused by simultaneous block of the TXN system and the glutathione pathway. Our finding that genes enriched for both pathways are highly overexpressed in multiple cancers further supports this strategy of inhibiting both pathways simultaneously to achieve effective targeted anti-cancer therapy.

Transcription factors regulating the cancer AOS response genes and their clinical relevance

NRF2

Our first analysis is based on gene expression data that reflects the sum activities of regulators of gene expression including those of transcription factors. We observed that in the genes list that predict poor outcome, 9 are known NRF2 targets (Table 1 and Figure S1-S3). These include genes involved in glutathione and TXN pathways, G6PD that is involved in NADPH generation (Figure 2) and *NQO1* and *HMOX1* that encode detoxification enzymes [68, 69, 72-79]. Because NRF2 promotes the expression of oxidative stress detoxifying proteins, it is not surprising that NRF2 depletion results in increased tumor formation in mice challenged with carcinogens [80-83]. However, cancer cells also exploit NRF2 to reduce oxidative stress and resist chemotherapy [84-87]. In line with these two seemingly opposing NRF2 functions, recent data provides evidence that NRF2 knockout mice develop more K-RAS induced tumors on the one hand, but these are less aggressive on the other hand [88]. These observations support the concept that cancer cells exploit NRF2 to adapt to oxidative stress and to resist chemotherapy. This concept gained support by identification of somatic mutations in *NRF2* itself and in its inhibitor, *KEAP1*, that lead to increased NRF2 activity in tumors (reviewed [13, 84, 87, 89, 90]). It is therefore an attractive strategy to block NRF2 in order to reduce the

expression of its downstream target genes that are involved in both the glutathione and TXN pathways. Interestingly, the natural compound Brustatol was recently found to inhibit NRF2 in cells and to promote tumor sensitization to chemotherapy *in vivo* [91], suggesting that NRF2 is druggable and that using an NRF2 antagonist may be a feasible therapeutic strategy.

FOXM1

Another transcription factor we found to be deregulated in multiple cancers is FOXM1, an oncogenic protein known to control proliferation, DNA damage repair, angiogenesis, and AOS response [92, 93]. Indeed, our analysis showed that *FOXM1* is highly expressed in multiple cancers (Figure 1) and associated with bad prognosis in breast cancer (Table 1 and Figure S2). These findings further reinforce previous studies reporting highly abnormal expression of FOXM1 in vast number of cancers and its correlation with poor prognosis [92, 94-97].

FOXM1 is known to regulate the expression of important AOS genes including *catalase*, *superoxide dismutase 2 (SOD2)* and *PRDX3* [97, 98] which we found to be highly overexpressed in multiple cancers (group 6) (Table S1), at the exception of *catalase*, exclusively overexpressed in hepatocellular carcinoma (group 3) (Table S1). Like NRF2 [99], FOXM1 is induced by active RAS [97] and required for mutant RAS-mediated invasion, anchorage independent growth [100], and development of lung abnormalities *in vivo* [101].

FOXM1 can be inhibited by classic proteasome inhibitors [96, 102, 103], by piperlongumine that acts as a proteasome inhibitor [104] and promotes autophagic cell death [11], by a peptide derived from ARF [105] and by the CDK4/6 inhibitor PD0332991 [106]. Interestingly, PD0332991 is currently tested in clinical trials (phase II) in breast cancer patients emphasizing the importance of FOXM1 in breast cancer (for review see [95]). Because proteasome inhibitors are already used in the clinic to treat multiple myeloma [107, 108], it is possible that these inhibitors might prove being beneficial in breast cancers patients, whose tumors highly express FOXM1. Consistently, several ROS inducers effectively killed breast cancer cells when combined with proteasome inhibitors or siRNA-mediated knockdown of FOXM1 [103].

NF-kappaB

Our analysis revealed that among the cancer oxidative stress response genes identified (group 6), a number of them are NF-kappaB targets (Table 1). NF-kappaB is essential for proliferation, cell adhesion, inflammatory response and AOS response [109, 110], and its activity is deregulated in cancers [111]. Interestingly, a number of oxidative stress response genes are transcriptionally controlled by NF-kappaB including *SOD1*, *SOD2*, *GPX1*, *GSTP1* and the NRF2 targets *GCLC*, *GCLM*, *NQO1* and *HO-1* [112, 113]. This transcriptional

regulation forms the basis for the protective role of NF-kappaB under oxidative stress [112]. This is especially relevant in the tumor context as we found that a number of these NF-kappaB targets are highly upregulated in multiple cancers (group 6, Table 1), supporting the notion of an elevated NF-kappaB activity in cancers as a strategy to manage oxidative stress conditions.

Several targeting approaches are being developed to inhibit NF-kappaB activity in cancers. The current strategy is to block NF-kappaB to sensitize tumors to chemotherapy and radiotherapy, since previous reports showed that inhibiting NF-kappaB leads to radiosensitization in radioresistant cancer cells [114, 115]. This is in agreement with the capacity of NF-kappaB to support an antioxidant program of which tumor cells may take advantage to resist oxidative stress-inducing therapies [116]. Thus, few natural compounds, such as curcumin, resveratrol and genistein, have been shown to inhibit NF-kappaB and to enhance the response to chemotherapeutic agents (for review[117]). A specific inhibitor of NF-kappaB nuclear translocation, namely dehydroxy-methylepoxy-quinomicin (DHMEQ), was shown to increase antitumor activities of taxane in a mouse model of thyroid cancer [118]. In addition, NF-kappaB activity can be blocked by direct inhibition of its upstream activator IKK, and the IKK inhibitor Bay 11-7082 leads to enhanced efficacy of cisplatin or paclitaxel in an ovarian tumor model [119, 120].

The cancer oxidative stress response metabolic program: NADPH is a key factor

Our analysis showed that the TXN and glutathione pathways are up-regulated in multiple cancers at the transcriptional level and that high expression of a significant number of these genes is correlated with poor survival. Because both of these pathways rely on NADPH (Figure 3) it raises the possibility that cancer cells will be highly sensitive to NADPH depletion. Indeed, it was demonstrated that the survival of cancer cells requires activation of the AMPK pathway to maintain NADPH levels under metabolic stress, which is usually encountered within solid tumors [7, 121, 122]. Similarly, it was demonstrated that survival of cells under detachment conditions, a hallmark of transformation, is dependent on the pentose phosphate pathway that generates NADPH [10, 123]. Moreover, NRF2 was shown to promote cancer cell proliferation by increasing NADPH generation through transcriptional up-regulation of a number of enzyme-encoding genes including *G6PD* [74] (Figure 3). Another study showed that TAp73, a transcription factor that is a member of the p53 family [124-128], facilitates the growth of transformed and of cancer cells *in vitro* and *in vivo* by up regulating the expression of *G6PD* and therefore NADPH levels [129].

In our analysis, G6PD was found to be up-regulated in cancer (Figure 1) and bad prognosis in breast cancer (Table 1 and Figure S3). As *G6PD* fuels the TXN and glutathione pathways with NADPH (Figure 3), we speculate that G6PD might represent a highly attractive novel drug target. It is therefore encouraging that compounds that inhibit G6PD *in vitro* were synthesized recently [130]. However, more work is needed in order to find lead G6PD inhibitors as candidate anti-cancer drugs.

CONCLUSIONS AND FUTURE PERSPECTIVES

The concept that the AOS response is utilized by cancer cells to promote their proliferation, adaptation, and resistance is now widely accepted by the scientific community and, therefore, numerous attempts to target AOS response genes as a therapeutic approach have been reported [10, 116, 131]. However, targeting endogenous proteins raises the concern of adverse off-target effects. Thus it is required to determine which proteins play a critical role in cancer as compared with normal tissues, as these are expected to offer a sufficient therapeutic window for intervention. Owing to the increasing availability of patient-derived gene expression, mutation, epigenetic, and survival data, it is now possible to use bioinformatics tools to screen for such targets in large cohorts for individual cancer entities as well as across histological entities [132].

Here, we used publicly available patient-derived gene expression and survival data, and identified genes that belong to two major detoxification pathways. Specifically, we show that genes belonging to the glutathione and TXN pathways are highly overexpressed in multiple cancers versus normal tissues and demonstrate that their high expression correlates with worse patient survival, pointing to a possible role of these genes as drug targets. Moreover, transcription factors such as NRF2, FOXM1, and NF- κ B as well as key metabolic enzymes such as G6PD that altogether drive the activity of these pathways, were identified in our analysis providing further support to the argument that these are important drug targets. Because the TXN and glutathione pathways are hyperactive in multiple cancers, we hypothesize that simultaneous inhibition of both pathways via targeting common regulators such as NRF2 or common metabolic requirements such as NADPH, may be highly efficient and should be prioritized in drug development.

ACKNOWLEDGMENTS

This work has been supported by the Medical Research Council, United Kingdom and the German Research Foundation (DFG GR3728/2-1 to TG).

REFERENCES

1. Cairns RA, Harris IS and Mak TW. Regulation of cancer cell metabolism. *Nat Rev Cancer*. 2011; 11(2):85-95.
2. Leprivier G, Remke M, Rotblat B, Dubuc A, Mateo AR, Kool M, Agnihotri S, El-Naggar A, Yu B, Somasekharan SP, Faubert B, Bridon G, Tognon CE, Mathers J, Thomas R, Li A, et al. The eEF2 kinase confers resistance to nutrient deprivation by blocking translation elongation. *Cell*. 2013; 153(5):1064-1079.
3. Ward PS and Thompson CB. Metabolic reprogramming: a cancer hallmark even warburg did not anticipate. *Cancer Cell*. 2012; 21(3):297-308.
4. Grunewald TG, Herbst SM, Heinze J and Burdach S. Understanding tumor heterogeneity as functional compartments--superorganisms revisited. *Journal of translational medicine*. 2011; 9:79.
5. Venere M, Hamerlik P, Wu Q, Rasmussen RD, Song LA, Vasanji A, Tenley N, Flavahan WA, Hjelmeland AB, Bartek J and Rich JN. Therapeutic targeting of constitutive PARP activation compromises stem cell phenotype and survival of glioblastoma-initiating cells. *Cell Death Differ*. 2013.
6. Matassa DS, Amoroso MR, Agliarulo I, Maddalena F, Sisinni L, Paladino S, Romano S, Romano MF, Sagar V, Loreni F, Landriscina M and Esposito F. Translational control in the stress adaptive response of cancer cells: a novel role for the heat shock protein TRAP1. *Cell death & disease*. 2013; 4:e851.
7. Jeon SM, Chandel NS and Hay N. AMPK regulates NADPH homeostasis to promote tumour cell survival during energy stress. *Nature*. 2012; 485(7400):661-665.
8. Sanchez-Macedo N, Feng J, Faubert B, Chang N, Elia A, Rushing EJ, Tsuchihara K, Bungard D, Berger SL, Jones RG, Mak TW and Zaugg K. Depletion of the novel p53-target gene carnitine palmitoyltransferase 1C delays tumor growth in the neurofibromatosis type I tumor model. *Cell Death Differ*. 2013; 20(4):659-668.
9. Trachootham D, Alexandre J and Huang P. Targeting cancer cells by ROS-mediated mechanisms: a radical therapeutic approach? *Nature reviews Drug discovery*. 2009; 8(7):579-591.
10. Schweikert EM, Devarajan A, Witte I, Wilgenbus P, Amort J, Forstermann U, Shabazian A, Grijalva V, Shih DM, Farias-Eisner R, Teiber JF, Reddy ST and Horke S. PON3 is upregulated in cancer tissues and protects against mitochondrial superoxide-mediated cell death. *Cell death and differentiation*. 2012; 19(9):1549-1560.
11. Wang Y, Wang JW, Xiao X, Shan Y, Xue B, Jiang G, He Q, Chen J, Xu HG, Zhao RX, Werle KD, Cui R, Liang J, Li YL and Xu ZX. Piperlongumine induces autophagy by targeting p38 signaling. *Cell Death Dis*. 2013; 4:e824.
12. Gorrini C, Harris IS and Mak TW. Modulation of oxidative stress as an anticancer strategy. *Nature reviews Drug*

discovery. 2013; 12(12):931-947

13. Shelton P and Jaiswal AK. The transcription factor NF-E2-related factor 2 (Nrf2): a protooncogene? *Faseb J.* 2013; 27(2):414-423.
14. Joo MS, Lee CG, Koo JH and Kim SG. miR-125b transcriptionally increased by Nrf2 inhibits AhR repressor, which protects kidney from cisplatin-induced injury. *Cell death & disease.* 2013; 4:e899.
15. Shah NM, Rushworth SA, Murray MY, Bowles KM and MacEwan DJ. Understanding the role of NRF2-regulated miRNAs in human malignancies. *Oncotarget.* 2013; 4(8):1130-1142.
16. Antonov AV, Schmidt T, Wang Y and Mewes HW. ProfCom: a web tool for profiling the complex functionality of gene groups identified from high-throughput data. *Nucleic Acids Res.* 2008; 36(Web Server issue):W347-351.
17. Serrano M and Blasco MA. Cancer and ageing: convergent and divergent mechanisms. *Nature reviews Molecular cell biology.* 2007; 8(9):715-722.
18. Antonov AV, Schmidt EE, Dietmann S, Krestyaninova M and Hermjakob H. R spider: a network-based analysis of gene lists by combining signaling and metabolic pathways from Reactome and KEGG databases. *Nucleic Acids Res.* 2010; 38(Web Server issue):W78-83.
19. Foller M, Harris IS, Elia A, John R, Lang F, Kavanagh TJ and Mak TW. Functional significance of glutamate-cysteine ligase modifier for erythrocyte survival in vitro and in vivo. *Cell death and differentiation.* 2013; 20(10):1350-1358.
20. Antonov AV. BioProfiling.de: analytical web portal for high-throughput cell biology. *Nucleic Acids Res.* 2011; 39(Web Server issue):W323-327.
21. Dalleau S, Baradat M, Gueraud F and Huc L. Cell death and diseases related to oxidative stress:4-hydroxynonenal (HNE) in the balance. *Cell death and differentiation.* 2013; 20(12):1615-1630.
22. Song Z, Saghafi N, Gokhale V, Brabant M and Meuillet EJ. Regulation of the activity of the tumor suppressor PTEN by thioredoxin in *Drosophila melanogaster*. *Experimental cell research.* 2007; 313(6):1161-1171.
23. Bassi C and Stambolic V. PTEN, here, there, everywhere. *Cell death and differentiation.* 2013; 20(12):1595-1596.
24. Li C, Thompson MA, Tamayo AT, Zuo Z, Lee J, Vega F, Ford RJ and Pham LV. Over-expression of Thioredoxin-1 mediates growth, survival, and chemoresistance and is a druggable target in diffuse large B-cell lymphoma. *Oncotarget.* 2012; 3(3):314-326.
25. Lim JY, Yoon SO, Hong SW, Kim JW, Choi SH and Cho JY. Thioredoxin and thioredoxin-interacting protein as prognostic markers for gastric cancer recurrence. *World journal of gastroenterology : WJG.* 2012; 18(39):5581-5588.
26. Noike T, Miwa S, Soeda J, Kobayashi A and Miyagawa S. Increased expression of thioredoxin-1, vascular endothelial growth factor, and redox factor-1 is associated with poor prognosis in patients with liver metastasis from colorectal cancer. *Hum Pathol.* 2008; 39(2):201-208.
27. Kakolyris S, Giatromanolaki A, Koukourakis M, Powis G, Souglakos J, Sivridis E, Georgoulias V, Gatter KC and Harris AL. Thioredoxin expression is associated with lymph node status and prognosis in early operable non-small cell lung cancer. *Clin Cancer Res.* 2001; 7(10):3087-3091.
28. Cadenas C, Franckenstein D, Schmidt M, Gehrmann M, Hermes M, Geppert B, Schormann W, Macoux LJ, Schug M, Schumann A, Wilhelm C, Freis E, Ickstadt K, Rahnenfuhrer J, Baumbach JI, Sickmann A, et al. Role of thioredoxin reductase 1 and thioredoxin interacting protein in prognosis of breast cancer. *Breast cancer research : BCR.* 2010; 12(3):R44.
29. Zhu X, Huang C and Peng B. Overexpression of thioredoxin system proteins predicts poor prognosis in patients with squamous cell carcinoma of the tongue. *Oral oncology.* 2011; 47(7):609-614.
30. Kim JH, Bogner PN, Ramnath N, Park Y, Yu J and Park YM. Elevated peroxiredoxin 1, but not NF-E2-related factor 2, is an independent prognostic factor for disease recurrence and reduced survival in stage I non-small cell lung cancer. *Clin Cancer Res.* 2007; 13(13):3875-3882.
31. Chung KH, Lee DH, Kim Y, Kim TH, Huh JH, Chung SG, Lee S, Lee C, Ko JJ and An HJ. Proteomic identification of overexpressed PRDX 1 and its clinical implications in ovarian carcinoma. *Journal of proteome research.* 2010; 9(1):451-457.
32. Woolston CM, Storr SJ, Ellis IO, Morgan DA and Martin SG. Expression of thioredoxin system and related peroxiredoxin proteins is associated with clinical outcome in radiotherapy treated early stage breast cancer. *Radiotherapy and oncology : journal of the European Society for Therapeutic Radiology and Oncology.* 2011; 100(2):308-313.
33. Qiao B, Wang J, Xie J, Niu Y, Ye S, Wan Q and Ye Q. Detection and identification of peroxiredoxin 3 as a biomarker in hepatocellular carcinoma by a proteomic approach. *International journal of molecular medicine.* 2012; 29(5):832-840.
34. Chang KP, Yu JS, Chien KY, Lee CW, Liang Y, Liao CT, Yen TC, Lee LY, Huang LL, Liu SC, Chang YS and Chi LM. Identification of PRDX4 and P4HA2 as metastasis-associated proteins in oral cavity squamous cell carcinoma by comparative tissue proteomics of microdissected specimens using iTRAQ technology. *Journal of proteome research.* 2011; 10(11):4935-4947.
35. Ramanathan RK, Stephenson JJ, Weiss GJ, Pestano LA, Lowe A, Hiscox A, Leos RA, Martin JC, Kirkpatrick L and Richards DA. A phase I trial of PX-12, a small-molecule inhibitor of thioredoxin-1, administered as a 72-hour infusion every 21 days in patients with advanced cancers refractory to standard therapy. *Investigational new drugs.* 2012; 30(4):1591-1596.
36. Baker AF, Adab KN, Raghunand N, Chow HH, Stratton

SP, Squire SW, Boice M, Pestano LA, Kirkpatrick DL and Dragovich T. A phase IB trial of 24-hour intravenous PX-12, a thioredoxin-1 inhibitor, in patients with advanced gastrointestinal cancers. *Investigational new drugs*. 2013; 31(3):631-641.

37. Peng X, Zhang MQ, Conserva F, Hosny G, Selivanova G, Bykov VJ, Arner ES and Wiman KG. APR-246/PRIMA-1(MET) inhibits thioredoxin reductase 1 and converts the enzyme to a dedicated NADPH oxidase. *Cell death & disease*. 2013; 4:e881.

38. Gromer S, Arscott LD, Williams CH, Jr., Schirmer RH and Becker K. Human placenta thioredoxin reductase. Isolation of the selenoenzyme, steady state kinetics, and inhibition by therapeutic gold compounds. *J Biol Chem*. 1998; 273(32):20096-20101.

39. Kast RE, Boockvar JA, Bruning A, Cappello F, Chang WW, Cvek B, Dou QP, Duenas-Gonzalez A, Efferth T, Focosi D, Ghaffari SH, Karpel-Massler G, Ketola K, Khoshnevisan A, Keizman D, Magne N, et al. A conceptually new treatment approach for relapsed glioblastoma: coordinated undermining of survival paths with nine repurposed drugs (CUSP9) by the International Initiative for Accelerated Improvement of Glioblastoma Care. *Oncotarget*. 2013; 4(4):502-530.

40. Canas A, Lopez-Sanchez LM, Valverde-Estepa A, Hernandez V, Fuentes E, Munoz-Castaneda JR, Lopez-Pedrera C, De La Haba-Rodriguez JR, Aranda E and Rodriguez-Ariza A. Maintenance of S-nitrosothiol homeostasis plays an important role in growth suppression of estrogen receptor-positive breast tumors. *Breast cancer research : BCR*. 2012; 14(6):R153.

41. Dai B, Yoo SY, Bartholomeusz G, Graham RA, Majidi M, Yan S, Meng J, Ji L, Coombes K, Minna JD, Fang B and Roth JA. KEAP1-dependent synthetic lethality induced by AKT and TXNRD1 inhibitors in lung cancer. *Cancer Res*. 2013; 73(17):5532-5543.

42. Chandler JD, Nichols DP, Nick JA, Hondal RJ and Day BJ. Selective metabolism of hypothiocyanous acid by mammalian thioredoxin reductase promotes lung innate immunity and antioxidant defense. *J Biol Chem*. 2013; 288(25):18421-18428.

43. Fath MA, Ahmad IM, Smith CJ, Spence J and Spitz DR. Enhancement of carboplatin-mediated lung cancer cell killing by simultaneous disruption of glutathione and thioredoxin metabolism. *Clin Cancer Res*. 2011; 17(19):6206-6217.

44. Fricker SP. Strategies for the biological evaluation of gold anticancer agents. *Anti-cancer agents in medicinal chemistry*. 2011; 11(10):940-952.

45. Traverso N, Ricciarelli R, Nitti M, Marengo B, Furfaro AL, Pronzato MA, Marinari UM and Domenicotti C. Role of glutathione in cancer progression and chemoresistance. *Oxidative medicine and cellular longevity*. 2013; 2013:972913.

46. Calvert P, Yao KS, Hamilton TC and O'Dwyer PJ. Clinical studies of reversal of drug resistance based on glutathione. *Chem Biol Interact*. 1998; 111-112:213-224.

47. Estrela JM, Ortega A and Obrador E. Glutathione in cancer biology and therapy. *Critical reviews in clinical laboratory sciences*. 2006; 43(2):143-181.

48. Scieneay J, Liu MC, Chen A, Wong CS, Bowtell DD and Moller A. The antioxidant N-acetylcysteine prevents HIF-1 stabilization under hypoxia in vitro but does not affect tumorigenesis in multiple breast cancer models in vivo. *PLoS One*. 2013; 8(6):e66388.

49. Jardim BV, Moschetta MG, Leonel C, Gelaleti GB, Regiani VR, Ferreira LC, Lopes JR and de Campos Zuccari DA. Glutathione and glutathione peroxidase expression in breast cancer: An immunohistochemical and molecular study. *Oncology reports*. 2013; 30(3):1119-28. doi: 10.3892/or.2013.2540.

50. Tew KD. Glutathione-associated enzymes in anticancer drug resistance. *Cancer Res*. 1994; 54(16):4313-4320.

51. Boivin A, Hanot M, Malesys C, Maalouf M, Rousson R, Rodriguez-Lafrasse C and Ardail D. Transient alteration of cellular redox buffering before irradiation triggers apoptosis in head and neck carcinoma stem and non-stem cells. *PLoS One*. 2011; 6(1):e14558.

52. Benassi B, Marani M, Loda M and Blandino G. USP2a alters chemotherapeutic response by modulating redox. *Cell death & disease*. 2013; 4:e812.

53. Shiga H, Heath EI, Rasmussen AA, Trock B, Johnston PG, Forastiere AA, Langmacher M, Baylor A, Lee M and Cullen KJ. Prognostic value of p53, glutathione S-transferase pi, and thymidylate synthase for neoadjuvant cisplatin-based chemotherapy in head and neck cancer. *Clin Cancer Res*. 1999; 5(12):4097-4104.

54. Schumaker L, Nikitakis N, Goloubeva O, Tan M, Taylor R and Cullen KJ. Elevated expression of glutathione S-transferase pi and p53 confers poor prognosis in head and neck cancer patients treated with chemoradiotherapy but not radiotherapy alone. *Clin Cancer Res*. 2008; 14(18):5877-5883.

55. Boku N, Chin K, Hosokawa K, Ohtsu A, Tajiri H, Yoshida S, Yamao T, Kondo H, Shirao K, Shimada Y, Saito D, Hasebe T, Mukai K, Seki S, Saito H and Johnston PG. Biological markers as a predictor for response and prognosis of unresectable gastric cancer patients treated with 5-fluorouracil and cis-platinum. *Clin Cancer Res*. 1998; 4(6):1469-1474.

56. Tan KL, Jankova L, Chan C, Fung CL, Clarke C, Lin BP, Robertson G, Molloy M, Chapuis PH, Bokey L, Dent OF and Clarke SJ. Clinicopathological correlates and prognostic significance of glutathione S-transferase Pi expression in 468 patients after potentially curative resection of node-positive colonic cancer. *Histopathology*. 2011; 59(6):1057-1070.

57. Jardim BV, Moschetta MG, Gelaleti GB, Leonel C, Regiani VR, de Santi Neto D, Bordin-Junior NA, Perea SA and

Zuccari DA. Glutathione transferase pi (GSTpi) expression in breast cancer: an immunohistochemical and molecular study. *Acta histochemica*. 2012; 114(5):510-517.

58. Huang J, Tan PH, Thiagarajan J and Bay BH. Prognostic significance of glutathione S-transferase-pi in invasive breast cancer. *Modern pathology : an official journal of the United States and Canadian Academy of Pathology, Inc.* 2003; 16(6):558-565.

59. Kolwijk E, Zusterzeel PL, Roelofs HM, Hendriks JC, Peters WH and Massuger LF. GSTP1-1 in ovarian cyst fluid and disease outcome of patients with ovarian cancer. *Cancer epidemiology, biomarkers & prevention : a publication of the American Association for Cancer Research, cosponsored by the American Society of Preventive Oncology*. 2009; 18(8):2176-2181.

60. Laborde E. Glutathione transferases as mediators of signaling pathways involved in cell proliferation and cell death. *Cell death and differentiation*. 2010; 17(9):1373-1380.

61. Peroja P, Pasanen AK, Haapasaari KM, Jantunen E, Soini Y, Turpeenniemi-Hujanen T, Bloigu R, Lilja L, Kuittinen O and Karihtala P. Oxidative stress and redox state-regulating enzymes have prognostic relevance in diffuse large B-cell lymphoma. *Experimental hematology & oncology*. 2012; 1(1):2.

62. Jerome-Morais A, Wright ME, Liu R, Yang W, Jackson MI, Combs GF, Jr. and Diamond AM. Inverse association between glutathione peroxidase activity and both selenium-binding protein 1 levels and Gleason score in human prostate tissue. *The Prostate*. 2012; 72(9):1006-1012.

63. Ho JC, Chan-Yeung M, Ho SP, Mak JC, Ip MS, Ooi GC, Wong MP, Tsang KW and Lam WK. Disturbance of systemic antioxidant profile in nonsmall cell lung carcinoma. *The European respiratory journal*. 2007; 29(2):273-278.

64. Griffith OW. Mechanism of action, metabolism, and toxicity of buthionine sulfoximine and its higher homologs, potent inhibitors of glutathione synthesis. *J Biol Chem*. 1982; 257(22):13704-13712.

65. Bailey HH, Mulcahy RT, Tutsch KD, Arzumanian RZ, Alberti D, Tombes MB, Wilding G, Pomplun M and Spriggs DR. Phase I clinical trial of intravenous L-buthionine sulfoximine and melphalan: an attempt at modulation of glutathione. *Journal of clinical oncology : official journal of the American Society of Clinical Oncology*. 1994; 12(1):194-205.

66. Bahlis NJ, McCafferty-Grad J, Jordan-McMurry I, Neil J, Reis I, Kharfan-Dabaja M, Eckman J, Goodman M, Fernandez HF, Boise LH and Lee KP. Feasibility and correlates of arsenic trioxide combined with ascorbic acid-mediated depletion of intracellular glutathione for the treatment of relapsed/refractory multiple myeloma. *Clin Cancer Res*. 2002; 8(12):3658-3668.

67. Sobhakumari A, Love-Homan L, Fletcher EV, Martin SM, Parsons AD, Spitz DR, Knudson CM and Simons AL. Susceptibility of human head and neck cancer cells to combined inhibition of glutathione and thioredoxin metabolism. *PLoS One*. 2012; 7(10):e48175.

68. Moinova HR and Mulcahy RT. Up-regulation of the human gamma-glutamylcysteine synthetase regulatory subunit gene involves binding of Nrf-2 to an electrophile responsive element. *Biochem Biophys Res Commun*. 1999; 261(3):661-668.

69. Wild AC, Moinova HR and Mulcahy RT. Regulation of gamma-glutamylcysteine synthetase subunit gene expression by the transcription factor Nrf2. *J Biol Chem*. 1999; 274(47):33627-33636.

70. Ishii T, Itoh K, Takahashi S, Sato H, Yanagawa T, Katoh Y, Bannai S and Yamamoto M. Transcription factor Nrf2 coordinately regulates a group of oxidative stress-inducible genes in macrophages. *The Journal of biological chemistry*. 2000; 275(21):16023-16029.

71. Chan JY and Kwong M. Impaired expression of glutathione synthetic enzyme genes in mice with targeted deletion of the Nrf2 basic-leucine zipper protein. *Biochim Biophys Acta*. 2000; 1517(1):19-26.

72. Itoh K, Chiba T, Takahashi S, Ishii T, Igarashi K, Katoh Y, Oyake T, Hayashi N, Satoh K, Hatayama I, Yamamoto M and Nabeshima Y. An Nrf2/small Maf heterodimer mediates the induction of phase II detoxifying enzyme genes through antioxidant response elements. *Biochem Biophys Res Commun*. 1997; 236(2):313-322.

73. Kensler TW, Wakabayashi N and Biswal S. Cell survival responses to environmental stresses via the Keap1-Nrf2-ARE pathway. *Annual review of pharmacology and toxicology*. 2007; 47:89-116.

74. Mitsuishi Y, Taguchi K, Kawatani Y, Shibata T, Nukiwa T, Aburatani H, Yamamoto M and Motohashi H. Nrf2 redirects glucose and glutamine into anabolic pathways in metabolic reprogramming. *Cancer Cell*. 2012; 22(1):66-79.

75. Lim JH, Kim KM, Kim SW, Hwang O and Choi HJ. Bromocriptine activates NQO1 via Nrf2-PI3K/Akt signaling: novel cytoprotective mechanism against oxidative damage. *Pharmacological research : the official journal of the Italian Pharmacological Society*. 2008; 57(5):325-331.

76. Alam J, Stewart D, Touchard C, Boinapally S, Choi AM and Cook JL. Nrf2, a Cap'n'Collar transcription factor, regulates induction of the heme oxygenase-1 gene. *The Journal of biological chemistry*. 1999; 274(37):26071-26078.

77. Kim YC, Masutani H, Yamaguchi Y, Itoh K, Yamamoto M and Yodoi J. Hemin-induced activation of the thioredoxin gene by Nrf2. A differential regulation of the antioxidant responsive element by a switch of its binding factors. *J Biol Chem*. 2001; 276(21):18399-18406.

78. Kim YC, Yamaguchi Y, Kondo N, Masutani H and Yodoi J. Thioredoxin-dependent redox regulation of the antioxidant responsive element (ARE) in electrophile response.

Oncogene. 2003; 22(12):1860-1865.

79. Heasman SA, Zaitseva L, Bowles KM, Rushworth SA and Macewan DJ. Protection of acute myeloid leukaemia cells from apoptosis induced by front-line chemotherapeutics is mediated by haem oxygenase-1. *Oncotarget*. 2011; 2(9):658-668.

80. Ramos-Gomez M, Dolan PM, Itoh K, Yamamoto M and Kensler TW. Interactive effects of nrf2 genotype and oltipraz on benzo[a]pyrene-DNA adducts and tumor yield in mice. *Carcinogenesis*. 2003; 24(3):461-467.

81. Fahey JW, Haristoy X, Dolan PM, Kensler TW, Scholtus I, Stephenson KK, Talalay P and Lozniewski A. Sulforaphane inhibits extracellular, intracellular, and antibiotic-resistant strains of *Helicobacter pylori* and prevents benzo[a]pyrene-induced stomach tumors. *Proceedings of the National Academy of Sciences of the United States of America*. 2002; 99(11):7610-7615.

82. Jeong WS, Jun M and Kong AN. Nrf2: a potential molecular target for cancer chemoprevention by natural compounds. *Antioxidants & redox signaling*. 2006; 8(1-2):99-106.

83. Baird L and Dinkova-Kostova AT. The cytoprotective role of the Keap1-Nrf2 pathway. *Archives of toxicology*. 2011; 85(4):241-272.

84. Hayes JD and McMahon M. NRF2 and KEAP1 mutations: permanent activation of an adaptive response in cancer. *Trends in biochemical sciences*. 2009; 34(4):176-188.

85. Hayes JD, McMahon M, Chowdhry S and Dinkova-Kostova AT. Cancer chemoprevention mechanisms mediated through the Keap1-Nrf2 pathway. *Antioxid Redox Signal*. 2010; 13(11):1713-1748.

86. Lau A, Villeneuve NF, Sun Z, Wong PK and Zhang DD. Dual roles of Nrf2 in cancer. *Pharmacological research : the official journal of the Italian Pharmacological Society*. 2008; 58(5-6):262-270.

87. Rotblat B, Melino G and Knight RA. NRF2 and p53: Januses in cancer? *Oncotarget*. 2012; 3(11):1272-1283.

88. Satoh H, Moriguchi T, Takai J, Ebina M and Yamamoto M. Nrf2 prevents initiation but accelerates progression through the Kras signaling pathway during lung carcinogenesis. *Cancer Res*. 2013; 73(13):4158-4168.

89. Taguchi K, Motohashi H and Yamamoto M. Molecular mechanisms of the Keap1-Nrf2 pathway in stress response and cancer evolution. *Genes to cells : devoted to molecular & cellular mechanisms*. 2011; 16(2):123-140.

90. Kansanen E, Kuosmanen SM, Leinonen H and Levonen AL. The Keap1-Nrf2 pathway: Mechanisms of activation and dysregulation in cancer. *Redox biology*. 2013; 1(1):45-49.

91. Ren D, Villeneuve NF, Jiang T, Wu T, Lau A, Toppin HA and Zhang DD. Brusatol enhances the efficacy of chemotherapy by inhibiting the Nrf2-mediated defense mechanism. *Proceedings of the National Academy of Sciences of the United States of America*. 2011; 108(4):1433-1438.

92. Koo CY, Muir KW and Lam EW. FOXM1: From cancer initiation to progression and treatment. *Biochim Biophys Acta*. 2012; 1819(1):28-37.

93. De Craene B, Denecker G, Vermassen P, Taminau J, Mauch C, Derore A, Jonkers J, Fuchs E and Berx G. Epidermal Snail expression drives skin cancer initiation and progression through enhanced cytoprotection, epidermal stem/progenitor cell expansion and enhanced metastatic potential. *Cell death and differentiation*. 2013; doi: 10.1038/cdd.2013.148.

94. Wang M and Gartel AL. The suppression of FOXM1 and its targets in breast cancer xenograft tumors by siRNA. *Oncotarget*. 2011; 2(12):1218-1226.

95. Halasi M and Gartel AL. Targeting FOXM1 in cancer. *Biochemical pharmacology*. 2013; 85(5):644-652.

96. Gartel AL. The oncogenic transcription factor FOXM1 and anticancer therapy. *Cell Cycle*. 2012; 11(18):3341-3342.

97. Park HJ, Carr JR, Wang Z, Nogueira V, Hay N, Tyner AL, Lau LF, Costa RH and Raychaudhuri P. FoxM1, a critical regulator of oxidative stress during oncogenesis. *Embo J*. 2009; 28(19):2908-2918.

98. Kamarajugadda S, Cai Q, Chen H, Nayak S, Zhu J, He M, Jin Y, Zhang Y, Ai L, Martin SS, Tan M and Lu J. Manganese superoxide dismutase promotes anoikis resistance and tumor metastasis. *Cell Death Dis*. 2013; 4:e504.

99. DeNicola GM, Karreth FA, Humpton TJ, Gopinathan A, Wei C, Frese K, Mangal D, Yu KH, Yeo CJ, Calhoun ES, Scrimieri F, Winter JM, Hruban RH, Iacobuzio-Donahue C, Kern SE, Blair IA, et al. Oncogene-induced Nrf2 transcription promotes ROS detoxification and tumorigenesis. *Nature*. 2011; 475(7354):106-109.

100. Behren A, Muhlen S, Acuna Sanhueza GA, Schwager C, Plinkert PK, Huber PE, Abdollahi A and Simon C. Phenotype-assisted transcriptome analysis identifies FOXM1 downstream from Ras-MKK3-p38 to regulate in vitro cellular invasion. *Oncogene*. 2010; 29(10):1519-1530.

101. Wang IC, Snyder J, Zhang Y, Lander J, Nakafuku Y, Lin J, Chen G, Kalin TV, Whitsett JA and Kalinichenko VV. Foxm1 mediates cross talk between Kras/mitogen-activated protein kinase and canonical Wnt pathways during development of respiratory epithelium. *Mol Cell Biol*. 2012; 32(19):3838-3850.

102. Bhat UG, Halasi M and Gartel AL. FoxM1 is a general target for proteasome inhibitors. *PLoS One*. 2009; 4(8):e6593.

103. Halasi M, Pandit B, Wang M, Nogueira V, Hay N and Gartel AL. Combination of oxidative stress and FOXM1 inhibitors induces apoptosis in cancer cells and inhibits xenograft tumor growth. *The American journal of pathology*. 2013; 183(1):257-265.

104. Halasi M, Wang M, Chavan TS, Gaponenko V, Hay N and Gartel AL. ROS inhibitor N-acetyl-L-cysteine antagonizes the activity of proteasome inhibitors. *Biochem J*. 2013;

454(2):201-208.

105. Kalinichenko VV, Major ML, Wang X, Petrovic V, Kuechle J, Yoder HM, Dennewitz MB, Shin B, Datta A, Raychaudhuri P and Costa RH. Foxm1b transcription factor is essential for development of hepatocellular carcinomas and is negatively regulated by the p19ARF tumor suppressor. *Genes Dev.* 2004; 18(7):830-850.
106. Anders L, Ke N, Hydbring P, Choi YJ, Widlund HR, Chick JM, Zhai H, Vidal M, Gygi SP, Braun P and Sicinski P. A systematic screen for CDK4/6 substrates links FOXM1 phosphorylation to senescence suppression in cancer cells. *Cancer Cell.* 2011; 20(5):620-634.
107. Kortuem KM and Stewart AK. Carfilzomib. *Blood.* 2013; 121(6):893-897.
108. Reinstein E and Ciechanover A. Narrative review: protein degradation and human diseases: the ubiquitin connection. *Annals of internal medicine.* 2006; 145(9):676-684.
109. Perkins ND. The diverse and complex roles of NF- κ B subunits in cancer. *Nat Rev Cancer.* 2012; 12(2):121-132.
110. Chang CP, Su YC, Hu CW and Lei HY. TLR2-dependent selective autophagy regulates NF- κ B lysosomal degradation in hepatoma-derived M2 macrophage differentiation. *Cell death and differentiation.* 2013; 20(3):515-523.
111. DiDonato JA, Mercurio F and Karin M. NF- κ B and the link between inflammation and cancer. *Immunological reviews.* 2012; 246(1):379-400.
112. Morgan MJ and Liu ZG. Crosstalk of reactive oxygen species and NF- κ B signaling. *Cell Res.* 2011; 21(1):103-115.
113. Lu SC. Regulation of glutathione synthesis. Molecular aspects of medicine. 2009; 30(1-2):42-59.
114. Lin Y, Bai L, Chen W and Xu S. The NF- κ B activation pathways, emerging molecular targets for cancer prevention and therapy. Expert opinion on therapeutic targets. 2010; 14(1):45-55.
115. Ahmed KM and Li JJ. ATM-NF- κ B connection as a target for tumor radiosensitization. *Current cancer drug targets.* 2007; 7(4):335-342.
116. D'Anneo A, Carlisi D, Lauricella M, Puleio R, Martinez R, Di Bella S, Di Marco P, Emanuele S, Di Fiore R, Guercio A, Vento R and Tesoriere G. Parthenolide generates reactive oxygen species and autophagy in MDA-MB231 cells. A soluble parthenolide analogue inhibits tumour growth and metastasis in a xenograft model of breast cancer. *Cell death & disease.* 2013; 4:e891.
117. Shen HM and Tergaonkar V. NF- κ B signaling in carcinogenesis and as a potential molecular target for cancer therapy. *Apoptosis : an international journal on programmed cell death.* 2009; 14(4):348-363.
118. Meng Z, Mitsutake N, Nakashima M, Starenki D, Matsuse M, Takakura S, Namba H, Saenko V, Umezawa K, Ohtsuru A and Yamashita S. Dehydroxymethylepoxyquinomicin, a novel nuclear Factor- κ B inhibitor, enhances antitumor activity of taxanes in anaplastic thyroid cancer cells. *Endocrinology.* 2008; 149(11):5357-5365.
119. Mabuchi S, Ohmichi M, Nishio Y, Hayasaka T, Kimura A, Ohta T, Saito M, Kawagoe J, Takahashi K, Yada-Hashimoto N, Sakata M, Motoyama T, Kurachi H, Tasaka K and Murata Y. Inhibition of NF- κ B increases the efficacy of cisplatin in *in vitro* and *in vivo* ovarian cancer models. *J Biol Chem.* 2004; 279(22):23477-23485.
120. Mabuchi S, Ohmichi M, Nishio Y, Hayasaka T, Kimura A, Ohta T, Kawagoe J, Takahashi K, Yada-Hashimoto N, Seino-Noda H, Sakata M, Motoyama T, Kurachi H, Testa JR, Tasaka K and Murata Y. Inhibition of inhibitor of nuclear factor- κ B phosphorylation increases the efficacy of paclitaxel in *in vitro* and *in vivo* ovarian cancer models. *Clin Cancer Res.* 2004; 10(22):7645-7654.
121. Liu PP, Liao J, Tang ZJ, Wu WJ, Yang J, Zeng ZL, Hu Y, Wang P, Ju HQ, Xu RH and Huang P. Metabolic regulation of cancer cell side population by glucose through activation of the Akt pathway. *Cell death and differentiation.* 2013; doi: 10.1038/cdd.2013.131. Epub 2013 Oct 4.
122. Tedeschi PM, Markert EK, Gounder M, Lin H, Dvorzhinski D, Dolfi SC, Chan LL, Qiu J, Dipaola RS, Hirshfield KM, Boros LG, Bertino JR, Oltvai ZN and Vazquez A. Contribution of serine, folate and glycine metabolism to the ATP, NADPH and purine requirements of cancer cells. *Cell death & disease.* 2013; 4:e877.
123. Schafer ZT, Grassian AR, Song L, Jiang Z, Gerhart-Hines Z, Irie HY, Gao S, Puigserver P and Brugge JS. Antioxidant and oncogene rescue of metabolic defects caused by loss of matrix attachment. *Nature.* 2009; 461(7260):109-113.
124. Velletri T, Romeo F, Tucci P, Peschiaroli A, Annicchiarico-Petruzzelli M, Niklison-Chirou MV, Amelio I, Knight RA, Mak TW, Melino G and Agostini M. GLS2 is transcriptionally regulated by p73 and contributes to neuronal differentiation. *Cell Cycle.* 2013; 12(22).
125. Dotsch V, Bernassola F, Coutandin D, Candi E and Melino G. p63 and p73, the ancestors of p53. *Cold Spring Harb Perspect Biol.* 2010; 2(9):a004887.
126. Rufini A, Agostini M, Grespi F, Tomasini R, Sayan BS, Niklison-Chirou MV, Conforti F, Velletri T, Mastino A, Mak TW, Melino G and Knight RA. p73 in Cancer. *Genes & cancer.* 2011; 2(4):491-502.
127. McCubrey JA and Demidenko ZN. Recent discoveries in the cycling, growing and aging of the p53 field. *Aging.* 2012; 4(12):887-893.
128. Amelio I, Grespi F, Annicchiarico-Petruzzelli M and Melino G. p63 the guardian of human reproduction. *Cell Cycle.* 2012; 11(24):4545-4551.
129. Du W, Jiang P, Mancuso A, Stonestrom A, Brewer MD, Minn AJ, Mak TW, Wu M and Yang X. TAp73 enhances the pentose phosphate pathway and supports cell proliferation. *Nat Cell Biol.* 2013; 15(8):991-1000.
130. Hamilton NM, Dawson M, Fairweather EE, Hamilton NS, Hitchin JR, James DI, Jones SD, Jordan AM, Lyons AJ,

Small HF, Thomson GJ, Waddell ID and Ogilvie DJ. Novel steroid inhibitors of glucose 6-phosphate dehydrogenase. *J Med Chem.* 2012; 55(9):4431-4445.

131. Traba J, Del Arco A, Duchen MR, Szabadkai G and Satrustegui J. SCaMC-1 promotes cancer cell survival by desensitizing mitochondrial permeability transition via ATP/ADP-mediated matrix Ca(2+) buffering. *Cell death and differentiation.* 2012; 19(4):650-660.

132. Willier S, Butt E and Grunewald TG. Lysophosphatidic acid (LPA) signalling in cell migration and cancer invasion: a focussed review and analysis of LPA receptor gene expression on the basis of more than 1700 cancer microarrays. *Biology of the cell / under the auspices of the European Cell Biology Organization.* 2013; 105(8):317-333.

133. Roth RB, Hevezi P, Lee J, Willhite D, Lechner SM, Foster AC and Zlotnik A. Gene expression analyses reveal molecular relationships among 20 regions of the human CNS. *Neurogenetics.* 2006; 7(2):67-80.

134. Irizarry RA, Hobbs B, Collin F, Beazer-Barclay YD, Antonellis KJ, Scherf U and Speed TP. Exploration, normalization, and summaries of high density oligonucleotide array probe level data. *Biostatistics.* 2003; 4(2):249-264.

135. Grunewald TG, Willier S, Janik D, Unland R, Reiss C, da Costa OP, Buch T, Dirksen U, Richter GH, Neff F, Burdach S and Butt E. The Zyxin-related protein thyroid receptor interacting protein 6 (TRIP6) is overexpressed in Ewing's sarcoma and promotes migration, invasion and cell growth. *Biology of the cell / under the auspices of the European Cell Biology Organization.* 2013; 105(11):535-547, doi: 10.1111/boc.201300041

136. Miller IV, Raposo G, Welsch U, Prazeres da Costa O, Thiel U, Lebar M, Maurer M, Bender HU, von Luettichau I, Richter GH, Burdach S and Grunewald TG. First identification of Ewing's sarcoma-derived extracellular vesicles and exploration of their biological and potential diagnostic implications. *Biology of the cell / under the auspices of the European Cell Biology Organization.* 2013; 105(7):289-303.

137. Bentley AR, Emrani P and Cassano PA. Genetic variation and gene expression in antioxidant related enzymes and risk of COPD: a systematic review. *Thorax.* 2008; 63(11):956-961.

The Zyxin-related protein thyroid receptor interacting protein 6 (TRIP6) is overexpressed in Ewing's sarcoma and promotes migration, invasion and cell growth

Thomas G.P. Grunewald^{*1,2}, Semjon Willert¹, Dirk Janik[†], Rebekka Unland[§], Cora Reisst^{†||}, Olivia Prazeres da Costa[#], Thorsten Buch[#], Uta Dirksen[§], Günther H.S. Richter^{*}, Frauke Neff[†], Stefan Burdach^{*} and Elke Butt^{†,3}

^{*}Children's Cancer Research Center and Roman Herzog Comprehensive Cancer Center, Laboratory of Functional Genomics and Transplantation Biology, Klinikum rechts der Isar, Technische Universität München, Munich 80804, Germany, [†]Institute for Clinical Biochemistry and Pathobiochemistry, University Clinic of Würzburg, Würzburg 97080, Germany, [‡]Institute of Pathology, Helmholtz Center Munich, Neuherberg 85764, Germany, [§]Department of Pediatric Hematology and Oncology, University Hospital Muenster, Westphalian Wilhelms University, Muenster 48149, Germany, ^{||}Center for Thrombosis and Hemostasis, University Medical Center Mainz, Mainz 55131, Germany, and [#]Institute for Medical Microbiology, Immunology, and Hygiene, Technische Universität München, Munich 81675, Germany

Background information. Ewing's sarcoma (ES) is the second most common bone-associated malignancy in children and is driven by the fusion oncogene EWS/FLI1 and characterised by rapid growth and early metastasis. Here, we explored the role of the Zyxin-related protein thyroid receptor interacting protein 6 (TRIP6) in ES. The Zyxin family comprises seven homologous proteins involved in migration and proliferation of many cell types of which Zyxin has been described as a tumour suppressor in ES.

Results. By interrogation of published microarray data ($n = 1254$), we observed that of all Zyxin proteins, only TRIP6 is highly overexpressed in primary ES compared with normal tissues. Re-analysis of published EWS/FLI1 gain- and loss-of-function microarray experiments as well as chromatin-immunoprecipitation assays revealed that TRIP6 overexpression is not mediated by EWS/FLI1. Microarray and subsequent gene-set enrichment analyses of ES cells with and without RNA interference-mediated TRIP6 knockdown demonstrated that TRIP6 expression confers a pro-proliferative and pro-invasive transcriptional signature to ES cells. While short-term proliferation was not considerably affected by TRIP6 knockdown, silencing of the protein significantly reduced migration, invasion, long-term proliferation and clonogenicity of ES cells *in vitro* as well as tumourigenicity *in vivo*.

Conclusions. Taken together, our data indicate that TRIP6 acts, in contrast to Zyxin, as an oncogene that partially accounts for the autonomous migratory, invasive and proliferative properties of ES cells independent of EWS/FLI1.



Additional supporting information may be found in the online version of this article at the publisher's web-site

¹These authors contributed equally to this work.

²To whom correspondence should be addressed (email thomas.grunewald@lrz.tum.de)

³To whom correspondence should be addressed (email e.butt@klin-biochem.uni-wuerzburg.de)

Key words: Clonogenicity, Ewing's sarcoma, Invasion, Migration, TRIP6.

Abbreviations used: ChIP, chromatin-immunoprecipitation; EIOGES, EWS/FLI1-independent genes overexpressed in ES; ES, Ewing's sarcoma;

EWS/FLI1, Ewing sarcoma breakpoint region 1/friend leukaemia virus integration 1; FA, focal adhesion; FBS, foetal bovine serum; GEO, Gene Expression Omnibus; GSEA, gene-set enrichment analysis; HE, haematoxylin and eosin; PI, propidium iodide; qRT-PCR, quantitative real-time PCR; RNAi, RNA interference; SEM, standard error of the mean; shRNA, short hairpin RNA; siRNA, small interfering RNA; TRIP6, thyroid receptor interacting protein 6.

Introduction

Ewing's sarcoma (ES) is an aggressive bone-associated cancer of likely mesenchymal origin mostly affecting children and young adolescents (Mackintosh et al., 2010). Even though multimodal therapy has remarkably improved survival of patients with localised disease, prognosis of patients with metastatic disease still remains poor with an event-free survival of less than 25% (Haeusler et al., 2010; Ladenstein et al., 2010). ES is characterised by the expression of chimeric Ewing sarcoma breakpoint region 1/E-twenty-six (EWS/ETS) fusion proteins derived from chromosomal translocations with Ewing sarcoma breakpoint region 1/friend leukaemia virus integration 1 (EWS/FLI1) being the predominant mutation (85% of cases) (Delattre et al., 1992, 1994). *EWS/FLI1* encodes an oncogenic transcription factor that determines the complex and highly malignant phenotype of ES (May et al., 1993). Despite the great propensity of ES towards early metastasis, recent evidence showed that EWS/FLI1 expression rather reduces cellular adhesion and migration of ES cells (Chaturvedi et al., 2012). These data are consistent with previous reports demonstrating that the important focal adhesion (FA) remodelling protein Zyxin, which has strong pro-adhesive and pro-migratory functions, is constitutively down-regulated in ES (Amsellem et al., 2005). In fact, Zyxin was ascribed to have tumour-suppressor activity in ES as *ZYXIN* gene transfer in EWS/FLI1-transformed fibroblasts (that usually lack clonogenic potential unless being transformed [Alt et al., 2011]) and SK-N-MC ES cells decreased clonogenicity *in vitro* and tumorigenicity *in vivo* (Amsellem et al., 2005). In addition, Zyxin was shown to be up-regulated in ES cells upon antibody-mediated ligation of CD99 (Cerisano et al., 2004), a prominent ES biomarker that inhibits differentiation of ES cells (Rocchi et al., 2010), which was accompanied by increased cell–cell adhesion and subsequent apoptosis (Cerisano et al., 2004).

So far, the Zyxin-family consists of seven homologous and in many aspects functionally redundant proteins named Zyxin, filamin binding LIM protein 1, alias Migfilin (FBLIM1), Wilms tumour 1 interacting protein (WTIP), AJUBA, LIM domains containing 1 (LIMD1), LIM domain containing preferred translocation partner in lipoma (LPP) and thyroid receptor interacting protein 6 (TRIP6) (Ferrand et al., 2009; Grunewald et al., 2009; Willier et al., 2011).

Besides their scaffolding functions at sites of actin-remodelling in FAs and invadopodia, Zyxin proteins are potent signal transducers that shuttle between the cytoplasm and the nucleus mediated by specific import/export mechanisms to link FA signalling to the transcriptional machinery (Nix and Beckerle, 1997; Zheng and Zhao, 2007; Grunewald et al., 2009; Willier et al., 2011; Wang et al., 2012).

By analysing the gene expression patterns of all Zyxin-family members in over 900 microarrays of nine different paediatric cancer entities (including 161 primary ES) and in 353 normal tissues, we identified TRIP6 to be the only Zyxin-family member that is overexpressed in primary ES. The human *TRIP6* gene is located on chromosome 7q22 and encodes a protein of 476 aa (molecular weight 50.3 kDa) (Willier et al., 2011), which is highly conserved across species (86% identity with murine *TRIP6*) (Wang et al., 1999). TRIP6 is ubiquitously expressed in normal tissues with peak expression in thyroid gland and superior cervical ganglion (Willier et al., 2011). The protein is a versatile scaffold at FAs involved in cytoskeletal organisation, coordinated cell migration and tissue invasion (Willier et al., 2011). Via its LIM and TDC domains, TRIP6 interacts with different components of the lysophosphatidic acid, NF- κ B (nuclear factor κ B), glucocorticoid and AMPK (AMP-activated protein kinase) signalling pathways (Xu et al., 2004; Li et al., 2005; Solaz-Fuster et al., 2006). In the nucleus, TRIP6 has transcriptional cofactor activity and regulates the transcriptional responses of these pathways (Kassel et al., 2004; Diefenbacher et al., 2008, 2010; Willier et al., 2011). Moreover, intranuclear TRIP6, but not Zyxin, associates with proteins ensuring telomere protection and hence may play a role in genome stability (Sheppard and Loayza, 2010; Sheppard et al., 2011). Accordingly, TRIP6 is engaged in key cellular processes such as cell migration, invasion, proliferation, differentiation and survival. These diverse functions of TRIP6 are found to be deregulated in various cancers such as nasopharyngeal, ovarian and lung carcinoma as well as glioblastoma (Chastre et al., 2009; Fei et al., 2013; Lin et al., 2013).

Here, we show that – in contrast to Zyxin – TRIP6 expression confers a pro-proliferative and pro-invasive transcriptional signature to ES cells, which is consistent with the observed reduction of migration, invasion, long-term proliferation and clonogenicity upon

Role of TRIP6 in Ewing's sarcoma

TRIP6 knockdown *in vitro* as well as the impaired tumourigenic and metastatic phenotype *in vivo*. Therefore, TRIP6 might represent an attractive candidate for targeted therapy.

Results

TRIP6 is the only Zyxin-family member being highly overexpressed in primary ES compared with normal tissues

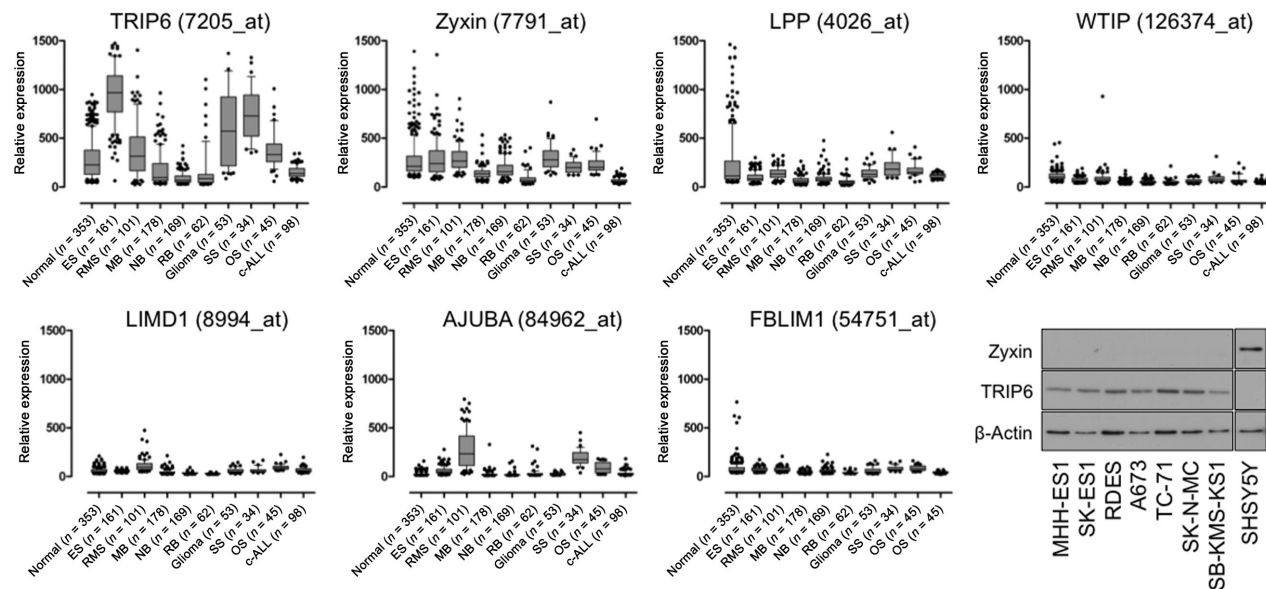
To investigate the gene expression pattern of the seven Zyxin-family members (TRIP6, Zyxin, AJUBA, LIMD1, LPP, WTIP and FBLIM1) publicly available microarray datasets for normal tissues [$n = 353$, GSE3526 (Roth et al., 2006)] were compared with datasets from nine different (mostly) paediatric cancer entities (total $n = 901$) comprising 161 ES (GSE12102, GSE17618 and GSE34620), 101 rhab-

domyosarcomas (E-TABM_1202), 178 medulloblastomas (GSE10327, GSE12992 and GSE37418), 169 neuroblastomas (GSE13136, GSE16237 and GSE16476), 62 retinoblastomas (GSE29683), 53 paediatric gliomas (GSE19578), 34 synovial sarcomas (GSE20196), 45 osteosarcomas (GSE33458, GSE14827) and 98 B-precursor acute lymphoblastic leukaemias (GSE28460). All data were generated on the same microarray platform (Affymetrix HG-U133plus2.0) and normalised simultaneously by Robust Multi-array Average (RMA) using custom brainarray CDF files (v15 ENTREZG).

As displayed in Figure 1, TRIP6 is the only Zyxin-family member being highly overexpressed in primary ES compared with normal tissues. Moreover, TRIP6 expression is considerably high in paediatric gliomas and synovial sarcomas, whereas all other Zyxin-family members, except AJUBA, show low

Figure 1 | TRIP6 is the only Zyxin-family member being highly overexpressed in primary ES compared with normal tissues

Normal, normal tissue; ES, Ewing's sarcoma; RMS, rhabdomyosarcoma; MB, medulloblastoma; NB, neuroblastoma; RB, retinoblastoma; glioma, paediatric glioma; SS, synovial sarcoma; OS, osteosarcoma; c-ALL, paediatric B-precursor acute lymphoblastic leukaemia. All datasets were normalised simultaneously using RMA and custom brainarray (v15 ENTREZG) CDF files. Data are depicted as box-plots. Whiskers indicate the 10th and 90th percentile. Outliers are displayed as dots. The data are presented in linear scale. Brainarray ENTREZG probeset IDs are given in brackets. Lower right: representative WBs of TRIP6 and Zyxin in seven ES cell lines (MHH-ES1, SK-ES1, RDES, A673, TC-71, SK-N-MC and SB-KMS-KS1). The neuroblastoma cell line SHSY5Y served as a positive control for Zyxin expression. In each lane of the gel, an equivalent of 1×10^5 cells was loaded. β -Actin served as a loading control.



basal levels in all analysed cancer entities. AJUBA is overexpressed in rhabdomyosarcoma, synovial sarcoma and to a lesser extent in osteosarcoma (Figure 1). The high expression of TRIP6 and the absence of Zyxin in ES were confirmed on protein level by Western blot (WB) in a panel of seven different ES cell lines (Figure 1, lower right).

To test whether this high overexpression of TRIP6 depends on the presence of the transcription factor EWS/FLI1, we re-analysed a published EWS/FLI1 loss-of-function microarray experiment (GSE14543, Affymetrix HG-U133A (Kauer et al., 2009). As displayed in Supplemental Figure 1A, RNA interference (RNAi)-mediated knockdown of EWS/FLI1 did not considerably and consistently alter the mRNA expression levels of TRIP6 in five different ES cell lines compared with known or likely EWS/FLI1 target genes such as *NKX2.2*, *NPY1R* and *STEAP1* (Smith et al., 2006; Körner et al., 2008; Grunewald et al., 2012a, 2012b). Conversely, re-analysis of a published time-course microarray study showed that EWS/FLI1 overexpression (gain-of-function) fails to induce TRIP6 in human mesenchymal stem cells, the most likely cells of origin of ES [GSE8665, Affymetrix HG-U133A (Miyagawa et al., 2008), Supplemental Figure 1B]. Consistently, no binding of EWS/FLI1 to a conserved ETS motif within the TRIP6 promoter could be detected in chromatin-immunoprecipitation (ChIP) (not shown).

Taken together, these data suggest that TRIP6 is the only Zyxin-related protein exclusively overexpressed in ES in an EWS/FLI1-independent manner.

TRIP6 confers a transcriptional signature related to invasiveness and proliferation

To gain insight in the role of TRIP6 for ES cells, we performed microarray analyses (Affymetrix Human Gene 1.0 ST) 48 h after transfection with two different small interfering RNA (siRNAs) targeting TRIP6 in two different ES cell lines (A673 and SK-N-MC). Knockdown efficacy of the siRNAs was confirmed by quantitative real-time PCR (qRT-PCR) and WB (Figures 2A and 2B).

As illustrated in Figure 2C, TRIP6 knockdown modulates the expression of 170 genes (36 up/134 down, minimum mean \log_2 FC of ± 0.4 , $P < 0.001$) in both cell lines (Supplemental Table 1). Among them, we chose the genes *CD164*, *RDX* and *CRYZ* for validation of the microarray data by qRT-PCR

(Figure 2D). Subsequent gene-set enrichment analysis (GSEA) of the microarray data indicated that TRIP6 expression is associated with the modulation of gene-sets involved in invasiveness (Bidus et al., 2006; Winneppenckx et al., 2006) and proliferation (Chang et al., 2004; Kong et al., 2007) of other cancers and mesenchymal cells, respectively (Figure 2E).

Knockdown of TRIP6 impairs migration and invasiveness of ES cells *in vitro*

To validate the GSEA prediction, we subjected ES cells to migration and invasion assays. Using a transwell-system (modified Boyden chamber), we observed that TRIP6 knockdown significantly reduced cell migration to about 80% of the controls (Figure 3A). Moreover, the cellular invasiveness of ES cells in a Matrigel-covered transwell-system was reduced even more pronounced after TRIP6 knockdown (Figure 3B). These data confirm that TRIP6 overexpression enhances the migratory and invasive properties of ES cells.

Knockdown of TRIP6 reduces long-term proliferation and clonogenicity of ES cells *in vitro* as well as tumourigenicity *in vivo*

Our microarray data predicted that TRIP6 plays a role in proliferation of ES cells. To validate this prediction, we performed RNAi experiments and tested the short- and long-term effects of TRIP6-suppression on ES proliferation. As seen from Figure 4A proliferation of ES cells with transient knockdown of TRIP6 was not considerably affected 48 h–60 h after transfection, as measured by Cell Titer assays. Similarly, short-term knockdown of TRIP6 (<72 h) had no significant impact on rates of apoptosis and cell cycle progression of ES cells as tested with AnnexinV/7AAD- and propidium iodide (PI) staining, respectively (Supplemental Figure 2). However, using xCELLigence, a system that records cell proliferation for a longer period of time, we observed a moderate but significant cell type-dependent decrease of proliferation upon knockdown of TRIP6 after 72 h–100 h (Figure 4B).

To analyse whether the knockdown of TRIP6 impacts the clonogenic properties of ES cells, we generated a Doxycycline-inducible short hairpin RNA (shRNA) expression system in the ES cell line A673 and seeded these cells and the corresponding nonsense-shRNA control cells at low density into

Figure 2 | TRIP6 confers a transcriptional signature related to invasiveness and proliferation

(A) Measurement of knockdown efficacy of TRIP6 siRNAs by qRT-PCR 48 h after transfection. Data are mean and standard error of the mean (SEM) of $n = 5$ experiments. (B) Confirmation of TRIP6 knockdown 48 h after transfection by WB in A673, SK-N-MC and SB-KMS-KS1 ES cells. (C) Heatmap of 170 differentially expressed genes (36 up/134 down, minimum mean \log_2 FC of ± 0.4 , $P < 0.001$) in A673 and SK-N-MC cells 48 h after transfection with siRNA. Arrows mark genes selected for validation. (D) Validation of microarray data by qRT-PCR with the genes *CD164*, *CRYZ* and *RDX*. Data are mean and SEM of $n = 3$ experiments. (E) Enrichment plots of significantly altered gene-sets as yielded by the GSEA of the microarray data (MSigDB, c2 curated gene-sets: chemical and genetic perturbations).

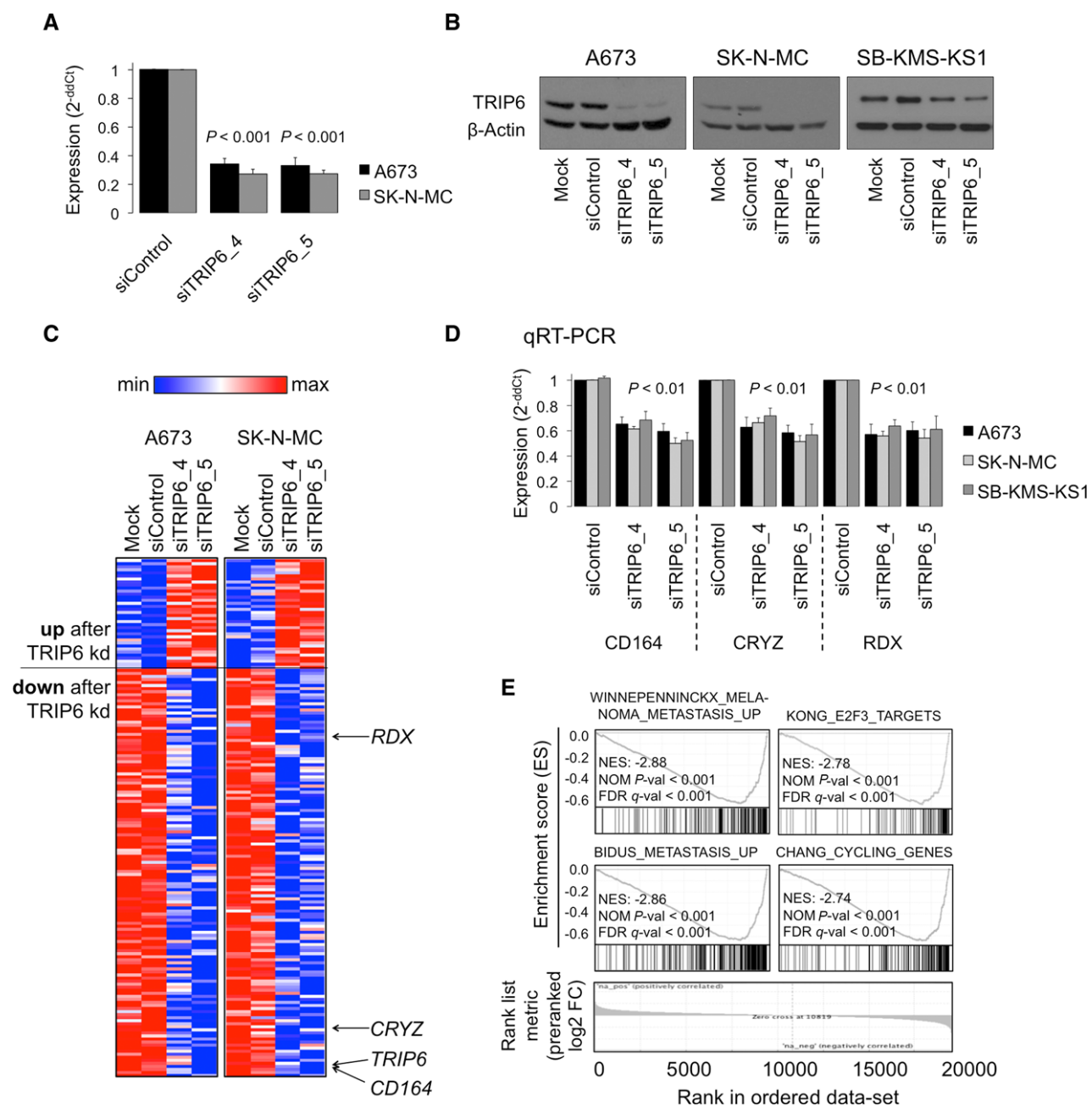
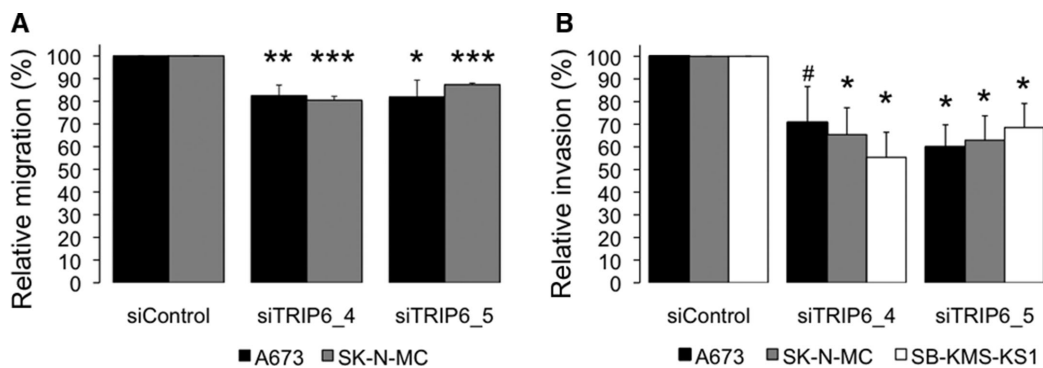


Figure 3 | Knockdown of TRIP6 impairs migration and invasiveness of ES cells *in vitro*

(A) Analysis of cellular migration using a transwell-system (modified Boyden chamber). Data are mean and SEM of at least three experiments. (B) Analysis of cellular invasiveness of ES cells after knockdown of TRIP6 in a Matrigel-covered transwell-system. Data are mean and SEM of $n = 4$ experiments. ${}^{\#}P < 0.08$, ${}^{*}P < 0.05$, ${}^{**}P < 0.01$, ${}^{***}P < 0.001$, *t*-test.



wells of 12-well plates. Upon Doxycycline-mediated knockdown of TRIP6 for 12 days, we observed a significant, more than five-fold decrease of colony numbers and colony size (expressed as clonogenicity index as described in the Materials and Methods section) (Figure 4C). This observation was validated in periodically re-transfected A673, SK-N-MC and SB-KMS-KS1 cells with two different siRNAs against TRIP6 (Figure 4D). The data suggest a TRIP6 concentration-dependent reduction of clonogenicity in these cells (Figure 4D).

Consistently, the tumourigenic potential of xenotransplanted A673 cells bearing a Doxycycline-induced TRIP6 knockdown, was significantly decreased *in vivo* without changing the rates of necrosis (as evidenced by serial sectioning of the xenografts and calculation of the ratios of necrotic versus total tumour area in haematoxylin and eosin (HE) staining Figures 4E and 4F). The persistence of the TRIP6 knockdown was confirmed by qRT-PCR in each xenograft *ex vivo* (Figure 4G). In addition, TRIP6 knockdown was associated with a considerable reduction in average size of liver metastases (equates *in vivo* colonies) after injection of A673 in the tail vein of immunocompromised mice (see arrows in Figure 4H).

Taken together, these data suggest that long-term knockdown of TRIP6 decreases proliferation, clonogenicity and tumourigenicity of ES cells.

Discussion

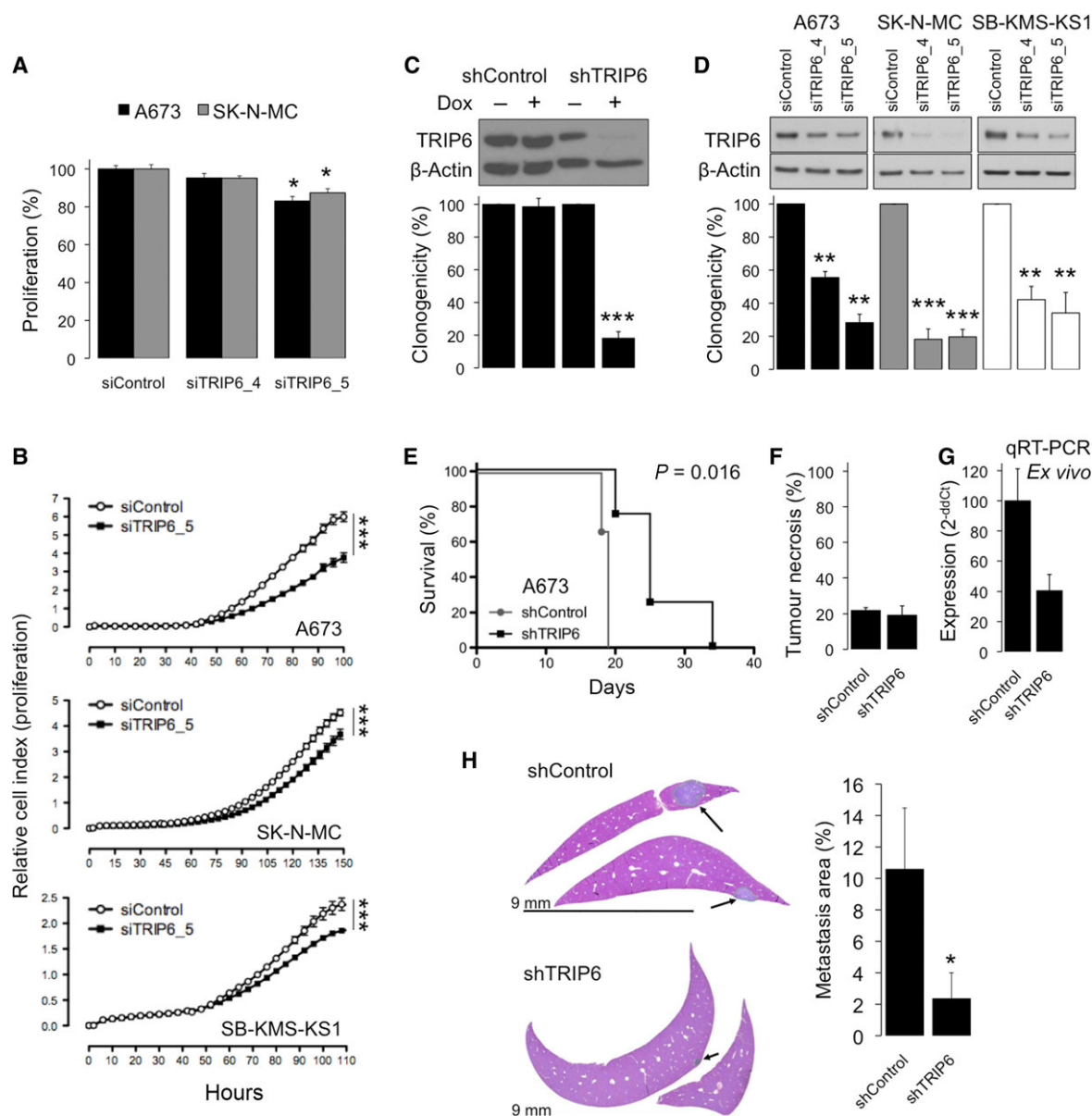
This study aimed to explore the relevance of TRIP6 for ES pathology. We showed that among all seven Zyxin-family proteins only TRIP6 is overexpressed in ES compared with normal tissues and that its expression appears to be independent of EWS/FLI1, the predominant oncogenic driver in ES (Kovar, 2010). Moreover, we demonstrate that TRIP6 expression confers a more aggressive phenotype to ES cells resulting in enhanced migration and invasion as well as accelerated proliferation and clonogenicity.

The role of Zyxin-family proteins in ES, especially of Zyxin itself, has been investigated previously in two independent studies (Cerisano et al., 2004; Amsellem et al., 2005). There, the absence of Zyxin correlated with enhanced cellular survival as well as inhibition of ES differentiation, and the authors concluded that Zyxin may act as a tumour suppressor in ES (Cerisano et al., 2004; Amsellem et al., 2005). In contrast, we now demonstrate that this conclusion might not hold true for all Zyxin-family proteins, as the Zyxin-related protein TRIP6 has rather oncogenic potential in this tumour entity.

This observation is consistent with recent data showing that TRIP6 can promote tumourigenesis in nasopharyngeal cancer cells upon binding and inactivation of p27 Kip1 – a tumour suppressor and inhibitor of cyclin-dependent kinase 2 (CDK2) – which ultimately stimulates cell

Figure 4 | Knockdown of TRIP6 reduces long-term proliferation and clonogenicity of ES cells *in vitro* as well as tumourigenicity *in vivo*

(A) Analysis of short-term proliferation using a Cell Titer assay (read-out at max. 60 h after transfection with siRNA as indicated). Data are mean and SEM of at least three experiments. (B) Results of long-term proliferation assays using the xCELLigence system (transfection of cells at 0 and 48 h). (C) Analysis of clonogenicity in A673 cells, stably transfected with Doxycycline-inducible shRNA expression system as indicated. Data are mean and SEM of $n = 3$ experiments. WB images show representative knockdown of TRIP6 after treatment of cells with Doxycycline at the experimental endpoint. (D) Validation of clonogenicity assay in three ES cell lines using transient (re)-transfection with two different siRNAs against TRIP6 as indicated. Data are mean and SEM of $n = 3$ experiments. Knockdown of TRIP6 was confirmed by WB on day 12. (E) Analysis of tumourigenicity of A673 shRNA infectants in $\text{Rag2}^{-/-}\text{yc}^{-/-}$ mice (3 shControl, 4 shTRIP6). Log-rank test. (F) Analysis of necrotic area per total tumour area by HE staining of formalin-fixed paraffin-embedded xenografts. (G) Confirmation of TRIP6 knockdown by qRT-PCR *ex vivo*. (H) Analysis of metastatic potential (four mice/group) by quantification of the average size of liver metastases (equals *in vivo* colonies) per total organ area. * $P < 0.05$, ** $P < 0.01$, *** $P < 0.001$, *t*-test.



proliferation (Lin et al., 2013). Our transcriptomic profiling and GSEA further support that TRIP6 expression is accompanied by a gene expression signature related to proliferation (Figure 2E). For instance, the gene-sets KONG_E2F3_TARGETS and CHANG_CYCLING_GENES were derived from two studies describing the pro-proliferative effect of these genes in mesenchymal cells (murine embryonic fibroblasts and human fibroblasts, respectively) (Chang et al., 2004; Kong et al., 2007). Moreover, we noted a down-regulation of the transcripts encoding Cyclin A1 (CCNA1), cyclin-dependent kinase 1 (CDK1) and their target E2F8 (Supplemental Table 1), all of which coordinate progression of the cell cycle (Lammens et al., 2009; Malumbres and Barbacid, 2009; Marlow et al., 2012).

These data suggest that in ES cells TRIP6 is, at least in part, involved in cell cycle regulatory processes. However, these effects are visible only after prolonged knockdown of TRIP6 since 48 h after siRNA transfection our cell cycle analyses did not result in considerable changes of the cell cycle phases (Supplemental Figure 2B), whereas long-term suppression of TRIP6 significantly reduced cell proliferation and, more pronounced, clonogenicity of ES cells (Figure 4). In this context, it is interesting to note that upon TRIP6 knockdown the spindle and kinetochore complex subunits 1 and 2 (SKA1/2) are down-regulated in ES cells (as seen by our microarray analysis, Supplemental Table 1). SKA1 and -2 are important players required for accurate cell division by establishing stable kinetochore–microtubule interactions (Jeyaprakash et al., 2012).

Consistent with results drawn from other cancer models (for review see Willier et al., 2011), we observed that TRIP6 expression enhances the migratory and invasive properties of ES cells. Recent evidence demonstrated that EWS/FLI1 suppression surprisingly reduces cell motility, which is unexpected as ES is a highly metastatic and aggressive tumour (Chaturvedi et al., 2012). This observation suggests that target genes of the transcription factor EWS/FLI1 in their overall function rather inhibit than stimulate cell motility (Chaturvedi et al., 2012). Hence, it is tempting to speculate that ES cells need to express genes in an EWS/FLI1-independent manner to maintain their basal migratory properties despite the expression of EWS/FLI1. In line with this hypothesis, our data indicate that TRIP6 might

be one representative of this group of pro-migratory and pro-invasive, EWS/FLI1-independent genes that are overexpressed in ES (EIOGES). Up-regulation of EIOGES may be due to the developmental stage of the cells in which the EWS/FLI1 translocation may occur (pre-translocational EIOGES). Alternatively, up-regulation of EIOGES may be caused by a selective advantage conferred by EIOGES in addition to the EWS/FLI1 translocation (post-translocational EIOGES). However, it remains to be determined why only TRIP6 is overexpressed in ES while all other Zyxin-family members are down-regulated – an effect possibly mediated by specific patterns of DNA-methylation and/or histone-modifications as well as expression of specific miRNAs (Brandl et al., 2009; Verrier et al., 2011; Bullock et al., 2012; Cock-Rada and Weitzman, 2013).

In summary, we show that TRIP6 expression confers a pro-proliferative and pro-invasive phenotype to ES cells, which suggests, that TRIP6, in contrast to Zyxin, acts as an oncogene in ES. TRIP6 might therefore represent an attractive candidate for targeted therapy.

Materials and methods

Cell lines and culture conditions

The A673 cell line was purchased from ATCC. The SB-KMS-KS1 cell line is an ES cell line with an EWS/FLI1 type 1 translocation, which was established and extensively functionally characterised in our laboratory (Richter et al., 2009, 2013; Grunewald et al., 2012a; Miller et al., 2013). All other cell lines were obtained from the German Collection of Microorganisms and Cell Culture (DSMZ). Cells were grown at 37°C in 5% CO₂ in a humidified atmosphere in RPMI 1640 medium (Invitrogen) containing 10% foetal bovine serum (FBS) (Invitrogen), 1% L-glutamine and 100 µg/ml gentamicin (both Invitrogen). Cell lines were checked routinely for presence of EWS/ETS translocation, surface antigen and/or HLA phenotype by PCR or flow cytometry, respectively. Mycoplasma contamination was ruled out with the MycoAlertTM Mycoplasma Detection Kit according to the manufacturer's instructions (Lonza).

RNAi with siRNA and generation of shRNA infectants

For transient protein knockdown, cells were transfected with siRNA using the HiPerFect transfection reagent (Qiagen) according to standard procedures for large-scale transfection in 100 mm dishes. 2 × 10⁶ cells were plated into 100 mm culture dishes at a final volume of 12 ml medium containing 5 nM siRNA and 36 µl transfection reagent and incubated at least 48 h. Concentration of media and reagents were adapted accordingly for transfection in smaller volumes. Knockdown efficacy was assessed by qRT-PCR and/or WB. Sequences of siRNAs used (all

Qiagen): siTRIP6-4 5'-GGCUGCUUUGUAUGUUUCUATT-3' (sense) and 5'-UAGAACAUACAAAGCAGCCCA-3' (antisense), siTRIP6-5 5'-GGAGGAGACUGUGAGAAUUTT-3' (sense) and 5'-AAUUCUCACAGUCUCCUCCTG-3' (antisense). The validated non-silencing Qiagen AllStars Negative Control siRNA was used as a control (siControl).

For generation of an inducible TRIP6 knockdown, A673 ES cells were infected with lentivirus (MOI: 1:10) containing a pTRIPZ vector with either a shRNA against TRIP6 (clone V3THS_315580, mature antisense sequence 5'-TCTCCGAGCCACCACACT-3'; Thermo Scientific) or respective non-targeting control shRNA. Single-cell cloned A673 infectants were selected in 0.5 µg/ml Puromycin (Invitrogen). Knockdown efficacy upon Doxycycline-treatment (0.5 µg/ml) was confirmed by WB.

Lentivirus production

5.5×10^6 HEK293T cells were seeded into a 100 mm cell culture dish one day before transfection and cultured in DMEM (Invitrogen) supplemented with 10% FBS, 100 units/ml penicillin and 100 µg/ml streptomycin (both Invitrogen). Arrest-In™ (Thermo Scientific) was used as transfection reagent. DNA/Arrest-In™ complexes were formed by mixing 9 µg of the particular pTRIPZ vector DNA, with 28.5 µg of optimised packaging plasmid mix (pTLA1-Pak, pTLA1-Enz, pTLA1-Env, pTLA1-Rev and pTLA1-TOFF; all Open Biosystems, Thermo Scientific). Supernatant was harvested 48 h after transfection and lentiviral particles were isolated by filtration and subsequent ultracentrifugation.

RNA extraction and reverse transcription

RNA extraction was performed with the RNeasy Mini Kit (Qiagen) according to the manufacturer's instructions. Isolated RNA was reversely transcribed using the High-Capacity cDNA Reverse Transcription Kit (Applied Biosystems) under these thermal conditions: 10 min at 25°C, 120 min at 37°C, 5 min at 85°C and terminal hold at 4°C.

Quantitative real-time polymerase chain reaction

qRT-PCR was performed by use of Maxima™ Probe/ROX qPCR Master Mix (2×) containing Hot Start Taq Polymerase, PCR buffer and dNTPs. Gene-specific expression assays were obtained from Applied Biosystems, which consisted of a FAM™ dye-labelled TaqMan® MGB probe and two unlabelled PCR primers (B2M Hs00984230_m1, CD164 Hs00174789_m1, CRYZ Hs01086229_m1, RDX Hs00988414_g1, TRIP6 Hs00377979_m1). qRT-PCRs were carried out in 96-well format in duplicate measurements. The final concentration of primers and probe were 900 and 250 nM, respectively. Fluorescence was measured with an AB 7300 Real-Time PCR System (Applied Biosystems). Gene expression values were normalised to that of the housekeeping gene *beta-2-microglobulin* (B2M) using the $\Delta\Delta Ct$ -method.

Microarray analyses

A673 and SK-N-MC cells were transfected with siRNA and cultivated for 48 h. Thereafter, RNA was extracted and RNA quality was checked using a Bioanalyzer (Agilent). Total RNA (200 ng) was amplified and labelled using Affymetrix GeneChip Whole Transcript Sense Target Labeling Kit. cRNA

was hybridised to Affymetrix Human Gene 1.0 ST arrays as described previously (Miller et al., 2013). Quality assessment consisted of RNA degradation plots, Affymetrix control metrics, sample cross-correlation and probe-level visualisations. Normalisation incorporated (separately for each RNA type dataset) background correction, quantile normalisation and probe-level summation by RMA (Irizarry et al., 2003). Data were normalised using custom brainarray CDF files (v15 ENTREZG) (Dai et al., 2005), analysed with the GENE-E software (<http://www.broadinstitute.org/cancer/software/GENE-E/>) and deposited at the Gene Expression Omnibus (GEO; GSE48010). GSEA was performed with the GSEA tool (<http://www.broad.mit.edu/gsea>) using a pre-ranked list and 1000 permutations. For the interrogation of publicly available microarray data, datasets were retrieved from the GEO and the Array Express platform of the EBI (<http://www.ebi.ac.uk/arrayexpress/>), manually checked for their correct annotations and simultaneously RMA-normalised using brainarray custom CDF files (v15 ENTREZG) as previously described (Willier et al., 2013). Individual data accession numbers are given in the results section.

Western blot

Cells were lysed in Laemmli-buffer containing 10% β -mercaptoethanol (Sigma-Aldrich). Equal amounts of cells were resolved by 10% SDS-PAGE. After blotting on a nitrocellulose membrane (Schleicher&Schuell), the membrane was blocked with 3% non-fat dry milk (Biorad) in TBS-T buffer [10 mM Tris, 150 mM NaCl, 0.1% (w/v) Tween, pH 7.5]. Then the membrane was incubated with the primary antibodies anti-TRIP6 (4B7 by Sigma-Aldrich, diluted 1:250) and anti-beta-Actin (SC-1616-R by Santa Cruz, diluted 1:2000), respectively. Finally, the membrane was washed with TBS-T and incubated with the secondary antibodies goat-anti-mouse and goat-anti-rabbit both horseradish peroxidase-coupled and diluted 1:5000 (both Biorad). The amount of detected protein was visualised by enhanced chemiluminescence (Amersham Biosciences) and autoradiography.

Chromatin-immunoprecipitation

The TRIP6 promoter contains one conserved ETS binding site –2281 bp upstream of the transcriptional start site (TSS). For ChIP, ES cells were fixed in 1% formaldehyde for 10 min. After neutralisation with glycine, nuclei were isolated using hypotonic lysis buffer (20 mM Tris-Cl pH 8, 185 mM KCl, 0.5% NP-40). The nuclear fraction was lysed in RIPA-buffer (50 mM Tris-Cl pH 7.4, 150 mM NaCl, 0.1% SDS, 0.5% Na-deoxycholate, 1% NP-40) supplemented with a protease inhibitor mix (Roche). Samples were sonicated to an average DNA length of 500 bp as estimated by gel-electrophoresis. ChIP was carried out with 3 µg of the following antibodies: anti-FLI1 (C19) and normal rabbit IgG (both Santa Cruz). Each ChIP was performed with 13 µg total DNA. qRT-PCR was performed using Power SYBR Green PCR Master Mix (Applied Biosystems). All ChIPs were normalised to IgG-IPs and to non-specific binding to an unrelated genomic region (–2845 bp away from the TSS of TRIP6). Primer sequences: –2281: forward 5'-GAGTGGACAGCATCCTCCTC-3', reverse 5'-CCACACACTGACAGCAAGGT-3'; –2845:

forward 5'-GGCTGATCTGAACCTCCAA-3', reverse 5'-AGACGCAGAGACCTCTTCCA-3'.

Proliferation assays

CellTiter 96® AQueous Non-Radioactive Cell Proliferation Assay (Promega): Cells were transfected with siRNA and subsequently seeded in 48-well plates. Per well 1.5×10^4 A673 or 3×10^4 SK-N-MC cells were seeded. After 48–60 h, cells were treated according to the manufacturer's protocol and absorbance was measured at 490 nm with an ELISA reader.

xCELLigence (Roche/ACEA Biosciences): Cell numbers were counted in real-time with a bioelectric xCELLigence instrument monitoring impedance across gold microelectrodes on the bottom of E-plates. Immediately after transfection with siRNA, 1.6×10^4 cells were seeded in 200 μ l medium containing 10% FBS and transfection reagents in 96-wells of E-plates. Cellular impedance was measured periodically every 4 h thereafter. Medium was changed and cells were re-transfected with siRNA after 48 h to maintain knockdown of TRIP6.

Analysis of migration and invasion

Cellular migration was assessed by a modified Boyden chamber assay (transwell chambers, Corning Star). Cells were serum-starved overnight, trypsinised, adjusted for viability, counted and re-suspended in serum-free medium to a concentration of 1×10^6 cells/ml. Before the experiment, the lower surface of the filter membrane (8 μ M pore size) was coated for 15 min with 100 μ l fibronectin solution (5 μ g/ml; Sigma–Aldrich) as a chemo-attractant. The inner filter chambers were coated with 100 μ l 10% FBS in RPMI medium for 30 min. Hundred microliters of cell suspension was placed in the upper filter chambers. The chambers were placed in 24-well plates and cultured in 500 μ l RPMI medium with 10% FBS for 4 h at 37°C to allow the cells to migrate through the porous membrane. Non-migrated cells from the top surface were removed using a cotton swab. Migrated cells at the lower surface of the membranes were stained in 200 μ l 1% (w/v) crystal violet in 2% ethanol in a 24-well plate for 30 s and rinsed twice afterwards in distilled water. Cell-associated crystal violet was extracted by incubating the membrane in 200 μ l 10% acetic acid for 20 min and measured at 595 nm absorbance using a plate reader. For analysis of cellular invasiveness, 5×10^4 transiently transfected cells were seeded in 500 μ l serum-free medium into the upper chambers of Matrigel-covered transwell plates (Becton Dickinson). Bottom chambers contained 500 μ l medium with 10% FBS. After 48 h, invaded cells were stained with 4 μ g/ml Calcein AM (Merck) in HBSS and photographed with an AxioCam MRM camera attached on an Axiovert 100 microscope (both Zeiss). The number of invaded cells was normalised to proliferation as assessed with xCELLigence (Roche/ACEA Biosciences).

Analysis of cell cycle and apoptosis by flow cytometry

Cell cycle phases of ES cells were analysed using PI (Sigma–Aldrich) as previously described (Grunewald et al., 2012a). 2×10^6 cells were harvested 48 h after transfection with siRNA by trypsinisation. Cells were washed twice with sample buffer (PBS with 0.5% FBS), fixed in 70% ethanol at 4°C and subsequently stained by resuspension in 300 μ l PI staining solution for 45 min in the dark before flow cytometry analysis. The annexin-V-PE/7-AAD apoptosis detection kit 1 (Becton

Dickinson) was used according to the manufacturer's protocol to assess apoptosis and necrosis 72 h after transfection with siRNA. Samples were analysed on a FACScalibur flow cytometer using Cellquest software (both Becton Dickinson).

Clonogenicity assays

Clonogenic assays were essentially performed as described (Franken et al., 2006). A673 shRNA infectants harbouring either an inducible non-silencing shRNA construct or an inducible TRIP6-silencing construct were seeded at 1×10^3 cells/well in 12-well plates and treated with 0.5 μ g/ml Doxycycline or vehicle. To assess clonogenicity after transient transfection with siRNA, cells were transiently transfected before seeding in 12-well plates (1×10^3 /well for A673, 2×10^3 /well for SK-N-MC and SB-KMS-KS1) and re-transfected on days 3, 6 and 9 to maintain the TRIP6 knockdown throughout the assay period. Knockdown efficacy was controlled at day 12 by WB. Colonies were methanol-fixed and stained with crystal violet. Colony number and area were quantified on scanned plates with the Image-J software (NIH). Relative clonogenicity is depicted as 'clonogenicity index', which is the product of the colony number and average colony size.

Histology

Formalin-fixed tumour and organ samples were processed and embedded in paraffin. For histology, 4 μ m sections were cut from paraffin blocks and stained with HE as a standardised staining for analysis of percentage of tumour necrosis. After scanning of the slides with a NanoZoomer-XR C12000 (Hamamatsu), the areas of organs and metastases were measured manually using the program NDP.view (Hamamatsu).

Mice and *in vivo* experiments

Immunodeficient $\text{Rag}^{2-/-} \gamma_c^{-/-}$ mice on a BALB/c background were obtained from the Central Institute for Experimental Animals (Kawasaki) and maintained under pathogen-free conditions in accordance with the German Animal Protection Law, institutional guidelines and approval by the Regierung von Oberbayern. Experiments were performed in 6–16 week-old mice. For *in vivo* tumour growth 2×10^6 ES cells in 200 μ l PBS were subcutaneously injected in groins. Once tumours were palpable, 1 mg/ml Doxycycline (Sigma–Aldrich) was added to the drinking water. Mice bearing tumours greater than 10 mm in diameter (determined with a caliper) were considered positive and sacrificed. Xenografts were excised and formalin-fixed for histology after removal of a small fraction for RNA extraction. To analyse metastatic potential, 2×10^6 cells were injected in the tail veins of male $\text{Rag}^{2-/-} \gamma_c^{-/-}$ mice, which received Doxycycline-containing drinking water throughout the time of the experiment. Five weeks after intravenous injection, mice were euthanised and metastasis was monitored in individual organs by HE staining. Metastases were counted by serial sectioning of individual organs and ratios of metastasis area over total organ area were calculated.

Statistical analyses

Differences in proportions between groups were evaluated by independent one-sample *t*-test, two-tailed Student's *t*-test or log-rank test as indicated. Statistical significance level was set at $P < 0.05$.

Author contribution

S.W., E.B. and T.G.P.G. designed the study, drafted and wrote the paper and designed the display items. S.W., R.U., E.B. and T.G.P.G. performed the experiments. D.J. and F.N. performed histological analyses. C.R. generated the shRNA infectants. U.D., G.H.S.R., F.N., S.B. and E.B. provided laboratory infrastructure. S.W., O.P.d.C., T.B. and T.G.P.G. carried out bioinformatic analyses.

Funding

This work was supported by grants from the Deutsche Forschungsgemeinschaft (DFG GR3728/1-1 to T.G.P.G., G.H.S.R. and S.B.; GR3728/2-1 to T.G.P.G.; SFB-TR22 to T.B.; and BU740/6-2 to E.B.) and the 'Dr. Sepp und Hanne Sturm Gedächtnissiftung' of the Ministry of Health of the City of Munich (to T.G.P.G., G.H.S.R. and S.B.), furthermore by grants from the Wilhelm-Sander-Stiftung (2009.901.2 to G.H.S.R. and S.B.), the Deutsche Krebshilfe DKH-108128 (to U.D.) and by the Federal Ministry of Education and Research of Germany (BMBF, TranSaRNet 01GM0869 to U.D., R.U., G.H.S.R. and S.B.; ENCCA EU-FP7; ERA-Net PROVABES to U.D., G.H.S.R. and S.B.).

Acknowledgement

We thank Mrs. Petra Thalheimer for excellent technical assistance.

Conflict of interest statement

The authors have declared no conflict of interest.

References

Alt, E., Yan, Y., Gehmert, S., Song, Y.-H., Altman, A., Gehmert, S., Vykoukal, D. and Bai, X. (2011) Fibroblasts share mesenchymal phenotypes with stem cells, but lack their differentiation and colony-forming potential. *Biol. Cell* **103**, 197–208

Amsellem, V., Kryszke, M.-H., Hervy, M., Subra, F., Athman, R., Leh, H., Brachet-Ducos, C. and Auclair, C. (2005) The actin cytoskeleton-associated protein zyxin acts as a tumor suppressor in Ewing tumor cells. *Exp. Cell Res.* **304**, 443–456

Bidus, M.A., Risinger, J.I., Chandramouli, G.V.R., Dainty, L.A., Litzi, T.J., Berchuck, A., Barrett, J.C. and Maxwell, G.L. (2006) Prediction of lymph node metastasis in patients with endometrioid endometrial cancer using expression microarray. *Clin. Cancer Res.* **12**, 83–88

Brandl, A., Heinzel, T. and Krämer, O.H. (2009) Histone deacetylases: salesmen and customers in the post-translational modification market. *Biol. Cell* **101**, 193–205

Bullock, M.D., Sayan, A.E., Packham, G.K. and Mirnezami, A.H. (2012) MicroRNAs: critical regulators of epithelial to mesenchymal (EMT) and mesenchymal to epithelial transition (MET) in cancer progression. *Biol. Cell* **104**, 3–12

Cerisano, V., Aalto, Y., Perdichizzi, S., Bernard, G., Manara, M.C., Benini, S., Cenacchi, G., Preda, P., Lattanzi, G., Nagy, B., Knuutila, S., Colombo, M.P., Bernard, A., Picci, P. and Scotlandi, K. (2004) Molecular mechanisms of CD99-induced caspase-independent cell death and cell-cell adhesion in Ewing's sarcoma cells: actin and zyxin as key intracellular mediators. *Oncogene* **23**, 5664–5674

Chang, H.Y., Sneddon, J.B., Alizadeh, A.A., Sood, R., West, R.B., Montgomery, K., Chi, J.-T., van de Rijn, M., Botstein, D. and Brown, P.O. (2004) Gene expression signature of fibroblast serum response predicts human cancer progression: similarities between tumors and wounds. *PLoS Biol.* **2**, E7

Chastre, E., Abdessamad, M., Kruglov, A., Bruyneel, E., Bracke, M., Di Gioia, Y., Beckerle, M.C., van Roy, F. and Kotelevets, L. (2009) TRIP6, a novel molecular partner of the MAGI-1 scaffolding molecule, promotes invasiveness. *FASEB J.* **23**, 916–928

Chaturvedi, A., Hoffman, L.M., Welm, A.L., Lessnick, S.L. and Beckerle, M.C. (2012) The EWS/FLI oncogene drives changes in cellular morphology, adhesion, and migration in ewing sarcoma. *Genes Cancer* **3**, 102–116

Cock-Rada, A. and Weitzman, J.B. (2013) The methylation landscape of tumour metastasis. *Biol. Cell* **105**, 73–90

Dai, M., Wang, P., Boyd, A.D., Kostov, G., Athey, B., Jones, E.G., Bunney, W.E., Myers, R.M., Speed, T.P., Akil, H., Watson, S.J. and Meng, F. (2005) Evolving gene/transcript definitions significantly alter the interpretation of GeneChip data. *Nucleic Acids Res.* **33**, e175

Delattre, O., Zucman, J., Plougastel, B., Desmaze, C., Melot, T., Peter, M., Kovar, H., Joubert, I., de Jong, P. and Rouleau, G. (1992) Gene fusion with an ETS DNA-binding domain caused by chromosome translocation in human tumours. *Nature* **359**, 162–165

Delattre, O., Zucman, J., Melot, T., Garau, X.S., Zucker, J.M., Lenoir, G.M., Ambros, P.F., Sheer, D., Turc-Carel, C. and Triche, T.J. (1994) The Ewing family of tumors – a subgroup of small-round-cell tumors defined by specific chimeric transcripts. *N. Engl. J. Med.* **331**, 294–299

Diefenbacher, M., Sekula, S., Heilbock, C., Maier, J.V., Litfin, M., van Dam, H., Castellazzi, M., Herrlich, P. and Kassel, O. (2008) Restriction to Fos family members of Trip6-dependent coactivation and glucocorticoid receptor-dependent trans-repression of activator protein-1. *Mol. Endocrinol.* **22**, 1767–1780

Diefenbacher, M.E., Litfin, M., Herrlich, P. and Kassel, O. (2010) The nuclear isoform of the LIM domain protein Trip6 integrates activating and repressing signals at the promoter-bound glucocorticoid receptor. *Mol. Cell. Endocrinol.* **320**, 58–66

Fei, J., Li, J., Shen, S. and Zhou, W. (2013) Characterization of TRIP6-dependent nasopharyngeal cancer cell migration. *Tumour Biol.* **34**, 2329–2335

Ferrand, A., Chevrier, V., Chauvin, J.-P. and Birnbaum, D. (2009) Ajuba: a new microtubule-associated protein that interacts with BUBR1 and Aurora B at kinetochores in metaphase. *Biol. Cell* **101**, 221–240

Franken, N.A.P., Rodermond, H.M., Stap, J., Haveman, J. and van Bree, C. (2006) Clonogenic assay of cells in vitro. *Nat. Protoc.* **1**, 2315–2319

Grunewald, T.G., Pasedag, S.M. and Butt, E. (2009) Cell adhesion and transcriptional activity – defining the role of the novel protooncogene LPP. *Transl. Oncol.* **2**, 107–116

Grunewald, T.G.P., Diebold, I., Esposito, I., Plehm, S., Hauer, K., Thiel, U., da Silva-Buttkus, P., Neff, F., Unland, R., Müller-Tidow, C., Zobylwalski, C., Lohrig, K., Lewandrowski, U., Sickmann, A., da Costa, O.P., Görlach, A., Cossarizza, A., Butt, E., Richter, G.H.S.

and Burdach, S. (2012a) STEAP1 is associated with the invasive and oxidative stress phenotype of Ewing tumors. *Mol. Cancer Res.* **10**, 52–65

Grunewald, T.G.P., Bach, H., Cossarizza, A. and Matsumoto, I. (2012b) The STEAP protein family: versatile oxidoreductases and targets for cancer immunotherapy with overlapping and distinct cellular functions. *Biol. Cell* **104**, 641–657

Haeusler, J., Ranft, A., Boelling, T., Gosheger, G., Braun-Munzinger, G., Vieth, V., Burdach, S., van den Berg, H., Juergens, H. and Dirksen, U. (2010) The value of local treatment in patients with primary, disseminated, multifocal Ewing sarcoma (PDMES). *Cancer* **116**, 443–450

Irizarry, R.A., Hobbs, B., Collin, F., Beazer-Barclay, Y.D., Antonellis, K.J., Scherf, U. and Speed, T.P. (2003) Exploration, normalization, and summaries of high density oligonucleotide array probe level data. *Biostat. Oxf. Engl.* **4**, 249–264

Jeyaprakash, A.A., Santamaria, A., Jayachandran, U., Chan, Y.W., Benda, C., Nigg, E.A. and Conti, E. (2012) Structural and functional organization of the Ska complex, a key component of the kinetochore-microtubule interface. *Mol. Cell* **46**, 274–286

Kassel, O., Schneider, S., Heilbock, C., Litfin, M., Göttlicher, M. and Herrlich, P. (2004) A nuclear isoform of the focal adhesion LIM-domain protein Trip6 integrates activating and repressing signals at AP-1- and NF- κ B-regulated promoters. *Genes Dev.* **18**, 2518–2528

Kauer, M., Ban, J., Kofler, R., Walker, B., Davis, S., Meltzer, P. and Kovar, H. (2009) A molecular function map of Ewing's sarcoma. *PLoS ONE* **4**, e5415

Kong, L.-J., Chang, J.T., Bild, A.H. and Nevins, J.R. (2007) Compensation and specificity of function within the E2F family. *Oncogene* **26**, 321–327

Körner, M., Waser, B. and Reubi, J.C. (2008) High expression of neuropeptide Y1 receptors in ewing sarcoma tumors. *Clin. Cancer Res.* **14**, 5043–5049

Kovar, H. (2010) Downstream EWS/FLI1 – upstream Ewing's sarcoma. *Genome Med.* **2**, 8

Ladenstein, R., Pötschger, U., Le Deley, M.C., Whelan, J., Paulussen, M., Oberlin, O., van den Berg, H., Dirksen, U., Hjorth, L., Michon, J., Lewis, I., Craft, A. and Jürgens, H. (2010) Primary disseminated multifocal Ewing sarcoma: results of the Euro-EWING 99 trial. *J. Clin. Oncol.* **28**, 3284–3291

Lammens, T., Li, J., Leone, G. and De Veylder, L. (2009) Atypical E2Fs: new players in the E2F transcription factor family. *Trends Cell Biol.* **19**, 111–118

Li, L., Bin, L.-H., Li, F., Liu, Y., Chen, D., Zhai, Z. and Shu, H.-B. (2005) TRIP6 is a RIP2-associated common signaling component of multiple NF- κ B activation pathways. *J. Cell Sci.* **118**, 555–563

Lin, V.T.G., Lin, V.Y., Lai, Y.-J., Chen, C.-S., Liu, K., Lin, W.-C. and Lin, F.-T. (2013) TRIP6 regulates p27 KIP1 to promote tumorigenesis. *Mol. Cell. Biol.* **33**, 1394–1409

Mackintosh, C., Madoz-Gúrpide, J., Ordóñez, J.L., Osuna, D. and Herrero-Martín, D. (2010) The molecular pathogenesis of Ewing's sarcoma. *Cancer Biol. Ther.* **9**, 655–667

Malumbres, M. and Barbacid, M. (2009) Cell cycle, CDKs and cancer: a changing paradigm. *Nat. Rev. Cancer* **9**, 153–166

Marlow, L.A., von Roemeling, C.A., Cooper, S.J., Zhang, Y., Rohl, S.D., Arora, S., Gonzales, I.M., Azorsa, D.O., Reddi, H.V., Tun, H.W., Döppler, H.R., Storz, P., Smallridge, R.C. and Copland, J.A. (2012) Foxo3a drives proliferation in anaplastic thyroid carcinoma through transcriptional regulation of cyclin A1: a paradigm shift that impacts current therapeutic strategies. *J. Cell Sci.* **125**, 4253–4263

May, W.A., Gishizky, M.L., Lessnick, S.L., Lunsford, L.B., Lewis, B.C., Delattre, O., Zucman, J., Thomas, G. and Denny, C.T. (1993) Ewing sarcoma 11;22 translocation produces a chimeric transcription factor that requires the DNA-binding domain encoded by FLI1 for transformation. *Proc. Natl. Acad. Sci. U.S.A.* **90**, 5752–5756

Miller, I.V., Raposo, G., Welsch, U., da Costa, O.P., Thiel, U., Lebar, M., Maurer, M., Bender, H.-U., von Luettichau, I., Richter, G.H.S., Burdach, S. and Grunewald, T.G.P. (2013) First identification of Ewing's sarcoma-derived extracellular vesicles and exploration of their biological and potential diagnostic implications. *Biol. Cell* **105**, 1–15

Miyagawa, Y., Okita, H., Nakajima, H., Horiuchi, Y., Sato, B., Taguchi, T., Toyoda, M., Katagiri, Y.U., Fujimoto, J., Hata, J.-I., Umezawa, A. and Kiyokawa, N. (2008) Inducible expression of chimeric EWS/ETS proteins confers Ewing's family tumor-like phenotypes to human mesenchymal progenitor cells. *Mol. Cell. Biol.* **28**, 2125–2137

Nix, D.A. and Beckerle, M.C. (1997) Nuclear-cytoplasmic shuttling of the focal contact protein, zyxin: a potential mechanism for communication between sites of cell adhesion and the nucleus. *J. Cell Biol.* **138**, 1139–1147

Richter, G.H.S., Plehm, S., Fasan, A., Rössler, S., Unland, R., Bennani-Baiti, I.M., Hotfilder, M., Löwel, D., von Luettichau, I., Mossbrugger, I., Quintanilla-Martinez, L., Kovar, H., Staegge, M.S., Muller-Tidow, C. and Burdach S. (2009) EZH2 is a mediator of EWS/FLI1 driven tumor growth and metastasis blocking endothelial and neuro-ectodermal differentiation. *Proc. Natl. Acad. Sci. U.S.A.* **106**, 5324–5329

Richter, G.H.S., Fasan, A., Hauer, K., Grunewald, T.G.P., Berns, C., Rössler, S., Naumann, I., Staegge, M.S., Fulda, S., Esposito, I., and Burdach, S. (2013) G-Protein coupled receptor 64 promotes invasiveness and metastasis in Ewing sarcomas through PGF and MMP1. *J. Pathol.* **230**, 70–81

Rocchi, A., Manara, M.C., Sciandra, M., Zambelli, D., Nardi, F., Nicoletti, G., Garofalo, C., Meschini, S., Astolfi, A., Colombo, M.P., Lessnick, S.L., Picci, P. and Scotlandi, K. (2010) CD99 inhibits neural differentiation of human Ewing sarcoma cells and thereby contributes to oncogenesis. *J. Clin. Invest.* **120**, 668–680

Roth, R.B., Hevezi, P., Lee, J., Willhite, D., Lechner, S.M., Foster, A.C. and Zlotnik, A. (2006) Gene expression analyses reveal molecular relationships among 20 regions of the human CNS. *Neurogenetics* **7**, 67–80

Sheppard, S.A. and Loayza, D. (2010) LIM-domain proteins TRIP6 and LPP associate with shelterin to mediate telomere protection. *Aging (Albany NY)* **2**, 432–444

Sheppard, S.A., Savinova, T. and Loayza, D. (2011) TRIP6 and LPP, but not Zyxin, are present at a subset of telomeres in human cells. *Cell Cycle* **10**, 1726–1730

Smith, R., Owen, L.A., Trem, D.J., Wong, J.S., Whangbo, J.S., Golub, T.R. and Lessnick, S.L. (2006) Expression profiling of EWS/FLI identifies NKX2.2 as a critical target gene in Ewing's sarcoma. *Cancer Cell* **9**, 405–416

Solaz-Fuster, M.C., Gimeno-Alcañiz, J.V., Casado, M. and Sanz, P. (2006) TRIP6 transcriptional co-activator is a novel substrate of AMP-activated protein kinase. *Cell. Signal.* **18**, 1702–1712

Verrier, L., Vandromme, M. and Trouche, D. (2011) Histone demethylases in chromatin cross-talks. *Biol. Cell* **103**, 381–401

Wang, Y., Dooher, J.E., Koedood Zhao, M. and Gilmore, T.D. (1999) Characterization of mouse Trip6: a putative intracellular signaling protein. *Gene* **234**, 403–409

Wang, Y.E., Pernet, O. and Lee, B. (2012) Regulation of the nucleocytoplasmic trafficking of viral and cellular proteins by ubiquitin and small ubiquitin-related modifiers. *Biol. Cell* **104**, 121–138

Willier, S., Butt, E., Richter, G.H.S., Burdach, S. and Grunewald, T.G.P. (2011) Defining the role of TRIP6 in cell physiology and cancer. *Biol. Cell* **103**, 573–591

Willier, S., Butt, E. and Grunewald, T.G.P. (2013) Lysophosphatidic acid (LPA) signaling in cell migration and cancer invasion: a focused review and analysis of LPA receptor gene expression on

the basis of more than 1700 cancer microarrays. *Biol. Cell* **105**, 317–333
Winneppenninckx, V., Lazar, V., Michiels, S., Dessen, P., Stas, M., Alonso, S.R., Avril, M.-F., Ortiz Romero, P.L., Robert, T., Balacescu, O., Eggermont, A.M., Lenoir, G., Sarasin, A., Tursz, T., van den Oord, J.J., Spatz, A.; Melanoma Group of the European Organization for Research and Treatment of Cancer. (2006) Gene expression profiling of primary cutaneous melanoma and clinical outcome. *J. Natl. Cancer Inst.* **98**, 472–482

Xu, J., Lai, Y.-J., Lin, W.-C. and Lin, F.-T. (2004) TRIP6 enhances lysophosphatidic acid-induced cell migration by interacting with the lysophosphatidic acid 2 receptor. *J. Biol. Chem.* **279**, 10459–10468
Zheng, Q. and Zhao, Y. (2007) The diverse biofunctions of LIM domain proteins: determined by subcellular localization and protein-protein interaction. *Biol. Cell* **99**, 489–502

Received: 30 June 2013; Accepted: 16 August 2013; Published online: 18 September 2013; Accepted article online: 23 August 2013

First identification of Ewing's sarcoma-derived extracellular vesicles and exploration of their biological and potential diagnostic implications

Isabella V. Miller*, Graca Raposo†‡, Ulrich Welsch§, Olivia Prazeres da Costa†, Uwe Thiel*, Maria Lebar||, Martina Maurer*||, Hans-Ulrich Bender*, Irene von Luettichau*||, Günther H. S. Richter*, Stefan Burdach*|| and Thomas G. P. Grunewald†#¹

*Children's Cancer Research Center and Roman Herzog Comprehensive Cancer Center, Department of Pediatrics, Klinikum rechts der Isar, Technische Universität München, 80804 Munich, Germany, †Institut Curie, Centre de Recherche, 75248 Paris, France, ‡Structure and Membrane Compartments CNRS, UMR144, 75248 Paris, France, §Anatomical Institute, Ludwig-Maximilians-Universität München, 80336 Munich, Germany, †Expression Core Facility, Institute of Medical Microbiology, Immunology, and Hygiene, Klinikum rechts der Isar, Technische Universität München, 81675 Munich, Germany, ||Max Planck Institute of Psychiatry, 80804 Munich, Germany, ¶Wilhelm Sander-Therapieeinheit für Knochen- und Weichteilsarkome, Klinikum rechts der Isar, Technische Universität München, 81675 Munich, Germany, and #Medical Life Science and Technology Center, TUM Graduate School, Technische Universität München, 85746 Garching, Germany

Background Information: Exosomes are small RNA- and protein-containing extracellular vesicles (EVs) that are thought to mediate hetero- and homotypic intercellular communication between normal and malignant cells. Tumour-derived exosomes are believed to promote re-programming of the tumour-associated stroma to favour tumour growth and metastasis. Currently, exosomes have been intensively studied in carcinomas. However, little is known about their existence and possible role in sarcomas.

Results: Here, we report on the identification of vesicles with exosomal features derived from Ewing's sarcoma (ES), the second most common soft-tissue or bone cancer in children and adolescents. ES cell line-derived EVs have been isolated by ultracentrifugation and analysed by flow-cytometric assessment of the exosome-associated proteins CD63 and CD81 as well as by electron microscopy. They proved to contain ES-specific transcripts including EWS-FLI1, which were suitable for the sensitive detection of ES cell line-derived exosomes by qRT-PCR in a pre-clinical model for patient plasma. Microarray analysis of ES cell line-derived exosomes revealed that they share a common transcriptional signature potentially involved in G-protein-coupled signalling, neurotransmitter signalling and stemness.

Conclusions: In summary, our results imply that ES-derived exosomes could eventually serve as biomarkers for minimal residual disease diagnostics in peripheral blood and prompt further investigation of their potential biological role in modification of the ES-associated microenvironment.



Additional supporting information may be found in the online version of this article at the publisher's web-site.

¹To whom correspondence should be addressed (email thomas.grunewald@curie.fr)

Key words: Biomarker, Extracellular vesicles, Exosomes, Ewing's sarcoma, Microarray.

Abbreviations: ES, Ewing's sarcoma; ETS, E-twenty six; EVs, extracellular vesicles; EWS, Ewing sarcoma breakpoint region 1; FBS, fetal bovine serum; FC, fold change; FLI1, Friend leukaemia virus integration 1; GEO, Gene Expression Omnibus; LPA, lysophosphatidic acid; LPARs, LPA receptors; miRNA, micro RNA; MRD, minimal residual disease; MVB, multivesicular body; qRT-PCR, quantitative real-time polymerase chain reaction.

Introduction

Extracellular vesicles (EVs) including exosomes and other microvesicles are 30–1000 nm sized, membranous vesicles, which are secreted by several cell types and which incorporate mRNA, micro RNA (miRNA) and proteins. By delivering this cargo to and into recipient cells, EVs have pleiotropic roles in intercellular communication (Pant et al., 2012). Especially cancer cells appear to manipulate their microenvironment via EVs, as tumour-derived EVs were shown to induce angiogenesis (Nazarenko et al., 2010; Umezawa et al., 2012), to prepare pre-metastatic niches (Hood et al., 2011; Peinado et al., 2012) and to modulate anti-tumour immune responses (Chaput and Thery, 2011). These effects are believed to be mediated, at least in part, through re-programming of stromal cells by horizontal transfer of mRNAs, such as that encoding the tyrosine kinase MET (Peinado et al., 2012), miRNAs inducing epigenetic changes (Umezawa et al., 2012) and proteins, for example the oncogenic receptor EGFRvIII (Al-Nedawi et al., 2008).

To enable this transfer of functional molecules, EVs are selectively packed with specific cargo during their biogenesis. Whereas so-called microvesicles are shed directly from the plasma membrane, exosomes are generated in the cells' late endosomes and multivesicular bodies (MVBs) before being released into the microenvironment during the fusion of MVBs with the plasma membrane (Michelet et al., 2010; Bobrie et al., 2011). The cell-specific cargo of EVs offers the possibility to use them as specific tumour biomarkers, which was already shown in glioblastoma (Skog et al., 2008; Noerholm et al., 2012), melanoma (Logozzi et al., 2009; Peinado et al., 2012), prostate (Duijvesz et al., 2011; Bryant et al., 2012), ovarian (Keller et al., 2009) and lung carcinoma (Rabinowitz et al., 2009). So far, the investigation of EVs and more specifically vesicles with features of exosomes was dominantly focused on those released by carcinomas. However, it is less clear whether human sarcomas also release exosome-like vesicles and if so: what is their functionally active cargo?

Ewing's sarcoma (ES) is the second most common soft-tissue or bone cancer in children and adolescents, which features high rates of early metastasis (Cotterill et al., 2000). The ES is characterised by a specific chromosomal translocation that generates a fusion oncprotein composed of the transcription factor EWS (Ewing sarcoma breakpoint region 1) and a

DNA binding domain of an ETS (E-twenty six) family member, in 85% FLI1 (Friend leukaemia virus integration 1) (Delattre et al., 1994). As a consequence, the transcriptional dysregulation caused by EWS-FLI1 dictates the malignant phenotype of ES (May et al., 1993; Toomey et al., 2010).

In an effort to identify highly upregulated genes in ES compared with normal tissues, we previously described a comprehensive microarray analysis yielding a signature of 37 genes (including *EZH2*, *STEAP1*, *NPY1R*, *DKK2* and *CCND1*) that are highly over-expressed in ES (Staege et al., 2004). This extremely high expression in ES renders them to be candidates for specific ES biomarkers, which, in addition to the detection of EWS-ETS transcripts, are eventually useful for diagnosis of minimal residual disease (MRD).

Indeed, some of these transcripts were qualified as surrogate markers for ES detection in bone marrow (Cheung et al., 2007). However, given the high instability of free mRNA in peripheral blood and the low frequency or even absence of circulating tumour cells (Vermeulen et al., 2006), detection of such transcripts in peripheral blood is challenging. In contrast, mRNA is conserved and protected in exosomes (Valadi et al., 2007). Hence, exosome enrichment in patient-derived plasma of peripheral blood could offer an advantage to detect specific mRNAs.

Generally, the reliable detection of such marker transcripts could help detecting residual disease earlier and thus potentially improve patients' outcome due to an earlier onset of rescue therapies. Furthermore, reliable screening of MRD in peripheral blood could partially replace testing by invasive bone marrow puncture. Moreover, the identification of ES cell line-derived exosomes as mediators of intercellular exchange of information would provide new insight in the underlying biology of this disease, which might accelerate the development of new biomarkers and therapeutic options.

Here, we report on the first identification of ES cell line-derived EVs with characteristics of exosomes, explore their diagnostic potential in a pre-clinical setting and define their transcriptional signature.

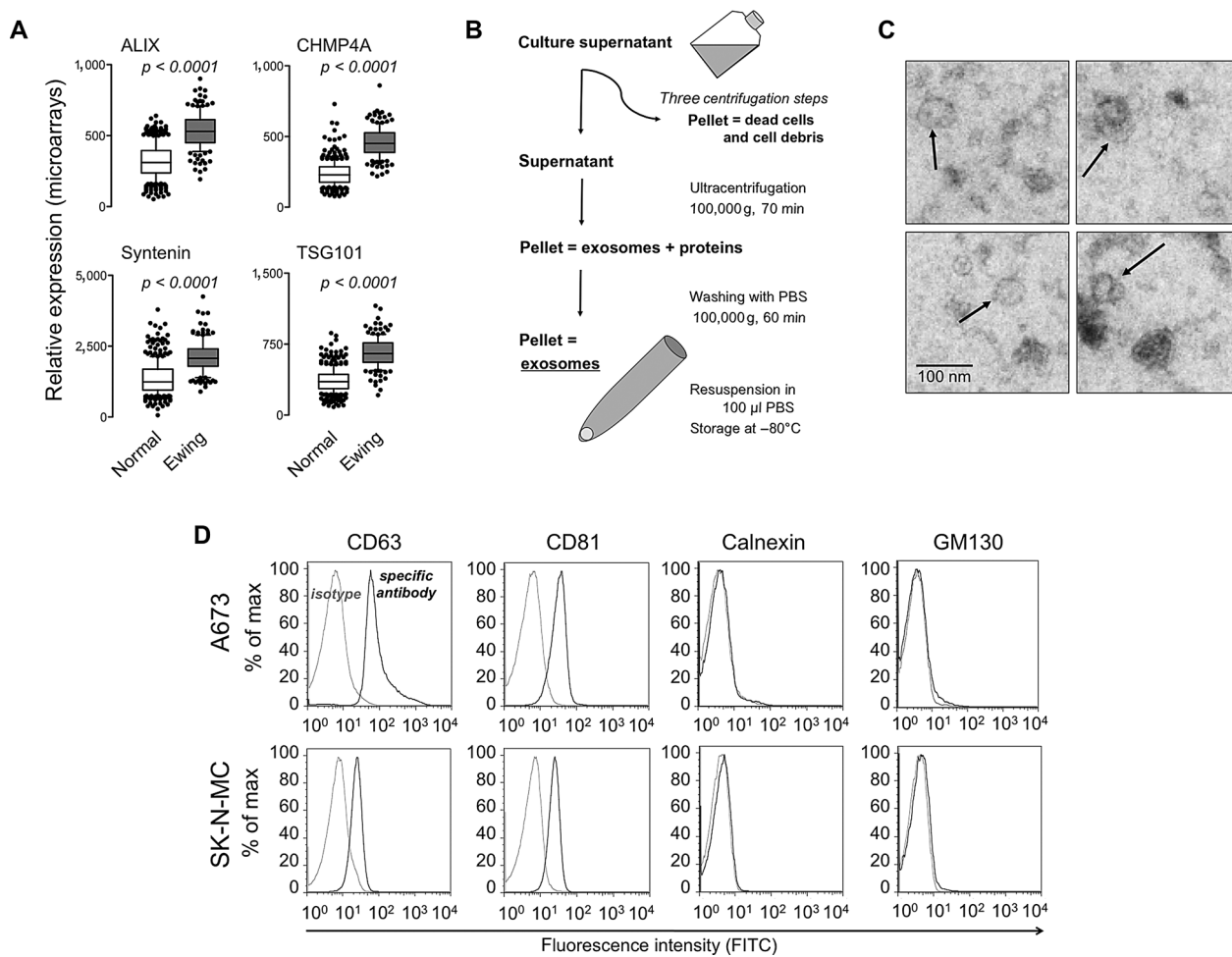
Results

ES cell lines release vesicles with characteristics of exosomes

The first indication that ES might release exosome-like vesicles was provided by re-analysis of published

Figure 1 | Ewing's sarcoma cell lines release vesicles with characteristics of exosomes.

(A) ES cell lines highly express enzymes necessary for exosome generation such as ALIX, CHMP4A, Syntenin and TSG101 (Baietti et al., 2012). Microarray data of 353 normal tissues and 161 primary ES are represented as box-plots. Whiskers indicate the 10th and 90th percentiles. Outliers are displayed as dots. Unpaired *t*-test with Welch's correction. (B) Schematic representation of the exosome preparation from supernatant of ES cell lines by ultracentrifugation. All exosomes enriched from cell culture supernatant were prepared according to this scheme. (C) Electron microscopy shows vesicles of 30–100 nm diameter corresponding to exosomes (arrows). (D) Flow cytometric analysis of the exosomal surface markers CD63 and CD81, as well as the endoplasmic reticulum marker Calnexin and the Golgi marker GM130. Exosomes were bound on 4 μ m latex beads before incubation with isotype control (grey colour) or specific antibodies (black colour), respectively. At least 30,000 events per group were recorded; two experiments per cell line.



microarray data of 353 normal tissues and 161 primary ES [GSE3526 (Roth et al., 2006), GSE34620 (Postel-Vinay et al., 2012), GSE12102 (Scotlandi et al., 2009) and GSE17679 (Savola et al., 2011)]. We observed a high expression of exosome-associated genes such as *CD63* and *CD81* (Thery et al., 2006) (Supplementary Figure 1). To examine this observation more closely, we investigated the expression

of typical exosomal marker genes as well as components necessary for exosome generation and release. Compared with normal tissue, several genes, especially from the Syntenin/ALIX pathway, are highly expressed in ES (Figure 1A). Of note, these genes have been recently reported to participate in exosome biogenesis/secrection (Baietti et al., 2012). We next isolated exosomes from cell culture supernatants

of the ES cell lines A673, SK-N-MC and SB-KMS-KS1 by ultracentrifugation (Figure 1B). Electron microscopy highlighted the presence of vesicles with the size of exosomes (30–100 nm) (Figure 1C). Additionally, the ES cell line-derived exosomes were detected by flow cytometry via staining for CD63 and CD81 (Figure 1D). In contrast, the endoplasmic reticulum marker Calnexin (alias CANX) and the Golgi matrix protein GM130 (alias GOLGA2) (Williams, 2006; Nakamura, 2010) were undetectable on exosomes, while being readily detectable within the parental A673 and SK-N-MC ES cells (Supplementary Figure 2), further confirming the endosomal origin and exosomal nature of these ES cell line-derived EVs (Figure 1D).

ES cell line-derived exosomes contain mRNAs highly specific for ES including EWS-FLI1

To investigate if the ES cell line-derived exosomes contain RNA, we profiled the product of an RNA extraction from exosome lysates with a Bioanalyzer (Agilent). This analysis demonstrated that the exosomes contain a broad spectrum of RNA, which consists especially of small RNAs. In contrast, RNA of the parental cells displayed the typical RNA profile with high abundance of ribosomal RNA (Figure 2A). The RNA profile of our exosome preparations is similar to that derived from murine mast cells as previously described (Valadi et al., 2007).

In order to examine whether this exosomal RNA harbours intact messenger RNAs, we performed quantitative real-time (qRT)-PCR analysis of a set of genes, which are highly overexpressed and thus specific for ES in comparison to normal tissues. Candidate genes fulfilling these criteria were identified in a two-step process using microarray data of us and others obtained from Affymetrix HG-U133A chips as a discovery cohort [$n = 63$ ES and $n = 36$ normal tissues; GSE1825 (Staege et al., 2004), GSE15757 (Burdach et al., 2009), GSE7007 (Tirode et al., 2007), E-MEXP-1142 (Schaefer et al., 2008) and GSE2361 (Ge et al., 2005)] and published microarray data of others derived from Affymetrix HG-U133plus2.0 chips as a validation cohort [$n = 161$ ES, $n = 353$ normal tissues; GSE34620 (Postel-Vinay et al., 2012), GSE12102 (Scotlandi et al., 2009), GSE17679 (Savola et al., 2011) and GSE3526 (Roth et al., 2006)].

Genes were ranked according to their linear fold change (FC) of the median expression levels in primary ES compared with normal tissue. Then, those 30 transcripts (corresponding to the top 0.25% of probe-sets) showing the highest FC in median gene expression in the discovery cohort were reassessed in the validation cohort. Finally, those 10 transcripts, which had a mean FC higher than 10 in both cohorts and which were previously implicated in ES pathology were selected as potential biomarkers (Table 1). The analysis of the validation cohort also identified *LIPI* as a promising candidate since the HG-U133plus2.0 microarrays contain probes for this gene (whereas the HG-U133A microarrays do not) (Figure 2B). In addition to these transcripts, EWS-FLI1 was examined in all continuative experiments as it constitutes the most specific marker for ES. Of note, these in total 12 potential marker transcripts could be readily and reproducibly detected in exosome preparations from cell culture supernatant (Figure 2C), suggesting that part of the RNA in ES cell line-derived exosomes is functional mRNA.

To assess whether these mRNAs are conserved and thus stabilised in exosomes, we treated ES exosomes with RNase. As expected, exosomal RNA was protected from RNase-mediated degradation in intact exosomes (Figure 2D). In contrast, the RNA of exosomes, whose membranes were disrupted by sonication before RNase-treatment, was completely degraded (Figure 2D). These experiments suggested that a considerable amount of RNA harvested from the supernatant of ES cells by ultracentrifugation is packed within exosomes. Furthermore, we enriched exosomes from cell culture supernatant in the presence of RNase (Supplementary Figure 3). Despite the continuous presence of RNase, we were still able to enrich our specific transcripts, further confirming that these transcripts are indeed packed within exosomes.

To challenge this observation, we tested if the enrichment of exosomes derived from supernatant of ES-cell lines would lead to a higher yield of RNA compared with isolation of RNA from an equal volume of supernatant without exosome enrichment when applying the same method of exosome enrichment and purification as described in Figure 1B. We observed a median 2.5-fold increase (range: 1.9–3.8) of detectable transcripts at a relation of supernatant volume to exosomal concentration volume

Figure 2 | See figure legend on next page

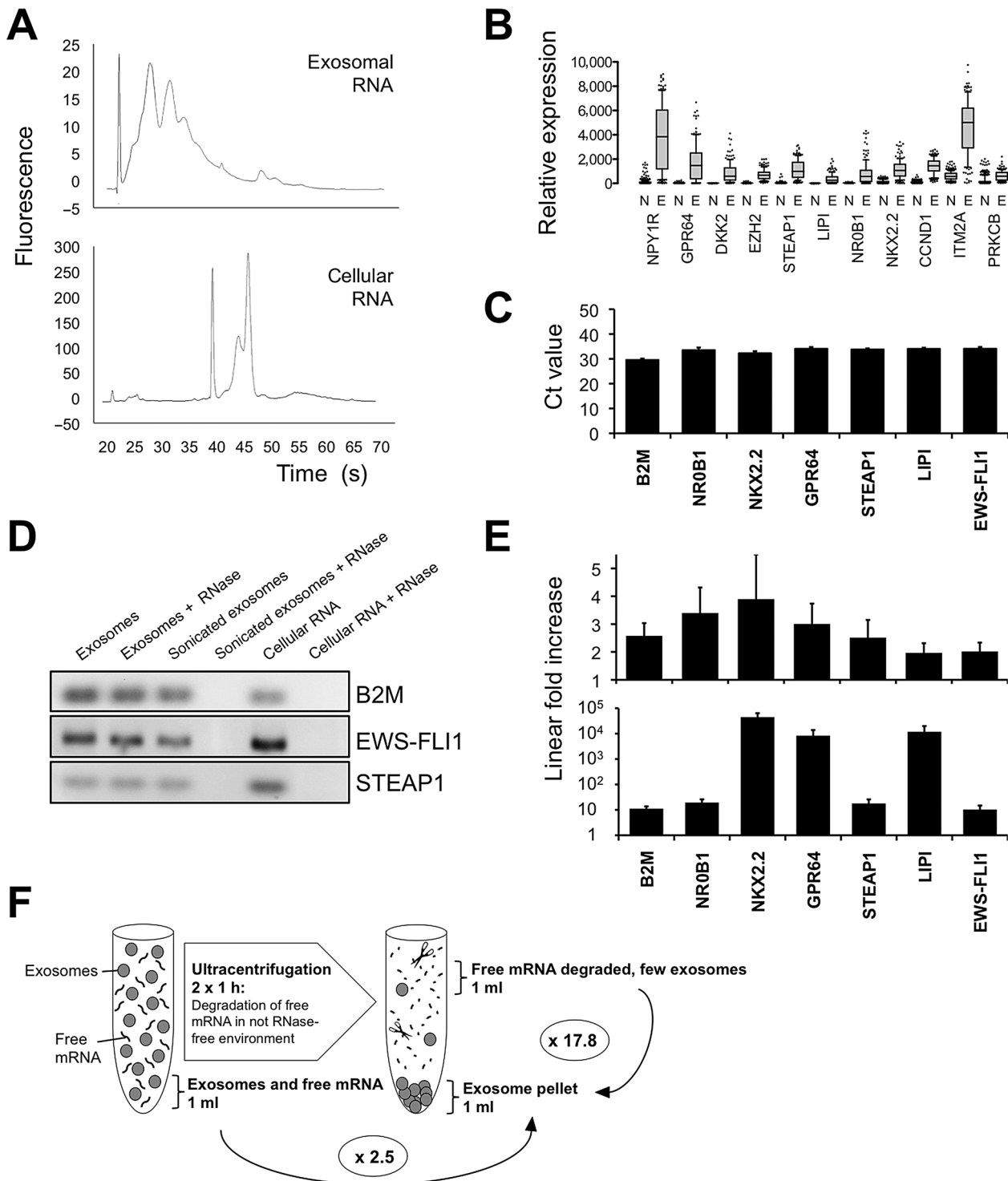


Figure 2 | ES derived exosomes contain functional mRNAs, including ES-specific transcripts

(A) Representative images of Bioanalyzer profiles of exosomal and cellular RNA from A673 cells. The spectrum of exosomal RNA contains a high amount of small RNAs, but few ribosomal RNAs. **(B)** Microarray analysis of the expression of candidate marker transcripts in 353 normal tissues (N) compared to 161 primary ES (E). **(C)** Representative qRT-PCR results of six potential marker transcripts and the housekeeping gene *B2M* showing their stable expression in ES cell line-derived exosomes. Similar results were obtained for the other marker transcripts (not shown). Data are mean \pm SEM of three experiments (duplicates/group). **(D)** RNase-treatment revealed no degradation of mRNA inside intact exosomes, but within exosomes which were sonicated to disrupt their membranes prior to RNase-treatment. As an additional control, isolated cellular RNA was treated with RNase to demonstrate full RNase activity. Representative DNA gel image of *B2M*, *EWS-FL1* and *STEAP1* after 50 cycles of PCR. **(E)** Upper panel: Gain of transcripts through exosome enrichment compared with an equal volume of supernatant measured by qRT-PCR. Lower panel: Yield of exosomal transcripts through exosome enrichment compared to an equal volume of supernatant after ultracentrifugation measured by qRT-PCR. Both experiments: mean \pm SEM of three experiments (duplicates/group). **(F)** Illustration of potential degradation of free mRNA during ultracentrifugation. All experiments shown in Figure 2 were performed with A673-derived exosomes.

Table 1 | Overview on the selected candidate marker genes based on their fold changes (FCs) in the discovery and validation cohort

| Entrez ID | Gene symbol | Description | FCs Ewing versus normal tissues | | |
|-----------|-------------|--|---------------------------------|------------|---------|
| | | | Discovery | Validation | Mean FC |
| 4886 | NPY1R | Neuropeptide Y receptor Y1 | 64.8 | 105.6 | 85.2 |
| 10149 | GPR64 | G-protein-coupled receptor 64 | 35.9 | 89.6 | 62.8 |
| 27123 | DKK2 | dickkopf homolog 2 | 20.5 | 78.8 | 49.7 |
| 4821 | NKX2.2 | NK2 homeobox 2 | 62.0 | 29.5 | 45.8 |
| 149998 | LIP1 | Lipase, member 1 | NA | 44.4 | 44.4 |
| 2146 | EZH2 | Enhancer of zeste homolog 2 | 17.8 | 59.9 | 38.9 |
| 26872 | STEAP1 | Six transmembrane epithelial antigen of the prostate 1 | 17.6 | 51.6 | 34.6 |
| 190 | NR0B1 | Nuclear receptor subfamily 0, group B, member 1 | 16.8 | 30 | 23.4 |
| 595 | CCND1 | Cyclin D1 | 10.7 | 19.5 | 15.1 |
| 5579 | PRKCB | Protein kinase C, beta | 19.7 | 6.7 | 13.2 |
| 9452 | ITM2A | Integral membrane protein 2A | 13.1 | 8.5 | 10.8 |

of 30:1 (Figure 2E upper panel). In contrast, the yield of RNA in exosome preparations compared with the supernatant after ultracentrifugation was considerably higher (median: 17.8-fold; range: 9.4–40,835.6), confirming that our applied exosome enrichment process is efficient and that the majority of the RNA containing exosomes is pelleted during ultracentrifugation (Figure 2E lower panel). The discrepancy of these two differential effects could be caused by free or protein-bound RNA in cell culture supernatant, which might be degraded in the possibly RNase-contaminated setting of ultracentrifugation (Figure 2F). Considering that human plasma contains active RNase (Tsui et al., 2002; Reddi and Holland, 1976), the substantial gain of transcripts by exosome enrichment and their protection from RNase

within exosomes suggest that this method could be a valuable approach to use these specific transcripts as stable biomarkers in peripheral blood.

Specific ES markers can be detected in ES cell line-derived exosomes re-suspended in healthy donor plasma

We then strove to assess the performance of our exosome enrichment method and the suitability of our candidate genes as potential ES biomarkers in peripheral blood. Accordingly, we first validated the specificity of the 12 potential marker transcripts by confirming their high expression (as predicted by microarrays) in ES cell lines by qRT-PCR. As negative controls we used neuroblastoma and leukaemia cell lines. Apart from EZH2 and CCND1, which are

expressed in many cancer entities (Diehl, 2002; Chang and Hung, 2012), as well as DKK2, which is upregulated in neuroblastoma (Revet et al., 2010), all other marker transcripts were rather specific for ES (Figure 3A).

Next, we tested for the presence of these marker transcripts in plasma of healthy donors to reject those, which can be unspecifically detected in plasma even before exosome enrichment. Of note, by qRT-PCR (50 cycles) five out of the 12 marker transcripts could neither be detected in all tested 20 healthy plasma samples (Figure 3B), nor in exosome preparations of 10 additional healthy plasma samples (not shown), indicating their high specificity for ES (which was anticipated for EWS-FLI1). Thus, the five markers NR0B1, NKX2.2, STEAP1, LIPI and EWS-FLI1 were eligible for further analysis.

To assess the sensitivity of these five markers in a pre-clinical setting, we designed a plasma model based on a calculation that involved data of our usual exosome yields (0.8 µg protein equivalent of 1×10^6 A673 cells in 48 h) as well as estimates about the possible behaviour of ES exosomes *in vivo*. Based on previously published data, we assumed that exosomes could be stable in blood for 8 days (Thery et al., 2006) and that more than 1% of the exosomes of a clinical ES would be released into the circulation. If a given ES comprised about 1×10^9 cells, which corresponds to a tumour volume of 1 cm³ (James et al., 1999), and the plasma volume was 2.7 l, we can calculate that the amount of exosomes in 10 ml plasma would account 0.24 µg. Accordingly, for the pre-clinical model, ES cell line-derived exosomes were serially diluted (range: 30–0.1 µg exosome equivalent) in 10 ml of plasma of a healthy donor and then isolated by ultracentrifugation (Figure 3C). Strikingly, all marker transcripts could be detected by qRT-PCR down to a concentration of 0.3 µg/10 ml plasma at least once in two experiments (Figure 3D) and to some extent even down to 0.1 µg/10 ml (not shown). Moreover, the packing of these transcripts within ES cell line-derived exosomes protected them from RNase-mediated degradation, as the additional incubation of re-suspended exosomes with active RNase had a negligible effect on the abundance and detectability of these specific marker transcripts (Supplementary Figure 4).

Taken together, these results indicate that NR0B1, NKX2.2, STEAP1, LIPI and EWS-FLI1 constitute specific and sensitive marker transcripts for detection of ES cell line-derived exosomes in peripheral blood.

ES cell line-derived exosomes share a common transcriptional signature

To gain insight into the potential (patho-)biological function of ES cell line-derived exosomes, we subjected RNA isolated from exosomes and their parental ES cell lines (A673, SK-N-MC and SB-KMS-KS1) to microarray analysis (Affymetrix Human Gene ST 1.0). We first filtered the microarray data for probe-sets annotating known genes that are at least minimally expressed (minimal average expression intensity ≥ 10 in natural scale across all six samples) yielding a total of 13,610 different probe-sets. This list of probe-sets was then filtered for those probe-sets which show an at least two-fold (\log_2) differential regulation between exosomes and their corresponding parental cell line. As seen in the Venn diagram in Figure 4A, exosomes from all three cell lines display a significant degree of overlap of in total 1382 strongly regulated probe-sets (10.15% of all probe-sets) corresponding to 1288 individual genes (Supplementary Data). Unsupervised hierarchical clustering of the samples and probe-sets further confirmed a strong match of the exosomal and the cellular RNA samples, respectively (Figure 4B).

We then performed a gene-set enrichment analysis (GSEA) with these commonly differentially regulated 1382 probe-sets and the remaining non-regulated probe-sets. GSEA demonstrated a significant enrichment of transcripts in exosomes that are involved in G-protein-coupled signalling, neurotransmitter signalling and stemness (Figure 4C). For instance, the 'MIKKELSEN_MEF_ICP_WITH_H3K27ME3' gene-set (Mikkelsen et al., 2008) describes a set of transcripts differentially expressed in murine embryonic fibroblasts with induced pluripotent stem cell characteristics that is associated with histone 3 lysine 27 tri-methylation, which has been previously reported to be implicated in the maintenance of a more immature phenotype of ES (Richter et al., 2009). In synopsis, these results indicate that ES cell line-derived exosomes are significantly enriched for a common set of transcripts involved in signal transduction and stemness.

Figure 3 | Evaluation of specificity and sensitivity of candidate marker transcripts

(A) qRT-PCR of selected 12 candidate marker transcripts in seven ES, two neuroblastoma (NBL) and two leukaemia (LK) cell lines. NTC: no-template-control. Mean \pm SEM of two experiments (duplicates/group). **(B)** Heatmap of marker transcript expression as measured by qRT-PCR normalised to B2M in 20 healthy plasma samples. White colour represents delta-Ct values equal or greater than 0, whereas black colour represents no detection of the corresponding transcript in 50 PCR cycles (triplicate measurements). The housekeeping genes *ACTB* and *GAPDH* were used as positive controls. Asterisks mark transcripts that were undetectable in all plasma samples. **(C)** Schematic representation of the dilution of ES cell line-derived exosomes in plasma of healthy donors. **(D)** Representative DNA gel images of qRT-PCR products of B2M, EWS-FLI1, STEAP1 and NR0B1 with or without exosome enrichment and progressive dilution of exosomes in healthy plasma. Similar results were obtained for LIP1 and NKX2.2 (not shown).

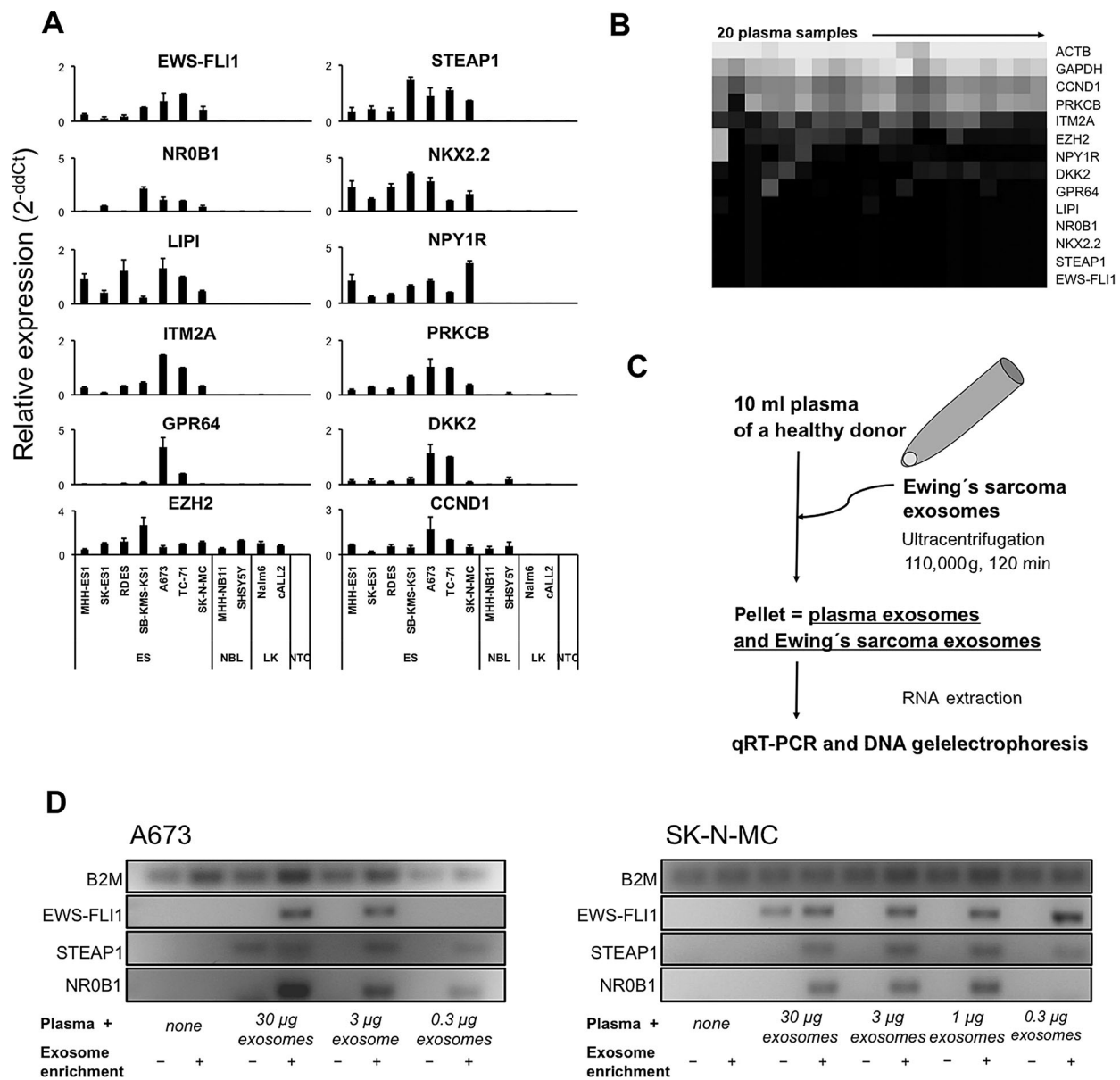
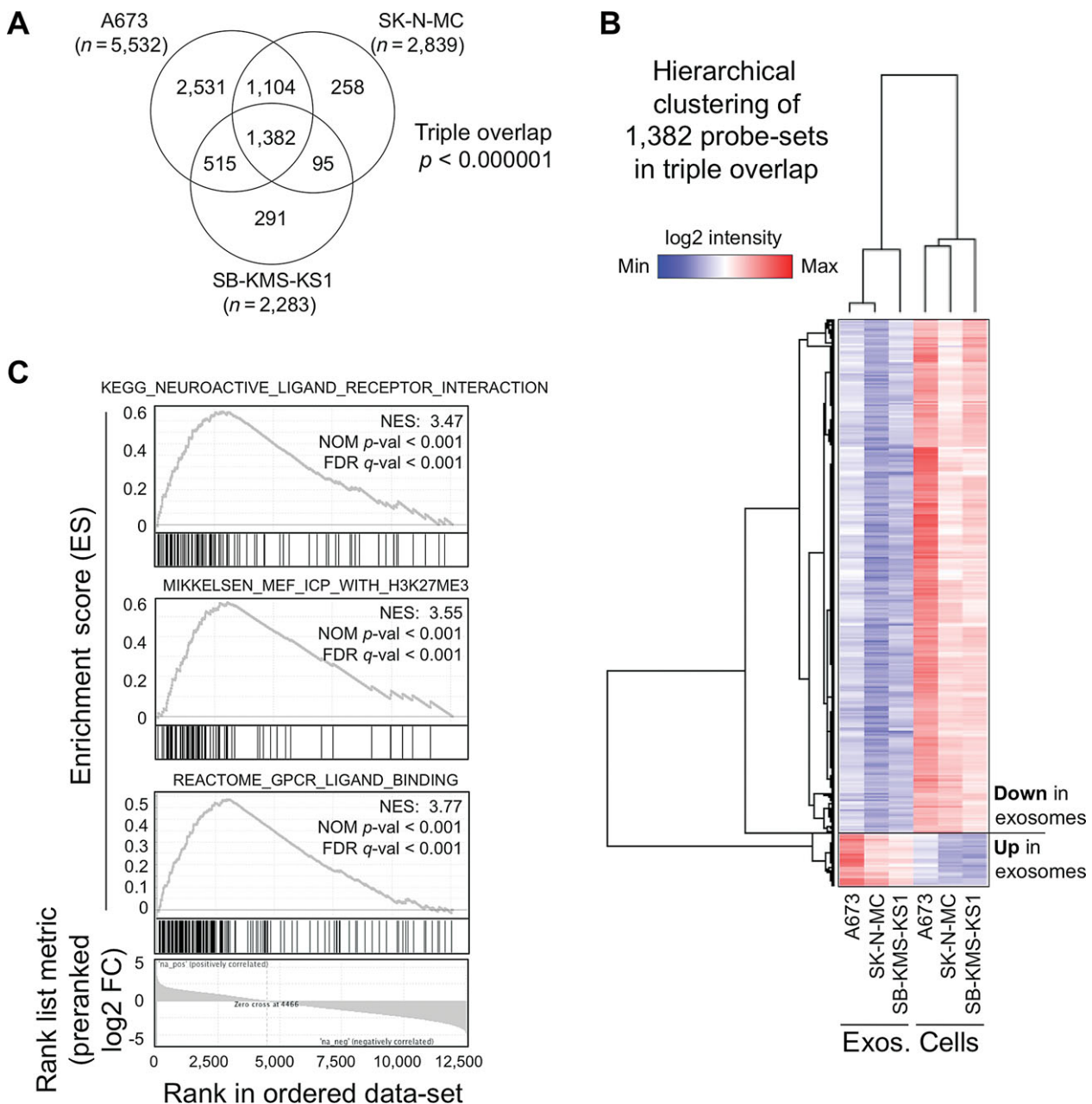


Figure 4 | ES cell line-derived exosomes share a common transcriptional signature

(A) Venn diagram of gene annotating probe-sets, which are differentially regulated between exosomes and their corresponding parental cell line (min. \log_2 FC ≥ 2), showing a significant degree of overlap (two-tailed chi-square test). (B) Unsupervised hierarchical clustering (average linkage) of the individual samples and the commonly differentially regulated 1382 probe-sets. Data were \log_2 -transformed and median-centred for depiction in a heatmap. (C) GSEA of the 1382 commonly differentially regulated and non-regulated probe-sets. NES: normalised enrichment score; NOM: nominal P value; FDR: false discovery rate.



Discussion

This study aimed to determine if ES secrete EVs, to characterise their RNA cargo and to explore in a pre-clinical setting, whether certain transcripts within the ES cell line-derived EVs might constitute suitable candidates for validation as biomarkers in a subsequent clinical study.

Here, we report on the identification of ES cell line-derived EVs, which show features of exosomes, such as the size of 30–100 nm in electron microscopy and the strong enrichment for CD63 and CD81—two tetraspanins associated with the internal vesicles of MVBs and consequently present on the surface of released exosomes (Escola et al., 1998). In addition, the endoplasmic reticulum and Golgi markers Calnexin and GM130 were undetectable on these ES cell line-derived EVs, further proving their endosomal origin and thus exosomal nature. We additionally demonstrate that these ES cell line-derived exosomes are packed with RNA, which is protected from degradation by RNases. Moreover, we show that they share a common set of transcripts that are potentially involved in intercellular communication, and provide pre-clinical evidence that these exosomes contain specific transcripts such as EWS-FLI1, which can be potentially used as ES markers in peripheral blood.

Interestingly, our set of the top five markers (NR0B1, NKX2.2, STEAP1, LIPI and EWS-FLI1) is similar to that of Cheung et al. (2007) who screened for highly overexpressed genes by microarrays to identify candidates for detection of occult ES bone marrow metastases. However, in comparison with their study, we additionally identified LIPI through the use of publicly available microarray data-sets built on a chip platform that contains probes for this gene.

Moreover, our analyses show that these transcripts are not detectable by qRT-PCR (50 cycles) in peripheral blood of 20 healthy donors. In contrast, they were readily detectable in plasma into which minute amounts of ES exosomes have been added. These results point to a high specificity of these five transcripts for ES and suggest that they might provide sufficient sensitivity for detection of MRD, which needs to be assessed in future clinical investigations.

NR0B1 (alias DAX1) is a key transcription factor highly expressed in embryonic development of the adrenal gland and only minimally or even not expressed in adult tissues. NR0B1 knockdown in ES cells significantly reduces their proliferative capacity

(Kinsey et al., 2006; Garcia-Aragoncillo et al., 2008). Similarly, the knockdown of the transcription factor NKX2.2 and the membrane-bound oxidoreductase STEAP1 impairs ES proliferation (Smith et al., 2006; Grunewald et al., 2012b) and both proteins proved to be valuable markers for ES in immunohistochemistry (Yoshida et al., 2012; Grunewald et al., 2012c). Interestingly, STEAP3 is actively involved in exosome production and release (Grunewald et al., 2012a), which might be also true for other STEAP proteins. Although little is known about the activity of the lysophosphatidic acid (LPA)-producing phospholipase LIPI in ES, recent work has shown that ES express different transcript variants of LIPI and the cognate LPA-receptors (LPARs) (Schmiedel et al., 2011), suggesting that ES could principally use the LPA/LPARs-signalling pathway to promote their growth, migration and invasiveness in an auto- and/or paracrine fashion as seen in other cancers (Willier et al., 2011).

Apart from these five markers, our microarray analysis identified a set of over 1200 transcripts that are either highly enriched or depleted in exosomes derived from ES cell lines. Especially the transcripts that are highly enriched in exosomes might constitute a means used by ES to communicate with other ES cells and/or the microenvironment by lateral transfer of mRNAs and miRNAs. In other cancers such as gastric and mammary carcinoma, recent evidence has shown that tumour-derived exosomes mobilise stromal cells and induce the differentiation of normal mesenchymal stem cells into cancer-associated fibroblasts by specifically delivering signalling molecules packed in exosomes into recipient cells (Gu et al., 2012; Luga et al., 2012). Moreover, in glioblastoma EVs serve as paracrine signalling molecules between tumour cells to promote dynamic adaptations on hypoxia by triggering G-protein-coupled receptors (Svensson et al., 2011). Notably, our GSEA demonstrated that the ES cell line-derived exosomes are significantly enriched for transcripts implicated in G-protein-coupled signalling, neurotransmitter signalling and stemness. Moreover, as the ES cell line-derived exosomes contain the mRNA of the ES-specific transcription factor EWS-FLI1, it would be interesting to document if EWS-FLI1 can be transferred to and expressed in recipient cells of the tumour-associated stroma, and if so, which role(s) this event might have regarding oncogenic

re-programming of the microenvironment? Since EWS-FLI1 is known to induce an endothelial gene expression signature in ES and mesenchymal stem cells (Staege et al., 2004; Tirode et al., 2007), it is tempting to speculate whether ES exosomes play a role in induction of neo-angiogenesis. Considering that ES display neuroectodermal features and a neuroectodermal transcriptional signature (Staege et al., 2004; von Levetzow et al., 2011), it is noteworthy that ES cell line-derived exosomes contain significantly more transcripts involved in neurotransmitter signalling than their parental cells, which might argue for an active role of ES exosomes in neuroectodermal differentiation. Although further experiments are required to understand the precise (patho-)biological role of ES exosomes, the identified set of commonly enriched transcripts presented in this study constitutes a initial step for future experiments. However, future proteomic analyses, for example by mass spectrometry, are warranted to fully characterise the exosomal cargo of ES. Additionally, it would be interesting to analyse if differently sized exosomes are packed with a distinct RNA and protein content, which is currently not accessible for investigation as there is as yet no established technique available that enables the definite distinction of exosomal subfractions (Minogue and Waugh, 2012).

Furthermore, if ES are indeed capable of delivering and receiving transcriptional cues via exosomes—perhaps mediated by specific cognate docking sites (Rana and Zoller, 2011)—a clinical application of exosomes might be considered too, for example by delivering short interfering RNAs against EWS-FLI1 specifically to ES cells.

In summary, this study describes the first identification of ES cell line-derived exosomes, pre-clinically explores their diagnostic potential and defines their transcriptional signature by microarrays. The fact that ES cell lines produce exosomes containing mRNAs such as EWS-FLI1 might have important implications in our understanding of how ES cells interact with each other and how they possibly re-program their microenvironment.

Materials and methods

Cell lines and culture conditions

All cell lines except for the A673 cell line, which was purchased from ATCC, and the SB-KMS-KS1 cell line were obtained from the German Collection of Microorganisms and Cell Cultures

(DSMZ). SB-KMS-KS1, previously named SBSR-AKS, is an ES cell line with an EWS-FLI1 type 1 translocation, which was established in our laboratory (Richter et al., 2009; Grunewald et al., 2012b). Cells were grown in RPMI 1640 media (Invitrogen) containing 10% fetal bovine serum (FBS) (Biochrom), 1% glutamine and 100 µg/ml gentamycin (Invitrogen) at 37°C in 5% CO₂ atmosphere. For experiments requiring FBS but exosome-free media, FBS was ultracentrifuged for 2 h at 100,000 x g before use to clear it from bovine serum exosomes. Cell lines were routinely checked for mycoplasma contamination and purity (status of EWS-ETS fusion transcript in ES cell lines).

Provenience of blood samples and plasma preparation

Human blood samples were obtained with IRB approval of the Faculty for Medicine of the Technische Universität München (TUM) in frame of the Neo-Ident study (approval no: 2562/09). All donors gave written informed consent. Peripheral blood samples were obtained from 20 healthy adult donors, whose health status was checked by a standardised questionnaire. Peripheral blood was drawn into EDTA-coated collection tubes (Sarstedt) and centrifuged for 7 min at 540 x g. Plasma was carefully transferred into a new tube, centrifuged for 15 min at 1,800 x g to remove platelets. Then, it was filtered through a 0.45 µm filter (Sartorius) and again centrifuged at 1,800g for 3 min to clear it from debris. All centrifugation steps were performed at 4°C. Plasma samples were stored at -80°C if they were not used *ad hoc* for exosome enrichment or RNA extraction.

Exosome preparation

Exosomes were prepared from the cell culture supernatant of A673, SK-N-MC and SB-KMS-KS1 ES cell lines using the classical ultracentrifugation protocol as described previously (Thery et al., 2006). ES cells at 80% confluence were washed with PBS and cultured in fresh RPMI 1640 media containing exosome-depleted FBS, 1% glutamine and 100 µg/ml gentamycin (both Invitrogen). After 48 h supernatant was collected and centrifuged at 300 x g for 10 min, at 2,000 x g for 10 min and at 10,000 x g for 30 min to clear it from debris. Subsequently, exosomes were collected by ultracentrifugation at 100,000 x g for 70 min, pooled, re-suspended in PBS and once more ultracentrifuged at 100,000 x g for 60 min using an Optima XL-90 ultracentrifuge with a 70.1 Ti rotor (both Beckman Coulter). Exosomes from human plasma samples were isolated by ultracentrifugation at 110,000 x g for 120 min using a SW 41 Ti rotor (Beckman Coulter). All exosome pellets were re-suspended in PBS and stored at -80°C if they were not used immediately for subsequent analyses.

The amount of harvested exosomes was estimated by measuring the protein content with a commercial Bradford assay (Bio-Rad). Briefly, 5 µl of the re-suspended exosome pellet were diluted with 5 µl of PBS. Then, 1 ml of Bradford solution (Bio-Rad) (diluted 1:5 in distilled water) was added. After 3 min, protein concentrations were measured photometrically at 595 nm and referenced to defined BSA standards. The average amount of exosomes harvested from supernatant of 1 × 10⁶ A673 cells after 48 h incubation was 0.8 µg.

Isolation of cellular and exosomal RNA

Cellular RNA was isolated using the RNeasy mini kit (Qiagen) according to the manufacturer's protocol. Exosomal and

free plasma RNA were extracted with the UltraSens Virus Kit (Qiagen). Here, the centrifugation step after the addition of the carrier RNA was performed for plasma at 660 $\times g$ and for exosomes at 830g in order to receive optimal results. To extract RNA from cells and exosomes for microarray analysis the miRCURY RNA isolation kit (Exiqon) was used according to the manufacturer's protocol and as described previously (Eldh et al., 2012). RNA concentration and quality were checked photometrically at 260 nm. RNA was stored at -80°C . To prove that the exosomal RNA is protected from RNases, RNase-treatment was performed with 0.1 $\mu\text{g}/\mu\text{l}$ RNase A (Fermentas) for 10 min at 37°C . As a negative control, exosomes were sonicated thrice for 10 s at 80% amplitude with a digital sonicator (Bransonic) to disrupt their membrane before RNase-treatment as described previously (Keller et al., 2011).

qRT-PCR and DNA gel electrophoresis

RNA (1 μg RNA/reaction) was reverse transcribed using the High-Capacity cDNA Reverse Transcription Kit (Applied Biosystems). For qRT-PCR, 1 μl cellular cDNA, 2 μl exosomal or 4 μl plasma cDNA were mixed with the TaqMan Universal PCR Master Mix (Applied Biosystems) and the corresponding primers (final volume: 20 μl). Primers were purchased as specific TaqMan Gene Expression Assays (Applied Biosystems): STEAP1 Hs00185180_m1, LIPI Hs01017703_m1, NR0B1 Hs00230864_m1, NKX2.2 Hs00159616_m1, GPR64 Hs00971379_m1, EZH2 Hs00544830_m1, NPY1R Hs00168565_m1, ITM2A Hs01011360_g1, DKK2 Hs00205294_m1, PRKCB Hs00176998_m1, B2M Hs00187842_m1, GAPDH Hs99999905_m1, ACTB Hs01060665_g1. For the detection of the EWS-FLI1 fusion transcript, the following primers were used: 5'-TAGTTACCCACCCCAAACCTGGAT-3' (sense), 5'-GGGCCGTTGCTCTGTATTCTTAC-3' (antisense) and probe 5'-FAM-CAGCTACGGGCAGCA-3'. qRT-PCR was performed with an AB 7300 Real-Time PCR System (Applied Biosystems). For DNA gel electrophoresis, a 2% agarose gel was prepared and a mix of 20 μl of cDNA and 2 μl of Blue Juice Gel Loading Buffer (Invitrogen) were loaded in each lane. DNA amplicons were visualised with a Gene Genius Bio imaging system (Syngene).

Microarray analysis

A673, SK-N-MC and SB-KMS-KS1 cells were cultivated for 48 h. Thereafter, RNA was extracted separately from the cells and the exosomes harvested from the supernatant as described in the section "Exosome preparation". RNA quality was checked using a Bioanalyzer (Agilent). Total RNA (200 ng) was amplified and labelled using Affymetrix GeneChip Whole Transcript Sense Target Labeling Kit. cRNA was hybridised to Affymetrix Human Gene 1.0 ST arrays. Arrays were RMA normalised. Quality assessment consisted of RNA degradation plots, Affymetrix control metrics, sample cross-correlation and probe-level visualisations. Normalisation incorporated (separately for each RNA type data-set) background correction, quantile normalisation and probe-level summation by RMA.

The microarray data were analysed with the GENE-E software package (<http://www.broadinstitute.org/cancer/software/GENE-E/>) and deposited at the Gene Expression Om-

nibus (GEO; GSE42282). GSEA was performed with the GSEA tool (<http://www.broad.mit.edu/gsea>) using a pre-ranked list and 1,000 permutations.

For the interrogation of publicly available microarray data, data-sets were retrieved from the GEO and the Array Express platform of the EMBL-EBI (<http://www.ebi.ac.uk/arrayexpress/>), manually revised for their correct annotations, and then simultaneously RMA-normalised using brainarray custom CDF files (v15 ENTREZG). Individual data accession numbers are given in the Results section.

Flow cytometry

For flow cytometry, exosomes derived from A673 and SK-N-MC ES cells were incubated with 4 μm aldehyde/sulphate latex beads (Invitrogen) overnight and blocked with 1 M glycine and 0.5% BSA in PBS before incubation with CD63 (sc-5275), CD81 (sc-7637) or corresponding isotype control antibodies (all Santa Cruz). The same procedure was applied for testing ES cell line-derived exosomes for the markers Calnexin (sc-80645, Santa Cruz) and GM130 (ab76154, Abcam). Before and after incubation with the secondary antibody [goat anti-mouse IgG1 FITC (sc-2078) and goat anti-rabbit IgG1 FITC (sc-2012); both Santa Cruz], three washing/blocking steps with 0.5% BSA in PBS were carried out. For positive control of the Calnexin and GM130 antibodies, intact A673 and SK-N-MC cells were fixed with 4% paraformaldehyde, permeabilised with 90% methanol and blocked with 0.5% BSA in PBS before incubation with specific antibodies. Samples were analysed on a FACScalibur flow cytometer using Cellquest Pro software (both Becton Dickinson). At least 30,000 events/sample were recorded.

Electron microscopy

Electron microscopy studies were performed as previously described (Raposo et al., 1996). Briefly, exosomes re-suspended in PBS were deposited for 20 min at RT on formvar-carbon coated electron microscopy grids. The samples were fixed for 20 min in PBS-2% PFA (Electron Microscopy Sciences), and quenched in PBS 50 mM glycine. After fixation in glutaraldehyde 1% (Electron Microscopy Sciences) grids were rinsed in water and contrast and embedding was performed with an ice-cold mixture of methylcellulose and uranyl acetate for 10 min. Grids were air-dried before observation. Samples were observed at 80 kV with a CM120 Twin FEIelectron microscope (FEI Company) and digital images were acquired with a numeric camera (Keen View, Soft Imaging System).

Statistical analyses

Differences in proportions between groups were evaluated by two-tailed chi-square test, unpaired *t*-test with Welch's correction or unpaired two-tailed Student's *t*-test. Statistical significance level was set at $P < 0.05$.

Author contributions

I.V.M., S.B. and T.G.P.G. designed the study. I.V.M. and T.G.P.G. performed the experiments, drafted and wrote the paper and designed the Figures and Tables. G.R. and U.W. carried out electron microscopy studies. M.L. helped with the ultracentrifugation procedures. M.M., U.T., H.U.B. and I.v.L. collected

blood samples. G.H.S.R. provided technical guidance and contributed to grant application. O.P.d.C. and T.G.P.G. carried out bioinformatic analyses. U.T., G.H.S.R., S.B. and T.G.P.G. wrote the application for the IRB approval of the current study. All authors read and approved the final manuscript before submission.

Acknowledgements

We thank Mrs. Colette Berns and Mrs. Sabine Tost for expert technical assistance and Dr. Maria Eldh (University of Gothenburg, Sweden) for her helpful advice on extracting RNA from exosomes.

Funding

This work was supported by grants from the Deutsche Forschungsgemeinschaft (DFG GR3728/1-1 to TGPG, GHSR and SB; GR3728/2-1 to TGPG; and SFB-TR22) and the 'Dr. Sepp und Hanne Sturm Gedächtnisstiftung' of the Ministry of Health of the City of Munich (to TGPG, GHSR and SB) and is part of the Translational Sarcoma Research Network supported by the BMBF (FK 01GM0870 and 01GM1104B to GHSR and SB).

Conflict of interest statement

The authors have declared no conflict of interest.

References

Al-Nedawi, K., Meehan, B., Micallef, J., Lhotak, V., May, L., Guha, A. and Rak, J. (2008) Intercellular transfer of the oncogenic receptor EGFRvIII by microvesicles derived from tumour cells. *Nat. Cell Biol.* **10**, 619–624

Baietti, M.F., Zhang, Z., Mortier, E., Melchior, A., Degeest, G., Geeraerts, A., Ivarsson, Y., Depoortere, F., Coomans, C., Vermeiren, E., et al. (2012) Syndecan-syntenin-ALIX regulates the biogenesis of exosomes. *Nat. Cell Biol.* **14**, 677–685

Bobrie, A., Colombo, M., Raposo, G. and Thery, C. (2011) Exosome secretion: molecular mechanisms and roles in immune responses. *Traffic* **12**, 1659–1668

Bryant, R.J., Pawlowski, T., Catto, J.W., Marsden, G., Vessella, R.L., Rhees, B., Kuslich, C., Visakorpi, T. and Hamdy, F.C. (2012) Changes in circulating microRNA levels associated with prostate cancer. *Br J Cancer* **106**, 768–774

Burdach, S., Plehm, S., Unland, R., Dirksen, U., Borkhardt, A., Staeghe, M.S., Muller-Tidow, C. and Richter, G.H. (2009) Epigenetic maintenance of stemness and malignancy in peripheral neuroectodermal tumors by EZH2. *Cell Cycle* **8**, 1991–1996

Chang, C.J. and Hung, M.C. (2012) The role of EZH2 in tumour progression. *Br J Cancer* **106**, 243–247

Chaput, N. and Thery, C. (2011) Exosomes: immune properties and potential clinical implementations. *Semin Immunopathol* **33**, 419–440

Cheung, I.Y., Feng, Y., Danis, K., Shukla, N., Meyers, P., Ladanyi, M. and Cheung, N.K. (2007) Novel markers of subclinical disease for Ewing family tumors from gene expression profiling. *Clin Cancer Res* **13**, 6978–6983

Cotterill, S.J., Ahrens, S., Paulussen, M., Jurgens, H.F., Voute, P.A., Gadner, H. and Craft, A.W. (2000) Prognostic factors in Ewing's tumor of bone: analysis of 975 patients from the European Intergroup Cooperative Ewing's Sarcoma Study Group. *J Clin Oncol* **18**, 3108–3114

Delattre, O., Zucman, J., Melot, T., Garau, X.S., Zucker, J.M., Lenoir, G.M., Ambros, P.F., Sheer, D., Turc-Carel, C., Triche, T.J., et al. (1994) The Ewing family of tumors—a subgroup of small-round-cell tumors defined by specific chimeric transcripts. *New Engl J Med* **331**, 294–299

Diehl, J.A. (2002) Cycling to cancer with cyclin D1. *Cancer Biol Ther* **1**, 226–231

Duijvesz, D., Luider, T., Bangma, C.H. and Jenster, G. (2011) Exosomes as biomarker treasure chests for prostate cancer. *Eur Urol* **59**, 823–831

Eldh, M., Lotvall, J., Malmhall, C. and Ekstrom, K. (2012) Importance of RNA isolation methods for analysis of exosomal RNA: evaluation of different methods. *Mol Immunol* **50**, 278–286

Escola, J.M., Kleijmeer, M.J., Stoorvogel, W., Griffith, J.M., Yoshie, O. and Geuze, H.J. (1998) Selective enrichment of tetraspan proteins on the internal vesicles of multivesicular endosomes and on exosomes secreted by human B-lymphocytes. *J Biol Chem* **273**, 20121–20127

Garcia-Aragoncillo, E., Carrillo, J., Lalli, E., Agra, N., Gomez-Lopez, G., Pestana, A. and Alonso, J. (2008) DAX1, a direct target of EWS/FLI1 oncoprotein, is a principal regulator of cell-cycle progression in Ewing's tumor cells. *Oncogene* **27**, 6034–6043

Ge, X., Yamamoto, S., Tsutsumi, S., Midorikawa, Y., Ihara, S., Wang, S.M. and Aburatani, H. (2005) Interpreting expression profiles of cancers by genome-wide survey of breadth of expression in normal tissues. *Genomics* **86**, 127–141

Grunewald, T.G., Bach, H., Cossarizza, A. and Matsumoto, I. (2012a) The STEAP protein family: versatile oxidoreductases and targets for cancer immunotherapy with overlapping and distinct cellular functions. *Biol Cell* **104**, 641–657

Grunewald, T.G., Diebold, I., Esposito, I., Plehm, S., Hauer, K., Thiel, U., da Silva-Buttkus, P., Neff, F., Unland, R., Muller-Tidow, C., et al. (2012b) STEAP1 is associated with the invasive and oxidative stress phenotype of Ewing tumors. *Mol Cancer Res* **10**, 52–65

Grunewald, T.G., Ranft, A., Esposito, I., da Silva-Buttkus, P., Aichler, M., Baumhoer, D., Schaefer, K.L., Ottaviano, L., Porembski, C., Jundt, G., et al. (2012c) High STEAP1 expression is associated with improved outcome of Ewing's sarcoma patients. *Ann Oncol* **23**, 2185–2190

Gu, J., Qian, H., Shen, L., Zhang, X., Zhu, W., Huang, L., Yan, Y., Mao, F., Zhao, C., Shi, Y., et al. (2012) Gastric cancer exosomes trigger differentiation of umbilical cord derived mesenchymal stem cells to carcinoma-associated fibroblasts through TGF-beta/Smad pathway. *PLoS ONE* **7**, e52465

Hood, J.L., San, R.S. and Wickline, S.A. (2011) Exosomes released by melanoma cells prepare sentinel lymph nodes for tumor metastasis. *Cancer Res.* **71**, 3792–3801

James, K., Eisenhauer, E., Christian, M., Terenziani, M., Vena, D., Muldal, A. and Therasse, P. (1999) Measuring response in solid tumors: unidimensional versus bidimensional measurement. *J Natl Cancer Inst* **91**, 523–528

Keller, S., Konig, A.K., Marme, F., Runz, S., Wolterink, S., Koensgen, D., Mustea, A., Sehouli, J. and Altevogt, P. (2009) Systemic presence and tumor-growth promoting effect of ovarian carcinoma released exosomes. *Cancer Lett* **278**, 73–81

Keller, S., Ridinger, J., Rupp, A.K., Janssen, J.W. and Altevogt, P. (2011) Body fluid derived exosomes as a novel template for clinical diagnostics. *J Transl Med* **9**, 86

Kinsey, M., Smith, R. and Lessnick, S.L. (2006). NR0B1 is required for the oncogenic phenotype mediated by EWS/FLI in Ewing's sarcoma. *Mol Cancer Res* **4**, 851–859

Logozzi, M., De Milito, A., Lugini, L., Borghi, M., Calabro, L., Spada, M., Perdicchio, M., Marino, M.L., Federici, C., Iessi, E., et al. (2009). High levels of exosomes expressing CD63 and caveolin-1 in plasma of melanoma patients. *PLoS ONE* **4**, e5219

Luga, V., Zhang, L., Viloria-Petit, A.M., Ogunjimi, A.A., Inanlou, M.R., Chiu, E., Buchanan, M., Hosein, A.N., Basik, M. and Wrana, J.L. (2012). Exosomes mediate stromal mobilization of autocrine Wnt-PCP signaling in breast cancer cell migration. *Cell* **151**, 1542–1556

May, W.A., Gishizky, M.L., Lessnick, S.L., Lunsford, L.B., Lewis, B.C., Delattre, O., Zucman, J., Thomas, G. and Denny, C.T. (1993). Ewing sarcoma 11;22 translocation produces a chimeric transcription factor that requires the DNA-binding domain encoded by FLI1 for transformation. *Proc Natl Acad Sci U.S.A.* **90**, 5752–5756

Michelet, X., Djeddi, A. and Legouis, R. (2010). Developmental and cellular functions of the ESCRT machinery in pluricellular organisms. *Biol Cell* **102**, 191–202

Mikkelsen, T.S., Hanna, J., Zhang, X., Ku, M., Wernig, M., Schorderet, P., Bernstein, B.E., Jaenisch, R., Lander, E.S. and Meissner, A. (2008). Dissecting direct reprogramming through integrative genomic analysis. *Nature* **454**, 49–55

Minogue, S. and Waugh, M.G. (2012). Lipid rafts, microdomain heterogeneity and inter-organelle contacts: impacts on membrane preparation for proteomic studies. *Biol. Cell* **104**, 618–627

Nakamura, N. (2010). Emerging new roles of GM130, a cis-Golgi matrix protein, in higher order cell functions. *J Pharmacol Sci* **112**, 255–264

Nazarenko, I., Rana, S., Baumann, A., McAlear, J., Hellwig, A., Tredelenburg, M., Lochnit, G., Preissner, K.T. and Zoller, M. (2010). Cell surface tetraspanin Tspan8 contributes to molecular pathways of exosome-induced endothelial cell activation. *Cancer Res* **70**, 1668–1678

Noerholm, M., Balaj, L., Limperg, T., Salehi, A., Zhu, L.D., Hochberg, F.H., Breakefield, X.O., Carter, B.S. and Skog, J. (2012). RNA expression patterns in serum microvesicles from patients with glioblastoma multiforme and controls. *BMC Cancer* **12**, 22

Pant, S., Hilton, H. and Burczynski, M.E. (2012). The multifaceted exosome: biogenesis, role in normal and aberrant cellular function and frontiers for pharmacological and biomarker opportunities. *Biochem Pharmacol* **83**, 1484–1494

Peinado, H., Aleckovic, M., Lavotshkin, S., Matei, I., Costa-Silva, B., Moreno-Bueno, G., Hergueta-Redondo, M., Williams, C., Garcia-Santos, G., Ghajar, C., et al. (2012). Melanoma exosomes educate bone marrow progenitor cells toward a pro-metastatic phenotype through MET. *Nat Med* **18**, 883–891

Postel-Vinay, S., Véron, A.S., Tirode, F., Pierron, G., Reynaud, S., Kovar, H., Oberlin, O., Lapoule, E., Ballet, S., Lucchesi, C., et al. (2012). Common variants near TARDBP and EGR2 are associated with susceptibility to Ewing sarcoma. *Nat Genet* **44**, 323–327

Rabinowitz, G., Gercel-Taylor, C., Day, J.M., Taylor, D.D. and Kloecker, G.H. (2009). Exosomal microRNA: a diagnostic marker for lung cancer. *Clin Lung Cancer* **10**, 42–46

Rana, S. and Zoller, M. (2011). Exosome target cell selection and the importance of exosomal tetraspanins: a hypothesis. *Biochem Soc Trans* **39**, 559–562

Raposo, G., Nijman, H.W., Stoorvogel, W., Liejendecker, R., Harding, C.V., Melief, C.J. and Geuze, H.J. (1996). B lymphocytes secrete antigen-presenting vesicles. *J Exp Med* **183**, 1161–1172

Reddi, K.K. and Holland, J.F. (1976). Elevated serum ribonuclease in patients with pancreatic cancer. *Proc Natl Acad Sci U.S.A.* **73**, 2308–2310

Revet, I., Huizinga, G., Koster, J., Volckmann, R., van Sluis, P., Versteeg, R. and Geerts, D. (2010). MSX1 induces the Wnt pathway antagonist genes DKK1, DKK2, DKK3 and SFRP1 in neuroblastoma cells, but does not block Wnt3 and Wnt5A signalling to DVL3. *Cancer Lett* **289**, 195–207

Richter, G.H., Plehn, S., Fasan, A., Rossler, S., Unland, R., Bennani-Baiti, I.M., Hotfilder, M., Lowel, D., von Luettichau, I., Mossbrugger, I., et al. (2009). EZH2 is a mediator of EWS/FLI1 driven tumor growth and metastasis blocking endothelial and neuro-ectodermal differentiation. *Proc Natl Acad Sci U.S.A.* **106**, 5324–5329

Roth, R.B., Hevez, P., Lee, J., Willhite, D., Lechner, S.M., Foster, A.C. and Zlotnik, A. (2006). Gene expression analyses reveal molecular relationships among 20 regions of the human CNS. *Neurogenetics* **7**, 67–80

Savola, S., Klami, A., Myllykangas, S., Manara, C., Scotlandi, K., Picci, P., Knuutila, S. and Vakkila, J. (2011). High expression of complement component 5 (C5) at tumor site associates with superior survival in ewing's sarcoma family of tumour patients. *ISRN Oncol* **2011**, 168712

Schaefer, K.L., Eisenacher, M., Braun, Y., Brachwitz, K., Wai, D.H., Dirksen, U., Lanvers-Kaminsky, C., Juergens, H., Herrero, D., Stegmaier, S., et al. (2008). Microarray analysis of Ewing's sarcoma family of tumours reveals characteristic gene expression signatures associated with metastasis and resistance to chemotherapy. *Eur J Cancer* **44**, 699–709

Schmiedel, B.J., Hutter, C., Hesse, M. and Staege, M.S. (2011). Expression of multiple membrane-associated phospholipase A1 beta transcript variants and lysophosphatidic acid receptors in Ewing tumor cells. *Mol Biol Rep* **38**, 4619–4628

Scotlandi, K., Remondini, D., Castellani, G., Manara, M.C., Nardi, F., Cantiani, L., Francesconi, M., Mercuri, M., Caccuri, A.M., Serra, M., et al. (2009). Overcoming resistance to conventional drugs in Ewing sarcoma and identification of molecular predictors of outcome. *J Clin Oncol* **27**, 2209–2216

Skog, J., Wurdinger, T., van Rijn, S., Meijer, D.H., Gainche, L., Sena-Esteves, M., Curry, W.T., Jr., Carter, B.S., Krichevsky, A.M. and Breakefield, X.O. (2008). Glioblastoma microvesicles transport RNA and proteins that promote tumour growth and provide diagnostic biomarkers. *Nat Cell Biol* **10**, 1470–1476

Smith, R., Owen, L.A., Trem, D.J., Wong, J.S., Whangbo, J.S., Golub, T.R. and Lessnick, S.L. (2006). Expression profiling of EWS/FLI identifies NKX2.2 as a critical target gene in Ewing's sarcoma. *Cancer Cell* **9**, 405–416

Staege, M.S., Hutter, C., Neumann, I., Foja, S., Hattenhorst, U.E., Hansen, G., Afar, D. and Burdach, S.E. (2004). DNA microarrays reveal relationship of Ewing family tumors to both endothelial and fetal neural crest-derived cells and define novel targets. *Cancer Res* **64**, 8213–8221

Svensson, K.J., Kucharzewska, P., Christianson, H.C., Skold, S., Lofstedt, T., Johansson, M.C., Morgen, M., Bengzon, J., Ruf, W. and Belting, M. (2011). Hypoxia triggers a proangiogenic pathway involving cancer cell microvesicles and PAR-2-mediated heparin-binding EGF signaling in endothelial cells. *Proc Natl Acad Sci U.S.A.* **108**, 13147–13152

Thery, C., Amigorena, S., Raposo, G. and Clayton, A. (2006). Isolation and characterization of exosomes from cell culture supernatants and biological fluids. *Curr Protoc Cell Biol*. Chapter 3, 30:3.22.1–3.22.29, John Wiley & Sons, Hoboken.

Tirode, F., Laud-Duval, K., Prieur, A., Delorme, B., Charbord, P. and Delattre, O. (2007). Mesenchymal stem cell features of Ewing tumors. *Cancer Cell* **11**, 421–429

Toomey, E.C., Schiffman, J.D. and Lessnick, S.L. (2010). Recent advances in the molecular pathogenesis of Ewing's sarcoma. *Oncogene* **29**, 4504–4516

Tsui, N.B., Ng, E.K. and Lo, Y.M. (2002). Stability of endogenous and added RNA in blood specimens, serum and plasma. *Clin Chem* **48**, 1647–1653

Umezawa, T., Ohyashiki, K., Kuroda, M. and Ohyashiki, J.H. (2012). Leukemia cell to endothelial cell communication via exosomal miRNAs. *Oncogene*, doi:10.1038/onc.2012.295

Valadi, H., Ekstrom, K., Bossios, A., Sjostrand, M., Lee, J.J. and Lotvall, J.O. (2007). Exosome-mediated transfer of mRNAs and microRNAs is a novel mechanism of genetic exchange between cells. *Nat Cell Biol* **9**, 654–659

Vermeulen, J., Ballet, S., Oberlin, O., Peter, M., Pierron, G., Longavenne, E., Laurence, V., Kanold, J., Chastagner, P., Lejars, O., et al. (2006). Incidence and prognostic value of tumour cells detected by RT-PCR in peripheral blood stem cell collections from patients with Ewing tumour. *Br J Cancer* **95**, 1326–1333

von Levetzow, C., Jiang, X., Gwyne, Y., von Levetzow, G., Hung, L., Cooper, A., Hsu, J.H. and Lawlor, E.R. (2011). Modeling initiation of Ewing sarcoma in human neural crest cells. *PLoS ONE* **6**, e19305

Williams, D.B. (2006). Beyond lectins: the calnexin/calreticulin chaperone system of the endoplasmic reticulum. *J Cell Sci* **119**, 615–623

Willier, S., Butt, E., Richter, G.H., Burdach, S. and Grunewald, T.G. (2011). Defining the role of TRIP6 in cell physiology and cancer. *Biol Cell* **103**, 573–591

Yoshida, A., Sekine, S., Tsuta, K., Fukayama, M., Furuta, K. and Tsuda, H. (2012). NKK2.2 is a useful immunohistochemical marker for Ewing sarcoma. *Am J Surg Pathol* **36**, 993–999

Received: 2 December 2012; Accepted: 19 March 2013; Accepted article online: 22 March 2013

Robust diagnosis of Ewing sarcoma by immunohistochemical detection of super-enhancer-driven EWSR1-ETS targets

Michaela C. Baldauf^{1,*}, Martin F. Orth^{1,*}, Marlene Dallmayer^{1,*}, Aruna Marchetto¹, Julia S. Gerke¹, Rebeca Alba Rubio¹, Merve M. Kiran², Julian Musa¹, Maximilian M. L. Knott¹, Shunya Ohmura¹, Jing Li¹, Nusret Akpolat³, Ayse N. Akatli³, Özlem Özgen⁴, Uta Dirksen⁵, Wolfgang Hartmann⁶, Enrique de Alava⁷, Daniel Baumhoer⁸, Giuseppina Sannino¹, Thomas Kirchner^{9,10,11} and Thomas G. P. Grünwald^{1,9,10,11}

¹ Max-Eder Research Group for Pediatric Sarcoma Biology, Institute of Pathology, Faculty of Medicine, LMU Munich, Munich, Germany

² Department of Pathology, Medical Faculty, Ankara Yildirim Beyazit University, Ankara, Turkey

³ Department of Pathology, Turgut Ozal Medical Center, Inonu University, Malatya, Turkey

⁴ Department of Pathology, Başkent University Hospital, Ankara, Turkey

⁵ Department of Pediatric Hematology and Oncology, University Hospital Essen, Essen, Germany

⁶ Gerhard-Domagk-Institute for Pathology, University Hospital Münster, Westfalian Wilhelms University, Münster, Germany

⁷ Institute of Biomedicine of Seville (IBiS), Hospital Universitario Virgen del Rocío/CSIC/Universidad de Sevilla, CIBERONC, Seville, Spain

⁸ Bone Tumour Reference Center, Institute of Pathology, University Hospital Basel, University of Basel, Switzerland

⁹ Institute of Pathology, Faculty of Medicine, LMU Munich, Munich, Germany

¹⁰ German Cancer Consortium (DKTK), Heidelberg, Germany

¹¹ German Cancer Research Center (DKFZ), Heidelberg, Germany

* These authors have contributed equally to this work

Correspondence to: Thomas G. P. Grünwald, **email:** thomas.gruenwald@med.uni-muenchen.de

Keywords: Ewing sarcoma, Ewing-like sarcoma, immunohistochemistry, BCL11B, GLG1

Received: July 18, 2017

Accepted: July 23, 2017

Published: August 04, 2017

Copyright: Baldauf et al. This is an open-access article distributed under the terms of the Creative Commons Attribution License 3.0 (CC BY 3.0), which permits unrestricted use, distribution, and reproduction in any medium, provided the original author and source are credited.

ABSTRACT

Ewing sarcoma is an undifferentiated small-round-cell sarcoma. Although molecular detection of pathognomonic EWSR1-ETS fusions such as EWSR1-FLI1 enables definitive diagnosis, substantial confusion can arise if molecular diagnostics are unavailable. Diagnosis based on the conventional immunohistochemical marker CD99 is unreliable due to its abundant expression in morphological mimics.

To identify novel diagnostic immunohistochemical markers for Ewing sarcoma, we performed comparative expression analyses in 768 tumors representing 21 entities including Ewing-like sarcomas, which confirmed that CIC-DUX4-, BCOR-CCNB3-, EWSR1-NFATc2-, and EWSR1-ETS-translocated sarcomas are distinct entities, and revealed that ATP1A1, BCL11B, and GLG1 constitute specific markers for Ewing sarcoma. Their high expression was validated by immunohistochemistry and proved to depend on EWSR1-FLI1-binding to highly active proximal super-enhancers. Automated cut-off-finding and combination-testing in a tissue-microarray comprising 174 samples demonstrated that detection of high BCL11B and/or GLG1 expression is sufficient to reach 96% specificity for Ewing sarcoma. While 88% of tested Ewing-like sarcomas displayed strong CD99-immunoreactivity, none displayed combined strong BCL11B- and GLG1-immunoreactivity.

Collectively, we show that ATP1A1, BCL11B, and GLG1 are EWSR1-FLI1 targets, of which BCL11B and GLG1 offer a fast, simple, and cost-efficient way to diagnose

Ewing sarcoma by immunohistochemistry. These markers may significantly reduce the number of misdiagnosed patients, and thus improve patient care.

INTRODUCTION

Ewing sarcoma is characterized by the presence of chimeric *EWSR1-ETS* fusion oncogenes [1]. Before the discovery of this unifying genetic hallmark, diagnosing Ewing sarcoma definitively was challenging [2] as Ewing sarcoma tumors are largely composed of undifferentiated cells displaying a small-round-cell phenotype [3, 4]. This phenotype is shared by many other tumor entities such as rhabdomyosarcoma and neuroblastoma [5]. Recently, several so-called Ewing-like sarcoma subtypes have been identified [6-9]. These tumors are characterized by distinct fusion oncogenes and transcriptomic signatures [6-12], as well as (most likely) by distinct clinical behavior [6, 12, 13].

Although Ewing sarcoma can usually be reliably distinguished from its morphological mimics by cytogenetic and molecular genetic analyses [14, 15], there is currently no robust biomarker available for routine histology. Substantial diagnostic confusion can arise because sophisticated cytogenetic and molecular diagnostic techniques are not universally available or too expensive for some diagnostic facilities (particularly in developing countries). While the widely used immunohistochemical biomarker CD99 shows high sensitivity for Ewing sarcoma, its low specificity and high expression in morphological mimics such as CIC- and BCOR-rearranged sarcomas, as well as in certain lymphoma subtypes and poorly differentiated synovial sarcoma, are problematic [3, 11-13, 16-18]. Thus, CD99 alone is unreliable to definitively diagnose Ewing sarcoma. Other studies identified auxiliary markers such as NKX2-2 and FLI1, which may help in some cases [19, 20]. However, a systematic and agnostic transcriptome-wide screen for auxiliary markers and testing of their value when used in combination has not been done so far. In the current study, comparative expression analyses revealed that *ATPIA1*, *BCL11B*, and *GLG1* constitute potential specific markers for Ewing sarcoma. Expression of these genes appeared to be induced by *EWSR1-FLI1*-bound super-enhancers, which showed high activity in reporter assays. Specific immunohistochemical staining of these proteins in comprehensive tissue microarrays (TMAs) combined with automated cut-off determination and combination-testing demonstrated that detecting high *BCL11B* and/or *GLG1* levels is sufficient to reach 96% specificity for Ewing sarcoma. In fact, these markers were extremely effective at discriminating Ewing sarcoma from Ewing-like sarcomas.

Hence, these results provide a fast, simple and cost-efficient means of diagnosing Ewing sarcoma by

immunohistochemistry (IHC), which is a considerable advantage for diagnostic facilities where molecular diagnostics are not available. This finding may significantly reduce the number of misdiagnosed patients and thus improve patient care.

RESULTS

ATPIA1, *BCL11B*, and *GLG1* are strongly overexpressed in Ewing sarcoma compared to tumor entities of differential diagnostic relevance

To identify highly specific diagnostic markers for Ewing sarcoma, we retrieved publicly available microarray gene expression data comprising genetically confirmed *EWSR1-ETS*-translocated Ewing sarcomas [21], 20 additional tumor entities of potential differential diagnostic relevance [5], and 71 normal tissue types. The set of morphological mimics also comprised *CIC-DUX4*-, *BCOR-CCNB3*-, and *EWSR1-NFATc2*-translocated sarcomas, which proved to be distinct entities as determined by unsupervised principal component analysis (PCA) (Supplementary Figure 1).

We then proceeded to perform comparative expression analysis on the entire dataset: Based on these microarray expression data the median expression of every gene represented on the Affymetrix HG-U133Plus2 microarray was determined. Next, we calculated the expression ratio (ER) for every gene based on its median expression in pairwise comparisons of Ewing sarcoma and the remaining tumor entities. Only genes, which were strongly overexpressed in Ewing sarcoma compared to all other tumor entities defined by a minimal log2-transformed ER of > 2 , were considered as diagnostically relevant. Of the 19,702 genes represented on the microarray platform, 51 had an ER of > 2 across all tested tumor entities. In parallel, the level of significance of the differential expression of all genes in pairwise comparisons of Ewing sarcoma relative to all other tumor entities was calculated. Only 10 genes exhibited a Bonferroni-corrected *P* value < 0.05 (Figure 1a, 1b). Next, both gene lists were crossed, which showed that only 3 genes, termed *ATPIA1* (ATPase Na^+/K^+ transporting subunit alpha1), *BCL11B* (B-cell CLL/lymphoma 11B), and *GLG1* (Golgi glycoprotein 1) were both strongly and highly significantly overexpressed in Ewing sarcoma compared to all other tumor entities (Figure 1b).

Then, the expression profiles of these three candidate biomarkers were compared to the conventional

Table 1: Composition of the TMA

| Entity | <i>n</i> |
|--------------------------------|------------|
| Ewing sarcoma | 47 |
| Alveolar Soft Part Sarcoma | 3 |
| Ewing-like sarcoma | 17 |
| Ganglioneuroblastoma | 7 |
| Leiomyosarcoma | 5 |
| Liposarcoma | 19 |
| Malignant Fibrous Histiocytoma | 3 |
| Nephroblastoma | 21 |
| Neuroblastoma | 16 |
| Osteosarcoma | 15 |
| Rhabdomyosarcoma | 11 |
| Synovial sarcoma | 10 |
| n total: | 174 |

Ewing sarcoma marker *CD99* across all tumor entities. While *CD99* showed broad expression in many different tumor entities, *ATP1A1*, *BCL11B*, and *GLG1* were only expressed at low levels in every tumor entity relative to Ewing sarcoma, indicating a higher specificity for this disease than *CD99* (Figure 1c).

Because commixture of tumor tissue with normal cells, which could express the three markers, could complicate immunohistochemical evaluation, we explored the expression levels of *ATP1A1*, *BCL11B*, and *GLG1* and that of *CD99* in Ewing sarcoma samples relative to 71 normal tissue types comprising 998 samples. As displayed in Supplementary Figure 2, *ATP1A1*, *BCL11B*, and *GLG1* were only lowly expressed in some normal tissue types, while *CD99* was rather broadly expressed across many normal tissue types. In fact, our three markers, except for *BCL11B* in thymus, were statistically significantly higher ($P < 0.05$) expressed in Ewing sarcoma as compared to any tested normal tissue type.

EWSR1-FLI1 induces *ATP1A1*, *BCL11B*, and *GLG1* expression by binding to GGAA-microsatellites found in super-enhancers

The specific expression of the three candidate biomarkers in primary Ewing sarcoma suggests a possible regulatory relationship between them and EWSR1-FLI1. In fact, *ATP1A1* and *GLG1* were previously shown to be upregulated after ectopic expression of *EWSR1-FLI1* in the rhabdomyosarcoma cell line RD [22]. Moreover, *BCL11B* was shown to be upregulated by EWSR1-FLI1 in Ewing sarcoma cell lines [23].

To further explore this regulatory relationship, available gene expression data were assessed, which showed that the ectopic EWSR1-FLI1 expression in

embryonic stem cells was sufficient to significantly induce the expression of *ATP1A1*, *BCL11B*, and *GLG1* (Figure 2a). Conversely, the shRNA-mediated knockdown of EWSR1-FLI1 in six different Ewing sarcoma cell lines significantly decreased their expression levels (Figure 2b). Such consistent EWSR1-FLI1-dependent regulation was not observed for *CD99* (Figure 2a, 2b).

These data in cell lines suggested that *ATP1A1*, *BCL11B*, and *GLG1* may be direct EWSR1-FLI1 target genes. Testing this hypothesis involved analyzing available ChIP-Seq and DNase-Seq data generated in Ewing sarcoma cell lines, which showed strong EWSR1-FLI1-binding to GGAA-microsatellites close to these genes. Notably, these GGAA-microsatellites exhibit characteristics of active EWSR1-FLI1-dependent enhancers (Figure 3a). In fact, EWSR1-FLI1 is known to convert non-functional GGAA-microsatellites into potent enhancers to steer a large proportion of its target genes [24-26]. Strong EWSR1-FLI1-dependent enhancer activity of these GGAA-microsatellites in luciferase reporter assays was consistently observed (Figure 3b). In agreement with previous observations [27], these EWSR1-FLI1-dependent enhancers showed the typical H3K27ac profile of so-called super-enhancers in the A673 and SK-N-MC Ewing sarcoma cell lines (Figure 3c, Supplementary Tables 1 & 2). Super-enhancers are often found near genes that have cell type-specific functions and contribute to cell identity [28, 29]. In addition to these findings *in vitro*, gene-set enrichment analyses of either *ATP1A1*-, *BCL11B*-, or *GLG1*-correlated genes within 166 primary Ewing sarcoma tumors revealed that the most significantly (min. NES = 3.08, $P < 0.001$, $q < 0.001$) associated gene expression signature among the 3,687 tested was for each candidate marker ‘ZHANG_TARGETS_OF_EWSR1-FLI1_FUSION’ [22] (Supplementary Table 3). Consistent with the previous finding that EWSR1-FLI1 and EWSR1-

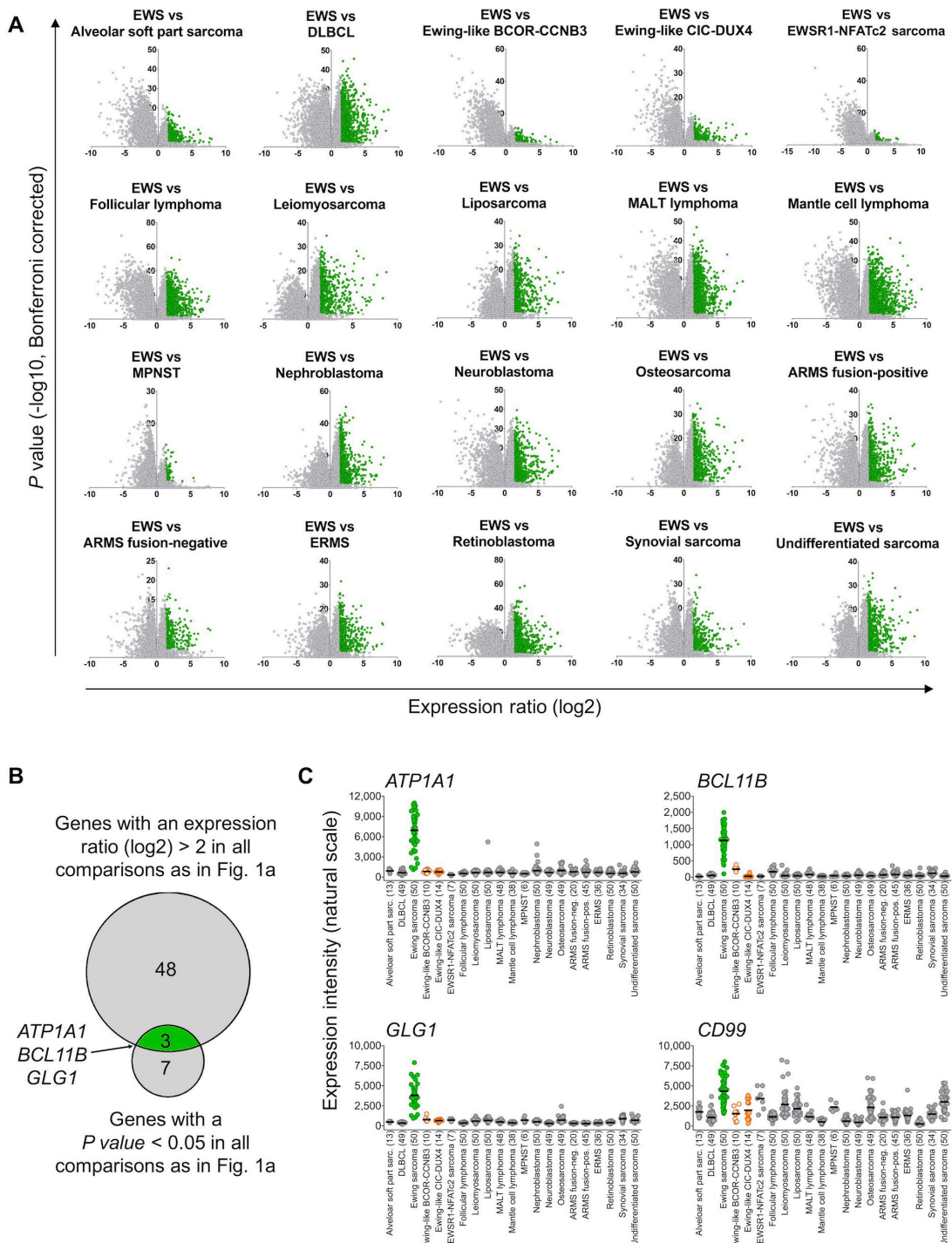


Figure 1: ATP1A1, BCL11B, and GLG1 are strongly overexpressed in Ewing sarcoma compared to tumor entities of differential diagnostic relevance. A. A. Volcano plots of pairwise comparison of gene expression in Ewing sarcoma (EWS) and indicated tumor entities. Diffuse large B-cell lymphoma (DLBCL); mucosa-associated lymphoid tissue (MALT) lymphoma; malignant peripheral nerve sheath tumor (MPNST); alveolar rhabdomyosarcoma (ARMS); and embryonal rhabdomyosarcoma (ERMS). Genes represented in green color had an expression ratio > 2 (log2) and a *P* value < 0.05 (Bonferroni-corrected). **B.** B. Size-proportional Venn diagram showing the overlap of genes differentially and significantly (minimal log2 expression ratio > 2; *P* value < 0.05, Bonferroni corrected) overexpressed in Ewing sarcoma relative to all other tumor entities given in A and C. **C.** C. Scatter dot plot depicting gene expression levels of *ATP1A1*, *BCL11B*, *GLG1*, and *CD99* as determined by Affymetrix HG-U133Plus2.0 microarrays in primary tumors of 21 different entities. Ewing sarcoma is highlighted in green, Ewing-like sarcomas (*CIC-DUX4* or *BCOR-CCNB3* translocation positive) are highlighted in orange. Horizontal bars represent median expression levels. The number of analyzed samples is given in parentheses.

ERG bind to highly similar DNA-motifs [30], all three genes are similarly highly expressed in Ewing sarcoma cell lines regardless of the specific *EWSR1-ETS* status (Supplementary Figure 3). Collectively, these data strongly suggest that *ATP1A1*, *BCL11B*, and *GLG1* are direct *EWSR1-ETS* target genes.

***ATP1A1* and *GLG1* may have prognostic relevance in Ewing sarcoma**

To explore the potential of *ATP1A1*, *BCL11B*, *GLG1*, and *CD99* as prognostic biomarkers, we analyzed the association of their expression levels with outcome in a

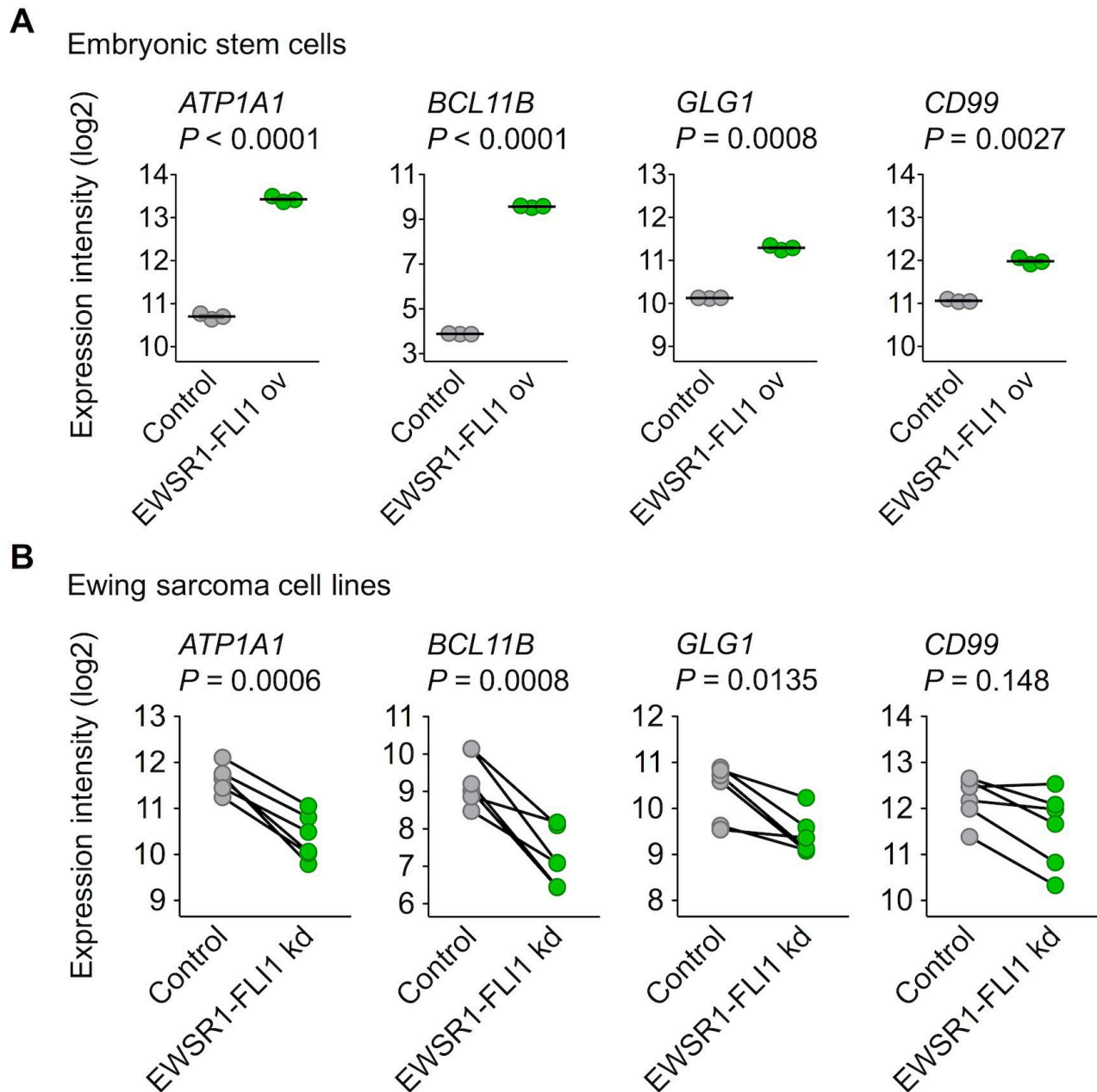


Figure 2: EWSR1-FLI1 is sufficient to induce *ATP1A1*, *BCL11B*, and *GLG1* expression. **A.** Analysis of gene expression levels of *ATP1A1*, *BCL11B*, *GLG1* and *CD99* by Affymetrix HG-U133Plus2.0 microarrays in human embryonic stem cells after ectopic expression of EWSR1-FLI1 (GSE64686). Bars represent the medians. Two-tailed student's *t* test. **B.** Analysis of gene expression levels of *ATP1A1*, *BCL11B*, *GLG1* and *CD99* by Affymetrix HG-U133A microarrays 96 h after short hairpin RNA-mediated knockdown of EWSR1-FLI1 in six different Ewing sarcoma cell lines (GSE14543 and GSE27524). Data are represented as before-after plots in which each dot represents a cell line. Two-tailed student's *t* test.

large cohort of Ewing sarcoma patients ($n = 166$). Whereas higher *ATP1A1* and *GLG1* expression levels showed a

significant correlation with better patient outcome ($P = 0.006$ and $P = 0.0028$, respectively), *BCL11B* and *CD99*

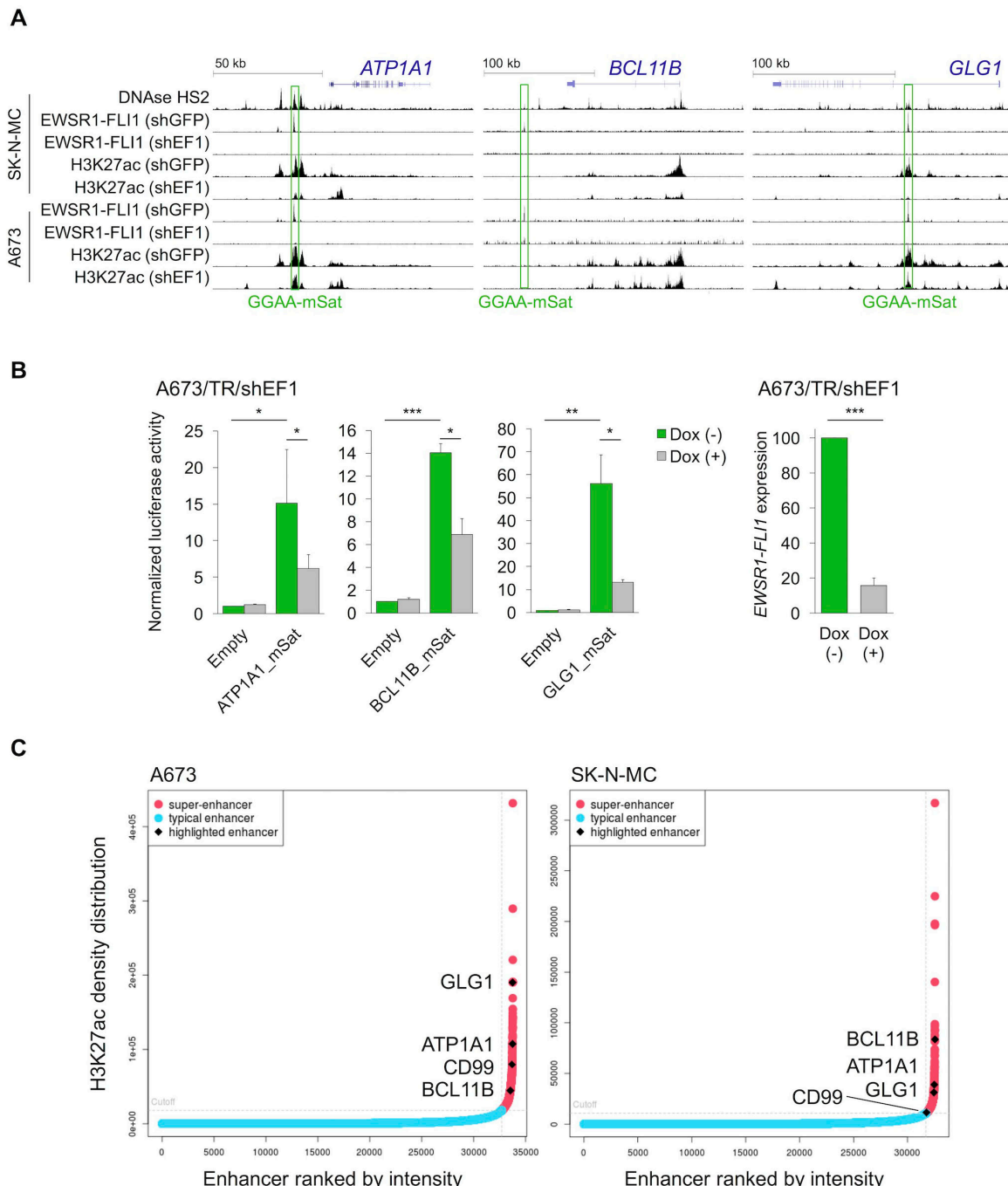


Figure 3: EWSR1-FLI1 binds to GGAA-microsatellites with enhancer activity located close to or within the *ATP1A1*, *BCL11B*, or *GLG1* gene. **A.** Published DNase-Seq and ChIP-Seq data generated in Ewing sarcoma cell lines were displayed in the UCSC genome browser. shGFP, control; shEF1, shEWSR1-FLI1. GGAA-mSat, GGAA-microsatellite. **B.** Luciferase reporter assays in A673/TR/shEF1 cells containing a doxycycline (Dox)-inducible shRNA against EWSR1-FLI1 confirmed the EWSR1-FLI1-dependent enhancer activity of cloned GGAA-microsatellites (1 kb fragments). EWSR1-FLI1 knockdown was confirmed by qRT-PCR 72 h after shRNA induction. Data are presented as mean and SEM of $n = 3$ independent experiments. Two-tailed student's *t*-test. * $P < 0.05$; ** $P < 0.01$; *** $P < 0.001$. **C.** Genome-wide analysis of published H3K27ac profiles of A673 and SK-N-MC Ewing sarcoma cell lines (GSE61944) identified super-enhancers proximal to *ATP1A1*, *BCL11B*, *GLG1*, and *CD99*. Enhancers are ranked by their H3K27ac density.

expression levels did not (Supplementary Figure 4).

High expression of BCL11B and/or GLG1 is sufficient to robustly diagnose Ewing sarcoma by IHC

To confirm the overexpression of ATP1A1, BCL11B, and GLG1 on the protein level, a comprehensive TMA

including many solid tumor entities closely resembling Ewing sarcoma and other sarcoma entities was generated (Table 1). Immunohistochemical staining of the TMAs was carried out with anti-ATP1A1, anti-BCL11B, anti-GLG1 and anti-CD99 antibodies, and immunoreactivity scores (IRS) were determined in analogy to the Remmle and Stegner [31] scoring system (IRS range from 0 to 12; Figure 4a, 4b). As displayed in Figure 4b, CD99 expression was not very specific for Ewing sarcoma

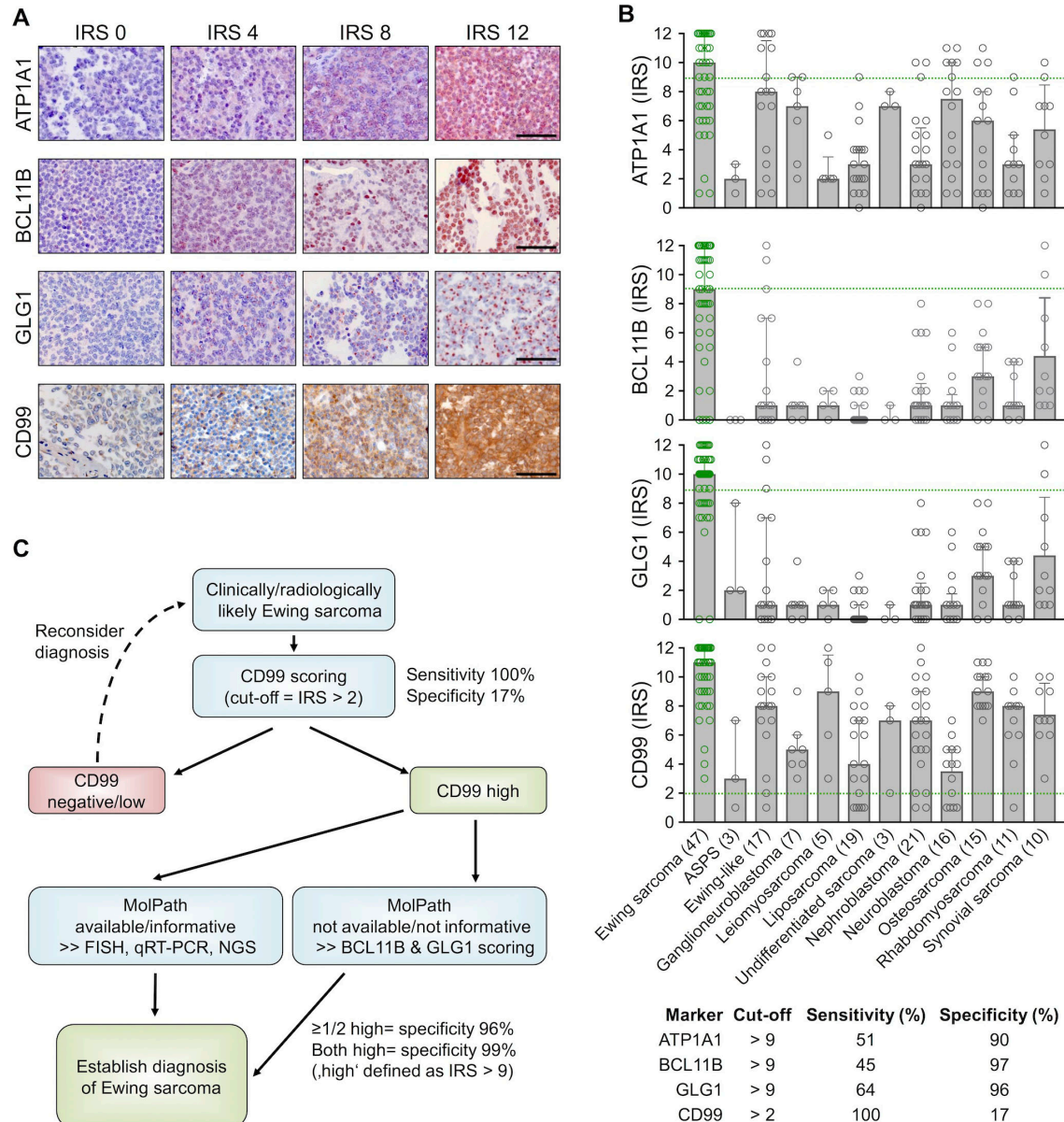


Figure 4: High expression of BCL11B and/or GLG1 is sufficient to robustly diagnose Ewing sarcoma by IHC. A. Representative IHC images for the indicated marker. ATP1A1 is expressed in the cytoplasm, BCL11B in the nucleus, GLG1 at the perinuclear Golgi apparatus, and CD99 at the membrane. Scale bars = 100 μ m. For ATP1A1, BCL11B, and GLG1 a red and for CD99 a brown chromogen was used. B. Scatter dot plots of the individual IRS for the indicated marker. The number of analyzed samples is given in parentheses. Bars represent mean IRS values, whiskers indicate the 95%-CI. Green dashed lines indicate the cut-offs to define sensitivity and specificity for detecting Ewing sarcoma as given in the table below. ASPS: alveolar soft part sarcoma. C. Proposed work-flow for establishing robust diagnosis of Ewing sarcoma.

compared to other sarcoma entities as well as Ewing-like sarcomas. However, CD99 reached 100% sensitivity for Ewing sarcoma in this TMA when applying a cut-off of IRS > 2. Compared to CD99, the three candidate markers were all less sensitive at any given cut-off, but much more specific (specificity 90 - 97%) when being highly expressed (defined as IRS > 9) (Supplementary Table 4).

Automated cut-off-finding and combination-testing algorithms were then applied to the samples and set of candidate markers to identify a minimal set of markers and optimal cut-offs for robustly diagnosing Ewing sarcoma by IHC. These analyses indicated that while CD99 is a very valuable marker for screening for Ewing sarcoma, it needs auxiliary markers to establish a robust diagnosis. Further analyses indicated that while ATP1A1 exhibited high specificity (90%), it had no additional value for establishing Ewing sarcoma diagnosis if it was combined with BCL11B and GLG1. In fact, detecting high BCL11B and/or GLG1 expression in CD99-high tumors reached a specificity for Ewing sarcoma of at least 96%, and of 99% if both markers were highly expressed (defined as IRS > 9). Strikingly, strong combined immunoreactivity for BCL11B and GLG1 was not observed in any of the tested Ewing-like sarcomas, while CD99 immunoreactivity was found in 15 of 17 cases (88%).

Thus, the following work-flow is proposed to establish a diagnosis of Ewing sarcoma (Figure 4c): In the case of clinically and/or radiologically suspected Ewing sarcoma, a biopsy should first be stained for CD99. If CD99 is positive (defined as IRS > 2), confirmatory molecular diagnostic procedures (such as FISH, qRT-PCR, and/or next-generation sequencing), if available, are preferred. If molecular diagnostic procedures are unavailable or the biopsy material is not suitable, an IHC-staining for BCL11B and GLG1 as well as subsequent scoring according to the Remmeli and Stegner system should be performed. Since high expression of BCL11B and/or GLG1 (defined as IRS > 9) was found in 79% of all Ewing Sarcoma cases and associated with a specificity of 96%, diagnosis of Ewing sarcoma should be strongly considered if one or both markers are highly expressed.

Collectively, our data provide evidence that fast and robust diagnosis of Ewing sarcoma is enabled by immunohistochemical detection of the super-enhancer-driven EWSR1-ETS targets BCL11B and GLG1.

DISCUSSION

Ewing sarcoma is genetically defined by pathognomonic *EWSR1-ETS* fusion transcripts [1]. To date, at least 18 types of chimeric *EWSR1-FLII* transcripts have been reported [6]. Alternatively, *EWSR1* can be fused with *ERG*, *ETV1*, *EIA-F* (alias *ETV4*) or *FEV* in Ewing sarcoma [6]. Although *CIC-DUX4*- and *BCOR-CCNB3*-translocated sarcomas were shown previously to be distinct from *EWSR1-ETS*-translocated Ewing sarcomas

[12, 32], the situation was less clear for *EWSR1-NFATc2*-translocated sarcomas. In fact, these tumors were until recently still considered by some authors as being simply a variant of Ewing sarcoma [33]. However, our PCA showed that *EWSR1-NFATc2*-translocated sarcomas are clearly distinct from *EWSR1-ETS*-translocated Ewing sarcomas, and confirm that *EWSR1-NFATc2*-translocated sarcomas also do not show any transcriptomic similarity with neither *CIC-DUX4*- nor *BCOR-CCNB3*-translocated sarcomas (Supplementary Figure 1).

Although several molecular diagnostic tools are available to identify Ewing sarcoma among morphological mimics by detecting these gene fusions (e.g. by FISH, qRT-PCR, and/or direct sequencing), there are several limitations: All these techniques require good-quality DNA or RNA, which is not available in more than 10% of cases [11]. In addition, FISH can sometimes yield non-informative results [14]. Moreover, there is a risk of falsely diagnosing a tumor as Ewing sarcoma based on FISH, because break-apart of the *EWSR1* gene can also be observed in other sarcoma entities such as desmoplastic small-round-cell tumor (DSRCT), clear cell sarcoma, angiomyxoid fibrous histiocytoma, extraskeletal myxoid chondrosarcoma, and a subset of myxoid liposarcoma [34]. Conversely, PCR-based assays can yield false negative results as the PCR may not cover the entire spectrum of different *EWSR1-ETS* fusions. Thus, some authors recommend combining FISH and qRT-PCR [11]. However, these sophisticated techniques are not available in all diagnostic facilities, especially in developing countries, which poses a significant obstacle to accurately diagnosing Ewing sarcoma.

To offer a simple, fast, and cost-effective way to reliably diagnose Ewing sarcoma by IHC, we combined *in silico*, *in vitro*, and *in situ* analyses, and found that the high expression of BCL11B and/or GLG1 is nearly diagnostic for this disease. It was shown that both genes are direct *EWSR1-FLII*-targets, which are specifically overexpressed in Ewing sarcoma. In fact, their genetic loci exhibit *EWSR1-FLII*-dependent super-enhancers that usually control the expression of tissue-defining genes [28]. In particular, the high expression of the chosen markers was highly effective in discriminating Ewing sarcoma from *EWSR1-ETS*-negative Ewing-like sarcomas, which expressed *CD99* at high levels in 88% of our cases. Nevertheless, it should be noted that some small-round-cell sarcoma subtypes such as DSRCTs could not be included in our primary screen as compatible gene expression microarrays were not publicly available. However, Surdez *et al.* published a transcriptomic comparison of DSRCTs and the same Ewing sarcoma samples as used in the current study, which proved that none of our markers ranges among the top 150 overexpressed probesets in DSCRT [35]. This finding was replicated in a subsequent study [25].

Previously, another *EWSR1-FLII* target gene,

NKX2-2, was proposed to serve in combination with CD99 as a useful immunohistochemical marker for Ewing sarcoma [36]. In our comparative microarray analyses, *NKX2-2* did not, however, meet the stringent selection criteria for further validation. Similarly, another report showed that *NKX2-2* is not fully specific for Ewing sarcoma [20].

Although most Ewing sarcoma tumors show little infiltration by lymphocytes [37], the fact that *BCL11B* is expressed in normal T cells (Supplementary Figure 2) should be taken into account when assessing immunoreactivity in small-round-cell tumors. In indeterminate cases, a CD3 staining may be helpful (Supplementary Figure 5).

In agreement with similar findings on different markers in other cancer entities [38, 39], *ATP1A1* and *GLG1* may have diagnostic as well as prognostic utility. However, this finding needs to be validated in an independent and larger cohort on the protein level.

Interestingly, all three original candidate markers play a role in fibroblast growth factor (FGF)-signaling. *ATP1A1* is required for unconventional secretion of FGF [40], *BCL11B* promotes FGF-signaling by transcriptional suppression of a negative feedback inhibitor [23, 41], and *GLG1* (alias cysteine-rich FGF receptor) is known to regulate intracellular levels of FGF [42]. Several studies have shown that FGF promotes *EWSR1-FLI1* expression [43] and growth of Ewing sarcoma cells *in vitro* and *in vivo* [25, 41], and that FGF-inhibitors could be used as a targeted treatment for Ewing sarcoma patients [44]. Although more work needs to be done to elucidate the precise role of *ATP1A1*, *BCL11B*, and *GLG1* in FGF-signaling, it is tempting to speculate that they could serve as predictive biomarkers for the efficacy of FGF-inhibitors.

Collectively, we propose utilizing *BCL11B* and *GLG1* as novel biomarkers for the diagnosis of Ewing sarcoma and recommend validating their diagnostic value in a prospective and multi-centered setting. It will be essential to further develop and characterize specific monoclonal antibodies directed against these proteins to improve and standardize their diagnostic utility.

MATERIALS AND METHODS

Human samples and ethics approval

Human tissue samples were retrieved from the archives of the Institute of Pathology of the LMU Munich (Germany), the Department of Pathology, Turgut Ozal Medical Center, Inonu University (Turkey), the Başkent University Hospital (Turkey), the Gerhard-Domagk-Institute for Pathology of the University of Münster (Germany), the Institute of Biomedicine of Seville (Spain),

and the Bone Tumour Reference Centre at the Institute of Pathology of the University Hospital Basel (Switzerland) with approval of the corresponding institutional review boards. The LMU Munich's ethics committee approved the current study (approval no. 550-16 UE).

Microarray analyses

Publicly available gene expression data generated with the Affymetrix HG-U133Plus2.0 DNA microarray for 1,790 samples comprising 21 tumor entities and 71 normal tissue types were retrieved from several repositories. Accession codes are given in Supplementary Table 5. All Ewing sarcoma samples were genetically verified to contain a specific *EWSR1-ETS* translocation as previously described [21]. After rigorous quality-checks (including the Relative Log Expression (RLE) and Normalized Unscaled Standard Error (NUSE)) and careful clinical annotation validation, expression intensities were calculated simultaneously with the Robust Multi-array Average (RMA) algorithm (including background adjustment, quantile normalization and summarization, using custom brainarray chip description file (CDF, ENTREZG, V19)), which yielded one optimized probe-set per gene [45]. The pairwise ER of every gene was calculated based on its median expression levels in primary Ewing sarcoma tumors and any of the 20 other remaining tumor entities. The differential gene expression's statistical significance was calculated with an unpaired, two-tailed Student's *t*-test. The resulting *P* values were adjusted for multiple testing with the Bonferroni method. Only genes with an ER of > 2 between Ewing sarcoma and any other tumor entity and a Bonferroni-corrected *P* value < 0.05 across all tumor entities compared with Ewing sarcoma were considered diagnostically relevant. PCA was performed in R [46]. Publicly available gene expression microarray data for ectopic *EWSR1-FLI1* expression in embryonic stem cells (Affymetrix HG-U133Plus2.0; GSE64686 [47]) and from Ewing sarcoma cell lines that were either transiently transfected with an shRNA directed against *EWSR1-FLI1* or a control shRNA (TC252, SK-N-MC, STA-ET-7.2, STA-ET-1, WE68; Affymetrix HG-U133A; GSE14543 [48]) or stably transduced with a doxycycline-inducible shRNA against *EWSR1-FLI1* (A673; Affymetrix HG-U133A 2.0; GSE27524 [49]) were normalized by RMA using custom brainarray CDF (ENTREZG, v19).

To identify the pathways and biological processes associated with a given gene present in normalized gene expression data from primary Ewing sarcoma tumors, gene-set enrichment analyses (GSEAs) were performed on ranked lists of genes in which all genes were ranked by their correlation coefficient with the given reference gene (MSigDB, c2.all.v5.1). GSEA was carried out with 1,000 permutations in default settings [50].

Analysis of DNase-Seq and ChIP-Seq data and genome-wide identification of super-enhancers

Publicly available data were retrieved from the Gene Expression Omnibus (GEO). ENCODE SK-N-MC DNase-Seq (GSM736570) [51] were analyzed in the Nebula environment [52] using Model-based Analysis of ChIP-Seq v1.4.2 (MACS) [53] and converted to *.wig format for display in the UCSC Genome Browser [54]. Preprocessed ChIP-Seq data from Riggi *et al.* [55] (GSE61944) were converted to *.wig format with the UCSC's bigWigToWig conversion tool.

The following samples were used in this study:

ENCODE_SKNMC_hg19_DNASeHS_rep2
GSM1517546 SKNMC.shGFP96.FLI1
GSM1517555 SKNMC.shFLI196.FLI1
GSM1517547 SKNMC.shGFP96.H3K27ac
GSM1517556 SKNMC.shFLI196.H3K27ac
GSM1517569 A673.shGFP48.FLI1
GSM1517572 A673.shFLI148.FLI1
GSM1517571 A673.shGFP96.H3.k27ac
GSM1517574 A673.shFLI196.H3K27ac

ChIP-seq data of the histone modification H3K27ac in A673 and SK-N-MC Ewing sarcoma cell lines (shGFP96) from a genome-wide chromatin analysis (GSE61944) conducted by Riggi *et al.* [55] were used for epigenetic analysis of enhancers. The already aligned Sequence Read Archives (*.sra) of both cell lines and the corresponding whole cell extracts were downloaded from GEO. Before peak calling with MACS2 [53], the data were prepared with SAMtools [56]. ChIP peak annotation was done with HOMER [57]. Super-enhancers were identified with ROSE [28, 58].

Cell culture, DNA constructs, and reporter assays

A673/TR/shEF1 Ewing sarcoma cells, which harbor a doxycycline-inducible shRNA against EWSR1-FLI1, were described previously [59] and kindly provided by J. Alonso (Madrid, Spain). Unmodified A673 cells were obtained from ATCC. All cells were grown at 37°C in 5% CO₂ in a humidified atmosphere in RPMI 1640 medium (Biochrom) containing 10% Tetracycline-free FCS (Biochrom), 100 U/ml penicillin, and 100 µg/ml streptomycin (both Biochrom). Cell line purity was confirmed by short tandem repeat profiling (latest profiling 15th December 2015), and cells were checked routinely for the absence of mycoplasma by PCR. Human GGAA-microsatellites close to the *ATP1A1*, *BCL11B*, or *GLG1* gene were cloned from the A673 Ewing sarcoma cell line into the pGL3-luc vector (Promega) upstream of the SV40 minimal promoter. qRT-PCRs-Primer sequences were as follows:

forward
5'-CTAGCCGGGCTCGAGAGCAA

CACAAGGACTCAATTAC-3' and reverse 5'-GATCGCAGATCTCGAGCTACTATGATGCAAA GCTGAGTG-3' for the *ATP1A1* associated GGAA-microsatellite;

forward 5'-CTAGCCGGGCTCGAG GCCGTCTCTGTTCTTAT-3' and reverse 5'-GATCGCAGATCTCGAGAAATCTCTGCTCCT TCATCCC-3' for the *BCL11B* associated GGAA-microsatellite; and

forward 5'-CTAGCCGGGCTCGAGGCTACTATAGCCAA ATGCAAAGAAGAA-3' and reverse 5'-GATCGCAGATCTCGAG TGCAGTGGTTATA-CAGAAAGAGTTTC-3' for the *GLG1* associated GGAA-microsatellite.

For the reporter assays, 3 × 10⁵ A673/TR/shEF1 cells per well of a six-well plate were seeded in 2.5 ml medium and transfected with pGL3-luc vectors and *Renilla* pGL3-Rluc (ratio, 100:1) using Lipofectamine LTX and Plus Reagent (Invitrogen). After 4 h transfection media were replaced by media with or without doxycycline (1 µg/ml). Cells were lysed after 72 h and assayed with a dual luciferase assay system (Berthold). *Firefly* luciferase activity was normalized to *Renilla* luciferase activity.

RNA extraction, reverse transcription, and quantitative real-time PCR (qRT-PCR)

RNA was extracted with the Nucleospin II kit (Macherey-Nagel) and reverse-transcribed using the High-Capacity cDNA Reverse Transcription Kit (Applied Biosystems). qRT-PCRs were performed using SYBR green (Applied Biosystems). Oligonucleotides were purchased from MWG Eurofins Genomics. Reactions were run on a Bio-Rad CFX Connect instrument and analyzed using Bio-Rad CFX Manager 3.1 software. Primer sequences for EWSR1-FLI1 and RPLP0 were reported previously [25].

Construction of TMAs and IHC

A total of 174 archival formalin-fixed and paraffin-embedded (FFPE) primary tissue samples with reviewed histological diagnosis were obtained from the participating institutions and collected at LMU Munich's Institute of Pathology. Representative FFPE tumor blocks were also selected for TMA construction at LMU Munich's Institute of Pathology. A detailed description of the TMA is given in Table 1.

All Ewing sarcoma FFPE samples showed cytogenetic evidence for a translocation of the *EWSR1* gene as determined by fluorescence *in situ* hybridization (FISH) and were reviewed by a reference pathologist. For this study, Ewing-like sarcomas were defined as small-

round-cell sarcomas being either positive for *CIC-DUX4* (8 cases) or *BCOR-CCNB3* (2 cases) or unclassified (7 cases) after extensive reference pathologist work-up. Each TMA slide contained three cores (each 1 mm in diameter) from every sample as well as internal controls.

For IHC, 4 μ m sections were cut, and antigen retrieval was performed with microwave treatment with 750W at pH7.5 TRIS buffer (2 x 15 min) using the antigen retrieval AR kit (DCS, HK057-5KE) for GLG1 or the Target Retrieval Solution (Dako, S1699) for BCL11B and ATP1A1. Blockage of endogenous peroxidase was performed using 7.5% aqueous H_2O_2 solution at room temperature and blocking serum from the corresponding kits for 20 min.

Slides were then incubated for 60 min with the primary antibodies anti-ATP1A1 (1:330 dilution, Proteintech, 14418-1-AP) [60], anti-BCL11B (1:1000 dilution, Abcam, ab70453) or anti-GLG1 (1:250 dilution, Sigma, HPA010815) [61]. Then slides were incubated with a secondary anti-rabbit IgG antibody (ImmPress Reagent Kit, Peroxidase-conjugated) followed by target detection using AECplus chromogen for 10 min (Dako, K3461).

For IHC of CD99, 4- μ m sections were cut and incubated for 32 min with an anti-CD99 antibody (1:40 dilution, Dako, 12E7) using the Roche UltraView detection kit.

Evaluation of immunoreactivity and automated cut-off finding

Semi-quantitative evaluation of marker immunostaining was carried out by three independent observers (MCB, MD, MFO) analogous to scoring of hormone receptor IRS ranging from 0-12 according to Remmele and Stegner [31], which is routinely used in surgical pathology to quantify hormone receptor expression in mammary carcinoma.

The percentage of cells with marker expression was scored and classified in five grades (grade 0 = 0-19%, grade 1 = 20-39%, grade 2 = 40-59%, grade 3 = 60-79% and grade 4 = 80-100%) after examination of 10 high-power fields (40 \times) of at least one section per sample. In addition, the intensity of marker immunoreactivity was determined (grade 0 = none, grade 1 = low, grade 2 = moderate and grade 3 = strong). The product of these two grades defined the final IRS. Sensitivity and specificity of each marker for Ewing sarcoma were calculated with an in-house generated VBA (Visual Basic for Applications) script implemented in Microsoft Excel (Microsoft). The script computed sensitivity and specificity for all possible combinations of markers and within these combinations, for all possible cut-offs for every marker. The best marker and cut-off combination was chosen based on the following criteria: high specificity (defined as > 95%), high sensitivity, and discriminability between positive

(IRS higher than the cut-off) and negative samples.

Survival analysis

Microarray data of 166 primary Ewing sarcoma tumors (GSE63157 [62], GSE34620 [21], GSE12102 [63], and GSE17618 [64]), which had well-curated clinical annotations available, were downloaded from the GEO. The data were generated on Affymetrix HG-U133Plus2.0 or Affymetrix HuEx-1.0-st microarray chips and normalized separately by RMA using custom brainarray CDF files (v20). Batch effects were removed using ComBat [65, 66]. Samples were stratified into two groups based on their median intra-tumoral gene expression levels. Significance levels were calculated with a Mantel-Haenszel test. *P* values < 0.05 were considered statistically significant.

Abbreviations

CDF-chip description file; DSRCT-desmoplastic small-round-cell tumor; GEO-gene expression omnibus; IRS-immunoreactivity score; PCA-principal component analysis; RMA-robust multi-array average; VBA-visual basic for applications; ChIP-Seq-chromatin immunoprecipitation followed by high-throughput sequencing; ER-expression ratio; FGF-fibroblast growth factor; GSEA-gene-set enrichment analysis; IHC-immunohistochemistry; MACS-Model-based Analysis of ChIP-Seq; qRT-PCR-quantitative real-time polymerase chain reaction.

Author contributions

MCB, MFO, MD, and TGPG conceived the study, wrote this paper, and drafted the figures and tables. MCB, JSG, MFO, and TGPG performed bioinformatic and statistical analyses. MMK, NA, ANA, ÖÖ, DB, EdA, UD, WH, and TK provided FFPE samples. MCB, MD, and MFO scored the TMAs. MMLK, RAR, SO, and JL helped in experimental procedures. TK provided laboratory infra-structure. AM, RAR, and GS cloned the GGAA-microsatellites and performed reporter assays. All authors read and approved the final manuscript.

ACKNOWLEDGMENTS

We would like to thank Mrs. Andrea Sendelhofert, Mrs. Anja Heier, and Mrs. Mona Melz for excellent technical assistance. The authors would like to thank all the donors and the Hospital Universitario Virgen del Rocío-Instituto de Biomedicina de Sevilla Biobank (Andalusian Public Health System Biobank and ISCIII-Biobank Platform PT13/0010/0056) for the human

specimens used in this study.

CONFLICTS OF INTEREST

The authors declare no conflict of interest.

FUNDING

This work was supported by the German National Academic Foundation (to M.C.B.), the Kind-Philipp-Foundation (to J.M., M.C.B., M.F.O., M.D., A.M, and G.S.), the ‘Deutsche Stiftung für Junge Erwachsene mit Krebs’ (to M.D.), the German National Academic Foundation (to M.C.B. and MMLK), the ‘Verein zur Förderung von Wissenschaft und Forschung an der Medizinischen Fakultät der LMU München’ (WiFoMed; to T.G.P.G.), the Daimler and Benz Foundation in cooperation with the Reinhard Frank Foundation (to T.G.P.G.), the Friedrich-Baur-Stiftung (to T.G.P.G.) by LMU Munich’s Institutional Strategy LMUexcellent within the framework of the German Excellence Initiative (to T.G.P.G.), the ‘Mehr LEBEN für krebskranke Kinder - Bettina-Bräu-Stiftung’ (to T.G.P.G.), the Fritz-Thyssen Foundation (FTF-40.15.0.030MN, to T.G.P.G. and G.S.), the Wilhelm-Sander-Foundation (2016.167.1 to T.G.P.G.), and the German Cancer Aid (DKH-111886 and DKH-70112257 to T.G.P.G.; DKH-108128 to U.D.), EU FP7 and TRANSCAN EraNet - PROVABES [01KT1310], EU-FP7 EEC [602856-2] to U.D.

Editorial note

This paper has been accepted based in part on peer-review conducted by another journal and the authors’ response and revisions as well as expedited peer-review in *Oncotarget*.

REFERENCES

1. Delattre O, Zucman J, Melot T, Garau XS, Zucker JM, Lenoir GM, Ambros PF, Sheer D, Turc-Carel C, Triche TJ. The Ewing family of tumors—a subgroup of small-round-cell tumors defined by specific chimeric transcripts. *N Engl J Med.* 1994; 331: 294-9. doi: 10.1056/NEJM19940804310503.
2. Machado I, Noguera R, Pellin A, Lopez-Guerrero JA, Piqueras M, Navarro S, Llombart-Bosch A. Molecular diagnosis of Ewing sarcoma family of tumors: a comparative analysis of 560 cases with FISH and RT-PCR. *Diagn Mol Pathol Am J Surg Pathol Part B.* 2009; 18: 189-99. doi: 10.1097/PDM.0b013e3181a06f66.
3. Doyle LA. Sarcoma classification: an update based on the 2013 World Health Organization Classification of Tumors of Soft Tissue and Bone. *Cancer.* 2014; 120: 1763-74. doi: 10.1002/cncr.28657.
4. Fletcher CDM. The evolving classification of soft tissue tumours - an update based on the new 2013 WHO classification. *Histopathology.* 2014; 64: 2-11. doi: 10.1111/his.12267.
5. Parham DM. Modern Diagnosis of Small Cell Malignancies of Children. *Surg Pathol Clin.* 2010; 3: 515-51. doi: 10.1016/j.path.2010.06.002.
6. Antonescu C. Round cell sarcomas beyond Ewing: emerging entities. *Histopathology.* 2014; 64: 26-37. doi: 10.1111/his.12281.
7. Pierron G, Tirode F, Lucchesi C, Reynaud S, Ballet S, Cohen-Gogo S, Perrin V, Coindre J-M, Delattre O. A new subtype of bone sarcoma defined by BCOR-CCNB3 gene fusion. *Nat Genet.* 2012; 44: 461-6. doi: 10.1038/ng.1107.
8. Italiano A, Sung YS, Zhang L, Singer S, Maki RG, Coindre J-M, Antonescu CR. High prevalence of CIC fusion with double-homeobox (DUX4) transcription factors in EWSR1-negative undifferentiated small blue round cell sarcomas. *Genes Chromosomes Cancer.* 2012; 51: 207-18. doi: 10.1002/gcc.20945.
9. Szuhai K, Ijszenga M, de Jong D, Karseladze A, Tanke HJ, Hogendoorn PCW. The NFATc2 gene is involved in a novel cloned translocation in a Ewing sarcoma variant that couples its function in immunology to oncology. *Clin Cancer Res Off J Am Assoc Cancer Res.* 2009; 15: 2259-68. doi: 10.1158/1078-0432.CCR-08-2184.
10. Kawamura-Saito M, Yamazaki Y, Kaneko K, Kawaguchi N, Kanda H, Mukai H, Gotoh T, Motoi T, Fukayama M, Aburatani H, Takizawa T, Nakamura T. Fusion between CIC and DUX4 up-regulates PEA3 family genes in Ewing-like sarcomas with t(4;19)(q35;q13) translocation. *Hum Mol Genet.* 2006; 15: 2125-37. doi: 10.1093/hmg/ddl136.
11. Machado I, Navarro L, Pellin A, Navarro S, Agaimy A, Tardío JC, Karseladze A, Petrov S, Scotlandi K, Picci P, Llombart-Bosch A. Defining Ewing and Ewing-like small round cell tumors (SRCT): The need for molecular techniques in their categorization and differential diagnosis. A study of 200 cases. *Ann Diagn Pathol.* 2016; 22: 25-32. doi: 10.1016/j.anndiagpath.2016.03.002.
12. Cohen-Gogo S, Cellier C, Coindre J-M, Mosseri V, Pierron G, Guillemet C, Italiano A, Brugières L, Orbach D, Laurence V, Delattre O, Michon J. Ewing-like sarcomas with BCOR-CCNB3 fusion transcript: a clinical, radiological and pathological retrospective study from the Société Française des Cancers de L’Enfant. *Pediatr Blood Cancer.* 2014; 61: 2191-8. doi: 10.1002/pbc.25210.
13. Machado I, Navarro S, Llombart-Bosch A. Ewing sarcoma and the new emerging Ewing-like sarcomas: (CIC and BCOR-rearranged-sarcomas). A systematic review. *Histol Histopathol.* 2016; 31: 1169-81. doi: 10.14670/HH-11-792.
14. Papp G, Mihály D, Sápi Z. Unusual Signal Patterns of Break-apart FISH Probes Used in the Diagnosis of Soft Tissue Sarcomas. *Pathol Oncol Res POR.* 2017; . doi: 10.1007/s12253-017-0200-z.

15. Peter M, Gilbert E, Delattre O. A multiplex real-time pcr assay for the detection of gene fusions observed in solid tumors. *Lab Investig J Tech Methods Pathol.* 2001; 81: 905-12.
16. Olsen SH, Thomas DG, Lucas DR. Cluster analysis of immunohistochemical profiles in synovial sarcoma, malignant peripheral nerve sheath tumor, and Ewing sarcoma. *Mod Pathol Off J U S Can Acad Pathol Inc.* 2006; 19: 659-68. doi: 10.1038/modpathol.3800569.
17. Lee SP, Park S, Park J, Hong J, Ko YH. Clinicopathologic characteristics of CD99-positive diffuse large B-cell lymphoma. *Acta Haematol.* 2011; 125: 167-74. doi: 10.1159/000322551.
18. Fisher C. Synovial sarcoma. *Ann Diagn Pathol.* 1998; 2: 401-21.
19. Rossi S, Orvieto E, Furlanetto A, Laurino L, Ninfo V, Dei Tos AP. Utility of the immunohistochemical detection of FLI-1 expression in round cell and vascular neoplasm using a monoclonal antibody. *Mod Pathol Off J U S Can Acad Pathol Inc.* 2004; 17: 547-52. doi: 10.1038/modpathol.3800065.
20. Hung YP, Fletcher CDM, Hornick JL. Evaluation of NKX2-2 expression in round cell sarcomas and other tumors with EWSR1 rearrangement: imperfect specificity for Ewing sarcoma. *Mod Pathol Off J U S Can Acad Pathol Inc.* 2016; 29: 370-80. doi: 10.1038/modpathol.2016.31.
21. Postel-Vinay S, Véron AS, Tirode F, Pierron G, Reynaud S, Kovar H, Oberlin O, Lapouble E, Ballet S, Lucchesi C, Kontny U, González-Neira A, Picci P, et al. Common variants near TARDBP and EGR2 are associated with susceptibility to Ewing sarcoma. *Nat Genet.* 2012; 44: 323-7. doi: 10.1038/ng.1085.
22. Hu-Lieskovan S, Zhang J, Wu L, Shimada H, Schofield DE, Triche TJ. EWS-FLI1 fusion protein up-regulates critical genes in neural crest development and is responsible for the observed phenotype of Ewing's family of tumors. *Cancer Res.* 2005; 65: 4633-44. doi: 10.1158/0008-5472.CAN-04-2857.
23. Wiles ET, Lui-Sargent B, Bell R, Lessnick SL. BCL11B is up-regulated by EWS/FLI and contributes to the transformed phenotype in Ewing sarcoma. *PloS One.* 2013; 8: e59369. doi: 10.1371/journal.pone.0059369.
24. Gangwal K, Sankar S, Hollenhorst PC, Kinsey M, Haroldsen SC, Shah AA, Boucher KM, Watkins WS, Jorde LB, Graves BJ, Lessnick SL. Microsatellites as EWS/FLI response elements in Ewing's sarcoma. *Proc Natl Acad Sci U S A.* 2008; 105: 10149-54. doi: 10.1073/pnas.0801073105.
25. Grünewald TGP, Bernard V, Gilardi-Hebenstreit P, Raynal V, Surdez D, Aynaud M-M, Mirabeau O, Cidre-Aranaz F, Tirode F, Zaidi S, Perot G, Jonker AH, Lucchesi C, et al. Chimeric EWSR1-FLI1 regulates the Ewing sarcoma susceptibility gene EGR2 via a GGAA microsatellite. *Nat Genet.* 2015; 47: 1073-8. doi: 10.1038/ng.3363.
26. Patel M, Simon JM, Iglesia MD, Wu SB, McFadden AW, Lieb JD, Davis JJ. Tumor-specific retargeting of an oncogenic transcription factor chimera results in dysregulation of chromatin and transcription. *Genome Res.* 2012; 22: 259-70. doi: 10.1101/gr.125666.111.
27. Tomazou EM, Sheffield NC, Schmidl C, Schuster M, Schönenberger A, Datlinger P, Kubicek S, Bock C, Kovar H. Epigenome mapping reveals distinct modes of gene regulation and widespread enhancer reprogramming by the oncogenic fusion protein EWS-FLI1. *Cell Rep.* 2015; 10: 1082-95. doi: 10.1016/j.celrep.2015.01.042.
28. Whyte WA, Orlando DA, Hnisz D, Abraham BJ, Lin CY, Kagey MH, Rahl PB, Lee TI, Young RA. Master transcription factors and mediator establish super-enhancers at key cell identity genes. *Cell.* 2013; 153: 307-19. doi: 10.1016/j.cell.2013.03.035.
29. Hnisz D, Abraham BJ, Lee TI, Lau A, Saint-André V, Sigova AA, Hoke HA, Young RA. Super-enhancers in the control of cell identity and disease. *Cell.* 2013; 155: 934-47. doi: 10.1016/j.cell.2013.09.053.
30. Wei G-H, Badis G, Berger MF, Kivioja T, Palin K, Enge M, Bonke M, Jolma A, Varjosalo M, Gehrke AR, Yan J, Talukder S, Turunen M, et al. Genome-wide analysis of ETS-family DNA-binding *in vitro* and *in vivo*. *EMBO J.* 2010; 29: 2147-60. doi: 10.1038/embj.2010.106.
31. Remmele W, Stegner HE. [Recommendation for uniform definition of an immunoreactive score (IRS) for immunohistochemical estrogen receptor detection (ER-ICA) in breast cancer tissue]. *Pathol.* 1987; 8: 138-40.
32. Specht K, Sung Y-S, Zhang L, Richter GHS, Fletcher CD, Antonescu CR. Distinct Transcriptional Signature and Immunoprofile of CIC-DUX4-Fusion Positive Round Cell Tumors Compared to EWSR1-Rearranged Ewing Sarcomas - Further Evidence Toward Distinct Pathologic Entities. *Genes Chromosomes Cancer.* 2014; 53: 622-33. doi: 10.1002/gcc.22172.
33. Charville GW, Wang W-L, Ingram DR, Roy A, Thomas D, Patel RM, Hornick JL, van de Rijn M, Lazar AJ. EWSR1 fusion proteins mediate PAX7 expression in Ewing sarcoma. *Mod Pathol Off J U S Can Acad Pathol Inc.* 2017; doi: 10.1038/modpathol.2017.49.
34. Romeo S, Dei Tos AP. Soft tissue tumors associated with EWSR1 translocation. *Virchows Arch Int J Pathol.* 2010; 456: 219-34. doi: 10.1007/s00428-009-0854-3.
35. Surdez D, Benetkiewicz M, Perrin V, Han Z-Y, Pierron G, Ballet S, Lamoureux F, Rédini F, Decouvelaere A-V, Daudigeos-Dubus E, Geoerger B, de Pinieux G, Delattre O, et al. Targeting the EWSR1-FLI1 oncogene-induced protein kinase PKC-β abolishes ewing sarcoma growth. *Cancer Res.* 2012; 72: 4494-503. doi: 10.1158/0008-5472.CAN-12-0371.
36. Shibuya R, Matsuyama A, Nakamoto M, Shiba E, Kasai T, Hisaoka M. The combination of CD99 and NKX2.2, a transcriptional target of EWSR1-FLI1, is highly specific

for the diagnosis of Ewing sarcoma. *Virchows Arch Int J Pathol.* 2014; 465: 599-605. doi: 10.1007/s00428-014-1627-1.

37. Kawaguchi S, Wada T, Tsukahara T, Ida K, Torigoe T, Sato N, Yamashita T. A quest for therapeutic antigens in bone and soft tissue sarcoma. *J Transl Med.* 2005; 3: 31. doi: 10.1186/1479-5876-3-31.
38. Iwahori K, Suzuki H, Kishi Y, Fujii Y, Uehara R, Okamoto N, Kobayashi M, Hirashima T, Kawase I, Naka T. Serum HE4 as a diagnostic and prognostic marker for lung cancer. *Tumour Biol J Int Soc Oncodevelopmental Biol Med.* 2012; 33: 1141-9. doi: 10.1007/s13277-012-0356-9.
39. Papale M, Vocino G, Lucarelli G, Rutigliano M, Gigante M, Rocchetti MT, Pesce F, Sanguedolce F, Bufo P, Battaglia M, Stallone G, Grandaliano G, Carrieri G, et al. Urinary RKIP/p-RKIP is a potential diagnostic and prognostic marker of clear cell renal cell carcinoma. *Oncotarget.* 2017; 8: 40412-24. doi: 10.18632/oncotarget.16341.
40. Zacherl S, La Venuta G, Müller H-M, Wegehingel S, Dimou E, Sehr P, Lewis JD, Erfle H, Pepperkok R, Nickel W. A direct role for ATP1A1 in unconventional secretion of fibroblast growth factor 2. *J Biol Chem.* 2015; 290: 3654-65. doi: 10.1074/jbc.M114.590067.
41. Cidre-Aranaz F, Grünewald TGP, Surdez D, García-García L, Carlos Lázaro J, Kirchner T, González-González L, Sastre A, García-Miguel P, López-Pérez SE, Monzón S, Delattre O, Alonso J. EWS-FLI1-mediated suppression of the RAS-antagonist Sprouty 1 (SPRY1) confers aggressiveness to Ewing sarcoma. *Oncogene.* 2017; 36: 766-76. doi: 10.1038/onc.2016.244.
42. Zuber ME, Zhou Z, Burrus LW, Olwin BB. Cysteine-rich FGF receptor regulates intracellular FGF-1 and FGF-2 levels. *J Cell Physiol.* 1997; 170: 217-27. doi: 10.1002/(SICI)1097-4652(199703)170:3 < 217::AID-JCP1 > 3.0.CO;2-R.
43. Girnita L, Girnita A, Wang M, Meis-Kindblom JM, Kindblom LG, Larsson O. A link between basic fibroblast growth factor (bFGF) and EWS/FLI-1 in Ewing's sarcoma cells. *Oncogene.* 2000; 19: 4298-301. doi: 10.1038/sj.onc.1203755.
44. Agelopoulos K, Richter GHS, Schmidt E, Dirksen U, von Heyking K, Moser B, Klein H-U, Kontny U, Dugas M, Poos K, Korschning E, Buch T, Weckesser M, et al. Deep Sequencing in Conjunction with Expression and Functional Analyses Reveals Activation of FGFR1 in Ewing Sarcoma. *Clin Cancer Res Off J Am Assoc Cancer Res.* 2015; 21: 4935-46. doi: 10.1158/1078-0432.CCR-14-2744.
45. Dai M, Wang P, Boyd AD, Kostov G, Athey B, Jones EG, Bunney WE, Myers RM, Speed TP, Akil H, Watson SJ, Meng F. Evolving gene/transcript definitions significantly alter the interpretation of GeneChip data. *Nucleic Acids Res.* 2005; 33: e175. doi: 10.1093/nar/gni179.
46. R Development Core Team. R: A language and environment for statistical computing [Internet]. Vienna, Austria; Available from <http://www.R-project.org>
47. Gordon DJ, Motwani M, Pellman D. Modeling the initiation of Ewing sarcoma tumorigenesis in differentiating human embryonic stem cells. *Oncogene.* 2016; 35: 3092-102. doi: 10.1038/onc.2015.368.
48. Kauer M, Ban J, Kofler R, Walker B, Davis S, Meltzer P, Kovar H. A molecular function map of Ewing's sarcoma. *PloS One.* 2009; 4: e5415. doi: 10.1371/journal.pone.0005415.
49. Bilke S, Schwentner R, Yang F, Kauer M, Jug G, Walker RL, Davis S, Zhu YJ, Pineda M, Meltzer PS, Kovar H. Oncogenic ETS fusions deregulate E2F3 target genes in Ewing sarcoma and prostate cancer. *Genome Res.* 2013; 23: 1797-809. doi: 10.1101/gr.151340.112.
50. Subramanian A, Tamayo P, Mootha VK, Mukherjee S, Ebert BL, Gillette MA, Paulovich A, Pomeroy SL, Golub TR, Lander ES, Mesirov JP. Gene set enrichment analysis: a knowledge-based approach for interpreting genome-wide expression profiles. *Proc Natl Acad Sci U S A.* 2005; 102: 15545-50. doi: 10.1073/pnas.0506580102.
51. Thurman RE, Rynes E, Humbert R, Vierstra J, Maurano MT, Haugen E, Sheffield NC, Stergachis AB, Wang H, Vernot B, Garg K, John S, Sandstrom R, et al. The accessible chromatin landscape of the human genome. *Nature.* 2012; 489: 75-82. doi: 10.1038/nature11232.
52. Boeva V, Lermine A, Barette C, Guillouf C, Barillot E. Nebula—a web-server for advanced ChIP-seq data analysis. *Bioinforma Oxf Engl.* 2012; 28: 2517-9. doi: 10.1093/bioinformatics/bts463.
53. Zhang Y, Liu T, Meyer CA, Eeckhoute J, Johnson DS, Bernstein BE, Nusbaum C, Myers RM, Brown M, Li W, Liu XS. Model-based analysis of ChIP-Seq (MACS). *Genome Biol.* 2008; 9: R137. doi: 10.1186/gb-2008-9-9-r137.
54. Meyer LR, Zweig AS, Hinrichs AS, Karolchik D, Kuhn RM, Wong M, Sloan CA, Rosenbloom KR, Roe G, Rhead B, Raney BJ, Pohl A, Malladi VS, et al. The UCSC Genome Browser database: extensions and updates 2013. *Nucleic Acids Res.* 2013; 41: D64-69. doi: 10.1093/nar/gks1048.
55. Rigg N, Knoechel B, Gillespie SM, Rheinbay E, Boulay G, Suvà ML, Rossetti NE, Boonseng WE, Oksuz O, Cook EB, Formey A, Patel A, Gymrek M, et al. EWS-FLI1 utilizes divergent chromatin remodeling mechanisms to directly activate or repress enhancer elements in Ewing sarcoma. *Cancer Cell.* 2014; 26: 668-81. doi: 10.1016/j.ccr.2014.10.004.
56. Li H, Handsaker B, Wysoker A, Fennell T, Ruan J, Homer N, Marth G, Abecasis G, Durbin R, 1000 Genome Project Data Processing Subgroup. The Sequence Alignment/Map format and SAMtools. *Bioinforma Oxf Engl.* 2009; 25: 2078-9. doi: 10.1093/bioinformatics/btp352.
57. Heinz S, Benner C, Spann N, Bertolino E, Lin YC, Laslo P, Cheng JX, Murre C, Singh H, Glass CK. Simple combinations of lineage-determining transcription factors prime cis-regulatory elements required for macrophage and B cell identities. *Mol Cell.* 2010; 38: 576-89. doi: 10.1016/j.molcel.2010.07.016.

molcel.2010.05.004.

58. Lovén J, Hoke HA, Lin CY, Lau A, Orlando DA, Vakoc CR, Bradner JE, Lee TI, Young RA. Selective inhibition of tumor oncogenes by disruption of super-enhancers. *Cell*. 2013; 153: 320-34. doi: 10.1016/j.cell.2013.03.036.
59. Carrillo J, García-Aragoncillo E, Azorín D, Agra N, Sastre A, González-Mediero I, García-Miguel P, Pestaña A, Gallego S, Segura D, Alonso J. Cholecystokinin down-regulation by RNA interference impairs Ewing tumor growth. *Clin Cancer Res Off J Am Assoc Cancer Res*. 2007; 13: 2429-40. doi: 10.1158/1078-0432.CCR-06-1762.
60. Yan X, Xun M, Dou X, Wu L, Zhang F, Zheng J. Activation of Na(+)–K(+)–ATPase with DRm217 attenuates oxidative stress-induced myocardial cell injury via closing Na(+)–K(+)–ATPase/Src/Ros amplifier. *Apoptosis Int J Program Cell Death*. 2017; 22: 531-43. doi: 10.1007/s10495-016-1342-2.
61. Morisaki T, Yashiro M, Kakehashi A, Inagaki A, Kinoshita H, Fukuoka T, Kasashima H, Masuda G, Sakurai K, Kubo N, Muguruma K, Ohira M, Wanibuchi H, et al. Comparative proteomics analysis of gastric cancer stem cells. *PloS One*. 2014; 9: e110736. doi: 10.1371/journal.pone.0110736.
62. Volchenboum SL, Andrade J, Huang L, Barkauskas DA, Kralio M, Womer RB, Ranft A, Potratz J, Dirksen U, Triche TJ, Lawlor ER. Gene Expression Profiling of Ewing Sarcoma Tumors Reveals the Prognostic Importance of Tumor-Stromal Interactions: A Report from the Children's Oncology Group. *J Pathol Clin Res*. 2015; 1: 83-94. doi: 10.1002/cjp2.9.
63. Scotlandi K, Remondini D, Castellani G, Manara MC, Nardi F, Cantiani L, Francesconi M, Mercuri M, Caccuri AM, Serra M, Knuutila S, Picci P. Overcoming resistance to conventional drugs in Ewing sarcoma and identification of molecular predictors of outcome. *J Clin Oncol Off J Am Soc Clin Oncol*. 2009; 27: 2209-16. doi: 10.1200/JCO.2008.19.2542.
64. Savola S, Klam A, Myllykangas S, Manara C, Scotlandi K, Picci P, Knuutila S, Vakkila J. High Expression of Complement Component 5 (C5) at Tumor Site Associates with Superior Survival in Ewing's Sarcoma Family of Tumour Patients. *ISRN Oncol*. 2011; 2011: 168712. doi: 10.5402/2011/168712.
65. Stein CK, Qu P, Epstein J, Buros A, Rosenthal A, Crowley J, Morgan G, Barlogie B. Removing batch effects from purified plasma cell gene expression microarrays with modified ComBat. *BMC Bioinformatics*. 2015; 16: 63. doi: 10.1186/s12859-015-0478-3.
66. Johnson WE, Li C, Rabinovic A. Adjusting batch effects in microarray expression data using empirical Bayes methods. *Biostat Oxf Engl*. 2007; 8: 118-27. doi: 10.1093/biostatistics/kxj037.

Chimeric EWSR1-FLI1 regulates the Ewing sarcoma susceptibility gene *EGR2* via a GGAA microsatellite

Thomas G P Grünewald^{1,2,17}, Virginie Bernard³, Pascale Gilardi-Hebenstreit⁴, Virginie Raynal^{1–3}, Didier Surdez^{1,2}, Marie-Ming Aynaud^{1,2}, Olivier Mirabeau^{1,2}, Florencia Cidre-Aranaz⁵, Franck Tirode^{1,2}, Sakina Zaidi^{1,2}, Gaëlle Perot⁶, Anneliene H Jonker^{1,2}, Carlo Lucchesi^{1,2}, Marie-Cécile Le Deley⁷, Odile Oberlin⁸, Perrine Marec-Bérard⁹, Amélie S Véron¹⁰, Stephanie Reynaud¹¹, Eve Lapouble¹¹, Valentina Boeva^{12,13}, Thomas Rio Frio³, Javier Alonso⁵, Smita Bhatia¹⁴, Gaëlle Pierron¹¹, Geraldine Cancel-Tassin¹⁵, Olivier Cussenot¹⁵, David G Cox¹⁰, Lindsay M Morton¹⁶, Mitchell J Machiela¹⁶, Stephen J Chanock¹⁶, Patrick Charnay⁴ & Olivier Delattre^{1–3,11}

Deciphering the ways in which somatic mutations and germline susceptibility variants cooperate to promote cancer is challenging. Ewing sarcoma is characterized by fusions between *EWSR1* and members of the ETS gene family, usually *EWSR1-FLI1*, leading to the generation of oncogenic transcription factors that bind DNA at GGAA motifs^{1–3}. A recent genome-wide association study⁴ identified susceptibility variants near *EGR2*. Here we found that *EGR2* knockdown inhibited proliferation, clonogenicity and spheroidal growth *in vitro* and induced regression of Ewing sarcoma xenografts. Targeted germline deep sequencing of the *EGR2* locus in affected subjects and controls identified 291 Ewing-associated SNPs. At rs79965208, the A risk allele connected adjacent GGAA repeats by converting an interspaced GGAT motif into a GGAA motif, thereby increasing the number of consecutive GGAA motifs and thus the *EWSR1-FLI1*-dependent enhancer activity of this sequence, with epigenetic characteristics of an active regulatory element. *EWSR1-FLI1* preferentially bound to the A risk allele, which increased global and allele-specific *EGR2* expression. Collectively, our findings establish cooperation between a dominant oncogene and a susceptibility variant that regulates a major driver of Ewing sarcomagenesis.

Ewing sarcoma is an aggressive pediatric malignancy that likely arises from neural crest- or mesoderm-derived mesenchymal stem cells (MSCs)^{5,6}. It is driven by oncogenic fusions between *EWSR1* and

genes in the ETS family (mostly *FLI1*)^{1–7}. *EWSR1-FLI1* binds DNA either at ETS-like consensus sites containing a GGAA core motif or, more specifically with respect to other ETS family members, at GGAA microsatellites, where the enhancer activity increases with the number of consecutive GGAA motifs^{2,3}. Notably, ~40% of *EWSR1-FLI1* binding occupancy maps to GGAA microsatellites⁸. Aside from *EWSR1-FLI1*, Ewing sarcoma is known for its paucity of recurrent somatic abnormalities^{9–11}.

Epidemiological studies have documented striking disparities in the incidence of Ewing sarcoma across human populations¹², implying a strong contribution of germline variation to Ewing sarcoma tumorigenesis. Our recent genome-wide association study (GWAS) identified three significant susceptibility loci with higher odds ratios (ORs) than commonly observed in adult cancers (OR > 1.5, compared with OR < 1.3 for adult cancers)^{4,13}. However, the potential oncogenic cooperation between the major *EWSR1-FLI1* somatic alteration and these Ewing sarcoma susceptibility loci remains to be elucidated. Here we focused on the chr10q21.3 susceptibility locus, which harbors two plausible candidate genes, *ADO* (2-aminoethanethiol dioxygenase), encoding a non-heme iron enzyme that converts cysteamine into taurine¹⁴, and *EGR2* (early growth response 2; also known as *KROX20*), encoding a conserved zinc-finger transcription factor that promotes proliferation, differentiation and/or survival in different cell types, including neural crest-derived Schwann cells and mesoderm-derived osteoprogenitors^{15,16}. Previous data showed that *ADO* and *EGR2* are overexpressed in Ewing sarcoma compared with other solid tumors

¹Genetics and Biology of Cancers Unit, Institut Curie, PSL Research University, Paris, France. ²INSERM U830, Institut Curie Research Center, Paris, France.

³Institut Curie Genomics of Excellence (ICGex) Platform, Institut Curie Research Center, Paris, France. ⁴École Normale Supérieure (ENS), Institut de Biologie de l'ENS (IBENS), INSERM U1024, CNRS UMR8197, Paris, France. ⁵Instituto de Investigación de Enfermedades Raras, Instituto de Salud Carlos III, Madrid, Spain.

⁶INSERM U916 Biology of Sarcomas, Institut Bergonié, Bordeaux, France. ⁷Département d'Epidémiologie et de Biostatistiques, Institut Gustave Roussy, Villejuif, France. ⁸Département de Pédiatrie, Institut Gustave Roussy, Villejuif, France. ⁹Institute for Pediatric Hematology and Oncology, Leon-Bérard Cancer Center, University of Lyon, Lyon, France. ¹⁰INSERM U1052, Léon-Bérard Cancer Centre, Cancer Research Center of Lyon, Lyon, France. ¹¹Unité Génétique Somatique (UGS), Institut Curie Centre Hospitalier, Paris, France. ¹²INSERM U900, Bioinformatics, Biostatistics, Epidemiology and Computational Systems Biology of Cancer, Institut Curie Research Center, Paris, France. ¹³Mines ParisTech, Fontainebleau, France. ¹⁴Institute for Cancer Outcomes and Survivorship, School of Medicine, University of Alabama, Birmingham, Alabama, USA. ¹⁵Centre de Recherche sur les Pathologies Prostatiques (CeRePP)-Laboratory for Urology, Research Team 2, UPMC, Hôpital Tenon, Paris, France. ¹⁶Division of Cancer Epidemiology and Genetics (DCEG), National Cancer Institute (NCI), Bethesda, Maryland, USA. ¹⁷Present address: Laboratory for Pediatric Sarcoma Biology, Institute of Pathology, LMU Munich, Munich, Germany. Correspondence should be addressed to O.D. (olivier.delattre@curie.fr).

Received 27 April; accepted 30 June; published online 27 July 2015; doi:10.1038/ng.3363

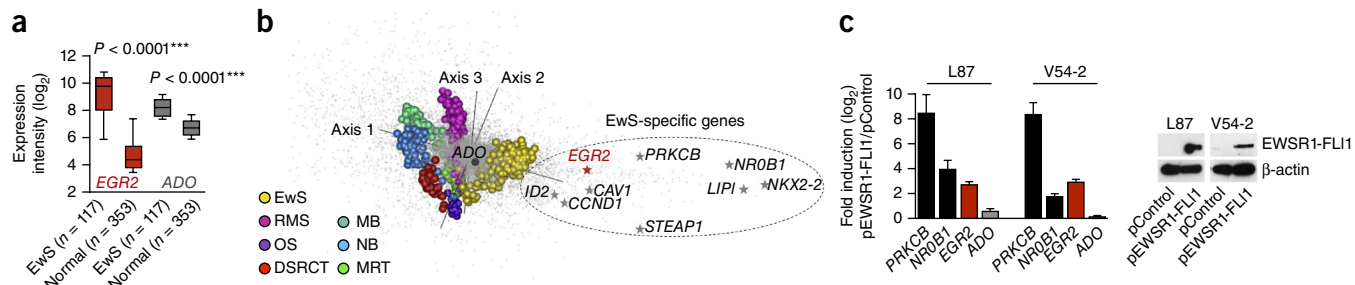


Figure 1 *EGR2* overexpression is mediated by *EWSR1-FLI1*. (a) *EGR2* and *ADO* expression levels in Ewing sarcoma (EwS, GSE34620) and normal tissue (GSE3526). The normal-body atlas consisted of 353 microarrays representing 63 individual tissue types (Supplementary Fig. 1). Data are shown as medians (horizontal bars) with ranges for the 25th–75th percentile (box) and 10th–90th percentile (whiskers). *P* values determined via two-tailed unpaired Student's *t*-test with Welch's correction. (b) Between-group analysis. Genes (gray dots) and tumor samples (colored spheres) are separated along three axes. EwS, Ewing sarcoma (*n* = 279); RMS, rhabdomyosarcoma (*n* = 121); OS, osteosarcoma (*n* = 25); DSRCT, desmoplastic small-round-cell tumor (*n* = 32); MB, medulloblastoma (*n* = 52); NB, neuroblastoma (*n* = 64); MRT, malignant rhabdoid tumor (*n* = 35). The main genes specifically overexpressed in Ewing sarcoma are indicated. (c) Quantitative real-time PCR analysis of *EGR2* and *ADO* expression in human MSC lines L87 and V54-2 after ectopic *EWSR1-FLI1* expression (pEWSR1-FLI1) as compared with empty vector (pControl). Data are shown as the mean and s.e.m.; *n* ≥ 9 independent experiments. The *EWSR1-FLI1* targets *NR0B1* and *PRKCB* served as positive controls^{17,35}. *EWSR1-FLI1* expression was confirmed by immunoblot (loading control: β-actin).

and that their elevated expression is associated with risk alleles⁴. *EGR2* and, to a lesser extent, *ADO* are also strongly overexpressed in Ewing sarcoma relative to their expression in normal tissues (Fig. 1a and Supplementary Fig. 1). Comparative analysis of microarray data from seven pediatric soft tissue and brain tumor types showed that *EGR2*, but not *ADO*, clusters with established *EWSR1-FLI1* target genes¹⁷ (Fig. 1b). To further explore the expression quantitative trait locus (eQTL) properties of the Ewing sarcoma chr10 susceptibility locus, we evaluated available genotype and matched expression data sets from Ewing sarcoma and other small-round-cell tumors, as well as from normal tissues^{4,18–23}. Interestingly, the Ewing sarcoma risk-associated rs1848797, which was genotyped in all data sets, was associated with higher *EGR2* and *ADO* expression only in Ewing sarcoma, and not in *EWSR1-FLI1*-negative tissues (Table 1, Supplementary Data and Supplementary Fig. 2). Moreover, ectopic *EWSR1-FLI1* expression in human MSCs specifically induced *EGR2* expression (Fig. 1c), whereas *EWSR1-FLI1* knockdown by specific small interfering RNA (siRNA) consistently reduced *EGR2* expression in four different Ewing sarcoma cell lines (Supplementary Fig. 3). Such regulation by *EWSR1-FLI1* was not observed for *ADO*. These data strongly suggest that *EGR2* and *ADO* are specifically regulated by eQTLs in Ewing sarcoma, but that only *EGR2* is *EWSR1-FLI1* dependent.

Knockdown experiments showed that inhibition of *EGR2*, but not of *ADO*, impaired the proliferation and clonogenicity of four different Ewing sarcoma cell lines, reduced cell cycle progression through

S-phase and reduced cell viability (Fig. 2a,b and Supplementary Fig. 4). To confirm the contribution of *EGR2* to Ewing sarcoma growth, we generated Ewing sarcoma cell lines with a doxycycline-inducible anti-*EGR2* small-hairpin RNA (shRNA) expression system. Long-term *EGR2* knockdown not only dramatically reduced anchorage-independent spheroidal growth *in vitro* but, even more strikingly, also induced the regression of Ewing sarcoma xenografts *in vivo* (Fig. 2c,d). Consistent with the hypothesis that *EGR2* acts downstream of *EWSR1-FLI1*, transcriptome profiling of Ewing sarcoma cells after knockdown of either gene showed highly significantly overlapping transcriptional signatures (Fig. 2e and Supplementary Data). Collectively, these data suggest that *EGR2* is an *EWSR1-FLI1*-induced target gene critical for Ewing sarcoma tumorigenicity.

As several reports have shown that *EGR2* acts downstream of the epidermal growth factor (EGF) and fibroblast growth factor (FGF) pathway^{15,24,25}, we explored a potential contribution of these pathways to Ewing sarcoma growth and *EGR2* regulation. Whereas EGF receptors (EGFRs) are minimally expressed in Ewing sarcoma, some FGF receptors (FGFRs), particularly FGFR1, are highly expressed (Supplementary Fig. 5a). Consistently, bFGF, but not EGF, strongly induced both proliferation of and *EGR2* expression in Ewing sarcoma cells (Supplementary Fig. 5b,c). These data indicate that *EWSR1-FLI1* and FGF signaling converge to upregulate the expression of *EGR2*.

To fine-map the chr10 susceptibility locus and to identify variants that potentially contribute to *EGR2* overexpression, we performed targeted deep sequencing across the chr10 susceptibility locus, including the flanking haplotype blocks, in the germline DNA of 343 individuals with Ewing sarcoma and 251 genetically matched controls (median target-region coverage ≥ 10×, 91.35%; median nucleotide coverage, 217×). Genetic matching was based on principal-component analysis⁴ of SNP array data (Supplementary Fig. 6). After quality control metrics had been applied to the sequencing data (for example, ≥10× coverage per position, genotype call rate of ≥90% and compliance with Hardy-Weinberg equilibrium), 290 common SNPs (minor allele frequency > 0.05) were identified that were significantly associated with Ewing sarcoma (*P* < 0.05; Fig. 3a, Supplementary Data and Supplementary Fig. 7). These included all 14 sentinel SNPs reported in our previous GWAS⁴. Haplotype and linkage disequilibrium (LD) analysis showed that this locus consists of discrete subhaploblocks (Fig. 3a and Supplementary Data).

Table 1 Overexpression of *EGR2* and *ADO* is mediated by Ewing sarcoma-specific eQTLs

| Tissue type | <i>n</i> | <i>P</i> value correlation with rs1848797 | |
|-------------|-------------------|---|------------|
| | | <i>EGR2</i> | <i>ADO</i> |
| Malignant | Ewing sarcoma | 0.0077 | 0.0023 |
| | Medulloblastoma | ns | ns |
| | Neuroblastoma | ns | ns |
| | AML | ns | ns |
| Normal | LCL | ns | ns |
| | Airway epithelium | ns | ns |
| | Broad GTEx | ns | ns |

eQTL analyses across tissue types identified Ewing sarcoma-specific correlations of *EGR2* and *ADO* expression with the risk allele at rs1848797. The Broad GTEx database comprised 13 normal tissue types (≥60 samples per tissue type). ns, not significant; AML, acute myeloid leukemia; LCL, lymphoblastoid cell lines.

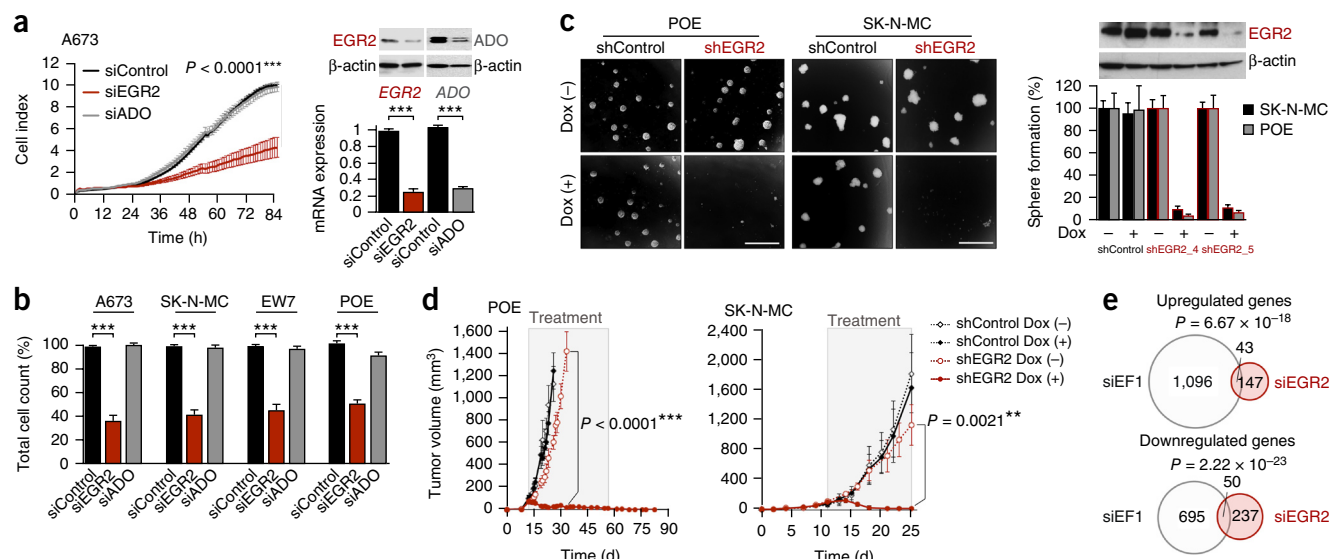


Figure 2 EGR2 is critical for the growth and tumorigenicity of Ewing sarcoma. **(a)** xCELLigence proliferation kinetics of A673 cells. Data shown are the mean \pm s.e.m. of results obtained with two different siRNAs against *EGR2* and three different siRNAs against *ADO*; $n \geq 6$ technical replicates. *EGR2* or *ADO* knockdown was confirmed at 48 h by quantitative real-time PCR (mean \pm s.e.m., $n \geq 4$ independent experiments) and immunoblot (loading control: β -actin). **(b)** Validation of xCELLigence results by cell counting (including supernatant) 96 h after transfection of A673, SK-N-MC, EW7 and POE cells. Data are mean and s.e.m. of results obtained with two different siRNAs against *EGR2* and three different siRNAs against *ADO*; $n \geq 3$ independent experiments. **(c)** Left, phase-contrast images of sphere-formation assays (scale bars, 1 mm). Right, mean and s.e.m. of $n \geq 3$ independent experiments performed with SK-N-MC and POE containing a doxycycline-inducible shRNA against *EGR2* (shEGR2_4 or shEGR2_5). Also shown is a representative *EGR2* immunoblot for POE cells (96-h doxycycline treatment; loading control, β -actin). **(d)** Growth curves for subcutaneously xenografted POE or SK-N-MC cells in mice (shControl and shEGR2_4). When tumors reached a volume of 75–100 mm³, doxycycline and sucrose (Dox +) or sucrose alone (Dox –) was added to the drinking water (treatment). Mean \pm s.e.m.; $n \geq 6$ mice per group. *P* values determined via two-tailed unpaired Student's *t*-test. **(e)** Size-proportional Venn diagrams of up- and downregulated genes 48 h after knockdown of *EWSR1-FLI1* (siEF1) or *EGR2* (siEGR2) in A673 and SK-N-MC cells (minimum \log_2 fold change ± 0.5 , Benjamini-Hochberg-corrected *P* < 0.05). Fisher's exact test.

To prioritize SNPs for functional assessment, we crossed our sequencing data with published chromatin immunoprecipitation (ChIP)-Seq, DNase-Seq and ENCODE data, with particular focus on Ewing sarcoma cell lines^{8,26,27}, as recent studies have suggested that most causal SNPs cluster in epigenetically active and cell-type-specific regulatory elements^{28,29} (Fig. 3a). We also included data on conserved *EGR2* regulatory elements previously mapped in animal models³⁰ (Fig. 3a and Supplementary Fig. 8). We observed activating chromatin marks, signals for formaldehyde-assisted isolation of regulatory elements (FAIRE) and/or DNaseI hypersensitivity at five main loci: two loci corresponding to known *EGR2* regulatory elements (MSE (myelinating Schwann cell enhancer)³⁰ and BoneE (bone enhancer) (unpublished data); Supplementary Fig. 8), one to the *ADO* promoter, and two to GGAA microsatellites (mSat1 and mSat2) that overlapped with *EWSR1-FLI1* ChIP-Seq signals (Fig. 3a). Because the *ADO* promoter does not contain Ewing sarcoma-associated SNPs, it was not further investigated. Luciferase reporter assays indicated that BoneE and MSE had no and weak activity in Ewing sarcoma, respectively (Fig. 3b,c). In contrast, both GGAA microsatellites exhibited strong *EWSR1-FLI1*-dependent enhancer-like activity (Fig. 3b,c). This activity corresponded to *EWSR1-FLI1*-dependent activating chromatin marks H3K4me1 and H3K27ac (Fig. 3a) and was consistent with recent evidence suggesting that *EWSR1-FLI1* can act as a pioneer transcription factor to create *de novo* enhancers at GGAA microsatellites²⁷.

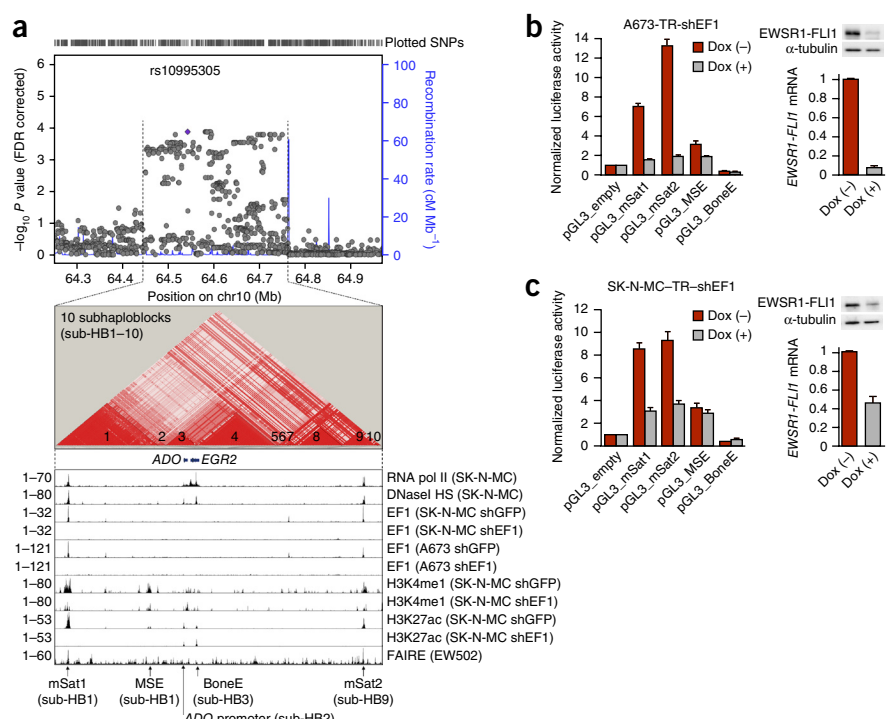
Because of its observed higher enhancer activity, relatively simpler structure compared with that of mSat1, and localization in the subhaploblock containing some of the most significant Ewing sarcoma-associated SNPs (Figs. 3a and 4a and Supplementary Fig. 9), we focused on mSat2 and carried out PCR-based targeted long-read

(300/300 nt) deep resequencing of all samples to analyze its genetic architecture. This yielded 1,158 analyzable mSat2 sequences, which revealed another SNP, rs79965208, in strong LD ($D' = 0.97$) with the nearby rs6479860, one of the strongest sentinel SNPs from our GWAS⁴ (Fig. 4a and Supplementary Data). The significant association of the A allele of rs79965208 with Ewing sarcoma ($P = 0.022$, logistic regression) was replicated in two independent cohorts, the first based on direct sequencing of this SNP in 156 additional Ewing sarcoma subjects and 184 controls of European descent ($P = 6.15 \times 10^{-3}$, logistic regression), and the second on imputation from the 1000 Genomes Project Phase 3 reference panel³¹ of 162 individuals with first primary Ewing sarcoma from the Childhood Cancer Survivor Study³² genotyped on Illumina HumanOmni5Exome arrays and 435 cancer-free controls from the Division of Cancer Epidemiology and Genetics ($P = 9.33 \times 10^{-6}$, logistic regression) (Supplementary Data).

Interestingly, rs79965208 converts a GGAT motif into a GGAA motif, thereby connecting two adjacent GGAA repeats (Fig. 4a). The first GGAA repeat is polymorphic and contains a median number of 11 GGAA motifs, whereas the second is not polymorphic and is composed of four GGAA motifs. The A allele at rs79965208 therefore increases the median number of consecutive GGAA motifs from 11 to 16.

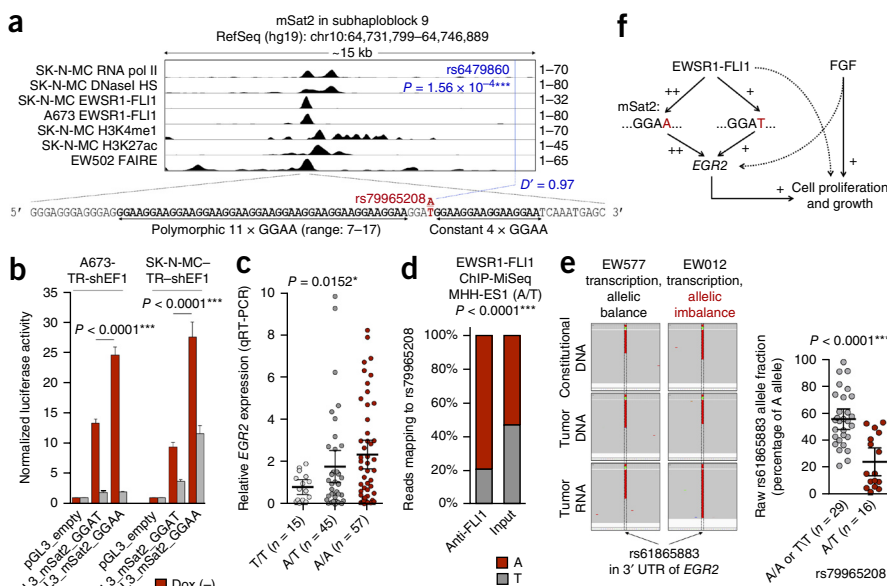
The previously described threshold for exponentially increasing *EWSR1-FLI1*-dependent enhancer activity is >12 consecutive GGAA motifs³. In the current study, a significantly larger proportion of Ewing sarcoma mSat2 sequences contained >12 GGAA motifs than did controls (65.88% versus 54.99%, $P = 2.10 \times 10^{-6}$, two-tailed Fisher's exact test). We subsequently examined the enhancer properties of mSat2 corresponding to the reference sequence (hg19) containing either the T or the A allele at rs79965208 in a luciferase assay. Relative to the T allele, the A allele increased the *EWSR1-FLI1*-induced enhancer

Figure 3 Fine-mapping and epigenetic profiling revealed candidate *EGR2* regulatory elements. (a) Top, Manhattan plot of 1,440 SNPs identified by targeted deep sequencing within the chr10 susceptibility locus and flanking haplotype blocks. rs10995305 was the SNP most significantly associated with Ewing sarcoma at this locus (false discovery rate (FDR)-corrected $P = 1.27 \times 10^{-4}$). The blue lines indicate the recombination-rate estimates from the HapMap project³⁶. Middle, LD plot of the chr10 susceptibility locus hotspot (chr10:64,449,549–64,756,872) based on the analysis of 290 significant Ewing sarcoma-associated SNPs in 343 affected subjects (a subset of the original GWAS cohort⁴) and 251 controls. Bottom, epigenetic profile of the chr10 susceptibility locus hotspot in the Ewing sarcoma cell lines SK-N-MC, A673 and EW502. Displayed are signals from published ChIP-Seq or DNase-Seq data for RNA polymerase II (pol II), DNase hypersensitivity (HS), EWSR1-FLI1 (EF1), H3K4me1 and H3K27ac in Ewing sarcoma cells transfected with either a control shRNA (shGFP) or a specific shRNA against *EWSR1-FLI1* (shEF1), and FAIRE^{8,26,27}. The read count is given on the left. mSat1 and mSat2 are GGAA microsatellites (Supplementary Fig. 8). (b,c) Normalized luciferase reporter signals in A673-TR-shEF1 and SK-N-MC-TR-shEF1 cells containing a doxycycline-inducible shRNA against *EWSR1-FLI1*. *EWSR1-FLI1* knockdown was confirmed by quantitative real-time PCR and immunoblot (loading control: α -tubulin). Data are shown as means and s.e.m.; $n \geq 5$ independent experiments.



activity of mSat2 (Fig. 4b). This transcription-activation property was observed in two Ewing sarcoma cell lines and was strictly dependent on *EWSR1-FLI1*, as its doxycycline-induced knockdown abrogated luciferase activity (Fig. 4b).

Figure 4 Germline variation at mSat2 modulates *EWSR1-FLI1*-dependent *EGR2* expression. (a) Coordinates, epigenetic profile and sequence of the mSat2 locus. Consistent with previous studies, H3K4me1 and H3K27ac signals peaked adjacent to the repetitive GGAA mSat^{8,27}. The P value reported for rs6479860 reflects the significance of its association with Ewing sarcoma. (b) Luciferase reporter signals of mSat2 with the T or A allele at rs79965208. Data are mean and s.e.m.; $n \geq 6$ independent experiments. P values determined via two-tailed unpaired Student's *t*-test. (c) *EGR2* expression measured by quantitative real-time PCR in 117 Ewing samples (103 primary tumors and 14 cell lines). *EGR2* expression was normalized to that of *RPLP0* and is displayed as expression relative to that of the median sample (set as 1). Horizontal bars represent means, and whiskers represent the 95% confidence interval boundaries. P value determined via linear regression. (d) Allele fraction of reads mapping to rs79965208 generated in a ChIP-MiSeq experiment in the A/T Ewing cell line MHH-ES1 (Supplementary Fig. 10 and Supplementary Data). (e) Left, representative Integrative Genomics Viewer³⁷ pile-up of reads covering the *EGR2* 3' UTR rs61865883 in matched constitutional or tumor DNA and tumor-derived RNA. The sample EW012 exhibited transcriptional allelic imbalance of *EGR2*, whereas EW577 did not. Right, raw rs61865883 allele fractions of targeted RNA deep sequencing in 45 Ewing sarcomas heterozygous (A/T) for the transcribed *EGR2* 3' UTR allelic marker rs61865883. Horizontal bars represent means, and whiskers show the 95% confidence interval boundaries. P values determined via parametric two-tailed Student's *t*-test. (f) Regulatory model of *EWSR1-FLI1* and mSat2 controlling *EGR2* expression and proliferation in convergence with the FGF pathway.



In accordance with the reporter assays, the A allele was associated with significantly higher *EGR2* expression in Ewing sarcoma tumors (Fig. 4c). Consistently, ChIP experiments in the A/T Ewing sarcoma cell line MHH-ES1 using a specific antibody to FLI1 followed by

quantitative real-time PCR and immunoblot (loading control: α -tubulin) confirmed that the A allele was associated with significantly higher *EGR2* expression in MHH-ES1 cells (Supplementary Fig. 10). Consistently, ChIP experiments in the A/T Ewing sarcoma cell line MHH-ES1 using a specific antibody to FLI1 followed by quantitative real-time PCR and immunoblot (loading control: α -tubulin) confirmed that the A allele was associated with significantly higher *EGR2* expression in MHH-ES1 cells (Supplementary Fig. 10). Consistently, ChIP experiments in the A/T Ewing sarcoma cell line MHH-ES1 using a specific antibody to FLI1 followed by quantitative real-time PCR and immunoblot (loading control: α -tubulin) confirmed that the A allele was associated with significantly higher *EGR2* expression in MHH-ES1 cells (Supplementary Fig. 10).

targeted deep sequencing of mSat2 identified significant enrichment of reads containing the A allele (Fig. 4d and **Supplementary Fig. 10**), indicating that EWSR1-FLI1 preferentially bound to the A allele of rs79965208. Moreover, taking advantage of a transcribed SNP in the 3' UTR of *EGR2* (rs61865883), we assessed allele-specific *EGR2* expression via targeted RNA deep sequencing. Across 45 individuals with heterozygosity for rs61865883, the transcriptional allelic imbalance was significantly higher in 16 tumors heterozygous for rs79965208 (A/T) than in 29 tumors homozygous (A/A or T/T) for this locus (Fig. 4e). Collectively, our results show that *EGR2* is an Ewing sarcoma susceptibility gene whose overexpression in tumors is mediated by EWSR1-FLI1 through a risk-conferring enhancer-like polymorphic GGAA microsatellite (Fig. 4f).

Importantly, we noted that the chr10 signal was strongly reduced when we performed association testing conditionally on rs79965208, which indicated that this SNP is a major functional variant at this locus. However, some association signal was still observed, so it remains plausible that other SNPs could also have a regulatory effect on *EGR2* expression through other mechanisms (**Supplementary Fig. 11**). The relatively low *EGR2* expression observed in some Ewing sarcoma cases, particularly in cases with the T/T genotype, suggests that *EGR2* might not always be absolutely necessary for Ewing sarcoma growth, and that growth may thus rely on alternative 'transformation-facilitating genes', possibly linked to other Ewing sarcoma susceptibility loci. However, we could not test whether Ewing sarcoma cells with a T/T genotype at rs79965208 have decreased sensitivity to *EGR2* knockdown, as the T/T genotype was not observed across 21 different Ewing sarcoma cell lines (**Supplementary Data**).

As the incidence of Ewing sarcoma is higher in Europeans than in Africans¹², we investigated the frequency of the A allele at rs79965208 across human populations, as determined by the 1000 Genomes Project³¹ (**Supplementary Data**). Strikingly, the A risk allele is highly significantly more frequent in non-African human populations (mean, 0.64; range, 0.57–0.70; $n = 1,886$) than in Africans (0.25; $n = 691$) ($P = 2.20 \times 10^{-16}$, Fisher's exact test), which suggests that rs79965208 underwent a recent expansion in non-Africans and that it might contribute to the variable susceptibility to Ewing sarcoma across populations.

To our knowledge, this constitutes one of the first reports of how a germline variant highly correlated with the reported GWAS signal can inform our understanding of a cancer-specific acquired genetic abnormality²². Furthermore, our findings are in line with predictions that causal variants are not necessarily among the most significant variations leading to the identification of the susceptibility loci, but rather are in strong LD with them^{33,34}. Moreover, they illustrate the contribution of a common germline variant that alters one or more key biological pathways in Ewing sarcoma through the modification of transcription regulatory elements that mediate the effects of a dominant oncogene¹³.

URLs. <https://www.addgene.org/21915/>; <http://www.gtexportal.org/home/>; <http://www.r-project.org/>; <https://github.com/jstjohn/SeqPrep>; <http://broadinstitute.github.io/picard/>; <http://www.clustal.org/omega/>.

METHODS

Methods and any associated references are available in the [online version of the paper](#).

Accession codes. Primary microarray data are compliant with the MIAME guidelines and were deposited at the Gene Expression Omnibus (GEO) under accession [GSE62090](https://www.ncbi.nlm.nih.gov/geo/query/acc.cgi?acc=GSE62090).

Note: Any Supplementary Information and Source Data files are available in the online version of the paper.

ACKNOWLEDGMENTS

T.G.P.G. is supported by a grant from the German Research Foundation (DFG GR3728/2-1), by the Daimler and Benz Foundation in cooperation with the Reinhard Frank Foundation, by LMU Munich's Institutional Strategy LMUexcellent within the framework of the German Excellence Initiative and by the Mehr LEBEN für krebskranke Kinder–Bettina-Bräu-Stiftung. D.S. is supported by the Institut Curie–SIRIC (Site de Recherche Intégrée en Cancérologie) program. F.C.-A. is supported by a grant from the Asociación Pablo Ugarte and Instituto de Salud Carlos III RTICC RD12/0036/0027. D.G.C. is supported by a grant from the InfoSarcomes Association. The Childhood Cancer Survivor Study is supported by the National Cancer Institute (CA55727, G.T. Armstrong), with funding for genotyping from the Intramural Research Program of the National Institutes of Health, National Cancer Institute. This work was supported by grants from the Institut Curie; INSERM; the Agence Nationale de la Recherche (Investissements d'Avenir) (ANR-10-EQPX-03); the Cancéropôle Ile-de-France (ANR10-INBS-09-08); the Ligue Nationale Contre le Cancer (Equipe labellisée); the Institut National du Cancer (PLBIO14-237); the European PROVABES (ERA-649 NET TRANSCAN JTC-2011), ASSET (FP7-HEALTH-2010-259348) and EEC (HEALTH-F2-2013-602856) projects; and the Société Française des Cancers de l'Enfant. The following associations supported this work: Courir pour Mathieu, Dans les pas du Géant, Olivier Chape, Les Bagouzamanon, Enfants et Santé, et les Amis de Claire. The Charnay laboratory was financed by INSERM, the CNRS, the Ministère de la Recherche et Technologie, and the Fondation pour la Recherche Médicale. It has received support under the program "Investissements d'Avenir" launched by the French Government and implemented by the ANR, with the references ANR-10-LABX-54 MEMOLIFE and ANR-11-IDEX-0001-02 PSL* Research University. We thank J. Maris for providing genotype information for the neuroblastoma data set, and we thank L. Liang and W. Cookson for providing access to genotype data on the LCL data set. We thank H. Kovar (Children's Cancer Research Institute Vienna, Vienna, Austria) for providing cell lines STA-ET-1, STA-ET-3 and STA-ET-8, and F. Redini (University of Nantes, Nantes, France) for providing cell line TC-32. Human MSC lines L87 and V54-2 were kindly provided by P. Nelson (University Hospital LMU, Munich, Germany). We also thank the following clinicians and pathologists for providing samples used in this work: I. Aerts, P. Anract, C. Bergeron, L. Boccon-Gibod, F. Boman, F. Bourdeaut, C. Bouvier, R. Bouvier, L. Brugérias, E. Cassagnau, J. Champigneulle, C. Cordonnier, J. M. Coindre, N. Corradini, A. Coulomb-Lhermine, A. De Muret, G. De Pinieux, A.S. Defachelles, A. Deville, F. Dijoud, F. Doz, C. Dufour, K. Fernandez, N. Gaspard, L. Galmiche-Rolland, C. Glorion, A. Gomez-Brouchet, J.M. Guinebretière, H. Jouan, C. Jeanne-Pasquier, B. Kantelip, F. Labrousse, V. Laithier, F. Larousserie, G. Leverger, C. Linassier, P. Mary, G. Margueritte, E. Mascard, A. Moreau, J. Michon, C. Michot, F. Millot, Y. Musizzano, M. Munzer, B. Narciso, O. Oberlin, D. Orbach, H. Pacquement, Y. Perel, B. Petit, M. Peuchmaur, J.Y. Pierga, C. Piguet, S. Piperno-Neumann, E. Plouvier, D. Ranchor-Vince, J. Rivel, C. Rouleau, H. Rubie, H. Sartelet, G. Schleiermacher, C. Schmitt, N. Sirvent, D. Sommelet, P. Terrier, R. Tichit, J. Vannier, J.M. Vignaud and V. Verkarre. We also thank D. Darmon for technical assistance, S. Grossetete-Lalami for bioinformatic assistance, and V.R. Buchholz and E. Butt for critical reading of the manuscript.

AUTHOR CONTRIBUTIONS

T.G.P.G. coordinated and designed the study, performed all functional experiments, analyzed the sequencing data, performed bioinformatic analyses, wrote the paper, designed the figures and helped with grant applications. V. Bernard processed the sequencing data and performed bioinformatic analyses. P.G.-H. participated in the study design, cloned enhancer elements and contributed to data analysis. V.R. performed all sequencing experiments and helped analyze the bioinformatic data. D.S. contributed to the *in vivo* experiments, performed the ChIP-MiSeq experiments and provided experimental protocols. M.-M.A., F.C.-A., A.H.J. and S.Z. helped with functional experiments. O.M., F.T. and C.L. provided statistical advice and helped in the bioinformatic analyses. G. Perot assisted in generation of the shRNA constructs. M.-C.L.D., O.O. and P.M.-B. provided Ewing sarcoma samples and annotation. G. Pierron, S.R. and E.L. provided and prepared Ewing sarcoma samples. T.R.F. coordinated and supervised sequencing experiments. V. Boeve helped analyze ChIP-Seq data. J.A. provided the A673-TR-shEF1 and SK-N-MC-TR-shEF1 cell lines. A.S.V. performed principal-component analysis clustering of Ewing sarcoma subjects and controls. G.C.-T. and O.C. provided DNA from healthy controls. D.G.C. and S.J.C. provided genetic and statistical guidance. S.B., L.M.M., M.J.M. and S.J.C. provided data for the CCSS replication cohort and performed imputation analyses. P.C. provided advice on analyses concerning *EGR2* and laboratory infrastructure. O.D. initiated, designed and supervised the

study; provided biological and genetic guidance; analyzed the data; wrote the paper together with T.G.P.G.; and provided laboratory infrastructure and financial support. All authors read and approved the final manuscript.

COMPETING FINANCIAL INTERESTS

The authors declare no competing financial interests.

Reprints and permissions information is available online at <http://www.nature.com/reprints/index.html>.

1. Delattre, O. *et al.* Gene fusion with an ETS DNA-binding domain caused by chromosome translocation in human tumours. *Nature* **359**, 162–165 (1992).
2. Gangwal, K. *et al.* Microsatellites as EWS/FLI response elements in Ewing's sarcoma. *Proc. Natl. Acad. Sci. USA* **105**, 10149–10154 (2008).
3. Guillou, N. *et al.* The oncogenic EWS-FLI1 protein binds *in vivo* GGAA microsatellite sequences with potential transcriptional activation function. *PLoS One* **4**, e4932 (2009).
4. Postel-Vinay, S. *et al.* Common variants near *TARDBP* and *EGR2* are associated with susceptibility to Ewing sarcoma. *Nat. Genet.* **44**, 323–327 (2012).
5. von Levetzow, C. *et al.* Modeling initiation of Ewing sarcoma in human neural crest cells. *PLoS One* **6**, e19305 (2011).
6. Tirode, F. *et al.* Mesenchymal stem cell features of Ewing tumors. *Cancer Cell* **11**, 421–429 (2007).
7. Delattre, O. *et al.* The Ewing family of tumors—a subgroup of small-round-cell tumors defined by specific chimeric transcripts. *N. Engl. J. Med.* **331**, 294–299 (1994).
8. Patel, M. *et al.* Tumor-specific retargeting of an oncogenic transcription factor chimera results in dysregulation of chromatin and transcription. *Genome Res.* **22**, 259–270 (2012).
9. Brohl, A.S. *et al.* The genomic landscape of the Ewing sarcoma family of tumors reveals recurrent *STAG2* mutation. *PLoS Genet.* **10**, e1004475 (2014).
10. Crompton, B.D. *et al.* The genomic landscape of pediatric Ewing sarcoma. *Cancer Discov.* **4**, 1326–1341 (2014).
11. Tirode, F. *et al.* Genomic landscape of Ewing sarcoma defines an aggressive subtype with co-association of *STAG2* and *TP53* mutations. *Cancer Discov.* **4**, 1342–1353 (2014).
12. Worch, J. *et al.* Racial differences in the incidence of mesenchymal tumors associated with *EWSR1* translocation. *Cancer Epidemiol. Biomarkers Prev.* **20**, 449–453 (2011).
13. Chung, C.C. & Chanock, S.J. Current status of genome-wide association studies in cancer. *Hum. Genet.* **130**, 59–78 (2011).
14. Dominy, J.E. Jr. *et al.* Discovery and characterization of a second mammalian thiol dioxygenase, cysteamine dioxygenase. *J. Biol. Chem.* **282**, 25189–25198 (2007).
15. Chandra, A., Lan, S., Zhu, J., Siclari, V.A. & Qin, L. Epidermal growth factor receptor (EGFR) signaling promotes proliferation and survival in osteoprogenitors by increasing early growth response 2 (EGR2) expression. *J. Biol. Chem.* **288**, 20488–20498 (2013).
16. Topilko, P. *et al.* Krox-20 controls myelination in the peripheral nervous system. *Nature* **371**, 796–799 (1994).
17. Mackintosh, C., Madoz-Gúrpide, J., Ordóñez, J.L., Osuna, D. & Herrero-Martín, D. The molecular pathogenesis of Ewing's sarcoma. *Cancer Biol. Ther.* **9**, 655–667 (2010).
18. Gao, C. *et al.* HEFT: eQTL analysis of many thousands of expressed genes while simultaneously controlling for hidden factors. *Bioinformatics* **30**, 369–376 (2014).
19. Radtke, I. *et al.* Genomic analysis reveals few genetic alterations in pediatric acute myeloid leukemia. *Proc. Natl. Acad. Sci. USA* **106**, 12944–12949 (2009).
20. Moffatt, M.F. *et al.* Genetic variants regulating *ORMDL3* expression contribute to the risk of childhood asthma. *Nature* **448**, 470–473 (2007).
21. Northcott, P.A. *et al.* Subgroup-specific structural variation across 1,000 medulloblastoma genomes. *Nature* **488**, 49–56 (2012).
22. Wang, K. *et al.* Integrative genomics identifies *LMO1* as a neuroblastoma oncogene. *Nature* **469**, 216–220 (2011).
23. GTEx Consortium. The Genotype-Tissue Expression (GTEx) project. *Nat. Genet.* **45**, 580–585 (2013).
24. Labalette, C. *et al.* Hindbrain patterning requires fine-tuning of early *krox20* transcription by Sprouty 4. *Development* **138**, 317–326 (2011).
25. Weisinger, K., Kayam, G., Missulawin-Drillman, T. & Sela-Donenfeld, D. Analysis of expression and function of FGF-MAPK signaling components in the hindbrain reveals a central role for FGF3 in the regulation of *Krox20*, mediated by Pea3. *Dev. Biol.* **344**, 881–895 (2010).
26. ENCODE Project Consortium. *et al.* An integrated encyclopedia of DNA elements in the human genome. *Nature* **489**, 57–74 (2012).
27. Rigg, N. *et al.* EWS-FLI1 utilizes divergent chromatin remodeling mechanisms to directly activate or repress enhancer elements in Ewing sarcoma. *Cancer Cell* **26**, 668–681 (2014).
28. Ernst, J. *et al.* Mapping and analysis of chromatin state dynamics in nine human cell types. *Nature* **473**, 43–49 (2011).
29. Maurano, M.T. *et al.* Systematic localization of common disease-associated variation in regulatory DNA. *Science* **337**, 1190–1195 (2012).
30. Ghislain, J. *et al.* Characterisation of cis-acting sequences reveals a biphasic, axon-dependent regulation of *Krox20* during Schwann cell development. *Development* **129**, 155–166 (2002).
31. 1000 Genomes Project Consortium. *et al.* An integrated map of genetic variation from 1,092 human genomes. *Nature* **491**, 56–65 (2012).
32. Robison, L.L. *et al.* The Childhood Cancer Survivor Study: a National Cancer Institute-supported resource for outcome and intervention research. *J. Clin. Oncol.* **27**, 2308–2318 (2009).
33. Edwards, S.L., Beesley, J., French, J.D. & Dunning, A.M. Beyond GWAS: illuminating the dark road from association to function. *Am. J. Hum. Genet.* **93**, 779–797 (2013).
34. Faye, L.L., Machiela, M.J., Kraft, P., Bull, S.B. & Sun, L. Re-ranking sequencing variants in the post-GWAS era for accurate causal variant identification. *PLoS Genet.* **9**, e1003609 (2013).
35. Surdez, D. *et al.* Targeting the EWSR1-FLI1 oncogene-induced protein kinase PKC-β abolishes Ewing sarcoma growth. *Cancer Res.* **72**, 4494–4503 (2012).
36. International HapMap 3 Consortium. *et al.* Integrating common and rare genetic variation in diverse human populations. *Nature* **467**, 52–58 (2010).
37. Robinson, J.T. *et al.* Integrative genomics viewer. *Nat. Biotechnol.* **29**, 24–26 (2011).

ONLINE METHODS

Cell culture. Ewing sarcoma cell lines A673, SK-N-MC, RDES and SK-ES1 were obtained from the American Type Culture Collection (ATCC); lines MHH-ES1 and TC-71 were from the German Collection of Microorganisms and Cell Cultures (DSMZ); lines EW1, EW3, EW7, EW16, EW18, EW23, EW24 and ORS were from the International Agency for Research on Cancer (Lyon, France); lines STA-ET-1, STA-ET-3, and STA-ET-8 were from the Children's Cancer Research Institute Vienna (kindly provided by H. Kovar); lines ES7, EW22 and POE were from the Institut Curie Research Centre (Paris, France); and line TC-32 was from the University of Nantes (kindly provided by F. Redini). A673-TR-shEF1 and SK-N-MC-TR-shEF1 harbor a doxycycline-inducible shRNA against *EWSR1-FLI1* (ref. 38). Neuroblastoma: SK-N-SH, IMR-32; breast cancer: MDA-MB-231; alveolar rhabdomyosarcoma: SJ-RH30 (from ATCC). Human MSC lines L87 and V54-2 were kindly provided by P. Nelson (University Hospital LMU)^{39,40}. Cells were grown at 37 °C in 5% CO₂ in a humidified atmosphere in RPMI 1640 medium (Gibco) containing 10% FCS (Eurobio), 100 U/ml penicillin and 100 µg/ml streptomycin (Gibco). Cell line purity and authenticity were confirmed by deep sequencing of susceptibility loci and short tandem repeat profiling. Cells were checked routinely by PCR for the absence of mycoplasma.

Transient transfection. Cells were seeded at a density of 1×10^5 to 2×10^5 per well of a six-well plate in a volume of 2.1 ml medium. Cell numbers were adjusted accordingly for transfection in larger or smaller volumes, and cells were transfected with siRNA (15 nM) with RNAiMAX (Invitrogen). The Qiagen AllStars Negative Control non-targeting siRNA was used as a control. siRNAs are listed in the **Supplementary Data**. For transfection with plasmids, 3×10^5 cells per well of a six-well plate were seeded in 2.5 ml medium and transfected with Lipofectamine LTX and Plus Reagent (Invitrogen). The pCDH1-MCS1-Puro (pControl) (System Biosciences) and the pCDH1-EWSR1-FLI1 (pEWSR1-FLI1) vectors were described previously^{3,35}.

Doxycycline-inducible shRNA constructs. Negative-control and specific shRNAs against *EGR2* were purchased from Sigma-Aldrich (**Supplementary Data**) and cloned into the pLKO-Tet-On all-in-one system⁴¹ (Addgene). Lentivirus was produced in HEK293T cells (from ATCC). SK-N-MC and POE cells were infected with a multiplicity of infection of 10 and selected for 7 d using 1–2 µg/ml puromycin (Invitrogen). Puromycin-resistant clones were grown from single cells. Knockdown efficacy was assessed in individual clones by quantitative real-time PCR (qRT-PCR) 96 h after the addition of doxycycline (1 µg/ml).

RNA extraction, reverse transcription and qRT-PCR. RNA was extracted with the Nucleospin II kit (Macherey-Nagel) and reverse-transcribed using the High-Capacity cDNA Reverse Transcription Kit (Applied Biosystems). PCRs were performed either using TaqMan assays with qRT-PCR Mastermix Plus without UNG (Eurogentec) or using SYBR green (Applied Biosystems). Oligonucleotides were purchased from MWG Eurofins Genomics (**Supplementary Data**). Reactions were run on an ABI/PRISM 7500 instrument and analyzed using the 7500 system SDS software (Applied Biosystems).

DNA microarrays. RNA from A673 and SK-N-MC cells was extracted 48 h after transfection with siRNA. RNA quality was checked with a Bioanalyzer (Agilent). Total RNA (200 ng) was amplified and labeled with the Affymetrix GeneChip Whole Transcript Sense Target Labeling Kit. Antisense copy RNA was hybridized on Affymetrix Human Gene 2.1 ST arrays. Data were normalized by means of Probe Logarithmic Intensity Error (PLIER) estimation and custom brainarray CDF (v16)⁴², are compliant with the MIAME guidelines, and were deposited in the Gene Expression Omnibus (GEO; [GSE62090](https://www.ncbi.nlm.nih.gov/geo/)).

eQTL analyses. Microarray data retrieved from GEO were normalized by robust multiarray averaging using custom brainarray CDF (v18)⁴². Accession codes are listed in the **Supplementary Data**. Matched genotype data for rs1848797 were retrieved from the series-matrix files of the original studies, except for the neuroblastoma and LCL data sets, for which genotypes were kindly provided by J. Maris (Children's Hospital of Philadelphia, Pennsylvania, USA) or by L. Liang (Harvard School of Public Health, Boston, Massachusetts, USA).

USA) and W. Cookson (Imperial College, London, UK). Additionally, the Broad GTEx database²³ was assessed for associations of *EGR2* and *ADO* expression with the genotypes at rs1848797 (data censoring: July 8, 2014; 13 normal tissue types with at least 60 samples per tissue type, amounting to 1,421 samples). *P* values of linear regressions are reported.

Between-group analysis (BGA). BGA was performed as described³⁵. In total, 279 Ewing sarcomas ([GSE34620](https://www.ncbi.nlm.nih.gov/geo/), [GSE34800](https://www.ncbi.nlm.nih.gov/geo/), [GSE12102](https://www.ncbi.nlm.nih.gov/geo/), and unpublished data), together with 32 desmoplastic small-round-cell tumors (unpublished data), 52 medulloblastomas ([GSE12992](https://www.ncbi.nlm.nih.gov/geo/) and unpublished data), 64 neuroblastomas ([GSE12460](https://www.ncbi.nlm.nih.gov/geo/) and unpublished data), 121 rhabdomyosarcomas ([E-TABM-1202](https://www.ncbi.nlm.nih.gov/geo/) and unpublished data), 35 malignant rhabdoid tumors (unpublished data) and 25 osteosarcomas ([GSE14827](https://www.ncbi.nlm.nih.gov/geo/)), were included in the BGA, which was carried out with the made4 R package⁴³. All microarray data were generated on Affymetrix HG-U133Plus2.0 arrays and simultaneously normalized using the gcrma package version 2.18.1 in R.

Immunoblots. Immunoblots were done with rabbit polyclonal anti-*EGR2* (1/2,000, PRB-236P, Covance), mouse monoclonal anti-*FLI1* (1:5,000, clone 7.3)⁴⁴, rabbit polyclonal anti-*FLI1* (1:250, RB-9295-PCL, Thermo Scientific), rabbit monoclonal anti-*ADO* (1:1,000, EPR6581, Abcam), mouse monoclonal anti- α -tubulin (1:10,000, DM1A, Sigma-Aldrich), and mouse monoclonal anti- β -actin (1:10,000, A-5316, Sigma-Aldrich). Then membranes were incubated with an anti-rabbit or anti-mouse immunoglobulin G (IgG) horseradish peroxidase-coupled secondary antibody (1:3,000, NA934 or NXA931, respectively; Amersham Biosciences). Proteins were detected by enhanced chemiluminescence (Pierce).

Sequence alignments. Mouse and human DNA sequences of *EGR2* enhancers were aligned using Clustal Ω (v1.2.0)⁴⁵.

Immunohistochemistry. Analyses were done on archived tumors derived from xenografted Ewing sarcoma cell lines (A673, TC-71, SK-ES1), an alveolar rhabdomyosarcoma cell line (SJ-RH30), and a neuroblastoma cell line (IMR-32) grown in immunocompromised mice. Sections were stained with polyclonal rabbit anti-*EGR2* as the primary antibody (1:50, Covance, PRB-236P) and hematoxylin.

Proliferation assays. *xCELLigence*. Cells were counted in real time with an *xCELLigence* instrument (Roche/ACEA Biosciences) monitoring impedance across gold microelectrodes. 8.5×10^3 cells per well of a 96-well plate were seeded in 200 µl medium containing transfection reagents (hexaplicates per group). Medium and transfection reagents were refreshed after 48 h. For Coulter counting, cells were plated in six-well plates and transfected immediately after seeding with siRNA. After 96 h, cells (including supernatant) were harvested and counted in a Vi-CELL XR Cell Viability Analyzer (Beckman Coulter) (duplicates per group). For Resazurin assay, 3×10^3 to 5×10^3 cells per well of a 96-well plate were seeded in 100 µl medium containing the desired growth factor. After 72–96 h, Resazurin (Sigma-Aldrich) was added (20 µg/ml) and cells were incubated for another 2–6 h, depending on the cell line. Fluorescence signals proportional to the number of cells were recorded in a FLUOstar Omega plate reader (BMG labtech SARL).

Analysis of cell cycle and apoptosis. Cell cycle phases were analyzed using propidium iodide (PI) (Sigma-Aldrich). 96 h after transfection with siRNA, cells (including supernatant) were harvested, fixed in 70% ethanol at 4 °C, and stained with PI solution (40 µg/ml, with 100 µg/ml RNase A). For analysis of apoptosis, cells (including supernatant) were harvested 96 h after transfection and stained with the Annexin-V-FITC/PI Apoptosis Detection Kit II (Becton Dickinson). Samples were assayed on an LSR II flow cytometer (Becton Dickinson). Data were analyzed with FlowJo software (TreeStar).

Clonogenic growth assays. Assays were performed essentially as described⁴⁶. Depending on the cell line, 1.5×10^3 to 3×10^3 cells per well of a 12-well plate were seeded in 1 ml medium containing 5% FCS for A673 cells and 10% FCS for SK-N-MC, EW7 and POE cells. Cells were transfected with siRNA 24 h after seeding and re-transfected every 96 h. After 9–14 d, colonies were methanol-fixed

and stained with crystal violet. Colony number and area were quantified on scanned plates with ImageJ. Relative clonogenicity is reported as the product of the colony number and the average colony size.

Spheroidal growth assays. 2×10^2 cells per well of a 96-well plate were seeded in 120 μ l in an equal mix of 10% FCS-containing RPMI 1640 medium and AIM-V medium (Gibco) in plates covered with attachment-preventing poly-2-hydroxyethyl-metacrylate (20 mg/ml PolyHEMA, Sigma-Aldrich). Doxycycline (1 μ g/ml) was added for the induction of *EGR2* knockdown. We used the following clones: SK-N-MC shControl#19, shEGR2_4#31, shEGR2_5#2, POE shControl21b, shEGR2_4#22, and shEGR2_5#2. After 9–11 d, spheres were documented by phase-contrast microscopy (four individual images per well; octaplicates per group). Images were analyzed with ImageJ. The relative sphere-formation capacity is reported as the product of the sphere number and the average sphere size.

DNA constructs and mutagenesis. Human elements mSat1, mSat2, MSE and BoneE were PCR cloned using the primers listed in the **Supplementary Data** into the pGL3-luc vector (Promega) upstream of the SV40 minimal promoter. T-to-A mutagenesis of mSat2 at rs79965208 was done with the QuickChange Mutagenesis Kit (Clontech).

Reporter assays and constructs. A673-TR-shEF1 and SK-N-MC-TR-shEF1 (ref. 38) were transfected with pGL3-luc vectors and *Renilla* pGL3-Rluc (ratio, 100:1). After 4 h, transfection media were replaced by media with or without doxycycline (1 μ g/ml). Cells were lysed after 48 h and assayed with a dual luciferase assay system (Promega). *Firefly* luciferase activity was normalized to *Renilla* luciferase activity.

Chromatin immunoprecipitation. ChIP was done with rabbit polyclonal anti-FLI1 (C19-X, Santa Cruz Biotechnology) or a rabbit IgG control in MHH-ES1 cells using the iDeal ChIP-Seq Kit for Transcription Factors (Diagenode). DNA was sheared to an average size of 500 bp to enable mSat2 PCR amplification followed by deep sequencing in an Illumina MiSeq instrument (>42,000 \times). ChIP efficacy was validated by qRT-PCR using a *CCND1* EWSR1-FLI1 binding site⁴⁷ (positive control) and an intronic *CCND1* locus (negative control; **Supplementary Fig. 10**). Primers are listed in the **Supplementary Data**.

Xenotransplantation experiments and mice. 8×10^6 POE or 15×10^6 SK-N-MC cells containing either a doxycycline-inducible negative control shRNA (POE shControl#21b or SK-N-MC shControl#19) or a specific shRNA against *EGR2* (POE shEGR2_4#22 or SK-N-MC shEGR2_4#31) were injected subcutaneously in the flanks of 6-week-old female C.B-17/SCID mice (Charles River Laboratories) in an equal mix of PBS and Matrigel (BD Biosciences). When tumors reached a volume of 75–100 mm³, mice were randomly assigned to either the control (5% sucrose in drinking water) or the treatment (doxycycline (2 mg/l) and 5% sucrose in drinking water) group. Tumor growth was monitored with a caliper every 2–3 d. Mice were killed once tumors reached a volume of 1,500 mm³, calculated as $V = a \times b^2/2$, with a being the largest diameter and b the smallest. Doxycycline-induced *EGR2* knockdown was confirmed by qRT-PCR 72 h after the start of doxycycline treatment in aliquots of the injected cells that were grown in parallel *in vitro*. Experiments were conducted in accordance with the recommendations of the European Community (86/609/EEC), the French Competent Authority, and UKCCCR (guidelines for the welfare and use of animals in cancer research). The sample size was not predetermined.

Human samples. Ewing sarcoma patients from France have been referred to the Institut Curie Hospital for molecular diagnosis since 1990. All subjects included in this study had a specific *EWSR1-ETS* fusion. Constitutional DNA of adequate quality was available for 343 subjects. This study received approval by institutional review boards and ethics committees (Comité de Protection des Personnes Ile-de-France I). Consent was obtained through communication with patients or families either by the referring oncologists or by the Institut Curie Unité de Génétique Somatique. Genomic DNA was isolated from bone marrow or blood via proteinase K lysis and a phenol chloroform extraction

method. We included control samples from 251 French subjects originally obtained as part of the Cancer Genetic Markers of Susceptibility (CGEMS) prostate cancer project⁴⁸. All control subjects were male and recruited in the geographical areas close to Paris, Nancy and Brest through participation in a systematic health-screening program funded by the French National Health Insurance. All controls were determined to be unaffected by cancer through medical examination and blood tests for prostate-specific antigen. The sample size was not predetermined.

Analysis of population substructure. Principal-component analysis (PCA) was performed as described⁴ to select genetically matching cases and controls for sequencing and association testing. To ensure genetic homogeneity in populations of affected subjects and controls, we used an EM-fitted Gaussian mixture clustering method assuming one cluster and noise to exclude isolated subjects (**Supplementary Fig. 6**). Noise was initialized by the NNclean function in the prabclus R package, which determines whether data points are noise or part of a cluster on the basis of a Poisson process model. This was followed by definition of the partition between the core of the data (one cluster) and the noise using the mclustBIC function of the mclust R package. Clustering was carried out in two dimensions for cases versus controls on the basis of the relative contribution of the first two PCA vectors.

DNA capturing and next-generation sequencing. *Illumina HiSeq2500 (non-repetitive regions).* DNA capturing of all three susceptibility loci⁴ was done with a customized Nextera target-enrichment system (Illumina). For all loci, the given risk haploblock and the adjacent 5' and 3' haploblocks were captured, for a total target size of 993 kb (library size, 500 bp; 2,614 Nextera probes with a predicted average coverage of the target regions of 95%: chr1:11,023,000–11,088,000 (171 probes); chr10:64,252,000–64,967,000 (1,882 probes); chr15:40,203,000–40,416,000 (561 probes)). Repetitive regions such as GGAA microsatellites were omitted in the Nextera design. Constitutional DNA was captured from 343 Ewing sarcoma cases and 251 controls. In addition, DNA from 14 Ewing sarcoma cell lines was captured. Massive parallel-end deep sequencing was done in an Illumina HiSeq2500 instrument (rapid mode; 150/150 nt) yielding a median capturing rate of 91.35% with at least 10 \times across samples and target regions and a median read depth per sample of 217 \times (**Supplementary Fig. 6**).

Illumina MiSeq (GGAA microsatellites). The mSat2 region was amplified by PCR with the primers listed in the **Supplementary Data** and Phusion High-Fidelity DNA polymerase (Thermo Scientific). After barcoding (Fluidigm), massive parallel-end deep sequencing was done in an Illumina MiSeq instrument (300/300 nt). Paired-end reads were merged using SeqPrep tools with the default parameters (median coverage, 124 \times).

Variant calling, genotyping, and statistical assessment. HiSeq reads were mapped on hg19 (NCBI GhR36 build) using BWA 0.6.2 with up to 4% mismatches allowed. BAM files were preprocessed according to the recommendations of the Genome Analysis Toolkit (GATK) using Samtools 1.8 (ref. 49), Picard tools 1.97 and GATK2.2.16 (ref. 50). Variant calling was done with GATK, focusing on single-nucleotide variants (SNVs) supported by ≥ 2 identical alternative reads at positions with $\geq 10\times$ in 90% of the samples. Genotype calling was done with the GATK DepthOfCoverage function. SNVs were defined as homozygous if the alternative allele ratio (AAR) was < 0.2 or > 0.8 , whereas heterozygous SNVs were defined by an AAR within ± 2 s.d. of the mean AAR of the non-homozygous SNVs. SNVs that had a minor allele frequency of > 0.05 and that did not depart from Hardy-Weinberg equilibrium in the entire cohort were considered for further analyses. Regional association results were plotted using LocusZoom⁵¹. The workflow is summarized in **Supplementary Figure 7**.

Association testing and analysis of LD. Statistical differences in genotype distributions were assessed with a logistic regression. Associations were adjusted for significant PCA eigenvectors (EV1, EV5 and EV6). *P* values were adjusted by false discovery rate. Significantly different SNVs were annotated with information available from the dbSNPv137 and RefGene databases using ANNOVAR v2013. LD and haplotype analyses were done with PLINK and HaploView^{52,53} as described by Gabriel *et al.*⁵⁴. Association testing conditional to rs79965208

was done with PLINK⁵³ with a logistic regression including significant PCA eigenvectors (EV1, EV5 and EV6) and the 'condition' command option.

Analysis of mSat2 MiSeq reads. To avoid mapping errors, we aligned raw reads on specific 'anchor' sequences (**Supplementary Data**) flanking mSat2. We determined the sequence between these anchors using a custom script designed to report the two alleles of each sample, taking into account a PCR-based slippage bias generating $n - 1$ GGAA repeats co-occurring with n GGAA repeats and a lower PCR-amplification rate affecting long GGAA stretches (≥ 19 GGAA repeats). Only alleles supported by $\geq 10\times$ were reported. Comparison of results with matched mSat2 Sanger sequences in 57 subjects showed an accuracy rate of our custom script and MiSeq analysis of 97.4%.

Replication of association results. A first replication of the initial rs79965208 association result was conducted in an independent sample of individuals of European descent, which was part of our preceding GWAS⁴. The pool of affected subjects included 156 individuals of European descent. Controls were 184 unaffected women from the French E3N cohort⁵⁵. In this cohort, the mSat2 region containing rs79965208 was directly sequenced in an Illumina MiSeq instrument. A second replication of the association of rs79965208 with Ewing sarcoma was conducted in an independent sample of individuals of European descent from the United States. This group of affected subjects included 162 individuals identified from the Childhood Cancer Survivor Study (CCSS), a multi-institutional follow-up study of 5-year survivors of childhood cancer diagnosed between 1970 and 1986 (ref. 32). Subjects were genotyped on the Illumina HumanOmni5Exome array as part of a larger project within the CCSS, with 4,052,581 unique polymorphic loci and 5,324 unique samples from unrelated individuals of European descent passing quality control thresholds (missing rate < 0.1, locus genotype concordance > 0.99 in 539 blinded duplicate samples, sample missing rate < 0.08, sample heterozygosity of 0.11–0.16, and genotyped sex concordant with self-report). Controls were 435 individuals of European descent from the Division of Cancer Epidemiology and Genetics reference panel of cancer-free adults⁵⁶. A region of ± 1 Mb of rs79965208 was imputed using the 1000 Genomes Project Phase 3 reference panel in IMPUTE2 (ref. 57). The rs79965208 SNP was well imputed (info score = 0.952). Associations were assessed using logistic regression models and adjusted for significant PCA eigenvectors (EV1, EV2 and EV9). The sample size was not predetermined.

Analysis of allele-specific expression. Allele-specific *EGR2* expression was assessed via targeted RNA sequencing (Illumina HiSeq2500) in 45 individuals with Ewing sarcoma who were heterozygous in constitutional DNA for rs61865883 (located in the *EGR2* 3' UTR), serving as transcribed allelic marker. Recurrent loss of heterozygosity at the *EGR2* locus was ruled out previously^{4,11} and was further excluded by targeted DNA sequencing of 10 out of the 45 subjects for which matched tumor and constitutional DNA were available. For each of these 45 subjects, we statistically compared the raw rs61865883 allele fractions of 16 tumors heterozygous for rs79965208 (A/T) with those of 29 tumors that were homozygous for rs79965208 (A/A or T/T) using a parametric two-tailed Student's *t*-test.

Analysis of ChIP-Seq, DNase-Seq and FAIRE-Seq data. Publicly available data were retrieved from the GEO. *.bed files from Patel *et al.*⁸ (GSE31838) were generated in FAIRE-Seq experiments in EW502 Ewing cells (GSM790218) and converted to hg19. ENCODE²⁶ SK-N-MC DNase-Seq (GSM736570) and

RNA Pol II ChIP-Seq data (GSM1010793), together with the FAIRE-Seq data, were analyzed in the Nebula environment⁵⁸ using Model-based Analysis of ChIP-Seq v1.4.2 (MACS)⁵⁹ and converted to *.wig format for display in the UCSC Genome Browser⁶⁰. Preprocessed ChIP-Seq data from Rigg *et al.*²⁷ (GSE61944) were converted from *.bigwig to *.wig format using the UCSC bigWigToWig conversion tool. Samples used were GSM1517544 SK-N-MC_shGFP_48h_FLI1, GSM1517553 SK-N-MC_shFLI1_48h_FLI1, GSM1517569 A673_shGFP_48h_FLI1, GSM1517572 A673_shFLI1_48h_FLI1, GSM1517548 SK-N-MC_shGFP_96h_H3K4me1, GSM1517557 SK-N-MC_shFLI1_96h_H3K4me1, GSM1517545 SK-N-MC_shGFP_48h_H3K27ac, and GSM1517554 SK-N-MC_shFLI1_48h_H3K27ac.

38. Carrillo, J. *et al.* Cholecystokinin down-regulation by RNA interference impairs Ewing tumor growth. *Clin. Cancer Res.* **13**, 2429–2440 (2007).
39. Conrad, C., Gottgens, B., Kinston, S., Ellwart, J. & Huss, R. GATA transcription in a small rhodamine 123(low)CD34(+) subpopulation of a peripheral blood-derived CD34(–)CD105(+) mesenchymal cell line. *Exp. Hematol.* **30**, 887–895 (2002).
40. Thalmeier, K. *et al.* Establishment of two permanent human bone marrow stromal cell lines with long-term post irradiation feeder capacity. *Blood* **83**, 1799–1807 (1994).
41. Wiederschain, D. *et al.* Single-vector inducible lentiviral RNAi system for oncology target validation. *Cell Cycle* **8**, 498–504 (2009).
42. Dai, M. *et al.* Evolving gene/transcript definitions significantly alter the interpretation of GeneChip data. *Nucleic Acids Res.* **33**, e175 (2005).
43. Culhane, A.C., Thioulouse, J., Perrière, G. & Higgins, D.G. MADE4: an R package for multivariate analysis of gene expression data. *Bioinformatics* **21**, 2789–2790 (2005).
44. Melot, T. *et al.* Production and characterization of mouse monoclonal antibodies to wild-type and oncogenic FLI-1 proteins. *Hybridoma* **16**, 457–464 (1997).
45. Sievers, F. *et al.* Fast, scalable generation of high-quality protein multiple sequence alignments using Clustal Omega. *Mol. Syst. Biol.* **7**, 539 (2011).
46. Franken, N.A.P., Rodermond, H.M., Stap, J., Haverman, J. & van Bree, C. Clonogenic assay of cells *in vitro*. *Nat. Protoc.* **1**, 2315–2319 (2006).
47. Boeva, V. *et al.* *De novo* motif identification improves the accuracy of predicting transcription factor binding sites in ChIP-Seq data analysis. *Nucleic Acids Res.* **38**, e126 (2010).
48. Yeager, M. *et al.* Genome-wide association study of prostate cancer identifies a second risk locus at 8q24. *Nat. Genet.* **39**, 645–649 (2007).
49. Li, H. *et al.* The Sequence Alignment/Map format and SAMtools. *Bioinformatics* **25**, 2078–2079 (2009).
50. McKenna, A. *et al.* The Genome Analysis Toolkit: a MapReduce framework for analyzing next-generation DNA sequencing data. *Genome Res.* **20**, 1297–1303 (2010).
51. Pruijm, R.J. *et al.* LocusZoom: regional visualization of genome-wide association scan results. *Bioinformatics* **26**, 2336–2337 (2010).
52. Barrett, J.C., Fry, B., Maller, J. & Daly, M.J. Haploview: analysis and visualization of LD and haplotype maps. *Bioinformatics* **21**, 263–265 (2005).
53. Purcell, S. *et al.* PLINK: a tool set for whole-genome association and population-based linkage analyses. *Am. J. Hum. Genet.* **81**, 559–575 (2007).
54. Gabriel, S.B. *et al.* The structure of haplotype blocks in the human genome. *Science* **296**, 2225–2229 (2002).
55. Clavel-Chapelon, F. *et al.* E3N, a French cohort study on cancer risk factors. E3N Group. Etude Épidémiologique auprès de femmes de l'Education Nationale. *Eur. J. Cancer Prev.* **6**, 473–478 (1997).
56. Wang, Z. *et al.* Improved imputation of common and uncommon SNPs with a new reference set. *Nat. Genet.* **44**, 6–7 (2012).
57. Howie, B.N., Donnelly, P. & Marchini, J. A flexible and accurate genotype imputation method for the next generation of genome-wide association studies. *PLoS Genet.* **5**, e1000529 (2009).
58. Boeva, V., Lermine, A., Barette, C., Guillouf, C. & Barillot, E. Nebula—a web-server for advanced ChIP-seq data analysis. *Bioinformatics* **28**, 2517–2519 (2012).
59. Zhang, Y. *et al.* Model-based analysis of ChIP-Seq (MACS). *Genome Biol.* **9**, R137 (2008).
60. Meyer, L.R. *et al.* The UCSC Genome Browser database: extensions and updates 2013. *Nucleic Acids Res.* **41**, D64–D69 (2013).